HUNGARIAN

Journal of

INDUSTRIAL CHEMISTRY

Edited by

the Hungarian Oil & Gas Research Institute (MÁFKI),
the Research Institute for Heavy Chemical Industries (NEVIKI),
the Research Institute for Technical Chemistry of the
Hungarian Academy of Sciences (MÜKKI),
the Veszprém University of Chemical Engineering (VVE).
Veszprém (Hungary)

Volume 9. 1981 Number 1.

HU ISSN: 0133—0276
CODEN: HJICAI

The "Hungarian Journal of Industrial Chemistry" is a joint publication of the Veszprém scientific institutions of the chemical industry that deals with the results of applied and fundamental research in the field of chemical processes, unit operations and chemical engineering. The papers are published in four numbers at irregular intervals in one annual volume, in the English, Russian, French and German languages

Editorial Office:
Veszprémi Vegyipari Egyetem
"Hungarian Journal of Industrial Chemistry"
H–8201 Veszprém, P. O. Box: 28.
Hungary

Orders may be placed with
KULTURA
Foreign Trading Co. for Books and Newspapers
Budapest 62. POB 149
or with its represenatives abroad, listed on the verso of the cover

FELELŐS SZERKESZTŐ: DR. BODOR ENDRE

KIADJA A LAPKIADÓ VÁLLALAT, 1073 BP. VII., LENIN KRT. 9–11.
TELEFON: 221-285. LEVÉLCÍM: 1906 BP. PF. 223
FELELŐS KIADÓ: SIKLÓSI NORBERT IGAZGATÓ

HUNGARIAN

Journal of

INDUSTRIAL CHEMISTRY

Edited by

the Hungarian Oil & Gas Research Institute (MÁFKI),
the Research Institute for Heavy Chemical Industries (NEVIKI),
the Research Institute for Technical Chemistry of the
Hungarian Academy of Sciences (MÜKKI),
the Veszprém University of Chemical Engineering (VVE).
Veszprém (Hungary)

Volume 9. **1981** **Number 1—4.**

HU ISSN: 0133—0276
CODEN: HJICAI

The „Hungarian Journal of Industrial Chemistry" is a joint publication of the Veszprém scientific institutions of the chemical industry that deals with the results of applied and fundamental research in the field of chemical processes, unit operations and chemical engineering. The papers are published in four numbers at irregular intervals in one annual volume, in the English, Russian, French and German languages

Editorial Office:
Veszprémi Vegyipari Egyetem
„Hungarian Journal of Industrial Chemistry"
H—8201 Veszprém, P. O. Box: 28.
Hungary

Orders may be placed with
KULTURA
Foreign Trading Co. for Books and Newspapers
Budapest 62. POB 149
or with its represenatives abroad, listed on the verso of the cover

FELELŐS SZERKESZTŐ: DR. BODOR ENDRE

KIADJA A LAPKIADÓ VÁLLALAT, 1073 BP. VII., LENIN KRT. 9—11.
TELEFON: 221-285. LEVÉLCÍM: 1906 BP. PF. 223
FELELŐS KIADÓ: SIKLÓSI NORBERT IGAZGATÓ

INDEX

Egyetemi Nyomda — 82.7281 Budapest, 1982. Felelős vezető: Sümeghi Zoltán igazgató

THE FOLLOWING ARE PLEASED TO ACCEPT SUBSCRIPTIONS TO THIS JOURNAL:

AUSTRALIA

C.B.D. Library and Subscription Service
Box 4886 G.P.O.
Sydney 2000

Cosmos Book and Record Shop
145 Acland Street
St. Kilda 3182

Globe and Co.
694—696 George Street
Sydney 2000

AUSTRIA

Globus (VAZ)
Höchstädtplatz 3
A—1200 Wien XX

BELGIUM

"Du Monde Entier" S. A.
Rue du Midi 162
B—1000 Bruxelles

Office International de Librairie
Avenue Marnix 30
B—1050 Bruxelles

CANADA

Pannonia Books
P.O. Box 1017
Postal Station "B"
Toronto, Ontario M5T 2T8

DENMARK

Munksgaard's Boghandel
Norregade 6
DK—1165 Copenhagen K

FINLAND

Akateeminen Kirjakauppa
Keskuskatu 2, P.O.B. 128
SF—00 100 Helsinki 10

FRANCE

Office International de Documentation et Librairie
48 Rue Gay Lussac
75 Paris 5

GERMAN FEDERAL REPUBLIC

Kubon und Sagner
Pf 68
D—8 München 34
BRD

GREAT BRITAIN

Bailey Bros and Swinfen Ltd.
Warner House, Folkestone
Kent CT 19 6PH England

HOLLAND

Martinus Nijhoff
Periodicals Department
P.O. Box 269
The Hague

Swets and Zeitlinger
Keizersgracht 487
Amsterdam C

ITALY

Licosa
P.O.B. 552, Via Lamarmora 45
50121 Firenze

JAPAN

Igaku Shoin Ltd.
Foreign Department
Tokyo International P.O. Box 5063
Tokyo

Maruzen Co. Ltd.
P.O. Box 5050
Tokyo International 100—31

Nauka Ltd.
Yasutomi Bldg. 5F 2—12 Kanda
Jinbocho, Chiyoda-ku
Tokyo 101

NORWAY

Tanum—Cammermayer
Karl Johangt. 41—43
Oslo 1

SWEDEN

Almqvist and Wiksell Förlag A. B.
Box 2120
S—103 13 Stockholm 2

Wennegren—Williams AB
Subscription Department Fack
S—104 Stockholm 30

SWITZERLAND

Karger Libri A. G.
Petersgraben 31
CH—4011 Basel

USA

Ebsco Subs. Services
1 st Ave North at 13th street
Birmingham, Ala. 35201

HUNGARIAN JOURNAL
OF INDUSTRIAL CHEMISTRY
VESZPRÉM
Vol. 9. pp. 1–12 (1981)

EXAMINATION OF THE COMPOSITION OF BARIUM ALKYLTHIOPHOSPHONATE LUBRICATING OIL ADDITIVE

S. Börzsönyi*, B. Markó-Monostory*, M. J. Abed**,
and K. Bélafy-Réthy*

(*Hungarian Oil and Gas Research Institute, Veszprém and
**Egyptian Petroleum Research Unstitute, Nasr City)

Received: February 16, 1981

In order to gain information about the composition of alkylthiophosphonic acids formed in the reaction of polyisobutylene and P_4S_{10} extraction of gasoline, solutions of thiophosphonic acids prepared at different conditions were made with methanol. The obtained fractions as well as their barium salts were investigated by elemental analysis, dialysis and infrared spectrometry. Barium alkylthiophosphonate was further fractionated in an ultracentrifuge. Characteristics of the acids prepared by the conventional process and the presence of P_4O_{10} respectively and that of their barium salts are discussed

An important group of lubricating oil additives are detergent-dispersant additives, having a hindering effect on the deposit formation from oils during the operation of the motor. Thiophosphonates are employed throughout the world for this purpose and are also produced in Hungary.

Procedures for preparing oil-soluble thiophosphonates, starting from hydrocarbons of high molecular mass (700–3000), reacting them at temperatures of 200–250 °C with tetraphosphorus decasulphide (P_4S_{10}), hydrolysing the product with steam and neutralising the formed acids with alkali earth metal oxides or hydroxides, have been published since the 1940s [1–7]. Nevertheless very little information is to be found in literature concerning the exact composition and structure of the products.

Based on the structure of the product identified by Fay and Lankelma [8] in the reaction of ciklohexene and P_4S_{10} the reaction product of higher olefins like polyisobutylene (PIB) and P_4S_{10} are fomulated as thioanhydrides of alkylene trithiophosphoric acids [9]:

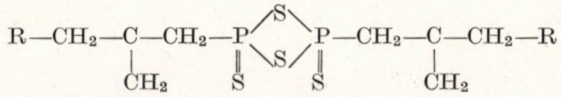

R being a polyisobutyl group.

According to Lacoste et al. [10] the additive is the salt of acids having the composition $RPS(OH)_2$. Abott and Stewart [11] found that the bulk of the

additive consists of thiopyrophosphates [$(RPO_2)_2(S)Ba$] sometimes being accompanied by a 10–25 mol percentage of thiophosphonates and phosphonates.

In a process developed by MÁFKI [12], polyisobutylene having an average molecular mass of 1000–1300 is reacted with tetraphosphorus decasulphide at 160 °C in the presence of tetraphosphorus decaoxide (P_4O_{10}). The acidic product formed is neutralized with crystalline barium hydroxide [$Ba(OH)_2 \times 8H_2O$]. The advantage of this procedure is that a lower reaction temperature can be employed in the first reaction step and that the other treating operations preceding the salt forming can be omitted.

We also tried earlier to explain the role of P_4O_{10} in the reaction and to obtain data about the composition of the compounds formed. It was shown [13] that PIB also reacts in this procedure only with P_4S_{10}, P_4O_{10} having an accelerating effect on the conversion. According to IR, ^1H- and ^{13}C—NMR spectral data the olefinic double bond can be involved in the reaction [14, 15].

The composition of the reaction product formed in the reaction of olefins and P_4S_{10} depends to a large extent on the starting molar ratios [13, 14]. In addition, PIB is a mixture of homologous and isomeric hydrocarbons. So the reaction product is a complicated system of related compound groups that also differ in their molecular masses.

Separation of the products obtained in the reaction of PIB and P_4S_{10}, as well as that of the former and P_4O_{10} by liquid chromatography (LC) [16] gave main fractions [24–44%] containing no oxygen and having a phosphorus to hydrocarbon molar ratio of 1.5–2, the S/P atomic ratio being between 2 and 3. The presence of metaphosphoric acid polymers was further rendered probable in the reaction product formed in the presence of P_4O_{10}.

The aim of the experiments discussed here was to gain information about the role of the different component groups present in the alkyl thiophosphonic acids on the composition of the additive.

Separation of Alkyl Thiophosphonic Acids by Extraction

The acidic products of the reaction of PIB and P_4S_{10} as well as that of the latter compounds and P_4O_{10} were aimed to separate by liquid-liquid extraction in order to gain fractions of different composition to be used as starting materials in barium salt formation. Extraction was chosen for this purpose, instead of LC, the amount of sample which can be separated being restricted in the latter method by the dimensions of the column applied.

On the basis of the experiences obtained with LC—where the PIB is not converted and the compounds containing no oxygen were eluable with hydrocarbons and the oxygen-containing ones with more polar eluents—to solvents of significantly different polarity: gasoline (b.p. 58–98 °C) and methanol were used in the extractions. The samples of alkyl thiophosphonic acids were dissolved in two volumes of gasoline and extracted with four volumes of methanol.

a) *Examination of the Reaction Products Formed in the Reaction of Polyisobutylene and Tetraphosphorus Decasulphide*

Alkyl thiophosphonic acids were prepared at temperatures between 160 and 240 °C, with the same starting molar ratio (0.48 mol of P_4S_{10} per mol of PIB having an average molecular mass of 1070), with a reaction time of 5 hours.

After four extraction steps carried out at room temperature, the methanol extracts were combined and both phases were freed from solvents by distillation in vacuum. The amounts of the obtained fractions and their composition are summarized in *Table 1.*

Table 1.

Composition of alkyl thiophosphonic acids obtained in the reaction of polyisobutylene and P_4S_{10} and that of their fractions

	Sample	Thiophosphonic acid		$\overline{M}$	P%	S%	O%	Acid number mg KOH/g	Saponification number	S/P at/at	Acid/P equ/at	Saponifiable equ/at
		temperature of preparation °C	amount %									
Starting alkyl thiophosphonic acid	6	160	100	–	1.2	2.8	1.5	10.3	18.7	2.3	0.43	0.86
	7	180	100	–	2.9	5.0	2.0	21.1	51.4	1.7	0.40	0.98
	8	200	100	–	3.0	6.5	2.5	22.2	49.6	2.1	0.41	0.91
	9	220	100	–	3.6	7.1	2.7	24.2	59.4	1.9	0.37	0.91
	10	240	100	–	4.4	7.8	3.2	35.0	85.9	1.7	0.44	1.1
Gasoline fraction	6/1	160	87.8	1620	0.8	2.5	0.0	5.5	16.8	3.0	0.38	1.2
	7/1	180	85.0	1600	1.7	4.4	0.0	9.4	22.1	2.5	0.30	0.72
	8/1	200	82.8	1560	2.1	5.3	0.4	12.0	24.0	2.4	0.31	0.63
	9/1	220	79.3	1520	2.2	5.8	0.3	13.2	27.0	2.6	0.33	0.68
	10/1	240	79.5	1560	2.6	5.3	0.7	16.6	32.3	2.0	0.35	0.69
Methanol fraction	6/2	160	12.2	–	3.2	5.9	–	28.5	38.7	1.8	0.49	0.67
	7/2	180	15.0	1040	5.8	10.2	4.5	81.7	122	1.7	0.78	1.2
	8/2	200	17.2	×	6.8	12.1	–	81.2	126	1.7	0.66	1.0
	9/2	220	20.7	–	7.7	10.7	–	126	159	1.3	0.90	1.1
	10/2	240	20.5	–	10.5	13.2	–	146	180	1.2	0.77	1.0

$\overline{M}$ = average molecular mass (by vapour pressure osmometry)
at. = gram-atom
equ. = gram-equivalent

Sulphur and phosphorus content of the starting alkyl thiophosphonic acids increased with the temperature of their preparation. The concentration of the mentioned elements and that of the functional groups generally decreased in the gasoline and increased in the methanol fractions. The compounds containing oxygen formed by hydrolysis with the water content of air during the operations were concentrated in the methanol fraction. The S/P atomic ratios in the gasoline fractions—like in the main fraction obtained by LC—were between 2 and 3, those of the methanol fractions—in accordance with their oxygen content—below 2.

The IR spectra support the tendencies outlined before. *Fig. 1* represents the spectrum of an alkyl thiophosphonic acid and the spectra of its fractions. The intensities of the absorptions originating from the valence vibration of P=S and P—O bonds, decrease in the gasoline and increase in the methanol fraction relative to the same intensities in the starting acid, the absorption due to P—O bonds being more significant in the methanol fraction.

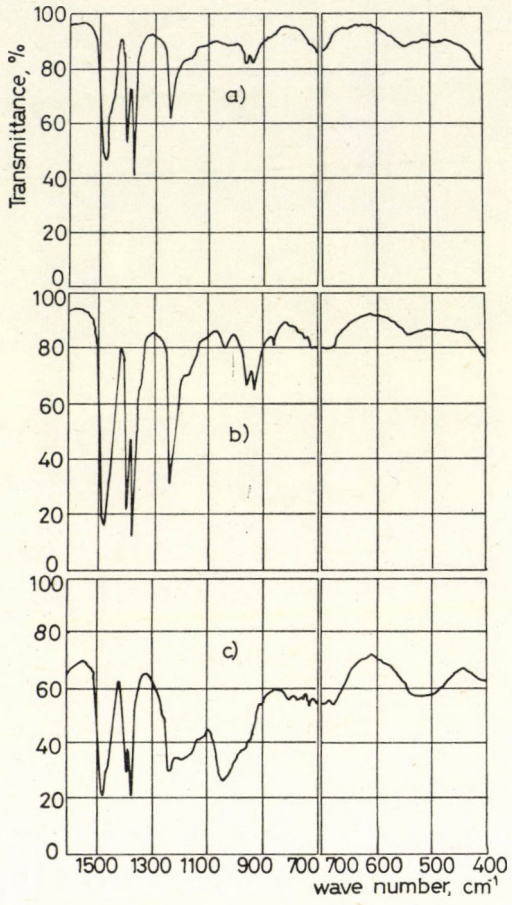

Fig. 1
a) IR spectrum of alkylthiophosphonic acid prepared at 220 °C without P_4O_{10} and the spectra of its fractions:
b) gasoline fraction *c)* methanol fraction

The polar and nonpolar fractions also differ in respect of their molecular mass, the average molacular mass of the gasoline fractions being higher. Regarding the unreacted PIB ($\overline{M} = 1070$) content of these fractions, the difference in molecular mass of the reaction products between the two type of fractions is certainly larger than measured.

b) *Examination of the Product Formed in the Reaction of Polyisobutylene and Phosphorus Decasulphide Prepared in the Presence of Phosphorus Decaoxide*

The alkyl thiophosphonic acid to be extracted was prepared at a temperature of 160 °C, in 5 hours of reaction time, with a starting molar ratio of 0.36 P_4S_{10}: 0.38 P_4O_{10}:1.00 PIB. Five-step extraction was made here, expecting a larger

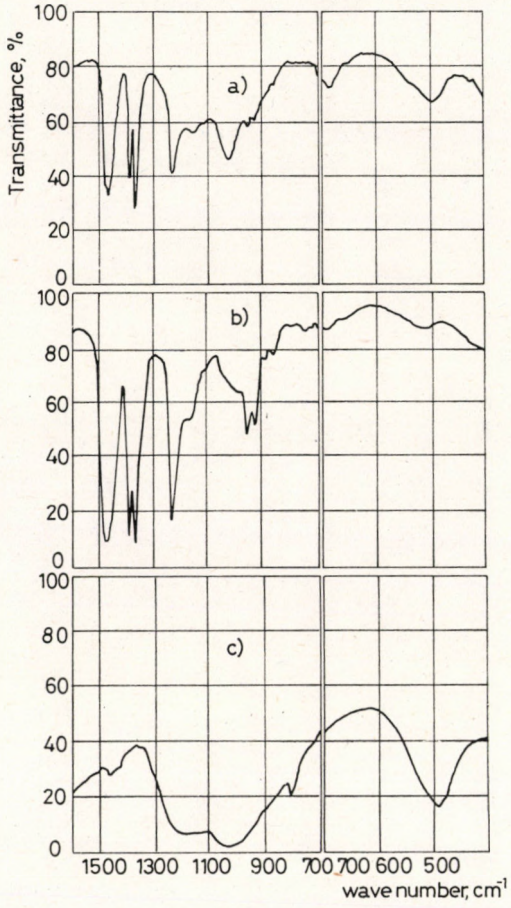

Fig. 2
a) IR spectrum of an alkylthiophosphonic acid pepared in the presence of P_4O_{10} and the spectra of its fractions:
b) gasoline fraction *c)* methanol fraction

content of polar compounds and the product obtained in the third step was treated with steam. The amount and composition of the fractions obtained up to the 3rd and 5th extraction steps respectively are represented in *Table 2*.

The tendency of distribution of sulphur and phosphorus content as well as that of the "acidic" functional groups between the fractions is the same as discussed in the former section; the differencies observed in the numeric data are due to the presence of inorganic phosphoric acids in methanol fractions.

In accordance with the differences in elemental and functional group composition, the IR spectra show the same tendency as established from the spectra of the samples prepared without P_4O_{10}, the presence of the bands originating from P–O bonds in the methanol fraction being here much more explicit. A supplementary band characteristic to P=O valence vibration in the spectrum of the latter fraction was observed.

Table 2.

Composition of alkyl thiophosphonic acid obtained in the reaction of polybutylene and P_4S_{10} in the presence of P_4O_{10} and that of its fractions

	Sample	Amount %	P %	S %	O %	Acid number mg KOH/g	Saponification number mg KOH/g	S/P at/at	Acid/P equ/at	Saponifiable equ/at
Starting alkyl-thio-phospho-nic acid	0	100	3.7	5.2	6.6	57.7	88.2	1.5	0.86	1.3
Gasoline fraction	3/1	74.8	1.5	2.9	–	13.3	13.3	1.9	0.50	0.50
	5/1	68.9	1.0	1.4	–	8.0	8.0	1.4	0.45	0.45
Methanol fraction	1–3/2	25.2	10.8	11.7	–	205	279	1.0	1.0	1.3
	4–5/2	5.9	6.4	4.1	–	150	150	0.6	1.3	1.3

at. = gram-atom
equ. = gram-equivalent

c) *Conversion of Polyisobutylene*

In order to determine the unreacted PIB present in gasoline fractions, they were converted to their barium salt, the hydrocarbon content of which can be separated by dialysis [17]. The PIB content of the fractions shown in *Table 3* were calculated on the basis of the assumption that the gasoline fractions contain practically all the nonreacted PIB content of the alkyl thiophosphonic acids.

According to the data shown, the nonreacted PIB content of the samples increases with the temperature of preparation, the amount of the polar com-

Table 3.

Amount and composition of the extraction fractions considering the content of polybutylene not converted

Sample	Preparation of alkyl thiophosphonic acid		Gasoline fraction			Methanol fraction %
	P_4O_{10}	temperature °C	PIB not converted %	reaction product %	P/PIB in reaction product at/mol	
6	–	160	57.3	30.5	0.9	12.2
7	–	180	31.0	54.0	1.0	15.0
8	–	200	30.1	52.7	1.3	17.2
9	–	220	20.0	59.3	1.1	20.7
10	–	240	20.3	59.2	1.4	20.5
5	+	160	25.0	44.0	0.6	31.0

at. = gram-atom

pounds also increasing in the same order. The addition of P_4O_{10} to the reaction mixture increases the conversion of PIB at the same temperature. The simultaneous increase of the amount of the polar fraction is due to the presence of some inorganic hydrolysis products of P_4O_{10} concentrating in this fraction.

There is an important difference between the gasoline fractions in respect of the atoms of phosphorus per mol of reacted PIB. This ratio is the lowest in the fraction of the acid prepared in the presence of P_4O_{10}, increasing otherwise with the reaction temperature of the synthesis. On the basis of the differencies in P/PIB ratios measured in the gasoline fractions (1.0 ± 0.4) and the ratio calculated in the methanol fraction 7/2 (P/mol = 2.0) the concentration of compounds having a lower molecular mass and containing more functional groups in the "polar" fractions may be regarded as a general tendency.

Preparation of Barium Salts from the Fractions Obtained by Extraction

Barium salts were prepared from alkyl thiophosphonic acids and from some chosen fractions obtained by extraction in order to gain information, about their solubility. This property is important, because only the oil-soluble thiophosphonates are suitable as lubricant additives.

Composition of the starting alkylthiophosphonic acids and their barium salt, as well as the part of the acidic fractions forming oil-soluble salt is summarized in *Table 4*. The fraction marked 1/2 is the first methanol extract of an alkyl-thiophosphonic acid synthetised in the presence of P_4O_{10}, consisting in the bulk of inorganic phosphoric acids.

According to the data, only a small part of this fraction formed salts soluble in oil. The other methanol fraction, at the same time, converted almost quantitatively to an oil-soluble barium salt. According to the composition of the

Table 4.

Composition of barium salts prepared from alkyl thiophosphonic acids and from their fractions

Type of ATA	P_4O_{10} at preparation of ATA	Alkyl thiophosphonic acid				Barium salt				
		sample	P,%	saponification number mg KOH/g	converted to oil-soluble salt %	sample	Ba,%	P,%	TBN mg KOH/g	Ba/P at/at
Without extraction	–	9	3.6	59.4	–	9/Ba	9.5	3.5	81.6	0.61
	+	0	3.7	88.2	–	0/Ba	12.0	2.4	80.7	1.13
Gasoline fraction	–	8910/1	2.3	27.8	82.4	8910/1Ba	4.0	1.3	31.9	0.69
	+	11/1	1.8	26.5	83.0	11/1Ba	5.2	1.5	45.7	0.78
Methanol fraction	–	8910/2	8.4	161	93.0	8910/2Ba	18.9	5.9	132	0.72
	+	1/2	26.4	650	4.7	1/2Ba	1.2	2.3	8.1	0.12

ATA alkyl thiophosphonic acid
TBN = total basic number
at. = gram-atom

starting acid, this salt has a higher barium and phosphorus content than the salts obtained from the gasoline fractions.

The difference between the barium content and Ba/P ratios of the salts prepared without preliminary extraction of the acids shows that inorganic phosphates can also be present (sample O/Ba) in spite of the fact that inorganic phosphate itself does not dissolve in oil.

In the IR spectra of the barium salts prepared without preliminary extraction of the acids *(Fig. 3)*, the relative intensities of the bands due P–O–(Ba)

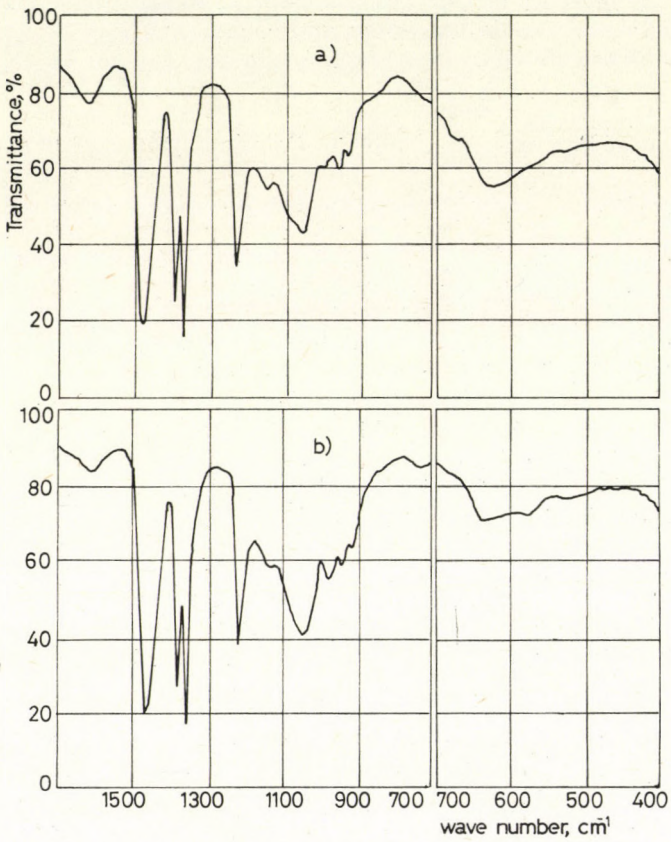

Fig. 3
IR spectra of barium salts obtained from alkylthiophosphonic acids
a) salt of alkylthiophosphonic acid prepared without P_4O_{10}
b) salt of alkylthiophosphonic acid prepared in the presence of P_4O_{10}

bonds are approximately the same. The differences appearing in the region of the valence vibration of the P=S bonds and in the absorption due to the deformation vibration of PO_xS_y groups, support the presence of inorganic phosphates in the salt of the thiophosphonic acid prepared in the presence of P_4O_{10}. The spectra shown in *Fig. 4* demonstrate the differences between the salts of gasoline and methanol fractions discussed earlier.

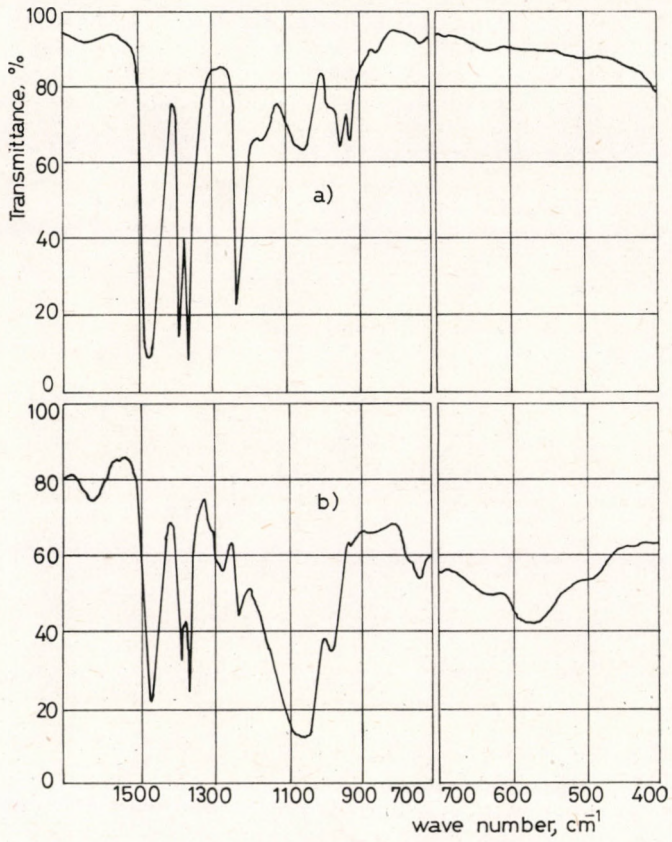

Fig. 4
IR spectra of barium salts obtained from the fractions of an alkylthiophosphonic acid prepared without P_4O_{10}:
a) salt from the gasoline fraction
b) salt from the methanol fraction

Separation of Barium Salts by the Application of an Ultracentrifuge

The conclusions concerning the composition of barium salts outlined in the previous section are in agreement with earlier results obtained in our laboratory. From the data of investigations carried out with alkyl thiophosphonic acids prepared in the presence of P_4O_{10} containing a phosphorus isotope of ^{32}P [13] it was established that alkyl thiophosphonic acids and their barium salts form rather stable colloid systems with the derivatives of P_4O_{10}. It was not possible to separate these inorganic compounds by centrifuging (r.p.m. = 6,000) the gasoline solutions of alkylthiophosphonic acids and those of their barium salts for several hours.

These experiences prompted us to try the separation of inorganic barium salts from organic thiophosphonates under more vigorous conditions. The maximum r.p.m. of the centrifuge rotor applied was 50,000 ($R_{max} = 187.265$ g).

The sample was dissolved in 20 volume of gasoline and centrifuged during 4 hours. Four phases formed as result, which were separated and dialysed in order to gain fractions containing no hydrocarbon (PIB). The composition of the fractions obtained and their amounts are given in *Table 5.*

Table 5.

Composition of fractions obtained by separation of a barium alkyl thiophosphonate additive in an ultracentrifuge

Sample	Vol. %	Ba %	TBN mg KOH/g	S %	P %	C %	H %	O* %	Ba	P	S	O
									atoms per mol of PIB			
Starting additive	–	5.0	50.6	1.1	0.8	–	–	–	–	–	–	–
Upper phase	9	13.6	86.4	3.2	3.3	66.9	11.7	1.6	1.7	1.7	1.7	1.7
Middle phase 1	44	14.9	94.6	3.3	3.2	64.1	10.8	3.7	1.9	1.7	1.7	4.0
Middle phase 2	44	17.8	112.8	3.9	3.5	60.5	10.6	3.7	2.4	2.0	2.0	4.0
Lower phase	3	29.3	185.7	3.5	6.2	47.3	8.2	5.5	5.0	4.5	2.5	8.0

*estimated from the sum of the other elements

According the data, nearly 90 per cent of the starting material concentrated in the two middle layers. Their composition was about the same and could be characterized with the formula $R(PSO_2Ba)_2$, R being an alkyl group corresponding to the average molecular mass of the starting polybutylene. The reason for the separation of these two middle phases may be the different association degree of the individual molecules included. The upper phase differed from the middle phases in the oxygen content.

Regarding its amount, the lowest not very important phase according to the IR spectrum contained a significant amount of inorganic phosphates. Formulating these latter as $BaHPO_4$ and supposing otherwise organic compounds similar to that found in the middle phases, 25–30% of inorganic phosphates can be present accordint to the elemental composition. This amount indicates less than 1% of inorganic compounds separated from the starting additive.

The ability of barium alkylthiophosphonates to disperse inorganic phosphates was further confirmed by an experiment in which phosphoric acid was added

Table 6.

Effect of phosphoric acid on the composition of the barium alkyl thiophosphonate additive

Experiment	Addition of % H_3PO_4	Composition of the product	
		Ba %	TBN mg KOH/g
12	–	4.4	46.2
13	10%	10.1	92.3

to the alkyl thiophosphonic acid and barium salt was prepared from the mixture. The same organic acid was parallel converted to its barium salt without any addition of phosphoric acid. On the basis of the difference measured in barium content of the samples purified by centrifugation *(Table 6)* barium alkyl thiophosphonate was able to disperse about 8–10% of barium phosphates.

Conclusions

Applying liquid — liquid extraction, mixtures of compounds containing 0.6–2 phosphorus atoms per mol of the starting PIB were separated from alkyl thiophosphonic acids. The number of functional group per hydrocarbon chain increases with the temperature used in the synthesis of the acids. The "polar" fraction separated from the alkyl thiophosphonic acids and which contains more than one functional group per mol could also be converted almost quantitatively to an oil-soluble barium salt.

The conversion of PIB increased if the alkyl thiophosphonic acid was prepared in the presence of P_4O_{10}.

A main fraction with the composition of $R(PSO_2Ba)_2$ was separated by ultracentrifuging and dialysis from the barium alkyl thiophosphonate additive prepared with MÁFKI technology. This product contains twice as many functional groups per mol of hydrocarbon as the product described in literature.

It could be shown that barium alkyl thiophosphonate disperses, a significant part of the salts formed from the hydrolysis products of P_4O_{10} in the form of a stable colloidal system. This is in accordance with our recent ^{32}P tracer experiments.

REFERENCES

1. U.S. Pat. 847,339
2. U.S. Pat. 936,650
3. U.S. Pat. 910,738
4. U.S. Pat. 903,950
5. U.S. Pat. 962,574
6. U.S. Pat. 958,520
7. BRD Pat. 1.053,125
8. Fay, P. and Lankelma, H. P.: J. Amer. Chem. Soc., *1952*, 74, 4933.
9. Indopol Polybutenes. Amoco Chemicals Corporation, Bulletin 12 G, 12 F.
10. U.S. Pat. 2.935,505
11. Advances in Petroleum Chemistry and Refining. Vol. 7., Ed. McKetta Jr., J. J., Interscience, New York — London 1963.
Stewart, W. T. and Stuart, F. A.: Lubr. Oil Additives. p. 25—26.
12. Hung. Pat. 156,066.
13. Markó-Monostory, B. and Bencze, P.: Ropa a Uhlie, *1980*, 22, 205.
Markóné-Monostory, B. and Bencze, P.: MÁFKI Közl. *21*, (in press).
14. Babóczky, K., Markó, B. and Bencze, P.: V. Internat. Conference of Organic Phosphorus Chemistry. Gdansk, September 16—21, 1974.
15. Babóczky-Kampós, K. and Bencze, P.: MÁFKI Közl. *1975*, 16, 132.
16. Markó-Monostory, B. and Wittmann, Zs.: MÁFKI Közl. *1977*, 18, 39.
17. Ifcsics, M., Bélafy-Réthy, K. and Kerényi, E.: MÁFKI Közl. *1978*, 20, 29.

РЕЗЮМЕ

Проводили экстракцию при различных условиях газолинового раствора тиофосфорных кислот с целью определения состава алкилтиофосфорных кислот путем реакции P_4S_{10} с полиизобутиленом. Полученные фракции и их бариевые соли изучали элементарным анализом, диализом и инфракрасной спектрометрией. Алкилтиофосфонат бария разделяли на фракции с помощью ультрацентрифуги. В данной стати приведены результаты анализа хатактерных свойств кислот и бариевых солей произведенных традиционным способом и в присуствии P_4O_{10}.

HUNGARIAN JOURNAL
OF INDUSTRIAL CHEMISTRY
VESZPRÉM
Vol. 9. pp. 13–20 (1981)

ABGASREINIGUNG IN DER STICKSTOFFINDUSTRIE MIT ZEOLITH ABSORBENTIEN

J. Sütő, G. Klopp, und I. Szebényi

(Technische Universität Budapest, Lehrstuhl für Chemische Technologie

Eingegangen am 17. Juli 1980.

Die Stickstoffoxyde gelten auch heute für schädlichste Komponenten der Luftverschmutzung. Ihre Emissionsraten liegen in meisten Betrieben mindestens um eine Größenordnung höher als der Sollwert. Zur Verminderung der Emission ist in vielen Fällen der einzige Weg der Einbau bzw. die Neugestalltung der Abgasreinigungsanlagen. In diesem Bericht wird ein Überlick über verschiedene Reinigungsmethoden gegeben. Darüber hinaus werden die Versuchsergebnisse der Herstellung und Anwendung zeolithhaltiger Adsorbentien einheimischer Herhunft erörtert.

Die Stickstoffindustrie ist eine gut bekannte Quelle von Luftschmutzung in der chemischen Industrie. Die in den Abgasen der Salpetersäure-Herstellung vorhandenen Stickstoff-Oxyde (NO und NO_2) gehören zu den schädlichsten Luftverunreinigungskomponenten. Diese verursachen schon im ppm-Konzentrationsbereich chronische Erkrankungen der Atmungsorganen und im Konzentrationsbereich von 100–1000 ppm kann die Einatmung der Stickstoff-Oxyde, zu Unfällen mit tödlicher Auswirkung führen [1, 2].

Die Stickstoff-Oxyd-Konzentration der Abgase von Salpetersäure-Betrieben beträgt auch heute in einigen Fällen 0,3—0,4 Vol.%. In Ungarn erreicht die Menge des emittierten Stickstoff-Monoxyds dieser Betriebe ungefähr 20 000 t/Jahr. Das bedeutet nicht nur eine schädliche lokale Verunreinigungsquelle sondern auch einen beträchtlichen Verlust für die Betriebe.

Wegen der schädlichen Wirkung der Stickstoff-Oxyde wird die Emission der Salpetersäure-Betriebe in vielen Ländern geregelt [3, 4, 5]. Die Konzentration der Stickstoff-Oxyde im Abgas muß heute in einem modernen Betrieb unter 2000 ppm liegen. Um diese Forderung einhalten zu können, muß man die Betriebe mit Umsicht planen und bauen mit besonderer Rücksicht auf die Abgasreiniegung.

Die einfachste Lösung für wirksame Abgasreinigung väre die effektive Stickstoff-Oxyd-Absorption. Es ist aber nicht einfach durch Absorption eine Stickstoff-Oxyd-Konzentration im Abgas unter 200 ppm zu erreichen. Bisher

war es nur dann möglich, wenn der Absorptionsdruck bedeutend erhöht wurde. Im allgemeinen ist ein Betriebsdruck von 6,5—15 bar nötig, um den vorher genannten Grenzwert zu erreichen [5, 6]. Solche Druckwerte waren aber früher in Salpeter-Säure-Betrieben nicht typisch. Deshalb muß man in unseren Betrieben für die Abgasreinigung einen anderen Weg einschlagen.

Abgasreinigungsmethoden

Zur absorptiven Abgasreinigung wurden früher verschiedene wässerige Lösungen von NaOH, Na_2CO_3, $Ca(OH)_2$, $Mg(OH)_2$, NH_3, dann Schwefelsäure, verdünnte oder konzentrierte Salpetersäure usw. verwendet. Hier sind vor allem zwei Probleme zu bemerken. Die Absorption ist in meisten Fällen nicht wirksam genug, und in den verwendeten alkalischen Lösungen entstehen unter anderen auch Nitrite, die explosiv, korrosiv und giftig sind. Die nitrat- und nitrithaltigen Lösungen finden meistens keine Verwendungsgebiete. Die Schwefelsäure kann man wegen Wassergehaltes des Abgases nicht vorteilhaft werwenden. Die Literatur der Abgasreinigund durch Absorption wurde von H. Vogel und W. Teske [7, 8] zusammengefaßt.

In Japan verwendet man neuestens auch alkalische $MKnO_4$-Lösungen für Stickstoff-Oxyd-Absorption [9]. Die verschiedenen Verfahren wurden von allem für die Reinigung von Rauchgasen ausgearbeitet. Als Nebenprodukt bekommt man in diesen Prozessen K_2SO_4 und KNO_3, die als Düngemittel verwendet werden können. Das aus dem $KMnO_4$ entstehende MnO_2 muß bei diesen Reinigunsprozessen regeneriert werden.

In den Salpetersäure-Betrieben hat sich meistens die katalytische Reduktion für die Reinigung der Abgase durchgesetzt. Man unterscheidet selektive und nicht selektive Reduktion. Bei selektiver Reduktion wird NH_3 als Reduktionsmittel benützt. Ammoniak reagiert im Abgas nur mit den Sickstoff-Oxyden im Gegensatz zu der häufiger benutzten nicht selektiven Reduktion, wo man Erdgas und wasserstoffhaltige Gase als Reduktionsmittel verwendet. Erdgas und wasserstoffhaltige Gase reagieren zuerst mit dem freien Sauerstoff und mit dem Stickstoff-Dioxyd, und die Reduktion des Stickstoff-Monoxyds kann nur mit Gasüberschuß und bei einer verhältnismäßig hohen Temperatur erreichet werden.

Die katalytische Stickstoff-Oxyd-Reduktion wurde zuerst in den Vereinigten Staaten in der Mitte der 60-er Jahren an die Reduktion des Stickstoff-Monoxyds angepaßt, obgleich diese Reduktion als katalytische Nachverbrennung schon früher für zusätzliche Energiegewinnung verbreitet angewandt wurde [10]. Die Stickstoff-Monoxyd-Reduktion führt in einigen Fällen, vor allem wenn die Sauerstoff-Konzentration im Abgas zu hoch ist, zu einer so hochen Abgas-Temperatur, die den Katalysator und die Konstruktionsbaustoffe beschädigt. In diesen Fällen ist vortleilhaft zweistufige katalytische Reduktion oder eine Abgas-Rezirkulation einzusetzen. So kann man die zur Reduktion erforderliche Temperatur mit weniger Fremdenergie erreichen und auch die Abgastemperatur herabsetzen.

Im *Bild 1* wird das katalytische Reduktionssystem der Firma Engelhard Minerals and Chemicals Corp. gezeigt. Das System ist vollautomatisiert und enthält auch einen adsorptiven Entschwefelungsapparat [3].

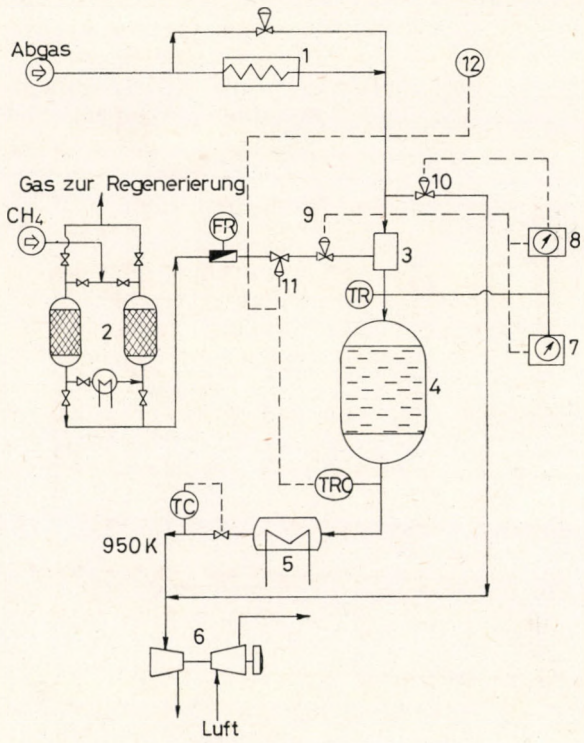

Bild 1

Katalytische Abgasreinigungsanlage für Salpetersäure-Betriebe der Firma Engelhard *1.* Abgasvorheizer; *2.* Molekularsieb-Entschwefelungsapparat für Erdgas; *3.* Gasmischer; *4.* Reaktor für die Reduktion der Stickstoff-Oxyde; *5.* Dampfkessel; *6.* Energie-Rückgewinnung; *7.* Methananalysator; *8.* Sauerstoffanalysator; *9.* CH_4/O_2 Verhältnisregler; *10.* Umleitung, geöffnet wenn der O_2-Gehalt im Abgas zu hoch ist; *11.* Möglichkeit zum Eingriff, wenn die Reaktortemperatur zu hoch ist; *12.* Möglichkeit zur Stillegung der Methaneinführung, wenn eine Störung im Salpetersäure-Betrieb auftritt; FR: Strömungsmeßung und -Registrierung; TR: Temperatur-Meßung und -Registrierung; TRC: Temparatur-Meßung, -Registrierung und -Regelung; TC: Temperatur-Regelung

Die Problemanalyse der katalytischen Abgasreinigung zeigt, dieses Verfahren kann nur in den Hochdruckbetrieben Anwendung finden. Die Absorption ist in diesen Betrieben wirksamer, und man kann die bei der reduktion entstehende Energie nicht nur zur Dampfherstellung, sondern auch zur Gewinnung elektrischer Energie anwenden. Der Energiehaushalt kann also in diesen Betrieben wirksamer gestaltet werden. Diese Situation ist bei uns in Ungarn bei Pétfürdő gegeben, wo der modernste Salpeter-Säure-Betrieb mit 8 bar Betriebsdruck zu finden ist. Dem Betrieb gehört auch eine katalytische Abgasreinigungsanlage.

Die selektive katalytische Reduktion wurde vor allem in Japan zur Reduktion der Stickstoff-Oxyde von Rauchgasen entwickelt unter Anwendung verschiedener Katalysatoren [9].

Für selektive Reduktion der Stickstoff-Oxyde in Abgasen der Salpetersäure-Betriebe hat die Firma Mitsubishi Chemical Industries ein Verfahren entwickelt. Das *Bild 2* zeigt das Prinzipschema einer zum gegebenen Salpetersäure-Betrieb gekoppelten Abgasreiningunsanlage [4].

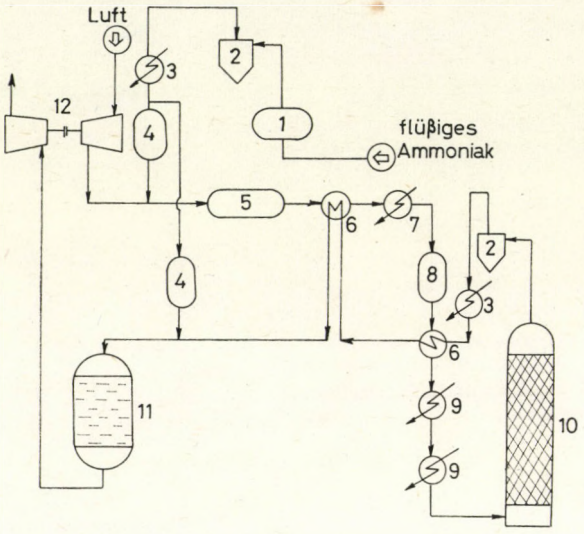

Bild 2
Mitsubishi Salpetersäure-Betrieb mit katalytischem Abgasreiniger (Reduktionsmittel: Ammoniak)
1. Ammoniakverdampfer; *2.* Separator; *3.* Vorheizer; *4.* Ammoniakfilter; *5.* Ammoniakbrenner; *6.* Wärmeaustauscher; *7.* Dampfkessel; *8.* Pt-Filter; *9.* Kühler; *10.* Absorber; *11.* Reaktor für die Reduktion der Stickstoff-Oxyde; *12.* Energie-Rückgewinnung

Das Verfahren wurde in einem unter 8 bar Druck arbeitenden Salpetersäure-Betrieb mit einer Kapazität von 120 t/Tag realisiert. Der Ammoniak-Verbrauch der Reduktion beträgt 2—3% bezogen auf den Ammoniakbedarf des Salpetersäure-Betriebes.

Unserer Meinung nach kann man obiges Verfahren auch nicht in den üblichen, unter niedrigem Druck arbeitenden Salpetersäure-Betrieben anwenden. Der Ammoniakverbrauch müßte hier noch bedeutend höher liegen und deshalb väre die Kosten der Abgasreinigung nicht verträglich.

Zur Reinigung des Abgases der Salpetersäure-Betriebe versuchte man schon seit langer Zeit auch Adsorbentien zu benützen. Mit Hilfe der Adsorption kann man einen Rezirkulationsprozeß entwickeln. Durch die Rezirkulation der Stickstoff-Oxyde steigert sich die Säure-Produktion in Salpetersäure-Betrieben engefähr um 2—3%. Die früher bekannten Adsorbentien, das Silikagel, Aluminium-Oxyd und die Aktivkohle waren aber nicht wirksam genug für die Adsorption der Stickstoff-Oxyde. Diese Lage hat sich nur in den letzten Zeiten mit der Anwendung der Zeolith-Adsorbentien verändert. Mit diesen Adsorbentien können wir um eine Größenordnung höhere spezifische Adsorptionskapazität als früher mit dem Silikagel erreichen. Bei der Adsorption entstehen keine

schädlichen Nebenprodukte. Diese Verfahren sind aber von größerem Energieaufwand.

Zur Zeit kennen wir zwei Adsorptionverfahren für die Reinigung von Abgasen der Salpetersäure-Betriebe. Diese sind: das PuraSiv-*N*-Verfahren der Firma UNION CARBIDE [11, 12], und das NORTON-Verfahren [13]. Diese Rezirkulations-Verfahren verfügen über zwei Adsorptionskolonnen und verwenden zur Regenerierung einen Teil des gereinigten Abgases.

Bei dem PuraSiv-*N*-Prozeß benütz man zwei verschiedene Adsorbentien in jeder Kolonne. Am Abgaseintritt funktionieren die Kolonnen als Trockner. Die Stickstoff-Oxyd-Adsorption findet in weiterem Sektor der Kolonnen statt. Die Leistung der Adsorptionseinheiten ändert sich von 6 000—25 000 Nm^3/h Abgas.

Das *Bild 3* zeigt das Schema des NORTON-Verfahrens.

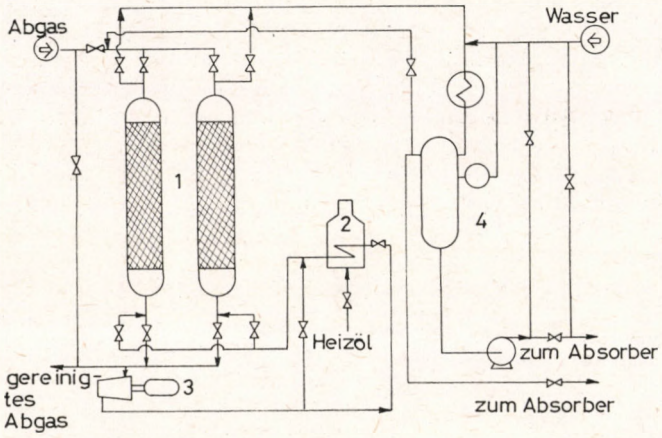

Bild 3
Norton Molekularsieb-Adsorptionsbaterien für Abgasreinigung in Salpetersäure-Betrieben
1. Adsorber; *2.* Rohrofen; *3.* Kompressor dür Regenerierungsgas-Zirkulation; *4.* Regenerierungsgasbehandlung

Die Zeolith-Adsorptionsanlagen können auch nicht leicht in die gegenwärtigen Salpetersäure-Betriebe eingebaut werden. Die Abgasreinigung durch Adsorption führt zu einem Rezirkulations-Gasstrom von 20—25% bezogen auf den Abgasstrom. Dieses Gasstrom sollte man zur Absorption zurückführen, aber in den ungarischen Betrieben bedeutet eben die Absorption einen Engpaß.

Die Reinigung mit Adsorption erfordert also auch eine Rekonstruktion der Absorptionsanlage.

Einheimische Zeolith-Adsorbentien zur Abgasreinigung

Wenn man gegen die schädliche Stickstoff-Oxyd-Emission in Ungarn etwas tun will, muß man eine andere Lösung finden. Am Lehrstuhl für Chemische Technologie der Technischen Universität Budapest haben wir mit Forschungs-

arbeiten für die Aufklärung des Stickstoff-Oxyd-Adsorptionvermögens einheimischer Zeolitgesteine vulkanisches Ursprungs begonnen. Diese Rhiolit-Tuffe enthalten zwei Zeolithsorten: Klinoptilolith und Mordenit. Das Mordenit ist ein bekanntes Stickstoff-Oxyd-Adsorbens. Die Adsorptionseigenschaften des Klinoptiloliths für Stickstoff-Oxyde waren aber zu dieser Zeit unbekannt.

In unseren Laborversuchen wurde festgestellt, daß sowohl klinoptilolith- als auch mordenithaltige Tuffe die Stickstoff-Oxyde adsorbieren. Im gereinigten Gas können wir eine Stickstoff-Oxyd-Konzertration unter 10 ppm erreichen. Da sich das spezifische Stickstoff-Oxyd-Adsorptionsvermögen der Tuffe in natürlichem Zustand nicht hoch genug erwies, bereiteten wir auch verschiedene Modifikationen durch Ionenaustausch und Aufschließung mit Säuren. Wir stellten fest, daß der Ionenaustausch für das spezifische Stickstoff-Oxyd-Adsorptionsvermögen dann vorteilhaft gestalltet wird, wenn damit gleichzeitig eine Porenmaßeerweiterung erreicht werden kann. Weil die säure Aufschließung das Porenmaß immer erweitert, war die Wirkung der Aufschließung bezogen auf die spezifische Stickstoff-Oxyd-Adsorption fast immer günstig. Durch geeignete chemische Behandlungen ist es gelungen die spezifische Stickstoff-Oxyd-Adsorptionsvermögen zu Anfang dieser Adsorbentien ums Mehrfache zu erhöhen.

Die optimalen dynamischen Bedingungen der Stickstoff-Oxyd-Adsorption wurden auch unter Anwendung dieser Adsorbentien in gefüllten Adsorberkolonnen untersucht.

Unsere besten Stickstoff-Oxyd-Adsorbentien wurden auch in einem Salpetersäure-Betrieb in Leninváros in einem Versuchsapparat, der zwei Adsorber von je 30 *l* Rauminhalt hat, geprüft. Im *Bild 4* wird das Schaltschema des Apparates gezeigt.

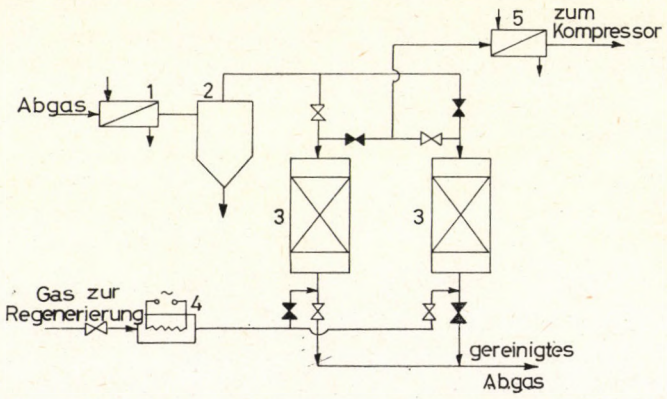

Bild 4
Adsorptionsversuchsapparat für Abgasreinigung in Salpetersäure-Betrieben
1. Abgaskühler; *2.* Tropfenabscheider; *3.* Adsorber; *4.* Regenerierungsgaserhitzer; *5.* Regenerierungsgaskühler

Unseren Erfahrungen nach können wir mit diesen Adsorbentien auch aus einem echten Abgas, das einen Druck von 2 bar und einen Taupunkt von 272 K hat, die Stickstoff-Oxyde bei 313—333 K adsorbieren. Zur Regenerierung können wir das von der Ammoniak-Oxydation stammende warme Gas mit einem

Stickstof-Oxyd-Gehalt von 7% benützen. Wir haben nach einer Regenerierung bei 603 K im allgemeinen eine Durchbruchkapazität von 3 Gew. % bezogen auf das Stickstoff-Dioxyd in Adsorberbetten erreicht. Optimale Ergebnisse haben wir mit mordenithaltigen Adsorbentien gefunden. Die Kapazität der Adsorbentien hatte während der von uns durchgeführten ungefähr 40 Adsorptionszyklen keine ungünstige Veränderung gezeigt.

Unserer Meinung nach ist es technisch möglich, die Abgase der Salpetersäure-Betriebe unter Anwendung dieser Adsorbentien zu reinigen. Der Konstenfrage muß noch nachgegangen werden, die bedeutend davon abhängen wie groß die spezifische Adsorptionskapazität vom Adsorbens ist. Der Mordenitgehalt unserer Adsorbentien war bisher nicht größer als 50%. Wir hoffen, daß die Mineralforschung in Ungarn in nächster Zukunft auch konzentriertere zeolithhaltige Tuffe zur Adsorbensherstellung bereitstellen kann. Damit können die Dimensionen des Adsorbers und die Kosten der Reinigung viel günstiger gestaltet werden.

LITERATUR

1. Ambio *1977*, 6, (5) 290.
2. Ricci, J. L.: Chem. Eng. *1977*, 84, (4) 33.
3. Gillespie, G. R., Boyum, A. A. and Collins, M. F.: Chem. Eng. Progress *1972*, 68, (4) 72.
4. Yamaguchy, M., Matsushita, K. and Takami, K.: Hydrocarbon Proc. *1976*, 55, (8) 101.
5. European Chem. News *1974*, 25, 38.
6. Hydrocarbon Proc. *1977*, 56, (11) 187–188.
7. Vogel, H.: Chemiker Ztg. Chemische Apparatur *1965*, 89, 632.
8. Teske, W.: The Chemical Engineer *1968*, 221, CE 263.
9. Ushio, S.: Chem. Eng. *1975*, 82, (15) 70.
10. Newmann, D. J.: Europe and Oil *1971*, 10, (5) 44.
11. Environment Sci. and Techn. *1974*, 8, (2) 106.
12. Chemical Week *1972*, 111, (24) 45.
13. Kiovsky, J. R., Koradia, P. B. and Hook, D. S.: Chem Eng. Progress *1976*, 72, (8) 98.

SUMMARY

The nitrogen oxides are the most harmful air polluting compounds. In most cases the NO_x emission of nitric acid plants are well above the allowed limits. For the reduction of the emission generally the onliest solution is the removal or destruction of nitrogen oxides. The authors deal with the various methods used for the cleaning of nitric acid stack gases. Data are presented on experiments carried out with natural zeolite adsorbents of Hungarian origin.

РЕЗЮМЕ

Окиси азота являются одними из самых вредных, загрязняющих воздух соединений. Степень загрязнения у большинства заводов производящих азотную кислоту превышает допустимое предельное значение. С целью уменьшения эмиссии в большинстве случаев строят и эксплуатируют оборудования для газоочистки.

В сообщении описаны различные методы очистки газа, кроме этого приведены основные результаты экспериментов проведенных адсорбентами изготовленных из минеральных цеолитов добываемых в Венгрии.

HUNGARIAN JOURNAL
OF INDUSTRIAL CHEMISTRY
VESZPRÉM
Vol. 9. pp. 21–36 (1981)

ACTIVITY INVESTIGATION ON ION-EXCHANGED ZEOLITES

GY. GÁRDOS, J. KRISTÓF*, L. PÉCHY and Á. RÉDEY

(Department of Hydrocarbon and Coal Processing,
*Department of Analytical Chemistry,
Veszprém University of Chemical Engineering)

Received: July 31. 1980.

The ion-exchange characteristics of synthetic *Y*-zeolites were investigated. The ion-exchanged forms of *Y*-zeolites have been characterized by various analytical methods. *Y*-zeolites were converted to NH_4Y, MgY and LaY; while in further experiments the NH_4Y zeolites were converted to NH_4MgY, NH_4LaY and NH_4MgLaY forms. Analytical measurements showed that conversion rates obtained for the ammonium, magnesium and lanthanum forms were 94%, 69% and 72%, respectively.

The heat-induced acidity of ion-exchanged zeolite catalysts was examined by IR spectroscopy along with their catalytic activity shown in the *1*-butene alkylating reaction of *i*-butane. Magnesium and lanthane were found to display strong stabilizing effects, while NH_4LaY and NH_4MgY prepared from NH_4Y were found to display high heat stability and favourable catalytic activity.

Generally, the term "zeolite" refers to a group of naturally occurring hydrated metal aluminosilicates. Many of them can be prepared artificially. The *Y*-type zeolite is a synthetic crystalline zeolite, which is similar to the faujasite occurring in nature. The principal building unit of the *Y*-type zeolite is the truncated octahedra (sodalite cage), which consists of a 3-dimensioned framework of SiO_4 and AlO_4^- tetrahedra [1, 2].

The tetrahedra are cross-linked by the sharing of oxygen atoms, so that the ratio of oxygen atoms to the total of the aluminium and silicon atoms is equal to two. The sodalite units are connected along two six-membered rings, resulting in a hexagonal prism. In this way, the polyhedra enclose a supercage with an internal diameter of 1.25 nm and is accessible through twelve-membered rings of oxygen atoms with a free aperture of 0.75 nm.

The negative electrovalance of tetrahedra containing aluminium is balanced by the inclusion of cations. Different cation sites can be distinguished depending on the position of the cation. The occupation of the cation sites is determined by the type of the cation and by the silicon-aluminium ratio. The type of the cation and its position are the principal factors, which determine the catalytic activity. In the case of the *Y*-type zeolite, the composition of the unit cell calculated on dehydrated basis can be given as follows:

$$Na_{57}(AlO_2)_{57}(SiO_2)_{135}.$$

One of the consequences of the higher silicon-aluminium ratio of the *Y*-type zeolite compared to the *X*-type zeolite is that less cation site is available. However, the advantage of the *Y*-type zeolite having a higher silicon-dioxide content appears in stability and activity, consequently the *Y* zeolite is widely used in catalytic cracking, isomerization and alkylation as the catalyst.

Hydrogen *Y* zeolites can be prepared by ammonium ion-exchange followed by a calcination step. During the calcination, ammonia is removed and a proton remains attached to the lattice oxygen [3].

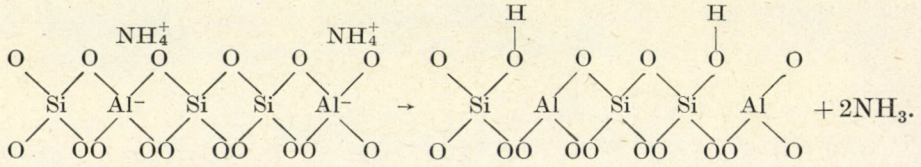

The calcination can be carried out in vacuum, or in a dry gas stream in the temperature-range of 300–500 °C. On the basis of Ward's experimental work, it can be stated that the Brönsted acidity remains constant, if the catalyst is activated in the given temperature range. In the case of activations carried out at higher temperatures than 500 °C, the Brönsted acid sites gradually cease to exist and during water removal, Lewis acid sites are formed [4].

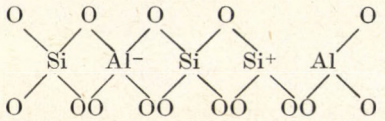

According to the above scheme, two Brönsted sites are converted into one Lewis acid site. The application of IR spectroscopy is the best method to ensure the identification and characterization of the active sites in zeolite. The results of the IR absorption studies demonstrated three types of hydroxyl groups. The band occurring at a wave number of 3745 cm^{-1} can be assigned to hydroxyl (silanol) groups at the edge of crystallites or present in amorphous material. The 3745 cm^{-1} band does not correlate with catalyst activity.

The 3640 cm^{-1} band is an indicator of Brönsted acidity [5]. In the pyridine absorption investigations, the decrease in the intensity of the 3640 cm^{-1} band, and the appearance of a new band at 1545 cm^{-1} as a consequence of the formation of pyridinium ion were observed. The intensity of the 3640 cm^{-1} band can be brought into connection with catalytic activity. The 3540 cm^{-1} hydroxyl band can react only with the stronger base piperidine forming a carbonium ion [3, 5, 6]. The maximum intensity of the 3640 cm^{-1} band can be attained at 375 °C, and it remains constant until 500 °C. The effect of calcination temperature on the acidic character of the *Y*-type zeolite was studied with chemisorbed pyridine.

The band at 1545 cm^{-1} can be used to indicate proton acidity (Brönsted), while the 1455 cm^{-1} band shows Lewis acidity. It can be stated that Brönsted acidity increases with the calcination temperature up to about 325 °C, and remains constant to 500 °C, and above 500 °C it begins to decrease. Lewis

acidity appears at 450 °C, and above 550 °C it increases rapidly, while the extent of BRÖNSTED acidity decreases.

The cracking of toluene was investigated on HY-zeolite. It can be stated that the change in the activity of the catalyst follows the intensity of the 3640 cm^{-1} band, so BRÖNSTED acid sites can be considered to be active sites. On the basis of the experimental results, it can be stated that hydroxyl groups appearing at a wave number of 3540 cm^{-1} are located in relatively inaccessible regions of the zeolite, while the hydroxyl groups appearing at 3640 cm^{-1} are in accessible regions.

Furthermore, the zeolites ion-exchanged with multivalent cations can be stated to be more active compared to zeolites containing univalent cations [5, 7, 8]. The activity of the zeolites increased with the silicon-to-aluminium ratio, and in the case of alkaline earth zeolites the activity increased with decreasing ionic radius (increasing field strength). It is assumed that the structural hydroxyl groups are formed by the solvation of the multivalent cation:

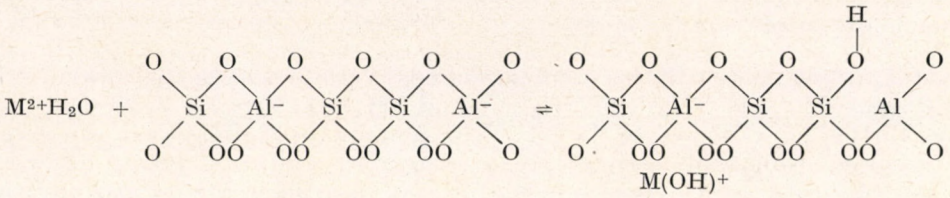

LEWIS acid sites are formed when zeolites containing multivalent ions are heat treated at temperatures above 500 °C. The hydroxyl bands appear near those frequencies observed on *HY*-zeolite. The hydroxyl groups associated with the cations have no acidic character. It was concluded that in the case of alkaline earth cations, the catalytic activity can be brought into connection with the concentration of the BRÖNSTED acid sites. BRÖNSTED acidity changed linearly with the electrostatic field and potential [5]. The rare earth ion-exchanged *Y*-type zeolites show similar characteristics, except that their activities and stabilities are more favourable compared to those of zeolites containing bivalent cations.

This probability can be explained by the higher electrostatic field potential and field strength of the rare earth cations [9, 10].

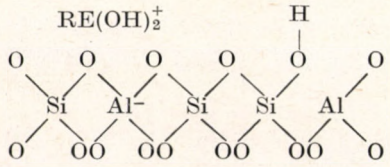

According to WARD's investigation, the concentration of the BRÖNSTED acid sites of the REY zeolite is between the values of *HY* and MgY measured beside the same condition. WARD stated that for every six exchange sites in *HY* 6, in REY 4 and in MgY 3 BRÖNSTED acid sites are formed [9].

Experimental

The aim of the experimental work was to prepare alkylating catalysts from *Y*-type zeolite by ion-exchange and to study the effects of the composition and calcination on the catalytic activity.

Synthetic *Y*-type zeolite produced by the Union Carbide Corporation was used as starting material. The composition of the *Y*-type zeolite on anhydrous base can be given as follows:

Al_2O_3	22.2 w%
SiO_2	64.5 w%
Na_2O	12.7 w%

The SiO_2/Al_2O_3 molar ratio of the starting material was 4.51. On the basis of thermogravimetric analysis, the water content of the zeolite sample was 24.4 w% beside air-dry condition. The *X*-ray diffraction measurements showed the samples to be highly crystalline. Its surface area was 902 m^2/g.

The ion-exchange of Y zeolite

NH_4Y, MgY, LaY forms were prepared by the exchange process of the *Y*-type zeolite and NH_4MgY, NH_4LaY and NH_4MgLaY types were formed by the further ion-exchange of the NH_4Y form according to the procedures given in literature [3, 4, 5]. During the laboratory experiments, the quantity of NH_4^+, Mg^{2+} and La^{3+} cations was sufficient to provide 3–5 equivalents of the cation per equivalent of total base-exchange capacity.

The scheme of the ion-exchange is given in *Fig. 1.*

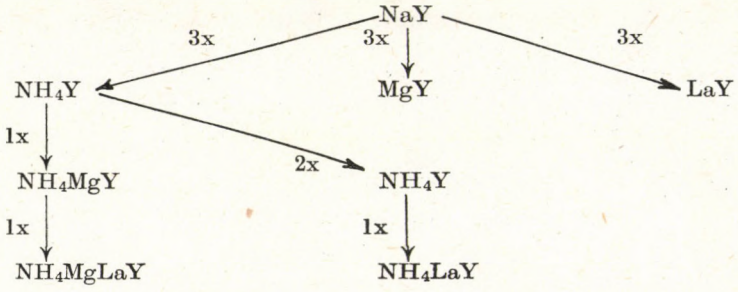

Fig. 1
The scheme of the ion-exchange

(the numbering given on the arrows shows the number of the ion-exchanges). The zeolite samples were dissolved for the quantitative determination of the components constituting the zeolite.

This was carried out in two different ways.

Digestion with hydrogen-fluoride: 400 mg of powdered zeolite sample was placed into a beaker. Concentrated hydrogen-chloride and hydrogen-fluoride helped to digest the zeolite, and the solution obtained was evaporated in a water bath. Then it was dissolved again in HCl and the solution was poured into a normal flask. Another digesting method was also applied in the experiments.

Digestion with hydrogen-fluoride in the presence of sulphuric acid: 100 mg of zeolite sample was placed in a platinium crucible and after adding 1 cc of H_2SO_4 it was dissolved in hydrogen-fluoride. The forming SiF_4 and the residual H_2F_2 were evaporated. The sample was repeatedly dissolved in hydrogen-fluoride and evaporated. The material digested was washed into a flask with distilled water.

The water content of the zeolites was determined by derivatograph. The derivatographic studies were carried out in static air atmosphere. The total water content of the basis zeolite was removed until 350 °C. The main part of the water content of the zeolite samples ion-exchanged with Mg^{2+} and La^{3+} respectively was removed until 200 °C. In both cases, the TG curves showed well perceptible changes, so the water removal lasts until 650 °C. Studying the NH_4Y form it can be stated that the removal of the ammonia and water takes place in more steps. The water content of the ion-exchanged zeolites calculated on the basis of the TG curves was as follows:

NaY	24.4 w%
NH_4Y	24.1 w%
MgY	26.2 w%
LaY	23.4 w%

Having digested the zeolite samples and determined the water content by derivatographic analysis, the ammonium, magnesium, and lanthanum-contents of the zeolites were determined. The experimental results are summarized in *Table 1.*

Table 1.

The results of the determinations of ammonia

Sample	Number of the NH_4^+ ion-exchanges	NH_3 content w %	The extent of the ion-exchange %
NH_4Y 1	1	3.2	64
NH_4Y 2	2	4.0	79
NH_4Y 3	3	4.4	88
NH_4Y 4	4	4.6	93
NH_4Y 5	5	4.7	94
NH_4MgY	3	1.6	32

The magnesium content was determined by the atom absorption method. The disturbing effect of Al^{3+} ions was eliminated by the application of 5 w% La^{3+} solution. The La^{3+} content of the rare-earth ion-exchanged zeolites was determined by spectrophotometric analysis with the use of arsenase colouring agent.

The results of the ion-exchanges carried out with Mg^{2+} and La^{3+} are given in *Table 2.*

On the basis of the experimental results, it can be stated that the extent of the exchanges approach the data given in technical literature. The NH_4MgY, NH_4LaY and NH_4MgLaY zeolites formed by the further exchanges of NH_4Y were analysed and the results are summarized in *Table 3.*

Table 2.

The rate of the ion-exchanges

Number of the ion-exchanges	Ion-exchange carried out with			
	Mg^{2+}		La^{3+}	
	The extent of the ion-exchange, %			
1	MgY 1	48.8	LaY 1	60.9
2	MgY 2	59.3	LaY 2	67.1
3	MgY 3	66.7	LaY 3	72.0

Table 3.

The results of the ion-exchanges carried out with different types of cations

The type of the zeolite	The extent of the ion-exchange, %		
	NH_4^+	Mg^{2+}	La^{3+}
NH_4MgY	32.0	57.7	—
NH_4MgLaY	18.7	35.6	38.1
NH_4LaY	45.1	—	49.2

On the basis of the analytical determinations it can be concluded that in the cases of NH_4MgLaY, NH_4LaY and NH_4MgY the extent of the ion-exchanges were 92.4%, 94.3% and 89.7% respectively.

Infrared spectroscopic studies

The spectroscopic studies were carried out in the Central Chemical Research Institute of the Hungarian Academy of Sciences. Before the spectroscopic studies, the zeolite samples were ground and pelletized. The thickness of the wafers was about 7 mg/cm^2. The spectral resolution was about 3 cm^{-1}. The windows of the infrared cell were made of CaF_2, and the furnace section of the cell was prepared from quartz. The infrared cell was attached to a conventional vacuum system. During the activation, the sample wafers were placed in the furnace section of the cell and the system was evacuated. The temperature was raised slowly to 110 °C and held until a vacuum of 0.0133 Pa was maintained. After this the temperature of the furnace was increased to the calcination temperature, and the sample was evacuated for 2 hours. The sample was cooled to room temperature and the spectrum was recorded. This procedure was repeated for each calcinaton temperature. The peak heights of the absorption bands due to water, ammonium ion and structural hydroxyl groups were measured. The intensities expressed by the peak heights related to sample mass were plotted in the function of the activation temperature. During the infrared spectroscopic studies, the changes of the 3630, 3530 cm^{-1} hydroxyl bands, the 1640 cm^{-1} water band and 1440 cm^{-1} ammonium band were followed in the function of calcination temperature. From these only the intensity of the

3630 cm^{-1} absorption band is given, since the hydroxyl band occurring at 3630 cm^{-1} can be brought into connection with the BRÖNSTED acidity.

Pyridine adsorption studies were not carried out to determine the formation of the BRÖNSTED and LEWIS acid sites. For the formation of the LEWIS acid sites, conclusions were drawn from the literature given.

Activity studies

The catalytic activity of the ion-exchanged *Y*-type zeolites was studied in the alkylating reaction of isobutane with *1*-butene. The alkylating reaction was carried out in liquid phase at a temperature of 343 *K*, alongside a molar ratio of 5:1, a pressure of 20 bar and a reaction time of 2 hours. The experimental technique was given in detail in previous publications [11, 12]. The zeolite catalysts investigated (NH_4Y, MgY, LaY, NH_4MgY, NH_4LaY, NH_4MgLaY) were prepared by the method mentioned in the previous part.

A freshly activated catalyst was used in every experiment. The zeolite catalysts were activated in flowing helium, applying a step-like temperature increase until 200 °C, and were held at this temperature for 2 hours. After having activated the zeolits in helium gas stream, they were activated in vacuum at the desired calcination temperature. The activating temperatures were as follows: 350, 400, 450, 500, 550, 600 °C. Experiments were carried out with the zeolites activated at different temperatures and the effects of the ion-exchange and the activation temperature on the alkylating reaction were studied.

The examination of the NH_4Y

The activation of the NH_4Y type zeolite catalyst was carried out in the temperature-range of 300–600 °C, and the activity values were calculated. The activity means that the percentage value which was calculated on the basis of the amount of the heavier hydrocarbons (C_5^+) formed in the alkylating reaction of isobutane with *1*-butene and related to the charged olefin. The infrared spectroscopic studies were carried out after the calcinations effectuated at 200, 300, 430 and 600 °C in vacuum. The spectrum was recorder in the wave number ranges of 1200–1800 cm^{-1} and 2600–4000 cm^{-1}. The absorbed water present on the zeolites is expected to absorb at about 1640 cm^{-1}. The decrease of the intensity of the 1640 cm^{-1} band can be observed with the increase of the activation temperature due to the desorption of the water absorbed. The intensity of the 1640 cm^{-1} band is in good connection with the amount of water absorbed on the zeolite. On the basis of the experimental results, it can be seen that most of the absorbed water is removed by 300 °C. The ammonium ion has a characteristic band intensity of about 1480 cm^{-1}. The amount of ammonium ions significantly decreases in the case of activation carried out at higher temperatures than 200 °C. Most of the ammonium is decomposed until 400 °C.

The hydroxyl groups absorb at 3540, 3640 and 3740 cm^{-1}. The changes of the hydroxyl groups occurring at 3540 and 3640 cm^{-1} were followed *(Fig. 2)*. It can be stated that these hydroxyl groups are located at different crystallographic sites. On the basis of chemisorption studies carried out with pyridine it was concluded that the hydroxyl groups located in the supercage can be con-

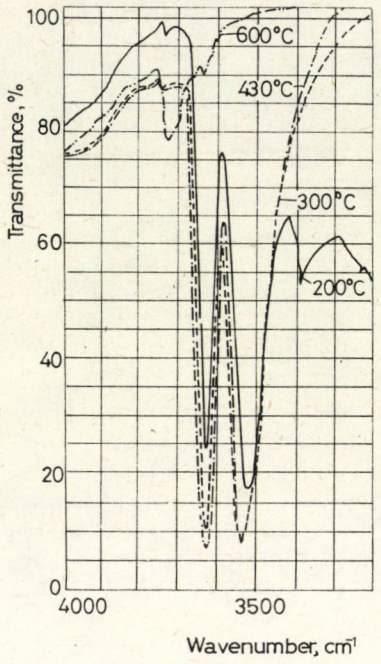

Fig. 2
Infrared spectra of NH_4Y after calcination at various temperatures

sidered to be BRÖNSTED acid sites. The 3540 cm^{-1} band be attributed to hydroxyl groups located in the sodalite unit. The absorption bands of the hydroxyl groups show maximum intensity at a temperature of 350 °C, and above 500 °C it begins to decrease. The intensity of the 3640 cm^{-1} absorption band in the function of the calcination temperature and the catalytic activity measured in the alkylating reaction of isobutane and 1-butene are plotted in *Fig. 3*. On the basis of the *Fig. 3 it* can be concluded that the activity of the NH_4Y type zeolite increases with the calcination temperature, but it begins to decrease above 500 °C. The plot of the activity in the function of the calcination temperature follows the change of the BRÖNSTED acid sites, and with the decrease of BRÖNSTED acidity and with the increase of LEWIS acidity it begins to decline. According to the data published in literature, it is well known that in the case of activation carried out at higher temperatures than 500 °C, LEWIS acid sites are formed by dehydroxylation and above 550 °C it increases rapidly as BRÖNSTED acidity decreases.

The examination of the MgY

The magnesium was chosen for the exchange procedure among the bivalent cations, since according to the data in literature the electrostatic potential and field strength of the bivalent cations has an important effect on the catalytic activity. The smaller the radius of the bivalent cation, the higher the electro-

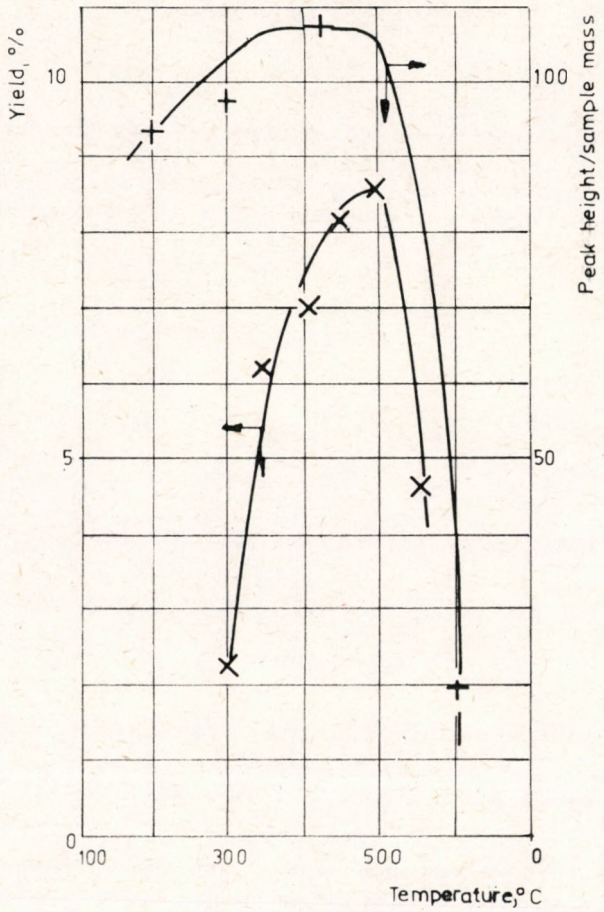

Fig. 3
The variation of the activity of NH_4Y with the calcination temperature

static field of the cation and so the activity of the ion-exchanged zeolites increases. The experimental results showed *(Fig. 4)* that the adsorbed water was removed until 300–350 °C. The intensity of the 3640 cm^{-1} hydroxyl band reaches a maximum at 300 °C and it begins to decline *(Fig. 4)*. Studying the alkylation of isobutane with *1*-butene it was inferred that the highest yield value (5%) was attained at 300 °C. Activating the MgY at higher temperatures than 300 °C, the activity of the ion-exchanged zeolite decreased and, at a temperature of 600 °C it showed one tenth of its maximum absorption band intensity.

Activating the zeolites at this temperature, the formation of LEWIS acid sites come into prominence. The gas-chromatographic analyses showed that C_8 olefin hydrocarbons were present to a significant extent, which can be explained by the polymerization of *1*-butene taking place simultaneously with the alkylation of isobutane.

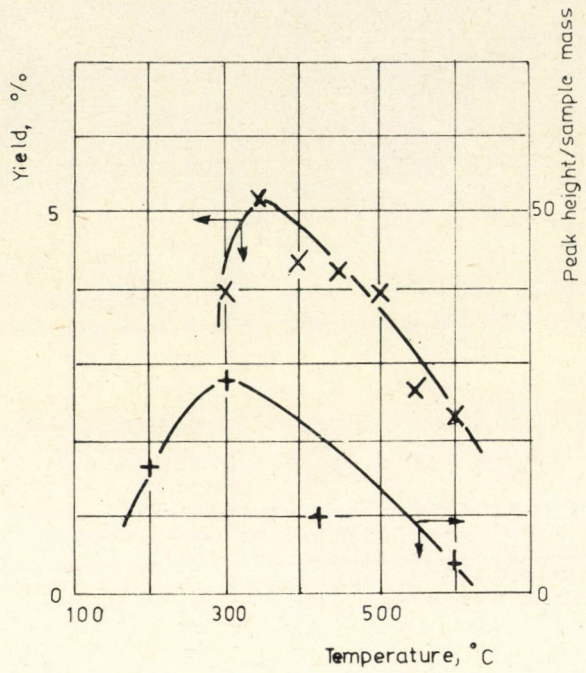

Fig. 4
The variation of the activity of MgY with the calcination temperature

The examination of the LaY

The results of the alkylating reaction of isobutane with *1*-butene carried out in the presence of LaY zeolite catalyst are summarized in *Fig. 5*. The intensity of the 3640 cm^{-1} hydroxyl band was near constant in the temperature range of 300–500 °C, and above this temperature it decreases. The activity of the LaY is highest at 550 °C and with the conversion of BRÖNSTED acid sites into LEWIS acid sites it diminishes. The incorporation of the lanthanum has a stabilizing effect, the intensity of the 3640 cm^{-1} absorption band was constant in a relatively wide temperature range. It should be noted that the alkylation is accompanied by the polymerization of *1*-butene.

The examination of the NH_4MgY

The infrared spectroscopic absorption bands of the NH_4MgY zeolite were investigated in the temperature-range of 300–600 °C. The absorbed water on the zeolites was expected to absorb at 1640 cm^{-1}, while the ammonium ion occurred at 1460 cm^{-1}. The hydroxyl groups were absorbed from 3750 to 3400 cm^{-1} The experimental results show that most of the absorbed water removed until 300 °C. The alternation of the intensity of the ammonium band as a function of calcination temperature shows that the removal of the ammonia takes place between 200–300 °C. Similar results were found in the case of NH_4Y type

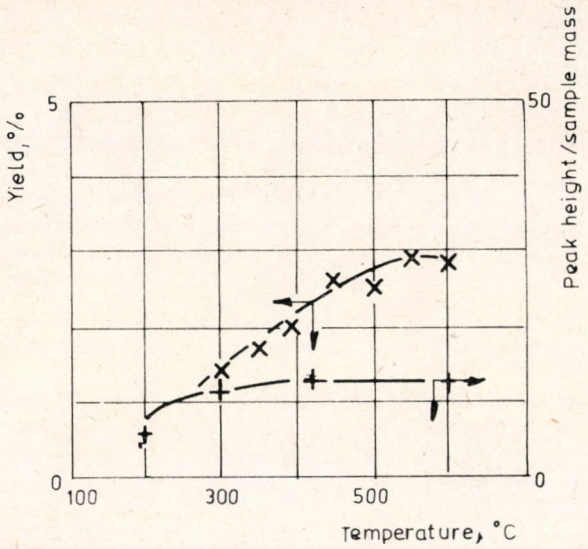

Fig. 5
The variation of the activity of LaY with the calcination temperature

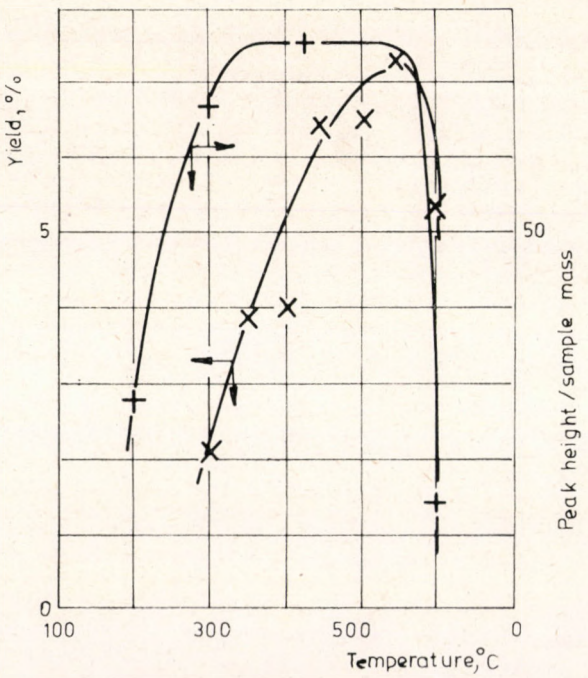

Fig. 6
The variation of the activity of NH_4MgY with the calcination temperature

zeolite. The absorption bands due to structural hydroxyl groups were observed at 3540 and 3640 cm^{-1}. The intensity of the 3640 cm^{-1} hydroxyl band increases as the calcination temperature is raised, the intensity reaches its maximum at temperatures in excess of 400 °C, it remains constant and above 550 °C the intensity declines *(Fig. 6)*. The intensity of the 3640 cm^{-1} band at 600 °C is about one fifth of its maximum intensity. The intensity of the hydroxyl band occurring at 3540 cm^{-1} is highest at 300 °C, it decreases as the calcination temperature is raised. It should be emphasized that coincidently with the data given in literature, the magnesium has a stabilizing effect on the structure and on the formation of BRÖNSTED acid sites, and the magnesium ammonium *Y* type zeolite is stable up to 550 °C compared to the NH_4Y which were stable up to 500 °C. On the basis of the activity values it can be concluded that zeolite pretreated at a temperature of 550 °C has the highest activity; this temperature coincides with the maximum concentration of the BRÖNSTED acid sites. Activating the catalyst at higher temperatures than 550 °C, the activity values diminish, similarly to the decrease of the concentration of the BRÖNSTED acid sites, which can be brought into connection with the formation of the LEWIS acid sites.

The examination of the NH_4LaY

The change of the infrared spectra of the NH_4LaY zeolite was studied after pretreatments carried out at 200, 300, 420, and 600 °C in vacuum. The activity

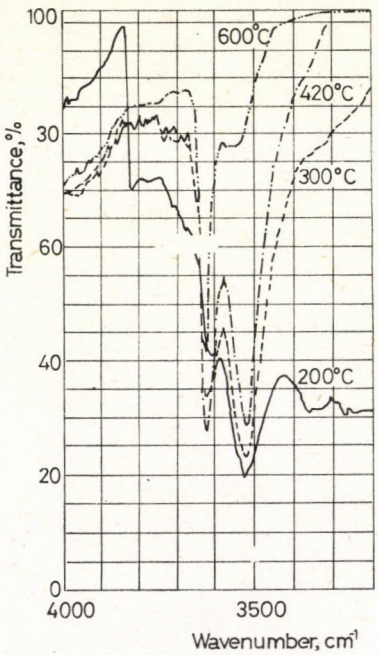

Fig. 7
Infrared spectra of NH_4LaY after calcination at various temperatures

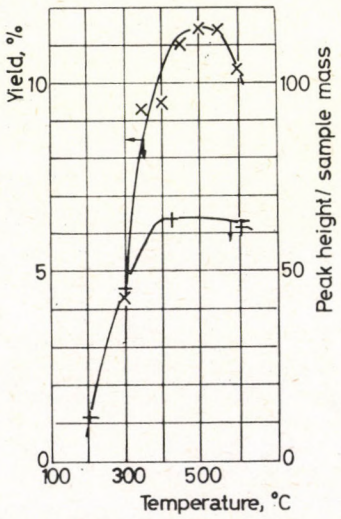

Fig. 8
The variation of the activity of NH_4LaY with the calcination temperature

investigations were effectuated in the temperature range of 300–600 °C. The experimental results are given in *Fig. 7, 8*. The change of infrared spectra of NH_4LaY after calcination at various temperatures is illustrated in *Fig. 7*. The change of the intensity of the absorption band measured at 3640 cm^{-1} and the variation of the activity are plotted in *Fig. 8*. It can be stated that the 3640 cm^{-1} band shows a constant intensity in the temperature range of 400–600 °C, which can be brought into connection with the BRÖNSTED acidity. After pretreating, the catalyst at temperatures from 450 to 550 °C the catalyst showed good activity, and the C_5^+-yield was about 11%.

The investigation of the NH_4MgLaY

The investigation of the NH_4MgLaY was carried out in the temperature range given in the previous part. On the basis of the intensity of the 3640 cm^{-1} band it can be deduced that maximum hydroxyl content can be attained bet-

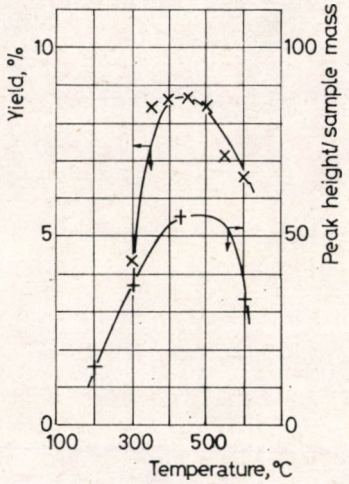

Fig. 9
The variation of the activity of NH_4MgLaY with the calcination tem perature

ween 400–500 °C. Considering the alkylating reaction of isobutane with *1*-butene it should be noted that catalysts pretreated at temperatures from 400 to 450 °C presented the highest activities. In this case, the C_5^+-yield is about 8.5%. Applying higher activation temperatures, the reduction of the intensity of the 3640 cm^{-1} band and simultaneously the loss of activity can be observed. The decrease of activity shows that the LEWIS acid sites formed at temperatures from 600 °C are unfavourable for the alkylation.

Conclusions

Different types of ion-exchanged zeolites were studied in the alkylation reaction of the isobutane with *1*-butene at 70 °C, alongside an isobutane-*1*-butene molar ratio of 5:1, and a pressure of 20 bar applying a reaction time of

2 hours. During our experimental work, the effects of the activation temperature of the ion-exchanged zeolites on the infrared spectra, on the Brönsted acidity and on the activity shown in alkylating reaction were studied. The features of the NH_4Y, MgY, LaY, NH_4MgY, NH_4LaY and NH_4MgLaY types were investigated. It can be stated that the intensity of the 3640 cm^{-1} band increases as the activation temperature is raised. The maximum band intensity is constant in a temperature-range depending on the stabilizing effect of the cations. Activating the zeolites at higher temperatures than 500 °C, the catalysts show a decrease in the intensity of the 3640 cm^{-1} band, which can be explained by the formation of the Lewis acid sites. The incorporations of the magnesium in lanthanum cations have a favourable effect on the thermal stability. The plots of the activity with the temperature have maximum values which coincide with the sections of the highest intensity of the 3640 cm^{-1} absorption band. Above these temperatures, the Brönsted acid sites are formed into Lewis acid sites and the activity decreases. This makes it probable that the alkylation reaction of isobutane with *1*-butene takes place in the Brönsted acid sites. The NH_4Y, NH_4MgY, NH_4LaY, and NH_4MgLaY are important considering the activity values. From these, the NH_4LaY and NH_4MgLaY have to be emphasized, because they are stable in a wider temperature range, and the NH_4LaY shows higher activity in the alkylating reaction.

ACKNOWLEDGEMENTS

The authors are indebted to Dr. E. Detrekőy for his excellent assistance in the infrared spectroscopic studies and are grateful for his helpful comments, and also thank Mrs. J. de Jonge for her help with the analytical determinations of the zeolites.

REFERENCES

1. Breck, D. W.: Zeolite Molecular Sieve, John Wiley and Sons, New York, 1974.
2. Jacobs, P. A.: Carboniogenic activity of zeolites, Elsevier Scientific Publ. Co., Amsterdam, 1977.
3. Ward, J. W.: Journal of Catalysis, *1967*, 9, 225.
4. Ward, J. W.: Journal of Catalysis, *1967*, 9, 396.
5. Haynes, H. W.: Catal. Rev.-Sci. Eng., *1978*, 17, (2), 273.
6. Ward, J. W.: Journal of Catalysis, *1968*, 11, 2259.
7. Ward, J. W.: Journal of Catalysis, *1968*, 11, 251.
8. Ward, J. W.: Journal of Catalysis, *1972*, 26, 470.
9. Ward, J. W.: Journal of Catalysis, *1969*, 13, 321.
10. Bielanski, A., Berak, J. M., Datka, J. and Drelinkiemiez, A.: Bull. De L'Academie Polonaise Des Sciences. Ser. des sci. chim. *1975*, 23, (5) 455.
11. Gárdos, Gy., Péchy, L., Rédey, Á. and Okonji, Ch.: Hung. J. Ind. Chem., *1980*, 8, 363.
12. Gárdos, Gy., Péchy, L., Rédey, Á. and Sokorai, I.: Hung. J. Ind. Chem., *1980*, 8, 371.

РЕЗЮМЕ

В ходе экспериментов авторы изучали ионнообменную способность синтетических цеолитов типа *Y* и также состав образцов цеолитов заполненных с другими ионами.

Цеолиты типа *Y* преобразовали в форму NH_4Y, MgY и LaY и используя цеолит NH_4Y производили типы NH_4LaY, NH_4MgY.

Путем аналитических исследований установили, что уровнь обмена с ионом аммония достигает 94%, а ионами магнезия и лантана 69 и 72%. Кислотный характер цеолитов возникающий в результате термической обработки изучали инфракрасной спектрофотометрией попутно оценивали каталитические свойства и активность цеолитов реакцией алкилизации изобутана и I бутена. Авторами установлено, что лантан и магнезий увеличивает устойчивость, а NH_4LaY и NH_4MgY нечивствительны на повышение температуры (термостойкие), в то же время имеют достаточную активность для катализации реакции алкализации.

HUNGARIAN JOURNAL
OF INDUSTRIAL CHEMISTRY
VESZPRÉM
Vol. 9. pp. 37–44 (1981)

МАТЕМАТИЧЕСКОЕ МОДЕЛИРОВАНИЕ ПРОЦЕССА СИНТЕЗА ЭФИРОВ α, β-НЕНАСЫЩЕННЫХ КИСЛОТ КАРБОНИЛИРОВАНИЕМ АЦЕТИЛЕНА II.

КАТАЛИТИЧЕСКАЯ СИСТЕМА PdI_2 – NaI – HCl – *н*-БУТАНОЛ

А. Н. Гарцман, Г. М. Шуляковский*, А. Ермакова, Н. И. Рассадникова, О. Н. Темкин**

(Институт катализа СО АН СССР, Новосибирск, 630 090, СССР)

Поступила в редакцию 20 окт. 1980

В работе рассмотрены различные способы осуществления процесса синтеза бутиловых эфиров акриловой, пропионовой, малеиновой, фумаровой и янтарной кислот карбонилированием ацетилена. Рассмотрение проведено на основании математической модели, предложенной в предыдущем сообщении [1].

В предыдущем сообщении [1] предложена математическая модель и на ее основе рассмотрены различные способы осуществления процесса синтеза 2-этилгексиловых эфиров ненасыщенных карбоновых моно- и дикислот карбонилированием ацетилена в каталитической системе $PdBr_2$ — HBr — $P(C_6H_5)_3$ — диметилформамид — 2-этилгексанол.

Дальнейшие исследования процесса карбонилирования позволили установить, что активность каталитической системы PdI_2 — NaI — HCl — *н*-бутанол при синтезе бутиловых эфиров моно- и дикислот в 1,5—2 раза выше активности упомянутой системы на основе бромидных комплексов палладия. Реакция карбонилирования в этой системе протекает с суммарной средней скоростью 0,005—0,007 моля продуктов на моль палладия в секунду. Предполагается, что в данной каталитической системе одновременно реализуются гидридный и алкоголятный механизмы [2], приводящие к протеканию сопряженных окислительно-восстановительных реакций, продуктами которых являются бутиловые эфиры акриловой, пропионовой, малеиновой, фумаровой и янтарной кислот. Эти реакции описываются следующей брутто-схемой:

$$CO + C_2H_2 + ROH \rightarrow CH_2{-}CH{=}COOR$$

$$2\,CO + C_2H_2 + 2\,ROH + PdI_2 \rightarrow (=CH{-}COOR)_2 + HPdI + HJ$$

$$CO + C_2H_2 + ROH + HPdJ + HJ \rightarrow CH_3CH_2COOR + PdI_2 \qquad (1)$$

* — Саратовский филиал НИИПолимеров им. академика В. А. Каргина, г. Саратов.

** — Московский институт тонкой химической технологии им. М. В. Ломоносова, г. Москва.

Цель настоящей работы состояла в исследовании кинетических закономерностей протекания процесса в указанной каталитической системе, создании его математической модели, выборе и расчете оптимального реактора для осуществления процесса.

Кинетику процесса исследовали в проточном по газу термостатированном реакторе, установленном на быстроходной качалке. Число качаний в секунду было равно 9—11. При такой скорости перемешивания достигалась кинетическая область протекания процесса. Исследования проводились при $C_{PdI_2}=$ $=0{,}022$—$0{,}080$ Кмоль/м^3; $C_{HCl}=0{,}16-0{,}44$ Кмоль/м^3; $T=322{,}15$—$364{,}15$ К и в интервале соотношений $CO : C_2H_2=1 : 3{,}25$ — $3{,}25 : 1$.

При обработке результатов кинетического эксперимента по методу, описанному в работах [3, 4], была выбрана следующая кинетическая модель процесса, адекватно описывающая скорости образования бутиловых эфиров акриловой (БА), пропионовой (БП) кислот и суммы эфиров дикислот (ДЭ):

$$r_{БА}=K_1 C^2_{ROH} \quad (1)$$

$$r_{БП}=K_2 C^2_{ROH} \quad (2)$$

$$r_{ДЭ}=K_3 C^2_{ROH} \quad (3)$$

Значения констант скоростей параллельных реакций K_1, K_2 и K_3 при $C_{PdI_2}=$ $=0{,}044$ Кмоль/м^3; $C_{HCl}=0{,}441$ Кмоль/м^3; $T=343{,}15$ К и $CO : C_2H_2=1 : 1$ оказались равны:

$$K_1=(2{,}84\pm0{,}36)\cdot10^{-6}\ \text{м}^3/(\text{Кмоль сек})$$

$$K_2=(1{,}02\pm0{,}42)\cdot10^{-6}\ \text{м}^3/(\text{Кмоль сек})$$

$$K_3=(6{,}14\pm0{,}48)\cdot10^{-6}\ \text{м}^3/(\text{Кмоль сек})$$

В общем случае эти константы являются некоторыми функциями состава каталитической системы и газовой смеси, однако, в силу сложности и недостаточной изученности истинного механизма процесса определить вид этих функций в настоящее время не удается. Поскольку концентрации компонентов каталитической системы в ходе процесса не изменяются, равно как не изменяется и состав газовой смеси (вследствие того, что при исходном составе $CO : C_2H_2=$ $=1 : 1$ газы поглощаются в соотношении 1 : 1), брутто-уравнения (1)—(3) с указанными значениями констант скоростей реакций описывают кинетику рассматриваемого процесса с достаточной для практических целей точностью. В настоящее время проводятся интенсивные исследования, цель которых — выявить истинный механизм процесса.

При осуществлении процесса карбонилирования ацетилена в указанной каталитической системе следует соблюсти ряд технологических требований к нему. Во-первых, необходимо обеспечить высокую степень превращения компонентов газовой фазы ($X_{CO}=0{,}9$ или $X_{C_2H_2}=0{,}9$). Во-вторых, для обеспечения возможности отделения БА от близкокипящего БП в составе азеотропа с бутанолом целесообразно проводить процесс до конверсии *н*-бутанола $X_{ROH}\approx0{,}3$. При этом концентрация БА в выходящем из реактора растворе составит около 10% мольных.

В предыдущем сообщении [1] отмечалось, что процессы жидкофазного карбонилирования ацетилена осуществляются при высоких газосодержаниях, по-

скольку отношение $Q^0_г/Q_ж$ велико (в настоящем случае оно равно 110), вследствие чего объем реактора используется нерационально. Из обсуждавшихся в этом сообщении способов увеличения эффективности использования реакционного объема для данного процесса приемлемым является распределение подаваемого в реактор газа по длине реактора (подпитка). Реализация же полупериодической схемы с циркуляцией катализаторного раствора в системе является затруднительной, поскольку кинетическая модель процесса состоит из трех параллельных реакций второго порядка по концентрации *н*-бутанола. Из-за этого необходимо увеличивать время каждого последующего цикла при фиксированных $Q^0_А$ и Q^0_{CO}. По этой же причине оптимальным режимом работы реактора для проведения рассматриваемого нами процесса будет режим идеального вытеснения.

В настоящей работе кроме расчетов реактора идеального вытеснения и реактора идеального вытеснения с подпиткой проведен расчет оптимального каскада реакторов идеального смешения и сравнение его с двумя вышеупомянутыми реакторами.

Математическая модель процесса в реакторе идеального вытеснения, подробно обсуждавшаяся в [1], записывается в следующем виде:

$$\frac{dX^Г_А}{d\tau'}=\frac{Q_ж RT}{P_А Q^0_А}\left(C^0_{ROH}\frac{dX_{ROH}}{d\tau'}+\frac{dC^ж_А}{d\tau'}\right) \tag{4}$$

$$\frac{dX^Г_{CO}}{d\tau'}=\frac{Q_ж RT}{P_{CO} Q^0_{CO}}\left(C^0_{ROH}\frac{dX_{ROH}}{d\tau'}+\frac{dC^ж_{CO}}{d\tau'}\right) \tag{5}$$

$$\frac{dC_{ROH}}{d\tau'}=-(K_1+K_2+K_3)C^2_{ROH}(1-\varphi);\qquad \frac{dX_{ROH}}{d\tau'}=\frac{1}{C^0_{ROH}}\frac{dC_{ROH}}{d\tau'} \tag{6}$$

$$\frac{dC_{БА}}{d\tau'}=K_1C^2_{ROH}(1-\varphi) \tag{7}$$

$$\frac{dC_{БП}}{d\tau'}=K_2C^2_{ROH}(1-\varphi) \tag{8}$$

$$\frac{dC_{ДЭ}}{d\tau'}=K_3C^2_{ROH}(1-\varphi) \tag{9}$$

$$\frac{dC^ж_А}{d\tau'}=\frac{6D_А}{d^2_п}\varphi K\left(\frac{P_А}{H_А}-C^ж_А\right)-(K_1+K_2+K_3)C^2_{ROH}(1-\varphi) \tag{10}$$

$$\frac{dC^ж_{CO}}{d\tau'}=\frac{6D_{CO}}{d^2_п}\varphi K\left(\frac{P_{CO}}{H_{CO}}-C^ж_{CO}\right)-(K_1+K_2+2K_3)C^2_{ROH}(1-\varphi) \tag{11}$$

с начальными условиями

$$\tau'=0;\quad X^Г_А=X^Г_{CO}=C^ж_А=C^ж_{CO}=C_{БА}=C_{БП}=C_{ДЭ}=0; \tag{12}$$

$$C_{ROH}=C^0_{ROH}$$

Модель, кроме того, дополняется соотношениями, с помощью которых учитывается изменение в ходе процесса газосодержания, диаметров газовых пузырей и безразмерного коэффициента массопередачи:

$$Q_A = Q_A^0(1 - X_A^\Gamma); \quad Q_{CO} = Q_{CO}^0(1 - X_{CO}^\Gamma) \tag{13}$$

$$\varphi = 0{,}833\frac{Q_A + Q_{CO}}{Q_A + Q_{CO} + Q_Ж} \tag{14}$$

(формула Арманда—Невструевой [5])

$$K = K^0\sqrt{\frac{d_п}{d_п^0}} \tag{15}$$

$$d_п = \sqrt[3]{\frac{6(Q_A + Q_{CO})}{\pi N}}. \tag{16}$$

Система уравнений (4)—(12) с дополнительными соотношениями (13)—(16) была решена численно на ЭВМ с помощью полунеявного метода Михельсена [6, 7]. С целью выбора оптимальных начальных значений диаметра пузырей газа $d_п^0$ и безразмерного коэффициента массопередачи K^0 были проведены специальные расчеты, в которых их значения, а также значения $Q_Ж$ варьировали в следующих пределах: $d_п^0 = 10^{-3} - 10^{-2}$ м; $K^0 = 10^2 - 10^5$; $Q_Ж = 5{,}56 \cdot 10^{-6} - 5{,}56 \cdot 10^{-4}$ м³/сек. Остальные параметры модели принимали такие значения: $T = 343{,}15$ К; $P_A = P_{CO} = 49$ КПа; $Q_A^0 = Q_{CO}^0 = 3{,}06 \cdot 10^{-4}$ м³/сек; $H_A = 4{,}9 \cdot 10^2$ (КПа м³)/кмоль; $H_{CO} = 8{,}09 \cdot 10^3$ (КПа м³)/кмоль; $D_A = D_{CO} = 0{,}36 \cdot 10^{-9}$ м²/сек. В процессе решения уравнений модели определялись концентрации компонентов в жидкой фазе и время контакта, необходимое для достижения заданной степени превращения $X_{ROH} = 0{,}3$.

Данные о зависимости фиктивного времени контакта τ' (связь истинного и фиктивного времени контакта дана уравнением (16) работы [1]) от параметров $d_п^0$ и K^0 представлены в *таблице 1*. Из этих данных следует, что при $K^0 \geq 10^4$ и $d_п^0 \leq 5 \cdot 10^{-3}$ м процесс протекает в кинетической области — время контакта практически не зависит от значений K^0 и $d_п^2$. Заметим, что значение K^0, при котором

Таблица 1

Зависимость фиктивного времени пребывания от параметров

$d_п^0$ и K^0 при $Q_Ж = 5{,}56 \cdot 10^{-6}$ м³/сек

K^0	$\tau' \cdot 10^4$–, сек при		
	$d_п^0 = 10^{-3}$ м	$d_п^0 = 5 \cdot 10^{-3}$ м	$d_п^0 = 10^{-2}$ м
10^5	1,314	1,314	1,314
$5 \cdot 10^4$	1,314	1,314	1,314
10^4	1,318	1,327	1,389
10^3	1,328	1,496	1,625
$5 \cdot 10^2$	1,382	1,598	1,640
10^2	1,401	1,620	1,730

достигается кинетическая область, для данного процесса на порядок выше, чем для процесса, протекающего в бромидной системе [1]. В кинетической области модель процесса значительно упрощается и состоит из уравнений (6)—(9) с соответствующими начальными условиями.

Результаты расчета реактора идеального вытеснения и реактора идеального вытеснения с подпиткой приведены в *таблице 2*. Заметим, что при осуществле-

Таблица 2

Сравнение различных способов осуществления процесса карбонилирования ацетилена в реакторе идеального вытеснения при

$Q_A^0 = Q_{CO}^0 = 3{,}06 \cdot 10^{-4}$ м³/сек; $D_p = 0{,}2$ м; $X_{ROH} = 0{,}3$; $K^0 = 10^4$; $d_п^0 = 5 \cdot 10^{-3}$ м; $C_{БА} = 0{,}59$ Кмоль/м³; $C_{БП} = 0{,}17$ Кмоль/м³; $C_{ДЭ} = 1{,}14$ Кмоль/м³

Способ осуществления процесса	$Q_Ж$, м³/сек	$W_Ж$, м/сек	φ^*	$\tau \cdot 10^{-4}$, сек	$L_{p'}$, м	Число точек подпитки
Реактор идеального вытеснения	$5{,}56 \times 10^{-6}$	$1{,}9 \times 10^{-4}$	0,80	1,314	2,37	—
Реактор идеального вытеснения с подпиткой	$2{,}78 \times 10^{-4}$	$9{,}5 \times 10^{-3}$	0,43	0,461	43,80	34

нии процесса по второму из упомянутых способов точки подпитки по длине реактора будут расположены неравномерно в силу принятой кинетической модели (второй порядок по C_{ROH}).

Математическая модель рассматриваемого процесса, осуществляемого в реакторе идеального смешения, состоит из уравнений (6)—(9).

Задачу расчета оптимального каскада реакторов идеального смешения можно сформулировать следующим образом: найти такое распределение времени контакта по реакторам каскада, при котором заданная степень превращения *н*-бутанола достигается при минимальном суммарном времени контакта, то есть критерий оптимальности в данном случае имеет вид:

$$\Psi = \min \sum_{i=1}^{N} \tau_i \tag{17}$$

при выполнении условия

$$X_N - X = 0 \tag{18}$$

Для решения этой задачи использовался метод неопределенных множителей Лагранжа [8]. Вместо независимых переменных τ_i введем новые переменные

$$\Theta_i = I - X_{ROH_i} \tag{19}$$

с помощью которых можно рассчитать долю непрореагировавшего *н*-бутанола на выходе из последнего реактора каскада

$$\Theta_N = \prod_{i=1}^{N} \Theta_i \tag{20}$$

Подставляя в уравнения (6)—(9) выражения τ_i через Θ_i, получим [9]:

$$\Theta_{i+1} = \sqrt{\frac{\Theta_i}{2-\Theta_i}} \tag{21}$$

С использованием выражения (21) были рассчитаны значения τ_i для каскадов, состоящих из различного числа реакторов идеального смешения. Результаты расчета приведены в *таблице 3*, где они сравниваются с результатами, получен-

Таблица 3

Распределение времени контакта и степени превращения X_{ROH} в каскадах реакторов идеального смешения

$Q_Ж = 5{,}56 \cdot 10^{-6}$ м³/сек; $Q^0_A = Q^0_{CO} = 3{,}06 \cdot 10^{-4}$ м³/сек; $C_{БА} = 0{,}59$ Кмоль/м³; $C_{БП} = 0{,}17$ Кмоль/м³; $C_{ДЭ} = 1{,}14$ Кмоль/м³.

Число реакторов в каскаде	Суммарное истинное время контакта в каскаде $\tau \times 10^{-3}$, сек	Распределение степени превращения (первое число) и истинного времени контакта $\tau \cdot 10^{-3}$, сек (второе число) по реакторам каскада						
		1	2	3	4	5	6	7
1	3,793	0,30	—	—	—	—	—	—
		3,793	—	—	—	—	—	—
2	3,172	0,169	0,157	—	—	—	—	—
		1,520	1,652	—	—	—	—	—
3	2,990	0,118	0,112	0,106	—	—	—	—
		0,941	0,997	1,052	—	—	—	—
4	2,903	0,091	0,087	0,083	0,080	—	—	—
		0,679	0,710	0,742	0,772	—	—	—
5	2,852	0,074	0,071	0,069	0,066	0,065	—	—
		0,531	0,551	0,570	0,590	0,610	—	—
6	2,818	0,062	0,060	0,058	0,057	0,055	0,054	—
		0,436	0,450	0,463	0,476	0,490	0,503	—
7	2,793	0,053	0,052	0,051	0,050	0,048	0,047	0,046
		0,369	0,379	0,389	0,399	0,409	0,419	0,429
Реактор идеального вытеснения	2,560	0,300						

ными для реактора идеального вытеснения. Как следует из этой таблицы, уже каскад из четырех реакторов идеального смешения достаточно хорошо приближает условия осуществления процесса в реакторе идеального вытеснения.

Сравнивая все рассмотренные способы осуществления процесса карбонилирования ацетилена в каталитической системе PdI_2 — NaI — HCl — *н*-бутанол, отметим, что в каскаде из четырех реакторов идеального смешения суммарное истинное время контакта лишь на 343 секунды больше, чем в реакторе идеального вытеснения.

Как уже отмечалось выше, недостатком реактора идеального вытеснения является нерациональное использование его объема вследствие высокого газосодержания. Недостатком реактора идеального вытеснения с подпиткой является большое число точек подпитки (34 точки). Кроме того, в этих точках необходимо обеспечить равномерное распределение газовой фазы по сечению аппарата и пузырей газа по размерам.

В результате математического моделирования процесса для его промышленной реализации рекомендуется каскад из четырех реакторов идеального смешения, суммарное истинное время контакта в котором составляет $2{,}903 \cdot 10^3$ секунд.

ОБОЗНАЧЕНИЯ

C — концентрация, Кмоль/м³;
$d_п$ — диаметр газового пузыря, м;
D — коэффициент молекулярной диффузии, м²/сек;
$D_р$ — диаметр реактора, м;
H — константа Генри (КПа м³)/Кмоль;
K — безразмерный коэффициент массопередачи;
K_1, K_2, K_3, — константы скоростей параллельных реакций второго порядка, м³/(Кмоль сек);
$L_Р$ — длина реактора, м;
N — число газовых пузырей, поступающих в реактор в единицу времени; число реакторов в каскаде;
P — давление, КПа;
Q — объемный расход, м³/сек;
r — скорость реакции, Кмоль/(м³ сек);
R — универсальная газовая постоянная (КПа м³)/(град Кмоль);
T — температура, К;
$W_Ж$ — линейная скорость жидкости в аппарате, м/сек;
$X=(Q^0-Q)/Q^0$ — степень превращения компонентов в реакторе идеального вытеснения;
$X=(C^0-C^1)/C^0$ — то же в каскаде реакторов идеального смешения;
τ, τ' — время контакта, сек;
φ — газосодержание;
φ^* — среднее значение газосодержания по длине реактора;
Ψ — критерий оптимальности, определяемый уравнением (17);
Θ — переменная, определяемая уравнением (19).

Индексы

А — ацетилен;
СО — окись углерода;
БА — бутиловый эфир акриловой кислоты;
БП — бутиловый эфир пропионовой кислоты;
ДЭ — бутиловые эфиры малеиновой, фумаровой и янтарной кислот;
ROH — *н*-бутанол;
г — газовая фаза;
ж — жидкая фаза;
о — начальное значение;
I — значение на выходе из реактора;
i — индекс *i*-того реактора каскада реакторов идеального смешения.

ЛИТЕРАТУРА

1. Гарцман, А. Н., Шуляковский, Г. М., Ермакова, А. и Темкин, О. Н.: Hung. J. Ind. Chem., *1980*, 8, 407.
2. Темкин, О. Н., Калия, О. Л., Жир-Лебедь, Л. Н., Голодов, В. Л., Брук, Л. Г. и Мехрякова, Н. Г.: Труды ИОКЭ, *1978*, 17, 3.
3. Himmelblau, D. M., Jones, C. R. and Bischoff, K. B.: Ind. Eng. Chem. Fundam., 6., 539. *1967*.
4. Vajda S.: Magyar Kémikusok Lapja, *1976*. 31, 437.
5. Кутателадзе, С. С., Стырикович, М. А.: Гидродинамика газожидкостных систем, „Энергия", М., 1976.
6. Michelsen, M. L.: AIChE J. *1976*. 22, 594.
7. Гарцман, А. Н., Черкашин, В. В. и Панкова, Г. А.: Алгоритмы и программы, Информ. бюлл., № 2, 41 (1979).
8. Смирнов, В. И.: Курс высшей математики, т. 1, „Физматгиз", М., 1958.
9. Бояринов, А. И. и Кафаров, В. В.: Методы оптимизации в химической технологии, „Химия", М., 1969.

SUMMARY

The paper deals with the different synthesis methods of acrylic, propionic, maleinic, fumarolic and resinic acid butylesters, to the synthesis of the previous compounds carbonylized acetylene was used. The applied mathematical model is described in the previous paper [1].

Опудликованные в журнале НЛС *1980*, 8 (4) 407—416 *обнаружены следующие опечатки:*

Страница	Строка	Напечатано	Следовало напечатать
407	5 сверху	2-ЕТИЛГЕКСАНОЛ	2-ЭТИЛГЕКСАНОЛ
408	10 сверху	(2-ЕГС)	(2-ЭГС)
408	4 снизу	$\varkappa_{ЭД}$	$\varkappa_{ДЭ}$
409	1 снизу	d^2	d_n^2
410	1 сверху	d^2	d_n^2
410	3 сверху	$C_{2-ЕГА}$	$C_{2-ЭГА}$
410	12 сверху	$(I-X_{CO})$	$(I-X_{CO}^{\Gamma})$
410	11 снизу	$K^0=10^2-10^4\,K$	$K^0=10^2-10^4$
410	7 снизу	ДМФ-2-ЭГС-НВ$_\varkappa$	ДМФ-2-ЭГС-НВг
411	9 сверху	$K^0>800$	$K^0=800$
412	*Рис. 3*, ось абсцисс	T, K	K^0
412	12 снизу	от параметра $T(K)$ при	от параметра K^0 при
412	6 снизу	кажбого	каждого
412	1 снизу	$X_A^2=0{,}9$	$X_A^{\Gamma}=0{,}9$
413	7 сверху	Ф	φ

HUNGARIAN JOURNAL
OF INDUSTRIAL CHEMISTRY
VESZPRÉM
Vol. 9. pp. 45–54 (1981)

PARTICLE FORMATION FROM SOLUTIONS IN GAS FLUIDISED BEDS. V.

THE MATHEMATICAL MODEL OF THE STEADY-STATE PROCESS IN THE CASE OF PARTICLE ADDITION

B. Dencs and T. Blickle

(Research Institute for Technical Chemistry
of the Hungarian Academy of Sciences, Veszprém, Hungary)

Received: February 1, 1981.

In the case of particle formation from solutions in gas fluidised beds, steady state conditions are often brought about by the addition of particulate material. The mathematical model of this process has been developed in the form of balance equations using the dispersion characteristics (numerousness, size, surface area and volume of the particles). The balance equations contain input and output convective flows and source terms. The solution method of the model is shown. The major characteristics calculated from the model (e.g. average particle size, and specific surface area) are compared with measured values. The accuracy of the model is sufficient for industrial purposes. The model can be used to estimate the major physical characteristics of the material leaving the apparatus.

Introduction

As it is well known, fluidisation can be used for the continuous production of particulate material from liquid phases (solution, suspension, slurry, and melt). There is an ever growing interest in this aspect of fluidisation demonstrated by the large number of types of continuous, industrial fluidisation apparatus and technologies developed in the past few years (e.g. 1–10, etc.). The major reason for this upsurge of activity is that the economic indicators of this operation are often more favourable than those of the multistage technologies (e.g. crystallization-filtration-drying, and evaporation-spray-drying, etc.) [8–10].

The essence of particle formation from solution in a gas fluidised bed (or in brief: direct particle formation) was detailed earlier [11]. Briefly, it means that a particulate mass, the composition of which is identical with that of the material dissolved or suspended in the solution, is fluidised by hot gas (generally air) in a suitable fluidised bed. The solution is sprayed onto the surface (or the interior) of the fluidised layer. The matted, fluidised particles dry while they are in constant motion. The fluidising air carries away the solvent vapours, while

the solid material content of the solution sprayed into the bed remains on the particles. Particulate material is continuously discharge from the layer at a rate equivalent to the solid material feed-in rate.

Size-changes of the particles taking place in the fluidised bed profoundly influence the establishment of steady-state operation conditions, and primarily that of a steady-state particle size distribution.

The size of the fluidised particles increases, due to the addition of the solution or suspension, either via surface layering or agglomeration [12]. A particle-size diminution also takes place in the fluidised bed, caused either by mechanical wear in the fluidised layer [11] or the temperature fluctuation at the surface of the particles [13, 14].

Product discharge and agglomeration decrease the number of particles present in the fluidised layer. In order to establish a steady-state particle size distribution, the number of particles in the layer has to be kept at a constant value [15] and certain conditions relating to the heat and mass flows have to be fulfilled. In most cases, particle-size-diminution processes are negligible. Steady-state particle size distribution can be ensured either by increasing the extent of size-diminution [13, 14, 15], or by introducing additional particulate material into the fluidised layer (e.g. by recirculating the "undersize" fraction of the product) [1–3, 17], or by both.

Several papers deal with the mathematical description of this process (e.g. [12, 15, 18–20], etc.). One of the major research areas of the Research Institute for Technical Chemistry is the investigation of chemical operations in which dispersed phases are involved, and more specifically, in which the aim of the given operation is the alteration of the characteristics of the dispersed phase (number, size, surface area, and volume, etc., of the particles). The latter include grinding, granulation, crystallization, dissolution, direct particle formation operations and so on. These and similar operations can be mathematically described by combining the conventional balance equations and the characteristics of the dispersed particles.

Development of the Mathematical Model

The principle of the studied process is shown in *Fig. 1.* Steady-state conditions can be brought about by adding additional particulate material.

The granules (as dispersed particles) present in the fluidised layer (as dis-

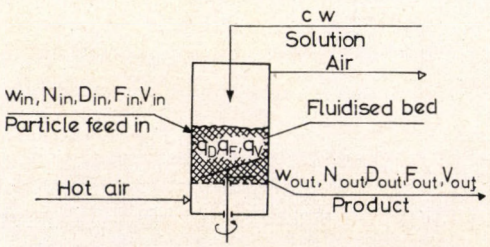

Fig. 1
Particle formation from solutions in gas-fluidised beds

persion) can be characterised by the following extensive and intensive quantities:

- number of particles ($\tilde{N}$), and the number of particles in unit dispersion volume (N),
- overall size of the particles ($\tilde{D}$), and the overall size of the particles in unit dispersion volume (D),
- overall surface area of the particles ($\tilde{F}$), and the overall surface area of the particles in unit dispersion volume (F),
- overall volume of the particles ($\tilde{V}$), and the overall volume of particles in unit dispersion volume (V).

The following simplifying assumptions were used for the development of the model:

1. The particles are at least approximately spherical.
2. Neither size diminution, nor agglomeration take place in the fluidised bed.
3. The fluidised layer is perfectly mixed.

The volume-increase-rate of a particle can be given as:

$$d\frac{\frac{\delta^3\pi}{6}}{dt}=\frac{\delta^2\pi}{\tilde{F}}w'c' \tag{1}$$

The left-hand side of Eq. 1 can be rewritten as:

$$\frac{\pi}{6}\frac{d\delta^3}{d\delta}\frac{d\delta}{dt}=\frac{\pi}{2}\delta^2\frac{d\delta}{dt} \tag{2}$$

This expression can be substituted into Eq. 1 yielding, after rearrangement, an expression for the linear-size-growth-rate of the particle:

$$\frac{d\delta}{dt}=\frac{2w'c'}{\tilde{F}} \tag{3}$$

Particle growth occurring during the average residence time can be obtained from Eq. 3:

$$a=\delta-\delta_0=2w'c'\int_0^{\tau}\frac{dt}{F} \tag{4}$$

Making use of the particle size growth expression, the extensive characteristics of the dispersion can be defined as:

$$\tilde{N}=\int_0^{\infty}n(\delta_0)d\delta_0 \tag{5}$$

$$\tilde{D}=\int_0^{\infty}(a+\delta_0)n(\delta_0)d\delta_0=a\tilde{N}+D_0 \tag{6}$$

$$\tilde{F} = \int_0^\infty \pi(a+\delta_0)^2 n(\delta_0) d\delta_0 = \pi a^2 \tilde{N} + 2\pi a \tilde{D}_0 + \tilde{F}_0 \tag{7}$$

$$\tilde{V} = \int_0^\infty \frac{\pi}{6}(a+\delta_0)^3 n(\delta_0) d\delta_0 = \frac{\pi}{6} a^3 \tilde{N} + \frac{\pi}{2} a^2 D_0 + \frac{1}{2} a \tilde{F}_0 + \tilde{V}_0 \tag{8}$$

where:

$$\tilde{D}_0 = \delta_0 \tilde{N} \tag{9}$$

$$\tilde{F}_0 = \pi \delta_0^2 \tilde{N} \tag{10}$$

$$\tilde{V}_0 = \frac{\pi}{6} \delta_0^3 \tilde{N} \tag{11}$$

The Source Terms

The source terms of the extensive characteristics of the particles present in the fluidised bed can be formulated as:

— Source term for the number:

This expression is derived from the 2nd simplifying assumption as:

$$q_N = \frac{d\tilde{N}}{dt} = 0 \tag{12}$$

— Source term for the size:

$$q_D = \frac{d\tilde{D}}{dt} = \frac{d\tilde{D}}{da} \frac{da}{dt} \tag{13}$$

"$\tilde{D}$" and "a" can be expressed from Eq. 6 and Eq. 4, respectively. After differentiation we obtain:

$$\frac{d\tilde{D}}{da} = \frac{d(a\tilde{N} + \tilde{D}_0)}{da} = \tilde{N} \tag{14}$$

$$\frac{da}{dt} = \frac{2w'c'}{\tilde{F}} \tag{15}$$

The source term for size then becomes, from Eq. 13–15:

$$q_D = \frac{2\tilde{N}w'c'}{\tilde{F}} \tag{16}$$

The source terms of surface area and volume can also be derived in this manner.

— The source term of surface area:

$$q_F = \frac{4\pi\tilde{D}w'c'}{\tilde{F}} \tag{17}$$

— The source term of volume:

$$q_V = w'c' \tag{18}$$

It is more advantageous to use the intensive dispersion characteristics, i.e. those which refer to unit dispersion volume. In the case of the size and surface area source terms, this requires only a formal operation. Since according to the simplifying assumptions the fluidised layer is perfectly mixed, the intensive dispersion characteristics of the material in the fluidised bed and in the discharge stream are identical. Therefore, the "out" subscript can be added to these quantities. The source terms expressed with the intensive dispersion characteristics are as follows:

$$q_N = 0 \tag{19}$$

$$q_D = \frac{2N_{\text{out}}w'c'}{F_{\text{out}}} \tag{20}$$

$$q_F = \frac{4\pi D_{\text{out}}w'c'}{F_{\text{out}}} \tag{21}$$

$$q_V = w'c' \tag{22}$$

Balance Equations in Steady-State Conditions

In steady-state conditions, the balance equations constructed with intensive dispersion characteristics and certain convective and source terms (i.e. the time-dependent changes of the intensive dispersion characteristics) are zero (cf. *Fig. 1*):

$$w_{\text{in}}N_{\text{in}} = w_{\text{out}}N_{\text{out}} \tag{23}$$

$$w_{\text{in}}D_{\text{in}} + \frac{2N_{\text{out}}w'c'}{F_{\text{out}}} = w_{\text{out}}D_{\text{out}} \tag{24}$$

$$w_{\text{in}}F_{\text{in}} + \frac{4\pi D_{\text{out}}w'c'}{F_{\text{out}}} = w_{\text{out}}F_{\text{out}} \tag{25}$$

$$w_{\text{in}}V_{\text{in}} + c'w' = w_{\text{out}}V_{\text{out}} \tag{26}$$

The void volume fraction of the input and output solid-gas dispersions are identical with that of the fluidised bed. Correspondingly:

$$V_{\text{in}} = V_{\text{out}} = 1 - \varepsilon \tag{27}$$

It should be noted here that either the mass or the volume related intensive dispersion characteristics can be used for the development of the model without limiting the scope and application field of the model. In this case $V_{\text{in}} = V_{\text{out}} = 1$, and the quantities w_{in} and w_{out} represent the volume and mass flows of the dispersed particles, while $c'w'$ is the volume or mass of the solid material introduced with the feed-liquid.

The intensive characteristics defining and uniquely characterizing the dispersion (N_{out}, D_{out}, F_{out}) can be calculated from balance equations Eq. 23–26 as follows. The volume flow rate of the dispersion entering the fluidised bed is

w_{in}, its characteristics are N_{in}, D_{in} and F_{in}, the void volume fraction is ε, the concentration of the solution (suspension) is c′ and spraying rate is w'. These characteristics are known parameters either given, or freely selectable aimed at the achievment of a given technological goal. w_{out} can be calculated from Eq. 26, and with it N_{out} from Eq. 23. Substituting these values of N_{out} and w_{out} into Eq. 24 and 25, a two variable equation set is obtained for D_{out} and F_{out}. Either of them can be obtained as the root of a third-order equation. The major physical characteristics of the particulate material leaving the fluidised bed — average particle size, d_{out}; average particle surface area, f_{out} and the so-called specific surface area, F^*_{out} can be calculated with the intensive dispersion characteristics determined from the model:

$$d_{out}=\frac{D_{out}}{N_{out}} \tag{28}$$

$$f_{out}=\frac{F_{out}}{N_{out}} \tag{29}$$

$$F^*_{out}=\frac{F_{out}}{1-\varepsilon} \tag{30}$$

Application of the Model

Experiments were carried out with urea as model material in a laboratory-scale cylindrical fluidisation apparatus (inner diameter: 0.106 m). Steady-state operation conditions were brought about by adding extra particulate material [17, 21]. The particulate product discharged in steady-state conditions was subjected to sieve-analysis. The intensive dispersion characteristics were calculated from the experimental data and the sieve analysis results. The average particle size, average particle surface area and specific surface area values were calculated from Eq. 28, 29 and 30.

From the technological parameters used for the experiments and Eq. 23–26 the intensive dispersion characteristics, the average particle size, average particle surface area and specific surface area values were calculated. These data

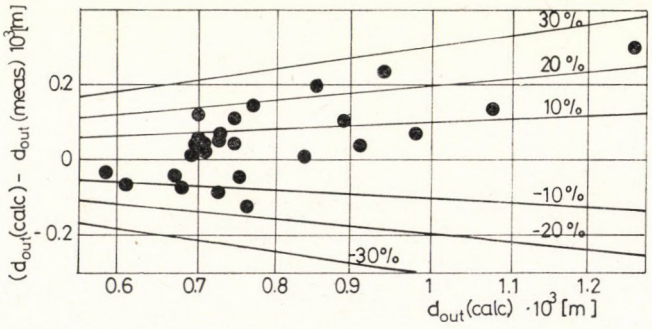

Fig. 2
Deviation of calculated and measured average particle size as a function of the calculated value

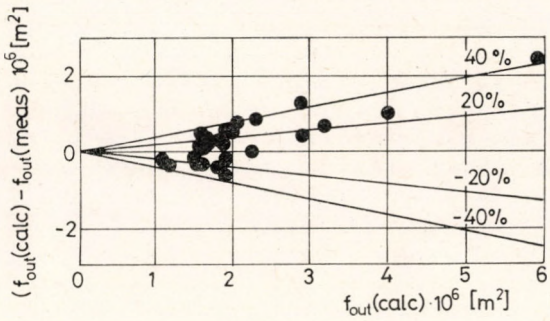

Fig. 3
Deviation of calculated and measured average particle surface area as a function of the calculated value

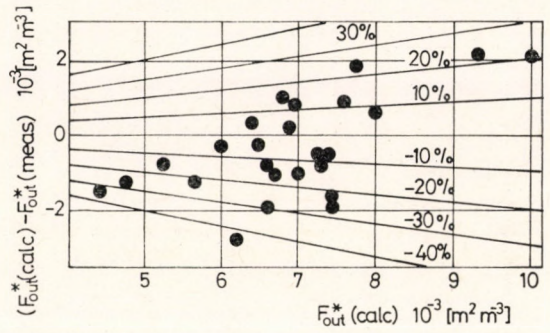

Fig. 4
Deviation of calculated and measured specific surface area as a function of the calculated value

were compared with those calculated from the sieve analysis of the steady-state product *(Fig. 2–4)*.

It can be seen from the comparisons that the average particle size calculated from the model and determined from sieve analysis agree within a -25% error. The deviation of the average particle surface area is less than 30% in at least 80% of the cases, while the largest deviation observed is 44%. (cf. *Fig. 3*). The specific surface area values deviate less than 30% in about 90% of the cases (cf. *Fig. 4*).

Summary

From the examination of the mathematical model of direct particle formation from solutions in a gas-fluidised bed, and the comparison of the data calculated from the model and measured in separate experiments, it can be concluded that the accuracy of the model developed is sufficient for most industrial purposes. The accuracy can be improved by accounting for the slight porosity of the particles and the deviation of the particles from the assumed spherical shape.

It has to be noted that the average particle size calculated from the model (and average particle size in general) does not in itself characterize the particulate material unambiguously, for widely different distribution curves can belong to the very same average particle size. Both the experimental results [21] and literature references confirm that the particle size distributions of various products are very similar, independently from their chemical identity, provided particle growth takes place via surface layering and there is no, or only very slight, agglomeration. The major part of the product mass is also within narrow particle size limits. The lower limit of this size range primarily depends on the conditions of fluidisation (gas velocity), while the upper limit is controlled by the size of the added particles and their growth rate. Taking into account this auxiliary information, one can predict whether the solid material to be produced really meets the requirements.

The model developed for direct particle formation using external particle addition can be used directly (without measurements or experimental data) for the calculation/prediction of the major physical characteristics of the particulate material discharged from the fluidised bed in steady-state conditions. The model can also be used for the estimation of the technological parameters necessary for the formation of products with predetermined characteristics (for the calculation of added external particle size, its mass or volume flow-rate, and solvent feed rate, etc.).

SYMBOLS

a particle growth occurring during the average residence time, m
c' concentration of the solution (suspension), m^3/m^3
d average particle size, m
D overall size of the particles in unit volume dispersion, $m \cdot m^{-3}$
$\tilde{D}$ overall size of the particles in the dispersion, m
f average particle surface area, m^2
F overall surface area of the particle in unit volume dispersion, m^2/m^3
$\tilde{F}$ overall surface area of the particles in the dispersion, m^2/m^3
F^* overall surface area of the particles in unit particle volume, so-called specific surface area, m^2/m^3
$n(\delta_0)$ size-distribution density function according to particle number at $t=0$, m^{-1}
N number of particles in unit volume dispersion, m^{-3}
$\tilde{N}$ number of particles in dispersion, —
q_N number source in the fluidised bed, s^{-1}
q_D size source in the fluidised bed, $m \cdot s^{-1}$
q_F surface area source in the fluidised bed, $m^2 s^{-1}$
q_V volume source in the fluidised bed, $m^3 s^{-1}$
t time, s
V overall volume of particles in unit volume dispersion, m^3/m^3
$\tilde{V}$ overall volume of the particles in the dispersion, m^3
w volumetric flow-rate of the dispersion, m^3/s^{-1}
w' spraying rate (volumetric rate) of the solution (suspension), m^3/s^{-1}
δ particle size, m
ε void volume fraction of the fluidised bed, —
τ average residence time, s

Subscripts

o initial value
∞ limiting value
out output value
in input value

REFERENCES

1. Shakhova, N. A. et. al.: Khim. Prom., *1973*, 49, 299.
2. Volkov, V. F. et. al.: Khim. Prom., *1966*, 42. 450.
3. Shakhova, N. A. et. al.: Khim. Prom., *1968*, 44, 446.
4. Repenkova, T. G., Kopilov, V. A.: Khim. Prom., *1965*, 41, 462.
5. Groshev, G. L. et. al.: Khim. Prom., *1967*, 43, 456.
6. Mortensen, S. and Hovmand, S.: Production of non-dusty granular products by fluid bed spray granulation. 18th Chemical Engineering Exhibition-Congress, 20th to 26th June, 1976, Frankfurt/Main, ACHEMA 76.
7. Danov, S. M. et. al.: Khim. Prom., *1966*, 42, 453.
8. Pictor, J. W.: Process Eng., *1974*, June, 66.
9. Christmann, G.: Chem. Anlagen Verfahren, *1973*, January, 42.
10. Kaspar, J. and Rosch, M.: Chem. Ing. Tech., *1973*, 45, 736.
11. Dencs, B. and Ormós, Z.: Hung. J. Ind. Chem. *1978*, 6, 301.
12. Volkov, V. F. et. al.: Khim. Prom., *1967*, 43, 452.
13. Nalimov, S. P., Kaganovic, V. A., Kozlovskij, V. V.: Zh. Prikl. Khim. *1970*, 43, 581.
14. Kozlovskij, V. V., Kaganovic, V. A. and Nalimov, S. P.: Khim. Prom., *1970*, 46, 122.
15. Todes, O. M. et. al.: Gidrodin, Teplo-Massoobmen Psevdoozhizhennom sloe, *1974*, 69.
16. Najmr, S., Zak, J. and Dorbohlov, R.: Czech. Pat. 134, 975 (1968).
17. Dencs, B. and Ormós, Z.: Hung. J. Ind. Chem. *1978*, 6, 313.
18. Todes, O. M. et. al.: Teor. Osn. Khim. Tekhnol., *1973*, 7, 126.
19. Sahova, N. A.: Khim. Prom., *1967*, 43. 459.
20. Todes, O. M.: Krist. Tech., *1972*, 7, 729.
21. Dencs, B. and Ormós, Z.: Hung. J. Ind. Chem., *1978*, 6, 323.

РЕЗЮМЕ

С целью произведения частиц из растворов в псевдоожиженном слое для получения установившегося процесса в аппарат часто загружают сыпучий материал. На основе уравнений равновесия содержащих характерные свойства частиц (рапределение, размер, удельная поверхность и удельный объем) авторы составили математическую модель процесса. Уравнения равновесия содержат конвективные потоки и источники. В стати обсуждается методика решения модели. Расчетные значения характерных свойств (средний размер и удельная поверхность) сопоставляют экспериментальными данными. Точность модели удовлетворяет требованиям промышленной практики. Применением модели становится возможным оценка основных физических свойств полученного в аппарате продукта.

HUNGARIAN JOURNAL
OF INDUSTRIAL CHEMISTRY
VESZPRÉM
Vol. 9. pp. 55–72 (1981)

EIN VERALLGEMEINERTES HOLDUP-MODELL FÜR DIE VERTIKALE ZWEIPHASEN-RING-TROPFEN-STRÖMUNG*

M. Reitz

(Ingenieurhochschule Köthen, 4370 Köthen, DDR)

Eingegangen am 5. November 1980

Mit Hilfe des Pitotrohr-Meßverfahrens wurden in einem quadratischen Kanal mit der Seitenlänge 72 mm im aufwärtsgerichteten Zweiphasen-Gleichstrom Flüssigkeits-Holdup-Profile ermittelt. Mit den über den Querschnitt gemittelten Holdup-Werten konnten Holdup-Profile über die Kanallänge aufgestellt werden, die ein Minimum bei etwa $l/d \approx 3$ aufweisen und bei $l/d > 15$ einen Gleichgewichts- bzw. Grenzwert annehmen. Dieser Sachverhalt wird analysiert und modelliert. Dazu ist eine fiktive Aufteilung des Gesamt-Holdup in einen Beschleunigungsanteil und einen Koaleszenzanteil notwendig. Das erhaltene Gesamtmodell stellt eine Superposition der Teilprozesse dar. Es beschreibt die Meßwerte adäquat, d.h. mit einem Fehlerbereich von $+10\%$ bzw. -20%.

Einleitung

Gegenstand dieser Betrachtung ist die aufwärtsgerichtete Zweiphasen-Ring-Tropfen-Strömung. Solche Strömungsformen treten beispielsweise bei Verdampfungs-, Absorptions- und Chemosorptionsprozessen in Gas-Flüssigkeits-Rohrreaktoren auf. Trotz gleicher Strömungsform unterscheiden sich diese Prozesse wesentlich durch die Erzeugung des Strömungszustandes bzw. die Art der Dispergierung der Flüssigphase. Bei Verdampfungsprozessen bildet sich der Tropfenstromanteil hauptsächlich als Entrainment aus dem Flüssigkeitsfilm [1, 2] im Gegensatz zu Absorptions- oder Chemosorptionsprozessen, speziell Hochgeschwindigkeitskontaktierung (HGK) [3, 4], wo ein großer Tropfenstromanteil durch Versprüheinrichtungen erzeugt wird und der Wandfilm sich mit zunehmender Kanallänge bildet. Oberhalb einer charakteristischen Kanallänge [4] geht im letztgenannten Fall die Phasenverteilung sowohl bei vertikaler als auch bei horizontaler Strömung in einen Gleichgewichtszustand über, d. h. die Änderung des Tropfenmassenstromes mit der Kanallänge ist gleich Null

$$\frac{d\dot{m}_T}{dl} = 0. \tag{1}$$

* Erweiterte Fassung eines auf dem 4. Internationalem Symposium „Thermische Stofftrennung" vom 26/27. August 1980 in Magdeburg gehaltenen Vortrages.

Erst unter dieser Bedingung sind die Strömungszustände bei adiabater Dampf-Flüssigkeits-Strömung und Prozessen mit mechanischer Flüssigkeitsdispergierung identisch.

Nach Angaben von Grundke, u. a. [5] erfolgt etwa 50% des Stoffaustausches bei der Absorption infolge der großen Relativgeschwindigkeit zwischen den Phasen schon nach kurzen Kanallänge, etwa $l/d < 2$. Der Gleichgewichtsbereich in der Phasenverteilung beginnt etwa bei einem Verhältnis $l/d \approx 15$ [4]. Wegen der Unsicherheit der Größe der Phasengrenzfläche bei Ring-Tropfen-Strömungen, besonders in dem Nichtgleichgewichtsbereich bei $l/d < 15$, wird die Intensitätsgröße β bei der Modellierung der Stoffübertragung häufig auf das Flüssigkeits-Holdup bezogen. Diese Größe ist aber in dem betrachteten Bereich bei konstanten Gas-Flüssigkeits-Belastungsverhältnissen längenabhängig. Das Flüssigkeits-Holdup wird als bezogene Größe verwendet und läßt sich bei konstantem Rohr- oder Kanalquerschnitt zu einem Querschnittsverhältnis reduzieren

$$(1-\varepsilon) = \frac{A_L}{A_K}. \tag{2}$$

Damit ist der Zusammenhang zwischen Flüssigkeits-Holdup und mittlerer Flüssigphasengeschwindigkeit durch die Kontinuitätsgleichung gegeben.

Unmittelbar aus dem Holdup kann die mittlere Verweilzeit der flüssigen Phase ermittelt werden

$$\bar{t} = \frac{\overline{(1-\varepsilon)} \cdot V_K}{\dot{V}_L} \tag{3}$$

die beispielsweise bei Anwendung der Penetrationstheorie häufig als Näherung benutzt wird. Da aber das Holdup, wie es in *Gl.* (2) definiert ist, eine von der Kanallänge abhängige Größe ist, muß für ein bestimmtes Kontaktzonen- bzw. Rohrvolumen V_K in *Gl.* (3) ein äquivalenter gemittelter Holdup-Wert eingesetzt werden. Die Mittelwertbildung kann nach *Gl.* (4) erfolgen

$$\overline{(1-\varepsilon)} = \frac{1}{l} \int_0^1 (1-\varepsilon)\,(l)\,dl. \tag{4}$$

Gleichfalls von Bedeutung ist das Holdup für die Ermittlung hydrostatischer Druckdifferenzen, da hierbei dei Gravitationsdichte [6] zu verwenden ist

$$\Delta p_{stat} = g\varrho_Z \Delta H = g(\varepsilon\varrho_G + (1-\varepsilon)\varrho_L)\Delta H. \tag{5}$$

Im Folgenden wird versucht, qualitative und quantitative Aussagen über das Holdup im Nichtgleichgewichtsbereich sowie dessen Modellierung zu treffen.

Literatur

Es kann davon ausgegangen werden, daß der hier betrachtete Anfangsbereich der Zweiphasenströmung mit mechanischer Flüssigkeitsdispergierung in der Literatur bisher kaum bzw. nicht behandelt wurde. In den meisten Fällen erstrecken sich die Untersuchungen der Literatur auf statische oder quasistatische Verhältnisse in der Phasenverteilung entlang des Strömungsweges. Aus

eingangs genannten Gründen stellen sich erst ab einer bestimmten Kanallänge diese Gleichgewichtsverhältnisse ein.

Für diesen Gleichgewichtsfall existieren eine Vielzahl von Berechnungsmethoden für Flüssigkeits- oder Gas-Holdup. Am bekanntesten ist das Verfahren von LOCKHART und MARTINELLI [7]. Der sogenannte LOCKHART/MARTINELLI-Parameter,

$$X_{LM} = X_{tt} = \left(\frac{1-\dot{x}}{\dot{x}}\right)^{0,9} \left(\frac{\eta_L}{\eta_G}\right)^{0,1} \left(\frac{\varrho_G}{\varrho_L}\right)^{0,5} \tag{6}$$

der die Gas-Flüssigkeits-Belastungsverhältnisse sowie die stoffspezifischen Verhältnisse berücksichtigt, wurde von DAVIS [8] für eine vertikale Zweiphasenströmung unter den Bedingungen $Re_L > 8000$ bzw $Re_L < 8000$ und $Fr > 100$ mittels einer mittleren Froude-Zahl korrigiert

$$X_{tt} = X_D = 0{,}19 \left(\frac{1-\dot{x}}{\dot{x}}\right)^{0,9} \left(\frac{\eta_L}{\eta_G}\right)^{0,1} \left(\frac{\varrho_G}{\varrho_L}\right)^{0,5} \left(\frac{\overline{w}^2}{g \cdot d}\right)^{0,185}. \tag{7}$$

Nach SARMA, u. a. (9) gilt dann für das Flüssigkeits-Holdup unter der Bedingung der Ring-Tropfen-Strömung, also bei $(1-\varepsilon) \ll 1$

$$(1-\varepsilon) \approx X_D. \tag{8}$$

Für eine horizontale Zweiphasenströmung hat WALLIS [10] eine Abhängigkeit des Gas-Holdup vom Parameter X_{tt} gefunden,

$$\varepsilon = (1 + X_{tt}^{0,8})^{-0,378} \tag{9}$$

aus welcher sofort das Flüssigkeits-Holdup folgt.

Weitere wesentliche Modelle sollen kurz vorgestellt werden. Das Verfahren von CHAWLA [11] ist für horizontale und vertikale Zweiphasenströmung abgeleitet, wobei die Stoffwertverhältnisse und Belastungsverhältnisse in weiten Bereichen variiert wurden. Es wird ein sogenannte. Zweiphasen-Austauschparameter gebildet in Anlehnung an den Lockhart/Martinelli-Parameter

$$\varepsilon_C = 9{,}1 \cdot \frac{1-\dot{x}}{\dot{x}} \cdot \left(\frac{\varrho_G}{\varrho_L}\right)^{0,9} \cdot \left(\frac{\eta_G}{\eta_L}\right)^{0,5} \cdot (Re_L \cdot Fr_L)^{-1/6}. \tag{10}$$

Die Holdup-Bestimmung kann zweckmäßig auch grafisch erfolgen. Die Kennzahlen Re_L und Fr_L beziehen sich auf die Flüssigphase und die Geschwindigkeit ist auf den gesamten Rohrquerschnitt bezogen

$$Re_L = \frac{w_L \cdot d \cdot \varrho_L}{\eta_L} \qquad Fr_L = \frac{w_L^2}{g \cdot d}. \tag{11}$$

Das Verfahren von HUGHMARK [12] ist ebenfalls für waagerechte und senkrechte Luft-Wasser-Strömungen gültig. Der Nachteil dieses Verfahrens besteht in der iterativen Berechnung des Gas-Holdup. Es ist ein Anfangswert für das Gas-Holdup entsprechend der zu erwartenden Strömungsform vorzugeben. Mit den über beide Phasen gemittelten Kennzahlen

$$Re = \frac{\dot{m}' \cdot d}{(1-\varepsilon)\eta_L + \varepsilon \cdot \eta_G} \quad \text{und} \quad Fr = \frac{\overline{w}^2}{g \cdot d} = \frac{(\Sigma \dot{V}_i)^2}{A_k^2 \cdot g \cdot d} \tag{12}$$

werden die Hilfsfunktionen

$$Y = Re^{1/6} \cdot Fr^{1/8} \cdot (1-\varepsilon)^{-1/4} \tag{13}$$

und

$$K = 0{,}75545 + 0{,}00358\ Y - 0{,}1436 \cdot 10^{-4} \cdot Y^2; \quad Y > 10 \quad [13] \tag{14}$$

gebildet, woraus das Gas-Holdup bestimmt wird

$$\varepsilon = \frac{K}{1 + \frac{\varrho_G}{\varrho_L}\left(\frac{1-\dot{x}}{\dot{x}}\right)}. \tag{15}$$

Die Anwendung hat gezeigt, daß schon beim 2. Iterationsschritt die Abweichung gegenüber dem Grenzwert kleiner als 1% ist. Bei dem Verfahren von Rouhani [14] werden zwei Modelle unterschieden, wobei nach [4] für den betrachteten Anwendungsfall nur das Modell I befriedigende Werte liefert. Nach [13] sind folgende drei Gleichungen heranzuziehen

$$C = 1 + 0{,}12(1-\dot{x}), \tag{16}$$

$$w' = \left(\frac{1{,}18}{\sqrt{\varrho_L}}\right)(g\sigma(\varrho_L - \varrho_G))^{0{,}25}, \tag{17}$$

$$\varepsilon = \frac{\left(\frac{\dot{x}}{\varrho_G}\right)}{\left[C(\dot{x}\varrho_G + (1-\dot{x})\varrho_L + \frac{w'}{\dot{m}'}\right]}. \tag{18}$$

Von Bedeutung sind noch die Berechnungsgleichungen für das Flüssigkeits-Holdup von Jagota, u. a. [15] und Ledinegg [16]. Jagota, u. a. gehen von einem physikalisch begründeten Ansatz aus im Gegensatz zu den anderen empirischen bzw. halbempirischen Modellen. Gemäß *Gl.* (2) wird das Querschnittsverhältnis angesetzt

$$(1-\varepsilon) = \frac{A_L}{A_K} = \frac{\dot{V}_L\left(\frac{z}{w_T} + \frac{1-z}{\overline{w}_F}\right)}{A_K}. \tag{19}$$

Voraussetzung für die Anwendung dieser Gleichung ist die Kenntnis von Tropfenstromanteil z, mittlerer Tropfengeschwindigkeit w_T und mittlerer Filmgeschwindigkeit w_F. Für die durchgeführte Vergleichsrechnung wurden diese Werte aus (4) entnommen. Ledinegg [16] gibt ein Modell an, welches sich unter der Bedingung großer Massenstromdichten $\dot{m} \geq 100 \frac{\text{kgs}}{\text{m}^2\text{s}}$ und bei konstantem Druck vereinfacht wie folgt darstellt,

$$C = \frac{1}{1 + \frac{K+1}{K}\sqrt{\frac{d_S \cdot \beta}{d_R \cdot \beta^*}}}; \quad K = \sqrt{\frac{\varrho_G}{\varrho_L}}, \tag{20}$$

$$(1-\varepsilon)=\frac{1-\dot{x}}{\dot{x}\left(\frac{C\varrho_L}{\varrho_G}-1\right)+1}, \tag{21}$$

wobei es gerechtfertigt ist bei dem vorliegenden relativ großen Kanalquerschnitt infolge $d_S \approx d_R$ und $\beta \approx \beta^*$ den entsprechenden Wurzelausdruck in Gl. (20) gleich Eins zu setzen.

Für die gezeigten Modelle wurden Parameterkombinationen ausgewählt, die den Arbeitsbereich der untersuchten Hochgeschwindigkeitsabsorptionsstufe [4] etwa überdecken, um einen Vergleich der Modelle durchzuführen (Gasgeschwindigkeiten w_G von 14 $\frac{m}{s}$, 18 $\frac{m}{s}$, 22 $\frac{m}{s}$ bei Flüssigkeitsdurchsätzen $\dot{V}_L$ von 1,0 m³/h und 2,0 m³/h). Das Resultat ist über dem Gasmassenstromanteil in Bild 1 aufgetragen. Dabei zeigt sich ebenso wie in [4] und [13], daß das Modell von HUGHMARK [12] bei großen Gas-Holdup-Werten und damit kleinen Flüssigkeits-Holdup starke Ungenauigkeiten aufweist. Natürlich ist es auch, daß die Berechnungsergebnisse für die horizontale Zweiphasenströmung am niedrigsten liegen, da kein Schwerkrafteinfluß vorliegt. Die Holdup-Ergebnisse für die vertikale Zweiphasenströmung der übrigen Autoren liegen im Bereich der ausgeprägten Ring-Tropfen-Strömung verhältnismäßig eng beieinander. Die vom Autor ermittelten Gleichgewichts-Holdup-Werte $(1-\varepsilon)^*$ (vgl. *Bild 4*) ordnen sich in diesem Bereich ebenfalls gut ein. Mit sinkendem Gasmassenstromanteil wird die Strömungsform instabil und schwallartig, d. h. von Rezirkulationen in der Flüssigphase überlagert [4]. Der aufwärtsgerichtete Gleichstrom verhält sich Belastungsveränderungen gegenüber bedeutend empfindliche, als der abwärtsgerichtete Gleichstrom. Der Verlauf der Meßpuntke (x) in *Bild 1* zeigt dies deutlich. Außerdem beschreiben die Berechnungsmodelle das Flüssigkeits-Holdup bei schwallartiger Ring-Tropfen-Strömung in der Nähe des Inversionspunktes nicht exakt, da zwar dei Belastungsverhältnisse eingehen aber die Erhöhung der Flüssigkeitsbelastung durch Rezirkulation nicht er-

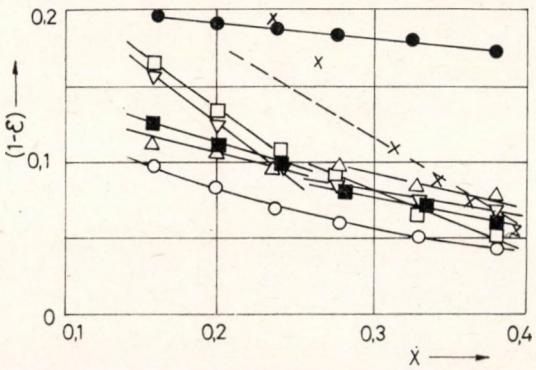

Bild 1
Modellergebnisse für das Flüssigkeits-Holdup bei konstanter Phasenverteilung im Vergleich zu Meßwerten × — Meßwerte Autor; ○, ■ — nach [7,8]; ○ — nach [12]; △ — nach [14]; ▽ — nach [15]; □ — nach [16]

faßt ist. Besonders im Bereich des Inversionspunktes (Umschlag von Gleich- in Gegenstrom) kommt es zur Ausbildung überhöhter Reibungsdruckverluste und eines überhöhten Holdup. Für die Ermittlung des Flüssigkeits-Holdup bei Gleichgewicht in der Phasenverteilung können bei $\dot{x}$-Werten oberhalb 0,3 die Modelle von LOCKHART und MARTINELLI [7], ROUHANI [14], JAGOTA, u.a. [15] und LEDINEGG [16] verwendet werden. Bei aufwärtsgerichtetem Gleichstrom sollte jedoch bei $\dot{x}$-Werten $< 0{,}3$ auf Messungen zurückgegriffen werden, da dieser Bereich der schwallartigen Ringströmung noch zu starke Abweichungen zwischen Meßwert und Modellwert aufweist.

Meßmethodik

Für die Ermittlung der Phasenverteilung über den Querschnitt (örtliches Holdup) und des daraus folgenden mittleren Holdup wurde die Pitotrohr-Methode herangezogen [17, 18].

Der Vorteil dieses Verfahrens besteht in dem geringen apparativen Aufwand und in der Möglichkeit Holdup-Profile über den Querschnitt zu erhalten. Nachteilig ist die abnehmende Meßgenauigkeit im Bereich der schwallartigen Ringströmung bzw. in der Nähe des Wandfilmes.

Das Meßprinzip ist in *Bild 2* dargestellt. Es wurde bei sieben verschiedenen Kanallängen das Flüssigkeits-Holdup bestimmt. Bei einer Kanalbreite (quad-

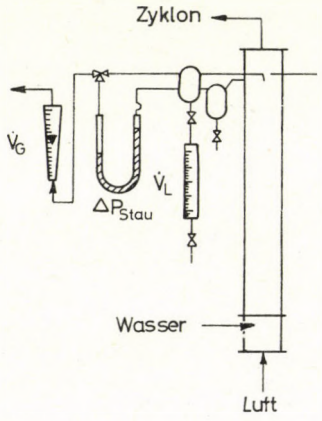

Bild 2
Meßprinzip zum Pitotrohr-Verfahren

ratischer Querschnitt) von 72 mm ergaben sich die l/d-Verhältnisse* 1,73; 2,9; 4,3; 6,2; 8,3; 10,5; 12,6. Die verwendete Sonde hatte einen Innendurchmesser von 3 mm. Kleiner sollte dieser Durchmesser nicht gewählt werden, da sonst das Meßergebnis von Kapillarkräften beeinflußt wird. Der Flüssigkeitsvolumenstrom wurde bei $\dot{V}_L = 1{,}0$ m³/h konstant gehalten und die Gas-

* Da diese Untersuchungen Teil eines umfangreicheren Versuchsprogrammes auch mit veränderten Kanalbreiten sind, wurde das l/d-Verhältnis eingeführt, obwohl bei dieser Betrachtung die Kanalbreite konstant bleibt.

geschwingidkeit zwischen 14 $\frac{m}{s}$ und 24 $\frac{m}{s}$ variiert. Somit ergaben sich F/G-Verhältnisse (Flüssigkeits-Gas-Massenstromverhältnisse) zwischen 1,8 und 3,2. Naturgemäß sind bei diesem Meßverfahren dei Meßfehler bei der Staudruckmessung am größten. Sie lagen je nach Meßort (Rand oder Kernströmung) zwischen 8% und 35%. Bei der Messung der Gas- bzw. Flüssigkeitsvolumenströme liegen die Meßfehler niedriger im Bereich zwischen 5% und 20%. Weitere Angaben zum Meßverfahren sind in der oben angegebenen Literatur sowie bei BANERJEE [19] zu finden.

Meßergebrisse

Die Gesamtheit der Meßergebnisse ist in *Bild 3* gezeigt. In diesem *Bild* sind die Holdup-Profile für die Reihenfolge der l/d-Verhältnisse mit der Gasgeschwindigkeit als Parameter aufgetragen. Dabei gilt sowohl für *Bild 3* wie auch für

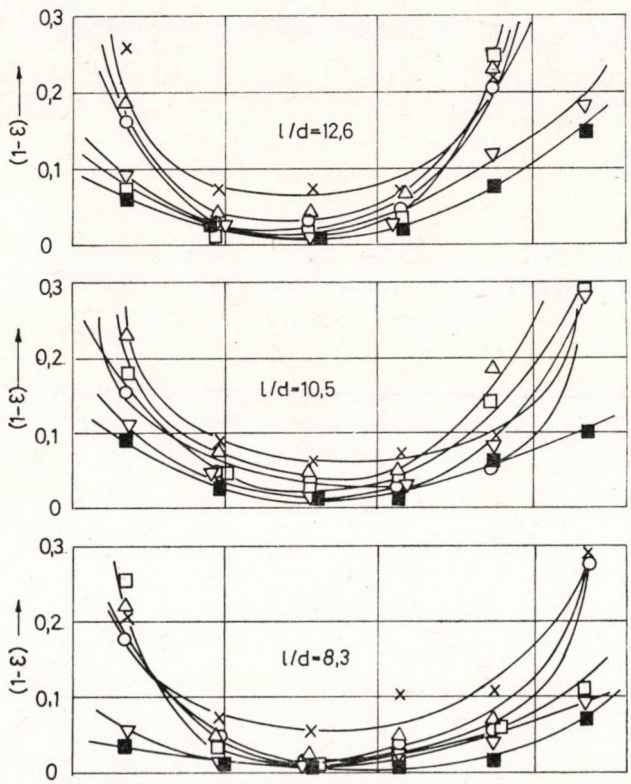

Bild 3
Holdup-Profile über den Kanalquerschnitt mit der Gasgeschwindigkeit und derKanallänge als Parameter
w_G Werte: × — 14 m/sec; △ — 16 m/sec; ○ — 18 m/sec: □ — 20 m/sec; ▽ — 22 m/sec; ■ — 24 m/sec.

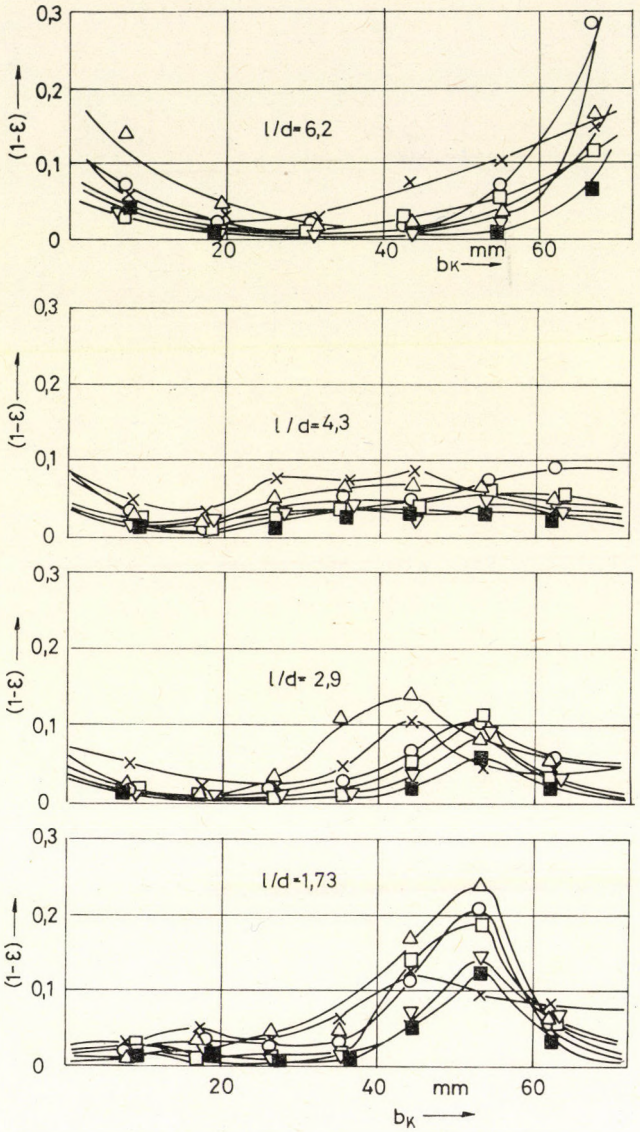

Bild 3. (Fortsetzung)

Bild 4 folgende Symbolik für die Geschwindigkeitsabstufung: x 14 m/s; △ 16 m/s; ○ 18 m/s; □ 20 m/s; ▽ 22 m/s; ■ 24 m/s. In *Bild 3* erkennt man im Kerngebiet der Strömung ein Maximum der Holdup-Werte, welches auf einen durch den Einfluß der Versprüheinrichtung erzeugten hohen Flüssigkeitsanteil zurückzuführen ist. Die erhaltene Asymetrie ist eine Spezifik der Versprüheinrichtung [4] und im Zusammenhang mit dieser Betrachtung von untergeordnetem Interesse. Mit steigendem l/d-Verhältnis wird das Maximum der

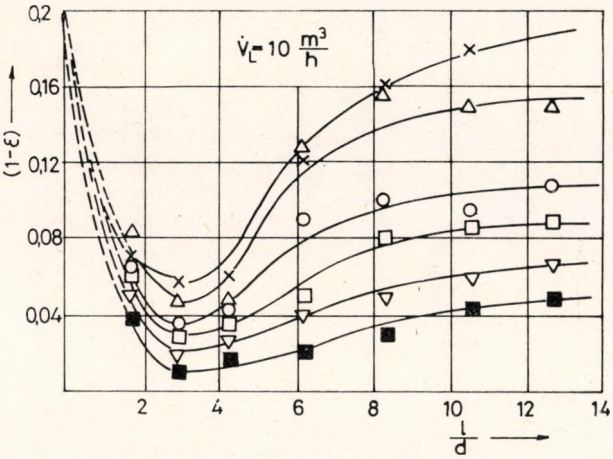

Bild 4
Holdup-Längeprofile mit der Gasgeschwindigkeit als Parameter
w_G Werte: × — 14 m/sec; △ — 16 m/sec; ○ — 18 m/sec;
□ — 20 m/sec; ▽ — 22 m/sec; ■ — 24 m/sec.

Holdup-Profile abgebaut unter gleichzeitiger Zunahme der Randgängigkeit, d. h. Ausbildung eines Wandfilmes unter Tropfenaufnahme.

Bei sehr großen Kanallängen in der Nähe des Gleichgewichtes in der Phasenverteilung erhält man in Randnähe sehr große Holdup-Werte die bei niedrigen Gasgeschwindigkeiten $>0{,}2$ sind und hauptsächlich auf Flüssigkeitsrezirkulation zurückzuführen sind. Für die weitere Bearbeitung sind die mittleren Holdup-Werte im Querschnitt erforderlich. Ein Vergleich zwischen einer integralen Mittelwertbildung unter Verwendung von Polynomanpassungen für die Profile nach Gl. (22)

$$(1-\varepsilon)=\frac{1}{b_K}\int_0^{b_K}(1-\varepsilon)\,(b_K)db_K \tag{22}$$

und einer arithmetischen Mittelwertbildung ergab nur Unterschiede von maximal 5% bezogen auf den Holdup-Wert.

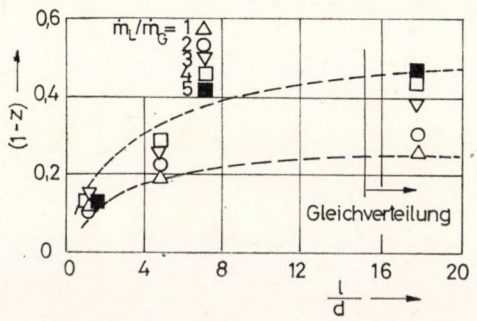

Bild 5
Abhängigkeit des Filmvolumenstromanteiles vom l/d — Verhältnis

Die erhaltenen Holdup-Werte (Holdup-Längenprofile) sind wiederum mit der Gasgeschwindigkeit als Parameter über dem l/d-Verhältnis aufgetragen *(Bild 4)*. Es zeigt sich, daß das Flüssigkeits-Holdup mit zunehmendem l/d-Verhältnis einem Grenzwert zustrebt, der etwa bei $l/d \approx 15$ erreicht ist. Der Beginn von konstantem Flüssigkeits-Holdup sowie des Gleichgewichtes in der Phasenverteilung wird durch Messungen des Filmvolumentsromanteiles $(1-z)$ (4) ebenfalls bei $l/d \approx 15$ bestätigt, wie *Bild 5* zeigt. Die Holdup-Längenprofile werden im Folgenden ausführlicher diskutiert und modelliert.

Modellierung

Die erhaltenen Ergebnisse in *Bild 4* weisen neben dem Anstreben eines Gleichgewichtswertes des Flüssigkeits-Holdup $(1-\varepsilon)^*$ auch auf ein je nach Belastungsverhältnissen mehr oder minder ausgeprägtes Minimum hin. Diese eigenartige Tatsache ist das Resultat zweier gleichzeitig auftretender physikalischer Vorgänge. Die Flüssigkeitseinführung erfolgt in allgemeinen über eine Vorrichtung, die einen konstanten Querschnitt besitzt. Setzt man voraus, daß dieser Querschnitt von der zuzuführenden Flüssigkeit vollständig ausgefüllt wird, so ergibt sich die Austrittsgeschwindigkeit entsprechend dem Flüssigkeitsdurchsatz und den hydrodynamischen Bedingungen. Somit erhält man den Anfangswert des Holdup $(1-\varepsilon)_0$ belastungsunabhängig als Verhältnis von Zuführungsquerschnitt bzw. Summe der Zuführungsquerschnitte und Kanalquerschnitt.

Schubspannungen zwischen Gas- und Flüssigphase führen zu einer Zerstäubung der Flüssigkeit, wobei sich der charakteristische Tropfendurchmesser des erzeugten Spektrums nach NUKIJAMA und TANASWA (20) berechnen läßt

$$\bar{d}_{T0} = 0{,}585 \sqrt{\frac{\sigma}{\varrho_L \cdot w_r^2}} + 53{,}2 \left(\frac{\dot{V}_L}{\dot{V}_G}\right)^{1{,}5} \cdot \left(\frac{\eta_L}{\sqrt{\varrho_L \cdot \sigma}}\right)^{0{,}45}. \tag{23}$$

Die parallel ablaufenden Vorgänge sind die Tropfenbeschleunigung und die überlagerte Tropfenkoaleszenz. Die Tropfenbeschleunigung führt zu einer sehr starken Holdup-Abnahme schon nach kurzer Kanallänge (1). Die Koaleszenz, die eine Folge des Tropfen- bzw. Geschwindigkeitsspektrums ist, bewirkt dagegen eine Tropfenvergrößerung mit gleichzeitiger Reduzierung der Beschleu-

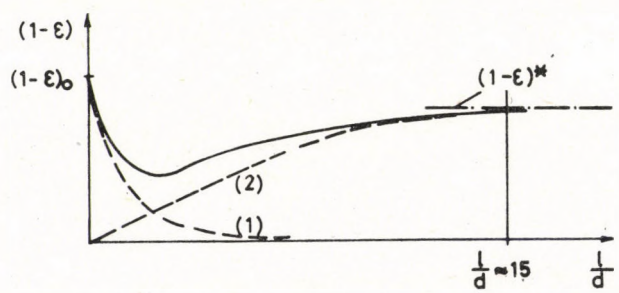

Bild 6
Modellvorstellung zum Holdup-Längeprofil

nigung und der Tropfengeschwindigkeit. Dies hat eine Holdup-Zunahme (2) zur Folge. Qualitativ sind beide Vorgänge in *Bild 6* dargestellt. Durch Superposition beider Prozesse ergibt sich zwischen dem Holdup-Anfangswert und dem Gleichgewichtswert ein Minimum. Die Meßergebnisse des *Bildes 4* zeigen, daß die Holdup-Schwankung sehr erheblich ist.

Koaleszenzeinfluß

Betrachtet man den ansteigenden Teil der Kurven in *Bild 4*, so lassen sich zunächst Schlußfolgerungen bezüglich des Tropfendurchmessers treffen. Geht man davon aus, daß die Holdup-Zunahme gleichermaßen im Wandfilm wie im Tropfenkern stattfindet, so läßt sich schreiben

$$A_{\mathrm{L}} \sim \left(\frac{l}{d}\right) \quad \text{bzw.} \quad A_{\mathrm{LT}} \sim \left(\frac{l}{d}\right). \tag{24}$$

Unter der Annahme, daß die Tropfenanzahl im Kanalquerschnitt konstant bleibt, führt die Verringerung der Tropfengeschwindigkeit [4] zwangsläufig zur Tropfenvergrößerung (Koaleszenz). Für *Gl.* (24) kann man schreiben

$$N \cdot d_{\mathrm{T}}^3 \approx N \cdot d_{\mathrm{T0}}^3 \cdot \left(\frac{l}{d}\right) \tag{25}$$

mit N als Tropfenanzahl.

Wie die Analyse der Tropfenbewegung und Phasenverteilung im Kanalquerschnitt in [4] zeigt, ist es gerechtfertigt, nicht nur von einer konstanten Tropfenanzahl im Querschnitt, sondern sogar von einer Verringerung zu sprechen. Damit ergibt sich die Ungleichung

$$d_{\mathrm{T}} \geq d_{\mathrm{T0}} \cdot \sqrt[3]{\frac{l}{d}} \quad \text{für} \quad \begin{matrix} (l/d) < 15 \\ N \leq N_0 \end{matrix}. \tag{26}$$

Die Konstanz des Holdup bei $l/d < 15$ bzw. das Gleichgewicht in der Phasenverteilung wird durch ein Gleichgewicht zwischen Koaleszenz und Tropfenzerfall sowie zwischen Tropfenaufnahme in den Wandfilm und Tropfenabgabe bewirkt.

Eine Abschätzung der Widerstandsbeiwerte für die Tropfenbewegung wird möglich unter Verwendung der kritischen Weberzahl, der aus Meßwerten ermittelten Relativgeschwindigkeiten [4] und *Gl.* (26)

Nach der Gleichung

$$\zeta = \frac{\zeta \cdot \sigma}{d_{\mathrm{T0}} \cdot \sqrt[3]{\left(\frac{l}{d}\right)_{\max}} \cdot \varrho_{\mathrm{G}} \cdot w_{\mathrm{r}}^2} \tag{27}$$

ergeben sich ζ-Werte $\leq 1{,}5$, d. h. der Prozeßverlauf liegt im Übergangsbereich bzw. nahe dem Newton'schen Bereich. Die Gleichung (27) ist für die Berechnung des Beschleunigungsvorganges von Bedeutung.

Für den Holdup-Verlauf infolge Koaleszenz, kurz Koaleszenzanteil* genannt, wurde in [4] aus einer phänomenalogischen Überlegung ein Ansatz gebildet, der keine empirische Korrektur erforderte und das Holdup auch unter den Verhältnissen einer Drallströmung relativ genau wiedergibt ($\pm 20\%$).

Die Gleichung lautet

$$(1-\varepsilon) = 1 - \exp\left(-\frac{l}{d}\cdot\frac{F}{G}\cdot\frac{2}{Fr}\right), \qquad \frac{l}{d} < 12. \tag{28}$$

Der Nachteil dieses Ansatzes besteht in der begrenzten Gültigkeit nur für den Koaleszenzanteil. Er beschreibt auch nicht den Übergang zum Holdup-Grenzwert.

Die *Gl.* (28) kann allgemeingültiger formuliert werden, wobei der Holdup-Grenzwert und eine empirische Korrektur des Einflusses des l/d-Verhältnisses erforderlich ist. Man erhält dann die Form

$$(1-\varepsilon_K) = (1-\varepsilon)^* \left(1 - \exp\left(-\left(\frac{l}{d}\right)^{1,3}\cdot\frac{F}{G}\cdot\frac{2}{Fr(1-\varepsilon)^*}\right)\right) \tag{29}$$

Gl. (29) enthält die wesentlichen Einflußgrößen in physikalisch sinnvoller Weise. Die Fr-Zahl wird dabei mit der Gasgeschwindigkeit gebildet. Auf die Ermittlung des Holdup-Grenzwertes wurde unter Punkt 2 eingegangen.

Beschleunigungseinfluß

Bei der Behandlung des Beschleunigungsprozesses muß zunächst auf den Modellcharakter hingewiesen werden. Die Komplexität der beim Tropfenflug auftretenden Wechselwirkungen kann durch eine Bewegungsgleichung nicht vollständig erfaßt werden, zumal eine relative hohe Tropfenkonzentration vorliegt.

Eine wesentliche Annahme besteht darin, daß für die Berechnung Einzeltropfen angenommen werden, deren Durchmesser dem mittleren Tropfendruchmesser des Tropfenspektrums entsprechen. Überschlagsrechnungen haben weiterhin gezeigt, daß die Änderung der Relativgeschwindigkeit mit der Kanallänge etwa durch die Änderung des Tropfendurchmessers nach *Gl.* (26) kompensiert wird, sodaß die Re-Zahl annähernd konstant bleibt. Damit kann von einem näherungsweise konstanten Widerstandsbeiwert ausgegangen werden.

Der Ansatz für die Berechnung der Tropfenbeschleunigung lautet dann

$$m_T \frac{dw_T}{dt} = \frac{\pi}{8}\cdot\varrho_G\cdot d_T^2\zeta\cdot(w_G - w_T)^2 + m_T\cdot g. \tag{30}$$

Da eine eindimensionale Aufwärtsbewegung betrachtet wird, ist eine spezielle Indizierung nicht erforderlich.

Mit der Vereinfachung

$$C = \frac{A_T}{m_T} = \frac{3\cdot\varrho_G}{4\cdot\varrho_L\cdot d_T} \tag{31}$$

* Die Aufteilung des „Gesamt-Holdup" in einen „Beschleunigungsanteil" und „Koaleszenzanteil" trägt fiktiven Charakter zum Zwecke der Modellierung.

läßt sich *Gl.* (30) umformen zu

$$\frac{dw_T}{(w_G - w_T)^2 + \frac{g}{C \cdot \zeta}} = C \cdot \zeta \cdot dt \tag{32}$$

wobei eine geschlossene Lösung dieser Differentialgleichung möglich ist, die zu *Gl.* (33) führt

$$w_T = w_G - \sqrt{\frac{g}{C \cdot \zeta}} \cdot \tan\left[\arctan\left(\frac{C \cdot \zeta}{g} \cdot w_G\right) - \sqrt{C \cdot \zeta \cdot g} \cdot t\right]. \tag{33}$$

Gl. (33) gilt für das Geschwindigkeitsverhältnis $w_G/w_T > 1$. Der Nachteil der Lösung besteht darin, daß es in der Nähe des stationären Zustandes, also bei

$$\frac{dw_T}{dt} \to 0 \quad \text{bzw. } w_T \to (w_G - w_S) w_S \ldots \text{Sinkgeschwindigkeit},$$

zu einer Inversion des Geschwindigkeitsverhältnisses kommt, was auf die tan-Operation zurückzuführen ist (vgl. WATZEL [21]). Da der Bereich großer Flugzeiten ($t > 0{,}1$ s) nicht von Interesse ist, kann dieser Nachteil unberücksichtigt bleiben.

Durch eine abschnittsweise Berechnung [4] kann zur Tropfengeschwindigkeit die entsprechende Kanallänge, ausgedrückt im l/d-Verhältnis, bestimmt werden.

Somit kann die Holdup-Änderung durch Beschleunigung nach

$$(1 - \varepsilon_B) = \frac{\dot{V}_L}{w_T \cdot A_K} \tag{34}$$

berechnet werden. Dabei beinhaltet *Gl.* (34), daß der gesamte Flüssigkeitsvolumenstrom in Tropfen dispergiert vorliegt. Der Wandfilm übt bei $l/d < 2$ nur einen unwesentlichen Einfluß auf das Holdup aus. Seine Zunahme mit der Kanallänge wird durch den Koaleszenzanteil miterfaßt.

Dieser Lösungsweg ist jedoch sehr aufwendig und von zahlreichen vereinfachenden Annahmen gekennzeichnet. Aus diesem Grund soll eine direkte Abhängigkeit des Holdup-Beschleunigungsanteils $(1-\varepsilon)_B$ vom l/d-Verhältnis vorgeschlagen werden.

Zweckmäßig erscheint ein Exponentialansatz, analog zur Berechnung des Koaleszenzanteils, einzuführen. Der Verlauf des Beschleunigungsanteils (1) in *Bild 6* läßt folgende Beschreibung zu

$$\frac{d(1-\varepsilon)_B}{d\left(\frac{l}{d}\right)} = -k \cdot (1-\varepsilon)_B, \tag{35}$$

woraus sofort folgt

$$(1-\varepsilon)_B = (1-\varepsilon)_0 \cdot \exp\left(-k \cdot \left(\frac{l}{d}\right)\right). \tag{36}$$

Die Größe k wurde empirisch aus den Holdup-Meßergebnissen unter Abzug des Koaleszenzanteiles bestimmt. Entsprechend den Abhängigkeiten

$$(1-\varepsilon) \sim \frac{1}{\dot{m}_G} \quad \text{und} \quad (1-\varepsilon) \sim \dot{m}_L \tag{37}$$

konnte der Koeffizient k mit dem Flüssigkeits-Gas-Massenstromverhältnis, welches die Belastungsveränderung der beiden Phasen ausdrückt, korreliert werden

$$k = 2{,}19 \left(\frac{F}{G}\right)^{-0{,}87}. \tag{38}$$

Es ergibt sich somit als Resultat für den Beschleunigungsanteil der Ausdruck

$$(1-\varepsilon)_B = (1-\varepsilon)_0 \cdot \exp\left(-2{,}19 \left(\frac{F}{G}\right)^{-0{,}87} \left(\frac{l}{d}\right)\right). \tag{39}$$

Der Anfangswert $(1-\varepsilon)_0$ ist, wie oben erwähnt, konstruktionsbedingt.

Ein Vergleich der Berechnungsmodelle für den Beschleunigungsanteil des Holdup nach *Gl.* (34) und *Gl.* (39) ist in *Bild 7* dargestellt. Die den Bereich der

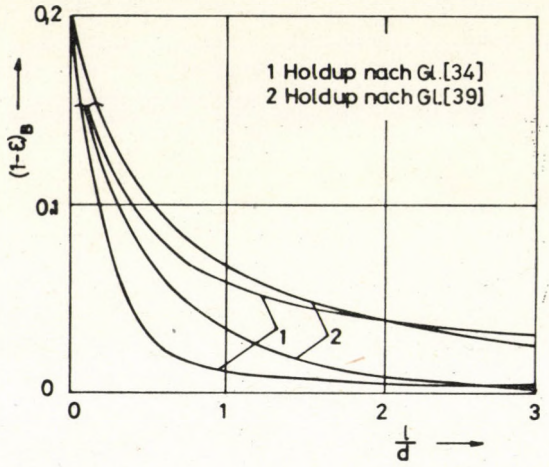

Bild 7
Holdup-Verlauf in der Beschleunigungsphase

Ergebnismenge eingrenzenden Kurven (1) zeigen einen stärkeren Holdup-Abfall bei kleinen Kanallängen ($l/d < 1$) als der Bereich (2), der auf der Auswertung der Meßergebnisse basiert. Hier zeigt sich deutlich die Auswirkung der idealisierenden Bedingungen unter denen *Gl.* (33) nur angewendet werden kann (Einzeltropfen, konstanter Widerstandsbeiwert, Vernachlässigung von Wechselwirkungen zwischen den Tropfen und den Phasen). Real liegt jedoch eine geringere Anfangsbeschleunigung der Tropfenphase vor. Erst im Bereich $l/d > 1{,}5$ beginnt eine gute Übereinstimmung beider Berechnungsansätze.

Insgesamt bewertet, zeigt sich zwischen beiden Ansätzen eine tendenziell gute Übereinstimmung, wobei der auf den Meßwerten basierende Ansatz nach *Gl.* (39) eine größere Adäquatheit bezüglich des Realverhaltens aufweist.

Holdup-Modell

Nachdem die Anteile am Gesamt-Holdup diskutiert werden und in den *Gl.* (29) und (39) mathematisch formuliert sind, kann ein Gesamtmodell durch Superposition bzw. Addition der Anteile gemäß

$$(1-\varepsilon)=(1-\varepsilon)_{\mathrm{B}}+(1-\varepsilon)_{\mathrm{K}} \tag{40}$$

gebildet werden.

Explizit erhält man die Form

$$(1-\varepsilon)=(1-\varepsilon)_0 \exp\left(-2{,}19\left(\frac{F}{G}\right)^{-0{,}87}\left(\frac{l}{d}\right)\right)+(1-\varepsilon)^*\left(1-\exp\left(-\left(\frac{l}{d}\right)^{1{,}3}\left(\frac{F}{G}\right)\frac{2}{Fr(1-\varepsilon)^*}\right)\right). \tag{41}$$

Die wesentlichen Einflußgrößen auf das Holdup, nämlich Gasgeschwindigkeit, Flüssigkeitsbelastung und Kanallänge, sind in den *Gl.* (29), (39) und (41) in dimensionsloser Form enthalten. Ebenso ist das Dichteverhältnis beider Phasen als stoffspezifische Größe mit im F/G-Verhältnis erfaßt. Bezüglich des Viskositätsinflusses können noch keine quantitativen Aussagen getroffen werden. Die Verwendung des l/d-Verhältnisses ist zweckmäßig im Hinblick auf den Übergang zu veränderten Kanalquerschnitten, da sich mit dem Rohrdurchmesser bzw. der Kanalbreite auch die Kanallänge für die Erreichung des Gleichgewichtes in der Phasenverteilung ändert. Dabei muß bezüglich der Anwendung von *Gl.* (41) auf die Notwendigkeit eines Mindestrohrdurchmessers bzw. einer Mindestkanalbreite bei eckigen Querschnitten hingewiesen werden, der etwa mit $d_{\min}=30$ mm angegeben wird. Dies ist erforderlich, da eine Unterschreitung des Minimalwertes Strömungsformen des Zweiphasengemisches erzeugt, die starke Wechselwirkungen zwischen Tropfen und Film hervorrufen, die nicht mehr den Voraussetzungen für das Holdup-Modell entsprechen [22]. Beispielsweise existiert bei kleinen Kanalquerschnitten schon unmittelbar hinter der Flüssigkeitseinführung ein starker, schwallartiger Wandfilm, der die Ausbildung eines Holdup-Minimums verhindert. Ein Vergleich der *Bilder 4* und *7* hinsichtlich des Einflusses der Gasgeschwindigkeit zeigt, daß der Koaleszenzanteil bedeutend stärker von Änderungen der Gasgeschwindigkeit abhängt als der Beschleunigungsanteil. Aus diesem Grund geht die Gasgeschwindigkeit im Koaleszenzanteil nicht nur im F/G-Verhältnis ein, sondern zusätzlich durch die Fr-Zahl.

Die Ergebnisse einer Nachrechnung der Meßwerte von *Bild 4* sind in *Bild 8* enthalten. Die Adäquatheit des Modells, die sich in den Fehlergrenzen $+10\%$ bzw. -20% ausdrückt, ist positiv zu bewerten. Die etwas größere negative Fehlergrenze ist durch das asymptotische Annähern des Modells an den Grenzwert $(1-\varepsilon)^*$ begründet, während dieser in einigen Fällen durch die Meßwerte schon bei $l/d=8\ldots12$ erreicht ist.

Der Gültigkeitsbereich für das Holdup-Modell umfaßt das Gebiet der stabilen, aufwärtsgerichteten Zweiphesan-Ring-Tropfen-Strömung, wobei die genannten Einschränkungen bezüglich der Viskositätsverhältnisse und der Kanalabmessung zu berücksichtigen sind.

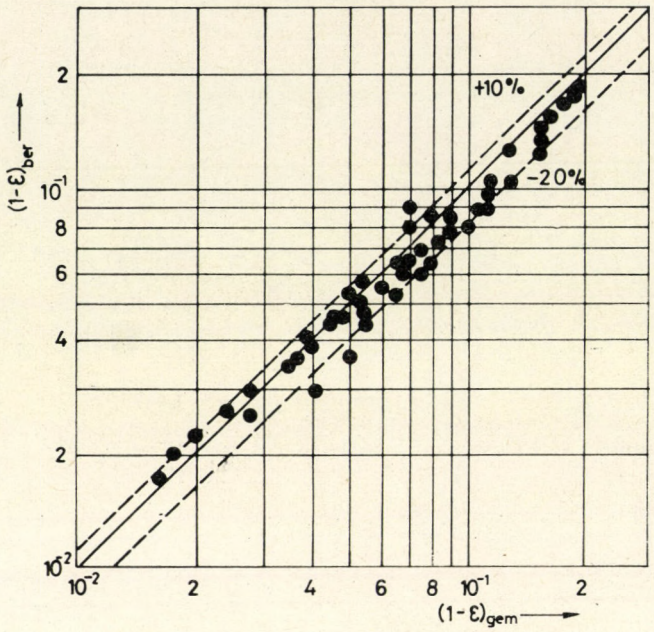

Bild 8
Zusammenhang zwischen gemessenen und berechneten Holdup-Werten

NOMENKLATUR

A	Querschnitt, Fläche	m^2
b_K	Kanalbreite	m
d	Rohrdurchmesser bzw. gleichwertiger Durchmesser	m
$\frac{F}{G}=\frac{\dot{m}_L}{\dot{m}_G}$	Flüssigkeits-Gas-Massenstromverhältnis	$kg \cdot kg^{-1}$
Fr	Froude-Zahl	
g	Erdbeschleunigung	$m\ s^{-2}$
ΔH	Höhendifferenz	m
l	Kanallänge, Rohrlänge	m
$\dot{m}$	Massenstrom	$kg\ s^{-1}$
$\dot{m}$	Massenstromdichte	$kg\ m^{-2}\ s^{-1}$
Δp_{stat}	statische Druchkdifferenz	Pa
Re	Reynolds-Zahl	
$\bar{t}$	mittlere Verweilzeit	s
V	Volumen	m^3
$\dot{V}$	Volumenstrom	$m^3\ s^{-1}$
w	Geschwindigkeit	$m\ s^{-1}$
$\dot{x}$	Gasmassenstromanteil	
z	Tropfenstromanteil	
$(1-\varepsilon)$, ε	Flüssigkeits-Holdup, Gas-Holdup	
ζ	Widerstandsbeiwert	
η	Viskosität	$kg\ m^{-1}\ s^{-1}$

ϱ	Dichte	kg m^{-3}
σ	Oberflächenspannung	N m^{-1}

Indices

A	Austausch
B	Beschleunigung
F	Film
G	Gas
K	Koaleszenz
K	Kanal, Kontaktzone
L	Flüssigkeit
T	Tropfen
r	relativ
°	Anfangswert
*	Gleichgewicht

1. Langner, H. und Mayinger, F.: Chemie-Ing.-Techn., *1978*, 50 (7) 554
2. Huhn, J.: Dissertation A, TU Dresden, 1971.
3. Zahn, A.: Dissertation A, AdW der DDR, ZIPC, 1978.
4. Reitz, M.: Dissertation A, IHS Köthen, 1980.
5. Grundke, E., Schneider, J. und Nett, J.: Chem. Techn., in Vorbereitung
6. Heckle, M.: Chemie-Ing.-Techn., *1970*, 42 (5) 304–310.
7. Lockhart, R. W. and Martinelli, R. C.: Chem. Engng. Progr. *1949*, 45 (1) 39–48.
8. Davis, W. J.: Brit. Chem. Engng. *1963*, 8 (7) 462–465.
9. Sarma, P. V. S. C., Sarma, P. K. and Voukata Apparao, K.: Indian. J. Technol *1973*, 11 (5) 199–201.
10. Wallis, G. B.: One-dimensional two-phase flow, New York, Mc Graw Hill, 196
11. Chawla, J. M.: Chemie-Ing.-Techn., *1969*, 41, 328–330.
12. Hughmark, G. A.: Chem. Eng. Progr. *1962*, 58 (4) 62–65.
13. Friedel, L.: Chemie-Ing.-Techn. *1978*, 50 (3) 167–180.
14. Rouhani, Z.: AE-RTV-841, 1969
15. Jagota, A. K., Rhodes, E. and Scott, D. S.: Canad. J. Chem. Engng. *1973*, 51, 393–399.
16. Ledinegg: Brennstoff-Värme-Kraft, *1978*, 30 (10) 400–406.
17. Cravarolo, L. and Massid, A.: CISE-Report, Nr. 98, Milano, 1963.
18. Barthels, H.: Chemie-Ing.-Techn., *1968*, 40, 530–537.
19. Banerjee, S. and Nguyen, D. M.: AIChE J. *1977*, 23 (3) 385–387.
20. Nukijama, S. U. and Tanasawa, Y.: Trans. Soc. Mech. Eng. Japan, *1938*, 5, 63.
21. Watzel, G. V. P.: VDI-Forschungsheft 541, Düsseldorf, 1970, S. 13.
22. Siegel, R. and Kruschke, D.: Diplomarbeit, IHS Köthen, 1978

SUMMARY

With the help of the Pitot tube measuring method liquid holdup profiles were found out in a quadratic channel length of side 72 mm — in the upwards directed two-phase continuous current. Through the holdup values found out with the help of the cross section holdup profiles of the length of channel showing a minimum at about $l/d \approx 3$ and reaching an equilibrium or limiting value at $l/d \approx 15$ could be made out. This state is analysed and modelled. For this a fictive division of the total holdup into a velocity part and a coagulation part is necessary. The obtained general model represents a superposition of the subprocesses. It describes the measured values adequately, i.e. with an error zone of +10% and −20%.

РЕЗЮМЕ

С помощью способа измерения трубки Пито в квадратном канале с боковой длиной 72 мм в наверх направленном двухфазном прямом течении были установлены профили боли объема жидкости. Средними по поперечному сечению значениями боли объема жидкости смогло было установить профили боли объема жидкости над длиной канала, показывающие минимум при примерно $l/d \approx 3$ и принимающие равновесное или предельное значение при $l/d \approx 15$. Этот факт анализируется и моделируется. Для этого необходимо фиктивное разделение общего боли объема жидкости на долю ускорения и коагуляции. Полученная общая модель представляет суперпозицию частичного процесса. Она описывает значения измерения адекватно, т. е. с областью ошибок $+10\%$ или -20%.

HUNGARIAN JOURNAL
OF INDUSTRIAL CHEMISTRY
VESZPRÉM
Vol. 9. pp. 73–88 (1981)

TRANSFER PROCESSES UPON PRESSURE SWING ADSORPTION. I.

L. Kotsis and J. Argyelán
(Department of Chemical Process Engineering
Veszprém University of Chemical Engineering)

Received: December 9, 1980

Transport processes taking place in gas separation processes based on pressure swing adsorption PSA have been examined experimentally. Energy transfer has been found negligible in the case of permanent gases. The unsteady state hydrodynamics of compressible fluids flowing in packed tubes has been studied. The adsorption kinetics have been determined from pressure change data using a constant volume apparatus. The authors conclude that transport rates primarily depend on the pore structure of the adsorbent particles. The basic unit of PSA operation, and gas separation achieved by pressure swing were studied. The authors conclude that the kinetic characteristics of the adsorbent and the hydrodynamic features of the adsorber have to be matched. The validity of the conclusions relating to the sub-processes are substantiated by separation measurements.

Introduction

The so-called pressure-swing adsorption (PSA) processes are used to an ever growing extent for the adsorption-based separation of the components of permanent gas mixtures. A number of patent applications have been filed disclosing various industrial applications [1–6].

A common feature of these processes is the filling of the evacuated column packed with an adsorbent by pressurized gas mixture. During the filling-up step, the adsorbent and the gases interact. In agreement with the principles of closed-space chromatography [7–9], a concentration distribution develops along the tube in both the gas and adsorbent phase. The components that are not retained by the adsorbent accumulate at the end of the column opposite to the feeding-point. When part of the gas mixture is vented from the column its composition changes with time.

In order to simplify the analysis of adsorbent-gas interaction, some authors prefer equilibrium treatment [10–12]. Others, however, point out that transport processes should [13–16] be ignored during the calculations.

This paper deals with the transfer phenomena occurring in the basic unit of PSA, i.e. in packed tubes.

Kadlec et al. [17, 18] studied the separation abilities of an adsorbent column, equipped with a flow restriction manifold at its end opposite to the feeding-

point, using periodically changing pressure. The optimum period-length with respect to product discharge was determined experimentally. An equilibrium model was used to model this short-period (3 second) process. The existence of an optimum period-length unequivocally supports the importance of the transfer processes. Thus, the experimental results presented in this paper can be generalized in this respect, and also applied for the PSA operations.

Experimental

Mass transfer processes occurring in packed tubes essentially consist of three dominant parts:

- convective filling of an evacuated column, closed at its end opposite to the filling-point, by a compressible medium
- mass transfer between the gas and the solid phase,
- local changes in the gas and solid phase.

Axial diffusion in the gas phase should also be examined since it can adversely influence the concentration profile developed in the separation process.

The same sub-processes also influence the momentum transfer. Heat transfer during separation is neglected since it is our experience that heat changes and corresponding temperature changes are negligable in the course of PSA separation of permanent gases. This is the reason why PSA is called heatless adsorption [7].

Filling-up Experiments with Inactive Packing

Hydrodynamics plays an important role in mass transfer processes. In order to achieve sufficient separation, the rates of convective component transfer and mass transfer into the solid phase have to be commensurable.

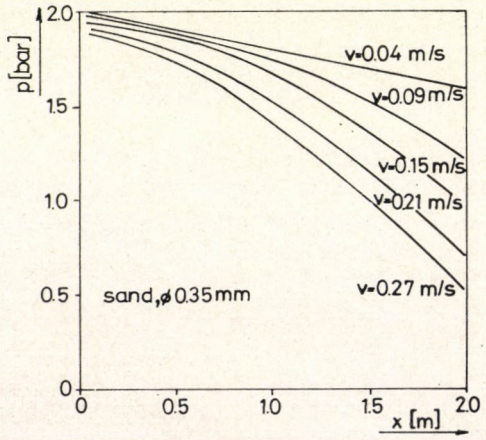

Fig. 1
Steady state pressure distributions in a tube packed with an inert packing of various gas loadings

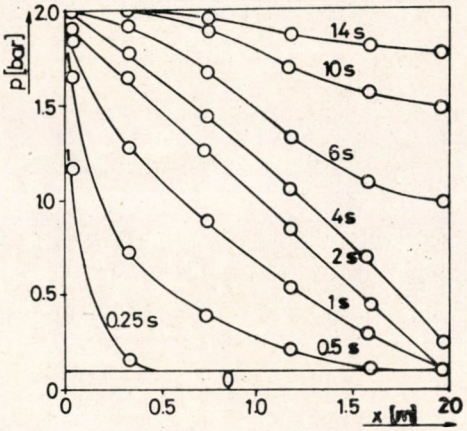

Fig. 2
Non-steady-state filling of a tube packed with an inert packing

Flow processes occurring in a 2 m long, 50 mm I.D. tube packed with sand of 0.35 mm average particle diameter were studied under steady-state and non-steady-state conditions. Filling-up was initiated by turning a 15 mm bore spherical valve connecting to a constant-pressure vessel.

The pressure profile along the column is shown *Fig. 1* at different gas (air) loadings. The major conclusion of the experiments is that contrary to assentations by MORRISON [19], the Darcy equation cannot be used for the description of momentum transfer in the flow of compressible media. Due to its expansion, the density and linear velocity slightly even the temperature of the medium change along the column. The velocities shown in Fig. 1 are considerably smaller than those observed during the filling of evacuated tubes (i.e. the sound-velocity). A nonsteady-state filling of the sand-packed column is shown in *Fig. 2*. It can be seen that the filling process is practically complete in 10 seconds. A considerable pressure drop takes place at the beginning of the filling process.

Calculations show that the gas velocity in the smallest flow cross-sections is in the range of the sound velocity during the first stage of the filling procedure. This finding is of considerable importance for the definition of the boundary conditions used for the mathematical description of the problem.

The length of the filling period is almost an order of magnitude smaller when coarser packing is used. Due to experimental problems, this time cannot be readily measured. The filling velocity is considerably smaller when the tube is packed with an active adsorbent. The time required to achieve a 90% filling is almost three times as long with 0.4 mm average particle diameter NUXIT Al than with sand. This shows, on the one hand, that a larger amount of gas is required to fill up the adsorbent system, and it requires additional time, and on the other hand, the gas components carry their momentum, i.e. sorption effects the friction coefficient in the packed bed.

The major finding of the experiments discussed so-far is that the filling time of conventional columns (1...2 m long columns packed with 1...3 mm diameter

particles) is in the range of a couple of seconds, provided the flow cross sections are sufficiently wide to transer the amount of gas required. If a restriction is used in the inlet line, the packed tube itself becomes practically free of pressure gradients [15].

When an evacuated tube packed with an adsorbent is filled up with a gas mixture, the fresh mixture flowing into the tube progressively displaces the gas phase already present in the tube. This assumption can be justified experimentally as shown in *Fig. 3*. Nitrogen, then oxygen was introduced into the above

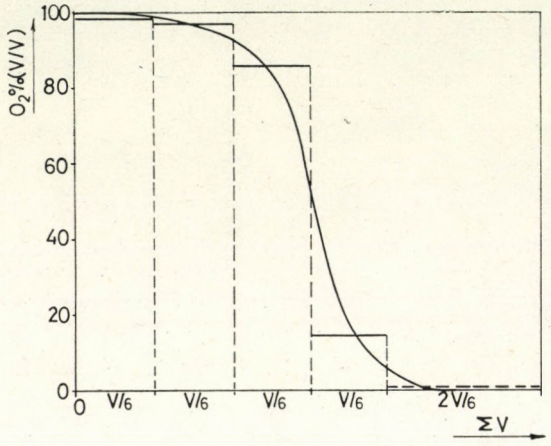

Fig. 3
Examination of the mixing processes in a tube packed with an inert packing caused by the non-steady-state filling and discharge steps

mentioned tube packed with sand until pressure p and $2p$ was achieved, respectively. When the gas volume enclosed in the tube was released in several portions, the concentration distribution shown in the *Fig. 3* was obtained. The distribution changed only slightly with the feed rate and the diameter of the packing. Therefore the longitudinal concentration distribution could not be used for the detection of the mixing effects taking place in the tube, because separation filling was always followed by gas discharge and the latter always caused mixing in the gas phase.

The mixing tests indicated that for a first approximation, flow could be considered free of mixing, though for a more accurate description turbulent diffusion characterized by a velocity-dependent diffusion coefficient might also be considered.

Characteristics of the Adsorbents

This project deals with the adsorption transfer processes connected with the components of air. Correspondingly, natural and synthetic zeolites, as well as a 5*A* molecular sieve activated charcoal was used for the experiments. Due to its specific pore structure, a Hungarian made activated charcoal NUXIT Al was also studied.

The major characteristics of the adsorbents studied are summarized in *Table 1* Their mercury porosimetry curves are shown in *Fig. 4.*

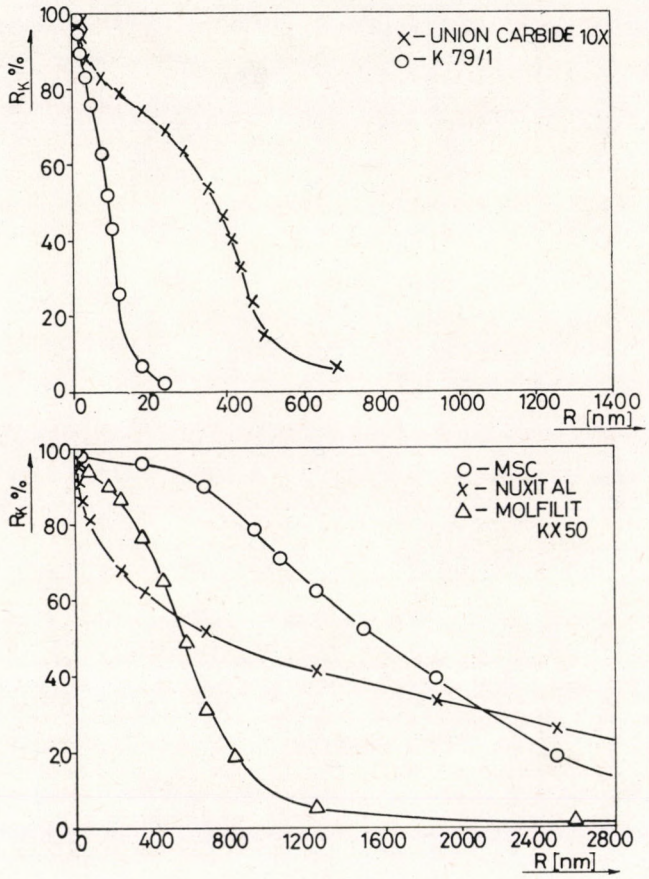

Fig. 4
Mercury porosimetric data of the adsorbents

UNION CARBIDE 10*X* is a cylindrical Type *X* synthetic zeolite of 0.8 mm diameter and 3 mm length; MOLFILIT KX50 is a Hungarian-made cylindrical Type 5*A* synthetic zeolite of 2.5 mm diameter and 8–15 mm length. The granules are composed of regular cubic zeolite crystallites of 3–6 μm size. *K* 79/1 is a natural rhiolite tuff mined at Tokaj, Hungary, which contains 40% clinoptilolite. It is ground to an average particle size of 1–3 mm [20]. The size of the clinoptilolite crystallites in this tuff is 0.1 μm, the diameter of the pores separating the crystallites is also about 0.1 μm, so the tuff is a hard-to-permeate, solid structure not readily suited for adsorption purposes.

The Type 5*A* molecular sieve activated charcoal was developed by KADLEC [21] of the HEYROWSKY Institute, Prague, Czechoslovakia. The micropores in

Table 1

The major characteristics of the adsorbents tested

Adsorbent	Density [g/cm³]	Specific surface area (by BETO-GRAF) [m²/g]	Porosity up to 7.5 nm [cm³/g]	Specific surface area of pores above 7.5 nm [m²/g]	Packing density in the column [kg/m³]	Void volume fraction [m³/m³]	Separation factor for O_2-N_2 at 3 bars [—]	Active ingredient
UNION CARBIDE 10X	2.586	148.9	0.4102	8.956	615	0.510	1.603	90% (m/m) x zeolit
MOLFILIT KX 50	2.457	20.0	0.3629	3.428	670	0.484	1.692	80% (m/m) A zeolit
K 79/1	2.440	41.2	0.1889	19.412	899	0.514	1.394	40% (m/m) clinoptilolit
MSC	1.878	820*	0.3764	1.17	612	0.326	0.337	—
NUXIT A1	2.406	1047.0	0.2781	6.552	521	—	—	—

* private communication [21]

this charcoal, which act as a molecular sieve, are difficult to approach, correspondingly the internal mass transfer is severly limited kinetically. The pore-size distribution of the Hungarian-made NUXIT A1 activated charcoal is broad, and varies widely. Its high specific surface area can be approached by diffusion over a distance of a couple of manometers.

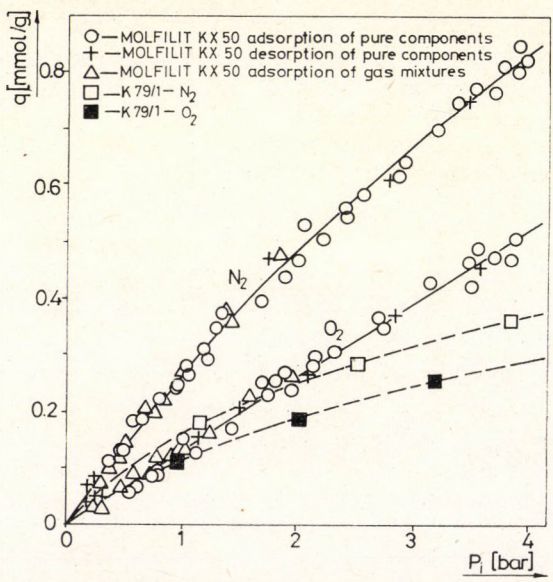

Fig. 5
Oxygen and nitrogen equilibrium isotherms of MOLFILIT *KX*50 and *K* 79/1

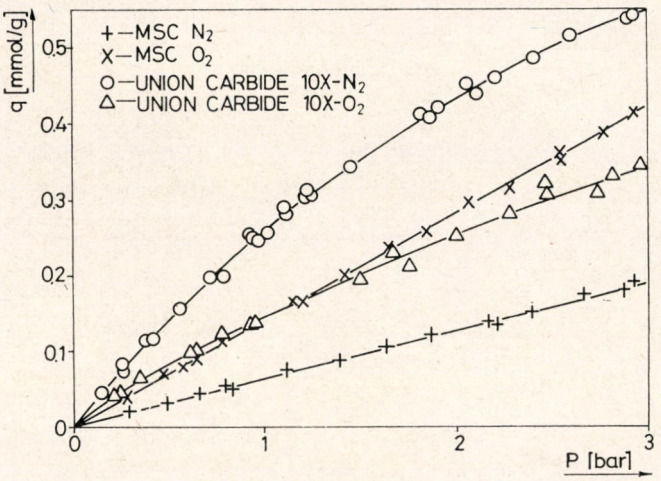

Fig. 6
Oxygen and nitrogen equilibrium isotherms of MSC and UNION CARBIDE 10*X*

The oxygen and nitrogen binding capacities of the adsorbents listed above are shown in *Fig. 5* and *6*. The isotherms were obtained at 293 *K*. Since the specific adsorption capacity values are low, equilibrium had to be detected on the basis of pressure measurements in a constant volume system. The densitivies of the adsorbents were determined in a He picnometer. At any given pressure, the zeolites could adsorb almost twice as much nitrogen than oxygen. The separation factors α, at a pressure of 3 bars (as defined by WOLF anf KÖNIG [22]) are listed in *Table 1*. At any given pressure, the molecular sieve charcoal adsorbs oxygen more readily than nitrogen. This characteristic of the adsorbent is of special value for the production of nitrogen rich gases, because in this case low amounts of oxygen have to be removed from the gas mixture. The separation factors do not vary widely, i.e. from an equilibrium point of view, the adsorbents listed (except NUXIT Al) are suitable for separation of the components of air.

Kinetic Tests

Due to technical problems, these tests were restricted to the adsorption period. However, it has to be noted that in our experience the desorption rates are of the same order of magnitude as adsorption rates though somewhat lower. The high rates preclude the use of mass measurements for the monitoring of the progress of the process, so the method advocated by WINFIELD [23] had to be applied. Essentially the evacuated adsorbent (10–20 mbar) was brought suddenly into contact with the pressurized gas mixture in a constant volume vessel. Evacuation to some 10 mbars was sufficient, since the separations presently in operation use this pressure in the regenerating cycle.

The experimental apparatus is shown schematically in *Fig. 7*. The system was tested using inert packing [9] and its transfer capability was found to be 100 Hz. This means that pressure changes taking longer than 0.01 s could be detected reliably.

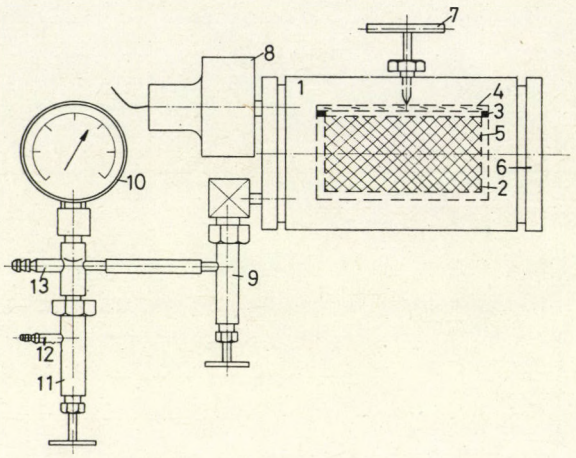

Fig. 7
Schematics of the constant volume pressure changes detecting apparatus used for the kinetical experiments. *1* — constant volume vessel, *2* — sample storage vessel, *3* — rubber gasket; *4* — glass plate, *5* — adsorbent; *6* — removable cover, *7* — breaking device; *8* — electric manometer; *9* — needle valve; *10* — control manometer; *11* — needle valve, *12* — vacuum, *13* — gas feed

The dimensionless transient curves obtained in kinetical measurements with pure gases and various adsorbents are shown in *Figs. 8*, *9* and *10*. In this *Figures* p stands for the actual pressure, p_0 for the system pressure at the moment of contact, and p_∞ for the so-called equilibrium pressure detected after a sufficiently long contact time. The major finding of the adsorption experiments is that the separation rates observed at the moment of contact between the pressurized gas and evacuated adsorbents can differ with orders of magnitude for different adsorbents [9].

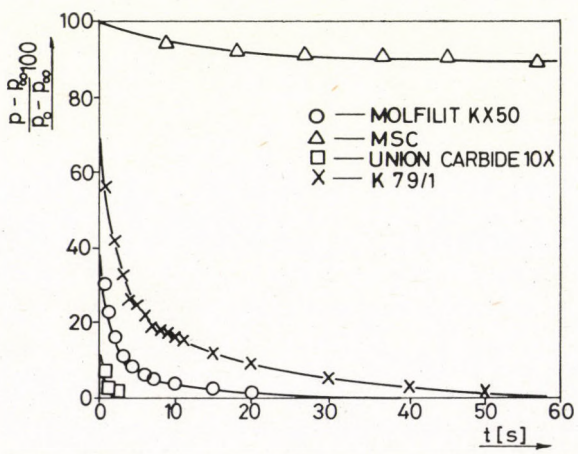

Fig. 8
Dimensionless transient curves of N_2 adsorption on various adsorbents

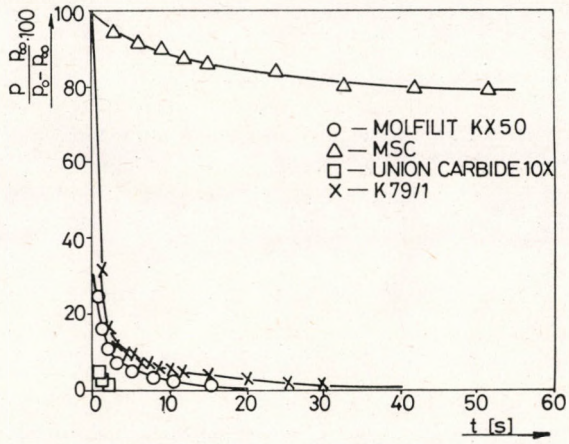

Fig. 9
Dimensionless transient curves of oxygen adsorption on various adsorbents

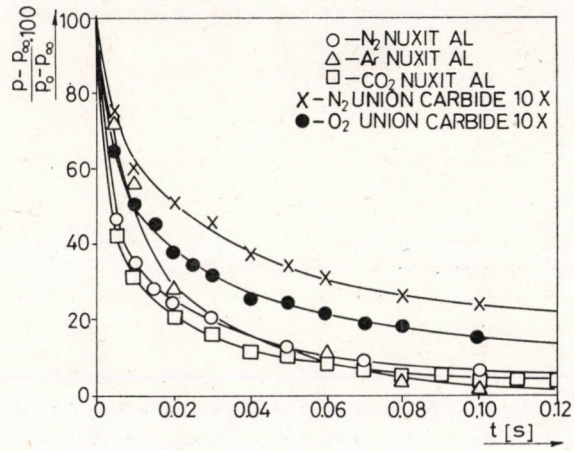

Fig. 10
Adsorption transients of a few selected gas — adsorbent pairs

In the case of NUXIT Al with its loose pore-structure, a quasi-equilibrium is attained in a couple of tenths of a second. On the other hand, in the case of molecular sieves, composed of crystallites and characterized by a bi-disperse pore distribution, the equilibrium time ranges from a few seconds to ten to fifty seconds. The equilibration time of MSC, which is extremely solid, is longer than an hour.

It is worth mentioning that the transport rate for any given adsorbent depends only slightly on the type of gas examined, i.e. the major rate controlling factor is the pore structure of the adsorbent. The Type 10*X* synthetic zeolite produced by Union Carbide is almost an order of magnitude faster than MOLFILIT *KX*50 A zeolite, which is composed of identical crystallites. The

rate difference is obviously due to the different crystalline structure of zeolite *A* and *X*.

The pore-structure-dependent kinetics indicates that viscous flow, gas diffusion, Knudsen diffusion and vacancy transfers are all present and are interrelated in a complex manner in the pores of the sorbent [24–26].

For any given gas-solid system the transients measured at different initial pressures do not differ significantly. However, it should be noted that initial pressures were always beyond the critical values as defined by flow through the throttle.

The adsorption transport rate of oxygen was larger for each adsorbent than that of nitrogen. The equilibration time for nitrogen was almost twice as long as for oxygen. This work has not dealt with the internal characteristics of adsorption kinetics. The major conclusion of the kinetical examinations concerning the separation process proper is that in the majority of cases the adsorption rate is comparable with the time required for the filling of the tube, so both phenomena have to be taken into consideration for the description of the separation process. The assumptions drawn from the equilibrium model are valid only in those cases when the rate of mass transfer is several orders of magnitudes higher than that of the conventive mass transport.

Investigations on the Effects of the Tube

The two sub-processes discussed in the previous paragraphs occur simultaneously in a tube packed with an adsorbent, in the basic unit of PSA gas separation.

Experiments were carried out in a 1000 mm long, 25 mm I.D. tube, closed at both ends by stopcocks. Gas pressure in the tube was monitored at the end of the tube opposite the gas-inlet point. A filling pressure of 3 bars [27], the common value for air separation, was used throughout the experiments. This pressure ensures a sufficiently high amount of gas, while the separation factor, α does not yet decrease significantly due to the curvature of the isotherms. Gas was discharged four times at the end of the tube opposite the inlet point at pressures above the ambient. The concentration and amount of oxygen in these samples were determined. Since the amount of air introduced was known, the composition at the fifth point could be obtained from the mass balance equation. The results of the experiments are shown in *Fig. 11* and *12*. The concentration distributions corresponding to the filling-up time (generally less than 1 s) determined by the internal resistance of the bed are shown in *Fig. 11*. Practically, there is no separation in the case of the slow MSC adsorbent, i.e. the composition of the gas phase after a sufficiently long time approaches the equilibrium composition corresponding to the given pressure. The role of the internal hydrodynamical resistance is shown in *Fig. 11* by the curves obtained with two different size fractions of UNION CARBIDE 10*X*. With increasing resistance (decreasing particle size) the extent of separation improves.

The effects of external flow resistance are shown in *Fig. 12*. It can be seen that a practically pressure gradient free filling operation with a filling time of 160 s results in considerable separation for MSC (MSC prefers oxygen). Similar results were obtained with MOLFILIT *KX* 50*A* as well.

The results of tube effect investigations agree with those of the hydrody-

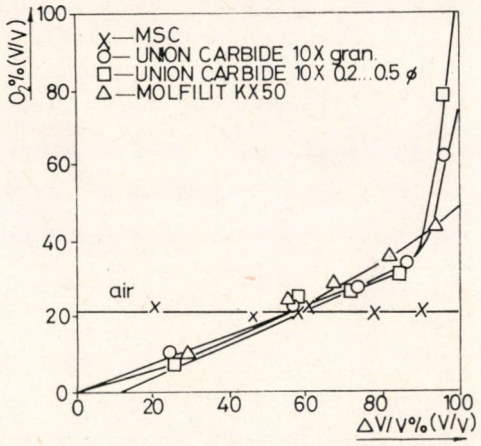

Fig. 11
Examination of the tube-effect with air for filling conditions controlled by the internal resistance of the bed

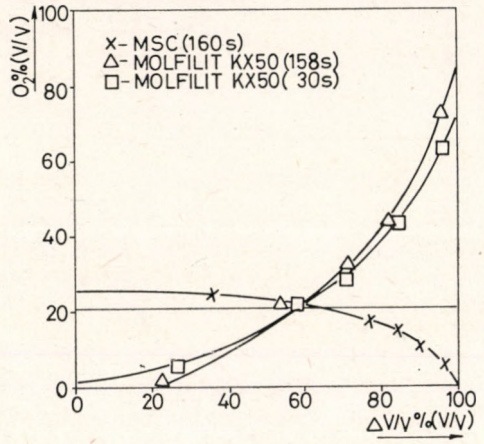

Fig. 12
Examination of the tube-effect with air for filling conditions controlled by an external flow resistance

namical and kinetical measurements. It should be noted that the selection of filling-up and discharge times are of considerable importance for design of successful PSA separators. The patent literature generally neglects this question or emphasizes that cycle time is determined by the length of the evacuation period. Based on the above experimental evidence it can be concluded that selection and design of paper equilibration time during filling up is of considerable importance. The selection of this time becomes a complex optimation problem including all aspects of equilibrium, hydrodynamics and kinetics.

Air Separation Experiments

Based on the findings of the hydrodynamical and kinetical experiments, the description given in Hungarian patent, No. 172.738 [6] separation experiments were carried out in a dual column apparatus using pressure equilibration. (Patent owners are the Department of Chemical Process Engineering, University of Chemical Engineering, and the Design Institute for Chemical Plants — Vegyterv, Budapest). The schematics of the apparatus is shown in *Fig. 13.*

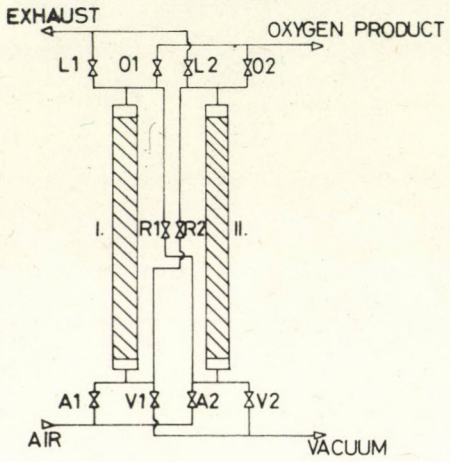

Fig. 13
Schemetics of a dual-column PSA gas separator with pressure equalization as disclosed by Hungarian Patent No. 172.738

The operation parameters of the system are as follows:

- packing: cylindrical MOLFILIT *KX*50, 1.4 kg/column
- filling pressure: 3 bar
- evacuation pressure: 26 mbar
- oxygen-rich product discharge (Δp) 0.5 and 1 bar.

The results of the filling experiments are shown in *Table 2.* In the first experiment, the internal resistance of the packed bed determined the time required to achieve a filling pressure of 3 bar. In the second, third and fourth experiments, external flow resistances were used to obtain increasing filling times.

It is apparent from the data in *Table 2* that at identical product discharge levels the oxygen concentration, i.e. the oxygen yield increases with the filling-time. In the third and fourth experiments, the longest step is the filling-up step, and not the evacuation step, as before. Correspondingly, the product obtained met the standards of high quality gas purification. This also means that the 80% oxygen concentration, commonly accepted as economically achievable in PSA oxygen separation could be met at higher product discharge and lower air consumption levels, i.e. with higher yields.

Another important feature of the fourth experiment is that 55% of all nitrogen introduced into the system can be recovered with a purity of 98.3%.

Table 2

Results of the separation experiments

Characteristics		1.	2.	3.	4.
Filling time of the evacuated column, s		5	30	100	100
Full cycle time, s		180	180	210	210
p, bar		0.5	0.5	0.5	1.0
Air feed rate, l/h		330	345	310.5	312.5
Oxygen enriched product	Volumetric flow rate l/h	45	47	40.5	62
	Oxygen conc. % V/V	71	90.6	99.1	86.7
End gas	Volumetric flow rate l/h	153	152	136	110
	Oxygen conc. % V/V	16	14.3	13	8.7
Gases removed by vacuum	Volumetric flow rate l/h	132	146	134	138.5
	Oxygen conc. % V/V	10	5.6	5.4	1.7
Oxygen production yield % V/V		46.1	58.8	61.6	81.9

Conclusion of the Experiments

It can be concluded from the experimental results discussed in the previous sections that the mass transfer processes occurring in a tube packed with an adsorbent have two major components, the non-steady-state hydrodynamics of the compressible medium and the mass transfer between the gas and solid phases.

In our opinion it is not advantageous to increase the hydrodynamical resistance of the columns by decreasing the particle size of the packing, because above a certain level resistance unfavourably influences the product dischange and evacuation processes. The use of an external flow resistance matched to the kinetical properties of the adsorbent seems more desirable. In this case, the flow in the packed column is free of pressure gradients.

The PSA process requires better adsorbents. For a given adsorbent and gas mixture, favourable equilibrium behaviour is not sufficient, the kinetical characteristics also have to be suitable. This means, in the case of zeolites, that small crystallites of 1–3 μm size and pores of similar magnitude have to be secured. This work does not deal with the design of the crystallite size of zeolites, however, it should be mentioned that the size of the crystallites cannot be

decreased infinitely, rather only to a certain value, because below a critical value the resistance of the transport process becomes the rate determining the factor.

ACKNOWLEDGEMENT

The authors are indebted to K. PATAKI of the Research Institute for Technical Chemistry of the Hungarian Academy of Sciences and to G. SZIKLAI of the Veszprém University of Chemical Engineering for their contributions to experimental work.

REFERENCES

1. GFR Pat. D.T. 25 48 291
2. FRENCH Pat. 1.601.126; 2.157.053; 2.157.054; 2.157.056; 2.157.057; 2.157.058; 2.157.059
3. US Pat. 3,546,816; 4,013,429
4. GFR Pat. DE 2 207 117; 2 702 784; 2 702 785
5. GFR Pat. DE 2 347 574
6. Hung. Pat. 172 738
7. SZOLCSÁNYI, P.: Magyar Kémikusok Lapja *1980*, 35 (7) 344 – 346.
8. ARGYELÁN J., KOTSIS L., SZÁNYA T. és SZOLCSÁNYI P.: Magyar Kémikusok Lapja, *1980*, 35, 11
9. KOTSIS L.: Magyar Kémikusok Lapja *1980*, 35 (12) 643 – 648
10. SZOLCSÁNYI P., HORVÁTH G., KOTSIS L. and SZÁNYA T.: V. International Congress of Chem. Engng. Chem. Equip. Des. and Aut. CHISA '75 J. 26.
11. USTINOV, E. A. Zh. Prikl. Khim. (Leningrad) *1980*, 53, (1) 136 – 141.
12. BEKKER, B. I., TOROCSESNIKOV, N. S., SUMJACKIJ M. I.: *1975*, 9, 771.
13. COONEY, D. O.: Ind. Eng. Chem. Proc. Des. Dev. *1974*, 13 (4) 368 – 373.
14. RAVILOV, R. G., SKLYAEV, A. A., BOGUSLAVSKII, E. G., VASILIEVA, L. M., ANUFRIENKO, V. F.: Izv. Sib. Otd. Akad. Nauk. SSSR. Ser. Khim. *1979*, 4, (9) 40 – 42.
15. USTINOV, E. A., AKULOV, A. K.: Zh. Prikl. Khim. (Leningrad) *1979*, 52, (10) 2291 – 5.
16. GFR pat. B01 D 53/02, DE 28 14 442;
17. TURNOCK, P. H. and KADLEC, R. H.: AIChE J. *1971*, 17, 335.
18. KOWLER, D. E. and KADLEC, R. H.: AIChE J. *1972*, 18, 1207.
19. MORRISON, Jr. A.: Ind. Eng. Chem. Fundam. *1972*, 11, 2, 191 – 197.
20. BLICKLE, T. et MAHÁCS M.: Non-waste technology and production (International seminar UN-ECE), Paris, 29. 11 – 4.12 1976.
21. KADLEC, O.: Prague, Heyrowsky Institut of Physical Chemistry and Electrochemistry CAS; private communication.
22. WOLF, F. und KÖNIG, P.: Chem. Techn. *1974*, 26, (12) 761 – 763.
23. WINFIELD, M. E.: Australian Journal of Chemistry *1953*, 6, 221 – 233.
24. TIMOFEJEV, D. P.: Adsorptionskinetik VEB Deutsche Verlag für Grundstoffindustrie. Leipzig. *1967*, 197 – 246.
25. WICKE, E. and WOLLMER, W.: Chem. Engng. Sci. *1952*, 1 (6) 282 – 291.
26. DUBININ, M. M., ERASHKO, I. T., KADLEC, U. and ULIN, V. I.: Carbon, *1975*, 13, 193 – 200.
27. SPRINGMANN, H.: Chemie-Ing. Techn. *1974*, 46, 21, 881 – 93.

РЕЗЮМЕ

Авторы изучали транспортные процессы адсорбционной сепарации газа (PSA) при колебании давления на базе экспериментальных данных. Установили, что в случае неконденсирующихся газов энерготранспортом в процессах можно пренебречь. Изучали нестационарную гидро-

динамику заполненных труб при течении в них сжимающихся сред. В аппарате постоянного объема работающего на принципе измерения давления изучали кинетику адсорбции и установили, что скорость транспортных процессов определяется структурой пор частиц адсорбента. Изучали основной элемент метода PSA, т. е. заполненную адсорбентом трубу и газовую сепарацию при заполнении газовой смесью трубу. Указали на необходимость согласования кинетических свойств частиц адсорбента и гидродинамических свойств трубы. На основе сепарационных измерений доказали правильность выводов установленных при изучении элементарных процессов. На основе экспериментальных данных авторы предлагают составлять математическое описание метода.

HUNGARIAN JOURNAL
OF INDUSTRIAL CHEMISTRY
VESZPRÉM
Vol. 9. pp. 89–98 (1981)

A CRITICAL REVIEW OF BUBBLE DETECTION IN GAS-SOLIO FLUIDISED BEDS USING QUASI PUNCTUAL PROBE TECHNIQUE

H. MASSON
(Faculté des Sciences Appliquées, Université Libre
de Bruxelles, Belgium)

Received: December 10, 1980.

The properties of gas-solid fluidised beds are strongly dependent on bubble behaviour. It is important to measure the bubble sizes, their velocity, and the visible flow, etc. For large scale installations, the use of punctual probes seems to be the most convenient way to completely characterize the local properties of the bubbles. However, the interpretation of the signals obtained by the probes is difficult and is based on a cascade of hypotheses, which even appear at times to be implicit.

The present work is a tentative aim to present the different approaches published on probe signal interpretation as a coherent "hypothesis tree". It also contains some suggestions for further tests of some of the more crucial hypotheses.

Introduction

Recent mathematical models for gas solid fluid beds explicitly use the local values of properties, such as bubble size, velocities, flow and volume fraction occupied by bubbles.

This fact has induced a considerable experimental effort to measure these properties.

Several experimental techniques have been used: two dimensional beds [10, 12, 28, 29], high speed cinematography of bubbles following the wall, or of eruption diameters at the top of the bed [6, 16], external probes [2, 13, 33], internal probes [1, 3, 5, 8, 11, 14, 15, 17, 18, 19, 20, 30] or radiocinematography [25, 26, 27].

Radiocinematography is actually limited to layers having a diameter less than 30 cm, due to radiation absorption by the fluidised solid.

Extrapolation from 2D measurements to 3D beds is far from evident [9].

The only method permitting a complete description of the local bubble phenomenon thus remains the use of internal quasi punctual probes.

Several *physical principles* have been used for this purpose: pressure probes [15], capacitive [1, 14, 30], resistive [3, 20] or inductive probes [5], hot wires [19] and light probes [17, 33].

Table 1.

Complementary checks to be done by X ray cinematography	Interpretation: chain of hypothesis	existing checking methods
	① signal/noise separation is possible	amplitude probability analysis (WERTHER)
	② permanency of bubble phenomenon	time series analysis (MASSON)
	③ random arrival of bubbles	exponential time interval distribution (WERTHER)
	yes / no	
	computation of bubble chain length (WERTHER)	
	④ bubble shape described by only one shape factor, bubble completely described by the $[n_{jjl}]$ matrix	
	⑤ local homogeneity of the bubbles near the tip of the probe	
	yes / no	
	definition of the distribution, i.e.: wall effect assimilating bubbles to rigid spheres (NAKAMURA et al.)	
	x_{ijkl} describes the measurements	
	only bubble size information needed?	
	no / yes	
	variable horizontal gap probe (PUTT et al.)	
	⑥ known D distribution D, σ_D (PUTT et al.)	χ^2 adjustment test on X ray films (ROWE and YACONO)
Check 4: $\Phi = \Phi(D)$	⑦ constancy of the shape factor with bubble size at a given point	
	yes / no	
Check 5: representativity of selectes bubbles as sample of the total population	use of a 5 leg probe to eliminate bubble having an oblique motion and eccentrated or coalescing bubbles BURGESS et al. individual measurement of the bubble size, velocity and shape for *some* of the bubbles passing at the tip of the probe.	

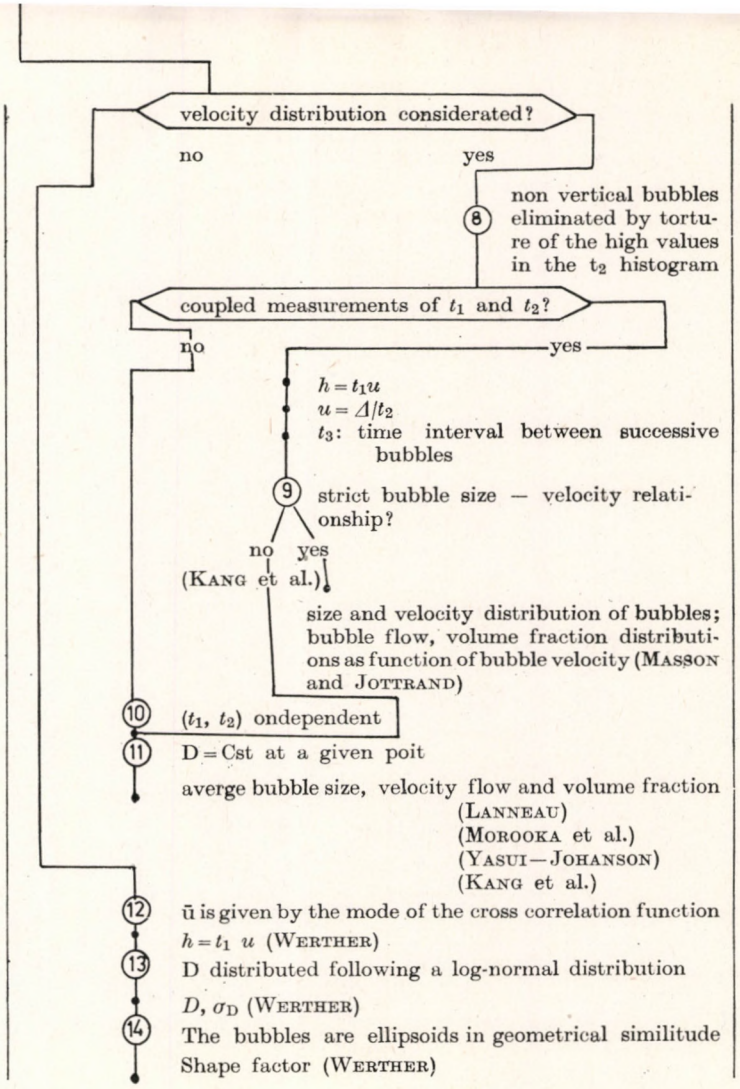

Check 6: χ^2 test on the h and the t_1 distribution in freely fluid beds

Some immediate criticism may be advanced against some of these techniques. The signal generated by a pressure probe is a rather complicated one [22] and has a time duration longer than the actual travel time of the bubble at the tip of the probe.

Impedance probes always present an electrical field and are thus progressively sensitive to the approach of a bubble. The detection volume is not well defined and the punctuality of the probe is questionable.

The slopes of the pulses obtained are generally not very sharp and the amplitude of the signal depends on the size of the detected bubbles.

Time interval measurements on such pulses are thus sensitive to the voltage level at which the measurement is made.

Several authors have investigated the *interpretation of probe signals*. The present work is a tentative aim to present in a coherent way these approaches and to put forward the associated explicit and often implicit hypotheses. The discussion is synthetized under the form of *Table 1*.

The common point to the different investigators is that they admit the stochastic nature of the bubble phenomenon and that they use, as a consequence, a statistical analysis approach.

Signal—Noise Separation

In the present case, a noise is any contribution to the signal which is not directly due to a bubble. If the fluctuations due to bubbles are larger than the parasitical ones, an amplitude probability analysis may be used [30].

PARK et al. [20] chose, without more justification, their detection level at 1/2 of the maximum peak amplitude. However, they checked that slightly changing the measurement level did not induce an appreciable difference in the results.

Description of the Local Values of the Bubble Population

To be significative the measurements of bubble properties must be independent on the initial instant of measurement and on the duration of the measurements. This point may be checked using classical time series analysis methods.

Secondly, the characteristics of successive bubbles must be independent on their respective properties or on the time interval separating their passage at the probe. WERTHER [32] has shown that for a short sojourn time at the tip of the probe, and for the random arrival of bubbles, the time interval distribution between successive bubbles must be exponential. In fact it appears that bubbles have a tendency to move in chains of 4 or 5 bubbles.

The third step consists in admitting that the bubbles shape may be defined by only one shape factor.

If we then call n_{ijl} the number of bubbles per unit volume having a diameter between Di and $Di+\Delta D$, a velocity between U_j and $U_j+\Delta U$ and a shape factor between φ_l and $\varphi_l+\Delta\varphi$, the (n_{ijl}) matrix completely describes, the bubble phenomenon.

At this stage of development, it is interesting to know to which extent the probe support affects the bubble properties (check 1).

Excentricity

The bubble volume is quite large, and all the detected bubbles are not obligatory centred on the tip of the probe. Only a chord may be intercepted.

Experimentally, we thus have to handle a 4 dimensional (x_{ijkl}) matrix. Each element of this matrix describes the number of bubbles detected per time unit, under a chord of which the length is between h_k and $h_k+\Delta h$, having a diameter between Di an $Di+\Delta D$, a velocity between U_j and $U_j+\Delta U$ and a shape factor between w_1 and $\varphi_1+\Delta\varphi$.

One then needs to assess the spatial distribution of the bubble centres around the tip of the probe.

The simplest possible hypothesis is to assume that this repartition is locally homogeneous, at the scale of a bubble diameter. It is noticable that this often means exactly at the scale of the vessel for laboratory installations.

Some published results reveal the existence of radial non-uniformities in bubble profiles [12, 30]: bubbles preferentially follow the wall in the bottom of the bed and then progressively concentrate in the axis of the vessel for small scale installations (≤ 30 cm in diameter).

The probe support itself may exercise an attractive or a repulsive effect on the bubble trajectories. X ray cinematography would be an ceasy way to assess this point (check 2).

On the other hand, the presence of the wall inhibits a uniform bubble spatial distribution around a measurement point in the vicinity of the wall. PARK et al. [21] assimilated the bubbles to rigid spheres. The bubble centres must then be at more than one bubble radius from the wall. This hypothesis leads to the conclusion that the bubbles must appear as points when observed through the transparent side wall of a 3 D bed.

In fact, as visual observation reveals, the bubbles are more or less deformed near the wall, following a law which has not yet been specified.

The radiocinematographical technique can be used to assess eventual combined wall and probe effects on bubbles moving near the wall (check 3).

Distribution of Horizontal Bubble Chords

This point may be investigated using a probe with a variable horizontal gap as suggested by PUT et al. [22].

If one then specifies the shape of the bubble size distribution, the mean bubble diameter and its variance may be defined.

Relationship between Spatial and Detected Bubble Properties

The relationship between the number of bubbles per unit volume n_{ijl} and the number of bubbles detected by the probe per time unit x_{ijkl} is given by:

$$\frac{x_{ijkl}}{N}=\frac{n_{ijl}}{N}\,P_1(D_i,\ U_j)\times P_2(D_i,\ h_k) \tag{1}$$

$$\text{where} \quad N=\sum_i \sum_j \sum_l n_{ijl} \tag{2}$$

$P_1(D_1, U_j)$ is the probability to detect a bubble having a diameter D_i and a velocity U_j; while $P_2(D_i, h_k)$ is the probability to detect following a chord h_k a bubble having a diameter D_i.

$P_1(D_i, U_j)$ is proportional to the volume covered by the bubble per time unit:

$$P_1(D_i, U_j) = \frac{\pi}{4} D_i^2 U_j \tag{3}$$

Equation (1) may be rewritten as:

$$x_{ijkl} = n_{ijl} \frac{\pi}{4} D_i^2 U_j P_2(D_i, h_k) \tag{4}$$

An analytical expression may be deduced for $P_2(D_i, h_k)$ in the unrestrained 3D case, after the acceptance of the local homogeneity hypothesis *(Fig. 1)*.

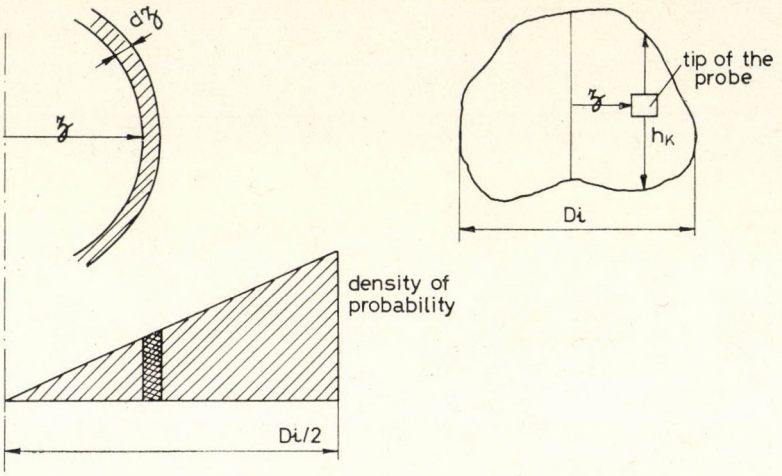

Fig. 1
Eccentricity probability function in unrestrained 3 *D* beds for a vertically moving bubble

For a given size and shape factor of the bubble, there is a strict relationship between the bubble eccentricity z and the length of the intercepted chord h_k. The detection probability is proportional to the horizontal area in which the centre of the bubble having a diameter D_i must be detected under a chord h_k:

$$P_2(D_i, h_k) = \frac{2\pi z \, dz}{\frac{\pi}{4} D_i^2} \tag{5}$$

Considered globally, the problem remains very large. Different simplifications have been advanced.

1° BURGESS and CALDERBANK [3] using a 5 legs probe and an on line computer developed a centring procedure. They selected the bubbles having a ver-

tical trajectory, being centred on the probe and undergoing no coalescence. The results are presented as distributions of size, velocity and shape factor.

This approach indicates that the selected bubbles are representative of the total population, which remains to be proven (check 5).

2° All the other approaches are based on the hypothesis that the shape factor remains constant at the measurement point.

This assumption is certainly an oversimplification of the reality; the shape of the bubbles is strongly affected by coalescence or splitting of the bubbles, eventually by the bubbles size (check 4) or even by the presence of the probe support.

However, the distribution of the shape factors does not seem to have a strong effect on fluid bed performances. It may thus appear legitimate to neglect the fluctuations of the shape factor. We then have to handle (x_{ijk}) and (n_{ij}) matrices each having a dimension less than the respective initial matrices.

The Method of Characteristic Times

The technique consists in recording the signals obtained by two vertically alignated probes, separated by a distance Δ.

The time duration of a pulse t_1 and the time shift between the two signals t_2 are of especial interest: they permit the bubble velocity to be defined:

$$U_j = \Delta / t_2 \tag{6}$$

and intercepted chord

$$h_k = U_j \times t_1 = \Delta t_1 / t_2 \tag{7}$$

The bubble roof or bottom velocity would be defined, then following this we measure the time shift on the ascending or descending slopes of the pulses, as far as the trajectory remains vertical.

In a same way, h_k may eventually be the measure of an oblique chord when the bubble trajectory is not vertical.

The measurements may be synthetized as a (U_j, h_k) frequency matrix of which each element x_{jk} is defined by:

$$x_{jk} = \sum_{i:k}^{i\,max} x_{ijk} \tag{8}$$

Two remarks must be advanced concerning the relationship (8). The upper limit of the sum is the maximum bubble size at the measurement level, which must be defined. The lower limit starts at a value of $D_i = h_k$; indeed a bubble may not be detected under a chord h_k greater than its diameter D_i.

Equations (4) and (8) define a system of equations of which the n_{ij}, appear as the unknowns.

The n_{ij} values must be non negative and an a priori estimation of the bubble shape is necessary to define $P_2(D_i, h_k)$ in Equation (4).

Non Vertical Bubble Trajectories

This accident is responsible for non biunivocal correspondence between the pulses detected on the 2 channels of a double probe.

The measurement of t_2 may thus be in error: instead of recording the true value of t_2, one may detect t_2+t_3, where t_3 is the time interval between successive bubbles.

Coalescence of bubbles between the measurement levels leads to the same effect. To minimize this kind of mistake, PARK et al. [20] proposed to cut the upper part of the t_2 histogram. If this histogram is bimodal, at the *valley* between the 2 modes: otherwise, at a maximum value of t_2 corresponding to a realistic minimum value of the bubble velocity ($u \geq 10$ cm/s).

It is finally noticeable that for bubbles having only a slight obliquity, the bubbles may cut the 2 measurement levels different oblique chords which leads to errors in the estimation of the bubble size and velocity. This effect has not yet been taken in consideration in literature.

Further Simplifications

Three different approaches are reported in literature.

1° In some of the earliest work on the subject [18, 19] the mean value of t_1 and t_2 are measured independently;

The average bubble chord is defined by: $\overline{h} = \Delta \overline{t}_1 / \overline{t}_2$

and the average bubble velocity by $\overline{u} = \Delta / \overline{t}_2$

This determination of $\overline{h}$ postulates that the t_1 and the t_2 distributions are statisticaly independent; otherwise, second order corrections must be added.

2° PARK et al. [20] performed coupled measurements of t_1 and t_2 and synthetized this result in a (x_{jk}) matrix. They defined the marginal distributions of h_k and U_j and calculated their mean values. Postulating then $\frac{h}{D} = 0.516$, they calculated the mean bubble diameter. According to the relationship (2) this approach is not completely correct when the bubble diameters and velocities are distributed, due to the preferential detection of large bubbles, as underlined by WERTHER [31].

3° The third approach [31] assumes that the bubble velocity is independent of their size in a freely fluidized bed.

One may then write:

$$h_k = \overline{u} \times t_1 \tag{11}$$

Following this relationship the h_k and the t_1 distributions differ only by a scale factor $\overline{u}$ (check 6).

Then assuming a log-normal distribution for the bubble diameter, a mean bubble size may be defined.

Finally, assimilating the bubbles to ellipsoids in geometrical similitude, a shape factor may be defined by cross correlation of the signals coming from two probes in the same horizontal plane.

Bubbles Volume Fraction ε_β and Visible Bubble Flow q'_β

The 3 characteristic times also permit the bubble volume fraction to be calculated:

$$\varepsilon_\beta = \bar{t}_1/\bar{t}_3 \tag{12}$$

and the visible bubble flow

$$q'_\beta = \varepsilon_\beta \times \bar{u} = \overline{\Delta t_1}/\bar{t}_2 \times \bar{t}_3 \tag{13}$$

Choice of the Mean Values of the Characteristic Times

Each of the three times is largely distributed and considerable differences exist between the estimations of their "central tendency".

Table II summarizes the choices made in literature. These choices seem to be linked more to experimental facility considerations than to theoretical support.

Table 2.

Author	t_1	$\bar{t}_2$	$\bar{t}_3$
Yasui—Johanson [33]	arithm	arithm	harmonic (frequency)
Morooka et al [19]	arithm	arithm	arithm
Park et al [20]	arithm	harmonic	arithm
Werther—Molerus [30]	median	cross correlation mode (= median if symmetrical histogram)	harmonic

In fact, as shown by Masson and Jottrand [17], the choice of the correct mean value depends on the nature of the bubble velocity-size relation and on the physical quantity to be defined.

Most of the checks suggested in *Table 1* were performed with the X ray facility of the University College of London and are presented as a separate publication [34].

ACKNOWLEDGEMENT

This work was performed during a sojourn at the University College of London, and the author is inbedted to Professor P. N. Rowe for his encouragement and the interest shown in this work.

REFERENCES

1. Bakker, P. J. and Heertjes, P. M.: Brit. Chem. Eng. *1958*, 1 (10) 240.
2. Baumgarten, P. K. and Pigford, K. P.: AICHE J. *1960*, 6 (1) 115.
3. Burgess, J. M. et. al.: Chem. Eng. Sci. *1975*, 30, 1107.
4. Clift, R. and Grace, J. R.: Chem. Eng. Progr. Symp. Ser. *1970*, 66 (105) 14 – 27.
5. Cranfield, R. R.: Chem. Eng. Sci. *1972*, 27, 239.
6. Cranfield, R. R. and Geldart, D.: Chem. Eng. Sci. *1974*, 29, 935.

7. DONSI, G. et. al.: Ing. Chim. Ital. *1974*, 10 (12) 185.
8. DOTSON, J. M.: AICHE J. *1959*, 5, 169.
9. GELDART, D.: Powder Technology *1970*, 4, 41.
10. GODARD, K. and RICHARDSON, J. F.: Chem. Eng. Sci. *1969*, 24, 663.
11. GOLDSCHMITT, D. and LEGOFF, P.: Trans. Inst. Chem. Engrs. *1967*, 45, 169.
12. GRACE, J. R. and HARRISON, D.: Inst. Chem. Engrs. Symp. Ser. *1968*, 30, 105.
13. KÖLBEL, H. et. al.: Chem. Ing. Tech. *1972*, 41, 697.
14. LANNAU, K. P.: Trans. Inst. Chem. Engrs. *1960*, 38, 125.
15. LITTMAN, H. and HOMOLKA, G. A. J.: Chem. Eng. Progr. Symp. Ser. *1970*, 66 (105) 37 – 46.
16. MCGRAITH, L. and STREATFIELD, R. E.: Trans. Inst. Chem. Engrs. *1971*, 49, 70.
17. MASSON, H. and JOTTRAND, R.: Proc. Int. Congr. on Fluidization. Cambridge. 1978. p. 1.
18. MIWA, K. et. al.: Int. J. Chem. Eng. *1972*, 12, 187.
19. MOROOKA, S. et. al.: Int. J. Chem. Eng. *1972*, 12, 168.
20. PARK, W. H. et. al.: Chem. Eng. Sci. *1969*, 24, 851.
21. PARK, W. H. et. al.: Chem. Eng. Sci. *1974*, 29, 339.
22. PUT, M. et. al.: Proc. Int. Congress "Fluidization and Applications". Toulouse. 1973.
23. PYLE, D. L. and MARISSON, D.: Chem. Eng. Sci. *1967*, 22, 1199.
24. REUTER, H.: Chem. Eng. Techn. *1963*, 35, 98.
25. ROWE, P. N. and EVERETT, D. J.: Trans. Inst. Chem. Engrs. *1972*, 50, 42.
26. ROWE, P. N. and WIDMER, A. J.: Chem. Eng. Sci. *1973*, 28, 980.
27. ROWE, P. N. and YACONO, G.: Trans. Inst. Chem. Engrs. *1975*, 53, 59.
28. TOOI, R. and MATSUNO, R.: Int. J. Chem. Eng. *1968*, 8, 351.
29. TOOI, R. et. al.:Int. J. Chem. Eng. *1969*, 9, 358.
30. WERTHER, J. and MOLERUS, O.: Int. J. Multiphase Flow *1973*, 1, 123.
31. WERTHER, J.: Trans. Inst. Chem. Engrs. *1974*, 52, 149.
32. WERTHER, J.: Int. J. Multiphase Flow *1977*, 3, 367.
33. YASUI, G. and JOHANSON, L. N.: AICHE J. *1958*, 4, 445.
34. ROWE, P. N. and MASSON, H.: Trans. Inst. Chem. Engrs. (to be published).

РЕЗЮМЕ

Свойства двухфазных (газ-твердое вещество) кипящих слоев во многом зависят от свойств газовых пузырей. Важно знать размер, скорость и внешний вид течения пузырей. В случае аппаратов больших размеров для охарактеризования локальных свойств пузырей целесообразно применять метод точечных измерений, т. е. зондирующий метод. В то же время расшифровка сигналов предоставленных зондами довольно сложна и установленные на основе этих данных гипотезы носят инстинктный характер.

Целью данной работы является обобщение опубликованных методов установления гипотез на основе зондирующих измерений. Автором предложены некоторые новые пути для установления более обоснованных гипотез.

HUNGARIAN JOURNAL
OF INDUSTRIAL CHEMISTRY
VESZPRÉM
Vol. 9. pp. 99–112 (1981)

ИССЛЕДОВАНИЕ ЛОКАЛЬНОГО МАССОПЕРЕНОСА ОТ ЧАСТИЦЫ К ЖИДКОСТИ. I

Экспериментальная проверка математической модели, основанной на полуэмпирической теории турбулентности

Ермакова А., Кузьмин В. А., Скоморохов В. Б., Умбетов А. С.
(Институт катализа СО АН СССР г. Новосибирск)

Поступила в редакцию: 23 декабрь 1980 г.

С использованием известных в литературе подходов, основанных на полуэмпирической теории турбулентности, выведено уравнение математической модели, описывающей массоперенос между реагирующей твердой частицей и жидкостью. Предполагается, что пограничный слой в окрестности твердой частицы подвергается периодическим возмущениям, вызванным барботажом газовых пузырей через псевдоожиженный слой суспензии.

С целью подтверждения теоретических зависимостей числа $\overline{Sh}$ от критериев $\overline{Pe}$ и Pe', отражающих соответственно вклад основного и пульсационного составляющего в относительную скорость движения твердой частицы, проводилось экспериментальное исследование массопереноса к частице (датчику) совершающей колебательное движение в жидкости. Измерение диффузионного тока проводилось электрохимическим методом. Дано сопоставление экспериментальных и теоретических зависимостей.

Постановка задачи исследования

Перенос реагентов к внешней поверхности катализатора является одним из основных физических процессов, влияющих на скорость и избирательность протекания сложных реакций в трехфазном псевдоожиженном слое (ТПС). Следовательно при математическом моделировании реактора закономерности протекания массообменных процессов в масштабе одного зерна катализатора должны быть отражены в модели как можно более точно.

Исследование массопереноса от частицы к жидкости — в теоретическом плане — путем аналитических, качественных и численных решений уравнений гидродинамического и диффузионного пограничного слоя, выполнено в ряде работ [1—12]. К первой группе исследований можно отнести работы, основанные на анализе ламинарного пограничного слоя [1—7]. В других теоретических работах [8—12] решается задача турбулентного массопереноса в пограничном слое, совершающем высокочастотное колебательное движение с малой амплитудой. Эти специфические условия позволяют сильно упрощать исходные уравнения нестационарной гидродинамики и массопереноса, и в результате полу-

чить аналитические решения задачи. В принципе идеи этих работ нам представляются интересными, и после соответствующих модификаций постановки — с учетом особенностей ТПС — могут быть использованы при составлении математической модели.

Экспериментальные исследования массопереноса между жидкостью и твердой частицей выполнены в основном в двухфазных псевдоожиженных слоях, и в трехфазных системах с неподвижным слоем катализатора [13—30]. Полученные авторами эмпирические корреляции могут быть полезными для нас только в первом приближении, когда режим работы ТПС близок к одному из вышеупомянутых крайних режимов.

Из литературы известно [31], что характер течения жидкости в ТПС является турбулентным, вследствие периодических возмущений основного стационарного течения цепочкой поднимающихся газовых пузырей. Следует отметить особо две известные нам работы, посвященные экспериментальному исследованию турбулентного массопереноса в ТПС [32, 33]. Авторы этих работ в независимых экспериментах исследовали пульсацию относительной скорости жидкости, и локальный массоперенос при растворении твердых частиц. Полученная между этими величинами эмпирическая корреляция является физически обоснованной, инвариантной к масштабу реактора. Продолжая идею авторов [32, 33] можем отметить, что следующим моментом в теоретическом и экспериментальном исследовании массопереноса должно быть изучение зависимости локальных турбулентных характеристик от макроскопических характеристик трехфазного слоя. Последние определяются расходными соотношениями фаз, их физическими свойствами, и геометрическими особенностями реактора.

В итоге приведенного выше краткого литературного обзора можем сказать, что в настоящее время отсутствуют математические модели массопереноса, которые в достаточной мере отражают особенности ТПС, и в то же время имеют простой вид, удобный для практического пользования.

В связи с этим общую задачу исследования локального массопереноса между частицей и жидкостью в ТПС сформулируем следующим образом:

1. Вывод и анализ уравнений математической модели, учитывающей влияние локальной турбулентности пограничного слоя.
2. Экспериментальное исследование массопереноса от одной частицы в стандартных условиях, когда характеристики турбулентного пограничного слоя могут быть заданы заранее как условия эксперимента.
3. Исследование взаимосвязи локальных и макроскопических гидродинамических характеристик ТПС.

Основное внимание в данной работе будет уделено решению задач 1 и 2.

Вывод и анализ математической модели

Предположим, что проскок газовой фазы в виде пузырей через слой жидкости приводит к периодическим возмущениям скорости течения последней относительно твердой частицы. Возмущенное движение характеризуется определенным спектром амплитуд и частот, которые непосредственно связаны с конкретной гидродинамической обстановкой в ТПС, а именно: размером пузыря, скоростью и частотой его проскока в рассматриваемой точке пространства.

Принимая во внимание периодический характер локальных возмущений жидкости, любая переменная величина $(Z(t))$ процесса массопереноса может быть охарактеризована средним значением $(\overline{Z})$ и отклонением от среднего или пульсацией $(Z'(t))$:

$$Z(t)=\overline{Z}+Z'(t) \tag{1}$$

где

$$\overline{Z}=\frac{1}{\tau^*}\int_0^{\tau^*} Z(t)\,dt; \qquad Z'(t)=Z(t)-\overline{Z} \tag{2}$$

Величина τ^* определяется как характерный период колебательного движения.

Как известно, в настоящее время наиболее удобным инструментом для описания турбулентного массопереноса является т. н. полуэмпирическая теория турбулентности, с помощью которой рассматриваемую задачу в терминах средних величин $\overline{Z}$ можно сформулировать математически в виде замкнутой системы уравнений [34].

Рассмотрим осесимметричную частицу катализатора, движущуюся в ТПС в турбулентном потоке жидкости. Обозначение координат показано на *рисунке*

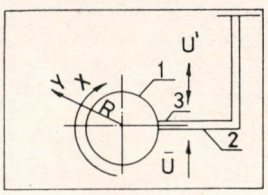

Рис. 1.

Схема обтекания датчика потоком жидкости. *1* — датчик (сфера, ∅ 0,4 см); *2* — державка; *3* — изоляция

1. Предположим, что на поверхности частицы протекает бесконечно быстрая химическая реакция. Начало координат закрепим в центре тяжести частицы. Используя известный метод Рейнольдса [34], уравнение массопереноса для осредненных величин $\overline{Z}$ может быть представлено в следующем, безразмерном виде:

$$\frac{\overline{Pe}}{2}\left(\overline{U}\frac{\partial\overline{c}}{\partial x}+V\frac{\partial\overline{c}}{\partial y}\right)=\frac{\partial^2\overline{c}}{\partial x^2}-\frac{Pe'}{2}\left[\frac{\partial}{\partial x}\langle u'c'\rangle+\frac{\partial}{\partial y}\langle u'c'\rangle\right] \tag{3}$$

граничные условия

$$y=1 \qquad c=0 \tag{4}$$

$$y=б_y \qquad c=1 \tag{5}$$

$$x=0 \qquad c=1 \tag{6}$$

Обычно граничное условие (5) задают на расстоянии $y\to\infty$, хотя на самом деле оно выполняется уже на определенном, конечном расстоянии σ_y, которое будем считать неизвестным параметром задачи.

Уравнение (3) должно быть дополнено соответствующими уравнениями гидродинамики, описывающими распределения $\bar{u}(x, y)$, и $\bar{v}(x, y)$.

Безразмерные переменные уравнения (3) получены делением размерных переменных на масштабы:

$$M_x = M_y = R; \qquad M_c = C_0; \qquad M_{\bar{u}} = M_{\bar{v}} = \overline{U}; \qquad M_{u'} = M_{v'} = \overline{U}$$

Безразмерные параметры определены следующим образом:

$$\overline{Pe} = \frac{2\overline{U}R}{D_M} = \overline{R_E} \cdot S_c; \qquad P'_E = \frac{2\overline{U}'R}{D_M} = Re' \cdot S_c \tag{7}$$

Характерный масштаб пульсационной скорости $\bar{u}'$ определяем как корень квадрат из среднеквадратичного значения скорости пульсаций „внешнего" потока, т. е. на расстоянии $y \geq \sigma_y$

$$\bar{u}' = \left[\frac{1}{\tau^*} \int_0^{\tau^*} (u(t))^2 \, dt \right]^{1/2} \tag{8}$$

Хотя в статистической теории турбулентности [34] дано более строгое определение „масштаба" и "интенсивности" турбулентности, на наш взгляд они с хорошим приближением, — без потери физического смысла — могут быть заменены соответственно характерным линейным размером частицы: R, и масштабом скорости: $\bar{u}'$. В соответствии с этим параметр $Pe'/2$ приобретает физический смысл безразмерного коэффициента турбулентной диффузии во внешнем потоке

$$\frac{Pe'}{2} = \frac{D_T}{D_M}, \qquad \text{где} \qquad D_T = \overline{U}' \cdot R \tag{9}$$

Возвращаясь к уравнению (3) отметим, что оно содержит неизвестные функции $\langle u'c' \rangle$ и $\langle v'c' \rangle$, представляющие собой осредненные во времени конвективные потоки, возникающие в результате пульсации скорости. Используя основное допущение полуэмпирической теории турбулентности, функция $\langle v'c' \rangle$ может быть заменена эмпирической функцией, имеющей смысл безразмерного турбулентного потока массы:

$$Sh_T(y) = -\langle v'c' \rangle \equiv \left(\frac{y-1}{\sigma_y - 1} \right)^n \frac{d\bar{c}}{dy} \tag{10}$$

удовлетворяющей основным требованиям на границах:

$$y = 1 : Sh_T(1) = 0; \qquad y = \sigma_y : Sh_T = 1 \tag{11}$$

где

$$Sh_T(y) = \frac{J_T(y) \cdot R}{C_0 D_T}$$

Вкладом пульсаций конвективного потока по направлению x пренебрегаем ($\langle u'c' \rangle \approx 0$).

Коэффициент n, фигурирующий в выражении (10), характеризует скорость затухания турбулентных пульсаций по мере приближения к межфазной поверхности. Численное значение n может быть оценено исходя из различных теорети-

ческих предпосылок [35], но чаще всего оно определяется как эмпирическая константа.

Результатом решения уравнения (3) с учетом (10) является выражение для осредненного по поверхности безразмерного диффузионного потока:

$$Sh \equiv \frac{2R\bar{J}}{C_0 D_M} = \frac{1}{\pi} \int_0^{\pi} \left(\frac{d\bar{c}}{dy} \right)_{y=1} dx \tag{12}$$

В общем случае эта задача не допускает аналитического решения. Однако, большой практический интерес представляет анализ асимптотических решений, ограничивающих область изменения общего решения. В частности, если приравнять Pe' нулю, то мы приходим к классической задаче конвективного массопереноса в невозмущенном пограничном слое. Более подробно эта задача будет рассмотрена при обсуждении результатов эксперимента.

Рассмотрим другой предельный случай, $\overline{Pe} \approx 0$. Этот режим имеет важное практическое значение для реакторов с ТПС. Он может иметь место, например:

1. в реакторах, работающих в режиме „транспорта" катализатора, когда скорость жидкости равна скорости уноса частиц [36],

2. в трехфазных реакторах с механическим перемешиванием суспензии,

3. в непроточных по жидкой фазе трехфазных реакторах, в которых псевдоожижение осуществляется с помощью барботируемого газа.

В первых двух случаях условие $\overline{Pe} \approx 0$ выполняется вследствие полного захвата частиц потоком жидкости, а в третьем случае — из-за отсутствия основного потока. Главную роль в процессе массопереноса играет при этом пульсация скорости.

Поделив обе части уравнения (3) на $Pe'/2$, и имея в виду условие:

$$\varepsilon = \overline{Pe} / P_e' \ll 1$$

мы приходим к задаче с малым параметром. Однако — в силу граничного условия (5) решение полной модели (3) быстро сходится к решению соответствующей одномерной модели, полученной из уравнения (3) при $\varepsilon \equiv 0$.

Уравнение турбулентного массопереноса при $\overline{Pe} \equiv 0$ для частиц различной геометрической формы имеет следующий вид:

$$\frac{1}{y^{\alpha}} \frac{d}{dy} \left\{ y^{\alpha} \left[2 + Pe' \left(\frac{y-1}{\sigma_y - 1} \right)^n \frac{d\bar{c}}{dy} \right] \right\} = 0 \tag{13}$$

граничные условия

$$\begin{aligned} y &= 1: \quad c = 0 \\ y &= \sigma_y: \quad \bar{c} = 1 \end{aligned} \tag{14}$$

($\alpha = 0, 1, 2$ соответственно для плоской пластинки, цилиндра и шара).

Выражение для числа $\overline{Sh}$ в данном случае можно получить сразу из аналитического решения уравнения (13):

$$Sh = \frac{1}{\sigma_y - 1} \left[\int_0^1 \frac{d\xi}{[\xi(\sigma_y - 1) + 1]^{\alpha} [2 + Pe' \xi^n]} \right]^{-1} \tag{15}$$

Путем несложного анализа интеграла (15) можно убедиться в том, что при $Pe' \gtrsim 10^4$ число Sh стремится к простому предельному выражению:

$$Sh = 2^{\frac{n-1}{n}} \cdot \frac{Cn}{\sigma_y - 1} \cdot \sqrt[n]{Pe'} \tag{16}$$

где числовой коэффициент Cn приблизительно равен интегралу:

$$C_n \approx \left[\int_0^\infty \frac{dx}{1+x^n} \right]^{-1} \tag{17}$$

следовательно не зависит от геометрического фактора α и параметра σ_y. Например, при $n=2$ $C_n \approx 2/\pi$, а при $n=3$ $C_n \approx 2/(\pi\sqrt{3})$.

Основную задачу экспериментального исследования массопереноса в данной работе сформулируем следующим образом:

1. Проверка справедливости асимптотических закономерностей для числа Sh при $\overline{Pe}=0$, $Pe' \neq 0$ и при $Pe=0$, $\overline{Pe} \neq 0$.

2. Исследование массопереноса для общего случая $\overline{Pe} \neq 0$ и $Pe' \neq 0$.

3. Определение граничных соотношений $Pe'/\overline{Pe}$, при которых общая зависимость числа $\overline{Sh}$ от $\overline{Pe}$ и Pe приближается к той или другой асимптотической зависимости.

Экспериментальная часть

Исследования массопереноса от частицы к жидкости проводили в условиях, когда характеристики турбулентности (частота и амплитуда пульсации относительной скорости) задавались искусственно, путем вынужденного колебания частицы в потоке жидкости. Измерение скорости массопереноса проводилось электрохимическим методом [28]. Датчик, имитирующий реагирующую частицу, размещался в вертикальной колонне диаметром 0,1 м, через которую с заданным расходом протекала рабочая жидкость (щелочный раствор желтой и красной кровяной соли). С помощью специального устройства (пульсатора) датчик совершал колебательное движение в вертикальном направлении. Амплитуда и частота колебаний измерялись с точностью до 0,01 см и 0,05 гц соответственно. Датчики были изготовлены из никеля в виде тонкого цилиндра диаметром 0,029 см. длиной 0,48 см, и в виде сферы диаметром 0,4 см.

Непрерывный сигнал от датчиков после усиления поступал на вход аналоговой части гибридной ЭВМ ГВС-100. Математическая обработка сигнала проводилась на цифровой части ЭВМ с помощью пакета программ, включающий в себя полную статистическую обработку и фурье-анализ. В ходе эксперимента варьировали скорость основного потока жидкости, амплитуду и частоту колебаний датчика.

Условия экспериментов приведены в *таблице 1.*

Расчет коэффициента массопереноса проводили по формуле:

$$\overline{k}_T = \overline{V}_B (R_\Omega \cdot K_y \cdot F \cdot C_0 \cdot \Phi_g)^{-1}; \qquad \overline{Sh} = \frac{2\overline{k}_T R}{D_M}; \tag{18}$$

Таблица 1

Условия экспериментов

Характеристика раствора:

$C_0 = 2{,}56 \cdot 10^{-6} \frac{\text{г экв.}}{\text{см}^3}$, $D_M = (5{,}82 - 6{,}02) \cdot 10^{-6}$ см^2/сек;

$\nu = (1{,}115 - 1{,}150) \cdot 10^{-2}$ см^2/сек.

Средняя скорость потока жидкости, см/сек U	Амплитуда смещения датчика, см A_x	Частота колебания датчика, 1/сек. Φ	Осредненная пульсационная скорость датчика $(A_x\omega)/\sqrt{2}$ см/сек
0 ÷ 54	0 ÷ 1,0	0 ÷ 8,4	0 ÷ 39

Результаты эксперимента

Согласно исходной постановке задачи, выведенные нами математические модели описывают закономерности массопереноса в терминах средних величин. В связи с этим в данном сообщении мы не будем обсуждать ту информацию, которую получили о флуктуации сигнала во времени, и приводим только корреляции для осредненного значения диффузионного потока.

Рассмотрим сначала опыты, проведенные с неподвижным датчиком ($Pe' = 0$).

Экспериментальная зависимость числа $\overline{Sh}$ от $\overline{Pe}$ при $\overline{Re} < 20$ представлена на *рисунке 2*.

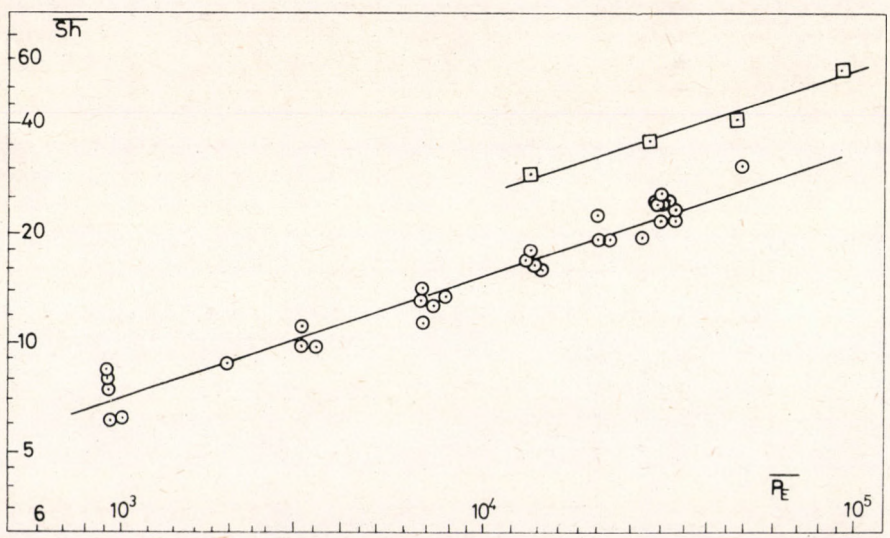

Рис. 2.

Зависимость числа $\overline{Sh}$ от $\overline{P}_E$ при $\overline{Re} < 20$ и $Re' = 0$. □ — шар, $d = 0{,}4$ см; ○ — цилиндр, $d = 0{,}03$ см

Из литературы известно, что в области $\overline{Re}<1$ обтекание частицы является безотрывным. Если при этом число $\overline{Pe}$ достаточно велико ($\overline{Pe}>10^3$), то в приближении диффузионного пограничного слоя модель (3) допускает аналитическое решение в виде:

$$\begin{aligned} &Sh=0{,}99\overline{Pe}^{1/3} && \text{для сферы [1]} \\ &Sh\approx 0{,}71\overline{Pe}^{1/3} && \text{для тонкого цилиндра [12]} \end{aligned} \qquad (19)$$

Из графиков рисунка 2 следует, что в указанной области значений $\overline{Pe}$ и Re экспериментальные данные с точностью до постоянного коэффициента удовлетворяют уравнению (19). Найденные из экспериментов значения коэффициентов пропорциональности равны 1,17 и 0,68 соответственно для шара и цилиндра.

В области $\overline{Re}>20$ обтекание твердой частицы происходит с отрывом пограничного слоя. Для этого случая точных аналитических решений уравнений гидродинамики и массопереноса не имеем. Приближенные качественные оценки предсказывают следующую зависимость числа $\overline{Sh}$ от $\overline{Re}$ и Sc [37]:

$$\overline{Sh}\sim Re^{1/2}\cdot Sc^{1/3} \qquad (20)$$

Структура этой зависимости подтверждается многочисленными литературными данными [33, 37], которые, как правило, обрабатываются в виде зависимости:

$$\overline{Sh}=2+B\overline{Re}^{1/2}\cdot Sc^{1/3} \qquad (21)$$

Значение коэффициента B — в зависимости от условий эксперимента — изменяется в пределах $0{,}55\div 0{,}95$.

На *рисунке 3* представлена экспериментальная зависимость комплекса

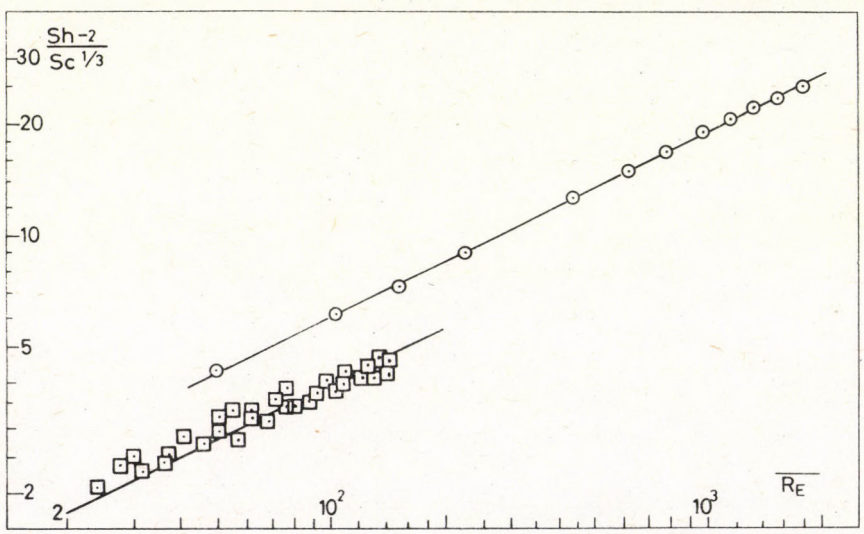

Рис. 3.
Зависимость числа Sh от $\overline{R}_E$ при $\overline{Re}>20$, $Re'=0$. ○ — шар, $d=0{,}4$ см; □ — цилиндр, $d=0{,}03$ см.

$(\overline{Sh}-2)/Sc^{1/3}$ от $\overline{Re}$, полученная нами для цилиндра и шара соответственно, в области $\overline{Re}=20\div 2000$. Из графиков следует, что экспериментальные данные удовлетворяют уравнению (21) при $B=0{,}4$ и $0{,}6$ соответственно для цилиндра и шара.

Вышеприведенные результаты свидетельствуют о том, что используемая нами методика измерения скорости массопереноса с хорошей точностью воспроизводит известные в литературе классические закономерности.

Переходим к анализу другого предельного случая: $Re=0$, $Re'\neq 0$. (Колебательное движение датчика в неподвижной жидкости.)

Если перемещение датчика относительно точки покоя описываем синусоидальным законом:

$$x(t)=A_x \sin(\omega t) \tag{22}$$

тогда мгновенная скорость (см/сек) пульсации выражается в виде:

$$u'(t)=A_x\cdot\omega\cdot\cos(\omega t)\,2c \quad \text{где} \quad \omega=2\pi\Phi \tag{23}$$

Соответственно, выражение для $\bar{u}'$ и P'_E — согласно определениям (7) и (8):

$$\bar{u}'=\frac{A_x\cdot\omega}{\sqrt{2}}; \qquad P'_E=\frac{A_x\cdot\omega\cdot\sqrt{2}\cdot R}{\nu}\cdot Sc \tag{24}$$

Зависимость числа Sh от параметра Pe' — в области $Pe'=10^3\div 4{,}10^5$ —

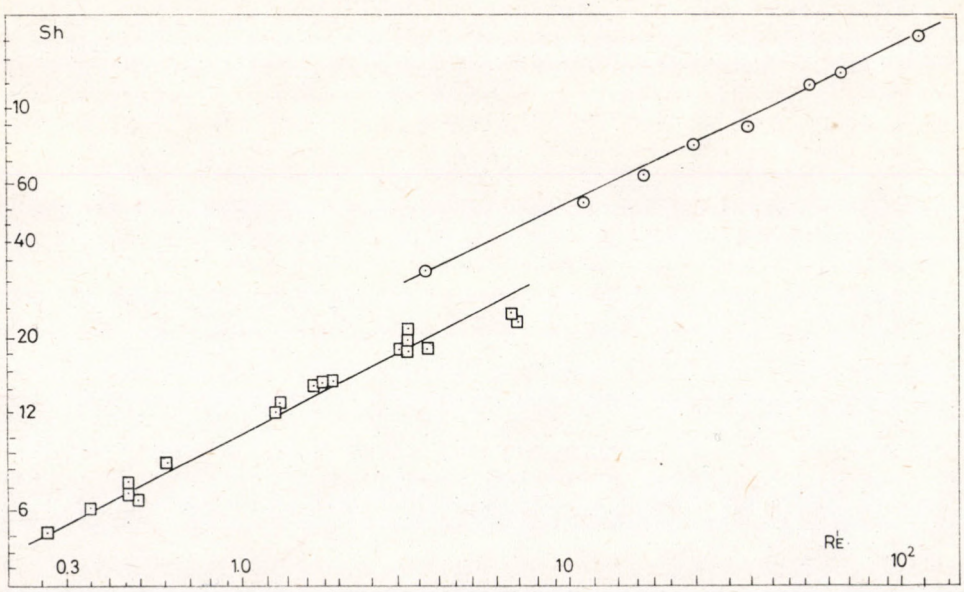

Рис. 4.

Зависимость числа $\overline{Sh}$ от $\dfrac{Re'}{2\pi}$ при $\overline{Re}=0$. ○ — шар, $d=0{,}4$ см; □ — цилиндр, $d=0{,}03$ см.

представлена на *рисунке 4*. Графики показывают, что экспериментальные данные с большой точностью описываются уравнениями:

$$\overline{Sh}=0{,}14\sqrt{Pe'}$$

для цилиндра (25)

$$\overline{Sh}=0{,}20\sqrt{Pe'}$$

для шара

Сравнивая выражение (25) с теоретической формулой (16) можно отметить следующее: во-первых, действительно параметр Pe' является единственным безразмерным критерием, определяющим среднюю скорость массопереноса в рассматриваемых условиях. Амплитуда и частота колебаний в отдельности не оказывают влияния, а только их произведение, определяющее численное значение Pe'. Во-вторых, степень затухания пульсаций n оказалась равной 2. Это значение характерно для подвижной границы раздела фаз, на которой компоненты скорости $\bar{u}$ и $\bar{v}$ не обращаются в нуль. Приближенные теоретические оценки, приведенные в литературе [35], предсказывают, что $n=3$ или 4 для твердой поверхности.

В цитированной выше экспериментальной работе [32] при исследовании растворимости борной кислоты в воде в условиях ТПС, получена следующая эмпирическая зависимость:

В области $Pe' \approx 10^4 \div 10^5$

$$Sh=2+(1{,}07 \div 1{,}16)Pe'^{1/3} \tag{26}$$

При этом среднеквадратичная скорость $\bar{u}'$, входящий в параметр Pe', была найдена в реальных условиях ТПС, как функция расходной скорости газа. Очевидно, в области больших Pe' уравнение (26) хорошо согласуется с теоретической зависимостью (16) при $n=3$.

Повидимому, завышенное значение n в наших экспериментах является следствием искусственно создаваемых возмущений внешнего потока, затухающих в пограничном слое медленнее, чем это можно было бы ожидать в естественных условиях. Эта гипотеза должна быть проверена экспериментально.

Сравнивая числовые коэффициенты уравнений (25) и (26) с расчетными значениями по модели (16) при $n=2$ и 3 соответственно, можем вычислить параметр $\sigma_y - 1 = (L_y - R)/R$, или соответствующую размерную „толщину" пограничного слоя. Получены следующие значения:

для цилиндра	$L_y - R = 1{,}03 \cdot R$
для шара	$L_y - R = 0{,}72 \cdot R$
для таблетки [32]	$L_y - R = 1{,}401 \cdot R$

Эти три значения являются величинами одного порядка и они свидетельствуют о том, что характерная область затухания турбулентных пульсаций в окрестности твердой частицы локализована на расстоянии, соизмеримой с радиусом частицы.

Наконец, представляет интерес проанализировать промежуточные режимы массопереноса, когда на колебательное движение датчика, описываемое выражениями (22) и (23), накладывается основное стационарное течение жидкости.

Обобщенные зависимости числа $\overline{Sh}$ от критерия $\overline{Re}$ при различных значениях Re', полученные для цилиндра и шара, представлены на *рисунках 5 и 6* соответ-

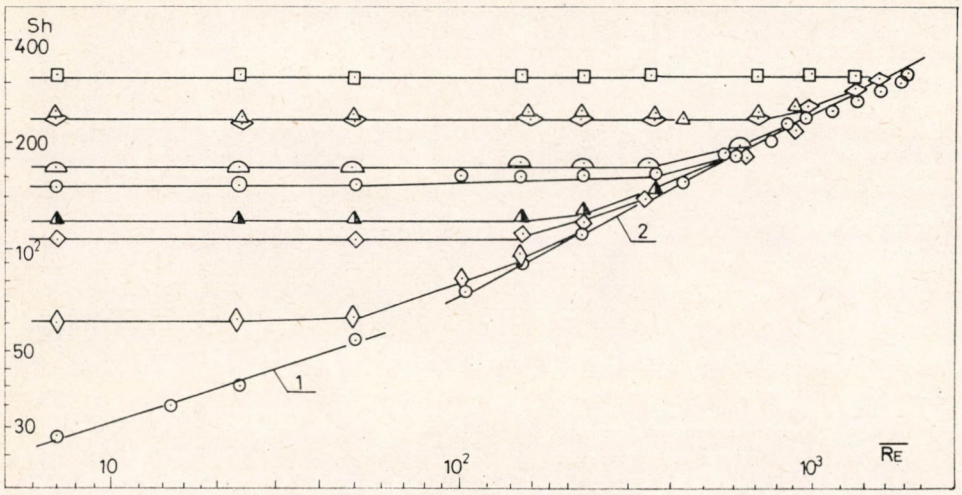

Рис. 5

Обобщенная зависимость числа $\overline{Sh}$ от $\overline{R}_E$ при различных значениях $\frac{Re'}{2\pi}$. Шар. Линии 1 и 2: асимптотические кривые, описывающиеся уравнениями (19) и (21) соответственно. Условия экспериментов:

A_x, см	0,5	0,5	1	0,5	1	0,5	1	1
Φ, сек$^{-1}$	0,6	1,8	1,4	3,8	2,86	8,4	5,3	8,8
$Re'/2\pi$	7,5	23,0	34,5	48,2	72	107	134	223
Знак	◇	◇	◭	⊙	⌓	◇	△	⊡

ственно. Нижние огибающие кривые характеризуют предельные зависимости (19) и (21). Параллельные линии для $\overline{Sh}$, принадлежащие различным значениям Re' удовлетворяют другой предельной зависимости (25).

Интересно отметить, что переход одной асимптотической зависимости числа $\overline{Sh}$ в другую происходит в очень узкой области. Уже при $Re'/\overline{Re} \gtrsim 0{,}6$, влиянием $\overline{Re}$ на число $\overline{Sh}$ можно пренебречь, и скорость массопереноса подчиняется закономерности (25). При $Re'/\overline{Re} < 0{,}6$ вступает в силу другая асимптотическая закономерность, выраженная уравнениями (19) и (21). Широкая область значений параметров $\overline{Pe}$ и Pe', при которых процесс целиком описывается с помощью простой модели типа (16), позволяет принять эту модель в качестве основной для описания процесса массопереноса в ТПС.

Как уже было отмечено выше, для решения прямой задачи расчета

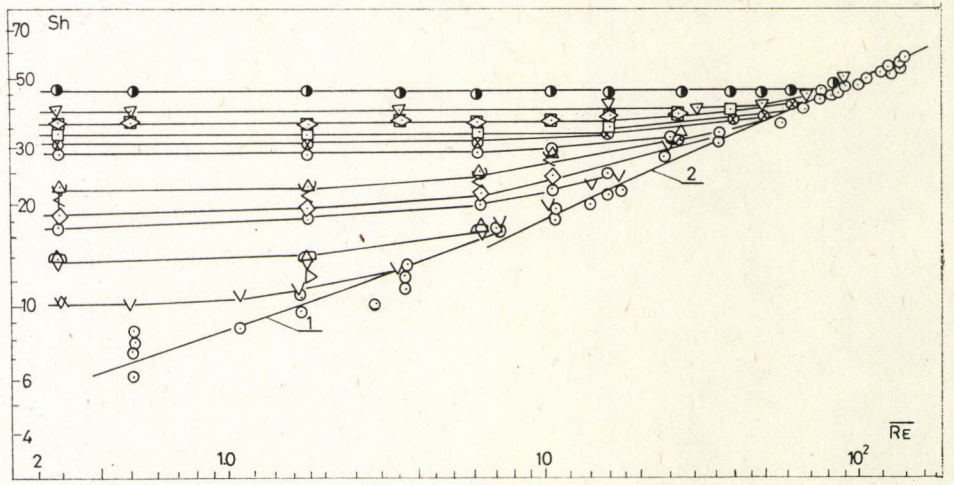

Рис. 6.

Сообщенная зависимость числа Sh от $\overline{Re}$ при различных значениях $\frac{Re'}{2\pi}$. Цилиндр. Линии 1 и 2: асимптотические кривые, описывающиеся уравнениями (19) и (21) соответственно. Условия экспериментов:

Ax, см	0,5	0,25	0,5	0,5	0,75	0,25	1	0,5	0,25	0,5	0,5	0,75	0,5	0,5	1	0,75
Φ, сек$^{-1}$	0,6	1,6	1,2	1,3	1,0	4,2	1,4	2,8	7,1	3,8	4,3	4,0	6,7	7,2	3,6	7,8
$\frac{Re'}{2\pi}$	0,55	0.76	1,14	1,24	1,43	2,0	2,6	2,7	3,4	3,6	4,1	5,7	6,4	6,9	6,9	11,1
Знак																

числа $\overline{Sh}$ с помощью выражения (25), следующим этапом эксперимента является нахождение взаимосвязи амплитудно-частотных характеристик пульсации скорости с расходными скоростями фаз и другими макроскопическими свойствами трехфазного псевдоожиженного слоя. Решению этой задачи будут посвящены следующие сообщения.

СПИСОК ОБОЗНАЧЕНИЙ

A_x — амплитуда смещения датчика
C — концентрация примеси в жидкости
C_0 — та же, на бесконечной удаленности от частицы
D_M, D_T — коэффициент молекулярной и турбулентной диффузии
Φ — частота колебания датчика
f_g — геометрическая поверхность датчика
F — число Фарадея
J — диффузионный поток массы
K_y — коэффициент усиления сигнала ($Ky=83$ для цилиндра, $Ky=83$ для шара)
L_y — расстояние по радиусу частицы
R радиус частицы (цилиндра, шара)
R_Ω — сопротивление нагрузки ($R_\Omega=500$ ом для цилиндра, $R_\Omega=100$ ом для шара)
t — время
u, v — компоненты относительной скорости u по направлениям x и y
U — относительная скорость жидкости во внешнем потоке
$\overline{V}_B$ — осредненное во времени значение напряжения электрического сигнала
x, y — координаты вдоль поверхности тела и по радиусу
$\sigma_y=L_y/R$ — параметр
ν — кинематическая вязкость раствора
$\xi=\dfrac{y-1}{\sigma_y-1}$ — безразмерная координата по толщине пограничного слоя.

СПИСОК ЛИТЕРАТУРЫ

1. Yaron I. and Gal-or B.: Int. J. Heat Mass Transf., *1971*, 14, 387.
2. Гупало Ю. П., Рязанцев Ю. С.: Прикладная математика и механика, *1971*, 35 (2).
3. Гупало Ю. П., Рязанцев Ю. С., Улин В. И.: Прикладная математика и механика, *1975*, 39 (3) 497.
4. Сергеев Ю. А.: Прикладная математика и механика *1976*, *40* (5) 892.
5. Полянин А. Д., Сергеев ЮА. А.: Прикладная математика и механика, *1977*, 41 (4) 667.
6. Brauer H.: Int. J. Heat Mass Transfer. *1978*, 21, 445.
7. Fedkiw P. and Newman: J. Chem. Eng. Sci. *1978*, 33, 1043.
8. Бурдуков А. П., Накоряков В. Е.: ПМТФ, *1969*, (2) 62.
9. Бурдуков А. П., Накоряков В. Е.: ПМТФ, *1967* (3) 198.
10. Болдарев А. М., Бурдуков А. П., Накоряков В. Е., Сосунов В. Н.: Инж. физ. Журнал, *1970*, 19, 5.
11. Болдарев А. М., Бурдуков А. П., Накоряков В. Е.: ПМТФ, *1970*, (4) 178.
12. Боголюбов Ю. Е., Гешев П. И., Михин В. А., Накоряков В. Е., Огородников И. А. В сб. „Тепло-массоперенос“, т. 1, часть 3, 291, Минск, 1972.
13. Tripathi G., Singh S. K., Upadhyay S. N.: Indian J. Technol. *1971*, 9, 285.
14. Levins D. M., Glastonbury J. R.: Chem. Eng. Sci., *1972*, 27, 537.
15. Upadhyay, S. N. and Tripathi, G.: Indian J. Technol *1972*, 10, 331.
16. Mochizuki, S. and Matsui, T.: Chem Eng. Sci. *1974*, 29, 1328.
17. Hughmark, G. A.: AICHE J. *1974*, 20, 202.
18. Lemay, Y., Pineault, G. and Ruether, J. A.: Ind. Eng. Chem. Proc. Des. Develop. *1975*, 14, 280.
19. Miyauchi, T., Matsumoto, K. and Yoshida, T.: J. Chem. Eng. Japan *1975*, 8, 228.
20. Nelson, P. A. and Galloway, T. R.: Chem. Eng. Sci. *1975*, 30, 1.
21. Rowe, P. N.: Chem. Eng. Sci. *1975*, 30, 7.
22. Tardos, G. I., Gurfinger, C. and Abuaf, N.: AICHE J. *1976*, 22, 1147.
23. Kmiec, A.: Chem. Eng. J. *1975*, 9, 221.
24. Tournie, P., Lagourie, C. and Couderc, J. P.: Chem. Eng. Sci. *1977*, 32, 1259.

25. Koloini, T., Sopcic, M. and Zumer, M.: Chem. Eng. Sci. *1977*, 32, 637.
26. Cono, J. and Böhm, U.: Chem. Eng. Sci. *1977*, 32, 213.
27. Mochizuki, S.: Chem. Eng. Sci. *1978*, 33, 623.
28. Valentin, G., Le Goff, P. and Vergness, F.: Chem. Eng. Journ. *1978*, 15, 185.
29. Specchia, V., Baldi, G. and Gianetto, A.: Ind. Eng. Chem. Proc. Des. Develop. *1978*, 17, 362.
30. Riba, J. P., Routie, R. and Couderc, J. P.: Fluidization Proc. 2 nd. Eng. Found. Conf., Cambridge *1978*, p. 157.
31. Ермакова А., Кириллов В. А., Стефогло Е. Ф., Берг Г. А.: ТОХТ, *1977*, 11, 688.
32. Евстропьева И. П., Таганов И. Н., Романков П. Г.: ТОХТ, *1972*, 6, 611.
33. Евстропьева И. П., Жуков В. Н., Таганов И. Н.: ФПХ, *1975*, 48, 1348.
34. Лойцянский Л. Г. „Механика жидкости и газа", „Наука", М., 1970.
35. Lin Sung P.: Ind. Eng. Chem. Fund., *1975*, 14, 246.
36. Стефогло Е. Ф., Ермакова А.: Хим. пром., *1974*, (5) 325.
37. Броунштейн Б. И., Фишбейн Г. А.: Гидродинамика, массо- и теплообмен в дисперсных системах. „Химия", Л., 1977.

SUMMARY

The liquid to particle turbulent mass transfer was theoretically investigated in the case of a three-phase fluidised bed. Using approximations permitted by the semiempirical theory of turbulency, a simple asymptotic dependences were obtained between the Sherwood number and the averaged and pulsation parameters. These relations were proved experimentally by measuring the diffusional current of a probe oscillated in the liquid (electrochemical method).

CONTENTS

Egyetemi Nyomda — 81.6295 Budapest, 1981. Felelős vezető: Sümeghi Zoltán igazgató

Ára: 250 Ft

THE FOLLOWING ARE PLEASED TO ACCEPT SUBSCRIPTIONS TO THIS JOURNAL:

AUSTRALIA

C.B.D. Library and Subscription Service
Box 4886 G.P.O.
Sydney 2000

Cosmos Book and Record Shop
145 Acland Street
St. Kilda 3182

Globe and Co.
694—696 George Street
Sydney 2000

AUSTRIA

Globus (VAZ)
Höchstädtplatz 3
A—1200 Wien XX

BELGIUM

"Du Monde Entier" S. A.
Rue du Midi 162
B—1000 Bruxelles

Office International de Librairie
Avenue Marnix 30
B—1050 Bruxelles

CANADA

Pannonia Books
P.O. Box 1017
Postal Station "B"
Toronto, Ontario M5T 2T8

DENMARK

Munksgaard's Boghandel
Norregade 6
DK—1165 Copenhagen K

FINLAND

Akateeminen Kirjakauppa
Keskuskatu 2, P.O.B. 128
SF—00 100 Helsinki 10

FRANCE

Office International de Documentation et Librairie
48 Rue Gay Lussac
75 Paris 5

GERMAN FEDERAL REPUBLIC

Kubon und Sagner
Pf 68
D—8 München 34
BRD

GREAT BRITAIN

Bailey Bros and Swinfen Ltd.
Warner House, Folkestone
Kent CT 19 6PH England

HOLLAND

Martinus Nijhoff
Periodicals Department
P.O. Box 269
The Hague

Swets and Zeitlinger
Keizersgracht 487
Amsterdam C

ITALY

Licosa
P.O.B. 552, Via Lamarmora 45
50121 Firenze

JAPAN

Igaku Shoin Ltd.
Foreign Department
Tokyo International P.O. Box 5063
Tokyo

Maruzen Co. Ltd.
P.O. Box 5050
Tokyo International 100—31

Nauka Ltd.
Yasutomi Bldg. 5F 2—12 Kanda
Jinbocho, Chiyoda-ku
Tokyo 101

NORWAY

Tanum—Cammermayer
Karl Johangt. 41—43
Oslo 1

SWEDEN

Almqvist and Wiksell Förlag A. B.
Box 2120
S—103 13 Stockholm 2

Wennegren—Williams AB
Subscription Department Fack
S—104 Stockholm 30

SWITZERLAND

Karger Libri A. G.
Petersgraben 31
CH—4011 Basel

USA

Ebsco Subs. Services
1 st Ave North at 13th street
Birmingham, Ala. 35201

HUNGARIAN

Journal of

INDUSTRIAL CHEMISTRY

Edited by

the Hungarian Oil & Gas Research Institute (MÁFKI),
the Research Institute for Heavy Chemical Industries (NEVIKI),
the Research Institute for Technical Chemistry of the
Hungarian Academy of Sciences (MÜKKI),
the Veszprém University of Chemical Engineering (VVE).
Veszprém (Hungary)

Volume 9. 1981 Number 3.

HU ISSN: 0133—0276
CODEN: HJICAI

The „Hungarian Journal of Industrial Chemistry" is a joint publication of the Veszprém scientific institutions of the chemical industry that deals with the results of applied and fundamental research in the field of chemical processes, unit operations and chemical engineering. The papers are published in four numbers at irregular intervals in one annual volume, in the English, Russian, French and German languages

Editorial Office:
Veszprémi Vegyipari Egyetem
„Hungarian Journal of Industrial Chemistry"
H—8201 Veszprém, P. O. Box: 28.
Hungary

Orders may be placed with
KULTURA
Foreign Trading Co. for Books and Newspapers
Budapest 62. POB 149
or with its represenatives abroad, listed on the verso of the cover

FELELŐS SZERKESZTŐ: DR. BODOR ENDRE

KIADJA A LAPKIADÓ VÁLLALAT, 1073 BP. VII., LENIN KRT. 9—11.
TELEFON: 221-285. LEVÉLCÍM: 1906 BP. PF. 223
FELELŐS KIADÓ: SIKLÓSI NORBERT IGAZGATÓ

HUNGARIAN JOURNAL
OF INDUSTRIAL CHEMISTRY
VESZPRÉM
Vol. 9. pp. 209–220 (1981)

LOGICAL STRUCTURE OF THE SYSTEM OF THE THERMODYNAMICAL MATERIAL CHARACTERISTICS. I.

G. FÁY and R. TŐRÖS

(Research Institute for Technical Chemistry of the Hungarian Academy of Sciences, Veszprém)

Received: March 23, 1981.

All the logically possible relations of the material characteristics of two variable homogeneous thermodynamic systems are algebraically calculated. The second part of paper contains the verification by which the equations were determined.

Introduction

The present paper shows which of the characteristics can be determined by the other ones, and also given the algebraic functions.

It is known for instance that:

$$\varkappa_S = \varkappa_T \frac{c_v}{c_p}$$

but it cannot be easily seen whether with the help of the characteristics c_p, c_v, $\varkappa_T$ the values

$$\alpha_S,\ \alpha_p,\ \beta_v,\ \beta_S$$

can also be determined and if so, which are the further characteristics of the same quality [1], [2]. To illustrate these results, it can be assumed that c_p, c_v, $\varkappa_T$ are values by which the following quantities can be determined in the following way, as can be seen later in the Table:

$$\alpha_p = \sqrt{\frac{\varkappa_T(c_p - c_v)}{T \cdot v}} \qquad \alpha_S = c_v \sqrt{\frac{\varkappa_T}{T \cdot v(c_p - c_v)}}$$

$$\beta_v = \frac{1}{p}\sqrt{\frac{c_p - c_v}{v \cdot T \cdot \varkappa_T}} \qquad \beta_S = \frac{c_p}{T}\sqrt{\frac{1}{T \cdot v \cdot \varkappa_T(c_p - c_v)}}$$

Not all groups of three functions chosen from the characteristics are of this quality.

Preliminary Remarks

The state of a homogeneous thermodynamic system is uniqually determined by its pressure p and its volume v. The system can also be characterized by another two variables depending on p and v: by the entropy S and the temperature T. According to the basic principles of thermodynamics, any chosen two of these variables determine the values of the remaining ones. From the variables

$$p,\ v,\ T,\ S \tag{1}$$

$\binom{4}{2} = 6$ pairs can be chosen:

$$p, v; \quad p, T; \quad p, S; \quad v, T; \quad v, S; \quad T, S. \tag{2}$$

Each of the variables in (1) can be produced with the help of the remaining variables according to the possible combinations (2) in three different ways. Therefore, twelve different functions may exist, namely:

$$\begin{aligned} &T(p, v); \quad S(p, v); \quad v(p, T); \quad S(p, T); \quad v(p, S); \quad T(p, S); \\ &p(T, S); \quad v(T, S); \quad p(v, S); \quad T(v, S); \quad p(v, T); \quad S(v, T). \end{aligned} \tag{3}$$

In the second line the inversions of the pairs of functions with two variables can be found.

If the functions in (3) have continuous second derivatives and the following relationships are valid: if $y_1(x_1, x_2)$ and $y_2(x_1, x_2)$ are any chosen two functions of the functions in (3) and

$$D \equiv \frac{\partial(y_1, y_2)}{\partial(x_1, x_2)} \neq 0$$

then the inverse system exists:

$$x_1(y_1, y_2); \quad x_2(y_1, y_2) \tag{4}$$

and

$$\begin{aligned} &\left(\frac{\partial x_1}{\partial y_1}\right)_{y_2} = \frac{1}{D}\left(\frac{\partial y_2}{\partial x_2}\right)_{x_1}; \qquad \left(\frac{\partial x_1}{\partial y_2}\right)_{y_1} = -\frac{1}{D}\left(\frac{\partial y_1}{\partial x_2}\right)_{x_1} \\ &\left(\frac{\partial x_2}{\partial y_1}\right)_{y_2} = -\frac{1}{D}\left(\frac{\partial y_2}{\partial x_1}\right)_{x_2}; \qquad \left(\frac{\partial x_2}{\partial y_2}\right)_{y_1} = \frac{1}{D}\left(\frac{\partial y_1}{\partial x_1}\right)_{x_2} \end{aligned} \tag{5}$$

where the indices show the other variables and

$$D = \frac{\partial(y_1, y_2)}{\partial(x_1, x_2)} = \begin{vmatrix} \left(\frac{\partial y_1}{\partial x_1}\right)_{x_2} & \left(\frac{\partial y_2}{\partial x_2}\right)_{x_1} \\ \left(\frac{\partial y_2}{\partial x_1}\right)_{x_2} & \left(\frac{\partial y_1}{\partial x_2}\right)_{x_1} \end{vmatrix} \tag{6}$$

is the *Jacobian* of the functions y_1, y_2.

For experimental reasons the following derivatives of the functions in (3) are distinguished, because it is possible to directly measure them, and they are frequently constants. These are called thermodynamic material characteristics and are the following:

$$
\begin{aligned}
c_p &= T\left(\frac{\partial S}{\partial T}\right)_p & \beta_v &= \frac{1}{p}\left(\frac{\partial p}{\partial T}\right)_v \\
c_v &= T\left(\frac{\partial S}{\partial T}\right)_v & \beta_S &= \frac{1}{p}\left(\frac{\partial p}{\partial T}\right)_S \\
\alpha_p &= \frac{1}{v}\left(\frac{\partial v}{\partial T}\right)_p & -\varkappa_T &= \frac{1}{v}\left(\frac{\partial v}{\partial p}\right)_T \\
\alpha_S &= \frac{1}{v}\left(\frac{\partial v}{\partial T}\right)_S & -\varkappa_S &= \frac{1}{v}\left(\frac{\partial v}{\partial p}\right)_S
\end{aligned}
\tag{7}
$$

The next study shows all the possible relationships between them.

With the assistance of those groups of three functions, the further five characteristics (7) can be expressed, which will henceforth be called the *basis*. To give an example a basis was shown in the first part. Many types of baiss are possible and not every group of three functions is a basis. For example:

$$\alpha_S \quad \beta_S \quad \varkappa_S$$

do not form a basis, and later it will be shown why not.

This paper contains every basis and all those groups of functions which do not form a basis. (7) is called the total system of material characteristics, while the individual characteristics are called the *members* of the system.

In order to show the connections between the characteristics the following facts have to be proved.

Thesis

1. Every basis consists of three members.
2. Every system of three members forms a basis, except:

$$c_p,\ \alpha_p,\ \beta_S$$

$$v_v,\ \alpha_S,\ \beta_v$$

$$\alpha_p,\ \beta_v,\ \varkappa_T$$

$$\alpha_S,\ \beta_S,\ \varkappa_S.$$

3. In each exception mentioned in 2. there exists an invertible relationship of functions between the members of the group.
4. A compendium of formulas gives all the possible algebraic interconnections.

The order of succession of the characteristics is the following:

$$c_p,\ c_v,\ \alpha_p,\ \alpha_S,\ \beta_v,\ \beta_S,\ \varkappa_T,\ \varkappa_S$$

The basis of three members are shown in lexigraphic order:

$c_p c_v \alpha_p$	$\alpha_S = \alpha_p \dfrac{c_v}{c_p - c_v}$	$\beta_v = \dfrac{c_p - c_v}{pvT\alpha_p}$
$c_p c_v \alpha_S$	$\alpha_p = \alpha_S \dfrac{c_p - c_v}{c_v}$	$\beta_v = \dfrac{c_v}{pvT\alpha_S}$
$c_p c_v \beta_v$	$\alpha_p = \dfrac{c_p - c_v}{pvT\beta_v}$	$\alpha_S = \dfrac{c_v}{pvT\beta_v}$
$c_p c_v \beta_S$	$\alpha_p = \dfrac{c_p}{pvT\beta_S}$	$\alpha_S = \dfrac{c_p c_v}{pvT\beta_S(c_p - c_v)}$
$c_p c_v \varkappa_T$	$\alpha_p = \sqrt{\dfrac{\varkappa_T(c_p - c_v)}{vT}}$	$\alpha_S = c_v \sqrt{\dfrac{\varkappa_T}{vT(c_p - c_v)}}$
$c_p c_v \varkappa_S$	$\alpha_p = \sqrt{\dfrac{\varkappa_S c_p (c_p - c_v)}{vT c_v}}$	$\alpha_S = \sqrt{\dfrac{c_p c_v \varkappa_S}{vT(c_p - c_v)}}$
$c_p \alpha_p \alpha_S$	$c_v = c_p \dfrac{\alpha_S}{\alpha_p + \alpha_S}$	$\beta_v = \dfrac{c_p}{pvT(\alpha_p + \alpha_S)}$
$c_p \alpha_p \beta_v$	$c_v = c_p - pvT\alpha_p\beta_v$	$\alpha_S = \alpha_p \left(\dfrac{c_p}{pvT\alpha_p\beta_v} - 1 \right)$
$c_p \alpha_p \beta_S$ not *basis*		$c_p = pvT\alpha_p\beta_S$
$c_p \alpha_p \varkappa_T$	$c_v = c_p - \dfrac{\alpha_p^2 vT}{\varkappa_T}$	$\alpha_S = \dfrac{c_p \varkappa_T}{vT\alpha_p} - \alpha_p$
$c_p \alpha_p \varkappa_S$	$c_v = \dfrac{c_p}{1 + \dfrac{vT\alpha_p^2}{c_p \varkappa_S}}$	$\alpha_S = \dfrac{c_p \varkappa_S}{vT\alpha_p}$
$c_p \alpha_S \beta_v$	$c_v = pvT \cdot \alpha_S \beta_v$	$\alpha_p = \alpha_S \left(\dfrac{c_p}{pvT\alpha_S\beta_v} - 1 \right)$
$c_p \alpha_S \beta_S$	$c_v = \dfrac{c_p}{1 + \dfrac{c_p}{pvT\alpha_S\beta_S}}$	$\alpha_p = \dfrac{c_p}{pvT\beta_S}$
$c_p \alpha_S \varkappa_v$	$c_v = \dfrac{vT\alpha_S}{\varkappa_T} \left(-\dfrac{\alpha_S}{2} + \sqrt{\left(\dfrac{\alpha_S}{2}\right)^2 + \dfrac{c_p \varkappa_T}{vT}} \right)$	$\alpha_p = -\dfrac{\alpha_S}{2} + \sqrt{\left(\dfrac{\alpha_S}{2}\right)^2 + \dfrac{c_p \varkappa_T}{vT}}$
$c_p \alpha_S \varkappa_S$	$c_v = \dfrac{c_p}{1 + \dfrac{c_p \varkappa_S}{vT\alpha_S^2}}$	$\alpha_p = \dfrac{c_p \varkappa_S}{vT\alpha_S}$

$\beta_S = \dfrac{c_p}{pvT\alpha_p}$	$\varkappa_T = \dfrac{\alpha_p^2 vT}{c_p - c_v}$	$\varkappa_S = \dfrac{\alpha_p^2 vT}{c_p - c_v}\dfrac{c_v}{c_p}$
$\beta_S = \dfrac{1}{pvT\alpha_S\left(\dfrac{1}{c_v} - \dfrac{1}{c_p}\right)}$	$\varkappa_T = \dfrac{\alpha_S^2(c_p - c_v)vT}{c_v^2}$	$\varkappa_S = vT\alpha_S^2\left(\dfrac{1}{c_v} - \dfrac{1}{c_p}\right)$
$\beta_S = \dfrac{c_p}{c_p - c_v}\beta_v$	$\varkappa_T = \dfrac{c_p - c_v}{p^2 vT\beta_v^2}$	$\varkappa_S = \dfrac{c_p - c_v}{p^2 vT\beta_v^2}\dfrac{c_v}{c_p}$
$\beta_v = \beta_S\dfrac{c_p - c_v}{c_p}$	$\varkappa_T = \dfrac{c_p^2}{p^2 vT\beta_S^2(c_p - c_v)}$	$\varkappa_S = \dfrac{c_p c_v}{p^2 vT\beta_S^2(c_p - c_v)}$
$\beta_v = \dfrac{1}{p}\sqrt{\dfrac{c_p - c_v}{vT\varkappa_T}}$	$\beta_S = \dfrac{c_p}{p\sqrt{vT\varkappa_T(c_p - c_v)}}$	$\varkappa_S = \varkappa_T\dfrac{c_v}{c_p}$
$\beta_v = \dfrac{1}{p}\sqrt{\dfrac{c_v(c_p - c_v)}{vTc_p\varkappa_S}}$	$\beta_S = \dfrac{1}{p}\sqrt{\dfrac{c_p c_v}{vT\varkappa_S(c_p - c_v)}}$	$\varkappa_T = \varkappa_S\dfrac{c_p}{c_v}$
$\beta_S = \dfrac{c_p}{pvT\alpha_p}$	$\varkappa_T = \dfrac{vT}{c_p}\alpha_p(\alpha_p + \alpha_S)$	$\varkappa_S = \dfrac{vT}{c_p}\alpha_p\alpha_S$
$\beta_S = \dfrac{c_p}{pvT\alpha_p}$	$\varkappa_T = \dfrac{\alpha_p}{p\beta_v}$	$\varkappa_S = \dfrac{\alpha_p}{p\beta_v} - \dfrac{vT\alpha_p^2}{c_p}$
$\beta_v = \dfrac{\alpha_p}{p\varkappa_T}$	$\beta_S = \dfrac{c_p}{vpT\alpha_p}$	$\varkappa_S = \varkappa_T - \dfrac{vT\alpha_p^2}{c_p}$
$\beta_v = \dfrac{c_p\alpha_p}{pc_p\varkappa_S + pvT\alpha_p^2}$	$\beta_S = \dfrac{c_p}{pvT\alpha_p}$	$\varkappa_T = \varkappa_S\left(1 + \dfrac{vT\alpha_p^2}{c_p\varkappa_S}\right)$
$\beta_S = \dfrac{\beta_v}{1 - \dfrac{pvT\alpha_S\beta_v}{c_p}}$	$\varkappa_T = \dfrac{c_p}{p^2 vT\beta_v^2} - \dfrac{\alpha_S}{p\beta_v}$	$\varkappa_S = \dfrac{\alpha_S}{p\beta_v} - \dfrac{vT\alpha_S^2}{c_p}$
$\beta_v = \beta_S\dfrac{c_p}{c_p + pvT\alpha_S\beta_S}$	$\varkappa_T = \dfrac{c_p + pvT\alpha_S\beta_S}{p^2 vT\beta_S^2}$	$\varkappa_S = \dfrac{\alpha_S}{p\beta_S}$
$\beta_v = \dfrac{-\dfrac{\alpha_S}{2} + \sqrt{\left(\dfrac{\alpha_S}{2}\right)^2 + \dfrac{c_p\varkappa_T}{vT}}}{p\varkappa_T}$	$\beta_S = \dfrac{c_p}{pvT\left(-\dfrac{\alpha_S}{2} + \sqrt{\left(\dfrac{\alpha_S}{2}\right)^2 + \dfrac{c_p\varkappa_T}{vT}}\right)}$	$\varkappa_S = \dfrac{vT\alpha_S}{c_p}\left(-\dfrac{\alpha_S}{2} + \sqrt{\left(\dfrac{\alpha_S}{2}\right)^2 + \dfrac{c_p\varkappa_T}{vT}}\right)$
$\beta_v = \dfrac{c_p\alpha_S}{pvT\alpha_S^2 + pc_p\varkappa_S}$	$\beta_S = \dfrac{\alpha_S}{p\varkappa_S}$	$\varkappa_T = \varkappa_S\left(1 + \dfrac{c_p\varkappa_S}{vT\alpha_S^2}\right)$

$c_p\beta_v\beta_s$	$c_v = c_p\,\dfrac{\beta_S-\beta_v}{\beta_v}$	$\alpha_p = \dfrac{c_p}{pvT\beta_S}$
$v_p\beta_v\varkappa_T$	$c_v = c_p - p^2vT\beta_v^2\varkappa_T$	$\alpha_p = p\beta_v\varkappa_T$
$c_p\beta_v\varkappa_S$	$c_v = \dfrac{c_p}{\dfrac{c_p}{2p^2vT\beta_S^2\varkappa_S}+\sqrt{\left(\dfrac{c_p}{2p^2vT\beta_S^2\varkappa_S}\right)^2-\dfrac{c_p}{p^2vT\beta_S^2\varkappa_S}}}$	$\alpha_p = \dfrac{c_p}{pvT}\left(\dfrac{1}{2\beta_v}+\sqrt{\left(\dfrac{1}{2\beta_v}\right)^2-\dfrac{p^2vT\varkappa_S}{c_p}}\right)$
$c_p\beta_S\varkappa_T$	$c_v = c_p - \dfrac{c_p^2}{p^2vT\beta_S^2\varkappa_T}$	$\alpha_p = \dfrac{c_p}{pvT\beta_S}$
$c_p\beta_S\varkappa_S$	$c_v = \dfrac{c_p}{1+\dfrac{c_p}{p^2vT\beta_S^2\varkappa_S}}$	$\alpha_p = \dfrac{c_p}{pvT\beta_S}$
$c_p\varkappa_T\varkappa_S$	$c_v = c_p\,\dfrac{\varkappa_S}{\varkappa_T}$	$\alpha_p = \sqrt{\dfrac{c_p(\varkappa_T-\varkappa_S)}{vT}}$
$c_v\alpha_p\alpha_S$	$c_p = c_v\,\dfrac{\alpha_S+\alpha_p}{\alpha_S}$	$\beta_v = \dfrac{c_v}{pvT\alpha_S}$
$c_v\alpha_p\beta_v$	$c_p = c_v + pvT\alpha_p\beta_v$	$\alpha_S = \dfrac{c_v}{pvT\beta_v}$
$c_v\alpha_p\beta_S$	$c_p = pvT\alpha_p\beta_S$	$\alpha_S = \dfrac{\alpha_p}{\dfrac{pvT\alpha_p\beta_S}{c_v}-1}$
$c_v\alpha_p\varkappa_T$	$c_p = c_v + \dfrac{vT\alpha_p^2}{\varkappa_T}$	$\alpha_S = \dfrac{c_v\varkappa_T}{vT\alpha_p}$
$c_v\alpha_p\varkappa_S$	$c_p = \dfrac{c_v}{-\dfrac{c_v\varkappa_S}{2vT\alpha_p^2}+\sqrt{\left(\dfrac{c_v\varkappa_S}{2vT\alpha_p^2}\right)^2+\dfrac{c_v\varkappa_S}{vT\alpha_p^2}}}$	$\alpha_S = \dfrac{1}{-\dfrac{1}{2\alpha_p}+\sqrt{\left(\dfrac{1}{2\alpha_p}\right)^2+\dfrac{vT}{c_v\varkappa_S}}}$
$c_v\alpha_S\beta_v$ not basis	$c_v = pvT\alpha_S\beta_v$	
$c_v\alpha_S\beta_S$	$c_p = \dfrac{c_v}{1-\dfrac{c_v}{pvT\alpha_S\beta_S}}$	$\alpha_p = \dfrac{\alpha_S}{\dfrac{pvT\alpha_S\beta_S}{c_v}-1}$

$\alpha_S = \frac{c_p}{pvT} \frac{\beta_S - \beta_v}{\beta_S \beta_v}$	$\varkappa_T = \frac{c_p}{p^2 vT \beta_S^2}$	$\varkappa_S = \frac{c_p}{p^2 vT} \frac{\beta_S - \beta_v}{\beta_S^2 \beta_v}$
$\alpha_S = \frac{c_p}{pvT\beta_v} - p\beta_v \varkappa_T$	$\beta_S = \frac{c_p}{p^2 vT \beta_v \varkappa_T}$	$\varkappa_S = \varkappa_T - \frac{p^2 vT \beta_v^2 \varkappa_T^2}{c_p}$
$\alpha_S = = \frac{p\varkappa_S}{\frac{1}{2\beta_v} + \sqrt{\left(\frac{1}{2\beta_v}\right)^2 - \frac{p^2 vT \varkappa_S}{c_p}}}$	$\beta_S = \frac{1}{\frac{1}{2\beta_v} + \sqrt{\left(\frac{1}{2\beta_v}\right)^2 - \frac{p^2 vT \varkappa_S}{c_p}}}$	$\varkappa_T = \varkappa_S \left(\frac{c_p}{2p^2 vT \beta_S^2 \varkappa_S}\right) + + \sqrt{\left(\frac{c_p}{2p^2 vT \beta_S^2 \varkappa_S}\right)^2 - \frac{c_p}{p^2 vT \beta_S^2 \varkappa_S}}$
$\alpha_S = p\beta_S \varkappa_T - \frac{c_p}{pvT\beta_S}$	$\beta_v = \frac{c_p}{p^2 vT \beta_S \varkappa_T}$	$\varkappa_S = \varkappa_T - \frac{c_p}{p^2 vT \beta_S^2}$
$\alpha_S = p\beta_S \varkappa_S$	$\beta_v = \frac{\beta_S}{1 + \frac{p^2 vT \beta_S^2 \varkappa_S}{c_p}}$	$\varkappa_T = \varkappa_S \left(1 + \frac{c_p}{p^2 vT \beta_S^2 \varkappa_S}\right)$
$\alpha_S = \varkappa_S \sqrt{\frac{c_p}{vT(\varkappa_T - \varkappa_S)}}$	$\beta_v = \frac{1}{p\varkappa_T} \sqrt{\frac{c_p(\varkappa_T - \varkappa_S)}{vT}}$	$\beta_S = \frac{1}{p} \sqrt{\frac{c_p}{vT(\varkappa_T - \varkappa_S)}}$
$\beta_S = \frac{c_v}{pvT} \left(\frac{1}{\alpha_S} + \frac{1}{\alpha_p}\right)$	$\varkappa_T = \frac{vT\alpha_p \alpha_S}{c_v}$	$\varkappa_S = \frac{vT\alpha_S}{c_v \left(\frac{1}{\alpha_S} + \frac{1}{\alpha_p}\right)}$
$\beta_S = \beta_v + \frac{c_v}{pvT\alpha_p}$	$\varkappa_T = \frac{\alpha_p}{p\beta_v}$	$\varkappa_S = \frac{\alpha_p c_v}{pc_v\beta_v + p^2 vT\alpha\beta_v^2}$
$\beta_v = \beta_S - \frac{c_v}{pvT\alpha_p}$	$\varkappa_T = \frac{vT\alpha_p^2}{pvT\alpha_p\beta_S - c_v}$	$\varkappa_S = \frac{\alpha_p}{\frac{p^2 vT \alpha_p \beta_S^2}{c_v} - p\beta_S}$
$\beta_v = \frac{\alpha_p}{p\varkappa_T}$	$\beta_S = \frac{\alpha_p}{p\varkappa_T} + \frac{c_v}{pvT\alpha_p}$	$\varkappa_S = \frac{1}{\frac{1}{\varkappa_T} + \frac{vT\alpha_p^2}{c_v \varkappa_T^2}}$
$\beta_v = \frac{c_v}{pvT} \left(-\frac{1}{2\alpha_p} + + \sqrt{\left(\frac{1}{2\alpha_p}\right)^2 + \frac{vT}{c_v \varkappa_S}}\right)$	$\beta_S = = \frac{1}{\varkappa_S p \left(-\frac{1}{2\alpha_p} + \sqrt{\left(\frac{1}{2\alpha_p}\right)^2 + \frac{vT}{c_v \varkappa_S}}\right)}$	$\varkappa_T = = \frac{\varkappa_S}{-\frac{c_v \varkappa_S}{2vT\alpha_p^2} + \sqrt{\left(\frac{c_v \varkappa_S}{2vT\alpha_p^2}\right)^2 + \frac{c_v \varkappa_S}{vT\alpha_p}}}$

$\beta_v = \frac{c_v}{pvT\alpha_S}$	$\varkappa_T = \frac{vT\alpha_S^2}{pvT\alpha_S\beta_S - c_v}$	$\varkappa_S = \frac{\alpha_S}{p\beta_S}$

$c_v \alpha_S \varkappa_T$	$c_p = c_v + \frac{c_v^2 \varkappa_T}{vT\alpha_S^2}$	$\alpha_p = \frac{c_v \varkappa_T}{vT\alpha_S}$
$c_v \alpha_S \varkappa_S$	$c_p = \frac{c_v}{1 - \frac{c_v \varkappa_S}{vT\alpha_S^2}}$	$\alpha_p = \frac{\alpha_S}{\frac{vT\alpha_S^2}{c_v \varkappa_S} - 1}$
$c_v \beta_v \beta_S$	$c_p = \frac{c_v \beta_S}{\beta_S - \beta_v}$	$\alpha_p = \frac{c_v}{pvT(\beta_S - \beta_v)}$
$c_v \beta_v \varkappa_T$	$c_p = c_v + p^2 vT \beta_v^2 \varkappa_T$	$\alpha_p = p \beta_v \varkappa_T$
$c_v \beta_v \varkappa_S$	$c_p = \frac{c_v}{1 - \frac{p^2 vT \beta_v^2 \varkappa_S}{c_v}}$	$\alpha_p = \frac{p c_v \beta_v \varkappa_S}{c_v - p^2 vT \beta_v^2 \varkappa_S}$
$c_v \beta_S \varkappa_T$	$c_p = p^2 vT \beta_S \varkappa_T \left(\frac{\beta_S}{2} + \sqrt{\left(\frac{\beta_S}{2}\right)^2 - \frac{c_v}{p^2 vT \varkappa_T}} \right)$	$\alpha_p = p \varkappa_T \left(\frac{\beta_S}{2} + \sqrt{\left(\frac{\beta_S}{2}\right)^2 - \frac{c_v}{p^2 vT \varkappa_T}} \right)$
$c_v \beta_S \varkappa_S$	$c_p = \frac{c_v}{1 - \frac{c_v}{p^2 vT \beta_S^p \varkappa_S}}$	$\alpha_p = \frac{p c_v \beta_S \varkappa_S}{p^2 vT \beta_S^2 \varkappa_S - c_v}$
$c_v \varkappa_T \varkappa_S$	$c_p = c_v \frac{\varkappa_T}{\varkappa_S}$	$\alpha_p = \varkappa_T \sqrt{\frac{c_v}{vT} \left(\frac{1}{\varkappa_S} - \frac{1}{\varkappa_T} \right)}$
$\alpha_p \alpha_S \beta_v$	$c_p = pvT \beta_v (\alpha_p + \alpha_v)$	$c_v = pvT \alpha_S \beta_v$
$\alpha_p \alpha_S \beta_S$	$c_p = pvT \alpha_p \beta_S$	$c_v = pvT \beta_S \frac{\alpha_p \alpha_S}{\alpha_p + \alpha_S}$
$\alpha_p \alpha_S \varkappa_T$	$c_p = \frac{vT}{\varkappa_T} \alpha_p (\alpha_p + \alpha_S)$	$c_v = \frac{vT}{\varkappa_T} \alpha_p \alpha_S$
$\alpha_p \alpha_S \varkappa_S$	$c_p = \frac{vT}{\varkappa_S} \alpha_p \alpha_S$	$c_v = \frac{vT}{\varkappa_S} \frac{\alpha_p \alpha_S^2}{\alpha_p + \alpha_S}$
$\alpha_p \beta_v \beta_S$	$c_p = pvT \alpha_p \beta_S$	$c_v = pvT \alpha_p (\beta_S - \beta_v)$
$\alpha_p \beta_v \varkappa_T$ not basis	$\alpha_p = p \beta_v \varkappa_T$	

$\beta_v = \dfrac{c_v}{pvT\alpha_S}$	$\beta_S = \dfrac{c_v}{pvT\alpha_S} + \dfrac{\alpha_S}{p\varkappa_T}$	$\varkappa_S = \dfrac{1}{\dfrac{1}{\varkappa_T} + \dfrac{c_v}{vT\alpha_S^2}}$
$\beta_v = \dfrac{c_v}{pvT\alpha_v}$	$\beta_S = \dfrac{\alpha_S}{p\varkappa_S}$	$\varkappa_T = \dfrac{\varkappa_S}{1 - \dfrac{c_v\varkappa_S}{vT\alpha_S^2}}$
$\alpha_S = \dfrac{c_v}{pvT\beta_v}$	$\varkappa_T = \dfrac{c_v}{p^2vT\beta_v(\beta_S - \beta_v)}$	$\varkappa_S = \dfrac{c_v}{p^2vT\beta_v\beta_S}$
$\alpha_S = \dfrac{c_v}{pvT\beta_v}$	$\beta_S = \beta_v + \dfrac{c_v}{p^2vT\beta_v\varkappa_T}$	$\varkappa_S = \dfrac{\varkappa_T}{1 + \dfrac{p^2vT\beta_v^2\varkappa_T}{c_v}}$
$\alpha_S = \dfrac{c_v}{pvT\beta_v}$	$\beta_S = \dfrac{c_v}{p^2vT\beta_v\varkappa_S}$	$\varkappa_T = \dfrac{\varkappa_S}{1 - \dfrac{p^2vT\beta_v^2\varkappa_S}{c_v}}$
$\alpha_S = \dfrac{c_v}{pvT\left(\dfrac{\beta_S}{2} + \sqrt{\left(\dfrac{\beta_S}{2}\right)^2 - \dfrac{c_v}{p^2vT\varkappa_T}}\right)}$	$\beta_v = \dfrac{\beta_S}{2} + \sqrt{\left(\dfrac{\beta_S}{2}\right)^2 - \dfrac{c_v}{p^2vT\varkappa_T}}$	$\varkappa_S = \dfrac{c_v}{p^2vT\beta_S\left(\dfrac{\beta_S}{2} + \sqrt{\left(\dfrac{\beta_S}{2}\right)^2 - \dfrac{c_v}{p^2vT\varkappa_T}}\right)}$
$\alpha_S = p\beta_S\varkappa_S$	$\beta_v = \dfrac{c_v}{p^2vT\beta_S\varkappa_S}$	$\varkappa_T = \dfrac{\varkappa_S}{1 - \dfrac{c_v}{p^2vT\beta_S^2\varkappa_S}}$
$\alpha_S = \sqrt{\dfrac{c_v}{vT}\,\dfrac{\varkappa_T\varkappa_S}{\varkappa_T - \varkappa_S}}$	$\beta_v = \dfrac{1}{p}\sqrt{\dfrac{c_v}{vT}\left(\dfrac{1}{\varkappa_S} - \dfrac{1}{\varkappa_T}\right)}$	$\beta_S = \dfrac{1}{p\varkappa_S}\sqrt{\dfrac{c_v}{vT}\,\dfrac{\varkappa_T\varkappa_S}{\varkappa_T - \varkappa_S}}$
$\beta_S = \beta_v\left(1 + \dfrac{\alpha_S}{\alpha_p}\right)$	$\varkappa_T = \dfrac{\alpha_p}{p\beta_v}$	$\varkappa_S = \dfrac{\alpha_p\alpha_S}{p\beta_v(\alpha_S + \alpha_p)}$
$\beta_v = \dfrac{\alpha_p\beta_S}{\alpha_p + \alpha_S}$	$\varkappa_T = \dfrac{\alpha_p + \alpha}{p\beta_S}$	$\varkappa_S = \dfrac{\alpha_S}{p\beta_S}$
$\beta_v = \dfrac{\alpha_p}{p\varkappa_T}$	$\beta_S = \dfrac{\alpha_p + \alpha_S}{p\varkappa_T}$	$\varkappa_S = \dfrac{\alpha_S\varkappa_T}{\alpha_p + \alpha_S}$
$\beta_v = \dfrac{\varkappa_S}{p}\,\dfrac{\alpha_p\alpha_S}{\alpha_p + \alpha_S}$	$\beta_S = \dfrac{\varkappa_S}{p}\,\alpha_S$	$\varkappa_T = \varkappa_S\,\dfrac{\alpha_p + \alpha_S}{\alpha_S}$
$\alpha_S = \alpha_p\left(1 - \dfrac{\beta_S}{\beta_v}\right)$	$\varkappa_T = \dfrac{\alpha_p}{p\beta_v}$	$\varkappa_S = \dfrac{\alpha_p}{p}\left(\dfrac{1}{\beta_v} - \dfrac{1}{\beta_S}\right)$

$\alpha_p\beta_v\varkappa_S$	$c_p = \dfrac{pvT\alpha_p^2\beta_v}{\alpha_p - p\beta_v\varkappa_S}$	$c_v = \dfrac{p^2vT\alpha_p\beta_v^2\varkappa_S}{\alpha_p - p\beta_v\varkappa_S}$
$\alpha_p\beta_S\varkappa_T$	$c_p = pvT\alpha_p\beta_S$	$c_v = \dfrac{vT\alpha_p}{\varkappa_T}(p\beta_S\varkappa_T - \alpha_p)$
$\alpha_p\beta_S\varkappa_S$	$c_p = pvT\alpha_p\beta_S$	$c_v = \dfrac{pvT\alpha_p\beta_S}{1 + \dfrac{\alpha_p}{p\beta_S\varkappa_S}}$
$\alpha_p\varkappa_T\varkappa_S$	$c_p = \dfrac{vT\alpha_p^2}{\varkappa_T - \varkappa_S}$	$c_v = \dfrac{vT\alpha_p^2}{\varkappa_T - \varkappa_S}\dfrac{\varkappa_S}{\varkappa_T}$
$\alpha_S\beta_v\beta_S$	$c_p = pvT\alpha_S\dfrac{\beta_S\beta_v}{\beta_S - \beta_v}$	$c_v = pvT\alpha_S\beta_v$
$\alpha_S\beta_v\varkappa_T$	$c_p = pvT\alpha_S\beta_v + p^2vT\beta_v^2\varkappa_T$	$c_v = pvT\alpha_S\beta_v$
$\alpha_S\beta_v\varkappa_S$	$c_p = \dfrac{pvT\alpha_S^2\beta_v}{\alpha_S - p\beta_v\varkappa_S}$	$c_v = pvT\alpha_S\beta_v$
$\alpha_S\beta_S\varkappa_T$	$c_p = pvT\beta_S(p\beta_S\varkappa_T - \alpha_S)$	$c_v = vT\alpha_S\left(p\beta_S - \dfrac{\alpha_S}{\varkappa_T}\right)$
$\alpha_S\beta_S\varkappa_S$ not basis	$\alpha_S = p\beta_S\varkappa_S$	
$\alpha_S\varkappa_T\varkappa_S$	$c_p = \dfrac{vT\alpha_S^2(\varkappa_T - \varkappa_S)}{\varkappa_S^2}$	$c_v = vT\alpha_S^2\dfrac{\varkappa_T - \varkappa_S}{\varkappa_T\varkappa_S}$
$\beta_v\beta_S\varkappa_T$	$c_p = p^2vT\beta_v\beta_S\varkappa_T$	$c_v = p^2vT\beta_v(\beta_S - \beta_v)\varkappa_T$
$\beta_v\beta_S\varkappa_S$	$c_p = p^2vT\beta_S\varkappa_S\dfrac{\beta_S\beta_v}{\beta_S - \beta_v}$	$c_v = p^2vT\beta_S^2\varkappa_S$
$\beta_v\varkappa_T\varkappa_S$	$c_p = p^2vT\beta_v^2\dfrac{\varkappa_S^2}{\varkappa_T - \varkappa_S}$	$c_v = p^2vT\beta_v^2\dfrac{\varkappa_T\varkappa_S}{\varkappa_T - \varkappa_S}$
$\beta_S\varkappa_T\varkappa_S$	$c_p = p^2vT\beta_S^2(\varkappa_T - \varkappa_S)$	$c_v = p^2vT\beta\varkappa_S\dfrac{\varkappa_T - \varkappa_S}{\varkappa_T}$

$\alpha_S = \dfrac{\alpha_p}{\dfrac{\alpha_p}{p\beta_v\varkappa_S} - 1}$	$\beta_S = \dfrac{\beta_v}{1 - \dfrac{p\beta_v\varkappa_S}{\alpha_p}}$	$\varkappa_T = \dfrac{\alpha_p}{p\beta_v}$
$\alpha_S = p\beta_S\varkappa_T - \alpha_p$	$\beta_v = \dfrac{\alpha}{p\varkappa_T}$	$\varkappa_S = \varkappa_T - \dfrac{\alpha_p}{p\beta_S}$
$\alpha_S = p\beta_S\varkappa_S$	$\beta_v = \dfrac{\beta_S}{1 + \dfrac{p\beta_S\varkappa_S}{\alpha_p}}$	$\varkappa_T = \varkappa_S + \dfrac{\alpha_p}{p\beta_S}$
$\alpha_S = \dfrac{\alpha_p\varkappa_S}{\varkappa_T - \varkappa_S}$	$\beta_v = \dfrac{\alpha_p}{p\varkappa_T}$	$\beta_S = \dfrac{\alpha_p}{p(\varkappa_T - \varkappa_S)}$
$\alpha_p = \dfrac{\alpha_S\beta_v}{\beta_S - \beta_v}$	$\varkappa_T = \dfrac{\alpha_S}{p(\beta_S - \beta_v)}$	$\varkappa_S = \dfrac{\alpha_S}{p\beta_S}$
$\alpha_p = p\beta_v\varkappa_T$	$\beta_S = \beta_v + \dfrac{\alpha_S}{p\varkappa_T}$	$\varkappa_S = \dfrac{\varkappa_T}{1 + \dfrac{p\beta_v\varkappa_T}{\alpha_S}}$
$\alpha_p = \dfrac{\alpha_S}{\dfrac{\alpha_S}{p\beta_S\varkappa_S} - 1}$	$\beta_S = \dfrac{\alpha_S}{p\varkappa_S}$	$\varkappa_T = \dfrac{\varkappa_S}{1 - \dfrac{p\beta_v\varkappa_S}{\alpha_S}}$
$\alpha_p = p\beta_S\varkappa_T - \alpha_S$	$\beta_v = \beta_S - \dfrac{\alpha_S}{p\varkappa_T}$	$\varkappa_S = \dfrac{\alpha_S}{p\beta_S}$

$\alpha_p = \alpha_S \dfrac{\varkappa_T - \varkappa_S}{\varkappa_S}$	$\beta_v = \dfrac{\alpha_S(\varkappa_T - \varkappa_S)}{p\varkappa_T\varkappa_T}$	$\beta_S = \dfrac{\alpha_s}{p\varkappa_S}$
$\alpha_p = p\beta_v\varkappa_T$	$\alpha_S = p(\beta_S - \beta_v)\varkappa_T$	$\varkappa_S = \varkappa_T\left(1 - \dfrac{\beta_v}{\beta_S}\right)$
$\alpha_p = \dfrac{p\beta_v\beta_S\varkappa_S}{\beta_S - \beta_v}$	$\alpha_S = p\beta_S\varkappa_S$	$\varkappa_T = \varkappa_S \dfrac{\beta_v}{\beta_S - \beta_v}$
$\alpha_p = p\beta_v\varkappa_T$	$\alpha_S = p\beta_v \dfrac{\varkappa_T\varkappa_S}{\varkappa_T - \varkappa_S}$	$\beta_S = \beta_v \dfrac{\varkappa_T}{\varkappa_T - \varkappa_S}$
$\alpha_p = p\beta_S(\varkappa_T - \varkappa_S)$	$\alpha_S = p\beta_S\varkappa_S$	$\beta_v = \beta_S \dfrac{\varkappa_T - \varkappa_S}{\varkappa_T}$

ACKNOWLEDGEMENT

The authors acknowledge the suggestions and advice given by the late Prof. I. FÉNYES and the help of Prof. T. BLICKLE, Director of the Research Institute for Technical Chemistry of the Hungarian Academy of Sciences.

SYMBOLS

p pressure, Pa
S entropy, Pa m^3 K^{-1}
v volume, m^3
T temperature, K
α_p volume coefficient at constant pressure, K^{-1}
α_S coefficient of aliabatic expension, K^{-1}
β_v coefficient of isochor thermal stress, K^{-1}
β_S coefficient of adiabatic thermal stress, K^{-1}
c_p specific heat at constant pressure, Pa m^3 K^{-1}
c_v specific heat at constant volume, Pa m^3 K^{-1}
$\varkappa_S$ coefficient of adiabatic expansion, Pa^{-1}
$\varkappa_T$ isothermal compressibility, Pa^{-1}

References

1. Modern Fizikai Kisenciklopédia. Gondolat Kiadó, Budapest. p. 357 (in Hungarian).
2. CALLEN, H. B.: Thermodynamics. John Wiley&Sons, New York, 1960. p. p. 51, 55.

РЕЗЮМЕ

Авторы установили логически возможные зависимости характеристик материалов двухпеременных однородных термодинамических систем алгебраическими методами. Вторая часть сообщения содержит подтверждение составленных уравнений.

HUNGARIAN JOURNAL
OF INDUSTRIAL CHEMISTRY
VESZPRÉM
Vol. 9. pp. 221–232 (1981)

LOGICAL STRUCTURE OF THE SYSTEM OF THE THERMODYNAMICAL MATERIAL CHARACTERISTICS II.

G. FÁY and R. TŐRÖS

(Research Institute for Technical Chemistry of the Hungarian Academy of Sciences, Veszprém, Hungary)

Received: March 23, 1981.

The first part of the present paper consisted of a theorem on the possible interconnections between thermodynamic material characteristics and all the formulas were also listed. This present (second) part of the paper contains the detailed proof of the theorem.

Introduction

The first part of the present paper consisted of a theorem about the formulas between thermodynamic characteristics. The state of a homogeneous thermodynamic system is determined by two variables f.e. p (pressure) and v (volume), or by the two functions $S(p, v)$, and $T(p, v)$.

Each chosen pair from the four quantities:

$$p,\ v{\cdot}T,\ S$$

determines the state of the system and all the other quantities can be calculated from the chosen two quantities. Twelve functions can be obtained altogether:

$$\left.\begin{array}{llllll} T(p, v); & S(p, v); & v(p, T); & S(p, T); & v(p, S) & T(p, S); \\ p(T, S); & v(T, S); & p(v, S); & T(v, S); & p(v, T); & S(v, T); \end{array}\right\} \tag{1}$$

The twelve functions in (1) have twenty-four derivatives. Twelve of these are, however, the reciprocals of the other twelve derivatives. Furthermore, on the basis of the relations of MAXWELL:

$$\left(\frac{\partial T}{\partial v}\right)_S = -\left(\frac{\partial p}{\partial S}\right)_v$$

$$\left(\frac{\partial S}{\partial v}\right)_T = \left(\frac{\partial p}{\partial T}\right)_v \tag{2}$$

$$\left(\frac{\partial S}{\partial p}\right)_T = -\left(\frac{\partial v}{\partial T}\right)_p$$
$$\left(\frac{\partial T}{\partial p}\right)_S = \left(\frac{\partial v}{\partial S}\right)_p \tag{2}$$

the examination of the further four derivatives seems unnecessary. Thus, using from now-on new symbols, eight derivatives are sufficient according to the full system of the characteristics. The proof suggests the symbols for the derivatives themselves and not for the characteristics slightly different from those. Let:

$$a = \frac{\partial S(p, T)}{\partial T} = \frac{1}{T} c_p; \qquad e = \frac{\partial T(p, S)}{\partial p} = \frac{1}{p} \beta_S$$
$$b = \frac{\partial v(p, T)}{\partial p} = -v\varkappa_T; \qquad f = \frac{\partial p(v, S)}{\partial S} = -\frac{1}{v}\frac{1}{\alpha_S}$$
$$c = \frac{\partial T(v, S)}{\partial S} = \frac{T}{c_v}; \qquad g = \frac{\partial p(v, T)}{\partial T} = p\beta_v \tag{3}$$
$$d = \frac{\partial p(v, S)}{\partial v} = -\frac{1}{v}\frac{1}{\varkappa_S}; \qquad h = \frac{\partial S(p, T)}{\partial p} = -v\alpha_p$$

A mathematical theorem has to be cited concerning the *Jacobian* determinant (see: Paper I.). Let us regard the following functions:

$$\begin{matrix} z_1(y_1, y_2) & z_2(y_1, y_2) \\ y_1(x_1, x_2) & y_2(x_1, x_2) \\ z_1(x_1, x_2) & z_2(x_1, x_2) \end{matrix} \tag{4}$$

If all these functions have continuous derivatives we get:

$$\frac{\partial(z_1, z_2)}{\partial(x_1, x_2)} = \frac{\partial(z_1, z_2)}{\partial(y_1, y_2)} \cdot \frac{\partial(y_1, y_2)}{\partial(x_1, x_2)}. \tag{5}$$

The *Jacobian* matrix is called the *object* if it is constituted from the two adequate functions in (1). A *Jacobian* matrix is a matrix with a *Jacobian* determinant. It can be seen from (1) that there are six Jacobian matrices. A *Jacobian* matrix can be denoted according to the two independent variables defining it. These two variables are called the *names of the object.* The six objects are being listed with the symbols of (3).

Object	Name	Occurring symbols
$\begin{pmatrix} \frac{1}{e} & \frac{1}{h} \\ -\frac{1}{f} & \frac{1}{g} \end{pmatrix}$	$\langle p, v \rangle$	(e, f, g, h)
$\begin{pmatrix} d & f \\ -f & c \end{pmatrix}$	$\langle p, T \rangle$	(c, d, f)

(6)

$$\begin{pmatrix} b & g \\ g & c \end{pmatrix} \qquad \langle p, S \rangle \qquad (b, c, g)$$

$$\begin{pmatrix} b & -h \\ h & a \end{pmatrix} \qquad \langle v, S \rangle \qquad (a, b, h)$$

$$\begin{pmatrix} \frac{1}{d} & e \\ e & \frac{1}{a} \end{pmatrix} \qquad \langle v, T \rangle \qquad (a, d, e) \qquad (6)$$

$$\begin{pmatrix} \frac{1}{g} & -\frac{1}{h} \\ \frac{1}{f} & \frac{1}{e} \end{pmatrix} \qquad \langle T, S \rangle \qquad (e, f, g, h)$$

It is easy to see that any object can be transformed into any other one, and that there exist as many transformations as pairs of objects, that is $\binom{6}{2} = 15$.

Not all of the transformations are independent, the basis of the theorem is to show their relationships. Let us denote a transformation by symbol t. Let A and B be two objects, their transformation can be written as:

$$A = t \cdot B$$

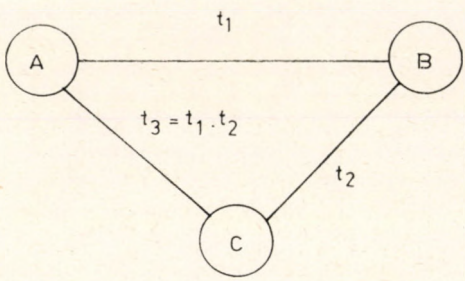

Fig. 1

Applying (5) it can be seen that if:

$$B = t_1 A$$

$$C = t_2 B$$

then:

$$C = t_3 A = t_1 t_2 A$$

An object can be symbolized by the points of a graph, the transformation by the directed edges connecting the points. Such a *diagram* is said to be commutative as it does not matter whether C is gained directly from A, or indirectly by B with a transformation.

Let us regard the following diagram *(Fig. 2)* to survey the logical relations of the transformations.

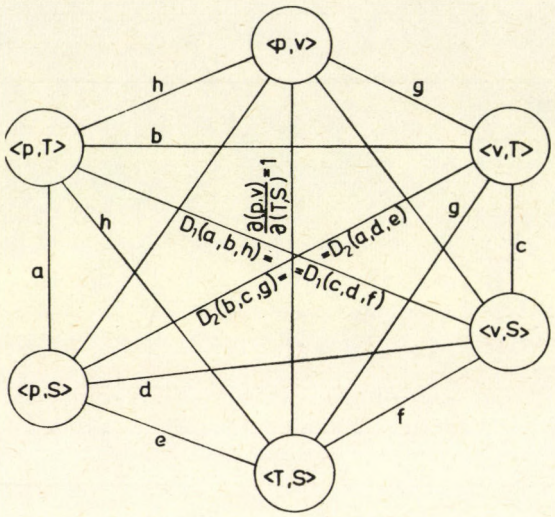

Fig. 2.

The orientation of the edges is neglected. The edges are called by those quantities, which determine one object from the other at the endpoint of the edge. The detailed method of the determination is, for the time being, not important. It is, however, very important that:

$$D_3 = \frac{\partial(p, v)}{\partial(T, S)} = \frac{\partial(T, S)}{\partial(p, v)} = 1 \tag{7}$$

following from the Maxwellian relations (2) or from equations (3). The formulas (6)—(7) show moreover, I—(5) that the transformations of the objects do form a group.

The graph-edges on *Fig. 2* are easily determined. For instance, in the edge belonging to the transformation of the pairs $\langle p, v\rangle$ and $\langle p, T\rangle$ we need:

$$\frac{\partial(p, v)}{\partial(p, T)} = \left(\frac{\partial v}{\partial T}\right)_p = -h$$

which depends only on h as can be seen in *Fig. 2.*

The not degenerated determinants are the following:

$$D_1 = \begin{vmatrix} \left(\frac{\partial v}{\partial p}\right)_T & \left(\frac{\partial v}{\partial T}\right)_p \\ \left(\frac{\partial S}{\partial p}\right)_T & \left(\frac{\partial S}{\partial T}\right)_p \end{vmatrix} = \begin{vmatrix} b & -h \\ h & a \end{vmatrix} = ab + h^2$$

The *Jacobian* determinant of the inverse transformation is the reciprocal of the original transformation, that is:

$$\frac{1}{D_1}=\begin{vmatrix} \left(\frac{\partial p}{\partial v}\right)_S & \left(\frac{\partial p}{\partial S}\right)_v \\ \left(\frac{\partial T}{\partial v}\right)_S & \left(\frac{\partial T}{\partial S}\right)_v \end{vmatrix} = \begin{vmatrix} d & f \\ -f & c \end{vmatrix} = dc+f^2$$

This means that D_1 is determined as a function of either a, b and h, or of c, d and f:

$$D_1(a, b, h) = D_1(d, c, f) \tag{8}$$

The determinant D_2 is:

$$D_2=\begin{vmatrix} \left(\frac{\partial v}{\partial p}\right)_S & \left(\frac{\partial v}{\partial S}\right)_p \\ \left(\frac{\partial T}{\partial p}\right)_S & \left(\frac{\partial T}{\partial S}\right)_p \end{vmatrix} = \frac{1}{ad}-e^2 = \begin{vmatrix} \frac{1}{d} & e \\ e & \frac{1}{a} \end{vmatrix}$$

and similarly according to the foregoing, function:

$$D_2(a, d, e) \qquad D_2(b, c, g) \tag{9}$$

and also their inverses can be formed simply. e.g. $a(D_2, d, e)$ and $b\ (D_2, c, g)$. Together with (8) the following functions are given:

$$\begin{aligned}
&D_1 = D_1(a, b, h) = D_1(c, d, f) = D_1 \\
&D_2 = D_2(b, c, g) = D_2(a, d, e) = D_2 \\
&a = a(D_2, d, e) = a(D_1, b, h) \\
&b = b(D_2, c, g) = b(D_1, a, h) \\
&c = c(D_2, b, g) = c(D_1, a, h) \\
&d = d(D_2, a, e) = d(D_1, c, f) \\
&e = e(D_2, a, d) \\
&f = \qquad\qquad = f(D_1, c, d) \\
&g = g(D_2, b, c) \\
&h = \qquad\qquad = h(D_1, a, b)
\end{aligned} \tag{10}$$

Now it is easy to make use of *Fig. 2*; if the edges x, y, z form a triangle then each can be determined by the remaining two. When repeatedly applying this rule, it can be decided from any set of edges if it determines all the other edges or not. It can be seen that the quadrangle a, b, c, d (in the following *internal quadrangle*) is of this type:

From *Fig. 3* and from the last equation of (10) it can be seen that if a, b, c, d and D_1 are determined, D_2 can be calculated, particularly two from a, b, c, d, and D_1 or D_2 determine the values of e, f, g, h. It can, therefore, be written:

$$\begin{aligned}
&(a, b, c, d) \xrightarrow{Fig.\ 3.} D_1, D_2 \qquad && (b, c, D_2) \xrightarrow{(10)} g \\
&(a, d, D_2) \xrightarrow{(10)} e && (a, b, D_1) \xrightarrow{(10)} h \\
&(c, d, D_1) \xrightarrow{(10)} f
\end{aligned} \tag{11}$$

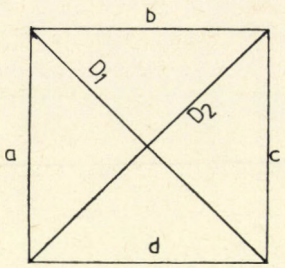

Fig. 3.

The numbers above the lines show the way of the determined relationship. *Fig. 3* shows that any three sides of a, b, c, d also determine the fourth side. e.g. in the case of a, b, c:

$$\begin{aligned} &(a, b) \xrightarrow{\text{Fig. 3.}} D_2 \\ &(c, D_2) \xrightarrow{\text{Fig. 3.}} d \end{aligned} \tag{12}$$

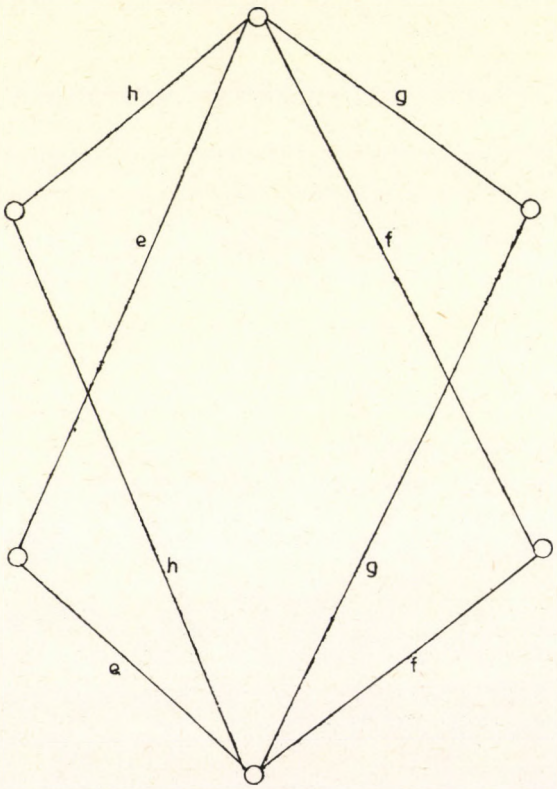

Fig. 4.

All three values of a, b, c, d form a base.

Let us see the double outer quadrangle formed by the edges e, f, g, h:

It can be seen that:

$$\begin{aligned} (e,f) &\xrightarrow{Fig.\ 5.} d \\ (f,g) &\xrightarrow{Fig.\ 5.} c \\ (g,h) &\xrightarrow{Fig.\ 5.} b \\ (h,e) &\xrightarrow{Fig.\ 3.} a \end{aligned} \tag{13}$$

Fig. 5 shows that the lower and upper angle points are connected with all four edges e, f, g, h and that the adjacent pairs of edges:

$$(e,f), \quad (f,g), \quad (g,h), \quad (h,e) \tag{14}'$$

always determine an internal (a, b, c, d) edge, while the other not-adjacent pairs of edges determine the edges belonging to Jacobian determinants. *Fig. 4* shows that in any three edges only two are adjacent. From the foregoing it can also be seen that if an internal edge is determined by n adjacent pair of edges it cannot be determined by a not-adjacent pair of edges. That is: any three outer edges determine three internal edges, and by (12):

All three values of e, f, g, h form a basis. (15)''

Three edges are surely no basis if they form a triangle, because this would mean that there also exists a basis of two elements which is impossible. According to *Fig. 5* there are four triangles of edges:

$$(a,e,h) \quad (b,g,h) \quad (c,f,g) \quad (d,e,f) \tag{16}$$

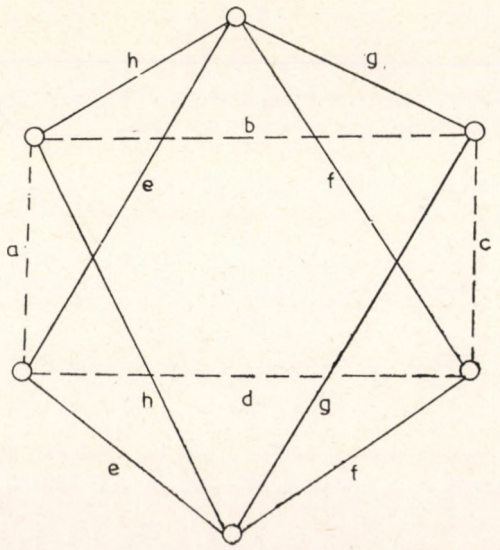

Fig. 5.

The question of the three internal edges has been discussed. The basic character of the outer edges with the exception of (16) has also been shown. In addition, further cases are also possible.

"Independent" means that the internal edge does not form a triangle with the two outer edges.

The groups of three edges forming a triangle were listed in (16). The case 3/a on *Table 1* can be separated into two parts:

$$\text{outer edges are } \begin{cases} \text{adjacent} \\ \text{not-adjacent} \end{cases} \tag{17}$$

The x, y adjacent edges are denoted by x, S, y.

Table 1

1	internal edges	its three edges are always a basis	
2	2 internal, 1 outer	a	adjacent internal edges
		b	not-adjacent internal edges
3	1 internal, 2 outer	a	one independent internal
		b	internal edges forming a triangle (24)
4	outer edges	with exception of (24) the three edges always are a basis	

The second line in *Table 1* is also separated. The following pairs of edges are not-adjacent:

$$a, b \quad b, c \quad c, d \quad d, a \tag{18}'$$

From (10) it can be seen that a pair of adjacent internal edges determines with D_1 or D_2 an outer edge. *Fig. 5* shows which two internal edges define the determinant. There are two cases:

$$\text{For the adjacent internal pair of edges is needed. } \begin{cases} 1/D_1 \\ 2/D_2 \end{cases} \tag{19}$$

That is:

$$\begin{aligned} &x, y = a, b, c, d \quad xSy \\ &(x, y, D_1) \rightarrow z = e, f, g, h \end{aligned} \tag{20}$$

or:

$$\begin{aligned} &x, y = a, b, c, d \quad xSy \\ &(x, y, D_2) \rightarrow z = e, f, g, h \end{aligned} \tag{21}$$

Equation (10) and *Fig. 5* show that two adjacent edges always form a determinant. Thus, if one determinant is needed the other one can be determined in the case of:

$$\begin{aligned} &x, y = a, b, c, -1 \quad xSy \\ &(x, y, D_1) \rightarrow z = e, f, g, h \end{aligned} \tag{22}$$

Whereas, in the case:

$$\begin{gathered} x, y \rightarrow D_2 \\ x, y = a, b, c, d \quad xSy \\ (x, y, D_2) \rightarrow z = e, f, g, h \\ x, y \rightarrow D_1 \end{gathered} \tag{23}$$

Let us denote the relationship of the determination with a symbol of function. If z is determined by x, y, D_1 let us write:

$$z = z(x, y, D_1) \tag{24}$$

or:

$$z = z(x, y, D_2) \tag{25}$$

A pair of two internal edges are called *complements* of the other pair of edges. The complement of (x, y) is denoted:

$$(\overline{x, y}) \tag{26}$$

With the symbols of (24) and (25):

$$(x, y) \rightarrow D_1 \quad (\overline{x, y}) \rightarrow D_2 \tag{27}$$

thus:

$$D_1 = D_1(x, y) \quad D_2 = D_2(\overline{x, y}) \tag{28}$$

The arrangement according to types depends on whether in the case of the three edges (x, y, z) the pair of relationship:

$$D_1(x, y) \quad z = z(x, y, D_2) \tag{29}$$

is valid or not.

If (29) is valid then:

$$(29) \xrightarrow{(10)} z = e, g$$

and:

$$(x, y, D_1) \xrightarrow{Fig.\ 2.} h$$

$$(x, y, D_1) \xrightarrow{Fig.\ 2.} f$$

Thus, (e, g) (h, f) are given. There also exists a pair of outer edges. According to (13) an internal edge was determined which is different from the given x, y. e.g. let $x = a$; $x = d$; $z = e$; and the adjacent pair of edges (g, h).

$$(a, d, e) \xrightarrow{(10)} D_2$$

$$(a, e) \xrightarrow{Fig.\ 2.} h$$

$$(D_2, e) \xrightarrow{Fig.\ 2.} g$$

$$(g, h) \xrightarrow{Fig.\ 2.} b$$

If it is not valid then similarily:

$$D_2 = D_2(x, y) \quad z = z(x, y, D_1)$$

Such groups of three edges also form a basis in this case.

From the second line of *Table 1* let us consider the case:
internal pair of nonadjacent edges, one outer edge. (30)′

This case can be handled by producing D_1, D_2 in different ways. According to (8) (9):

$$\frac{a}{d}=-\frac{h}{f}=\frac{b}{c}=D_1=ab+h^2=(dc+f^2)^{-1}$$
$$\frac{c}{d}=-\frac{e}{g}=\frac{b}{a}=D_2=\frac{1}{ad}-e^2=\left(\frac{1}{bc}-g^2\right)^{-1} \tag{31}$$

However, on the basis of theorem (15) calculated from *Fig. 2:*

$$h=bg; \quad f=ed; \quad h=ae; \quad f=-cg \tag{32}$$

According to (31) and (32):

$$D_1=ab+h^2=ab+(-ae)^2=aC_1D_1+a^2e^2$$
$$D_2=\frac{1}{ad}-e^2=\frac{1}{ad}-\left(\frac{f}{d}\right)^2=\frac{1}{\left(\frac{b}{D_2}\right)d}-\frac{f^2}{d^2}$$

solved for D_1, D_2:

$$D_1=D_1(a, c, e)$$
$$D_2=D_2(b, d, f)$$

From *Fig. 2* one can see that:

$$e=e(a, h)$$
$$f=f(e, d)$$

Therefore:

$$D_1=D_1(a, c, e)=D_1(a, c, h)$$
$$D_2=D_2(b, d, f)=D_2(b, d, e) \tag{33}$$

On the other hand from (31) we get:

$$D_1=D_1(a, c, f)=D_1(a, c, g)$$
$$D_2=D_2(b, d, e)=D_2(b, d, h) \tag{34}$$

According to (33), (34) in the case of a not adjacent internal pair of edges and any outer edge another internal diagonal line is also determined, and according to *Fig. 2* in each triangle every edge is determined, e.g. in the case of a, c, h from (33):

$$(a, c, h) \rightarrow D_1$$
$$(D_1, c) \rightarrow b$$

and:

$$(D_1, a) \rightarrow d$$
$$(a, h) \rightarrow e$$
$$(D_1, h) \rightarrow f$$
$$(b, h) \rightarrow g$$

This means that the type of (30)′ is always a basis. With this statement the problem of the 2nd line of *Table 1* is solved.

Let us consider the case of adjacent edges in the 3rd line: In case of type a) a further edge is added to the independent internal one, and thus the subtype of adjacent edges of type a), was reduced to the 2nd line of *Table 1.* In the case of non-adjacent edges [the other case of (17)] always an internal diagonal is obtained. In this case according to (14)′ we gain an internal diagonal.

For instance, let be given:

$$(h, f, b)$$

then:

$$(h, f) \rightarrow D_1$$

$$(D_1, b) \rightarrow c$$

There exists an adjacent pair of internal edges b and c, so that this case has been reduced to the 2nd line of *Table 1.*

With this case all the possibilities have been examined and our Theorem concerning basis has been proved by way of separation of different cases. The results of the calculations were shown in the *Tables* of the first part of this paper.

SYMBOLS

a, b, c, d, e, f, g, h	symbols defined in Equation (10)
p	pressure, Pa
S	entropy, Pa m^3 K^{-1}
v	volume, m^3
T	temperature, K
α_p	volume coefficient at constant pressure, K^{-1}
α_S	coefficient of aliabatic expension, K^{-1}
β_v	coefficient of isochor thermal stress, K^{-1}
β_S	coefficient of adiabatic thermal stress, K^{-1}
c_p	specific heat at constant pressure, Pa m^3 K^{-1}
c_v	specific heat at constant volume, Pa m^3 K^{-1}
$\varkappa_S$	coefficient of adiabatic expension, Pa^{-1}
$\varkappa_T$	isothermal compressibility, Pa^{-1}

РЕЗЮМЕ

Первая часть сообщения связана изложением теории возможных взаимосвязей между термодинамическими характеристиками материалов, и здесь перечислены принятые формулы. В настоящей стати приведены результаты утверждающие теоретические предпосылки.

HUNGARIAN JOURNAL
OF INDUSTRIAL CHEMISTRY
VESZPRÉM
Vol. 9. pp. 233–240 (1981)

ON THE SOLUTION OF SCHEDULING PROBLEMS WITH PROHIBITED INTERMEDIATE STORAGE

E. BIECHELE, G. BIESS, F. SCHMIDT and W. JÄNICKE*

(Technische Hochschule „Carl Schorlemmer" Leuna–Merseburg, 42 Merseburg, GDR)

Received: April 14, 1981.

In the production of paints, medicines and cosmetics, etc. production scheduling problems lead to machine allocation problems with prohibited intermetiate storage.

The problem is presented, simple known algorithms and couplings of algorithms are discussed, and numerical results for examples (14 machines and up to 30 jobs) are given.

This paper begins with the requirement to solve a machine allocation problem for a paint factory. This demand arose during the design of multiproduct plants for low tonnage chemical products, where given devices had to be weighted, and information about possible changes of these devices had to be obtained.

Multiproduct plants are complex systems consisting of multipurpose devices, auxiliary and secondary equipment, which can be connected simultaneously or in sequence to form various configurations for manufacturing the scheduled products.

In the following, the problem is treated generally for any multiproduct, multicharge, and multimachine plant, with the constraint of prohibited intermediate storage.

The prohibition of intermediate storage results from the technological necessity of manufacturing low tonnage chemical products.

Practical examples are devices for the manufacture of paints or their intermediate products, medicines, cosmetics, polymers, and primary products for the film industry, etc.

The problem having been presented, heuristic algorithms for its solution are reported, and an example with test calculations is discussed. The object

* Correspondence concerning this paper should be adressed to W. JÄNICKE.

of this paper is to provide some information about the solution of non-trivial machine allocation problems.

Rather than present new algorithms, the efficiency of simple heuristic solution procedures is demonstrated for a special class of examples.

The problem

The given plant consists of process units and connections between these process units.

This plant is represented by a directed graph $G=(X, U)$, where $X=\{x_1 \ldots x_n\}$ are vertices, and $U=\{u_1 \ldots u_m\}$ are arcs. Each arc $u_k=(x_i, x_j)$ is characterized by its starting vertex x_i and a final vertex x_j. The existence of an arc u_k means that the process unit x_i can be supplied with a product, which previously was in process unit x_j. Data concerning type, size, change-over time, and allocated process unit, etc., are assigned to each vertex.

The plant is to manufacture several products $P_1 \ldots P_p$. For these products, production specifications $H_1 \ldots H_p$ exist, which describe the required type of process units, their sequence and utilization time and further data. It is to be noted that the time of transition from one process unit to the other is specified; consequently, no intermediate storage is allowed.

To manufacture these products, jobs $A_1 \ldots A_q$ are given, which determine the volume of production expressed in batch numbers, and several supplementary conditions such as the release date and the due date.

For each single process unit, scheduling is sought, i.e. the calculation having been completed, it will be known, for each machine and for each time, which batch of which job will be processed on the machine considered. The optimization aims at minimizing the completion time T_{end} of the total production project.

A series of other tasks can be derived from this basic task; such as:

- determination of the completion time of a given production volume (e.g. as an aid in the design of a plant)
- determination of the processing sequence of the different batches.

For further information on scheduling see [4].

Concept of Solution

In most cases, scheduling problems of this kind with practically relevant problem size cannot be exactly solved. Hence it is the object of the present work to determine, by coupling heuristic algorithms, a permissible machine allocation plan, the completion time T_{end} of which is as short as possible. Experience with heuristic algorithms for solving other discrete optimization problems shows that the efficiency of such algorithms depends on the respective case.

Therefore, an attempt was made to develop strategies allowing the chemical engineer to influence the computation, e.g. by coupling the algorithms, by parameters and by job sequencing. These parameters and sequences can be

improved by the computation of the variants. To support these calculations, a programme system capable of extension was developed (cf. [1], [2]).

This system carries out basic operations occurring when machine scheduling problems are dealt with. Moreover, it contains several heuristic algorithms for solving scheduling problems with intermediate storage being prohibited. This programme system requires EC 1040 data processing equipment.

Realized Algorithms

Thus far, the following algorithms have been realized:

1. BE: A machine allocation plan is established according to a chosen batch sequence. The chemical engineer may use the BE as a partial programme of other algorithms, or alone.

2. FI: FI realizes the well-known heuristic principle of the "earliest successor". The batch which can begin at the earliest possible time is selected from among all batches still to be processed. This batch is inserted into the machine allocation plan, and the algorithm is again applied to the remaining batches.

3. SN: In this variant, the machine being used longest (bottleneck machine) is determined first (estimate calculation) in order to utilize the bottleneck machine as appropriately as possible. For this purpose, a batch of the job requiring this bottleneck machine is selected where appropriate as early as possible, i.e. a batch starting with this machine. The last job requires this machine as late as possible, i.e. the device is used until the batch is concluded, or a little shorter. The remaining jobs are ordered in a similar manner. All batches of a job are then fixed directly one after the other according to this pre-ordering.

4. BK: By analogy with the "travelling salesman" problem, the permutation algorithm used here might be termed "algorithm of successive inclusion of products" (cf. [3]). This aims at systematically generating some variants instead of the $k!$ possible permutations (k is the total charge number). We start from two different batches C_i and C_j and determine which sequence of processing is more favourable, i.e. whether C_i should be processed before or after C_j. This decision remains valid. The third batch is examined with respect to whether it should be put before, between, or after the two batches determined first. This is continued up to the nth batch, for which there are n possibilities of inclusion. However, this algorithm is too time-consuming to be utilized for solving practically relevant problems and will therefore be used only as a programme to be processed before other algorithms in order to determine favourable sequences of a partial number of jobs, which can then be combined to from the overall sequence.

5. BS: In this algorithm, the permutation algorithm is used in such a way that first a favourable sequence for the case of a single processing of all production specifications is found (i.e. use of the permutation

algorithm under the condition that exactly one batch of each product is required.)

In this way, a possibility of favourable arrangement of production specifications is found. In order to economize change-over time, all batches required to obtain one product are then processed in direct succession, with the sequence found by the permutation algorithm being maintained.

6. BNF: Let r be the smallest of all g occurring batch numbers. From each job, the partial amount rth is picked out and considered to be a representative of the total amount. In this way, the problem has been divided into r similar partial problems, of which only one is considered. Errors caused by this division are compensated for in the course of the computation. (This approach is effective especially for long-term scheduling problems in which a steady output of products is required.)

   The batch sequence of a partial amount is determined by the best successor method. It is maintained for all r partial amounts of the job.

7. BAB: Like BNF. Instead of the best successor method, however, the permutation algorithm is used.

8. HS: HS orders the jobs according to priority parameters which can be determined by the following factors: an importance parameter chosen for each job according to subjective aspects, the latest final date, the number of batches to be produced, and a value of the extent to which bottleneck machines are used. These factors are combined additively with chosen weighting parameters. The priority parameters established in this way are used to order the jobs. If required, the problem can be divided again into r partial problems, otherwise, $r = 1$.

   According to the sequence previously determined by weighting the single parameters, as many batches of the same job are now fixed successively as are given by the determined partial number of batches or the total batch number, respectively. The process is executed r times.

Description of the Modifications of Example

The test calculations were carried out with the aid of a realistic example, which was modified several times. The data available were those of a multiproduct device, which is at present being designed for the manufacture of low-tonnage chemical products. The chemical plant was taken as a graph containing 14 vertices (process units) and 24 arcs (connections between units) (cf. *Fig. 1*). The production specifications of 4 products were available. For simplification, the units used only pairwise are combined to form an abstract unit. Units required only for one product, but not for the longest step of its production specifications, were not included into the calculation. This reduction of the problem does not result in any important information

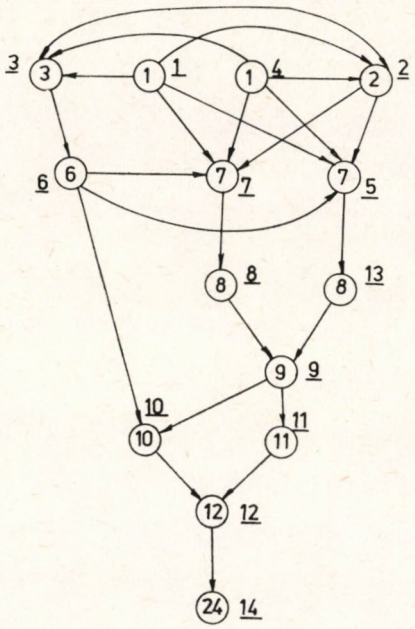

Fig. 1.

being lost. Examples of different dimensions were constructed simply by choosing different batch numbers for the 4 products (cf. *Table 1*).

Table 1

Designation of the example	Number of jobs	Batch number of job			
		1	2	3	4
B1	3	2	2	4	—
B2	4	2	2	4	1
B3	4	4	3	7	2
B4	4	14	7	8	1

The existing connections between these units are contained in the graph of *Fig. 1.*

The production specifications of the 4 products are characterized in *Table 3.*

Here, h_i denotes the number of activities of the i-th production specification, $j = 1(1)h_i$ is the number of the activity, l_{ij} the type of the unit required, d_{ij} the utilization time, and z_{ij} is the relative starting time, i.e. how many units of time after the first activity is to start.

Table 2

Data about the chemical plant

Number of device	Number of type of device	Change-over time when production is changed	Change-over time when batches are changed, with the same product being further processed	Designation
		(in hours)		
1	1	8	2	tank
2	2	8	2	tank
3	3	8	2	tank
4	1	8	2	tank
5	7	24	2	reactor 1a
6	6	24	2	reactor 2
7	7	24	2	reactor 1b
8	8	24	2	sediment vessel
9	9	8	2	filter
10	10	8	2	ML-receiver 16 m^3
11	11	8	2	ML-receiver 20 m^3
12	12	8	2	WL-receiver 10 m^3
13	8	24	2	sediment vessel
14	24	24	2	reactor 3

Table 3

$h_1 = 7$ (a)

j:	1	2	3	4	5	6	7
l_{1j}:	1	2	7	8	9	10	12
z_{1j}:	0	6	0	25	33	33	68
d_{1j}:	3	16	27	10	22	12	17

$h_2 = 9$ (b)

j:	1	2	3	4	5	6	7	8	9
l_{2j}:	1	2	3	6	7	8	9	11	12
z_{2j}:	0	14	4	0	13	49	75	75	85
d_{2j}:	3	32	6	16	41	37	23	12	12

$h_3 = 5$ (c)

j:	1	2	3	4	5
l_{3j}:	1	7	8	9	11
z_{3j}:	0	0	11	13	13
d_{3j}:	3	13	4	22	12

$h_4 = 6$ (6)

j:	1	2	3	4	5	6
j_{4j}:	1	3	6	10	12	24
z_{4j}:	6	0	5	225	240	25
d_{4j}:	3	7	12	17	17	148

Results of the Tests

The algorithms described were used to carry out test calculations whose results are contained in *Table 4*. This table gives the completion times for our test problems. To solve the test problems the EC 1040 required from 0.25 to 10 minutes. For instance example B2 required 15.90 seconds by algorithm FI.

Table 4

	BE	FI	SN	BK[1]	BS	BNF[2]	BAB[2]	HS[3]
B1	241	266	266	246	244	275	249	297
B2	276	269	271	257	275	269	275	322
B3	484	430	434	—	456	420	451	438
B4	1041	792	782	—	773	792	773	753

(1) Examples B3 and B4 were not treated by algorithm BK since the computing times were too long.

(2) In Examples B2 and B4, algorithm BNF corresponds to FI and BAB to BS.

(3) The results contained in this column were obtained after repeated variations of the weighting parameters for the jobs. Consequently, they depend on the experience and the skill of the chemical engineer.

Conclusions

The present algorithms provide a means for scheduling problems, which can be combined and used by the chemical engineer in a dialogue with the computer. General statements are not possible, since the quality of heuristic algorithms strongly depends on the respective problem. It appears to be desirable that a larger number of different strategies should be available, which can be fitted to the respective example problem.

SYMBOLS

$G=(X, U)$	graph
$X=\{x_1, \ldots, x_n\}$	vertices
$U=\{u_1, \ldots, u_m\}$	arcs
T_{end}	completion time
$P_1, \ldots, P_p$	products
$H_1, \ldots, H_p$	production specifications
$A_1, \ldots, A_q$	jobs

REFERENCES

1. Jänicke, W.: MB — Ein Programmsystem zur Maschinenbelegung. Chemische Technik, 1981. (in press).
2. Biechele, E.: Untersuchingen zu Maschinenbelegungsproblemen fuer Mehrprodukten-

anlagen der chemischen Verfahrenstechnik, Diplomarbeit. Technische Hochschule Leuna-Merseburg, Sektion Mathematik, 1980.
3. Muller-Merbach, H.: Operations Research — Methoden und Modelle der Optimalplanung, Verlag Franz Vahlen GmbH, Berlin und Frankfurt, 1969.
4. Noltemeier, H.: Graphentheorie mit Algorithmen und Anwendungen. Verlag Walter de Gruyter, Berlin und New York. 1976.

РЕЗЮМЕ

При проектировании циклов рабочего времени производства красителей, медикаментов, косметики и т. д. возникает проблема расстановки производственной аппаратуры включающая в себе недопустимость хранения полуфабрикатов между операциями. В сообщении излагается этот вопрос и даны простые алгоритмы и их соединения, и также приведены результаты расчетов на численных примерах.

HUNGARIAN JOURNAL
OF INDUSTRIAL CHEMISTRY
VESZPRÉM
Vol. 9. pp. 241—250 (1981)

PURIFICATION OF AMMONIUM NITRATE CONTAINING CONDENSED WATER BY ION-EXCHANGERS

I. Ország, F. Ratkovics and B. Szeiler

(University for Chemical Engineering, Veszprém and *Nitrogen Works, Pétfürdő, Hungary)

Received: April 17, 1981.

Synthetic ion exchangers — Varion KSM (cation exchanger) and Varion ADAM (anion exchanger) — were used for the removal of ammonium and nitrate ions from condensed water containing 2.5 g.dm^{-3} ammonium-nitrate. The useful capacity and regeneration of the resins were studied. The cation exchanger was regenerated by nitric acid and the anion exchanger with ammonium hydroxyde.

The NH_4NO_3 content could be decreased to below 10 mg.dm^{-3} using the VARION (NIKE, Balatonfűzfő) resins. The useful capacity of the cation exchanger was 1.6 mol.dm^{-3}, while that of anion exchanger was 1.2—1.3 mol.dm^{-3}.

Introduction

A large amount of condensed water is formed in the course of nitrogen fertilizer production, which contains only a few gram.dm^{-3} nitrogen compound. Formerly this water was directly discharged into various receiving water bodies. Nowadays, however, due to the advanced eutrophication of most surface waters, this condensed water has to be purified prior to discharge. There have been several attempts to develop a reasonable treatment technology for such condensed waters [1—7]. Most of them dealt specifically with NH_4NO_3 removal.

Bingham et al. [1] investigated in detail the use of various technological possibilities. The methods tested included:

— microbial nitrification,
— biological denitrification,
— ammonia stripping by air,
— ammonia precipitation as magnesium-ammonium phosphate,
— recovery of ammonia by reverse osmosis,
— recovery of ammonia by continuous ion-exchange.

They found that only the ion-exchange technologies met the concentration limits imposed by the water authorities and were also acceptable from an economical point of view. This conclusion is due to the fact that the NH_4NO_3 content is recovered in the regeneration cycle of the exchanger and it is returned to the evaporator as a solution containing more than 10% NH_4NO_3. 58% of the purified water is used as boiler feed-water, while 42 % is used as cooling water.

The Farmers' Chemical Association, Inc. and the Chemical Separations Co., reported a continuous method [8] in which a Chem-Seps or Higgins contactor was used. In this contactor, saturation-elution-washing takes place in compartments seprated by valves. The resin moves in a pulsating manner. The resin is moved by the feed-water, which also decreases the friction losses. Their pilot plant with a capacity of 9 $m^3.h^{-1}$ has been in operation since 1972. The NH_4NO_3 concentration in the influent and effluent is 2500 $mg.dm^{-3}$ and 5—50 $mg.dm^{-3}$, respectively.

In the closed-loop ammonium nitrate recovery system, the influent to be treated, first passes a hydrogen-form resin bed, where ammonium ions are exchanged for hydrogen ions. This dilute nitric acid solution then goes to the anion exchanger bed, which is in hydroxyde form. Nitrate ions are replaced here by hydroxide ions, i.e. salt-free water leaves the system.

After solution, the action and anion exchanger beds are regenerated by nitric acid and ammonium hydroxyde solutions, respectively. In both cases, the effluent contains ammonium nitrate.

The overall ion-exchange cycle consists of the saturation (exhaustion) — elution (regeneration) and washing (displacement of the regenerant) steps.

The saturation and regeneration steps were studied in the present experimental series to obtain information usable for industrial purposes.

Experimental

Materials, Methods and Apparatus

Strong acid cation exchangers and weak basic reticular anion exchangers can be used. Such resins are, e.g. the Dowex NC 2077, KU—2 (USSR), Amberlite 200, Wofatite KS 10 and Varion KSM cation exchangers and the Amberlite IRA—93 and Varion ADAM (NIKE, Fűzfőgyártelep) anion exchangers.

The Amberlite IRA—93 (Rohm and Haas, Pa, USA) and VARION (NIKE) resins were used for the experiments, the former one as reference material. The cation exchangers were obtained in sodium form, and the anion exchangers in chloride form.

The solutions used for the experiments were prepared from reagent grade NH_4NO_3 and distilled water.

The eluents were prepared from reagent grade nitric acid, ammonium hydroxide and distilled water. The procedure was tested in a stationary-bed column (cf. *Fig.* 1). Downward flow was used in each case. A peristaltic pump ensured a constant flow rate. The concentration of the effluent was continuously monitored by a recording conductometer. Specific conductivity of the solution was also determined by discontinuous sampling and measurement in a thermistatted cell. This served as a check on the reliability of the

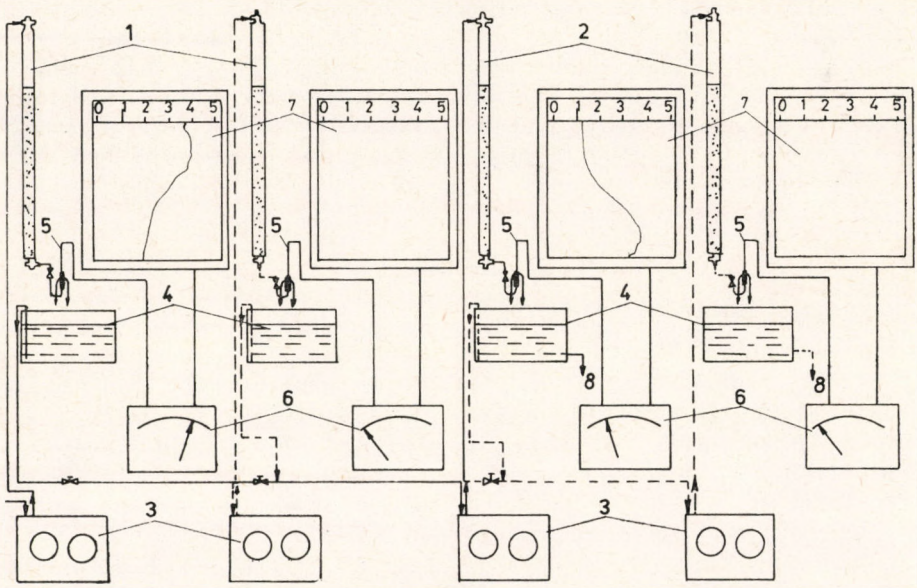

Fig. 1
Schematics of the ion exchanger
1 — cation exchanger column; *2* — anion exchanger column; *3* — pump; *4* — tank; *5* — electrode; *6* — meter conductivity; *7* — recorder; *8* — treated water; ═══ liquid flow; ─┤├─ electric conduit

recording system. At higher nitric acid concentrations, the acidity was also determined by acid-base titration, followed by the analysis of the neutral solution for NH_4NO_3. This method was used for the determination of the ammonium concentration of the effluents leaving the cation exchanger column. The photometric NESSLER method was used for the measurement of very low NH_4^+ concentrations.

The pH of the purified water leaving the anion exchanger was monitored by a combined glass electrode.

In most experiments, only a single cation and a single anion exchanger column were used. Either the effluent of the cation exchanger was directly introduced on top of the anion exchanger, or the latter was operated independently, using a nitric acid solution equivalent to what one could expect, assuming a complete ammonium exchange.

The NH_4NO_3 concentration in the influent of the cation exchanger was maintained at 2,500 g/l, while the HNO_3 concentration of the influent of the anion exchanger corresponded to that one of the effluent of the cation exchanger, or, if prepared sparately, it was 1,968 g/l.

The ion exchangers were activated before use. The cation exchanger was activated by a 10 % nitric acid solution, while the anion exchanger was activated either by a 4 % sodium hydroxide or 7 % ammonium hydroxide solution. The cation exchanger was activated with a 250 % stochiometric excess, while the anion exchanger required only a 150 % excess.

After activation the exchangers were washed with water until the effluent

was neutral. The quality of the activating acid or base did not influence the useful capacity of the resin.

The cation exchanger column was packed with 125 ml resin, while the anion exchanger with 140 ml. The inner diameter of the columns was 20 mm, and their lengths 400 and 450 mm, respectively. When the large internal diameter columns (I.D. = 30 mm) shown in *Fig. 1* were used, the bed heights were equal and the resin volumes 2.25 times larger then in the previous cases.

Results

The saturation and regeneration data are presented graphically. The data shown were obtained with the smaller columns, but practically identical results were obtained in the other experiments, for the height of the bed was kept constant, irrespective of the type of the resin.

In the saturation (water purification) cycle, the relationships between the useful capacity and loading flow rate was studied. The flow rate was changed in the 1—12 mh^{-1} (2.5—30 $cm^3.h^{-1}cm^{-3}$) range. The flow rate was kept constant for each experiment.

The isoplanes constructed from two experimental series are shown in *Fig. 2* for both the cation and anion exchanger columns. The measured specific conductivity values at ambient temperature are plotted on the ordinate. These values can be easily expressed as HNO_3 or NH_4NO_3 concentrations, because

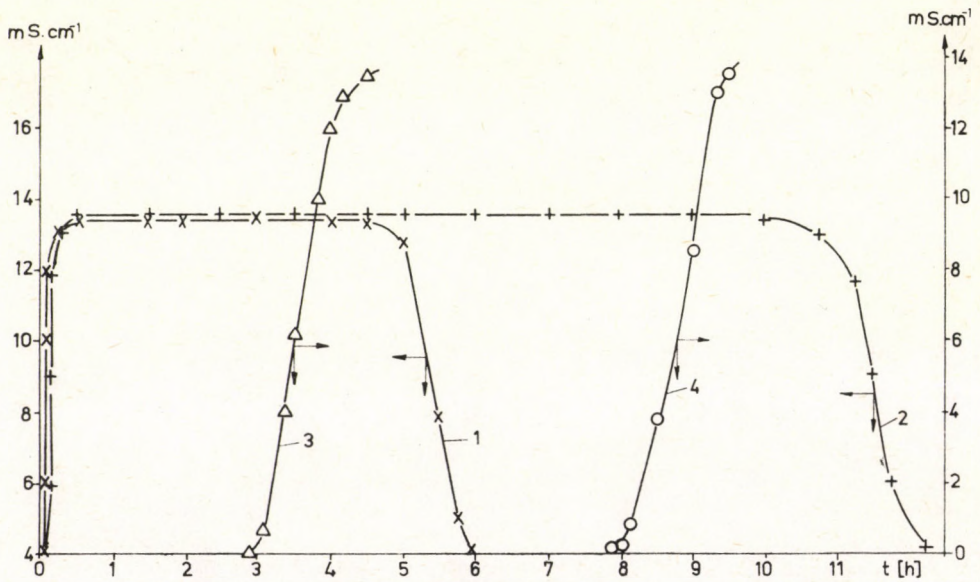

Fig. 2
Specific conductivity of the effluent as a function of time
1; *2* cation exchanger
3; *4* anion exchanger
Specific loading (cm^3 water·cm^{-3} resin·h^{-1}): 1—14.4; 2—7.7; 3—14.6; 4—6.0.

there is a linear relationship between the specific conductance and concentration values over the range tested. Both the useful and the overall capacities can be determined from these plots.

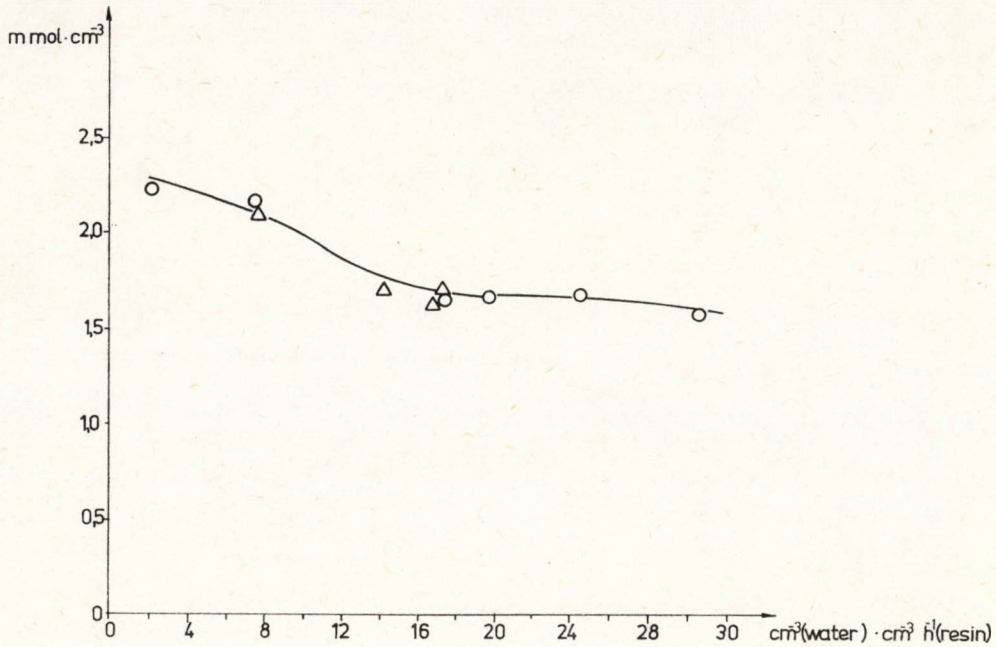

Fig. 3
Dependence of the useful capacity of VARION KSM resin upon the specific loading

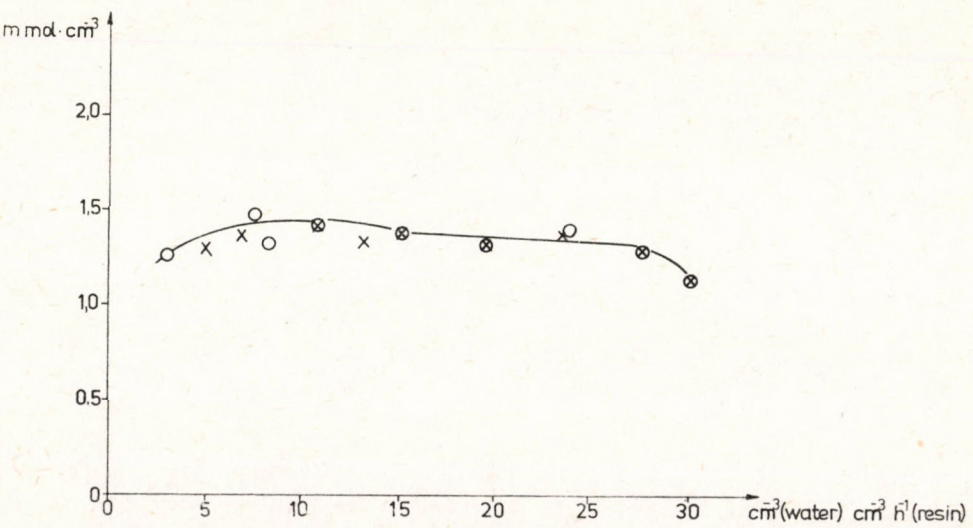

Fig. 4
Dependence of the useful capacity of VARION ADAM resin upon the specific loading

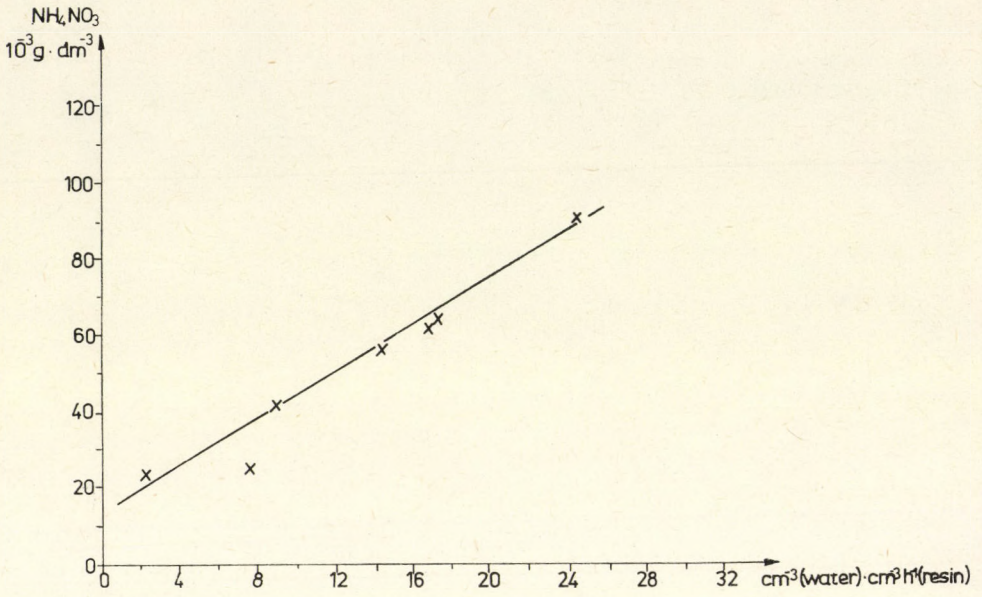

Fig. 5
Ammonium nitrate concentration in the effluent of the cation exchanger column as a function of the loading

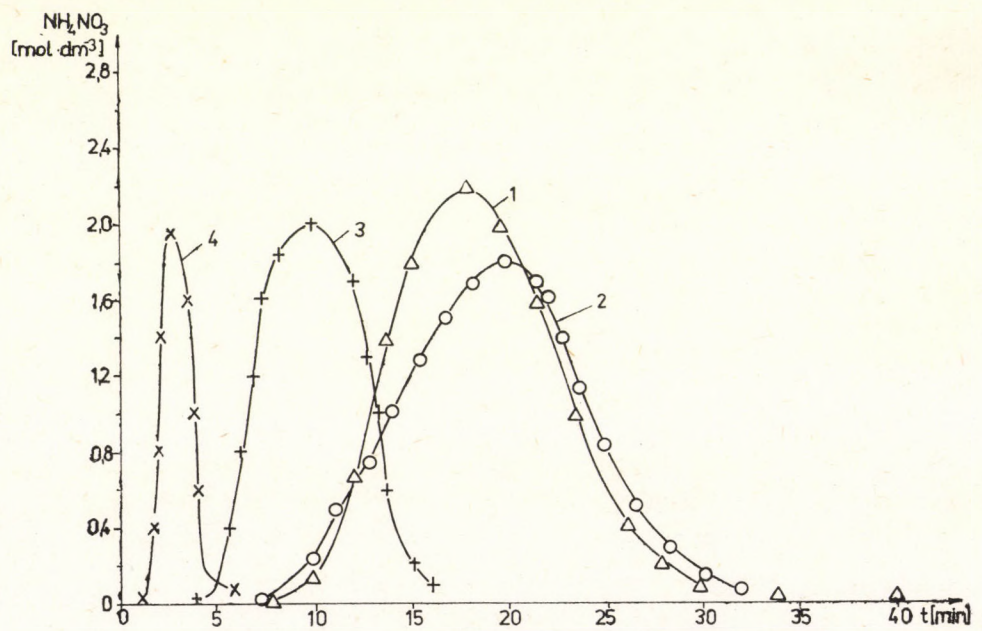

Fig. 6
Regeneration of the cation exchanger column Specific loading of the regenerant (cm^3 cm^{-3} resin h^{-1}) 1—4.8; 2—5.76; 3—9.6; 4—26.9
Acid concentration: 1—22%; 2—3.4—15%

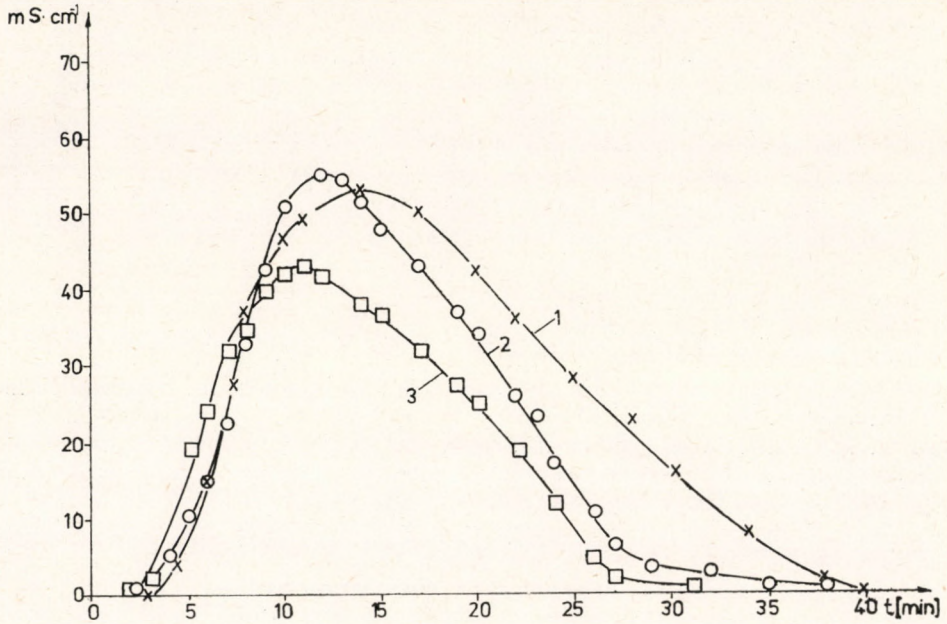

Fig. 7
Regeneration of the anion exchanger column. Specific conductivity of the regenerant leaving the column as a function of time specific loading: (cm^3 water cm^{-3} resin h^{-1}): 1—7.7; 2—9.9; 3—12
Acid concentration: 1.2—7%; 3—5%

The useful capacity could be calculated from the amount of ions retained up to the breakthrough point. Up to the breakthrough point, the specific conductance was constants. The useful capacities obtained this way are plotted in *Fig. 3* and *4* for the entire loading range studied. It can be seen that in this range the capacity of VARION KSM is more sensitive to loading than that of the VARION ADAM.

According to the experimental results, the useful capacity of the cation exchanger is 1.6 $mol.dm^{-3}$, while that of the anion exchanger is 1.28—1.30 $mol.dm^{-3}$.

The ammonium nitrate concentrations in the effluent of the cation exchanger are shown in *Fig. 5*. It is apparent that for the given bed height, the NH_4NO_3 concentration increases practically linearity with the specific loading.

With increasing bed height, the extent of NH_4NO_3 removal increases. Thus, if the effluent of the first column is introduced into the second column, then the NH_4NO_3 concentration in the final effluent decreases to 5.10^{-3}—15.10^{-3} $g.dm^{-3}$.

For *regeneration* (elution) 15 and 22 % nitric acid and 5—7 % ammonium hydroxide solutions were used, respectively. The specific loading was also changed. The results obtained are shown graphically in *Fig. 6* and *7*.

The measured specific conductivity and not the concentration values are plotted in the figures obtained for the regeneration of the anion exchanger. The concentration can be easily calculated from the $\varkappa = 1.12\ c$ relationship ($\varkappa$ in $ohm^{-1}\ cm^{-1}$).

The data for the cation exchanger come from experiments No. 7, 14, 27 and 33, and for the anion exchanger from No. 18, 36 and 39. This is worthwhile mentioning, because one judges the in-service changes of the resin.

The amount of NH_4NO_3 leaving the column with the regenerant and the mole number of ions removed from 1 cm^3 resin can also be calculated from the curves. The value obtained for the cation exchanger is 1.95 ± 0.12 mol.dm^{-3} and 1.52 ± 0.07 mol.dm^{-3} for the anion exchanger.

This means that the regenerant concentrations used are practically identical and each can be used with the same efficiency, and the capacity of the resins has also not been altered during 39 cycles.

From a practical point of view, the use of more concentrated solutions is more advantageous. Thus, for nitric acid 22 %, and for ammonium hydroxide 7 % solutions should be used. In fact, for ammonium hydroxide the solution containing 7 % NH_3 also gave identical results (and capacity), so this solution can also be used. Literature references [1, 2] substantiate this claim. However, the use of more concentrated nitric acid solutions does not seem advisable, because the resin may possibly deteriorate.

Technical-economical considerations

It can be concluded from the present experimental data that the required purification of NH_4NO_3 containing condensed water is possible using the Hungarian VARION KSM and VARION ADAM resins.

The useful capacity of the cation exchanger is 1.6 mol.dm^{-3}, and that of the anion exchanger is 1.28 mol.dm^{-3}. It follows that with a 2.5 g.dm^{-3} NH_4NO_3 influent 50 and 40 bed volumes of treated water can be obtained in a cycle on the cation and anion resins, respectively.

The value of the resin used for the water treatment, i.e. the value deprecation of the resin in the production of 1 m^3 water depended on the number of cycles achievable with a given resin. At present no such experimental data are available.

If the value given by the producer (NIKE) is taken, i.e. 1,200—1,500 cycles, then with a large safety margin, 1,200 cycles, at 1980 prices, the resin cost is 3.89 Ft.m^{-3} purified water.

REFERENCES

1. Bigham, E. C., Chopra, R. C.: A closed cycle water system for ammonium-nitrate procedurs. International Water Conference the Engineers Society of Western Pennsylvania 32 V D Annual Meeting Pittsburgh. 1971. Nov. 4.
2. Pavliuk, Sz. J., Livke, V. A., Arzamonostsova, V. S.: Khim. Prom. *1975*, 5., 42.
3. Pol. Pat. 88,262.
4. Barcicki, J., Pawlowski, L., Wimmicki, T.: Conservation et Recycling. Vol. I. pp 291—298. Pergamon Press. Printed in Great Britain. 1977.
5. Asirov, A.: Zh. Prihl. Khim. *1978*, (5) 991.
6. Pawlowski, L.: Ion Exhange Method for Recycling Water and Chemicals from Waste Water. 4. Symp. of Ion Exhange—Siófok 1980. May. 27—30.
7. Böhm, R. Application of Ion Exhanger for Cleaning Waste Waters of Fertilizer Production. 4. Symp. of Ion Exhange—Siófok 1980. May. 27—28.
8. Feser, R., Kelly, H. D., Kuncl, K. L.: Pollution Prevention. Chemical Processing. Reprinted 1977. jan.

РЕЗЮМЕ

Проведены эксперименты с целью удаления из конденсационных вод содержащих макс. 2,5% г/л нитрата аммония иона аммония и иона нитрата на синтетических катионообменных ианионообменных смолах типа VARION KSM и VARION ADAM. Изучали полезную мощность и восстановливающую способность смолей. Восстановление катионообменника осуществлялось азотной кислотой, а анионообменника гидроокисью аммония.

Авторами установлено, что содержание нитрата аммония с помощью ионнообменников типа VARION (NIKE, Fűzfőgyártelep) можно уменьшать до концентраций меньше чем 10 мг/г. Полезная мощность катионообменника 1,6 моль/дм^3, а анионообменника 1,2—1,3 моль/дм^3.

HUNGARIAN JOURNAL
OF INDUSTRIAL CHEMISTRY
VESZPRÉM
Vol. 9. pp. 251—262 (1981)

REMOVAL OF ORGANICS FROM WASTE WATER BY MACRORETICULAR RESINS. I.

ADSORPTION AND ELUTION EQUILIBRIA OF SEVERAL SOLUTES

GY. MARTON*, MRS. J. HAVAS-DENCS*, L. SZOKONYA*
and MISS ZS. ILLÉS**

*Veszprém University of Chemical Engineering,
Department of Chemical Process Engineering
**State Hospital, Balatonfüred, Hungary

Received: May 15, 1981.

The aim of the work reported here was the determination of multi-component phase-equilibria established on adsorption resins. Therefore, the well-known LANGMUIR and B.E.T. equations were modified and applied for the description of liquid-solid adsorption. The relationships derived fit well the adsorption isotherms obtained on charcoal as determined by OKAZAKI-KAGE and TOEI [1]. The major advantage of the model proposed, however, is that the adsorption isotherms of benzene and methyl-isobutylketone (MIBUK) mixtures dissolved in water and the elution isotherms of a mixture of benzene and methyl-iso-butyl ketone obtained with methanol as eluent can be described by expressions of similar structure. The difference between adsorption isotherms measured on a macroreticular resin, AMBERLITE XAD-4, and those calculated by the model proposed is less than 2—15%.

Introduction

The recovery of the slightly soluble organics dissolved in waste waters and fermentation broths (at 1—5 g/l concentration levels) is a frequent task in the chemical industry. The use of activated charcoal and polymer resin adsorbents for this purpose has often been mentioned in literature of the past two decades, especially for the solution of problems associated with the pharmaceutical and organic synthesis industry [2, 3].

The advantages of the ever more popular, high-quality synthetic resin adsorbents are often demonstrated by comparing the adsorption isotherms or break-through curves of the resin in question and a high-quality activated charcoal. Unfortunately, most comparisons include only single components (e.g. benzene or phenol). Relatively little is known about the simultaneous

adsorption of two or more compounds. Desorption equilibria, such as established, for example, during elution with alcohols have not been investigated in sufficient detail, either on activated charcoal, or on synthetic resins.

The Adsorption Isotherms In Solid-Liquid Systems

In the case of several solutes simultaneously adsorbed by a solid phase, the state-equation of liquid-phase adsorption is given by the isotherm-equations:

$$q_i = f_i(c_1; c_2; \ldots c_i, \ldots c_n; T) \tag{1}$$

best fitting the measured data. This task appears to be a simple one, because the thermodynamic relationships of the adsorption isotherms can be readily derived from the GIBBS—DUHEM equation. The GIBBS-isotherm reads, in the case of dilute aqueous solutions, as:

$$Ad\pi/RT = \sum_{i=n}^{n} (q_i/c_i)dc_i \tag{2}$$

Unfortunately, without the knowledge of the actual form of Eq.1, this isotherm (Eq. 2) cannot be integrated. Therefore, essentially, Eq. 2 does not help in the solition of the original problem.

Some of the isotherms used in daily practice, nevertheless, have a theoretical foundation. Such isotherms are the LANGMUIR isotherms, those derived by the TÓTH and REDLICH—PETERSON theory [4, 5], or those derived recently, by OKAZAKI-KAGE-TOEI [1]. The other group of isotherms is the FREUNDLICH-isotherm, or other similar power-functions [6]. Though these equations are essentially empirical, they are more accurate than the LANGMUIR isotherm, especially in the case of several simultaneously adsorbed solutes. The poor precision of the adsorption isotherms mentioned in literature is due to the extremely heterogeneous adsorbent surface provided by activated charcoal, the most frequently used adsorbent. So, even in the case of a single solute, adsorption may follow 4 or 5 different isotherms [7]. By increasing the number of model parameters this problem can be eliminated if only a single solute is involved, but the empirical nature of the model becomes more dominant. However, this approach is not feasible when several solutes are present.

The situation observed with synthetic resin adsorbents is different. The active surface of the synthetic resin adsorbents is energetically more homogeneous than that of the activated charcoals. Therefore, as expected, the LANGMUIR-type monomolecular adsorption concept applies better in dilute solutions. In concentrated solutions, the multi-layer adsorption models, as for exapmle, the B.E.T.-theory constructed from the LANGMUIR-principle, can be applied.

The essence of the work reported here can be summarized as the re-evaluation an extension of the LANGMUIR and B.E.T. isotherms, and their application for the description of simultaneous adsorption of several solutes.

The Langmuir-type adsorption of several, simultaneously adsorbed liquid components

WEBER [8] extended the original LANGMUIR isotherm to describe the simultaneous, monomolecular adsorption of two compounds. His well-known adsorption equation reads:

$$q_i = \frac{Q_i b_i c_i}{1 + \sum_{j=1}^{n} b_j c_j} \tag{3}$$

The equilibrium distribution of a component can be represented by the electric network shown in *Fig. 1.* In this network the partial capacities play an important role, as the limiting capacity is:

$$C_0^* = \frac{\sum_{i=1}^{n} C_i^*}{\sum_{j=1}^{n} C_j^*/Q_j} \tag{4}$$

and

$$C_i^* = Q_i b_i c_i, \tag{5}$$

and the resultant capacity is:

$$C^* = \sum_{i=1}^{n} q_i \tag{6}$$

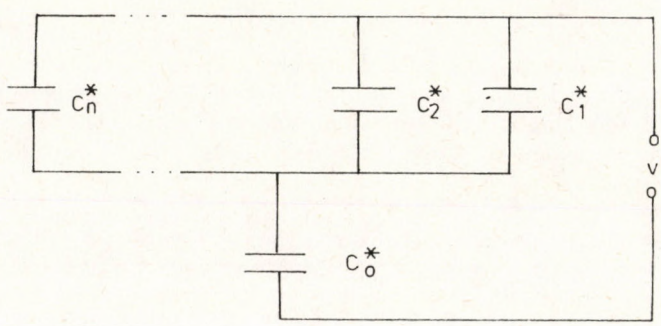

Fig. 1.
Electric network-analogy of adsorption from liquid phase

According to *Fig. 1* the reciprocal resultant capacity is:

$$\frac{1}{C^*} = \frac{1}{\sum_{i=1}^{n} C_i^*} + \frac{1}{C_0^*} \tag{7}$$

From Eq. 6 and 7:

$$\sum_{i=1}^{n} q_i = \frac{C_0^* \sum_{i=1}^{n} C_i^*}{C_0^* + \sum_{i=1}^{n} C_i^*} \tag{8}$$

and:

$$q_i = \frac{C_0^* C_i^*}{C_0^* + \sum_{i=1}^{n} C_i^*} . \tag{9}$$

The effective limiting adsorption capacity of the resin for two solutes can be obtained from Eq. 4 and 9:

$$C_0^* = \frac{Q_1 b_1 c_1 + Q_2 b_2 c_2}{b_1 c_1 + b_2 c_2}$$

The isotherm equations for solutes 1 and 2 become:

$$q_1 = \frac{Q_1 b_1 c_1 c_1}{1 + b_1 c_1 + b_2 c_2} \tag{9a}$$

and:

$$q_2 = \frac{Q_2 b_2 c_2}{1 + b_1 c_1 + b_2 c_2} . \tag{9b}$$

Thus, in a multi-component system, the limiting adsorption capacity of the adsorbent is weighted according to $b_i c_i$ and may never exceed the Q_i value obtained for the pure components. Essentially, this approach neglects the interaction of the components adsorbed, and considers them energetically similar. Therefore, Eq. 3 yields the isotherm with sufficient precision only when the components have approximately identical Q_i and b_i values. Even WEBER [8] noted these limitations of Eq. 3 when he studied the simultaneous adsorption of phenol and sodium dodecyl sulphonate on activated charcoal. Ha found that the limiting adsorption capacity of the binary mixture considerably exceeded the Q_i values derived for the single components. He thought that the phenomenon was due to the dissimilarity of the molecular structures involved.

Extension of the Langmuir and B.E.T. theory for the description of multi-component liquid-phase adsorption

According to the original LANGMUIR hypothesis the free area available for component i at adsorption is:

$$S_i = \tau_i z_i \sigma_{0i} N \left(Q_i - \sum_{j=1}^{n} S_i \right) \tag{10}$$

Let us assume that the ratio of free and occupied area of the adsorbent is:

$$\frac{S_i}{\sum_{j=1}^{n} S_j} = \frac{N \tau_i z_i \sigma_{0i} Q_i}{\sum_{j=1}^{n} N \tau_j z_j \sigma_{0j} (Q_j - \delta_{ij})} \tag{11}$$

where δ_{ij} is the surface-area-excess accounting for the difference in size and energy-state of the competing adsorbing components. By definition $\delta_{ij} = 0$ for each $i = j$, while for $i \neq j$ it may be a positive or negative number, or zero.

By substituting Eq. 11 into Eq. 10 we obtain:

$$S_i = \tau_i z_i \sigma_{0i} N \left[Q_i - \frac{S_i}{N \tau_i z_i \sigma_{0i} Q_i} \sum_{\substack{j=1 \\ i=1}}^{n} N \tau_j z_j \sigma_{0j} (Q_j - \delta_{ij}) \right] \tag{12}$$

Let us introduce:

$$\tau_i z_i \sigma_{0i} N = b_i c_i \,. \tag{13}$$

Let us make use of the statement of the B.E.T. theory, i.e. that at low concentrations the adsorption surface area is linearily related to the concentration of the adsorbed component:

$$S_i = \left(1 - \sum_{i=1}^{n} k_i c_i \right) q_i \tag{14}$$

By substituting Eq. 13 and 14 into Eq. 12 we obtain:

$$q_j = \frac{b_i c_i Q_i}{1 + \frac{1}{Q_i} \sum\limits_{\substack{j=1 \\ j=1}}^{n} b_j c_j (Q_j - \delta_{ij})} \cdot \frac{1}{\left(1 - \sum\limits_{i=1}^{n} k_i c_i \right)} \tag{15}$$

Let us introduce:

$$b_{ji} = \frac{b_j (Q_j - \delta_{ij})}{Q_i}$$

For three components Eq. 15 becomes:

$$q_1 = \frac{b_1 Q_1 c_1}{(1 + b_1 c_1 + b_{21} c_2 + b_{31} c_3)} \cdot \frac{1}{(1 - k_1 c_1 - k_2 c_2 - k_3 c_3)} \tag{15a}$$

$$q_2 = \frac{b_2 Q_2 c_2}{(1 + b_2 c_2 + b_{12} c_1 + b_{32} c_3)} \cdot \frac{1}{(1 - k_1 c_1 - k_2 c_2 - k_3 c_3)} \tag{15b}$$

$$q_3 = \frac{b_3 Q_3 c_3}{(1 + b_3 c_3 + b_{13} c_1 + b_{23} c_2)} \cdot \frac{1}{(1 - k_1 c_1 - k_2 c_2 - k_3 c_3)} \tag{15c}$$

Experience tells us that the values of k expressed in m^3/mole is between 5×10^{-5} and 3×10^{-2}, so the effective LANGMUIR constants, Q_i and b_i can be obtained from the data of mono-component solutions assuming that their concentration is below 1—2 mole/m^3. (Obviously so, since the value of $k_i c_i$ is practically zero.) Using the Q_i and b_i values thus obtained, the most probable k_i value can be calculated from isotherms taken in more concentrated solutions. Then, by using the mono-component data thus obtained, the b_{ij} value of multi-component systems can be obtained. Naturally, the more components that are present the higher the error in b_{ji}. The error is partly an analytical error, and partly the error of the model.

Application of Eq. 15 for the Calculation of the Binary Adsorption Isotherms on Activated Charcoal as Measured by Okazaki-Kage-Toei

OKAZAKI-KAGE-TOEI used [1] the CAL (Calgon Corp.)-type activated charcoal for the determination of simultaneous adsorption isotherms of phenol-p-nitrophenol and p-cresole-p-nitrophenol dissolved in water. Using their data, the

constants of Eq. 15a, 15b and 15c were determined for phenol (p) and p-nitro-phenol (n).

Measured and calculated q_i values (q_i^m and q_i^c, the latter obtained with Eq. 15) are compiled in *Table 1* along with the F error percentage calculated as:

$$F_i = 100 \left[\sum_{l=1}^{N} \{(q_{il}^c - q_{il}^m)/q_{il}^m\}^2 / N \right]^{1/2} \tag{16}$$

Table 1

Comparison of measured and calculated isotherms of phenol (p) and p-nitro-phenol (n) on activated charcoal

C_p mol/m³	C_n mol/m³	q_p^m mol/kg	q_p^c mol/kg	c_n mol/m³	c_p mol/m³	q_n^m mol/kg	q_n^c mol/kg
0.1	0	1.03	1.03	0.1	0	1.56	1.55
0.2	0	1.42	1.41	0.2	0	1.80	1.83
0.4	0	1.70	1.72	0.4	0	1.96	2.01
0.6	0	1.82	1.86	0.6	0	2.04	2.09
0.8	0	1.92	1.94	0.8	0	2.10	2.14
1.0	0	1.99	1.99	1.0	0	2.16	2.17
2.0	0	2.11	2.13	2.0	0	2.31	2.29
4.0	0	2.27	2.24	4.0	0	2.50	2.46
6.0	0	2.35	2.32	6.0	0	2.60	2.64
$q_p^c = \frac{19.545 c_p}{1 + 8.930 c_p (1 - 0.0124 c_p)}$				$q_m^c = \frac{52.490 c_n}{1 + 23.860 c_n (1 - 0.029 c_n)}$			
$F_p = 1.16\%$				$F_n = 1.67\%$			

It can be seen from *Table 1* that the model is adequate for those mono-component systems. In the case of binary systems the results do not agree so well; though the error is within 20%, a practically acceptable value (cf. *Table 2*).

Application of Eq. 15 for the Calculation of the Amount of Benzene and MIBUK Adsorbed by Amberlite XAD-4 from the Aqueous and Methanol Solution of their Mixture

Experiments were carried out with the macroreticular resin, Amberlite XAD-4, and the aqueous solutions of a mixture of benzene and MIBUK. These experiments were followed by elution experiments carried out with methanol. Equilibrium measurements were carried out in a mixed tank of 1 l capacity. The phase volume ratio of the adsorbent was kept at 5% in each experiment. The apparatus was thermostatted to 20 ± 0.2 °C. Concentration changes of both components in the aqueous phase were determined by UV spectrophotometry. The error of the measurement was less than 3%. No change could be detected in the concentrations after an equilibration period of 2.5 hours,

Table 2

Comparison of measured and calculated isotherms of phenol (p) and p-nitro-phenol (n) on activated charcoal (simultaneous adsorption)

c_p mol/m³	c_n mol/m³	b_{np} m³/mol	q_p^m mol/kg	q_p^c mol/kg	c_n mol/m³	c_p mol/m³	b_{pn} m³/mol	q_n^m mol/kg	q_n^c mol/kg
1.5	0.1	112.13	1.17	1.38	0.4	1	3.80	1.50	1.61
2	0.1	96.53	1.41	1.57	0.6	1	3.55	1.72	1.79
3	0.1	77.23	1.72	1.74	0.8	1	3.32	1.86	1.90
4	0.1	71.68	1.88	1.88	1	1	2.93	1.97	1.98
5	0.1	36.45	2.12	1.97	2	1	1.45	2.22	2.19
6	0.1	31.89	2.20	2.05	4	1	3.42	2.41	2.42
1	0.5	80.56	0.40	0.43	0.4	5	2.01	1.10	0.92
1.5	0.5	77.56	0.57	0.60	0.6	5	2.20	1.30	1.16
2	0.5	72.24	0.74	0.74	0.8	5	2.27	1.46	1.34
3	0.5	68.07	1.00	0.96	1.0	5	2.25	1.60	1.48
4	0.5	63.49	1.22	1.14	2	5	2.19	2.00	1.90
5	0.5	59.86	1.40	1.29	4	5	2.72	2.32	2.31
6	0.5	61.30	1.51	1.41	6	5	5.21	2.42	2.60
1	1	82.73	0.22	0.25	0.2	10	1.62	0.55	0.36
1.5	1	81.78	0.32	0.35	0.4	10	1.95	0.81	0.63
2	1	75.01	0.44	0.45	0.6	10	2.03	1.03	0.84
3	1	76.84	0.60	0.62	0.8	10	2.13	1.19	1.02
4	1	68.01	0.81	0.77	1	10	2.73	1.32	1.17
1	5	40.14	0.11	0.06	2	10	2.34	1.78	1.67
2	5	48.48	0.18	0.12	4	10	3.21	2.15	2.22
4	5	55.20	0.31	0.24	6	10	4.83	2.30	2.60

$$q_p^c = \frac{19.545 c_p}{1 + 8.930 c_p + 72.80 c_n} \cdot \frac{1}{(1 - 0.0124 c_p - 0.0288 c_p)}$$

$$q_n^c = \frac{52\,490 c_n}{1 + 23.860 c_n + 2.81 c_p} \cdot \frac{1}{(1 - 0.0288 c_n - 0.0124 c_p)}$$

$F_p = 19.70\%$ $F_n = 17.80\%$

so the conditions prevailing at 2.5 hours after the start of the experiment, could be considered equilibrium ones. Eq. 15 was applied for each equilibrium setting. The results of the measurements and calculations are summarized in *Tables 3...6.*

It is apparent from Tables 3...6 that in the system studied k_i is about 10^{-5} m³/mole for both benzene, MIBUK and methanol. This means that below $c_i = 10^3$ mole/m³ the isotherms are practically LANGUMIR-type ones. (It is at this concentration that the multiple $k_i c_i$ causes a correction amounting to 1%.)

It can be seen that in the case of elution carried out with methanol, the $k_i c_i$ multiple plays an important role ($c_A \sim 10^4$).

It also follows that in the multi-component system studied, MIBUK, which is bound to a lesser extent, acts upon benzene as a "salting out" agent. This means that on Amberlite XAD-4 the two components can be separated almost completely by using a frontal adsorption-elution process. Using two columns

Table 3

Comparison of measured and calculated isotherms of benzene (B) and MIBUK (M) on Amberlite XAD—4 resin (adsorption from 20 °C aqueous solutions)

c_B mol/m³	c_M mol/m³	q_B^m mol/kg	q_B^c mol/kg	c_M mol/m³	c_B mol/m³	q_M^m mol/kg	q_M^c mol/kg
0.462	0	0.487	0.453	0.10	0	0.091	0.036
0.756	0	0.750	0.765	0.21	0	0.073	0.070
1.051	0	0.979	0.932	0.35	0	0.128	0.118
1.282	0	1.147	1.096	1.05	0	0.307	0.300
1.308	0	1.160	1.114	1.20	0	0.347	0.335
1.923	0	1.540	1.494	1.50	0	0.395	0.395
2.167	0	1.670	1.594	4.20	0	0.709	0.729
2.691	0	1.870	1.884	6.20	0	0.821	0.860
3.641	0	2.227	2.271	12.70	0	1.068	1.066
3.782	0	2.301	2.371	15.37	0	1.178	1.108

$$q_B^c = \frac{1.071 c_B}{1 + 0.197 c_B} \qquad q_M^c = \frac{0.3684 c_M}{1 + 0.267 c_M}$$

$F_B = 2.56\%$ $F_M = 9.71\%$

Table 4

Comparison of measured and calculated isotherms of benzene (B) and MIBUK (M) on Amberlite XAD—4 resin (adsorption from 20 °C aqueous solutions). The case of simultaneous adsorption

c_B mol/m³	c_M mol/m³	b_{MB} m³/mol	q_B^m mol/kg	q_B^c mol/kg	b_{BM} m³/mol	q_M^m mol/kg	q_M^c mol/kg
0.833	3.30	+0.014	0.736	0.809	0.801	0.477	0.528
2.179	12.80	+0.013	1.464	1.954	0.528	0.847	0.854
2.308	17.50	−0.006	1.834	2.182	0.252	1.031	0.942
0.756	1.25	−0.041	0.738	0.719	0.722	0.245	0.268
1.795	1.50	−0.031	1.471	1.450	0.497	0.241	0.239
2.949	2.20	−0.061	2.183	2.050	0.662	0.229	0.263
4.077	2.65	−0.083	2.759	2.490	0.670	0.220	0.258
0.718	2.80	−0.278	0.739	0.706	0.522	0.486	0.488
2.077	4.05	+0.027	1.466	1.667	0.546	0.464	0.476
3.615	5.25	+0.012	2.182	2.396	0.511	0.455	0.456
5.256	6.10	−0.034	3.083	2.997	0.502	0.427	0.424

$$q_B^c = \frac{1.071 c_B}{1 + 0.197 c_B - 0.0184 c_M} \qquad q_M^c = \frac{0.3684 c_M}{1 + 0.267 c_M + 0.508 c_B}$$

$F_B = 13.7\%$ $F_M = 13.2\%$

of suitable size, connected in series, the first column would — expectedly — retain only benzene, and the second column would hold only MIBUK. By separate elution, the two compounds can be practically separated.

Table 5

Comparison of measured and calculated isotherm of benzene (B) and MIBUK (M). Elution from Amberlite XAD−4 at 20 °C, with $C_A = 23750$ mole/l methanol eluent

c_B mol/m³	c_M mol/m³	q_B^m mol/kg	q_B^c mol/kg	c_M mol/m³	c_B mol/m³	q_M^m mol/kg	q_M^c mol/kg
51.280	0	0.110	0.110	120	0	0.141	0.180
217.949	0	0.473	0.466	260	0	0.383	0.391
243.589	0	0.526	0.520	520	0	0.740	0.763
333.300	0	0.723	0.711	790	0	1.129	1.147
525.617	0	1.133	1.117	1000	0	1.433	1.432
589.701	0	1.272	1.252	1340	0	1.920	1.897
705.183	0	1.514	1.494	1600	0	2.310	2.248

$$q_B^c = \frac{1.071 c_B}{(1 + 0.97 c_B + 0.506 c_A)} \cdot \frac{1}{(1 - 4 \times 10^{-5} c_A)}$$

$$q_M^c = \frac{0.3684 c_M}{(1 + 0.267 c_M + 0.245 c_A)} \cdot \frac{1}{(1 - 4 \times 10^{-5} c_A)}$$

$F_B = 1.7\%$

$F_M = 3.3\%$

Table 6

Comparison of measured and calculated isotherms of benzene (B), MIBUK (M) and methanol (A) on Amberlite XAD−4 resin, at 20 °C. The case of simultaneous adsorption

c_B mol/m³	c_M mol/m³	c_A mol/m³	q_B^m mol/kg	q_B^c mol/kg	q_M^m mol/kg	q_n^c mol/kg
333.3	300	23,720	0.774	0.714	0.449	0.438
525.6	430	22,917	1.170	1.123	0.605	0.615
769.2	790	22,900	1.900	1.638	1.167	1.091
1079.9	920	23,100	1.920	2.182	1.208	1.234
117.9	520	23,483	0.249	0.253	0.817	0.766
282.0	530	23,617	0.644	0.605	0.775	0.770
371.8	460	23,727	0.919	0.796	0.690	0.665
237.2	1930	22,431	0.561	0.510	2.543	2.651
38.5	350	23,807	0.084	0.083	0.507	0.523

$$q_B^c = \frac{1.071 c_B}{(1 + 0.197 c_B - 0.0184 c_M + 0.504 c_A)} \cdot \frac{1}{(1 - 4 \times 10^{-5} c_A)}$$

$$q_M^c = \frac{0.3684 c_M}{(1 + 0.267 c_M + 0.508 c_B + 0.245 c_A)} \cdot \frac{1}{(1 - 4 \times 10^{-5} c_A)}$$

$F_B = 9.9\%$

$F_M = 5.9\%$

Conclusions

1. The isotherm proposed here (Eq. 15) can be used equally well for the modelling of isotherms of both the heterogeneous activated charcoal, and the more homogeneous synthetic resins.

2. The isotherm proposed here is at least as precise for mono-component adsorption as any of the other equations proposed in literature [1, 4, 5], and it is much more advantageous for multi-component adsorption than any of those proposed in literature.

3. The main advantage of the isotherm given by Eq. 15 is that the same model can be used for the description of both the adsorption and elution equilibria.

SYMBOLS

A specific surface area of adsorbent, m^2/kg
b adsorption energy coefficient, m^2/mol
c^* resultant capacity of adsorption system, mol/kg
C^* partial capacity (def. by Eq. 4.), mol/kg
C_0^{*i} partial capacity (def. by Eq. 5.), mol/kg)
c_i concentration of i-th solute, mol/m^3
k_i BET-constant, m^2/mol
N AVOGADRO's number, 1/mol
q_i amount of adsorbed component, mol/kg
Q ultimate uptake capacity, mol/kg
R universal gas coefficient, m^2 bar/K mol
S_i surface covered by i-th solute, m^2
T temperature, K
z_i collision frequency factor of i-th solute
π spreading pressure, bar m
σ_{0i} actual area of one adsorbed molecule, m^2
τ_i residence time on the surface of i-th solute, h

Subscripts

i, j . . ., . . ., n component
c calculated
m measured

REFERENCES

1. OKAZAKI, M., KAGE, H. and TOEI, R.: J. of Chem. Engng. of Japan, *1980*, 13, 286—291.
2. KENNEDY, D. C.: Ind. Eng. Chem. Prod. Res. Develop., *1973*, 12, 56—61.
3. RIZZO, L. J., and SHEPHERD, A. R.: Chem. Engineering, *1971*, 84, 95—100.
4 REDLICH, O. and PETERSON, D. L.: J. Phys. Chem., *1959*, 63, 1024.
5. TÓTH, J.: Acta Chim. Acad. Sci. Hung., *1971*, 69, 311—28.
6. JOSSENS, L., PRAUSNITZ, J. M., FRITZ, W. and SCHLÜNDER, E. V.: Chem. Eng. Sci., *1978*, 33, 1097—1106.
7. FRITZ, W. and SCHLÜNDER, E. U.: Chem. Eng. Sci., *1981*, 36, 721—730.
8. WEBER, W. J.: J. Appl. Chem., *1964*, 14, 565—572.

РЕЗЮМЕ

Целью авторов являлась точное определение равновесия фаз установившегося на многокомпонентных исскуственных смолах использованных в качестве адсорберев. Для достижения этой цели развили и использовали в модифицированном виде известные изотермические уравнения Лангмюира и В. Е. Т. Эти зависимости хорошо описывают адсорбционные изотермы измеренные на активном угле Оказаким-Каге и Толлем (I). Главным преимуществом предложенной модели является то, что адсорбционные изотермы смеси бензола растворимой в воде и метил-изобутил-кетона (МИБУК) и системы вензола, МИБУК и метанола описываются одинаковыми структурными формулами. Данные изотерм полученные на искусственной смоле типа AMBEPLITE-XAD—4 согласуются рассчитанными по модели данными в пределах ошибки 2—15%.

HUNGARIAN JOURNAL
OF INDUSTRIAL CHEMISTRY
VESZPRÉM
Vol. 9. pp. 263–272 (1981)

REMOVAL OF ORGANICS FROM WASTE WATER BY MACRORETICULAR RESINS. II.

SEPARATION OF TWO COMPONENTS BY LIQUID ADSORPTION

GY. MARTON, L. SZOKONYA, MRS. J. HAVAS-DENCS and MISS ZS. ILLÉS*

(Veszprém University of Chemical Engineering, Department of Chemical Process Engineering, Veszprém, and *State Hospital, Balatonfüred, Hungary)

Received: May 15, 1981.

Organic solvents, used as extractants and only rarely soluble in water, are quite common in waste waters in the fields of the chemical industry. These solvents include, among others, benzene, toluene, methyl-iso-butylketone (MIBUK), and ethylacetate, etc. Their concentration is generally less then a few grams per litre. In view of their negative effects on the environment, their removal is imperative. In the case of these compounds, adsorption on activated charcoal or synthetic resins is andoubtedly, one of the most popular pollution abatement method.

The separation of benzene and MIBUK, reclaimed from waste water by a dual-column system packed with Amberlite XAD–4 synthetic resin, has been studied in-depth. The kinetics of the process has been measured and identified. Based on these results, a frontal adsorption – elution model was developed.

Introduction

Liquid adsorption on 2–4 stationary-bed columns is frequently used for the frontal separation of compounds. The adsorption, elution and aqueous washing periods can easily be distinguished in this cyclic operation.

A common problem in adsorption-based pollution abatement processes is that the compounds to be removed from the waste water stream are often dissimilar in their adsorption characteristics. Recognition of this problem led to the study of frontal adsorption/elution experiments carried out with both bicomponent and multicomponent systems.

Mathematical Model of Frontal Adsorption and Elution

The complete listing of all the models described in literature would be virtually impossible. Some of the most common models used for the description of multicomponent adsorption are listed in *Table 1.*

Table 1

Mathematical models for frontal adsorption and elution

Denomination	Balance equations	Boundary conditions	Note
General model	$\frac{v}{\varepsilon}\frac{\partial s_i}{\partial x} - D_{Li}\frac{\partial^2 c_i}{\partial x^2} + A = -\frac{\partial c_i}{\partial t}$ $A = -\frac{\partial q_i}{\partial t}$	Four types of conditions are necessary	
Equilibrium model	$\frac{v}{\varepsilon}\frac{\partial c_i}{\partial x} + \frac{\partial q_i}{\partial t} + \frac{\partial c_i}{\partial t} = 0$ $q_i^* = f(c_i)$	$c_i(x, t) = 0;\quad 0 \le x \le L;\quad t = 0$ $q_i^*(x, t) = 0;\quad 0 \le x \le L;\quad t = 0$ $c_i(x, t) = 0;\quad x = 0;\quad t > 0$	$D_{L_i} = 0$ $A \to \infty$ $q_i^n = f(c_i)$ equilibrium
Solid film model [1]	$\frac{\partial c_i}{\partial t_i} + \frac{1-\varepsilon}{\varepsilon}\frac{\partial q_i}{\partial t} + \frac{v}{\varepsilon}\frac{\partial c_i}{\partial x} = 0$ $\frac{\partial q_i}{\partial t} = \beta\omega(q_i^* - q_i)$	$q_i(x, t) = q;\quad (x);\quad 0 \le x \le L;\quad t \le 0$ $c_i(x, t) = 0;\quad 0 \le x \le L;\quad t \le 0$ $c_i(x, t) = c_{0i};\quad x = 0;\quad x = 0$	$\beta\omega = f(c_i)$
General pore diffusion model [2, 3]	$\frac{\partial c_i}{\partial t} + \frac{1-\varepsilon}{\varepsilon}\frac{3}{R}(\beta\omega)_f \cdot (c_i - cp_i/r = R) = D_{Li}\frac{\partial^2 c_i}{\partial x^2} - \frac{v}{\varepsilon}\frac{\partial c_i}{\partial x}$	$c_i(t, x) = 0;\quad 0 \le x \le L;\quad t \le 0$ $\frac{v}{\varepsilon}c_{0i}(t) = \frac{v}{\varepsilon}c;\quad (t, x) - D_{Li}\left.\frac{\partial c_i}{\partial x}\right\|_{x=0};\quad t > 0;\quad x = 0$ $\left.\frac{\partial c_i}{\partial x}\right\|_{x=L} = 0;\quad t > 0;\quad x = L$	$\beta\omega \neq f(c_i)$ $D_{Li} \neq f(c_i)$ $Dp_{12} \neq f(c_i)$

In general, the pore diffusion model [2] best describes adsorption in the case of multicomponent systems. It has the added advantage, compared to the solid film model, that its parameters are independent of concentration. This model, however, is very difficult to realize. In general, the solid film models can be solved both numerically and analytically. Naturally, the relationship between the component transfer co-efficient and concentration has to be known. Therefore, the kinetics of adsorption had to be investigated.

The Kinetics of Adsorption and Elution

The rate-determining intermediary diffusion processes in adsorption and elution are:

1. internal or solid phase diffusion (diffusion in the adsorbent),
2. pore diffusion, i.e. diffusion in the liquid phase filling the pores of the particles, and
3. film diffusion, i.e. diffusion from the mobile phase into the outer surface of the adsorbent.

The differential equations describing the intermediary diffusion processes are summarized in *Table 2*.

Table 2

Descriptrion equations of the intermediary diffusion processes

Diffusion process	Differential equation	Boundary conditions
Internal diffusion	$D_{sz}\left(\frac{\partial^2 q_r}{\partial r^2}+\frac{2}{r}\cdot\frac{\partial q_r}{\partial r}\right)=\frac{\partial q_r}{\partial t}$	$D_{sz}\left.\frac{\partial q}{\partial t}\right\|_{r=R}=(\beta\omega)_f(c-c^*)$; $t>0$ $\left.\frac{\partial q}{\partial r}\right\|_{r=0}=0;\quad t>0$ $q=0;\quad 0>r>R;\quad t=0$
Pore diffusion	$Dp_0\left(\frac{\partial^2 c_r}{\partial r^2}+\frac{2}{r}\cdot\frac{\partial c_r}{\partial r}\right)=\frac{\partial q_r}{\partial t}$	$Dp_0\left.\frac{\partial c}{\partial r}\right\|_{r=R}=(\beta\omega)_f(c-c^*)$; $t>0$ $\left.\frac{\partial c}{\partial r}\right\|_{r=0}=0;\quad t>0$ $q=0;\quad 0>r>R;\quad t=0$
Film diffusion	$\frac{dq}{\partial t}=\frac{(\beta\omega)t}{\beta\varepsilon}(c-c^*)=$ $=(\beta\omega)_f(q-q^*)$ $(\beta\omega)_f=\frac{2.62(D_f\cdot v)^{0,5}}{d_{pa}^{1,5}}$	$q=q_0;\ t=0$

Internal diffusion is described by a polynomial [4], and pore diffusion by a trigonometric series [5]. For comparison purposes, GLUECKAUF [6] derived an approximative expression for both solid phase and pore diffusion. In these equations, the transfer coefficients are expressed in a manner very similar to that used for the film diffusion process. Failure to take into consideration the concentration dependence of the component-transfer coefficients causes detrimental consequences. VERMEULEN [4] solved this problem by proposing the following rate equation for approximating solid-phase and pore diffusion:

$$\frac{dq}{dt} \cong \frac{4D_{sz}\pi^2}{dp_0^2} \frac{q^* - 2q_0 + q}{2q - 2q_0} (q^* - q) \tag{1}$$

With respect to the others, this equation is an improvement, in that it takes into consideration the variation of the component-transfer coefficient with the concentration.

Kinetic Cascade Model

The basis of the kinetic cascade model is the solid-film model supplemented by accounting for the variation of the component-transfer coefficient with concentration. In this way, component-transfer has a finite rate, an idea which is in direct opposition to the provisions of the equilibrium cascade model.

The balance equation of the pth element and the ith component of the liquid phase reads as:

$$\frac{v}{\varepsilon} \frac{C_{i,p,s} - C_{i,p-1,s}}{\Delta x} + \beta\omega\left(q^*_{i,p,s} - q_{i,p,s}\right) = \frac{C_{i,p,s} - C_{i,p,s-1}}{\Delta t} \tag{2}$$

In the case of the solid phase we obtain:

$$\beta\omega\left(q^*_{i,p,s} - q_{i,p,s}\right) = \frac{q_{i,p,s} - q_{i,p,s-1}}{\Delta t} \tag{3}$$

where:

$$q_{i,p,s} = H(c_{1,p,s}; \ldots; c_{n,p,s}) c_{i,p,s}$$

The initial and boundary conditions for adsorption are:

$$\begin{aligned} &c_{i,p,s} = c(0)_i; && x = 0; && t > 0 \\ &c_{i,p,p} = 0; && 0 < x < l; && t = 0 \\ &q_{i,p,s} = 0; && 0 < x < l; && t = 0 \end{aligned} \tag{4}$$

The kinetic cascade model also gives a reasonably accurate description of the adsorption and elution processes. To a large degree the accuracy of the model depends on the accuracy of the equilibrium description of the multicomponent adsorption process.

Adsorption and Elution Equilibria

Despite the fact that several authors dealt with the description of multicomponent adsorption equilibria, no sufficiently accurate equation has yet been published. Literature on the elution equilibria is quite scarce. In Part 1

of this series [8] an equilibrium relationship, equally suitable for both adsorption and elution, was described:

$$q_i = \frac{b_i c_i Q_i}{\left[1 + \frac{1}{Q_i} \sum_{\substack{i=1 \\ j=1}}^{n} b_i c_i (Q_i - \delta_{i,j})\right] \left(1 - \sum_{i=1}^{n} b_i c_i\right)} \tag{5}$$

The above equation was derived from a variation of WEBER's improvenment on LANGMUIR's multicomponent isotherm equation [7], and from an improvenment on the B.E.T. multi-component adsorption equation.

In Part 1 [8] the equations of benzene, MIBUK and methanol on Amberlite XAD—4 were given as:

$$q_i = \frac{Q_b b_b c_b}{1 + b_b c_b + b_{MB} c_M + b_{Ab} c_A} \times \frac{1}{1 - k_A c_A}$$

$$q_M = \frac{Q_M b_M c_M}{1 + b_M c_M + b_{bM} c_b + b_{AM} c_A} \times \frac{1}{1 - k_A c_A} \tag{6}$$

The values of the constants at 20 °C are as follows:

$Q_b = 5.437$ mol/kg $b_M = 0.267$ m³/mol $b_{Ab} = 0.5069$ m³/mol,

$Q_M = 1.38$ mol/kg $b_{Mb} = 0.508$ m³/mol $b_{AM} = 0.249$ m³/mol,

$b_b = 0.197$ m³/mol $b_{bM} = 0.0184$ m³/mol $K_A = 4 \cdot 10^{-5}$ m³/mol.

The difference between the measured adsorption and elution data and those calculated by Eq. 6 is less than 15%. This equation was used for the solution of the kinetic cascade model.

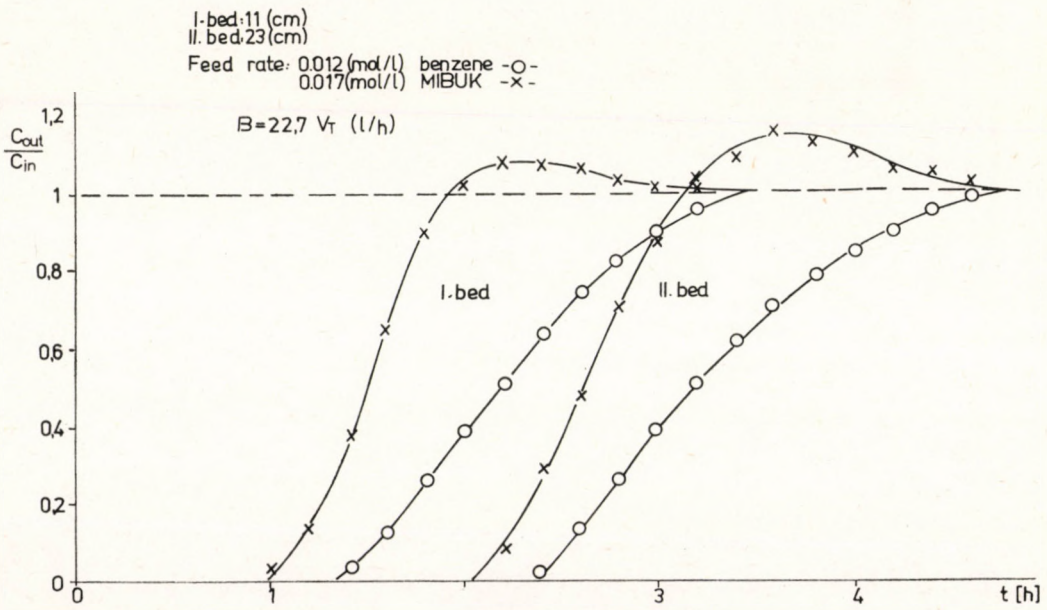

Fig. 1
Break-through curves of benzene and MIBUK

The Adequacy of the Model

In order to investigate the adequacy of the model, benzene and MIBUK were adsorbed on the Amberlite XAD 4—from their dilute aqueous solution. The calculated and measured curves are shown in Figure 1 for two different adsorbent layer thicknesses.

It can be seen in *Fig. 1* that the agreement between the calculated and experimental values is indeed very good. This might be attributed to the fact that bot the solid-phase and pore diffusion coefficients were determined from experimental values.

Benzene and MIBUK adsorbed on the resin could be separated by methanol elution. Two adsorption columns of equal volume were connected in series and

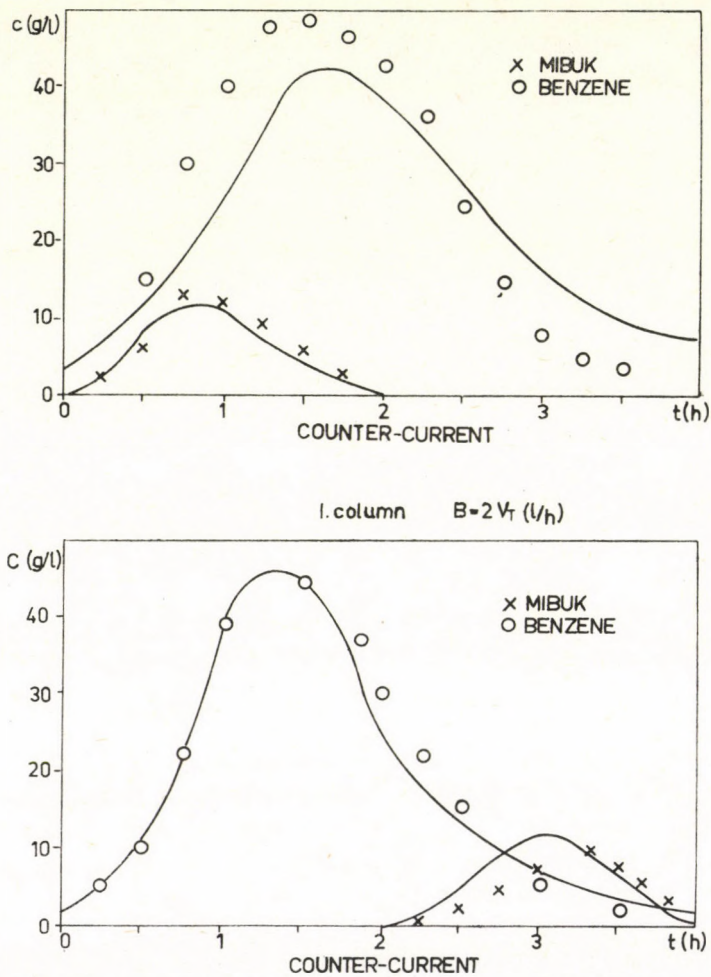

Fig. 2
Elution curves of the first column

loaded with benzene and MIBUK, respectively. Then the columns were eluted with methanol both con-currently and counter-currently.

The elution curves of the first and second colcmns are shown in *Fig. 2* and *3*, respectively. The experimentally determined values are shown along with the calculated curves.

It is apparent in *Fig. 2* that in the case of counter-current elution benzene, which is more readily adsorbed, is eluted first followed by MIBUK. In the

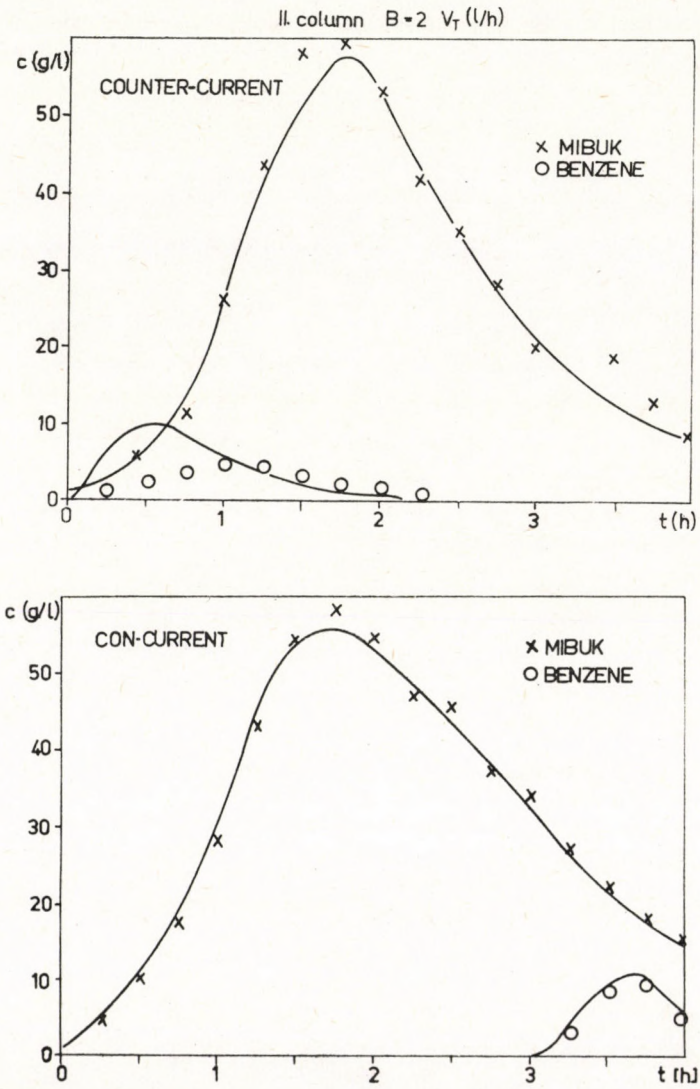

Fig. 3
Elution curves of the second column

case of con-current elution dissolution of both components takes place simultaneously.

Fig. 3, on the other hand, indicates that during the regeneration of the second column benzene and MIBUK can be separated.

Conclusions

The kinetic cascade model and the new equilibrium relationships derived in Part 1 [8] allow for a good description of both the liquid-phase adsorption and elution processes. With a judicial choice of the elution conditions, the components adsorbed in the multi-column adsorbent system can be separated.

REFERENCES

1. Glueckauf, E. and Coates, J. I.: Chem. Soc., *1947*, 1315.
2. Balzli, M. W., Liapis, A. I. and Rippin, D. W. T.: Trans. I. Chem. Eng., *1978*, 56, 145.
3. Liapis A. I., and Rippin, D. W. T.: Chem. Eng., *1974*, 32, 612.
4. Vernemulen, T.: Ind. Eng. Chem. *1953*, 45, 166.
5. Newmann, A. B.: Transact. of A. I. Ch. E., *1931*, 27, 310.
6. Glueckauf, E.: Trans. Farad. Soc., *1955*, 51, 1540.
7. Weber, W. J.: J. Appl. Chem., *1964*, 14, 565—572.
8. Marton, Gy., Mrs. Havas-Dencs, J., Szokonya, L. and Illés, Zs.: Hung. J. Ind. Chem., *1981*, 9, 251.

SYMBOLS

b adsorption energy coefficient, m^3/mol
c_i concentration of solute "i" in fluid phase, mol/m^3
D_{po} pore diffusion coefficient of solute "i", m^2/h
D_{sz} solid-phase diffusion coefficient of solute "i", m^2/h
d_{pa} particle diameter, m
k_i BET-coefficient for component "i", m^3/mol
L length of column, m
R radius of particle, m
Q ultimate uptake capacity, mol/kg
q_i actual amount of adsorbed component "i", mol/kg
q_i^* equilibrium amount of adsorbed component "i", mol/kg
t time, h
x axial distance in column, m
β film mass transfer coefficient, m/h
ε void fraction in the bed, m^3/m^3
ω specific surface area of the adsorbent, m^2/m^3

Subscripts

A methanol
b benzene
M MIBUK
i, ..., m, ..., n component
p−1; p; ...; P serial number of the cascade element
s−1; s; ...; S serial number of time-sharing

РЕЗЮМЕ

Сточные воды химической промышленности часто содержат такие малорастворимые вещества которые необходимо использовать в операциях экстракции. В большинстве случаев такими веществами являются следующие: бензол, толуол, метил-изобутилкетон (МИБУК) этиловый ацетат и. т. д; концентрация которых в сточных водах составит всего несколько граммов на литр. Так как органические вещества отравляют природные воды, животные и расстение в них, удаление таких веществ имеет первостепенное значение. Наиболее распространенным способом извлечения является адсорбция на активном угле или на исскуственных смолах.

Авторы изучали возможность очистки воды содержащей МИБУК использованием двух адсорбционных колонн заполненных искусственной смолой типа AMBERLITE-XAD-4. Измеряли и установили кинетику адсорбции. Построили модель фронтальной адсорбции и системы элюции.

HUNGARIAN JOURNAL
OF INDUSTRIAL CHEMISTRY
VESZPRÉM
Vol. 9. pp. 273–298 (1981)

EXTENSION OF A TRIDIAGONAL MATRIX METHOD TO SOLVE DESIGN PROBLEMS OF EXISTING DISTILLATION COLUMNS

L. Timár, and Z. Csermely

(Hungarian Oil and Gas Research Institute, Veszprém)

Received: May, 27, 1981.

In distillation modelling, the bubble point tridiagonal matrix method (BP), due to its moderate storage requirement, easy realization and good convergence characteristics over a relatively wide range of separation tasks, is often preferred even now to the all equations simultaneously solving approach. For the original BP-algorithm, however, no product parameters can be prescribed instead of the distillate rate. In order to extend the specification range of the BP-method, the Θ-convergence technique of the tray-to-tray calculation approach was attached to the tridiagonal matrix algorithm.

This combination makes it possible to solve some design-like problems without introducing an extra iteration level. Some selected examples illustrate. how efficiently the modified algorithm works.

Introduction

For operating distillation columns it is occasionally inevitable to readjust some parameters to maintain the desired product quality if the feed conditions undergo changes (control case) or to meet new product quality requirements in accordance with the changing demand (design case). Using mathematical modelling for the determination of the modified set of the parameters, the above requirements mean that usually output variables such as light, or heavy key concentration or the bubble point of the products must be specified as input for the rigorous simulation algorithms.

The equations simultaneously solving methods (e.g. [1, 2]) are theoretically suitable for treating any kinds of specifications. Nevertheless, they have the disadvantage that many partial derivates must be evaluated, which leads to a large computer storage requirement and long computation time. Moreover, the construction of such a programme is a rather hard work, in relation to the less complicated approaches based on the decomposition of the model equations. Among the decomposition algorithms, the classical tray-to-tray calculation approach, perfected by Holland and his co-workers [3], is also capable

of handling bubble point or purity specifications, due to the incorporated Θ-convergence method [4]. On the other hand, in the case of multiple feeds they are not competitive with the other class of decomposition approach represented by the tridiagonal matrix methods. The latter ones have a considerable flexibility concerning the number of feeds and side-draws, they exhibit a reliable convergence over a wide range of distillation problems and are easy to realize as a programme. Among them, the full-decomposition bubble point (BP) [3] method seems most popular especially for computers of moderate size. Unfortunately, it is not suitable for treating design-like or control-like specifications made on products. The standard set of the specifications consists of the reflux ratio and distillate rate or reboiler heat duty.

Some attempts so far have been made to extend this set of specifications to design cases. Hirose et al [6], while preserving the original tridiagonal structure, developed an effective iterative procedure, which permits the prescription of the condenser or reboiler heat duty, instead of the reflux ratio. The proposed method is easy to incorporate in existing programmes of any complexity. KORELITZ et al [7] formulated the design-like case as an optimization problem, wherein the light and heavy key quantities are prescribed and considered as constraints and the feed stage location and the reflux ratio must be varied to maximize these quantities. The relatively simple optimization scheme is superimposed on the bubble point algorithm.

The present modification discussed in the following makes it possible to specify the bubble point of any of the products or the mole fraction of the key component in the distillate or in the bottom, instead of the distillate rate. All this can be performed without introducing an external iteration loop, while the tridiagonal matrix structure also remains unchanged.

Modified Algorithm

Θ-method for Product Specifications

The experiences gained with the tray-to-tray calculation approach have convinced us of the excellent convergence characteristics of the so-called Θ-convergence method. In addition, the definition of the Θ-correction permits the prescription of the bubble point or purity of one of the products, instead of the distillate rate or reboiler heat duty. Moreover, all this can be performed without any external iteration loop, which would necessitate several repeated simulations for different values of the distillate rate being adjusted by the appropriate numerical method.

Though the tray-to-tray-specific Θ-correction seems to be alien to the tridiagonal matrix approach, nevertheless, we tried to couple the Θ-method with the bubble point algorithm in order to make use of the above-discussed design-like advantages.

Θ-correction for different specifications

The detailed description of the Θ-method is to be found in [3]. Nevertheless, for good measure, the basic equations are summarized below:

Θ-definition equation:

$$(b_i/d_i)_c = \Theta(b_i/d_i)_{ca} \tag{1}$$

or

$$(d_i/b_i)_c = \Theta(d_i/b_i)_{ca}.$$

Corrected overall material balances:

$$(b_i)_c = \sum_{j=1}^{n} (F_j z_{j,i})/[1 + \Theta(d_i/b_i)_{ca}] \tag{2}$$

or

$$(d_i)_c = \sum_{j=1}^{n} (F_j z_{j,i})/[1 + \Theta(b_i/d_i)_{ca}].$$

If associating the above formulation of the overall material balances with various product specifications, different forms of nonlinear equations of the same type can be derived:

$$g(\Theta) = 0. \tag{3}$$

These Θ-equations can be easily solved by NEWTON's method.

The special forms of the Θ-equations derived for prescribed product temperature or purity are as follows:

Distillate bubble point (T_D):

$$g(\Theta) = \sum_{i=1}^{c} [1 - K_i(T_D)] d_i(\Theta). \tag{4}$$

Bottom bubble point (T_B):

$$g(\Theta) = \sum_{i=1}^{c} [1 - K_i(T_B)] b_i(\Theta). \tag{5}$$

Distillate purity (mole fraction of the key component, y_k):

$$g(\Theta) = y_k - d_k(\Theta) \Big/ \sum_{i=1}^{c} d_i(\Theta). \tag{6}$$

Bottom purity (mole fraction of the key component, x_k):

$$g(\Theta) = x_k - b_k(\Theta) \Big/ \sum_{i=1}^{c} b_i(\Theta). \tag{7}$$

In the case of side products, the additional prescriptions naturally result in additional Θ-equations, so that instead of a single Θ-equation, a nonlinear equation set has to be solved simultaneously.

Insertion of the Θ-method into the BP-algorithm

Before coming to the point of the modification, let us summarize the main steps of the original version of the BP-algorithm, using vector-notation for its basic equations:

1. Input: n, nf, $\underline{F}$, R, D; estimates of $\underline{T}$, $\underline{V}$
2. Calculation of the liquid mole fractions from the material balances:

   $\underline{x}_i = \underline{x}_i(\underline{T}, \underline{V})$ $\quad i = 1, 2, \ldots, c$

3. Calculation of the temperatures of the equilibrium stages from the bubble point relationships:

$$T_j = T_j(\underline{x}_j^T) \qquad j = 1, 2, \ldots, n$$

4. Calculation of the vapour flow profile from the heat balances:

$$\underline{V} = \underline{V}(\underline{\underline{x}}, \underline{T})$$

5. Checking for convergence. If not converged, go to 2.
6. Output: $\underline{\underline{x}}$, $\underline{T}$, $\underline{V}$.

Since the Θ-correction applies component flows, it can be inserted after the material balancing. Of course this correction also leads, to a corrected distillate rate:

$$(D)_c = \sum_{i=1}^{c} d_i(\Theta). \tag{8}$$

The new D-value more or less corresponds to the modified values of the design specifications (x or T). A full correspondence is only reached at the solution point. Due to the decomposition of the equations according to their types in the BP-algorithm, the effect of the Θ-correction is somewhat different from that in the tray-to-tray approach. It means the propagation of the correction over the intermediate trays might be perceived only with some delay, in the following iteration cycles. Nevertheless, it was supposed that the changes of the D-values from iteration to iteration do not considerably interfere with the convergence of the original algorithm.

The numerous distillation runs show that 2—3 iterations with fix (estimated) D-value are usually sufficient to stabilize the convergence for the design case. Consequently, it is advisable to switch over to the product specifications only after some iterations carried out with estimated D (say in the 4th cycle).

Thus, the modified algorithm appears as follows:

1. Input: n, nf, F, R, $x_k(y_k, T_D, T_B)$; estimates of T, V and D
2. Calculation of the liquid mole fractions from material balances:

$$\underline{x}_i = \underline{x}_i(\underline{T}, \underline{V}) \qquad i = 1, 2, \ldots, c$$

3. If the number of the iterations is less than 3, go to 5
4. Θ-correction; new D-value
5. Calculation of the temperatures of the equilibrium stages from the bubble point relationships:

$$T_j = T_j(x_j^T) \qquad j = 1, 2, \ldots, n$$

6. Calculation of the vapour flow profile from the heat balances:

$$\underline{V} = \underline{V}(\underline{\underline{x}}, \underline{T})$$

7. Checking for convergence. If not converged, go to 2
8. Output: $\underline{\underline{x}}$, $\underline{T}$, $\underline{V}$.

If the mixture is strongly nonideal, then the step 2 has to be repeated 3—4 times as in [8], in order to take the concentration-dependency of the equilibrium coefficients into consideration.

Examples

The time-saving power of the Θ-modification will be illustrated with 3 selected examples taken from industrial practice. The aspects of the selection were to have possibly different column configurations and different mixtures for their nonideality. Hence, example 1 represents a conventional distillation problem with slightly nonideal mixture, example 2 is a case of a special column without a condenser, and example 3 demonstrates a strongly nonideal distillation task. The input data are tabulated in the Appendix.

The convergence speed was measured by the average deviation of the sum of the mole fractions:

$$E = \sum_{j=1}^{n} \left(\sum_{i=1}^{c} (x_{j,i} - 1)^2 \right) \Big/ n \tag{9}$$

and the criterium of the convergence was given as $E < 0.0001$.

With regard to the estimates of T and V, constant molar overflow and linear temperature profile were assumed.

For comparison, the calculations were also carried out with D-specification. *Table 1* contains the number of iterations obtained for the different, but corresponding specifications.

Table 1

Examples with different specifications

Example	Number of iterations		
	x_k	T_B	D
1	19	18	15
2	34	31	35
3	9	8	7

From the results, it can be concluded that the product specifications do not considerably increase the iteration number related to that of the D-specification case. In addition, for the special column (example 2) the convergence speed was somewhat enhanced in the event of T-specifications or x-specifications. Similar experiences were obtained for a number of distillation problems which were so far investigated. Evidently, the iteration surplus due to the delay of the Θ-correction effect, seems to be much smaller than the number of additional iterations required by any external NEWTON—RAPHSON-like procedure.

Conclusions

The combination of the Θ-method and the bubble point algorithm makes it possible to solve some design-like problems of existing distillation columns, without introducing any time-consuming extra iteration level. Experience showed that the combined method exhibits good convergence characteristics and its application yields a considerable saving of time as related to the

classical extra-iteration-loop calculation. Moreover, it is easy to insert the relatively simple Θ-method into existing programmes. A similar combination with no full-decomposition matrix algorithms (e.g. [9, 10]) also proved to be very useful. Of course, for those who possess a global, all equations simultaneously a solving programme, the whole procedure discussed in this paper, may lose its attraction.

Appendix

Input data of the examples

Example 1 (propane-butane column)

Feed	
Mass flow, kmol/h	140.8
Temperature, K	417.2
Components, kmol/kmol	
ethane	0.0005
propane	0.0655
butane	0.1111
pentane	0.1721
hexane	0.1714
heptane	0.1677
octane	0.1279
nonane	0.0849
decane	0.0989
Operation parameters	
Pressure, Pa	8×10^5
Number of theoretical trays	15
Feed location	7
Reflux ratio	4.5
Reflux temperature, K	bubble point
Condenser	total
Reboiler	partial
Mole fraction of butane in bottom, kmol/kmol	0.0200
(bubble point of bottom, K)	(439.5)
(distillate rate, kmol/h)	(23.86)
Equilibrium model	GRAYSON—STREED, HILDEBRAND, REDLICH—KWONG
Enthalpy	polynomial

Example 2 (reboiler absorber)

Feed	1	2
Mass flow, kmol/h	114.6	751.1
Temperature, K	250.0	279.0
Components	Mole fractions, kmol/kmol	
methane	0.1224	0.2638
ethane	0.4642	0.1168
propane	0.0566	0.1282
i-butane	0.0001	0.0454
n-butane	0.0001	0.0466
i-pentane	0.0003	0.0128
n-pentane	0.0015	0.0120

hexane	0.1207	0.1251
heptane	0.1271	0.1344
octane	0.0738	0.0791
nonane	0.0244	0.0263
decane	0.0088	0.0095

Operation parameters

Pressure, Pa	25×10^5
Number of theoretical trays	16
Location of feed 1	1
Location of feed 2	9
Reboiler	partial
Mole fraction of ethane in bottom, kmol/kmol	0.0070
(bubble point of bottom, K)	(442.7)
(distillate rate, kmol/h)	(358.6)
Equilibrium model	polynomial based on GPSA-charts
Convergence pressure, Pa	150×10^5
Enthalpy	pseudo-component principle; REDLICH–KWONG eq. of state

Example 3 (strongly nonideal mixture)

Feed

Mass flow, kmol/h	100
Temperature, K	352.3
Components, kmol/kmol	
ethanol	0.4205
water	0.5795

Operation parameters

Pressure, Pa	1.01×10^5
Number of theoretical trays	15
Feed location	10
Reflux ratio	3
Reflux temperature	bubble point
Condenser	total
Reboiler	partial
Mole fraction of ethanol in bottom, kmol/kmol	0.0890
(bubble point of bottom, K)	(360.3)
(distillate rate, kmol/h)	(44.52)
Equilibrium model	Wilson
Enthalpy	polynomial

SYMBOLS

b component mass flow in bottom, kmol/h
c number of components
d component mass flow in distillate, kmol/h
D distillate rate, kmol/h
F mass flow of feed, kmol/h
i component index
j tray index
K vapour-liquid equilibrium coefficient
n number of theoretical trays
nf location of feed
R reflux ratio

T temperature of equilibrium trays, K
T_D bubble point of distillate, K
T_B bubble point of bottom, K
V vapour mass flow, kmol/h
z mole fractions in feed, kmol/kmol
x liquid mole fraction, kmol/kmol
y vapour mole fraction, kmol/kmol
x_k mole fraction of key in bottom, kmol/kmol
y_k mole fraction of key in distillate, kmol/kmol
Θ variable to be iterated in Θ-equations

REFERENCES

1. NAPHTALI, L. M. and SANDHOLM, D. P.: A. I. Ch. E. J. *1971*, 17, 148.
2. BRANOCK, N. F., VERNEUIL, V. S. and WANG, Y. L.: Proceedings of Symp. CHEMDATA '77, 1977; Helsinki-Espoo, Finland, p. 69.
3. HOLLAND, C. D.: Multicomponent Distillation, New York, Prentice-Hall, 1963.
4. LYSTER, W. N., SULLIVAN, S. L., BILLINGSLEY, D. S. and HOLLAND, C. D.: Hydrocarbon Processing, *1959*, 38 (6) 221.
5. WANG, J. C. and HENKE, G. E.: Hydrocarbon Processing, *1966*, 45 (8), 155.
6. HIROSE, Y., KAWASE, Y. and FUNADA, I.: Ind. Eng. Chem. Process Des. Dev., *1980*, 19, 505.
7. KORELITZ, T. H. und HVANG, C. C.: Erdöl u. Kohle, *1976*, 29 (12), 549.
8. RENON, H., ASSELINEAU, L., COHEN, G. et RAIMBAULT, C.: Calcul sur ordinateur des equilibres liquid vapeur et liquid-liquid, Technip., Paris, 1972.
9. JEDLOVSZKY, P.: Chem. Eng. Sci. *1974*, 29, 287.
10. ISHII, Y. and OTTO, F. D.: Can. J. Chem. Eng., *1973*, 51, 601.

РЕЗЮМЕ

При моделировании ректификационных колонн и в наши дни метод известный как тридиагональный матричный покомпонентный подход (ВР) преимущественно используют вместо алгоритмов решающих одновременно все уравнения. Причина этого обьясняется с тем, что в этом случае требуется меньше памяти, легче можно составить программы и в сравнительно широкой области задач сходимость оказывается быстрей. Оригинальный вариант покомпонентного метода однако кроме количества дестиллята не разрешает учитывать специальные характеристики качества продукта. С целью расширения области спецификацией покомпонентного метода, т. н. Θ алгоритм сходимости потарелочного расчета соединили тридиагональным матричным методом.

Такая комбинация позволила трактовать дансе спецификацию некоторых параметров продуктов без введения допольнительного итерационного уровня. Эффективность модифицированного алгоритма иллюстрируется специальными примерами.

HUNGARIAN JOURNAL
OF INDUSTRIAL CHEMISTRY
VESZPRÉM
Vol. 9. pp. 281–298 (1981)

INVESTIGATION OF CARBON DIOXIDE ABSORPTION BY ABSORBENTS IMPREGNATED WITH ALKANOL AMINES

F. RATKOVICS and I. HORVÁTH

(Institute for Physical Chemistry, University of Chemical Engineering, Veszprém, Hungary)

Received: May 26, 1981.

Absorption of carbon dioxide by adsorbents impregnated with alkanol amines was investigated in a laboratory-scale packed column. The over all gas-phase mass transfer coefficients and the enhancement factors were determined in these systems.

Based on the examination of the mechanism of the chemical reaction taking place in the interfacial layer, a reaction model is proposed, which can account for the effect of the chemical reaction upon the absorption rate, better than any other model described in literature.

Introduction

For the design of absorption systems, a knowledge of the mass transfer coefficients prevalent in the given system is of prime importance. Since the chemisorption of carbon dioxide is a widely used operation, a large number of theoretical and practical papers dealt with the absorption of carbon dioxide in alkanolamines, alkaline hydroxide and carbonate-containing absorbents.

DANCKWERTS published an excellent review [1] dealing with the methods used for the estimation of the mass transfer coefficients and the absorption rate. Apparently, the methods based on the film-model, HIGBIE's and DANCKWERTS' mass transfer models can efficiently be used for the estimation of the effects of the reaction rate upon the mass transfer coefficients and the absorption rates, even though the mathematical apparatus involved is fairly simple.

Nevertheless, large differences were observed between actual absorption rate data determined in plant-scale columns and those calculated by the methods mentioned above, when carbon dioxide was absorbed by monoethanol and diethanol amine solutions [2].

Since the available experimental results were obtained, almost exclusively, in laboratory-scale model systems (laminar and turbulent jet, agitated cell, etc.), measurements were carried out with carbon dioxide-alkanolamine solutions using a laboratory-scale packed column. The results obtained were compared with both literature data and with values calculated by the models proposed.

Experimental

Apparatus

A laboratory-scale packed column was used throughout the experiments. Its schematics are shown in *Fig. 1.* The column consisted of 8 glass elements, with internal diameter, $d_k = 0.08$ m. The column was packed to a height of 0.9 m (h) with porcelain Raschig rings of nominal diameter, $d_p = 0.009$ m.

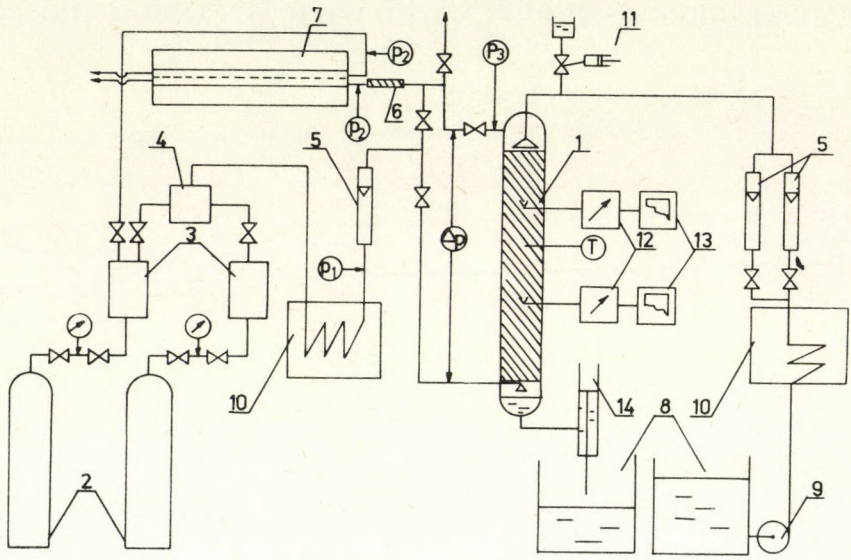

Fig. 1
Schematics of the experimental apparatus
1 — packed column, *2* — gas cylinders, *3* — pressure buffers, *4* — gas mixer, *5* — rotameters, *6* — P_2O_5 drying tube, *7* — gas interferometer, *8* — absorbent tanks, *9* — pump, *10* — thermostats, *11* — injection device, *12* — conductometers, *13* — recorders, *14* — overflow device

Thus, the h/d_k ratio corresponded to the value proposed by UCHIDA and FUJITA [12], and the d_k/d_p ratio was higher than the universally accepted minimum value as proposed by BAKER [13]. The column was packed by the so-called wet method. The measured void volume fraction was $\varepsilon = 0.63$, corresponding to literature values obtained for packings of similar geometry [14].

The argon and carbon dioxide gas mixture was immediately introduced under the packing support screen.

The absorbent was stored in a polypropylene tank of 0.1 m^3 capacity and fed in at the top of the column by a pump. A perforated liquid distributor was used at the top of the column. Visual inspection revealed that the distribution of the absorbent liquid was sufficiently uniform. An overflow device was used at the bottom of the column to maintain a constant liquid level. The temperature of both the gas and liquid phases was controlled in such a

manner that the nominal temperature could be measured at the centre of the column.

The design of the apparatus allowed for the determination of liquid-phase hold-up calculated from the measured residence time distribution functions. STEIGEL's method [15] was used for the residence-time distribution measurements. The modified version of the liquid sampler of ÁRVA and SZEIFERT [16] was used for the determination of conductance in the column.

Measured Quantities and the Calculations

Measurements were carried out at atmospheric pressure and $T = 293 \pm 0.5$ K. The nominal CO_2 concentration in the gas mixture entering the column was 18% v/v.

The volumetric flow rate of the thermostated gas and liquid flows was determined by calibrated rotameters. Gas rotameters were calibrated as a function of the carbon dioxide concentration in the input flow, while liquid rotameters were calibrated against the density of the liquid phase.

Gas pressure was measured in front of the rotameter, p_1, at the exit of the column, p_2, at the entrance of the analyser, p_3. The atmospheric pressure and the pressure drop along the column were also determined. The average gas volumetric flow rate could be calculated from the pressure data, the calibration curve of the rotameter and the extent of absorption. The CO_2-Ar mixture was considered an ideal one.

A thermostated ZEISS gas-interferometer was used for the determination of the carbon dioxide content of the gas phase. Therefore, the gas mixture entering the apparatus was not saturated with water vapour, rather it was dried prior to analysis.

The general gas-side mass transfer coefficients were determined for carbon dioxide in the course of experiments with ion-exchanged water, potassium carbonate-hydrocarbonate buffer, aqueous solution of diethanolamine, and potassium carbonate buffer solution of monoethanolamine and diethanolamine.

The $Ar/CO_2—H_2O$ System

In order to standardize the apparatus, the general gas-phase mass transfer coefficients and liquid-phase hold-up were determined for the $Ar/CO_2—H_2O$ system. The operation parameters were: $G = 0.5—2$ m^3 h^{-1}, $L = 50—150$ dm^3 h^{-1}.

SATER's and LEVENSPIEL's method [17] was used for the determination of the liquid-phase hold-up from the moments of the measured residence time distribution curve. A linear regression was applied between the measured values and liquid feed-rate. The correlation obtained was compared with that of GELBE [18]. As shown in *Fig. 2* the correspondance is satisfactory.

The ideal output flow model of the apparatus was used for the determination of the general gas-phase mass transfer coefficient [16]. It was assumed that the concentration of dissolved carbon dioxide in the distilled water entering the system was negligible:

$$K_G a = \frac{v_G}{h} \times \frac{1}{\frac{m v_G}{v_L} - 1} \ln \frac{Y(h)}{1 - \frac{m v_G}{v_L}[1 - Y(h)]} . \tag{1}$$

The regression relationship obtained is compared in *Fig. 3* with that of MATHUR and WELLEK [19], obtained on a column of similar geometry operated at 298 K in an identical hydrodynamic range.

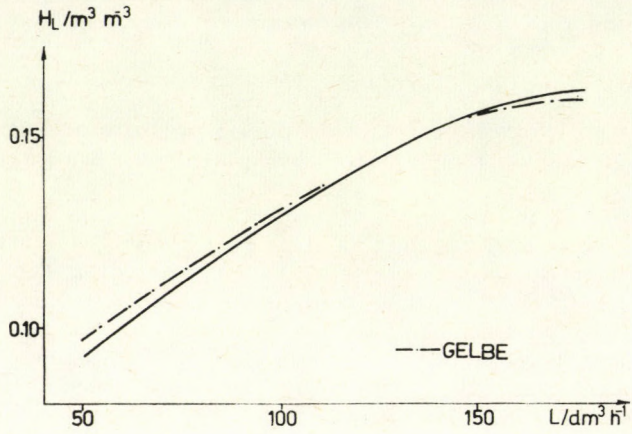

Fig. 2
Liquid hold-up — liquid loading correlation calculated from the residence time distribution

$$H_L = 1.327 \times 10^{-2}\ L^{0.5}/m^3\ m^{-3}$$

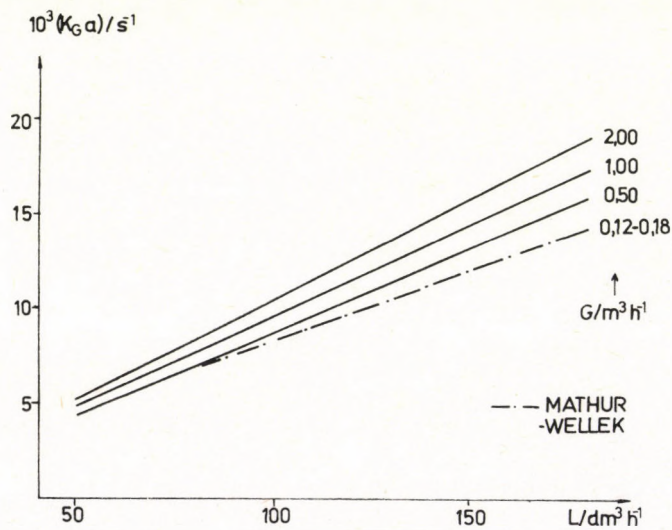

Fig. 3
Generalised gas phase mass transfer coefficient as a function of the gas and liquid load

$$K_G a = 3.646 \times 10^{-5}\ L^{1.012}\ G^{0.125}/s^{-1}$$

The $Ar/CO_2-K_2CO_3/KHCO_3/H_2O$ system

The usefulness of the physico-chemical quantities and the methods used for their estimation were tested in the $Ar/CO_2-K_2CO_3/KHCO_3$ system. The data and the relationships used are summarized in *Table 1.* Since no literature data were available, the density, viscosity and surface tension values of the absorbents used were measured.

The physico-chemical characteristics mentioned were determined at $T = 293 \pm 0.02$ K. Viscosity was determined by an OSTWALD-type capillary-viscosimeter, and surface tension by a stalagmometer. Surface tension was calculated from measurements carried out with materials of known surface

Table 1.a.

The physico-chemical quantities, hydrodynamical parameters and relationships used for the calculations

Quantity	Value	Calculation method	Ref.
D/m^2s^{-1} $T = 298$ K CO_2/H_2O	1.88×10^{-9}	—	[20]
D/m^2s^{-1} $T = 293$ K $CO_2/H_2O-K_2CO_3$	1.4×10^{-9}	STOKES—EINSTEIN's equation	[22]
D/m^2s^{-1} CO_2/Ar $T = 298$ K	1.47×10^{-5}	—	[21]
D/m^2s^{-1} CO_2/Ar $T = 293$ K	1.43×10^{-5}	FULLER's method	[22]
μ_G/Pa s $T = 293$ K	2.09×10^{-5}	GOLUBEV's method	[22]
a_p/m^{-1}	522	$a_p = 4.7/d_p$	[23]
$k_G/m\ s^{-1}$		$7.512 \times 10^{-3} \times G^{0.7}$	[24]
k_L		ONDA et al's correlation relationship	[23]
a/m^{-1}		$50.9 \times L^{0,323}$	[25]
m CO_2/H_2O	1.07		[14]
m $CO_2/K_2CO_3/H_2O$ $C_{K_2CO_3} = 0.8$ mol dm^{-1}	1.29		[26]
m		VAN KREVELEN's and HOFTIJZER method	[1]
k_{OH}, k_{Am}		Value published by DANCKWERTS and HIKITA	[26, 30]

Table 1.b

The physico-chemical characteristics of the absorbents used for the experiments

$T = 293 \pm 0.02$ K

c_{Am}/kmol m^{-3}	ϱ/kg m^{-3}	$10^3 \times \mu$/Pa s	$10^2 \times \sigma$/Nm^{-1}
	DEA/H_2O		
0	998.2	1.004	7.260
0.015	998.3	1.032	7.195
0.077	999.0	1.038	7.175
0.125	999.5	1.050	7.118
0.310	1001.2	1.113	7.042
0.325	1001.1	1.118	7.022
0.515	1001.5	1.190	6.977
	MEA/CO_3^{2-}/HCO_3^-/H_2O		
0	1069.1	1.183	7.272
0.008	1069.7	1.184	7.310
0.018	1070.5	1.191	
0.042	1070.8	1.200	7.321
0.096	1071.8	1.201	7.310
0.300			7.305
0.372	1073.0	1.218	
0.525	1073.4	1.325	
	DEA/CO_3^{2-}/HCO_3^-/H_2O		
0.013	1069.3	1.197	7.318
0.028	1069.4	1.203	7.316
0.061	1069.8		7.308
0.086	1070.0	1.216	7.302
0.300	1072.2	1.255	7.269
0.500	1072.4	1.319	7.257

tension (propionic acid [28]). Double-distilled water was used as reference material in the viscosity determinations. Density was determined by a DMA 20 C type instrument (Anton Paar, K.G., Graz, Austria). The results are shown in *Table 1.b*.

Liquid feed rate was identical with that of the previous run, while the gas flow rate was kept at $G = 0.5 - 1.5$ m^3 h^{-1}. The nominal total carbonate concentration was always $Q = 0.7$ mole dm^{-3}, while the CO_3^{2-}/HCO_3^- ratio, $P = 0.65 - 0.73$.

The following model was used for the calculation of the mass transfer coefficient.

Dissolved carbon dioxide reacts in a solution, which contains both carbonate and bicarbonate ions, as follows:

$$CO_2 + CO_3^{2-} + H_2O \rightleftharpoons 2\,HCO_3^- \qquad (2)$$

(Without catalysis the rate of the

$$CO_2 + H_2O \rightleftharpoons HCO_3^- + H^+$$

reaction is negligible compared with that of Eq. 2 in solutions of pH > 10.)

The reaction described by Eq. 2 takes place in two steps. The rate controlling reaction:

$$CO_2 + OH^- \xrightleftharpoons{k'_{OH^-}} HCO_3^- \tag{3}$$

is preceded by the immediate reaction:

$$CO_3^{2-} + H_2O \rightleftharpoons HCO_3^- + OH^- \tag{4}$$

Under given experimental conditions, assuming that reaction (3) is fast enough to establish an equilibrium for the bulk phase, the concentration of carbon dioxide dissolved in the bulk is sufficiently low. Thus, reaction (3) can be considered irreversible, and the driving force of mass transfer becomes equal with the carbon dioxide concentration in the gas phase. Also, assuming that reaction (4) establishes an equilibrium in the diffusion layer between local OH^-, CO_3^{2-} and HCO_3^- concentrations, hydroxyl ion concentration in the diffusion film becomes practically constant and approaches the OH^- concentration in the bulk. Its mathematical condition [1]:

$$c_L^i\left(\frac{1}{[CO_3^{2-}]} + \frac{2}{[HCO_3^-]}\right)\left(\sqrt{1+\frac{k'_{OH}D_{CO_2}[OH^-]}{k_L^2}}-1\right) \ll 1 \tag{5}$$

is fulfilled in our experimental conditions, and accordingly, reaction (3) can be considered a pseudo-first order, irreversible reaction.

Assuming that the concentration of physically dissolved carbon dioxide is zero in the liquid phase the general gas-phase mass transfer coefficient can be calculated by the following relationship, which is based on the ideal out-flow model of the system:

$$K_G a = \frac{v_G}{h} \ln \frac{1}{Y_{out}} \tag{6}$$

According to the general additivity of the resistances:

$$k_L a = \frac{m}{\frac{1}{K_G a} - \frac{1}{k_G a}} \tag{7}$$

Liquid hold-up, used for the calculation of the general gas-phase mass transfer coefficient, could be obtained by calculation from the values measured with the $Ar/CO_2—H_2O$ system, taking into consideration the density, viscosity and surface tension of the carbonate solution, and using the relationships of HOBLER [27].

The pH of the solution at the entrance and exit of the column was also measured. The logarithmic average (OH^-) value could be calculated from these data. Experimental values were accepted only when the mass balance equation of the gas phase was satisfied within $\pm 10\%$. The results are shown in *Table 2*.

Liquid-phase mass transfer coefficients can be estimated for absorption accompanied by an irreversible, pseudo-first-order reaction with the following equation [1]:

$$k_{L,R} = \sqrt{k_{L,0}^2 + k'_{OH}D_{CO_2}[OH^-]} \tag{8}$$

It is noted that exact values could be obtained from the integral average of the local values of the right-hand-side term, but since axial changes of the

Table 2

Generalised gas-phase mass transfer coefficients for the $Ar/CO_2-K_2CO_3/KHCO_3/H_2O$ system

$T = 293 \pm 0.5$ K
$p = (1.00 \pm 0.01) \times 10^5$ Pa

$\frac{G}{m^3\ h^{-1}}$	$\frac{L}{dm^3\ h^{-1}}$	$\frac{y(0)}{mol\ mol^{-1}}$	$\frac{y(h)}{mol\ mol^{-1}}$	$\frac{[OH^-]\times10^4}{mol\ dm^{-3}}$	$\frac{v_G\times10^2}{ms^{-1}}$	$\frac{K_Ga\times10^3}{s^{-1}}$
.508	50	0.184 96	0.158 18	1.60	5.19	9.02
1.045		0.186 27	0.174 13	1.05	10.67	8.00
1.053		0.178 75	0.166 82	1.28	10.75	8.25
1.588		0.182 43	0.174 70	0.91	16.21	7.79
1.515	96	0.184 23	0.150 88	1.94	5.61	12.45
1.056		0.179 96	0.163 28	1.44	11.50	12.43
1.081		0.178 45	0.163 32	1.12	11.77	11.60
1.579		0.187 52	0.177 35	1.02	17.19	10.65
0.509	145	0.176 50	0.138 33	1.42	5.86	15.87
1.053		0.180 40	0.160 16	1.61	12.13	16.04
1.045		0.180 00	0.161 65	1.10	12.03	14.37
1.581		0.182 75	0.169 30	1.25	18.21	15.47

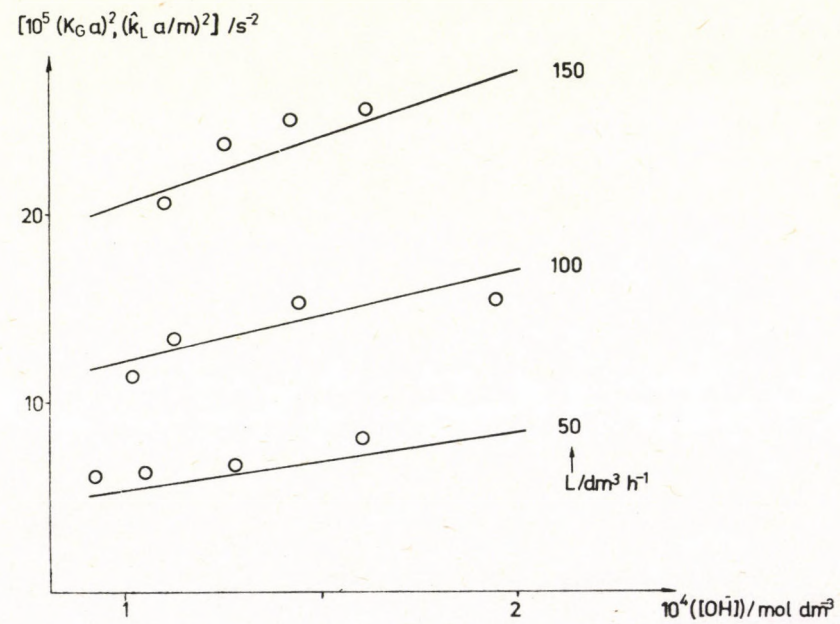

Fig. 4

Measured and estimated mass transfer coefficients for the $CO_2/Ar\text{-}H_2O/CO_3^{2-}/HCO_3^-$ system. $G = 0.50-1.50$ m³ h⁻¹. Full line indicates the k_La vs$[OH^-]$ relationship based on DANCKWERT's model

hydroxide concentration along the entire column were always within 20%, use of Eq. 8 probably does not introduce any significant error.

Mass transfer coefficients calculated from the measured values and also from the average hydroxyl ion concentration by Eq. 8 are compared in *Fig. 4*. $(K_G a)^2$ is plotted in the Figure, and not $(k_L a)^2$, because under the given conditions the gas phase resistance to mass transfer can be neglected in Eq. 7.

The acceptable agreement of the measured and calculated values indicates that the literature data used are indeed applicable for our system, and also the accuracy of the methods used for the estimation of physico-chemical characteristics and hydrodynamical parameters is acceptable.

The Ar/CO_2-alkanolamine/H_2O and Ar/CO_2-alkanolamine/$K_2CO_3/KHCO_3/H_2O$ Systems

Measurements with MEA and DEA were carried out in the same manner as described above. Liquid feed rate was $L=100$ and 150 $dm^3\ h^{-1}$, gas feed rate was $G=0.5$ and 1.0 $m^3\ h^{-1}$. In the case of carbonate-containing systems the overall carbonate content was $Q=0.7$ and the CO_3^{2-}/HCO_3^- ratio was 0.72 in the absorbent entering the system. Amine concentration in the absorbent was set by accurate weighing.

A number of difficulties were met in the evaluation of the experimental results, so these will be dealt with separately in the following chapter.

Evaluation

According to the earlier, universally accepted practice—as shown, e.g. by DANCKWERTS [1]—the reaction taking place between carbon dioxide and MEA or DEA was considered a second order one, i.e. a first order one for both carbon dioxide and the amine. The overall reaction is:

$$2\,R_1R_2NH + CO_2 \rightleftharpoons R_1R_2NCO_2^- + R_1R_2NH_2^+ \qquad (9)$$

Table 3

Generalised gas phase mass transfer coefficients for the $Ar/CO_2-MEA/K_2CO_3/KHCO_3/H_2O$ system

$T = 293 \pm 0.5$ K
$p = (1.00 \pm 0.01) \times 10^5$ Pa
$G = 0.500$ $m^3\ h^{-1}$
$L = 100$ $dm^3\ h^{-1}$
$Q = 0.7$ mol dm^{-3}
$P = 0.72$

c_{Am} / mol dm^{-3}	$[OH^-]\times 10^4$ / mol dm^{-3}	$y(0)$ / mol mol^{-1}	$y(h)$ / mol mol^{-1}	$v_G\times 10^2$ / ms^{-1}	$K_G a\times 10^3$ / s^{-1}
0.005	1.41	0.185 65	0.131 35	5.47	21.03
0.013	1.45	0.185 85	0.115 06	5.46	29.09
0.404	1.43	0.182 83	0.087 21	5.46	44.91
0.890	1.46	0.183 30	0.071 24	5.47	57.44
0.186	1.52	0.186 06	0.052 79	5.47	76.56

Table 4

Generalised gas phase mass transfer coefficients for the $Ar/CO_2-DEA/H_2O$ system

$T = 293 \pm 0.5$ K
$p = (1.00 \pm 0.01) \times 10^5$ Pa
$G = 0.500$ m³ h⁻¹
$L = 100$ dm³ h⁻¹

c_{Am} / mol dm⁻³	$y(0)$ / mol mol⁻¹	$y(h)$ / mol mol⁻¹	$v_G \times 10^2$ / ms⁻¹	$K_G a \times 10^3$ / s⁻¹
0.108	0.184 36	0.103 80	5.59	35.68
0.227	0.184 03	0.075 43	5.59	55.40
0.470	0.188 00	0.042 29	5.63	89.04
0.715	0.187 60	0.019 50	5.67	142.63
0.964	0.184 95	0.012 14	5.64	181.50

Table 5

Generalised gas phase mass transfer coefficients for the $Ar/CO_2-DEA/K_2CO_3/KHCO_3/H_2O$ system

$T = 293 \pm 0.5$ K
$p = (1.00 \pm 0.01) \times 10^5$ Pa
$G = 0.500$ m³ h⁻¹
$L = 100$ dm³ h⁻¹
$Q = 0.7$ mol dm⁻³
$P = 0.72$

c_{Am} / mol dm⁻³	$[OH^-] \times 10^4$ / mol dm⁻³	$y(0)$ / mol mol⁻¹	$y(h)$ / mol mol⁻¹	$v_G \times 10^2$ / ms⁻¹	$K_G a \times 10^3$ / s⁻¹
0.003	1.41	0.187 00	0.146 80	5.26	14.15
0.006	1.43	0.179 90	0.130 95	5.26	18.56
0.020	1.47	0.179 86	0.126 02	5.13	20.28
0.043	1.56	0.186 30	0.118 85	5.06	25.27
0.093	1.60	0.180 08	0.110 79	5.03	27.15

Table 6

Generalised gas phase mass transfer coefficients for the $Ar/CO_2-DEA/K_2CO_3/KHCO_3/H_2O$ system

$T = 293 \pm 0.5$ K
$p = (1.00 \pm 0.01) \times 10^5$ Pa
$G = 1.00$ m³ h⁻¹
$L = 145$ dm³ h⁻¹
$Q = 0.7$ mol dm⁻³
$P = 0.72$

c_{Am} / mol dm⁻³	$[OH^-] \times 10^4$ / mol dm⁻³	$y(0)$ / mol mol⁻¹	$y(h)$ / mol mol⁻¹	$v_G \times 10^2$ / ms⁻¹	$K_G a \times 10^3$ / s⁻¹
0.003	1.40	0.180 90	0.158 78	12.40	17.97
0.007	1.43	0.180 01	0.156 78	12.2	19.40
0.021	1.40	0.179 65	0.150 92	12.2	23.63
0.046	1.60	0.179 76	0.147 72	12.2	26.61
0.095	1.58	0.184 26	0.149 12	12.1	28.45

which follows the following mechanism:

$$R_1R_2NH + CO_2 \rightleftharpoons R_1R_2NHCO_2 \tag{10}$$

$$R_1R_2NHCO_2 + R_1R_2NH \rightleftharpoons R_1R_2NCO_2^- + R_1R_2NH_2^+ \tag{11}$$

If the proton-transfer reaction described by Eq. 11 can be considered momentary compared with Eq. 10, then the rate determining reaction is Eq. 10. If the amount of carbon dioxide physically dissolved is negligible, then the reaction between carbon dioxide and the amines is an irreversible, second-order one. The rate determining step is the reaction described by Eq. 10, while the reaction rate is expressed by Eq. 12:

$$r = k_2'[CO_2][Am] \tag{12}$$

Under such conditions the differential balance equations constructed for the boundary phase cannot be solved analytically. However, the growth coefficient can be calculated by the equation derived from the numerical solution of the equations of the film model. These equations were derived by van Krevelen and Hoftijzer, and published by Danckwerts [1]:

$$E = \sqrt{M\frac{E_i - E}{E_i - 1}} \tanh \sqrt{M\frac{E_i - E}{E_i - 1}} \tag{13}$$

Growth coefficients calculated by Eq. 13 and those calculated from the measured values are compared in *Fig. 5*.

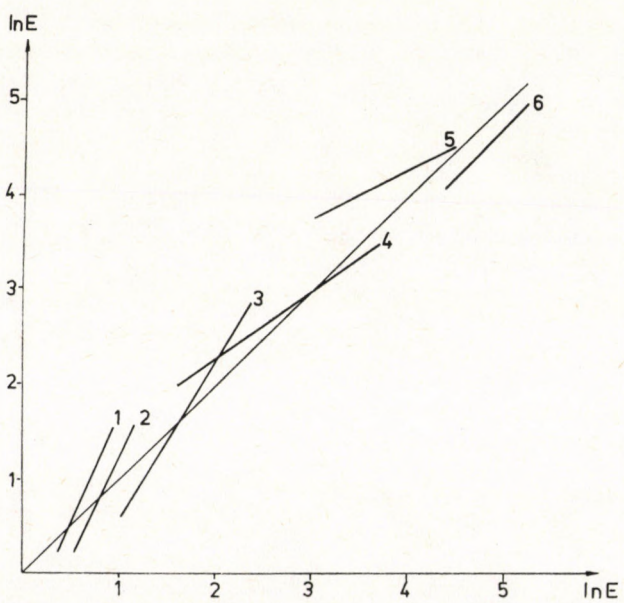

Fig. 5
Calculated (from measured data) and estimated growth coefficients
1 — DEA + carbonate, $L = 100$ dm³ h⁻¹ $G = 0.50$ m³ h⁻¹, *2* — DEA + carbonate, $L = 150$ dm³ h⁻¹, $G = 1.00$ m³ h⁻¹, *3* — MEA + carbonate, $L = 100$ dm³ h⁻¹, $G = 0.50$ m³ h⁻¹, *4* — DEA, $L = 100$ dm³ h⁻¹, $G = 0.50$ m³ h⁻¹, *5* — MEA + carbonate [31], *6* — MEA [32]

It can be seen that though the difference between the measured and calculated values is within the limits acceptable for design purposes, the estimated values have to be considered basically wrong, because there is a trend-like increase in the deviation. This deviation is a monotonous function of the growth coefficient, and as such, makes any extrapolation impermissible.

The fact, supported both by our experience, and a number of recent papers, that the difference between measured and calculated values is a monotonous function of the growth coefficient, prompted a more detailed investigation of the reaction mechanism.

Based on the critical analysis of literature references, DANCKWERTS [3] believed that the mechanism proposed by CAPLOW could be applied for both MEA and DEA. Accordingly, the reaction mechanism can be formulated as:

$$R_1R_2NH + CO_2 \underset{k'_{-1}}{\overset{k'_1}{\rightleftharpoons}} R_1R_2N^+HCO_2^- \tag{14}$$

$$R_1R_2N^+HCO_2^- + \xrightarrow{k'_B} R_1R_2NCO_2^- + BH^+ \tag{15}$$

where B is a BRONSTED-base. In our systems B is either H_2O, OH^- or the amine.

Assuming that the concentration of the very labile $[R_1R_2N^+HCO_2^-]$ is low and the BODENSTEIN principle can be applied, the reaction rate based on the elementary steps described by Eq. 14 and 15, can be given as:

$$r = k'_1[CO_2][Am] - k'_{-1}[R_1R_2N^+HCO_2^-] = [R_1R_2N^+HCO_2^-] \sum_i k'_{B,i}[B_i] \tag{16}$$

If the concentration term of the intermediate is eliminated, the concentrations of the probable bases are substituted into Eq. 16, and the co-current reaction taking place between CO_2 and OH^- is considered (Eq. 3), then the following expression is obtained:

$$r = [CO_2][Am]k'_1\left(\frac{k'_{H_2O} + k'_{B,Am}[Am] + k'_{B,OH}[OH^-]}{k'_{-1} + k'_{H_2O} + k'_{B,Am}[Am] + k'_{B,OH}[OH^-]}\right) + \frac{k'_{OH}}{k'_1}\frac{[OH^-]}{[Am]}\Bigg) \tag{17}$$

However the application of Eq. 17 is limited, because the rate constants are unknown, and also, its form does not allow for the usual, formal treatment, i.e. the reaction rate is given as the power multiple of the reactant concentrations.

Accordingly, a combination of the parameters in Eq. 17 was determined using an ODRA—1204 digital computer, which best fitted HIKITA's measurements [30]. Due to the large number of the parameters Eq. 17 was rearranged in such a manner that the parameters:

$$\frac{k'_{H_2O}}{k'_{B,Am}}, \quad \frac{k'_{OH}}{k'_{B,Am}}, \quad \frac{k'_{-1}}{k'_{B,Am}}, \quad k'_1$$

occurred in it.

In order to further decrease the number of parameters it was assumed that the BRONSTED relationship could be applied for the rate constants of the deprotonation reaction, Eq. 15.

$$\log \frac{k'_{B,i}}{k'_{B,j}} = \log\left(\frac{K_{B,i}}{K_{B,j}}\right)^{\beta} \tag{18}$$

where

$$K_{B,i} = \frac{1}{K_{BH,i}},$$

and

$$K_{BH} = \frac{[B]\,[H^+]}{[HB^+]}, \qquad \beta = \text{const.}$$

Thus, since K_B is known for the given components, the number of parameters could be reduced to three. Two conditions were examined in the course of the calculations simultaneously. The first requirement is the numerical agreement of the reaction rate with that calculated from HIKITA's measurements [30]. The other requirement is that for a given OH^- concentration, and amine concentration range the order of the reaction is constant and agrees with those established by HIKITA [30]. This means that the following conditions set has to be satisfied:

$$\frac{r}{[CO_2][Am]^n} = \text{const} \tag{19}$$

and $n=1$ if Am = MEA, $0.015 < [Am] < 0.177$ and $n=2$ if Am = DEA, $0.174 < [Am] < 0.719$ mole/dm^3.

Using the parameters obtained as described above, the reaction rate was calculated with Eq.17 for a given OH^- concentration as a function of the amine concentration. The reaction-rate — amine concentration relationship indicates that the order of reaction depends on the amine concentration. For any given OH^- concentration it can be accurately approximated by a power function of the amine concentration:

$$r = [CO_2] k'_\alpha [Am]^\alpha \tag{20}$$

where

$$\alpha,\ k'_\alpha = f([Am]) \tag{21}$$

Accordingly, the reaction rate can be given for the successive ranges as the usual power-multiple. This makes the calculation of the growth coefficient possible in a similar manner to Eq. 13.

According to HIKITA and ASAI [31] the growth coefficient of absorption, accompanied by a chemical reaction in the boundary phase, characterized by the rate equation:

$$r = k'_{n_1 n_2} b_1^{n_1} b_2^{n_2} \tag{22}$$

can be calculated as follows:

$$E = \sqrt{M}\left(\frac{E_i - E}{E_i - 1}\right)^{\frac{n_2}{2}} \Big/ \tanh \sqrt{M}\left(\frac{E_i - E}{E_i - 1}\right)^{\frac{n_2}{2}} \tag{23}$$

The growth coefficients were calculated by Eq. 23 and the rate equations determined by us. The values thus obtained were again compared with those calculated from the measured data. The comparison is shown in *Fig. 6*.

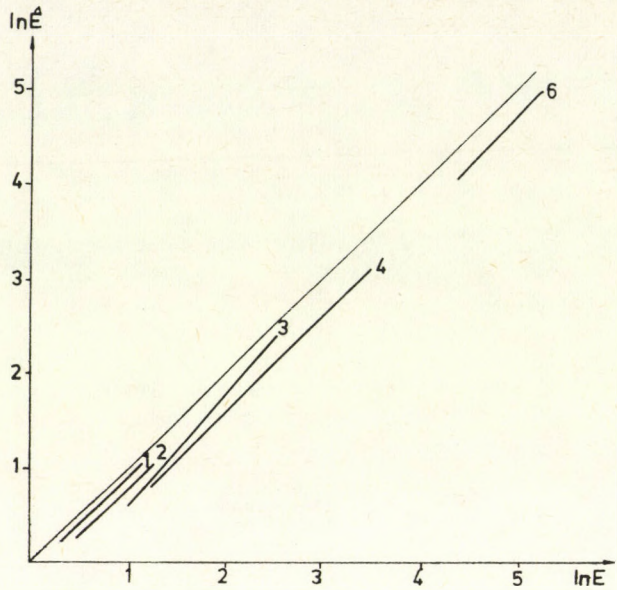

Fig. 6
Calculated (from measured data) and estimated (by the improved method) growth coefficients

$1,2 - 0.4 < \alpha < 1$; $3 - 0.7 < \alpha < 1.3$. $4 - \alpha = 2$, $6 - \alpha = 1$.

(Curve 5 cannot be evaluated, for pH > 11, thus further reactions could take place)

It can be concluded that though some differences between the calculated and measured values still exist, the curves obtained are approximately parallel with the $\hat{E} = E$ line. This indicates that the differences are due to the uncertainties of the physico-chemical quantities and the parameters, and that the model is correct.

Regarding the mechanism of the amine-carbon dioxide reaction, it can be concluded that the approximation offered by the mechanism formulated by Eq. 14 and 15 is better than formerly possible. Another advantage is that its elements are in agreement with experimental data obtained by other methods. The evaluation method described here allows for the estimation of growth coefficients by proven and widespread methods.

Discussion

Even though the model developed here, which considers the complicated mechanism of the reaction taking place between carbon dioxide and both MEA and DEA, is a better approximation of the reality than the earlier attempts, the estimated growth coefficients differ significantly from those determined in actual plant-scale systems [2]. This difference might be due to the inaccuracy of the physico-chemical data used for the calculation of the

mass transfer coefficients. (For example, the published rate constants of MEA and carbon dioxide at 298 K range from 5000 to 8500 $dm^3\ mole^{-1}\ s^{-1}$ [4]). Also, the effects of the chemical reaction upon the actual mass transfer surface area are not fully known, and this effect can be estimated only qualitatively.

Finally, it has to be mentioned that the amines used act not only as reactants, but also as surface active agents. During the absorption process convective flows are induced in the vincinity of the phase boundary layer [5, 6]. The hydrodynamical conditions thus created make the use of transfer models, based on diffusion into a stagnant liquid phase, at best questionable. Though there were several attempts to describe both physical absorption [8, 9] and chemical reaction-accompanied absorption [10] on the basis of turbulence at the phase boundary layer, only regression equations [11] can be used for the acceptably accurate description of the phenomenon.

In our view, the accuracy of the description can be increased by improving the physical model and studying the surface active effects of MEA and DEA.

SYMBOLS

b_1	liquid phase concentration of the component to be absorbed, mole dm^{-3}
b_2	liquid phase concentration of the reacting component, mole dm^{-3}
G	flow rate of the gas phase, $m^3\ h^{-1}$
L	flow rate of the liquid phase, $dm^3\ h^{-1}$
D	diffusion coefficient, $m^2\ s^{-1}$
K	generalized mass transfer coefficient, $m\ s^{-1}$
Q	overall carbonate content, mole dm^{-3}
k	partial mass transfer coefficient, $m\ s^{-1}$
k'	reaction rate constant
v	linear flow velocity of the phase, $m\ s^{-1}$
Y	dimensionless concentration in the gas phase, $y/y\ (0)$
y	gas phase concentration of CO_2, mole dm^{-3}
y (0, h)	gas phase CO_2 concentration at the entrance and exit points, mole dm^{-3}
m	HENRY coefficient, C_G^*/C_L^*, –
n, n_1, n_2	exponents defined by Eq. 19 and 22
c	concentration, mole dm^{-3}
P	buffer ratio, $[CO_3^{2-}]/[HCO_3^-]$
r	reaction rate, mole dm^{-3}, s^{-1}
K_B	basicity constant, $[H^+B]/[B]\,[H^+]$, $dm^3\ mole^{-1}$
E	growth coefficient, –
E_i	limiting value of the growth coefficient for immediate reactions
M	$r \cdot D_{CO_2}/(k_{L,0}^2 \times [CO_2^{i,p}])$, –
a	surface area of the effective boundary, m^{-1}
σ	surface tension, Nm^{-1}
μ	dynamic viscosity, Pas
ϱ	density, $kg\ m^{-3}$
H_L	liquid hold-up, $m^3\ m^{-3}$
d	diameter, m
h	height of the packing, m
ε	void volume coefficient, $m^3\ m^{-3}$

Subscripts

L	liquid
G	gas
i	component
R	in the case of chemical reaction

p	packing
k	column
Am	amine (=MEA and DEA)
O	without reaction
B	Bronsted base

Superscripts

i	phase boundary
*	equilibrium
i, p	boundary phase
∧	estimated

REFERENCES

1. DANCKWERTS, P. V.: Gas-Liquid Reactions. McGraw-Hill Co., New York [etc.], 1970.
2. DE COURSEY, W. J.: Absorption of Acid Gases by MEA: Comparison of Theory with Industrial Practice (Unpublished) (Dep. of Chem. and Chem. Eng., Univ. of Saskatchewan, Saskatoon S7N, OWO, Canada)
3. DANCKWERTS, P. V.: Chem. Eng. Sci., *1979*, 34, 443.
4. SADA, E.; KUMAZAWA, H.; BUTT, M. A. and HAYASHI, D.: Chem. Eng. Sci., *1976*, 31, 839.
5. BRIAN, P. L.; VIVIAN, J. E. and MATIATOS, D. C.: AlChE J., *1967*, 13, 28.
6. THOMAS, V. J. and NICHOLL, E. McK. N.: Chem. Eng. Sci., *1967*, 22, 1877.
7. SADA, E. and LOZANO, J. E.: Can. J. Chem. Eng., *1977*, 55, 293.
8. ANTONINI, V. and ZOULALIAN, A.: Chem. Eng. J., (Lausanne) *1979*, 17, 237.
9. HÖRNER, B.; ABBENSETH, R. J. and DIALER, K.: Vt "Verfahrenstechnik", *1979*, 13, 786
10. KOLAR, V. and BROZ, Z.: Coll. Czehoslov. Chem. Commun., *1975*, 44, 1388.
11. DIL'MAN, V. V.; AKSEL'ROD, J. V. and HUTORYANSKY, F. M.: Khim. Prom.-st. (Moscow), *1976*, 9, 693.
12. UCHIDA, S. and FUJITA, S.: J. Soc. Chem. Ind. (Japan) Suppl., *1943*, 37, 274; *1936*, 39, 432; *1938*, 41, 275.
13. BAKER, T.; CHILTON, T. H. and VERNON, A. C.: Trans. Am. Inst. Chem. Eng., *1935*, 31, 296.
14. PAVLOV, K. F.; ROMANKOV, P. V. and NOSZKOV, A. A.: Primeri i apparatov khimicheskoi tekhnologii "Khimiya", Leningrad, 1976.
15. STIEGEL, G. J. and SHAH, Y. T.: Ind. Eng. Chem. Process Des. Dev., *1977*, 16, 37.
16. ÁRVA, P. and SZEIFERT, F.: Hung. J. Ind. Chem., *1973*, 1, 271.
17. SATER, V. E. and LEVENSPIEL, D.: Ind. Eng. Chem. Fundam., *1966*, 5, 86.
18. GELBE, H.: Chem. Eng. Sci., *1968*, 33, 1401.
19. MATHUR, V. K. and WELLEK, R. M.: Can. J. Chem. Eng., *1976*, 54, 90.
20. MAZAREI, A. F. and SANDALL, O. C.: AlChE J., *1980*, 26, 154.
21. KESTIN, J. and SUNG TACK RO: Ber. Bunsenges. Phys. Chem., *1976*, 80, 619.
22. REID, R. C.; PRAUSNITZ, J. M. and SHERWOOD, T. K.: The Properties of Gases and Liquids McGraw Hill, Inc. 1977.
23. ONDA, K.; SADA, E. and OTUBO, F.: Chem. Eng. (Japan), *1958*, 32, 194.
24. ONDA, K.; SADA, E. and TAKEUCHI, H.: J. Chem. Eng. Jap., *1968*, 1, 62.
25. VIDWANS, A. D. and SHARMA, M. M.: Chem. Eng. Sci., *1967*, 33, 673.
26. DANCKWERTS, P. V. and MCNEIL, K. M.: Trans. Instn. Chem. Engrs., *1967*, 45, T32.
27. HOBLER, T.: Mass Transfer and Absorbers. Pergamon Press, London, 1966.
28. JUHÁSZ, É. and LELKESNÉ ERŐS M.: Felületaktív-anyagok zsebkönyve. Műszaki Könyvkiadó, Budapest. 1979.
29. CAPLOW, M.: J. Am. Chem. Soc., *1968*, 90, 6795.

30. Hikita, H.; Asai, S.; Ishikawa, H. and Honda, M.: Chem. Engng. J., *1977*, 13, 7.
31. Ellis, J. E.: Trans. Inst. Chem. Eng., *1960*, 38, 216.
32. Akselrod, Yu. V.; Dil'man, V. V. and Alekperova, L. V.: Gazov. Prom., *1968*, 13, 37.

РЕЗЮМЕ

Авторы изучали процесс адсорбции углекислого газа адсорбентами содержащими алканоламины в заполненной колонне лабораторного размера. Определили коэффициенты массопередачи и роста для упомянутых систем. Построили модель механизма химической реакции протекающей в пограничном слое учитывающую влияние реакции на скорость адсорбции. Модель дает лучшее приближение по сравнению известных методов расчета.

HUNGARIAN JOURNAL
OF INDUSTRIAL CHEMISTRY
VESZPRÉM
Vol. 9. pp. 299–312 (1981)

ИССЛЕДОВАНИЕ ЛОКАЛЬНОГО МАССОПЕРЕНОСА ОТ ЧАСТИЦЫ К ЖИДКОСТИ. III.

ДВУХФАЗНЫЕ СИСТЕМЫ: НЕПОДВИЖНЫЙ И ПСЕВДООЖИЖЕННЫЙ СЛОЙ

Ермакова А., Кузьмин В. А. и Умбетов А. С.

(Институт катализа СО АН СССР, Новосибирск)

В работе приведены результаты экспериментального исследования локального массопереноса от жидкости к частице в двухфазном неподвижном и псевдоожиженном слое. Измерения проводились электрохимическим методом. Получена зависимость осредненного и пульсационного значения коэффициента массопереноса от скорости жидкости при изменении порозности слоя от 0,38 до 1. Отмечено, что кривая зависимости дисперсии коэффициента массопереноса от скорости жидкости проходит через максимум в области начала псевдоожижения. Экстремальный характер этой зависимости дает возможность использовать электрохимический метод для определения скорости начала псевдоожижения.

Экспериментальные данные обобщены в виде критериального уравнения

$$Sh = F(\tilde{\varepsilon})Sh\big|_{\tilde{\varepsilon}=1}$$

которое справедливо для неподвижного и псевдоожиженного слоя, а также для единичной частицы. Вид функции $F(\tilde{\varepsilon})$ найден из рассмотрения геометрической модели упаковки зернистого слоя. Дано сравнение полученных результатов с литературными данными.

Постановка задачи

В предыдущем сообщении [1] — при исследовании локального массопереноса от жидкости к единичной частице, совершающей гармонические колебания со скоростью:

$$V(t) = (U_0 - A_v \cos \omega_0 t) \tag{1}$$

была получена следующая инвариантная связь между осредненными значениями скорости и коэффициента массопереноса:

$$\bar{k} = (0{,}739 \pm 0{,}021) \times 10^{-3} \bar{V}^{1/2} \frac{\text{см}}{\text{сек}} \tag{2}$$

где

$$V=A_v\left[\frac{2}{\pi}\sqrt{1-x^2}+x\left(1-\frac{2}{\pi}\arccos x\right)\right] \tag{3}$$

$$A_v=A_x\omega_0\,, \qquad x=U_0/A_v$$

Уравнение (2) имеет энергетический смысл, так как оно выражает трансформацию между средними составляющими частотных спектров мощности относительной скорости и коэффициента массопереноса.

Между дисперсиями этих величин также существует однозначная связь, которая выражается в следующем виде:

$$\sqrt{\sigma_k^2(x)}=[H(f)]\sqrt{\sigma_v^2(x)} \tag{4}$$

где

$$[H(f)] \text{ — коэффициент усиления;} \qquad f=\frac{\omega_0}{2\pi} \tag{5}$$

Соотношения (2) и (4) названы инвариантными, поскольку — как показали опыты — независимо от того, каким сочетанием параметров A_x, ω_0 и U_0 были достигнуты данные значения $\overline{V}$ и σ_v^2, уравнения связи (2) и (4) оставались справедливыми. Было показано [1], что структура этих соотношений базируется на решениях уравнений массопереноса и гидродинамики, описывающих процесс на уровне „элементарного акта“, т. е. в масштабе пограничного слоя.

В терминах безразмерных параметров уравнение (2) может быть записано в следующем виде:
в области

$$10<\overline{Re}<2000$$

$$Sh=(0{,}678\pm 0{,}018)\overline{Re}^{1/2}Sc^{1/3} \tag{6}$$

Целью настоящей работы является исследование локального массопереноса от частицы к жидкости в двухфазных — неподвижном и псевдоожиженном — слоях.

Имеющиеся в литературе аналогичные исследования [2, 4, 7—16] согласуются между собой тем, что отмечают существенную зависимость числа Sh от средней порозности слоя. В работе [7] эта зависимость получена из решения модели „обновления поверхности“ Данквертса. В других работах [8, 9, 12, 14] порозность слоя учитывается как эмпирическая поправка в критериальном уравнении массопереноса, полученной для единичной частицы:

$$Sh=\tilde{\varepsilon}^m(ARe_0^{1/2}Sc^{1/3}) \tag{7}$$

Уравнение (7) при $m=-1$ является достаточно удачным обобщением экспериментальных данных.

В работах [11, 15] используется другой подход к обобщению числа Sh. Например, авторы [15] предлагают следующую эмпирическую зависимость:
в области

$$0{,}4<\tilde{\varepsilon}\leq 0{,}9$$

$$Sh=0{,}267Ga^{0{,}33}Sc^{0{,}34}M_v^{0{,}37}, \tag{8}$$

В этом уравнении порозность слоя учитывается лишь в неявной форме. По-су-

ществу она зависит от критериев Ga, M_v, которые в свою очередь влияют на скорость начала псевдоожижения, следовательно и на степень расширения слоя. Интересно отметить, что в уравнении (8) отсутствует зависимость числа Sh от числа Re_0.

Учитывая имеющийся в литературе достаточно богатый экспериментальный материал по массопереносу в двухфазных системах и отсутствие единого подхода к его обобщению, возникает вопрос: можно ли найти хорошую инвариантную форму критериального уравнения, которая была бы справедливой для описания скорости массопереноса между частицей и жидкостью, независимо от состояния слоя. На наш взгляд такими обобщениями могут служить зависимости, подобные уравнению (6), выраженные в терминах локально-осредненных величин. Осредненные по всему объему макроскопические характеристики процесса или состояния слоя (например, средняя объемная порозность $\bar{\varepsilon}$) должны учитываться в этих уравнениях в виде параметров, влияющих на локально осредненные величины. Авторы работ [7, 8, 16] следуют аналогичному подходу. В качестве модели „элементарного акта" использована модель обновления Данквертса. „Локальным" параметром этой модели является частота обновления поверхности: „s". В свою очередь s выражают в виде эмпирических зависимостей от макроскопических параметров процесса, например,

$$s = D_M \alpha^2 Re_0 Sc^{2/3} (d\bar{\varepsilon}^m)^{-2} \tag{9}$$

$$m = 1, \quad \alpha = 0{,}6$$

К сожалению, модель Данквертса сама по себе является полуэмпирической и, входящий в нее коэффициент S скорее всего можно рассматривать лишь как некоторый подгоночный параметр. Повидимому, этим объясняется ограниченная область применимости этой модели для обобщения экспериментальных данных [12].

В данной работе — сохраняя рабочую гипотезу об инвариантности моделей типа (6), записанных в терминах локально осредненных величин, попытаемся найти некоторое, физически обоснованное обобщение для числа Sh, которое будет справедливым независимо от того, является ли слой неподвижным или псевдоожиженным.

Экспериментальная часть

Методика эксперимента

Эксперимент проводили в вертикальной колонне, изготовленной из органического стекла, внутренним диаметром 0,1 м, высотой 1,5 м. Зернистый слой состоял из стеклянных шариков диаметром 0,3 и 0,5 см. Высота неподвижного слоя была равна 13 см. Снизу слой поддерживался сеткой, выполненной из нержавеющей проволоки. Непосредственно перед слоем был установлен специальный участок гидродинамической стабилизации, позволяющий получить плоский профиль скорости на входе в реактор.

Измерение скорости массового потока проводили электрохимическим методом. В качестве анода использовали накопительный бак из нержавеющей стали, емкостью 0,4 м³. Датчиком-катодом служили полые никелевые шарики, имеющие тот же размер и, примерно, тот же вес, которым обладали частицы слоя. Датчики были либо закреплены на конце нержавеющего капилляра, с помощью которого перемещались по радиусу колонны, либо они были свободно подве-

шены на гибкой сдвоенной медной проволоке диаметром 0,0025 см, длиной 25 см. Визуальные наблюдения показали, что случайные блуждания гибко подвешенного датчика по псевдоожиженному слою мало отличается от хаотического движения инертных частиц слоя.

После предварительного усиления электрический ток с датчика подавался на аналогово-цифровой преобразователь ЭВМ ГВС—100, с последующим фурье-анализом сигнала на цифровой части ЭВМ. Длительность одного опыта была равна 41 сек, частота преобразования сигнала: 100 герц, каждый опыт повторялся 10 раз, а результаты повторных опытов усредняли. В результате были найдены средние из 10-и реализаций значения коэффициента массопереноса, дисперсия от среднего, амплитудно-частотный спектр мощности. Диспресия воспроизводимости повторных опытов составляла около 5% от осредненных значений.

Результаты эксперимента

Первичные результаты измерений, пересчитанные на коэффициент массопереноса, представлены на *рисунках 1* и *2*.

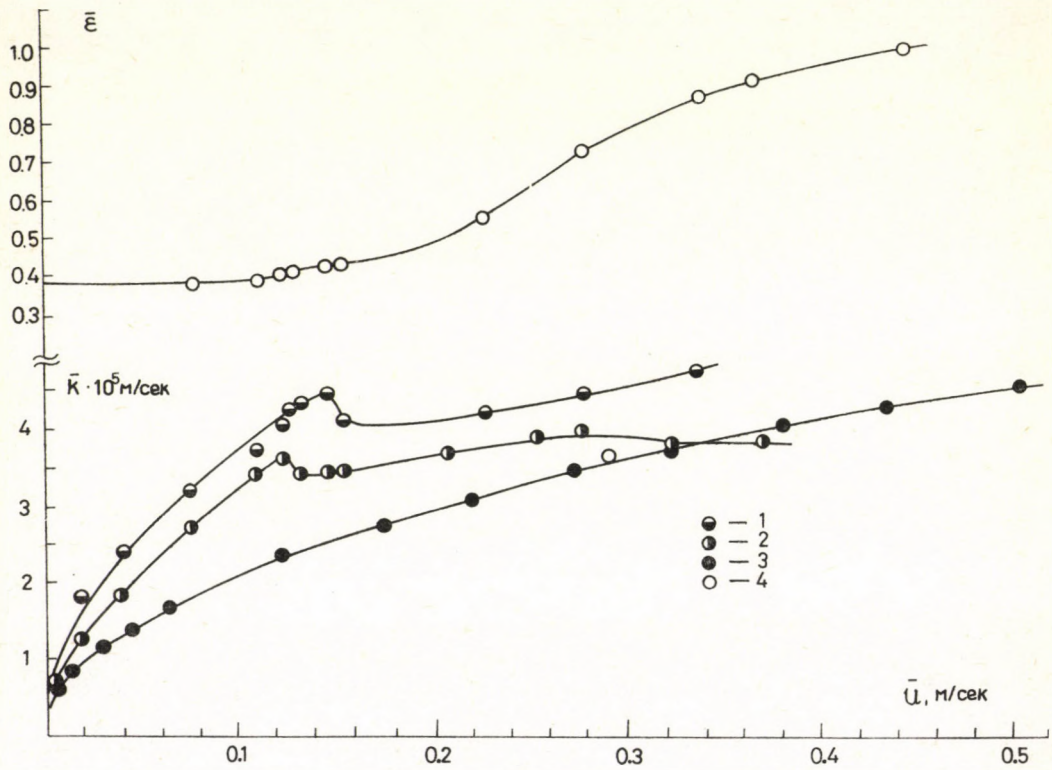

Рис. 1.
Зависимость среднего значения коэффициента массопереноса от средней скорости жидкости
1. Зернистый слой, d=0,4 см; 2. Зернистый слой, d=0,5 см; 3. Единичная частица, d=0,4 см; 4. Порозность в зависимости от $\bar{U}$

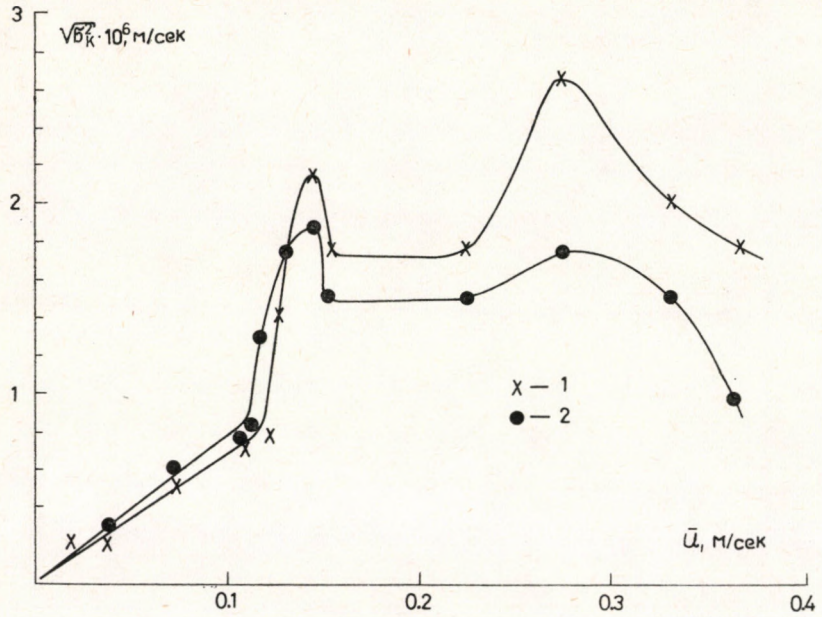

Рис. 2.
Зависимость дисперсии коэффициента массопереноса от средней скорости жидкости в зернистом слое
1. $d=0{,}5$ см; *2*—$d=0.4$ см

График рисунка 1 иллюстрирует зависимость среднего значения коэффициента массопереноса от средней скорости $\bar{U}$ в зернистом слое (кривые 1, 2), и в свободном потоке (кривая 3). На этом же рисунке приведена кривая средней порозности. На *рисунке 2* показаны аналогичные зависимости для пульсационной составляющей $(\sqrt{\sigma_k^2})$ коэффициента массопереноса.

Из графиков следует, что в области неподвижного слоя ($\bar{\varepsilon}=0{,}38$) как среднее значение, так и пульсационная составляющая коэффициента массопереноса возрастают с ростом $\bar{U}$. Кривые $\bar{k}$ в зернистом слое лежат выше кривой $\bar{k}$, измеренной в свободном потоке, и только по мере роста $\bar{\varepsilon}$ они приближаются друг к другу.

Интересно отметить два максимума на кривой $\sqrt{\sigma_k^2}$. Первый максимум — практически скачкообразное изменение — наблюдаем в области начала псевдоожижения, при порозности слоя $0{,}39-0{,}42$. (Аналогичный, но менее ярко выраженный максимум имеет место и на кривой $\bar{k}$). В этой области зернистый слой приобретает подвижность, хотя порозность слоя еще мало отличается от порозности неподвижного слоя. (Согласно наблюдениям авторов [5] частицы обладают максимальной кинетической энергией именно в области, близкой к началу псевдоожижения, при $\bar{\varepsilon}\approx 0{,}48$). Таким образом, исследование дисперсии коэффициента массопереноса электрохимическим методом при переходе от неподвижного слоя к псевдоожиженному может дать прекрасную информацию о скорости начала псевдоожижения.

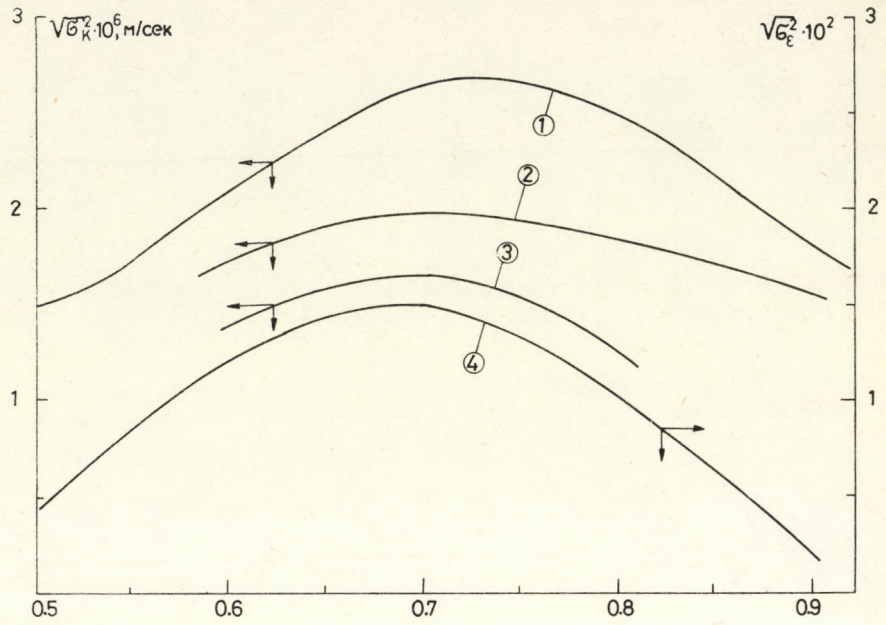

Рис. 3.
Зависимость дисперсии коэффициента массопереноса и пульсации порозности от средней скорости жидкости в зернистом слое
1 — наши данные, $d=0{,}5$ см; *2* — данные [16] $d=1$ см; *3* — данные [16] $d=0{,}7$ см; *4* — данные [6] $d=0{,}42$ см

Второй максимум на кривой $\sqrt{\sigma_к^2}$ принадлежит значению порозности $\tilde{\varepsilon}\approx 0{,}7-0{,}75$. Область этого максимума (зависимость $\sqrt{\sigma_к^2}$ от $\tilde{\varepsilon}$) приведена отдельно на *рисунке 3*. На этом же рисунке показаны аналогичные результаты, полученные в работе [16], а также кривая флуктуации порозности ($\sqrt{\sigma_\varepsilon^2}$), измеренная авторами работы [6]. Как и следовало ожидать, абсцисса точек экстремума ($\tilde{\varepsilon}_м$) на кривых $\sqrt{\sigma_к^2}$ и $\sqrt{\sigma_\varepsilon^2}$ совпадает. Она равна примерно 0,7. Пульсация коэффициента массопереноса невелика, она не превышает $4-5\%$ от среднего значения коэффициента массопереноса. Это свидетельствует об однородности структуры двухфазного псевдоожиженного слоя.

На рисунке 4 приведены частотные спектры мощности, полученные в результате Фурье-преобразования выходного сигнала датчика. Из графиков следует, что в области, близкой к началу псевдоожижения *(рис. 4а)* можно отметить определенную периодичность процесса. Основная мощность сигнала сконцентрирована в достаточно узкой области низких частот, в интервале 0,4—0,6 герц. В области псевдоожиженного слоя *(рис. 4б)* мы имеем более размытые спектры мощности. Частоты, несущие основную мощность сигнала, растянуты в интервале $0{,}4-2$ герц. Следовательно, пульсация массопереноса в псевдоожиженном слое носит скорее случайный чем периодический характер. Эти наблюдения хорошо согласуются с данными работы [16]. Авторы этой работы — в

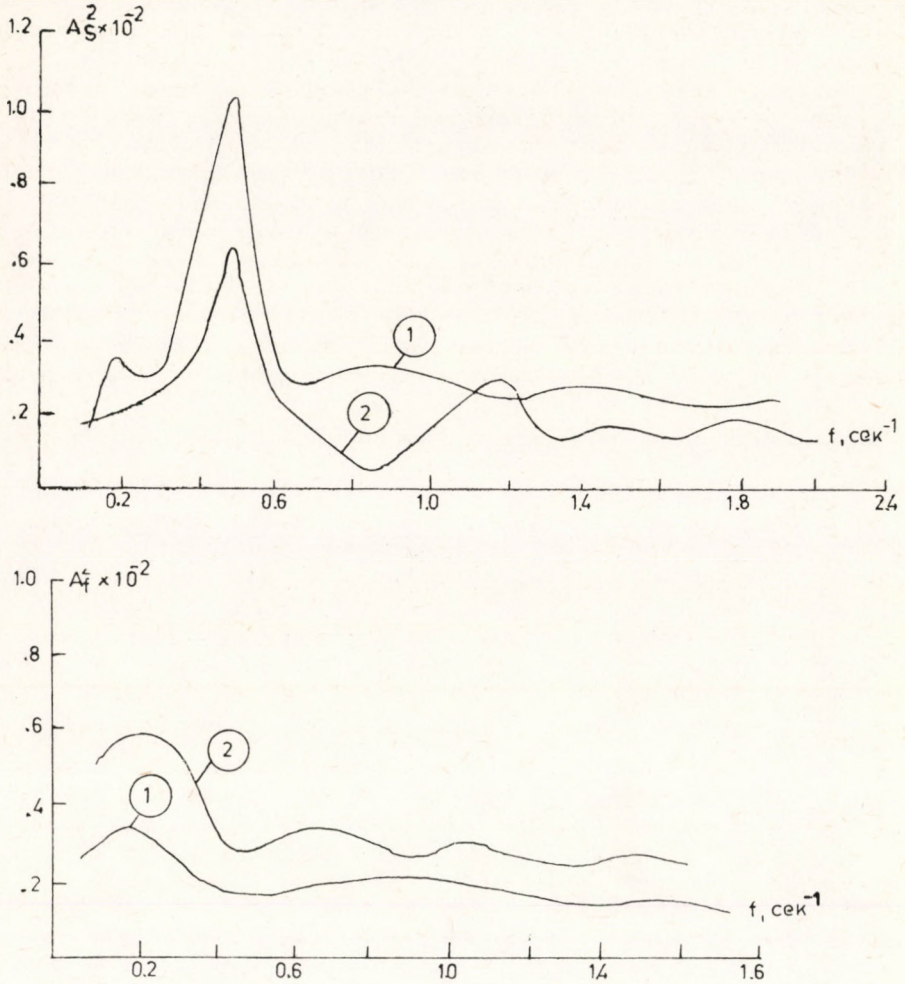

Рис. 4.
Спектры мощности сигнала от датчика
а) неподвижный слой, $\tilde{\varepsilon}=0{,}38$, кривая 1: $U_0=0{,}0448$ м/сек кривая 2: $U_0=0{,}00775$ м/сек
б) псевдоожиженный слой, кривая 1: $U_0=0{,}105$ м/сек, $\tilde{\varepsilon}=0{,}5$; кривая 2: $U_0=0{,}21$ м/сек, $\tilde{\varepsilon}=0{,}76$

результате исследования флуктуации коэффициента массопереноса электрохимическим методом — по характерному виду автокорреляционных функций пришли к аналогичному выводу.

Обсуждение результатов

Более высокие значения коэффициента массопереноса, наблюдаемые в зернистом слое, по сравнению с теми значениями, которые характерны для свободного потока, повидимому, объясняется локальной турбулентностью, возника-

ющей при протекании потока жидкости в каналах переменного сечения между частицами. Как мы убедились в этом в предыдущей части работы, флуктуации массового потока (следовательно, и скорости) незначительны. Поэтому, течение жидкости в каналах можно считать квазистационарным. Однако, из-за переменного сечения канала, квазистационарное течение характеризуется не только большими градиентами скорости но и резкими изменениями градиента вдоль канала. Это обстоятельство приводит к пространственному возмущению течения в локализованном объеме, размеры которого соизмеримы с размером свободного объема между двумя частицами. Мелкие вихри — как следствие возмущенного течения — являются дополнительными переносчиками массы. Согласно теории Колмогорова [18] энергия этих вихрей непосредственно связана с диссипацией энергии в локальном объеме жидкости. Следовательно, можно попытаться найти количественную оценку между локально-осредненным потоком энергии, рассеивающейся в рассматриваемом объеме, и локально-осредненным значением коэффициента массопереноса.

Прежде всего уравнение (7) представим в более общем виде:

$$Sh=F(\tilde{\varepsilon})\cdot ARe_0^{1/2}Sc^{1/3} \tag{10}$$

Функцию $F(\tilde{\varepsilon})$ пока будем считать неизвестной, удовлетворяющей двум граничным условиям: она имеет максимальное значение в неподвижном слое и равна единице при $\tilde{\varepsilon}=1$.

Далее, рассмотрим элементарную ячейку зернистого слоя, конфигурация которой соответствует либо гексагональной, либо кубической упаковке частиц (см. *рис. 5*). Локальную скорость жидкости на внешней границе пограничного

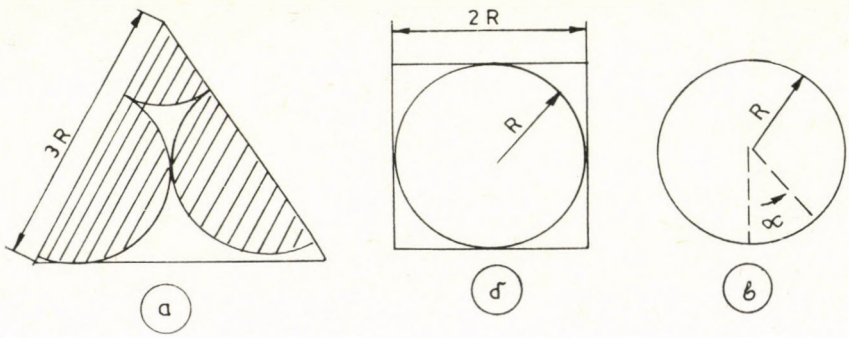

Рис. 5.
Модели элементарной ячейки зернистого слоя
а) гексагональная;
б) кубическая;
в) направление отсчета переменного угла α

слоя определим как отношение фиктивной скорости U_0 к доле свободного сечения канала:

$$\overline{V}(\alpha)=\frac{U_0}{\bar{\varepsilon}(\alpha)} \tag{11}$$

Свободное сечение характеризуется угловой координатой α, отсчет которого показан на *рисунке 5в*. Черта над переменными означает их осредненные во времени значения.

С использованием „теоремы энергии“ для пограничного слоя [19], и выведенных на ее основе известных интегральных соотношений, была получена следующая пропорциональность:

$$\langle \bar{J}_E \rangle \sim \langle \bar{V}^2(\alpha) \rangle = U_0^2 I^2 \tag{12}$$

$$I^2 = \int_0^{\pi/2} \frac{d\alpha}{\bar{\varepsilon}^2(\alpha)} \tag{13}$$

связывающая локально-осредненное значение диссипации энергии с осредненным значением квадрата локальной скорости вне пограничного слоя.

Для того чтобы заменить знак пропорциональности на знак равенства в уравнении (12), нам потребовалось бы задать явный вид функции $\left(\frac{\partial \bar{V}}{\partial y}(y, \alpha)\right)^2$, интеграл которой по y в пределах от 0 до ∞ определил бы коэффициент пропорциональности. Поскольку в стесненных условиях обтекания твердой частицы задать точный вид этой функции практически невозможно, мы ограничиваемся соотношением (12). Коэффициент пропорциональности можно найти с помощью экспериментальных данных.

Корень квадратный из левой части уравнения (12) обозначим через $\overline{W}$. Эту величину мы вправе считать той определяющей скоростью, на базе которой можно строить инвариантные, аналогичные уравнению (6), обобщения для числа *Sh*:

$$Sh = A \overline{Re}_w^{1/2} Sc^{1/3} \tag{15}$$

или, с учетом равенства (12)

$$Sh = I^{1/2} A Re_0^{1/2} Sc^{1/3} \tag{16}$$

Сравнивая выражения (16) и (10) находим функцию $F(\tilde{\varepsilon})$:

$$F(\tilde{\varepsilon}) = I^{1/2} \tag{17}$$

Для представления зависимости (17) в явном виде, вернемся к приведенным на *рисунке 5* геометрическим моделям ячейки зернистого слоя. Среднюю объемную порозность ячейки определим как отношение свободного объема к полному. Для гексагональной упаковки:

$$\tilde{\varepsilon}_\Delta = 1 - \frac{v_0}{v_\Delta} = 1 - 5{,}6429 \frac{R^2}{a^2} \tag{18}$$

для кубической упаковки:

$$\tilde{\varepsilon}_\square = 1 - \frac{v_0}{v_\square} = 1 - 4{,}1887 \frac{R^3}{a^3} \tag{19}$$

В неподвижном слое мы имеем самую плотную упаковку зерен. В этом случае $a_\Delta = 3R$, $a_\square = 2R$. Соответственно, значения объемной порозности равны 0,3730 и 0,4764. Первое значение хорошо согласуется с измеренным экспериментально значением, равным 0,38.

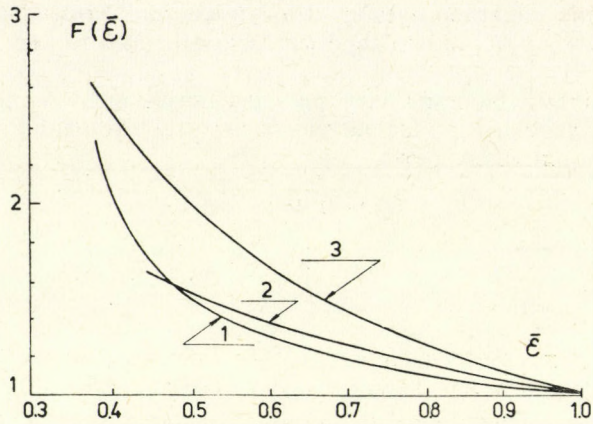

Рис. 6.
Обобщенная зависимость $Sh/F(\tilde{\varepsilon})$ от Re_0

— неподвижный слой, $d=0{,}5$ см;
— неподвижный слой, $d=0{,}4$ см;
— псевдоожиженный слой, $d=0{,}4$ см;
— псевдоожиженный слой, $d=0{,}5$ см;
— единичная частица, $d=0{,}4$ см.

Графики функции $L(\tilde{\varepsilon})$. Кривая 1: гексагональная модель Кривая 2: кубическая модель. Кривая 3: эмпирическая функция $1/\tilde{\varepsilon}$

Локальную порозность ячейки — согласно вышеприведенному определению — находим как отношение свободного сечения ячейки к полному:

$$\bar{\varepsilon}_{\Delta}(\alpha)=1-\frac{F_0(\alpha)}{F_{\Delta}}=1-8{,}4644\,\frac{R^2}{a_{\Delta}^2}\sin^2\alpha \tag{20}$$

$$\bar{\varepsilon}_{\square}(\alpha)=1-\frac{F_0(\alpha)}{F_{\square}}=1-\pi\,\frac{R^2}{a_{\square}^2}\sin^2\alpha \tag{21}$$

Предположим, что в расширенном псевдоожиженном слое геометрическая конфигурация ячейки сохраняется, и только отношения R/a_{Δ} или $R/a_{\square}$ будут изменяться в зависимости от средней объемной порозности слоя. Эту зависимость можно выразить из соотношений (18) и (19). В результате мы получим следующие уравнения связи между локальной и средней порозностью:

$$\bar{\varepsilon}_{\Delta}(\alpha)=1-1{,}499(1-\tilde{\varepsilon})\sin^2\alpha \tag{22}$$

$$\bar{\varepsilon}_{\square}=1-1{,}209(1-\tilde{\varepsilon})^{2/3}\sin^2\alpha \tag{23}$$

Подстановка выражений (22) или (23) в уравнение (13) позволяет вычислить функцию порозности $F(\tilde{\varepsilon})$

Результаты вычислений представлены на рисунке (6). На этом же рисунке изображен график эмпирической функции $1/\tilde{\varepsilon}$. Из графика видно, что кривые, построенные для двух разных геометрических моделей ячейки, в области псевдоожиженного слоя мало отличаются друг от друга. Кривая $1/\tilde{\varepsilon}$ по характеру адекватна им, но лежит несколько выше. Поскольку кубическая модель имеет

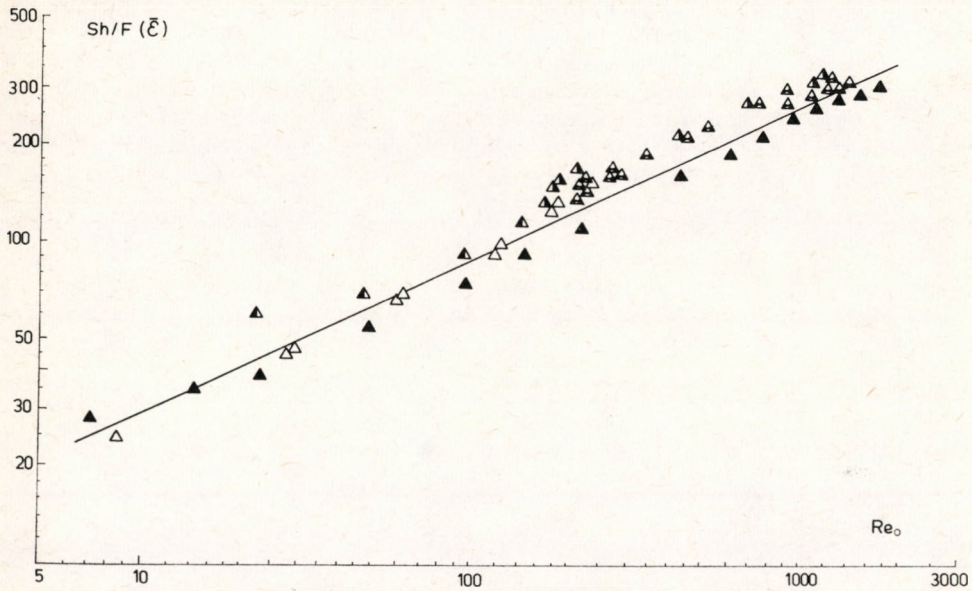

Рис. 7.

смысл только при $\tilde{\varepsilon} \geq 0{,}476$, в дальнейшем будем пользоваться гексагональной моделью.

Попытка обобщения экспериментальных данных в терминах $Sh/F(\tilde{\varepsilon}) - Re_0$ привела к графику, изображенному на *рисунке 7*. Прямая линия в логарифмических координатах описывается уравнением:

$$\frac{Sh}{F(\tilde{\varepsilon})} = (0{,}699 \pm 0{,}027) Re_0^{1/2} Sc^{1/3} \tag{24}$$

или

$$Sh = (0{,}699 \pm 0{,}027) \overline{Re}_w^{1/2} Sc^{1/3} \tag{25}$$

(с 95%-ной) доверительной вероятностью, и при постоянном значении Sc, равном 1910).

Точки на графике означают экспериментальные данные, полученные как в неподвижном, так и в псевдоожиженном слое, а также в свободном потоке. Как и следовало ожидать, коэффициент пропорциональности в уравнениях (24) и (25) в пределах погрешности эксперимента совпадает с коэффициентом пропорциональности уравнения (6). Уравнение (6) является предельным случаем уравнения (25), так как при $\tilde{\varepsilon} = 1$, осредненная во времени относительная скорость V не зависит от α. Следовательно,

$$\overline{W}\Big|_{\tilde{\varepsilon}=1} = \overline{V} \quad \text{и} \quad \overline{Re}_w\Big|_{\tilde{\varepsilon}=1} = \overline{Re} \tag{26}$$

С целью сравнения наших результатов с данными других авторов литературные данные [2, 17] обрабатывали по уравнению (16). В первую очередь мы обратились к тем литературным источникам, в которых одной и той же методикой измеряли коэффициент массопереноса в неподвижном, псевдоожиженном слое, и в свободном потоке. Значения коэффициента A вычислили методом наименьших квадратов. Результаты расчета представлены в *таблице 1*. Из таблицы

Таблинпа 1

Сравнение литературных данных с нашими результатами с помощью уравнения: $Sh = A \cdot F(\tilde{\varepsilon}) Re_0^{1/2} Sc^{1/3}$

№№ пп	Условия опытов	Метод исследования	Состояние слоя	Число опытных точек	Значение „A"	Ссылки на лит.
1	d =0,637, 0,48, 0,32, 0,207, 0,125 см Re_0=14,4–439 Sc =1189–1387 $\tilde{\varepsilon}$ =0,37–0,44	растворение нафталина в воде	неподвижный	36	0,7609± 0,0281	[2]
2	d =0,637, 0,32, 0,207, 0,125 см Re_0=6,8–666 Sc =1204–1286 $\tilde{\varepsilon}$ =0,52–0,95	растворение нафталина в воде	псевдоожиженный слой	26	0,7580± 0,1008	[2]
3	d =0,637, 0,480, 0,319 см Re_0=31,5–989 Sc =1211–1416, $\tilde{\varepsilon}$ =1	растворение нафталина в воде	единичная частица	21	0,6685± 0,1133	[2]
4	d =0,635 см Re_0=62–1342 Sc =1360–1440 $\tilde{\varepsilon}$ =0,37–0,64	растворение нафталина в воде	неподвижный и псевдоожиженный слой	54	1,183± 0,027	[17]
5	d =0,4 см Re_0=10–2000 Sc =1910 $\tilde{\varepsilon}$ =1	электрохимический метод	единичная частица с колебательным движением	65	0,6709± 0,0185	[1]
6	d =0,4 см Re_0=29–1320 Sc =1910 $\tilde{\varepsilon}$ =0,38–0,95	электрохимический метод	неподвижный и псевдоожиженный слой	58	0,6986± 0,0265	данная работа

видно, что данные Mc Cune и Wilhelm [2] хорошо обобщаются в рамках модели (16). Значение A для единичной частицы совпадает с нашим значением, для зернистого слоя оно несколько выше.

Данные Rowe и Claxton [17], измеренные в неподвижном и псевдоожиженном слое, также обобщаются в виде одного критериального уравнения, однако коэффициент пропорциональности существенно выше нашего значения.

Причины расхождения могут быть методологическими. Повидимому, электрохимический метод позволяет получить более точные результаты. Этот вопрос требует дальнейшего исследования.

В заключении можем отметить, что наши эксперименты, а также литературные данные достаточно убедительно подтверждают исходную предпосылку об инвариантности обобщений, представленных в виде уравнения (15) к состоянию зернистого слоя. Использованная при выводе уравнения (15) геометрическая модель и энергетическая интерпретация процесса массопереноса позволили найти физически обоснованный вид функции порозности, справедливость которой проверена экспериментально в области средних значений числа Re_0 ($10 < Re_0 < 2000$) и при изменении порозности в полном диапазоне от 0,38 до 1. В литературе известны и другие подходы к физической интерпретации функции порозности [20], справедливые для области малых чисел Re_0, ($Re_0 < 10$). Эта область представляет также практически важный интерес, и также требует дополнительного теоретического и экспериментального исследования.

СПИСОК ОБОЗНАЧЕНИЙ

A_x — амплитуда смещения твердой частицы, совершающей колебательное движение, L;
A_v — амплитуда скорости колебания, LT^{-1};
a — характерный геометрический размер элементарной ячейки зернистого слоя, L;
d — диаметр твердой частицы, L;
$D_м$ — коэффициент молекулярной диффузии, L^2T^{-1};
$F(\alpha)$ — переменное поперечное сечение элемента чяейки зернистого слоя, L^2;
I^2 — интеграл, определяемый уравнением (13);
$\overline{k}$ — локально-осредненное значение коэффициента массопереноса, LT^{-1};
R — радиус сферической частицы, L;
S — частота обновления поверхности, параметр модели Данквертса, T^{-1};
t — время, T;
U_0 — фиктивная скорость жидкости, отнесенная к полному сечению реактора, LT^{-1};
$\overline{U}$ — скорость жидкости, определяемая как $U_0/\bar{\varepsilon}$, LT^{-1};
v_0 — объем твердой фазы в элементе ячейки зернистого слоя, L^3;
v_Δ, $v_\square$ — объем элементарной ячейки зернистого слоя, L^3;
$V(t)$ — локальная скорость относительного движения твердой частицы и жидкости, LT^{-1};
$\overline{V}$ — осредненная во времени функция $\overline{V}(\alpha)$, LT^{-1};
$\overline{W}$ — корень квадрат из среднеквадратичного значения $\overline{V}(\alpha)$, LT^{-1};
y — радиальная координата, L.
$\overline{V}(y, \alpha)$ — продольная компонента осредненной скорости $\overline{V}$

Греческие символы:

$\dot{\varepsilon}(\alpha)$ — локальная порозность определенная уравнениями (15) и (16);
$\tilde{\varepsilon}$ — средняя объемная порозность зернистого слоя;
ν — кинематическая вязкость, L^2T^{-1};
M — динамическая вязкость, $M(LT)^{-1}$;
ϱ — плотность, ML^{-3};
σ_φ^2 — дисперсия переменной φ, определяемая как

$$\frac{1}{n-1}\sum_{i=1}^{n}(\varphi_i-\overline{\varphi})^2$$

ω_0 — круговая частота колебательного движения твердой частицы в жидкости, T^{-1};

Индексы:

„□" — кубическая модель;
„Δ" — гексагональная модель;
„K" — коэффициент массопереноса;
„V", „W" — скорость;
„ε" — порозность;
„э" — экспериментальное значение;
„L" — жидкая фаза;
„S" — твердая фаза.

Безразмерные числа;

$$Re_0=\frac{U_0 d}{\nu_L};\quad \bar{Re}=\frac{\bar{V}d}{\nu_L};\quad \bar{Re}_w=\frac{\bar{W}d}{\nu_L};\quad Sc=\frac{\nu_L}{D_M};$$

$$Sh=\frac{\bar{k}d}{D_M};\quad Ga=\frac{d^3\varrho_L^2 g}{M_L^2};\quad M_V=\frac{\varrho_S-\varrho_L}{\varrho_L}$$

СПИСОК ЛИТЕРАТУРЫ

1. Ермакова, А., Кузьмин, В. А., Скоморохов, В. Б., Умбетов, А. С.: Исследование локального массопереноса от частицы к жидкости. II. Трансформация кинетической энергии относительной скорости в массовый поток. Hung. J. Ind. Chem. *1981*, 9, 187.
2. McCune, L. K. and Wilhelm, R. H.: Ind. Eng. Chem. *1949*, 41, 1124.
3. Rowe, P. N., Claxton, K. T. and Lewis, J. B.: Trans Inst. Chem. Engrs. *1965*, 43, 14.
4. Coeuret, F. et Legoff, P.: Ind. Chem. Engr. *1967*, 207, CE 75.
5. Bordet, J., Borlai, O., Vergnes, F. and Legoff, P.: Ind. Chem. Eng. Symp. Ser. *1968*, 36, 165.
6. Trupp, A.: Ind. Chem. Eng., Symp. Ser. *1968*, 30, 182.
7. Nelson, P. A. and Galloway, T. R.: Chem. Eng. Sci. *1975*, 30, 1.
8. Rowe, P. N.: Chem. Eng. Sci. *1975*, 30, 7.
9. Kmiec, A.: Chem. Eng. J. *1975*, (3) 251.
10. Dwivedi, P. N. and. Upadhyay, S. N.: Ind. Eng. Proc. Des. Dev. *1977*, 16, (2) 57.
11. Tournie, P., Laguerie, E. and Couderc, J. P.: Chem. Eng. Sci. *1977*, 32, 1259.
12. Koloni, T., Sopcic, M. and. Zumer, M.: Chem. Eng. Sci. *1977*, 32, 637.
13. Valentin, G., Legoff, P. and. Vergnes, F.: Chem. Eng. Journ. *1978*, 15, 185.
14. Singh, A. N., Kisavan, S. and Gupta, P. S.: Int. J. Heat Mass Transfer *1980*, 23, 279.
15. Riba, J. P. and Couderc, J. P.: Int. J. Heat Mass Transfer *1980*, 23, 909.
16. Riba, J. P. and Couderc, J. P.: Chem. Eng. Sci. *1980*, 35, 1470.
17. Rowe, P. N. and Claxton, K. T.: Trans. Instn. Chem. Engrs. *1965*, 43, 321.
18. Хинце, И. О.: Турбулентность. Ее механизм и теория, М., Физматгиз, 1963.
19. Шлихтинг, Т.: Теория пограничного слоя. „Наука", Москва, 1974.
20. Буевич, Ю. А., Корнеев, Ю. А.: ИФЖ, *1973*, XX*V*, 594.

SUMMARY

Experimental data are given on the local particle fluid mass transfer in two-phase fixed and fluidized beds. Measurements were made by the electrochemical method. Dependence of the averaged and pulse values of the mass transfer coefficient on fluid velocity with variation of porosity from 0.38 to 1 was established. The relevant curve was shown to pass through the maximum in the region of the beginning of fluidization. An extreme character of this dependence enables the use of the electrochemical method for the determination of the velocity at the beginning of fluidization.

The experimental data obtained were generalized as the criterion equation:

$$Sh=F(\tilde{\varepsilon})Sh\Big|_{\tilde{\varepsilon}=1}$$

which is valid for the fixed, fluidized beds, and also for a single particle. The form of the function $F(\tilde{\varepsilon})$ was obtained from the geometric model of the packing of the grained bed. The results obtained are compared with the data in literature.

HUNGARIAN JOURNAL
OF INDUSTRIAL CHEMISTRY
VESZPRÉM
Vol. 9. pp. 313–322 (1981)

TAYLOR DIFFUSION WITH HOMOGENEOUS AND SURFACE REACTION IN MHD COMBINED FREE AND FORCED CONVECTIVE FLOW

R. K. PRABHAKAR RAM

(Department of Physics, National College, Basavangudi,
Bangalore 560004, India)

Received: June 17, 1981

TAYLOR dispersion of solute with homogeneous and surface reaction was considered in MHD combined free and forced convective laminar flow in a channel. It was found that the effective dispersion co-efficient decreases with the increase in the homogeneous reaction rate parameter (α) and HARTMANN number (M) for both heating ($G>0$) and cooling ($G<0$) of the plates, except for a small increase with heating of the plates and large values of the reaction rate parameter compared to the HARTMANN number. Even for dispersion with homogeneous and surface reaction, similar behaviour is exhibited by the effective dispersion co-efficient. The analysis confirms that a magnetic field regulates the rate of dispersion of a solute in an electrically conducting solvent.

Introduction

The dispersion of chemically reacting solute in a solvent is of interest in chemical engineering as evidenced by the processes of hydrolysis, gas absorption in an agitated tank, ester experiments and so on as pointed out by BIRD et al. [1]. Recently combined free and forced convection has been shown to be an important flow regime governing the conversion rates of acids used in oil well treatments, discussed by ROBERTS and GUIN [2] and in reverse osmosis studies, discussed by DERZANSKY and GILL [3]. Surface reaction is one of the causes which yields the combined forced and free convective regime as shown by CHANG, GUIN and ROBERTS [4]. Dispersion of solute in combined forced and free convective flow has very recently been analysed by MAZUMDER [5] without the effects of either homogeneous or surface reactions.

The effect of homogeneous and heterogeneous reactions on the dispersion of solute in MHD channel flow was analysed by NARASIMHAMURTHY and KRISHNAMURTHY [6]. MHD combined forced and free convective flow situations were analysed by GUPTA [7] and KANT [8] among others.

Very recently REIS, RAMAKRISHNA and LIGHTFOOT [9], LEE, EVANS and CUSSLEY [10], CHANG and GUIN [11] and KABADI, DOSHI and GILL [12] studied chemical engineering situations where dispersion with combined free and forced convection in conducting liquids was considered. The present paper reports on a study of the relative influences of homogeneous and heterogeneous reactions, buoyancy force and magnetic field on the dispersion of solute. The study was carried out using TAYLOR's analysis, which was also shown to be valid for falling films by PRENOSIL [13]. The study is expected to have some bearing on understanding magnetic field effects in regulating such processes as the selective recovery of metal ions, electrochemical reactions, and desalination of water.

Formulation of the Problem and Solution

The laminar flow of a viscous conducting fluid between two parallel plates, a distance $2d$ apart, is considered under the action of a uniform pressure gradient dp/dx^*. The walls are assumed non-conducting. Taking 'x^*'-axis along the mid-section of the channel, 'y^*'-axis perpendicular to the plates, the uniform magnetic field is assumed to act along the y^*-axis. Further, assuming a uniform axial temperature variation and utilising the BOUSSINESQ approximation, the velocity profile subject to the no-slip condition at the walls, following GUPTA [7] is:

$$u=\frac{1}{M^2}\left\{\frac{\cosh My}{\cosh M}-\frac{\sinh My}{\sinh M}-Gy+1\right\}, \tag{1}$$

in non-dimensional form, with:

$$G=\frac{g\beta d^4N}{\nu^2P_x}; \qquad M^2=\frac{\sigma B_0^2d^2}{\varrho\nu}, \tag{2}$$

being the GRASHOF and HARTMANN numbers and N and P_x are as used by MAZUMDER [5].

In terms of the average velocity $\bar{u}=\frac{1}{2}\int_{-1}^{1} u\,dy$ this can be written as:

$$\bar{u}_x=u-\bar{u}=\frac{1}{M^2}\left\{\frac{\cosh My}{\cosh M}-\frac{\sinh My}{\sinh M}-Gy-\frac{\tanh M}{M}\right\}. \tag{3}$$

Diffusion with a homogeneous first order reaction

Assuming that a solute diffuses and simultaneously undergoes a first order irreversible chemical reaction in the conducting liquid, the equation, for the concentration of the solute is:

$$\frac{\partial c}{\partial t}+u\frac{\partial c}{\partial x^*}=D\left[\frac{\partial^2 c}{\partial x^{*2}}+\frac{\partial^2 c}{\partial y^{*2}}\right]-K_1c \tag{4}$$

where D is the molecular diffusion co-efficient and K_1 is the first order reaction rate. Assuming:

$$\frac{\partial^2 c}{\partial x^{*2}} \ll \frac{\partial^2 c}{\partial y^{*2}}$$

and introducing the dimensionless quatities:

$$\Theta = \frac{t}{\bar{t}}; \quad \bar{t} = \frac{d}{\bar{u}}; \quad x = \frac{x^* - \bar{u}t}{d}; \quad y = \frac{y^*}{d}$$

in equation (4) we obtain:

$$\frac{1}{\bar{t}} \frac{\partial c}{\partial \Theta} + \frac{\bar{u}_x}{d} \frac{\partial c}{\partial x} = \frac{D}{d^2} \frac{\partial^2 c}{\partial y^2} - K_1 c. \tag{5}$$

Following the analysis of TAYLOR [14, 15, 16] we assume that a partial equilibrium can be established in any cross-section of the channel, so that the variation of c with y is obtained as:

$$-\frac{K_1 d^2}{D} c + \frac{\partial^2 c}{\partial y^2} = \frac{d\bar{u}_x}{D} \frac{\partial c}{\partial x}. \tag{6}$$

Substituting Equation (2) in Equation (6) and integrating twice, we get after using the boundary conditions:

$$\frac{\partial c}{\partial y} = 0 \quad \text{at} \quad y = \pm 1,$$

the concentration as:

$$c = \frac{a}{2\alpha^3}\left(\frac{\cosh \alpha y}{\cosh \alpha} - \frac{\sinh \alpha y}{\sinh \alpha}\right) + \frac{bG}{2\alpha^3}\left(\frac{\cosh \alpha y}{\sinh \alpha} - \frac{\sinh \alpha y}{\cosh \alpha}\right) + \frac{bG}{2\alpha^3}\left(\frac{\cosh \alpha y}{\cosh \alpha} + \frac{\sinh \alpha y}{\sinh \alpha}\right) -$$
$$- \frac{b(1 + M^2/\alpha^2)}{M^2\alpha^2}\left(\frac{\cosh My}{\cosh M} - \frac{\sinh My}{\sinh M}\right) - \frac{b}{\alpha^2}(1 - Gy), \tag{7}$$

where:

$$\left.\begin{aligned} a &= \frac{2b}{M}(1 + M^2/\alpha^2) \coth 2M, \\ b &= \frac{d}{D}\frac{\partial c}{\partial x}, \qquad \alpha^2 = \frac{K_1 d^2}{D}, \end{aligned}\right\} \tag{8}$$

α, being the reaction rate parameter.

The dimensionless volumetric flow rate at which the solute is transported, across the cross-section of the channel of unit breadth, is given by:

$$Q = \int_{-1}^{1} c\bar{u}_x \, dy$$

Using Equations (2) and (8) gives:

$$Q = \frac{\sinh(\alpha + M)}{(\alpha + M)M^2}\left(\frac{a_1}{\cosh M} + \frac{a_2}{\sinh M}\right) + \frac{\sinh(\alpha - M)}{M^2(\alpha - M)}\left(\frac{a_1}{\cosh M} - \frac{a_2}{\sinh M}\right) -$$

$$-\frac{2\sinh\alpha}{\alpha}\cdot\frac{a_1\tanh M}{M^3}+\frac{2a_2G}{M^2\alpha^2}(\alpha\cosh\alpha-\sinh\alpha)-$$

$$-\frac{\sinh 2M}{2M}\;\frac{b(M^2+\alpha^2)}{M^4\alpha^4}\left(\frac{1}{\cosh^2 M}+\frac{2}{\sinh^2 M}\right)+$$

$$+\frac{b}{M^2\alpha^2}\;\frac{2\tanh M}{M}\left\{\frac{(M^2+\alpha^2)}{\alpha^2}\cdot\frac{\tanh M}{M^3}-1\right\}+$$

$$+\frac{2Gb}{M^4\alpha^2}(1-M\coth M)\left\{\frac{(M^2+\alpha^2)}{M^2\alpha^2}+1\right\}-\frac{b(M^2+\alpha^2)}{M^4\alpha^4\sinh^2 M}(\tanh^2 M-2)+$$

$$+\frac{2b}{M^2\alpha^2}\left(\frac{\tanh M}{M}-\frac{1}{3}G^2\right), \tag{9}$$

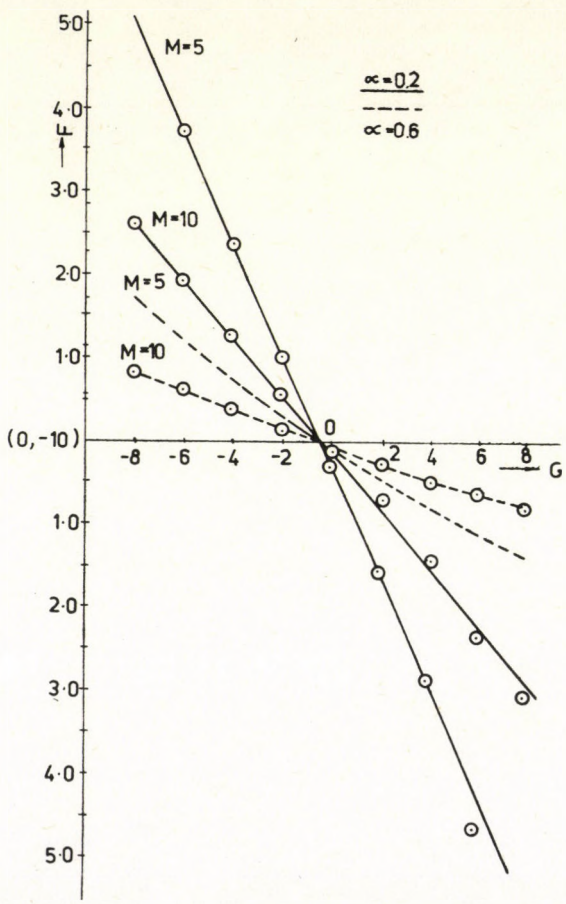

Fig. 1
Variation of "F" with G, α and M, when $\alpha > 1.0$

where:

$$a_1 = \frac{a \sinh \alpha + bG(\sinh \alpha + \cosh \alpha)}{\alpha^3 \sinh 2\alpha}, \tag{10}$$

$$a_2 = \frac{a \cosh \alpha + bG(\sinh \alpha - \cosh \alpha)}{\alpha^3 \sinh 2\alpha}, \tag{11}$$

comparing with FICK's Law of diffusion, we find that the solute is dispersed, relative to a plane moving with the mean speed of the flow, with an effective dispersion coefficient D^* given by:

$$D^* = \frac{D}{K_1 d^3} F(\alpha, M, G), \tag{12}$$

where:

$$F(\alpha, M, G) = -\frac{b}{\alpha^4} Q. \tag{13}$$

$F\ (\alpha, M, G)$ has been computed for different values of α, M and G and the results are represented in *Figure 1* and *2*.

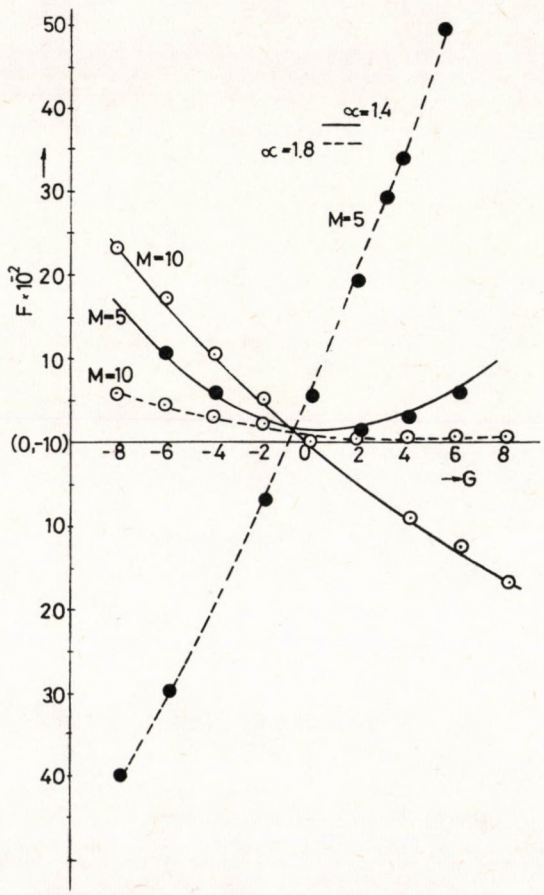

Fig. 2
Variation of "F" with G, α and M, when $\alpha < 1.0$

It can be observed that the effective dispersion coefficient F decreases with an increase in the reaction rate parameter, at moderate values of the reaction rate ($\alpha \leq 1$) and also with an increase in the HARTMANN number M for fixed G^*. This is in agreement with the result obtained earlier, without a temperature gradient, by NARASIMHAMURTHY and KRISHNAMURTHY [6]. It can also be observed that for fixed α and M an increase in GRASHOF number G causes a decrease in F, for moderate values of the reaction rate. However, when the reaction rate is large compared to the magnetic field, F increases with M- as seen for $\alpha = 1.4$ — and also with G, for $G > 0$, which shows that there are critical values of the parameters α and M. When M is small compared to α the variation of F with G is similar to that obtained by MAZUMDER [5] without the magnetic field or reaction, with the values for heating ($G > 0$) being lower then for cooling ($G < 0$) of the plates. These results agree with the general tendency of the magnetic field, which is to retard the onset of convection, as was first shown by CHANDRASEKHAR [4], in the absence of rotation.

Diffusion with combined homogeneous and surface reaction

Here we discuss the problem of diffusion in a channel with first order irreversible chemical reaction occurring both in the bulk of the fluid and at the walls, which are assumed catalytic to reaction and non-conducting to any electromagnetic effects.

Inthis case the diffusion Equation (4) subject to the boundary conditions:

$$\left.\begin{aligned} \frac{\partial c}{\partial y^*} + fc = 0 \quad &\text{at} \quad y^* = d \\ \frac{\partial c}{\partial y^*} - fc = 0 \quad &\text{at} \quad y^* = -d \end{aligned}\right\} \tag{14}$$

is to be solved.

Again introducing the dimensionless quantities as mentioned earlier and assuming limiting TAYLOR conditions, the diffusion equation is:

$$-\frac{K_1 d^2}{D} \cdot c + \frac{\partial^2 c}{\partial y^2} = \frac{d\bar{u}_x}{D} \frac{\partial c}{\partial x}, \tag{15}$$

with boundary conditions:

$$\left.\begin{aligned} \frac{\partial c}{\partial y} + \gamma c = 0 \quad &\text{at} \quad y = 1 \\ \frac{\partial c}{\partial y} - \gamma c = 0 \quad &\text{at} \quad y = -1 \end{aligned}\right\} \tag{16}$$

where $\gamma = fd$ is the surface reaction rate parameter. The solution of Equation (15) subject to the boundary conditions [16] is:

$$c = a_3 \cosh \alpha y - a_4 \sinh \alpha y - a_5 \cosh (\alpha + \alpha y) - a_6 \sinh (\alpha + \alpha y) + a_7 \cosh (\alpha - \alpha y) +$$
$$+ a_8 \sinh (\alpha - \alpha y) - \frac{b}{\alpha^2}(1 - Gy) - \frac{2b}{\alpha^2}\left(1 + \frac{M^2}{\alpha^2}\right)\frac{\sinh (M - My)}{M^2 \sinh 2M}, \tag{17}$$

where:

$$\left.\begin{aligned} a_3 &= \frac{2b\gamma(\alpha\cosh\alpha+\gamma\sinh\alpha)}{a_9}, \qquad a_4 = \frac{2bG(1+\gamma)(\alpha\sinh\alpha+\gamma\cosh\alpha)}{a_9}, \\ a_5 &= \frac{b_1M\alpha}{2\alpha^2a_9}, \qquad a_6 = \frac{b_1M\gamma}{2\alpha^2a_9}, \qquad a_7 = \frac{b_1\alpha(\gamma\sinh 2M+\alpha\cosh 2M)}{2\alpha^2a_9}, \\ a_8 &= \frac{b_1\gamma(\gamma\sinh 2M+\alpha\cosh 2M)}{2\alpha^2a_9}, \end{aligned}\right\} \tag{18}$$

with:

$$\left.\begin{aligned} a_9 &= (\alpha^2+\gamma^2)\sinh 2\alpha+2\alpha\gamma\cosh 2\alpha, \\ b_1 &= \frac{2b}{\alpha^2}\cdot\frac{(1+M^2/\alpha^2)}{M^2\sinh 2M}. \end{aligned}\right\}$$

Again, the volumetric rate at which the solute is transported across a section of the channel, of unit breadth, is:

$$Q = \int_1^1 c\bar{u}_x\,\mathrm{d}y$$

which on utilising (2) and (17) and comparing with FICK's law of diffusion, gives the effective dispersion coefficient, D^*, with which the solute is dispersed relative to a plane moving with the mean velocity of the flow, as:

$$D^* = \frac{D}{K_1d^3}H(\alpha,\gamma,M,G), \tag{19}$$

where:

$$\begin{aligned} H(\alpha,\gamma,M,G) = {} & \frac{\sinh 2M}{2M}(b_2m_1-2b_3m_2)+(b_2m_1+2b_3m_2)+\frac{2Im_4\sinh\alpha}{\alpha}+\frac{2}{3}b_5m_3- \\ & -\frac{\sinh(\alpha+M)}{(\alpha+M)}(Im_1+Jm_2)-\frac{\sinh(\alpha-M)}{(\alpha-M)}(Im_1-Jm_2)- \\ & -\frac{2Jm_3}{\alpha^2}(\alpha\cosh\alpha-\sinh\alpha)-\frac{2}{M}\sinh M(b_1m_4-b_4m_1)- \\ & -\frac{2}{M^2}(M\cosh M-\sinh M)(b_3m_3-b_5m_2), \end{aligned} \tag{20}$$

with:

$$\left.\begin{aligned} I &= \frac{b}{\alpha^4}(a_3-a_5\cosh\alpha-a_6\sinh\alpha+a_7\cosh\alpha+a_8\sinh\alpha), \\ J &= \frac{b}{\alpha^4}\{a_4+a_5\sinh\alpha+a_6\cosh\alpha+a_7\sinh\alpha+a_8\cosh\alpha\}, \\ m_1 &= \frac{1}{M^2\cosh M}, \qquad m_2 = \frac{1}{M^2\sinh M}, \qquad m_3 = \frac{G}{M^2}, \\ m_4 &= \frac{\tanh M}{M^3}, \qquad b_2 = 2b_1\sinh M, \qquad b_3 = 2b_1\cosh M, \\ b_4 &= \alpha^2, \qquad b_5 = G\alpha^2. \end{aligned}\right\} \tag{21}$$

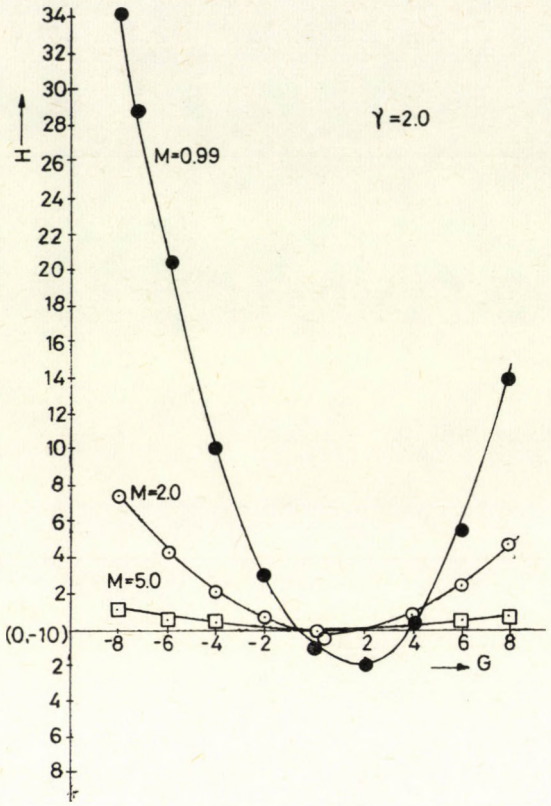

Fig. 3
Variation of "H" with G, and M, when $\alpha = 1.0$

We have computed $H(\alpha, \gamma, M, G)$ for $\alpha = 1$ and different values of γ, M and G. The results are represented in *Fig. 3* and *4*.

In this case it can also be observed that the effective dispersion coefficient decreases with an increase in the surface reaction rate parameter γ and the HARTMANN number M, in conformity with the results obtained by NARASIMHAMURTHY and KRISHNAMURTHY [6], for moderate values of the parameters γ, M and G. When γ and M exert comparable influences, it is found that the variation of H with G is similar to that obtained by MAZUMDER [5] with, however, the values for heating of the plates ($G > 0$)*. The results again show that there are critical values of the parameters, γ and M.

In any case the magnetic field exerts a regulating influence on the dispersion.

*Being again less than for cooling of the plates ($G < 0$).

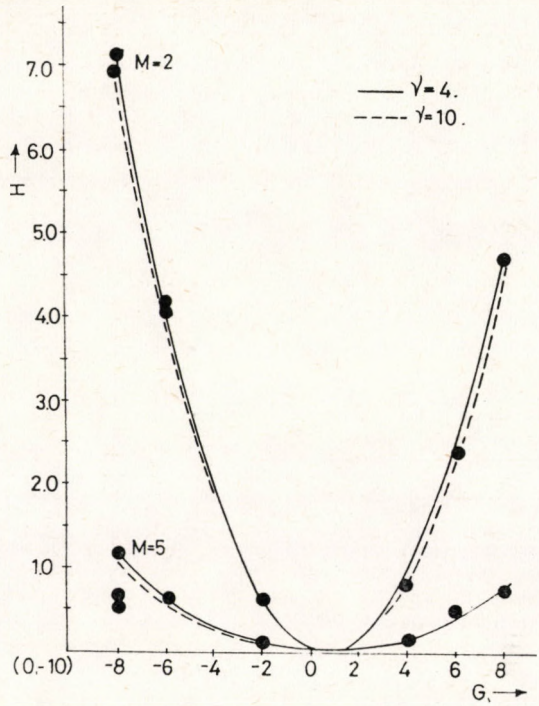

Fig. 4
Variation of "H" with G, μ and M when $\alpha = 1.0$

Conclusions

In this paper, the relative influence of homogeneous and surface reactions, and a magnetic field on the dispersion of solute in combined forced and free convective laminar flow in a channel have been considered. In the case of diffusion with a homogeneous first order reaction alone, it was found that the effective dispersion coefficient decreases with an increase in the reaction rate parameter, together with an increase in the HARTMANN number, with there being a critical value of the HARTMANN number for each value of the reaction rate. The value of the dispersion coefficient is lesser for heating ($G > 0$) of the plates than for cooling ($G < 0$) of the plates, when the other parameters are held fixed, and the influence of the magnetic field is less than that of the homogeneous reaction.

For diffusion with homogeneous and surface reaction, similar behaviour is exhibited by the effective dispersion coefficient for variations in the rate of first order surface reaction, HARTMANN number and the GRASHOF number. Once again a critical value of the HARTMANN number exists for any given value of the surface reaction rate when the homogeneous reaction rate is held fixed. The above analysis suggests that a magnetic field can regulate the rate of diffusion of a solute in an electrically conducting solvent, even in the presence of a temperature or density gradient and chemical reactions.

Acknowledgement

The author is grateful to DR. S. NARASIMHAMURTHY for helpful discussions and to DR. C. R. SUBRAHMANYA for assistance with the computations.

SYMBOLS

'd' — distance between plates,
p — pressure,
u — velocity along X-axis,
M^2 — Hartmann number,
B_0 — applied magnetic field,
σ — conductivity of fluid,
ϱ — density of fluid,
ν — kinematic viscosity,
g — acceleration due to gravity,
β_0 — coefficient of volume expansion,
N — constant representing temperature variation along x-axis,
p_x — dimensionless pressure gradient,
$\overline{u}$ — average velocity,
c — concentration gradient,
K_1 — first order reaction rate,
D — molecular diffusion coefficient,
α — first order reaction parameter,
Q — dimensionless volumetric flow rate,
K_2 — surface reaction rate,
γ — surface reaction rate parameter.

REFERENCES

1. BIRD, R. B., STEWART, W. E. and LIGHTFOOT, E. N.: Transport Phenomena. John Wiley and Sons, New York, 1960.
2. ROBERTS, O. O. and GUIN, J. A.:
3. DERZANSKY, L. J. and GILL, W. N.: AIChEJ *1974*, 20, 751.
4. CHING-YUAN CHANG, GUIN, J. A. and ROBERTS, O. O.: AIChEJ *1976*, 22, 252.
5. MAZUMDER, B. S.: Acta Mechanica *1979*, 32, 211.
6. NARASIMHAMURTHY, S. and KRISHNAMURTHY, M. R.: Ind. J. Phys. *1974*, 48, 634.
7. GUPTA, A. S.: ZAMP *1969*, 20, 506.
8. KANT, R.: Proc. Nat. Acad. Sci. Ind. A. *1977*, 102.
9. REIS, J. F. G., RAMAKRISHNA, D. and LIGHTFOOT, E. N.: AIChEJ *1978*, 24, 679.
10. LEE, K. H., EVANS, D. F. and CUSSLER, E. L.: AIChEJ *1978*, 24, 860.
11. CHANG, C. Y. and GUIN, J. A.: AIChEJ *1978*, 24, 1046.
12. KABADI, V. N., DOSHI, M. R. and GILL, W. N.: Chem. Engg. Commun. *1979*, 3, 339.
13. PRENOSIL, J.: Chem. Engg. Sci. *1973*, 28, 1763.
14. TAYLOR, G. I.: Proc. Roy. Soc. Lond. *1953*, A219, 186.
15. TAYLOR, G. I.: Ibid. *1954*, A223, 446.
16. TAYLOR, G. I.: Ibid. *1954*, A225, 473.
17. CHANDRASEKHAR, S.: Phil. Mag. Ser. *1953*, 7, 43, 501.

РЕЗЮМЕ

Автором изучено дисперсия Тейлора растворенного вещества полученного при поверхностной и однородной реакции в магнето-гидродинамическом (МГД) канале при ламинарным свободным и вынужденным течении. Установлено, что эффективный коэффициент дисперсии убывает если „альфа" параметр скорости однородной реакции и число Гартмана „M" увеличивается, в обеих случаяя если пластины нагреваются ($G>0$) или охлаждаются ($G>0$), исключением являются те случаи когда увеличение нагрева пластин незначительное или параметры реакции по сравнению числа Тартмана большие. Поведение дисперсии в случае однородной и поверхностной реакции одинаково, что подтверждается и численными значениями эффективных коэффициентов дисперсии. Проведенным анализом подтверждено, что магнитное поле имеет определенное влияние на скорость дисперсии вещества растворенного в электропроводящем растворителе.

Guide for authors

1. The "Hungarian Journal of Industrial Chemistry" is a joint publication of the Veszprém scientific institutions of the chemical industry that deals with the results of applied and fundamental research in the field of chemical processes, unit operations and chemical engineering in the form of original articles written in the English, Russian, German and French languages.

In addition to the scientific workers of the institutions at Veszprém, the Editorial Board of this publication also welcomes articles for inclucion in this periodical, which are written by authors who are engaged in the above mentioned fields.

2. Manuscripts should be sent—in duplicate—to the Editor-in-Chief:

Dr. Endre Bodor,
Veszprém University of Chemical
Engineering (VVE),
P.O.B. 28
Veszprém
H—8201 Hungary

3. In a brief letter attached to the manuscripts, authors should declare that:
   a) their work is original and has not previously been published elsewhere in its present format, and
   b) for the purposes of correspondence, they can be contacted at the address and telephone number which they give.

4. Manuscripts should be typed on paper of A/4 size.

The first page should give the title, the author's name, place of work and a brief summary of the article (maximum of 15 lines).

If possible the article should be presented with an introduction, experiments carried out, conclusions and discussion. Tables and Figures must be presented on separate sheets and their position in the text should be noted on the margin. A summary of the symbols used, the Tables and subscripts of the Figures should be attached separately to the manuscripts.

It is regretted that photographs cannot be included in the periodical.

The Tables and Figures should not exceed an A/4 size. If diagrams are presented, only the explanation and dimensions of the ordinate and abscissa, and marking numbers are required, while further explanatory texts can be given in the subscripts of the Figures. The equations used should be numbered, and Tables and Figures should be numbered and noted in the margin.

With regard to units, it is essential that an SI (Systeme International d'Unités) should be used.

References should be prepared in the following manner:

a) Publications which have appeared in periodicals:

Author's name and initials; title of the periodical (the abbreviation used by Chemical Abstracts is recommended); year of publication; volume number; (number of brochure if necessary); the first and last page number of the article, e.g.:

WAKAO, N. and SCHWARTZ, J. M.:
Chem. Eng. Sci., **1962**; 17 (3); 825—827.

b) Books:

Author's name and initials; title of book; publisher; place of publication; yera of publication, e.g.:

SATTERFIELD, C. N.:
Mass Transfer in Heterogeneous Catalysis.
MTI Press, Cambridge, Mass., 1951, pp. 26—32.

c) Patents:

Country where granted, and number of the patent, e.g.:
U.S. Pat. 3,425,442
Brit. Pat. 997,665
Hung. Pat. 553,243

d) Published lectures:

Author's name and initials; title of lecture; name of the conference; further information if necessary, e.g.:

HIH, S., HHU C. and LEECH, W. J.:
A Discrete Method to Heat Conduction Problems. 5th International Heat Transfer Conference, Tokyo, 1975. Co. 2.4.

5. Authors receive 50 complimentary copies of the in edition which their article appears.

Editorial Board
Hungarian Journal of Industrial Chemistry

CONTENTS

Egyetemi Nyomda — 81.7079 Budapest, 1981. Felelős vezető: Sümeghi Zoltán igazgató

Ára: 250 Ft

THE FOLLOWING ARE PLEASED TO ACCEPT SUBSCRIPTIONS TO THIS JOURNAL:

AUSTRALIA

C.B.D. Library and Subscription Service
Box 4886 G.P.O.
Sydney 2000

Cosmos Book and Record Shop
145 Acland Street
St. Kilda 3182

Globe and Co.
694—696 George Street
Sydney 2000

AUSTRIA

Globus (VAZ)
Höchstädtplatz 3
A—1200 Wien XX

BELGIUM

"Du Monde Entier" S. A.
Rue du Midi 162
B—1000 Bruxelles

Office International de Librairie
Avenue Marnix 30
B—1050 Bruxelles

CANADA

Pannonia Books
P.O. Box 1017
Postal Station "B"
Toronto, Ontario M5T 2T8

DENMARK

Munksgaard's Boghandel
Norregade 6
DK—1165 Copenhagen K

FINLAND

Akateeminen Kirjakauppa
Keskuskatu 2, P.O.B. 128
SF—00 100 Helsinki 10

FRANCE

Office International de Documentation et Librairie
48 Rue Gay Lussac
75 Paris 5

GERMAN FEDERAL REPUBLIC

Kubon und Sagner
Pf 68
D—8 München 34
BRD

GREAT BRITAIN

Bailey Bros and Swinfen Ltd.
Warner House, Folkestone
Kent CT 19 6PH England

HOLLAND

Martinus Nijhoff
Periodicals Department
P.O. Box 269
The Hague

Swets and Zeitlinger
Keizersgracht 487
Amsterdam C

ITALY

Licosa
P.O.B. 552, Via Lamarmora 45
50121 Firenze

JAPAN

Igaku Shoin Ltd.
Foreign Department
Tokyo International P.O. Box 5063
Tokyo

Maruzen Co. Ltd.
P.O. Box 5050
Tokyo International 100—31

Nauka Ltd.
Yasutomi Bldg. 5F 2—12 Kanda
Jinbocho, Chiyoda-ku
Tokyo 101

NORWAY

Tanum—Cammermayer
Karl Johangt. 41—43
Oslo 1

SWEDEN

Almqvist and Wiksell Förlag A. B.
Box 2120
S—103 13 Stockholm 2

Wennegren—Williams AB
Subscription Department Fack
S—104 Stockholm 30

SWITZERLAND

Karger Libri A. G.
Petersgraben 31
CH—4011 Basel

USA

Ebsco Subs. Services
1 st Ave North at 13th street
Birmingham, Ala. 35201

HUNGARIAN

Journal of

INDUSTRIAL CHEMISTRY

Edited by

the Hungarian Oil & Gas Research Institute (MÁFKI),
the Research Institute for Heavy Chemical Industries (NEVIKI),
the Research Institute for Technical Chemistry of the
Hungarian Academy of Sciences (MÜKKI),
the Veszprém University of Chemical Engineering (VVE).
Veszprém (Hungary)

Volume 9. 1981 Number 4.

HU ISSN: 0133—0276
CODEN: HJICAI

The "Hungarian Journal of Industrial Chemistry" is a joint publication of the Veszprém scientific institutions of the chemical industry that deals with the results of applied and fundamental research in the field of chemical processes, unit operations and chemical engineering. The papers are published in four numbers at irregular intervals in one annual volume, in the English, Russian, French and German languages

Editorial Office:
Veszprémi Vegyipari Egyetem
"Hungarian Journal of Industrial Chemistry"
H–8201 Veszprém, P. O. Box: 28.
Hungary

Orders may be placed with
KULTURA
Foreign Trading Co. for Books and Newspapers
Budapest 62. POB 149
or with its represenatives abroad, listed on the verso of the cover

FELELŐS SZERKESZTŐ: DR. BODOR ENDRE

KIADJA A LAPKIADÓ VÁLLALAT, 1073 BP. VII., LENIN KRT. 9–11.
TELEFON: 221-285. LEVÉLCÍM: 1906 BP. PF. 223
FELELŐS KIADÓ: SIKLÓSI NORBERT IGAZGATÓ

HUNGARIAN JOURNAL
OF INDUSTRIAL CHEMISTRY
VESZPRÉM
Vol. 9. pp. 325-332 (1981)

REACTORS FOR MULTIPHASE SYSTEMS

F. KASTANEK, M. RYLEK and J. NÉMETH*

(Institute of Chemical Process Fundamentals, Czechoslovak Academy of Sciences, Praha-Suchdol and *Research Institute for Technical Chemistry of the Hungarian Academy of Sciences, Veszprém)

Received: April 24, 1981.

This paper deals with the classification of reactors used for gas-liquid systems on the basis of the existing form of both phases in the reactor. The relationships of fluid mechanics for two phase and multiphase reactors are given, and methods used for the determination of the interfacial area existing in bubble type beds are discussed. A relationship was derived for the determination of the volumetric mass transfer coefficient assuming the validity of the penetration theory.

In general, the reactors used for gas-liquid systems can be classified according to the form the phases assumed in the reactor. This is essential for the modelling of heterogeneous multiphase systems. The classification is given in *Table 1.* The classification can be further expanded to individual types, taking the actual geometric arrangement of the reactor elements and the character of the flows inside the reactor (e.g. phase pulsation, etc.) into consideration [1]. These variants are discussed in patent literature and have commercial significance.

So-called bubble-type reactor are discussed here. Bubble-type reactors constitute an important group of multiphase reactors. In bubble-type reactors the small bubbles formed spontaneously on the distributor plate are dispersed in the bulk of the liquid phase.

Interfacial Area in Bubble-Type Reactors

The structure of the multiphase fluid system in a bubble-type reactor varies with the type of electrolyte present. This was also confirmed by our measurements. The quantitative relationships of air-to-liquid ratio (bed porosity) and operation parameters are still unknown. Therefore, the absolute value of the interfacial contact area, where actual contact takes place, cannot yet be calculated.

Table 1

Existence Forms of the Phases in the Reactor

No.	Continuous phase			Dispersed phase			Contact of Phases	Moving Elements	Type of Industrial Reactor
	Film	Jet	Bulk	Film	Bubbles	Drops			
1	Liquid		Gas				Across the surface of liquid film formed on the vertical plates, walls and packings		Wetted-wall reactors, wetted-spirals, etc.
2	Liquid		Gas				Through surface of liquid film on packings or oriented packings		Packed absorbers
3		Liquid	Gas				In the liquid jet in bulk of the reactor	Wiped film	Wiped-film reactors Multiple laminar jets, Venturi tube reactor
4			Liquid Gas		Gas		Through surface of the liquid charge	Stirrer situated at liquid surface	Reactors with surface vortex
5			Liquid		Gas		Between liquid and bubbles on the packing		Bubble-type packed reactors
6			Liquid		Gas		Between liquid and bubbles in reactor without packing or with oriented packing, e.g. plates, etc.		Bubble-type reactors, multistage bubble-type reactors
7			Liquid		Gas		Between bubbles and liquid in mechanically stirred bed or internals of plate type	Rotary stirrers on one axis, vibrating plates	Stirred bubble-type reactors, multistage stirred bubble-type react. with vibrating plates
8			Gas			Liquid	Through surface of droplets		Scrubbers, showers, react. with liquid sprayed of into the gas phase
9				Liquid	Gas	(Liquid)	Between liquid films in the bed, or between droplets and bubbles		Absorption columns

The air-liquid ratio is significantly different in certain electrolytes. For example, even though the air-liquid ratio is as different in aqueous solutions of Na_2CrO_4 and $NaClO_4$ as 0.27 and 0.16 at 0.1 m/s reference velocity, both values can be calculated with an average error of 6–10%. It seems likely that emprical, "practice-oriented" relationships can be better used to relate the basic flow parameters of the gas phase, and the interfacial contact area. Since interfacial contact area determinations are very difficult to carry out even today [2–4], the parameters used in the above correlation have to be—advantageously—easily obtainable. There is a correlation between the magnitude of interfacial contact area and the air-liquid ratio of the multiphase system. This relationship can be derived by the critical application of the "isotropic turbulence theory". Formerly KOLAR [5], CALDERBANK [6] and NAGEL [7] attempted a similar approach. By expanding NAGEL's approach a relationhip could be obtained for the expected average bubble diameter, $\bar{d}_B$.

When turbulent sheer stress is expressed according to the theory of isotropic turbulence and is substituted into the equation of the dissipation energy, a relationship is obtained for the expected average bubble diameter:

$$\bar{d}_B \sim (\sigma/\varrho_L)^{0.6} e_d^{-0.4} \tag{1}$$

Assuming that the mean and equivalent bubble diameters d_e are proportional, the expression for the specific interfacial contact area reads, in the case of spherical bubbles ($a = 6e/d_{eB}$), as:

$$a \sim (\varrho_L/\sigma)^{0.6} e_d^{0.4} e \tag{2}$$

where e is the average air-to-liquid ratio in the bed.

The total dissipated energy related to unit mass of liquid in the bed is $e_d = vg$.

Part of the total dissipated energy, dissipated only by the liquid, related to the unit mass of liquid is:

$$e_{wd} = v(\mu_G/\mu_L)\,(1-e)/e. \tag{3}$$

The specific interfacial contact surface area related to the volume of the reaction mixture is:

$$a \sim (\varrho_L/\sigma)^{0.6} (\mu_G/\mu_L)^{04.} v^{0.4} (1-e)^{0.4} e^{0.6}. \tag{4}$$

In agreement with REITH [8]:

$$a \approx K[v/(2v+0.2)]. \tag{5}$$

If REITH's expressions for the air-to-liquid ratio $e = v/(2v+c)$ is used then:

$$a \sim (v+c)^{0.4} e. \tag{6}$$

In this case Eq. 4–6 agree well with the experimentally found behaviour of the interfacial contact area [9, 10].

For small gas velocities the interfacial contact area is proportional to the air-to-liquid ratio, $a \sim e$. This conclusion is also in agreement with that physical interpretation, which states that for small gas velocities the bubble diameter is constant, even though the gas velocity increases. Since the number of bubbles increases, both the air-to-liquid ratio and the magnitude of the interfacial contact area increase. These conclusions agree with other authors' findings, and also with our results published earlier [11]. In the $v \leq 0.03$ m/s range the

magnitude of interfacial contact area can be estimated from the measured air-to-liquid ratio and mean bubble diameter data.

Another method used for the estimation of the interfacial contact area at $v > 0.02$ m/s gas velocities is based on the calculation of the constant, K. This, in turn, can be obtained from measured gas-to-liquid ratios. This value is then substituted into Eq. 5. This procedure is suitable for those systems which behave like on air-water system.

If both the momentum and force balance equations are applied to an infinitesimal volume of the bed, then a general relationship can be derived giving the magnitude of interfacial contact area in a bubble-type reactor. Practical application of this relationship depends on our ability to determine the gas-liquid friction coefficient, and also the spatial dependence of the gas-to-liquid ratio in the bed. Using simplifying assumptions, the relationship:

$$a = Cv(1-e) \tag{7}$$

can be obtained, which agrees well with the results of measurements carried out in electrolytes [10]. The value of coefficient C depends on the physico-chemical parameters of the system and also, slightly, on the diameter of the column.

Similarily to the estimation of the air-to-liquid ratio, $K = 1{,}500$ was chosen for a first approximation and the interfacial contact area, a was calculated from Eq. 5. In 0.2–1.0 M aqueous Na_2SO_3 solutions $K = 1{,}460$ corresponds to an equivalent bubble diameter of 4 mm.

Mass Transfer Coefficient

An expression could be derived for the mass transfer coefficient assuming that the penetration theory applies:

$$k_L \sim (2/\sqrt{\pi})\,(D_L/\nu_L)^{1/2}[g(\varrho_G/\varrho_L)\nu_G(v+c)]^{1/4}. \tag{8}$$

The principle of isotropic turbulence was used to derive the constant time-coefficient of the penetration theory. Dissipation energy was expressed by Eq. 3.

Eq. 8 could be obtained by substituting REITH's expression for the air-to-liquid ratio into the following general relationship:

$$k_L \sim (2/\sqrt{\pi})\,(D_L/\nu_L)^{1/2}[vg(\varrho_G/\varrho_L)\nu_G(1-e)/e]^{1/4}. \tag{9}$$

Eq. 8 demonstrates that the mass transfer coefficient is practically independent from the gas flow rate. This statement is in agreement with the experimental observations. In order to create an equation of practical use an empirical coefficient has to be introduced into the proportionality described by Eq. 9. matching the simplified model and the actual system.

The volume mass transfer coefficient, $k_L a$ can be determined more easily than k_L. Its knowledge is important for a number of applications of bubble-type columns, e.g. for fermentors, etc. The term $k_L a$ can be derived by combining Eq. 9 and 4:

$$k_L a \sim \frac{D_L^{1/2} g^{1/4} \nu_G^{13/20} \varrho_G^{13/20}}{\sigma^{3/5} \nu_L^{9/10} \varrho_L^{1/20}}\, v^{13/20} e^{7/20}(1-e)^{13/20} \tag{10}$$

If the air-to-liquid ratio is taken from Eq. 6 then Eq. 10 becomes:

$$k_L a \sim \frac{D_L^{1/2} g^{1/4} \nu_G^{13/20} \varrho_G^{13/20}}{\sigma^{3/5} \nu_L^{9/20} \varrho_L^{1/20}} [(v+c)^{13/20} v/(2v+c)] \tag{11}$$

$k_L a$ follows the shape of the term $(v+c)^{13/20}$. $v/(2v+c)$ in the $5<c<60$ range. These c values are more reasonable than the "universal" $c=20$ value generally used in Eq. 5 for various electrolytes. In the 0–0.2 m/s linear gas velocity range $k_L a$ can be approximated by the following expression:

$$k_L a \sim v^x \tag{12}$$

where $0.7<x<1.2$. This calculated exponent x agrees surprisingly well with that calculated from DECKWER's experimental data [13].

If v is expressed from Eq. 6 and is substituted here, then:

$$k_L a \sim e^y \tag{13}$$

The optimum theroretical value of y is 1.1. On the basis of experimental data AKITA and YOSHIDA [14] found that $y=1.16$. The fit between experimental $k_L a$ values and Eq. 10 or 11 is very good over a wide range of conditions, and in a number of various electrolytes.

A rough estimate for the absolute value of k_L can be obtained from CALDERBANK's and MOO-YOUNG's relationships. It has to be stressed that different methods used for the measurement of k_L and $k_L a$ yield different results. Generally, values of $k_L a$ derived by DANCKWERTS' method from measurements also involving a chemical reaction are larger than those obtained in the case of physical absorption only. For an air—weak-aqueous-electrolyte system $k_L a$ can be estimated by Eq. 14 assuming that there is no inter-phase turbulence.

$$k_L a \times 10^2 = 2.88 v^{0.65} e^{0.35} (1-e)^{0.65}, \quad s^{-1}. \tag{14}$$

Gas Hold-Up in a Bubble-Type Bed

Gas and liquid hold-up are important parameters significantly influencing the performance of bubble-type reactors.

In connection with the hold-up, our results can be summarized as follows:

- — prediction with good accuracy of the air-to-liquid ratio in non-electrolyte-filled bubble-type reactors is possible;
- — prediction of the air-to-liquid ratio is problematic in electrolytes because insufficiently known surface effects also come into play.

Assuming that the gas-phase pressure drop can be expressed by the relationship used in conduits with an equivalent diameter, d_e, an equation can be formulated:

$$\Delta p/H = 1/2(\Psi_G/\varrho_G)\,(1/d_e)\,(G/e)^2 \tag{15}$$

where $d_e = 4e/a$, $\Delta p/H = \varrho_L \cdot g$, and the friction coefficient, Ψ_G is a function of the Re number:

$$\Psi_G = k/Re_e^n, \qquad Re_e = v \times d_e \times \varrho_G/\mu_G.$$

The value of constants k and n can be determined from the experimentally determined air-to-liquid ratios (15):

$$e = BK^{7/15} v^{4/5} / (2v + 0.2)^{7/15} \tag{16}$$

where

$$B = 1/2^{4/5} \times 1/4^{1/5} (\varrho_G / \varrho_L g)^{4/15} k^{4/15} (\mu_G / \varrho_G)^{1/5} \tag{17}$$

with the value $K = 1.74 \times 10^3$ considered universal. (SI units are used throughout Eq. 16 and 17). Quantity K is characteristic for a given system and bed geometry.

In the case of non-electrolytes:

$$K = C \times \mu_L^{0.23} / \varrho^{0.077} \tag{18}$$

where $\mu_L = cP$, $\sigma = \text{dyn/cm}$ and $C = 1{,}042$ for a column of internal diameter 150 mm.

The validity of Eq. 19–21 was verified in the $780 < \varrho_L < 1{,}200$ (kg/m^3), $1 < \mu_L < 107$ (10^{-3} Ns/m^2), $22.3 < \varrho < 77$ (10^{-3} N/m) and $0.01 <$ linear gas-velocity < 0.15 (m/s) range. The average accuracy was 18%.

Similar dependence could not be obtained for electrolyte solutions. Air-to-liquid ratios calculated as the integral mean value along the bed significantly differ for the different electrolyte solutions. For a bed of 150 mm internal diameter, $K = 800$ for water and $680 < K < 2{,}960$ for 1 M electrolytes. (This means that the air-to-liquid ratio can be lower in electrolytes than in water!). It is stressed here that the e-v relationship shows a considerable hysteresis for the majority of electrolytes, depending on the manner the bed was brought to steady-state conditions.

Air-to-liquid ratios differ so considerably in various electrolytes and their dependency on the column diameter is so varied that for engineering purposes the effects of the changing diameter can be neglected at I.D. > 90 mm, though some effects were noted and correlated during the experiments.

The most reliable method to obtain a reliable air-to-liquid ratio is to measure an e-v pair on model equipment. The K is calculated from Eq. 16–18 and the e-v relationship is obtained.

For aqueous electrolytes of unknown concentration and composition $K = 1{,}500$ can be taken for the purpose of first estimation.

Regarding the concentration dependence of the air-to-liquid ratio it can be said that the ratio is approximately constant in the 0.2–2 M range, while a linear relationship exists in the 0–0.2 M range. The fit between the experimental data and the proposed correlation is satisfactory for linear gas velocities in the $v > 0.09$ m/s range. In the $0.02 < v < 0.09$ m/s range measured and calculated values differ by 20–30%.

Thus, it can be concluded from the correlations of interfacial contact area and mass transfer coefficient with e_{wd} and e that the volume mass transfer coefficient implicitly depends on the size of the reactor, as the air-to-liquid ratio depends on the dimensions of the apparatus. However, the latter dependency is often negligible.

Pressure Drop on the Bubbling Plates

Pressure drop of the gas flow passing the holes of a plate can be calculated as:

$$\Delta p = \sum_{n} (\Delta p_d + h\varrho_L g) \tag{19}$$

where h is the height of liquid on a plate prior to the start of the gas flow.

For thin plates ($T/d_0 < 2$) the pressure drop of dry plates can be calculated as

$$\Delta p_d = K^*/2[0.4(1.25 - \varphi) + (1 - \varphi^2] \times \varrho_G \times v_0^2 \tag{20}$$

where the value of K^* is taken from the plot *Fig. 1.*

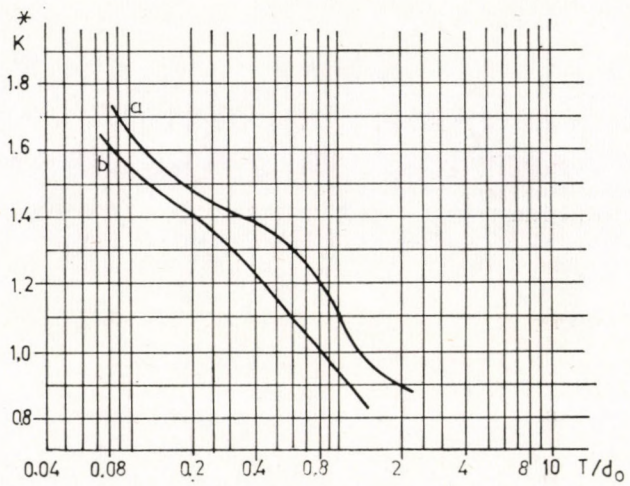

Fig. 1.
Function of the value K^* versus T/d_0
a — Sieve-plate, *b* — Turbogrid tray

In the case of co-current operation mode, pressure drop across the plates can become the limiting factor. The following plate-designs were examined: plates with circular holes, thin plates ($T/d_0 < 2$), $d_0 = 10$–25 mm, $T = 2$ mm, $\varphi = 0$–5%; thick plates, $d_0 = 10$–25 mm, $\varphi = 0$–14%, $T = 32$–80 mm. In the case of two-phase flow, pressure drop in orders of magnitude larger than in the case of single-phase flows [17]. For thin plates, pressure drop is minimum, and constant (392 $Pa = 40$ mm H_2O) for $\varphi \geq 4\%$. Regarding the pressure drop, the optimum value of free plate area is $11 < \varphi < 14\%$ for thick plates.

SYMBOLS

a	specific interfacial contact area per unit volume of the reaction ($g-l$) mixture
c, C	constants
$\overline{d}_B$	average bubble diameter
d_{eB}	equivalent bubble diameter
d_e	equivalent diameter

d_0	diameter of the holes on the sieve plate
D_L	diffusion coefficient of the dissolved compound
e	air-to-liquid ratio
e_d	total dissipated energy per unit of liquid mass
e_{wd}	fraction of total dissipated energy in liquid per unit of liquid mass
g	gravity constant
G	gas flow rate
H	bed height
k	constant
k_L	mass transfer coefficient in liquid
K	constant, characteristic for the given system
Δp	pressure drop
Δp_d	dry plate pressure drop
Re	Reynolds number
T	plate thickness
$v_0 = v/\varphi$	linear gas velocity related to free plate area
v	linear gas velocity in reactor
μ_G	gas viscosity
μ_L	liquid viscosity
ϱ_G	gas density
ϱ_L	liquid density
ν_G	kinematic viscosity of gas
ν_L	kinematic viscosity of liquid
σ	surface tension
φ	relative free plate area
Ψ_G	friction coefficient

REFERENCES

1. TURBA, J., NÉMETH, J.: Vegyipari készülékek és gépek tervezése, Műszaki Könyvkiadó, Budapest, 1973.
2. KOVÁCS, S., ÚJHIDY, A., NAGY, E., LAURENT, M., CHARPENTIER, J.-C.: 3rd Conf. on Applied Chemistry, Veszprém, 1977. p. 52.
3. LAURENT, A., CHARPENTIER, J.-C.: 3rd Conf. on Applied Chemistry, Veszprém, 1977. p. 39.
4. SASVÁRI, GY., HITES, F., BLICKLE, T.: Acta Chimica Acad. Sci. Hung. *1971*, 70, 395.
5. KOLÁR, V.: Ibid. *1961*, 26, 335; *1970*, 35, 3678; *1959*, 24, 3811.
6. CALDERBANK, P. H., MOO-YOUNG, M. B.: Chem. Eng. Sci. *1961*, 16, 39.
7. NAGEL, O., KÜRTEN, M., SINN, R.: Chem.-Ing.-Tech. *1972*, 44, 899.
8. REITH, T., BEEK, W. J.: Proc. Chem. React. Eng. Symp. p. 191, Bruxelles 1968.
9. KASTÁNEK, F.: Collection Czechoslov. Chem. Commun. *1976*, 41, 3709.
10. KASTÁNEK, F., NYVLT, V.: Ibid. *1974*, 39, 3068.
11. KASTÁNEK, F., KRATOCHVIL, J., ZAHRADNIK, J., RYLEK, M., CERMÁK, J.: Chemicky prumysl, in press (Czech.).
12. KASTÁNEK, F.: Collection Czechoslov. Chem. Commun, *1977*, 42, 2491.
13. DECKWER, W. D., BRUCKHAART, R., ZOLL, G.: Chem. Eng. Sci. *1974*, 29, 2177.
14. AKITA, K., YOSHIDA, F.: Ind. Eng. Chem., Process Des. Develop. *1973*, 12, 76.
15. KASTÁNEK, F., NYVLT, V., RYLEK, M.: Ibid. *1974*, 39, 528.
16. KASTÁNEK, F., RYLEK, M., KRATOCHVIL, J.: Ibid. *1976*, 41, 2010.
17. SISAK, CS., BALLA, L.: 3rd Conf. on Applied Chemistry, Veszprém, 1977. p. 35.

РЕЗЮМЕ

Авторы провели классификацию реакторов газово-жидкостных систем по форме проявления фаз. Анализировали наиболее важные гидродинамические зависимости и трактваны методы определения поверхности соприкосновения фаз. В стати описаны уравнения расчета коэффициента объемной массопередачи с учетом теории пенетрации.

HUNGARIAN JOURNAL
OF INDUSTRIAL CHEMISTRY
VESZPRÉM
Vol. 9. pp. 333–338 (1981)

SOLUTION OF THE DIFFERENTIAL EQUATION SET USED TO DESCRIBE THE COMPONENT TRANSFER BETWEEN A SOLID AND FLUID PHASE

ERROR ANALYSIS OF THE SOLUTION IN THE CASE OF SOLID-PHASE RESTRICTED PROCESS

J. ARGYELÁN

(Department for Chemical Process Engineering, University of Chemical Engineering, Veszprém, Hungary)

Received: June 15, 1981

An analytical solution of the differential equation set used to describe the component transfer process from a limited-capacity fluid phase into a limited-capacity solid phase was developed. A concentrated-parameter differential equation was used for the description of the fluid phase, while a distributed-parameter equation was used for the solid phase. It was assumed that transfer in the solid phase was due to diffusion only, and the initial concentration was not identically zero in any of the phases. An error analysis was given to show the relationship between the number of terms of the infinite series considered and the required precision of the solution.

If solid, spherical particles are suspended in a fluid phase and the concentrations are to be described—assuming that component transport in the solid phase is due to diffusion only—then the following differential equation set and boundary conditions, well known in literature, are obtained:

$$V\frac{dc}{dt} = -4R^2\pi D\frac{\partial q}{\partial r} \qquad r=R \tag{1}$$

$$\frac{\partial qr}{\partial t} = D\frac{\partial^2 qr}{\partial r^2} \qquad R \geq r \geq 0 \tag{2}$$

$$\frac{\partial q}{\partial r} = 0 \qquad r=0 \qquad t>0 \tag{3}$$

$$q = Kc \qquad r=R \qquad t>0 \tag{4}$$

The differential equation set, Eq. 1 to 4 is generally Laplace transformed [1, 2] using the following initial conditions:

$$c = C_0 \qquad t=0 \tag{5}$$

$$q = 0 \qquad R>r\geq 0 \qquad t=0 \tag{6}$$

$$q = KC_0 \qquad r=R \qquad t=0 \tag{7}$$

The solution of functions $c(t)$ and $q(r, t)$ are also known from literature:

$$c=\frac{C_0\alpha}{1+\alpha}+C_0\sum_{k=1}^{\infty}\frac{6\alpha e^{-D\omega_k^2 t}}{9+9\alpha+(\omega_k R)^2\alpha^2} \tag{8}$$

$$q=K\frac{C_0\alpha}{1+\alpha}+KC_0\sum_{k=1}^{\infty}\frac{6\alpha e^{-D\omega_k^2 t}}{9+9\alpha+(\omega_k R)^2\alpha^2}\frac{R}{\sin\omega_k R}\frac{\sin\omega_k r}{r}. \tag{9}$$

where $\alpha=3V/4R^3\pi$ and ω_k are the roots of Eq. 10:

$$\operatorname{tg}\omega_k R=\frac{3\omega_k R}{3+\alpha(\omega_k R)^2} \tag{10}$$

This type of solution is also similar under the following initial conditions:

$$q=Q_0 \qquad R>r>0 \qquad t=0 \tag{11}$$

$$q=0 \qquad r=R \qquad t=0 \tag{12}$$

$$c=0 \qquad t=0 \tag{13}$$

The solution becomes:

$$c=\frac{Q_0}{K(1+\alpha)}\left\{1-\sum_{k=1}^{\infty}\frac{6\alpha(1+\alpha)e^{-D\omega_k^2 t}}{9+9\alpha+(\omega_k R\alpha)^2}\right\} \tag{14}$$

$$q=\frac{Q_0}{1+\alpha}\left\{1-\sum_{k=1}^{\infty}\frac{6\alpha(1+\alpha)}{9+9\alpha+(\omega_k R\alpha)^2}\frac{R}{\sin\omega_k R}\frac{\sin\omega_k r}{r}\right\} \tag{15}$$

It is comparatively simple to produce both Eq. 8, 9 and Eq. 14, 15, because the initial concentration in one of the phases is zero. The condition system described by Eq. 5–7 and 11–13 can be derived from the more general condition system:

$$q=Q_0 \qquad R>r\geq o \qquad t=o \tag{16}$$

$$q=KC_0 \qquad r=R \qquad t=o \tag{17}$$

$$c=C_0 \qquad t=o \tag{18}$$

if the substitution $c=\tilde{c}+Q_0/K$ and $q=\tilde{q}+Q_0$ or $c=\tilde{c}+C_0$ and $q=\tilde{q}+KC_0$ are carried out. However, due to the sign of KC_0-Q_0, an alternative solution is obtained, for the substitution makes $\tilde{c}$ or $\tilde{q}$ zero at time zero.

Using the "separation of the variables" method the more general equation set, Eq. 1–4, 16–18 can also be solved. If c is eliminated from Eq. 1 using, as boundary condition, Eq. 4, and the time-derivate of the results is derived by Eq. 2, then following equation set is obtained:

$$\frac{\partial qr}{\partial t}=D\frac{\partial^2 qr}{\partial r^2} \tag{19}$$

$$\frac{\partial q}{\partial r}=0 \qquad r=0 \qquad t>o \tag{20}$$

$$V\frac{\partial^2 qr}{\partial r^2}=4R^3\pi K\frac{\partial q}{\partial r} \qquad r=R \qquad t>0 \tag{21}$$

$$q=Q_0 \qquad 0\leq r<R \qquad t=0 \tag{22}$$

$$q=KC_0 \qquad r=R \qquad t=0 \tag{23}$$

Let us seek the solution in the form of $f(r)g(t)$. Then:

$$\frac{\frac{dg}{dt}}{g}=\frac{\frac{d^2f}{dr^2}}{f}=-\gamma_i \tag{24}$$

where γ_i is a positive constant. Then:

$$g_i=e^{-\gamma_i t} \tag{25}$$

$$f_i=a_i \cos\sqrt{\frac{\gamma_i}{D}}\,r+b_i \sin\sqrt{\frac{\gamma_i}{D}}\,r \tag{26}$$

The boundary conditions become:

$$\lim_{r\to 0}\left(\frac{1}{r}\frac{df}{dr}-\frac{f}{r^2}\right)=0 \tag{27}$$

$$V\frac{d^2f}{dr^2}=4R^2\pi K\left(\frac{df}{dr}-\frac{f}{r}\right) \qquad r=R \tag{28}$$

If function f_i is substituted into the boundary conditions, the $a_i=0$ is obtained, so $f_i=b_i\cdot\sin\sqrt{\frac{\gamma_i}{D}}\,r=b_i \sin\,\omega_i r=b_i y_i$. It follows from the boundary conditions of Eq. 28 that:

$$tg\ \omega_i R=\frac{4R^3\pi K\omega_i R}{V(\omega_i R)^2+4R^3\pi K} \tag{29}$$

The last equation yields ω_i and this results in the eigen-value $\gamma_i=D\omega_i^2$. Then the qr function becomes:

$$qr=\sum_{i=1}^{\infty} b_i e^{-\gamma_i t}y_i+\frac{3VC_0+4R^3\pi Q_0}{3V+4R^3\pi K}\,Kr \tag{30}$$

Substituting the solution into initial conditions of Eq. 22, 23 we obtain, after rearrangement:

$$\sum_{i=1}^{\infty} b_i y_i=\left\{\begin{array}{ll} 3V\dfrac{Q_0-KC_0}{3V+4R^3\pi K}\,r & r<R \\ 4R^3\pi K\dfrac{KC_0-Q_0}{3V+4R^3\pi K}\,R & r=R \end{array}\right\}=u \tag{31}$$

The fact that function set y_i is not orthogonal over interval $0-R$ might pose a problem in the determination of coefficients b_i. This difficulty can be bridged by defining the scalar multiple of the two functions as follows:

$$<v,\ w>=\int_0^R v\cdot w\,dr+\frac{V}{4R^2\pi K}\,v(R)\cdot w(R) \tag{32}$$

With this scalar multiple function set y_i becomes orthogonal, so the solution-function u can be expressed as a series according to eigen-functions y_i. Let us now form the scalar multiple of u and functions y_k (32) as follows:

$$< u, y_k > = < y_k, \sum_i b_i y_i > = b_k \left\{ \int_0^R y_k^2 \, dr + \frac{V}{4R^2\pi K} y_k^2(R) \right\} = B_k b_k \tag{33}$$

On the other hand:

$$< u, y_k > = 3V \frac{Q_0 - KC_0}{3V + 4R^3\pi K} \int_0^R r y_k \, dr + R^2 V \frac{KC_0 - Q_0}{3V + 4R^3\pi K} y_k(R) = A_k \tag{34}$$

A_k and B_k can be expressed as:

$$A_k = \frac{V(C_0 K - Q_0)}{4\pi RK} \sin \omega_k R \tag{35}$$

$$B_k = \frac{V\omega_k^2 + 4\pi RK \sin^2(\omega_k R)}{2(V\omega_k^2 + 4\pi RK)} R + \frac{V}{4\pi R^2 K} \sin^2(\omega_k R) \tag{36}$$

Then the solution:

$$b_k = \frac{A_k}{B_k}$$

$$q(r, t) = \sum_{k=1}^{\infty} \frac{V(KC_0 - Q_0)R(V\omega_k^2 + 4\pi RK) \sin \omega_k R \sin \omega_k r}{2KVR^3\pi\omega_k^2 + (8\pi^2 R^4 K^2 + V^2\omega_k^2 + 4\pi RKV) \sin^2(\omega_k R) r} e^{-D\omega_k^2 t} + \\ + \frac{3VC_0 K + 4R^3\pi KQ_0}{3V + 4R^3\pi K} \tag{37}$$

Function $c(t)$ describing the concentration in the fluid phase can be obtained in two ways. One of them is that the q solution is substituted into boundary condition 4, so:

$$c = \frac{1}{K} \sum_{k=1}^{\infty} \frac{V(KC_0 - Q_0)(V\omega_k^2 + 4\pi RK) \sin^2(\omega_k R)}{2KVR^3\pi\omega_k^2 + (8\pi^2 R^4 K^2 + V^2\omega_k^2 + 4\pi RKV) \sin^2(\omega_k R)} e^{-D\omega_k^2 t} + \\ + \frac{3VC_0 + 4R^3\pi Q_0}{3V + 4R^3\pi K} \tag{38}$$

The other possibility is that the overall amount of material which entered the solid phase is expressed and it is subtracted from the amount initially present in the fluid phase:

$$c = C_0 - \frac{1}{V} \int_0^R (q - Q_0) 4r^2\pi \, dr \tag{39}$$

The functions expressed by Eq. 38 and 39 are identical, which proves that $q(r, 0)$ differens from Q_0 only in a few points, at the most.

Substituting $C_0 = 0$ and $Q_0 = 0$ into Eq. 37–39, they become Eq. 8, 9 and 14, 15, respectively.

If only the fluid phase concentration is interesting, and only N terms of the infinite series are considered, then the error, H is largest at $t=0$ and can be expressed as:

$$H=\frac{1}{K}\sum_{k=N+1}^{\infty}\frac{V(KC_0-Q_0)\left(V\omega_k^2+4\pi RK\right)\sin^2(\omega_k R)}{2KVR^3\pi\omega_k^2+\left(8\pi^2R^4K^2+V^2\omega_k^2+4\pi RKV\right)\sin^2(\omega_k R)}=$$

$$=\frac{1}{K}\sum_{k=N+1}^{\infty}\frac{2V(KC_0-Q_0)}{4R^3\pi K+3V+\dfrac{V^2\omega_k^2}{4\pi RK}} \tag{40}$$

Here $\sin(\omega_k R)$ was expressed by Eq. 29. When Eq. 29, relating to the eigen-value is examined, then it can be shown that there is an $\omega_k R$ root in each $k\pi-(k+1)\pi$ interval. If this root is substituted with $k\pi$, then Eq. 40 becomes:

$$H<\sum_{k=N+1}^{\infty}\frac{2V(KC_0-Q_0)4R^3\pi}{(4R^3\pi K)^2+12R^3\pi KV+(kV\pi)^2}=\frac{1}{K}\sum_{k=N+1}^{\infty}\frac{6\alpha(KC_0-Q_0)}{9+9\alpha+(\alpha\pi k)^2}<$$

$$<\frac{6(KC_0-Q_0)}{K\alpha\pi}\int_N^{\infty}\frac{dk}{\dfrac{9(1+\alpha)}{\alpha^2\pi^2}+k^2}=\frac{KC_0-Q_0}{K\sqrt{1+\alpha}}\left\{1-\frac{2}{\pi}\operatorname{arc\,tg}\frac{\alpha\pi N}{3\sqrt{1+\alpha}}\right\}. \tag{41}$$

It can be seen that by selecting an appropriate N value, error H can become as small as required. Thus, component transfer can be calculated in the case of solid-phase controlled processes without alternative equations and transformation of the variables.

ACKNOWLEDGEMENT

The author is indebted to S. Székely for valuable discussions.

SYMBOLS

$c, \tilde{c}$ concentration in the fluid phase, mmol/cm³
$q, \tilde{q}$ concentration in the solid phase, mmol/cm³
V volume of the fluid phase, cm³
R radius of the solid particle, cm
D diffusion coefficient, cm²/s
t time, s
r radius, cm
C_0 initial concentration in the fluid phase, mmol/cm³
Q_0 initial concentration in the solid phase, mmol/cm³
K equilibrium coefficient
α volume fraction, —
γ_i eigen-value, 1/s
ω_i eigen-value, 1/cm
H absolute error, mmol/cm³
a_i, b_i, A_i, B_i coefficients, mmol/cm²
N limiting value
i, k subscripts
g, f, u, v, w, y functions

REFERENCES

1. Crank, J.: The Mathematics of Diffusion, Clarendon Press, Oxford, 1964.
2. Carslaw, H. S.: Conduction of Heat in Solids, Oxford, 1947.

РЕЗЮМЕ

Описывается аналитическое решение системы дифференциальных уравнений перехода компонентов из жидкостной фазы конечной емкости в твердую фазу конечной емкости. Жидкостная фаза описывается системой дифференциальный уравнений с жатыми параметрами, а твердая фаза описывается уравнением с разделенными параметрами. Предпологается, что транспорт в твердой фазе обусловлено лишь диффузией и в начальный момент концентрация ни в одной фазе не равняется тождественно нулью. Проведен анализ ошибки насчёт порядка точности полученного в результате решения бесконечного ряда.

HUNGARIAN JOURNAL
OF INDUSTRIAL CHEMISTRY
VESZPRÉM
Vol. 9. pp. 339–346 (1981)

ISOCRATIC REVERSED PHASE LIQUID CHROMATOGRAPHIC SEPARATION OF INSULINS

MRS. Z. VARGA-PUCHONY, MRS. E. HITES-PAPP, J. HLAVAY and GY. VIGH*

(Department for Analytical Chemistry, University of Chemical Engineering, Veszprém, Hungary)
Received: July 31, 1981.

A simple, isocratic liquid chromatographic separation method was developed for the analysis of bovine and porcine insulins and their desamido decomposition products. The dependence of insulin retention upon the water concentration of the eluent and the chain-length of the tetraalkyl ammonium ion pair reagents was investigated. The applicability of the system for routine production control purposes was demonstrated by the analysis of crude insulin samples and a monocomponent insulin preparation.

Introduction

High perfomance liquid chromatography (HPLC) underwent spectacular development over the past ten years. With the advent of reliable reversed phase (RP) packings, and the introduction of ion pair reagents, HPLC entered such new fields as protein and polypeptide analysis, which in the past had been dominated by low performance gel chromatographic separation methods.

Insulins are large polypeptides with an approximate molecular mass of 6,000. The insulins of various species differ only slightly in their amino acid sequence, generally in 2 or 3 amino acids at the most. Since crude insulin batches may contain other biologically active components and decomposition products, a simple and fast separation as a first screening method is essential for insulin processing. So far most insulin separations were carried out by gel chromatography, e.g. [1–4] or by reversed phase HPLC with gradient elution, e.g. [5–9] requiring costly instrumentation. Only DINNER and LORENZ [10] and DAMGAARD and MARKUSSEN [11] published simple, isocratic insulin separation methods.

Some of the papers on gradient insulin separation [8, 12] indicate that tetramethyl ammonium cations have a favourable effect upon the peak shape of insulins and related large polypeptides, because the tetramethyl ammonium

* To whom correspondence should be addressed.

ions are believed to block the residual OH groups of the reversed phase packing, and also, possibly, form ion pairs with the polypeptides. However, the retention volume of insulins were apparently identical with and without tetramethyl ammonium ions.

Therefore, it seemed worthwhile to investigate the effects of tetraalkyl ammonium ions upon the retention volume of insulins, and based on these results, develop a simple, isocratic liquid chromatographic separation method suitable for fast quality-control purposes.

Experimental

A Varian LC 5020 liquid chromatograph (Varian, USA) connected to an LC 55 variable wavelength detector (Perkin-Elmer, USA) was used in the experiments. The thermosttated 250×4.0 mm I.D. s.s. column [13] was packed with 10 μm RP-18 octadecyl silica (Merck, FRG). Tetramethyl, tetraethyl and tetrabutyl ammonium hydroxide reagents were obtained from BDH (Britain), while phosphoric acid and methanol were from Reanal (Hungary). In order to check the hydrophobic eluting power of the eluent, nitroalkanes (Fluka, Switzerland) were also separated along with the insulins. The retention volumes of nitroalkanes were used as reference points, since their values mainly depended on the methanol content of the eluent. Since former experiments indicated [14] that the retention of insulins depended sensitively on the methanol content and the preparation method of the eluent, the latter was rigorously standardized. The calculated amount of methanol, ion pair reagent and phosphoric acid was weighed into a 1000 ml volumetric flask, then the flask—while kept at 25 °C—was brought almost to mark with double distilled water leaving a free space of about 500 μl. Then, the pH of the eluent was measured with a combined glass electrode and precision pH meter (Radelkis, Hungary), calibrated with pH 4 and 7 aqueous buffers. If necessary, final pH adjustment was achieved by adding a few drops of concentrated phosphoric acid. Then the flask was brought to the mark, the eluent was filtered, degassed ultrasonically and used immediately.

Retention was characterized by the k' values determined as:

$$k' = \frac{V_R - V_0}{V_0}$$

where V_R is the retention volume of the component in question and V_0 is the dead volume of the column determined as described in [15].

Results

1. Effects of the Chain-Length of the Tetraalkyl Ammonium Cation

pH 3.2 eluents were prepared, which contained 45.8 g methanol in 100 ml final volume, 0.1 mol/l phosphoric acid and also one of the following ion pair reagents:

a) none
b) 0,05 mol/l tetramethyl ammonium (TMA^+) cations

c) 0.05 mol/l tetraethyl ammonium (TEA^+) cations
d) 0,05 mol/l tetrabutyl ammonium (TBA^+) cations.

The k' values of nitroalkanes, bovine and porcine insulins obtained with these eluents are summarized in *Table 1.*

Table 1.

Effects of the chain-length of tetraalkyl ammonium cation upon the k' values of nitroalkanes, bovine and porcine insulins. Eluent: 45.8 g/100 cm^3 methanol, pH 3.2, tetraalkyl ammonium cation concentration: 0.05 mol/l, $T = 26$ °C

Tetraalkyl ammonium cation	k'			
	nitro-butane	nitro-pentane	bovine insulin	porcine insulin
none	1.22	2.50	8	—
tetramethyl	1.23	2.51	5.0	9.0
tetraethyl	1.23	2.51	5.1	9.0
tetrabutyl	1.22	2.50	0.6	1.1

It can be seen that in the range studied, the tetraalkyl ammonium cations do not influence the retention of the neutral nitroalkanes. In the absence of tetraalkyl ammonium ions the retention of the insulins is large, and the peaks are distorted by severe tailing.

With the addition of TMA^+ their retention decreases and the peak shapes improve. TEA^+ has a similar effect on the k' values of insulins and none upon the k' of nitroalkanes.

The k' of insulins are almost identical with both TMA^+ and TEA^+. However, upon the addition of TBA^+ the k' of insulins decreased dramatically, while those of the nitroalkanes remained constant.

The concept of classical ion pair formation between the positively charged tetraalkyl ammonium cations and the negative carboxylate groups of the insulins—as suggested in literature—cannot be maintained, for it would require an increase in k' with an increase in the chain length of the ion pair reagent and the opposite is true.

It is believed that the tetraalkyl ammonium cations are adsorbed on the hydrophobic packing and create a positively charged environment. This positive charge exercises a repulsive effect upon the positive charges of the insulins, which at this pH are in excess, compared to the negatively charged carboxylate groups. The more hydrophobic the tetraalkyl ammonium cation, the more pronounced this repulsion is, and the smaller the k' values are. Knox et al. postulated a similar retention mechanism for small peptide zwitterions [16]. The identical k' values obtained with TMA^+ and TEA^+ are not surprising, because as Hung et al. have shown [17] the adsorption isotherms of TMA^+ and TEA^+ on octadecyl silicas are almost identical and run much lower than that of TBA^+.

2. *Effects of the Eluent Composition*

The effects of the water concentration in the eluent upon the k' of insulins was also investigated. KARL-FISCHER titration with amperometric dead-stop end-point indication was used for water determination. The k' values of insulins as a function of the water concentration are shown in *Tables 2* and *3*. It can

Table 2.

k' values of bovine and porcine insulins on LiChrosorb RP-18 packing with pH 3.0, 0.05 mol/l tetraethyl ammonium hydroxide/phosphoric acid/methanol eluents containing varying amounts of water ($T = 24$ °C)

Water content g/100 cm³ (KARL–FISCHER titration)	k'	
	bovine insulin	porcine insulin
48.56	2.49	4.59
49.41	3.10	5.77
50.18	4.20	7.56
51.55	7.21	12.99
52.08	9.17	16.73

Table 3.

k' values of bovine and porcine insulins on LiChrosorb RP-18 packing with pH 2.6, 0.005 mol/l tetrabutyl ammonium hydroxide-phosphoric acid-methanol eluents containing varying amounts of methanol

g MeOH in 100 ml eluent	k'				
	nitro-butane	nitro-pentane	nitro-hexane	bovine insulin	porcine insulin
45.93	1.25	2.53	5.24	0.5	1.0
44.02	1,43	3.02	6.33	1.3	2.3
41.53	1.78	3.83	8.24	4.1	7.1

be seen that a mere 3 g/100 g change in the water concentration causes a threefold change in k', a behaviour entirely unknown with simple, neutral organic molecules [14]. This meant that for meaningful, quality-control-oriented separations, the methanol content of the eluent has to be kept absolutely constant.

3. *Isocratic Analysis of Insulin Samples*

From the methanol-dependence of the k' of insulins, and the effects of the ion pair reagents upon the peak shapes, the analysis conditions yielding satisfactory isocratic insulin separations could be determined. These are as follows:

column: 250 mm × 4.0 I.D., packed with 10 μm LiChrosorb RP-18
eluent:
composition: 456 g methanol,
46 ml 10 cm^3/100 cm^3 tetramethyl ammonium hydroxide,
0.9 ml 85% ortophosphoric acid, double distilled water to make up for a final eluent volume of 1000 ml.
flow rate: 1,0 ml/min
temperature: 30 °C

The system allows for routine, fast monitoring/screening of incoming crude insulin batches and insulin-containing products. As an example of the former, the chromatograms of two crude insulin batches are shown in *Fig. 1* and *2*. Both samples are mixtures of bovine and porcine insulins, but the amount of

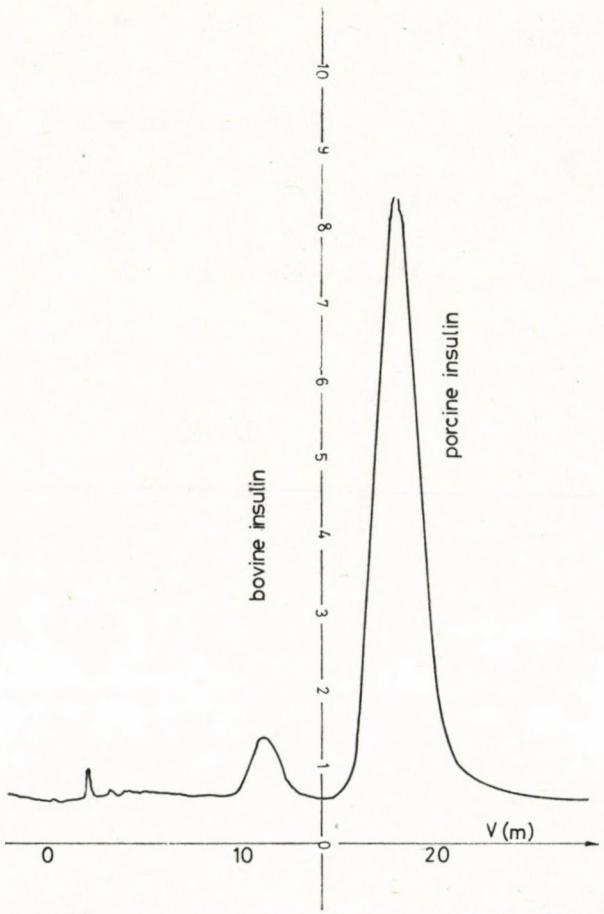

Fig. 1.
Chromatogram of a crude insulin batch. For analysis conditions see text
Error in Fig. 1: The correct dimension of abscissa is (ml).

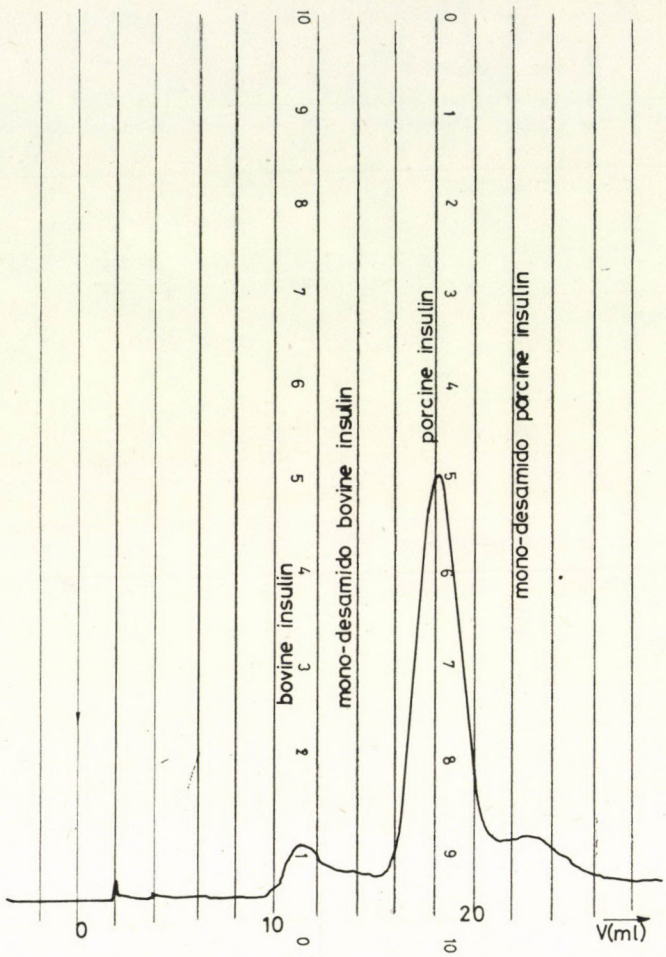

Fig. 2.
Chromatogram of a partially decomposed crude insulin batch.
For analysis conditions see text

decomposition products (monodesamido insulins) is higher in the second batch *(Fig. 2)*. The chromatogram of a monocomponent insulin injection (Monotard, NOVO, Denmark) is shown in *Fig. 3.*

Conclusions

It was shown that tetraalkyl ammonium ion pair reagents decrease the retention volume of insulins in pH 3.2 aqueous methanol eluents. However, the effects of tetramethyl and tetraethyl ammonium ions are much weaker than that of the tetrabutyl cation. The water concentration range in which insulin

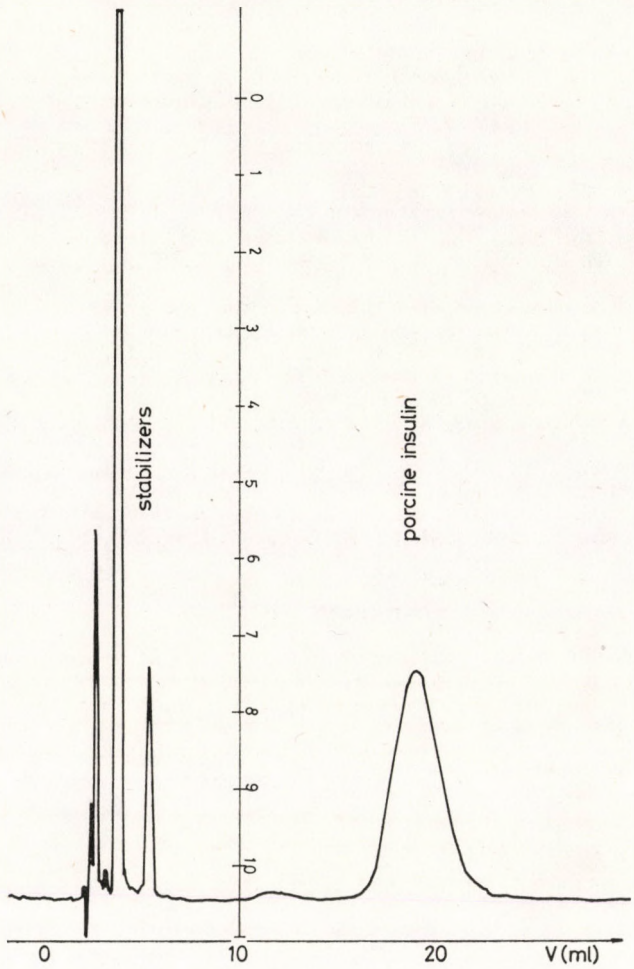

Fig. 3.
Chromatogram of a monocomponent insulin injection (Monotard, NOVO, Denmark). For analysis conditions see text

separation is possible proved to be very narrow. An isocratic reversed phase liquid chromatographic separation method was developed for the rapid screening analysis of insulin-containing samples.

ACKNOWLEDGEMENT

This work was partly supported by the Chemical Works of G. Richter, Budapest, Hungary. Permission to publish these results, and discussions with Dr. M. Gazdag and Dr. G. Szepesi are gratefully acknowledged.

REFERENCES

1. Gruber, K. A., Whitaker, M. and Morris, M.: Anal. Biochem. *1979*, 97, 176.
2. Imamura, T. and Konichi, K.: J. Biochem. (Tokyo). *1979*, 86, 639.
3. Rokushika, S., Ohkaea, T. and Hatano, H.: J. Chromatogr. *1979*, 176, 456.
4. Ui, N.: Anal. Biochem. *1979*, 97, 65.
5. Hancock, W. S., Bishop, C. A., Prestige, R. L. and Hearn, M. T. W.: Anal. Biochem. *1978*. 89, 203.
6. Hearn, M. T. W., Hancock, W. S., Hunell, J. G. R., Fleming, R. J. and Kemp, B.: J. Liquid Chromatogr. *1979*, 2, 919.
7. O'hare, M. J. and Nice, E. C.: J. Chromatogr. *1979*, 171, 209.
8. Biemond, M. E. F., Sipman, W. A. and Olivie, J.: J. Liquid Chromatogr. *1979*, 2, 1407.
9. Terabe, S., Konaka, R. and Inouye, K.: J. Chromatogr. *1979*, 172, 163.
10. Dinner, A. and Lorenz, L.: Anal. Chem. *1979*, 51, 1872.
11. Damgaard, V. and Markussen, J.: Metab. Res. *1979*, 11, 580.
12. Rivier, J. E.: J. Liquid Chromatogr. *1978*, 1, 343.
13. Vigh, Gy.: J. Chromatogr. *1976*, 117, 424.
14. Vigh, Gy., Varga-Puhony, Z., Hlavay, J. and Hites-Papp, E.: J. Chromatogr. *1981*, 236, 51.
15. Berendsen, G., Schoenmaker, P., de Galan, L., Vigh, Gy., Varga-Puhony, Z. and Inczedy, J.: J. Liquid Chromatogr. *1980*, 3, 1669.
16. Knox, J. H. and Hartwick, R. A.: J. Chromatogr. *1981*, 204, 3.
17. Hung, C. T. and Taylor, R. B.: J. Chromatogr. *1980*, 202, 333.

РЕЗЮМЕ

Авторами разработан кроматографический метод разделения простой жидкости с целью анализа скотского и свиного инзулина и их дезамидированных разложенных продуктов. Далее исследована зависимость ретенции инзулина от водяной концентрации, а также влияние длины цепи ионной пары тетраалкила аммония на ретенцию. На примере измерения проб сырого инзулина и однокомпонентных препаратов инзулина показаны возможности применения метода в контроле производственного процесса.

HUNGARIAN JOURNAL
OF INDUSTRIAL CHEMISTRY
VESZPRÉM
Vol. 9. pp. 347–364 (1981)

KINETICS OF THE VAPOUR-PHASE DEHYDRATION OF ALCOHOLS OVER ALUMINA AND RELATED CATALYSTS

M. RAVINDRAM and K. S. MURTHY*

(Department of Chemical Engineering Indian Institute of Science
Bangalore-560012, INDIA)

Received: August 6, 1981.

Kinetics of the vapour-phase dehydration of *iso*-propanol, *n*-butanol, *iso*-butanol, *s*-butanol and *t*-butanol has been studied over alumina, silica-alumina and molecular sieve catalysts in a fixed bed flow reactor under isothermal conditions in the temperature range 200–400 °C at atmospheric pressure. All the catalysts were characterized with respect to their physical properties. The reaction products essentially consisted of unreacted alcohol, water, propylene and butylene with traces of ether.

The dehydration reaction was found to be first order and the experimental and calculated conversions based on the proposed rate equations were found to be in good agreement. Acidity of the catalyst was found to significantly influence the catalyst dehydration activity. In general, a direct dependence was observed between catalyst acidity and dehydration rate. Rates of dehydration of the alcohols were compared, based on linear free energy relationship and stability of carbonium ions.

Catalytic vapour-phase dehydration of alcohols was studied over solid acids by many investigators from the standpoint of elucidating the reaction kinetics and mechanism [1–8]. Rate controlling mechanisms for alcohol dehydration based on LANGMUIR–HINSHELWOOD models for heterogeneous reactions were also proposed [9–15]. Some attempts were also made to explain the dehydration-dehydrogenation of alcohols based on the electronic theory of catalysis [16–18]. More often such studies were confined to the dehydration of ethyl alcohol over alumina with a view to determining whether ethylene formation takes place directly from alcohol or through the formation of ether as a true intermediate.

WHITMORE [19] was the first to propose a mechanistic model for explaining the dehydration of alcohols based on carbonium ion mechanism. This mechanism, which is similar to that proposed by ROSS and BENNETT [20], and others [21] for liquid phase reactions in acid media, was subsequently

* Present Address: Food and Nutrition Board, Sastri Bhawan, MADRAS 600 006, INDIA.

extended by BREMNER [22], DOWDEN [23], and WINSFIELD [24] for solid acid catalysts. More recently it was proposed that the reaction takes place by a converted mechanism, wherein both the acidic as well as basic sites present on the surface of the catalyst take part in the reaction [25]. The role played by acid sites on the catalyst surface in promoting reactions such as dehydration, isomerization, alkylation, and cracking, etc., was demonstrated by several investigators. PINES and HAAG [26] were the first to demonstrate the quantitative behaviour of catalyst acidity. However, very few comprehensive investigations were reported. This paper reports the results on the dehydration of several alcohols over alumina, silica-alumina and molecular sieve catalysts.

Experimental

Apparatus

The experimental set up employed in the kinetic studies is given in *Fig. 1.* It consisted of alcohol feeding unit, preheater, reactor and product collection unit. The reactor was made of 12 mm I.D. Pyrex glass tubing and was exter-

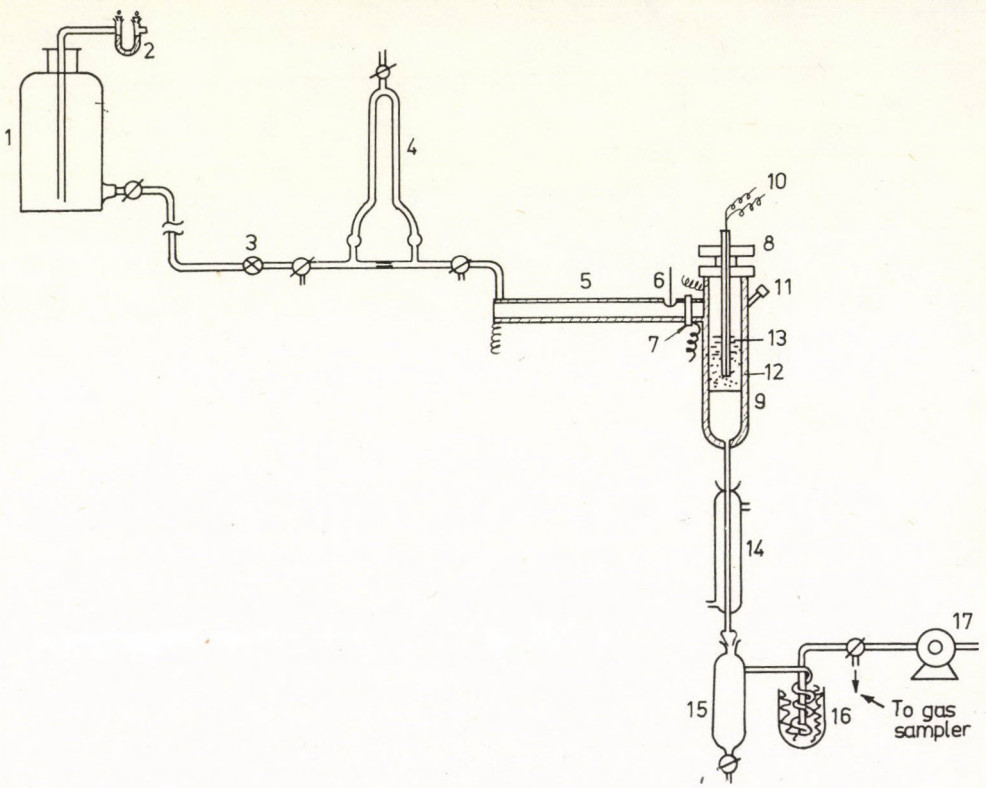

Fig. 1.
Schematic Diagram of the Experimental Set-Up.
1 — Alcohol storage; *2* — Calcium chlorid tube; *3* — Needle valve; *4* — Capillary flow meter; *5* — Pre-heater; *6* — Thermometer; *7* & *8* — Gland and nut joint; *9* — Reactor; 10 — Thermocouple; *11* — Catalyst loading point; 12 — Catalyst; *13* — Glass beads; *14* — Double surface condenser; *15* — Liquid receiver; *16* — Dewar flask; *17* — Wet gas meter

nally wound with a heating tape. The reactant feed was controlled by a fine adjustment valve and was measured by means of a rotameter. Temperature in the reactor was measured by a calibrated thermocouple and was controlled by means of a variable energy transformer. Reaction products were condensed in a double walled glass condenser. Uncondensable product gas was metered before it was vented.

Analysis

The liquid product mainly consisted of unreacted alcohol, water and ether with traces of carbonyl compounds (aldehydes and ketones). Quantitative estimation of the individual liquid products was done by vapour phase chromatography.

When iso-propyl ether and acetone were present together, these were estimated by chemical analysis. Uncondensable product gas consisting of propylene or butylene was estimated by Orsat gas analyser.

Catalyst Preparation and Characterization

Alumina was prepared from aluminium nitrate by precipitation technique. Silica-alumina was prepared by mixing the gels in the required proportion. Molecular sieve 10 x supplied by the Union Carbide Co, was used as such. All the catalysts were subjected to an activation treatment. Details of the method of preparation, treatment and characterization of catalysts were reported in an earlier communication [27]. Properties of the catalysts employed in the present study are listed in *Table 1.*

Table 1.

Physical properties of the catalysts

Notation	Catalyst	Temp. of activation °C	Surface area $m^2./g.$	Acidity		Total pore volume c.c./g.	Average pore radius Å
				m.mol/g.	m.moles/m^2.		
1	Alumina from aluminium nitrate	500	226.5	0.498	2.198×10^{-3}	0.3956	34,9
1(a)	— do —	630	160.6	0.427	2.659×10^{-3}	—	—
1(b)	— do —	730	126.6	0.337	2.662×10^{-3}	—	—
1(c)	Alumina from aluminium isopropoxide	500	224.8	0.141	0.627×10^{-3}	0.4525	40.2
2	10 × molecular sieve (MS)	500	615.5	0.597	0.970×10^{-3}	0.3318	10.8
3	Silica-alumina (81:19)	500	243.4	0.623	2.560×10^{-3}	0.3811	31.2

Mass Transfer Characteristics

Before undertaking detailed kinetic studies, the effect of the following variables on the reaction rate was studied.

i) Effect of clock time,
ii) Effect of bulk and pore diffusion.

The effect of clock time was studied at 310 °C by noting the conversion of alcohol as a function of time for a period of 24 hours under otherwise identical conditions. The conversion remained constant for a period of over 10 hours. Consequently, all the kinetic runs were conducted in the period of constant catalyst activity.

The effect of bulk diffusion was largely overcome by employing high enough velocities of the reactant. Subsequent calculations of partial pressure drop and temperature drop at the surface of the catalyst by the method of YOSHIDA, RAMASWAMY and HONGEN [28] have shown that under the operating conditions employed in the present study, the effect of intraphase diffusion could be considered to be negligible.

The effect of pore diffusion was assessed in an indirect manner by employing different particle sizes of the catalyst in the 0.4–1.0 mm range. It was found that the rate of dehydration remained essentially constant with particles of size 0.5 mm dia and below, thereby indicating the absence of intraparticle diffusion with this particle size. In the actual kinetic experiments catalyst particles of 0.4 mm dia were used.

Subsequent calculations of effectiveness factor by the method of MILLER and KIRK [29] have shown it to be near unity.

Kinetic Experiments

The range of variables employed in the present study is as follows:

Reaction temperature: 220–410 °C
Time factor (W/F): 0.5–3.0 g. cat. hr./g.mol.

Kinetic data on the dehydration of *iso*-propanol, *n*-butanol, *iso*-butanol, *s*-butanol and *t*-butanol were collected over alumina, silica-alumina and 10 x molecular sieve catalysts, by notting the conversion of alcohol as a function of time factor and reaction temperature.

Dehydration of iso-propanol led to the formation of propylene and diiso-propyl ether. Butylene was the main product with butanols except in the case of *n*-butanol where small quantities of ether also formed at lower temperatures. The dehydrogenation reaction leading to the formation of carbonyl compounds (aldehydes and ketones) was found to proceed to a negligible extent (less than 1 per cent). Even in the case of iso-propanol, ether formation never exceeded 10 per cent and hence was not taken into account in the kinetic analysis that follows.

Analysis of Kinetic Results

Dehydration of alcohol essentially resulted in olefin formation and was found to increase as a function of time factor as well as reaction temperature. Representative plots are given in *Fig. 2–4*.

Assuming alcohol dehydration to be first order with respect to the alcohol concentration, the reaction velocity constants could be computed using the following integrated rate expression:

$$k \cdot (W/F) = -\frac{RT}{P_T}[2 \ln(1-x) + x]. \qquad (1)$$

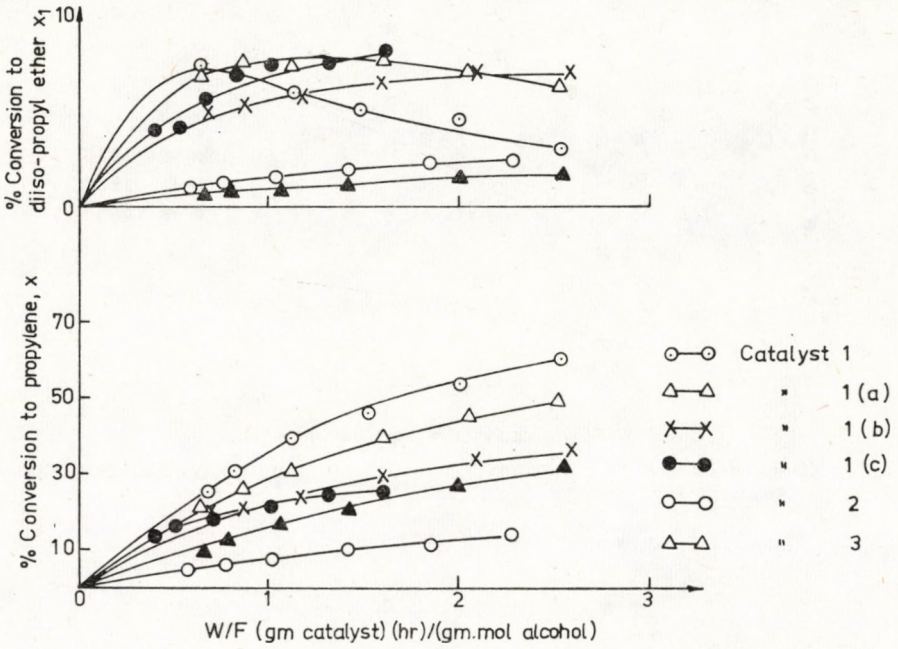

Fig. 2.
Effect of Time Factor on Conversion. Alcohol: *iso*-propanol, temperature 250 °C

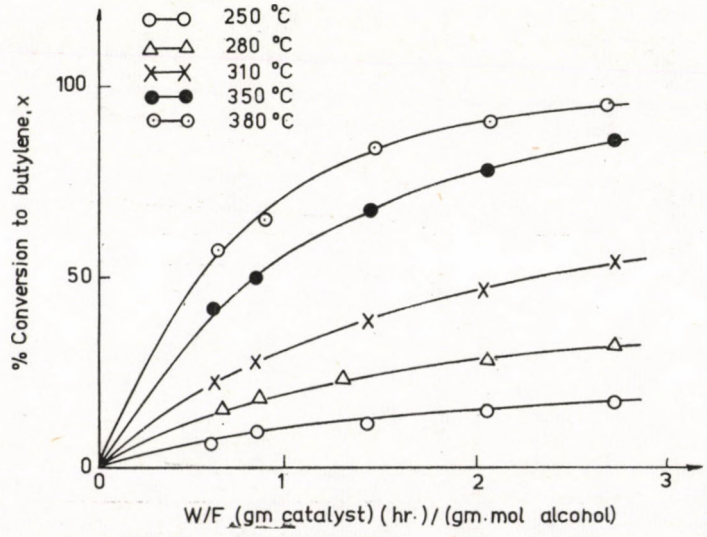

Fig. 3.
Effect of Time Factor on Conversion. Alcohol: *iso*-butanol, catalyst: Silica-Alumina

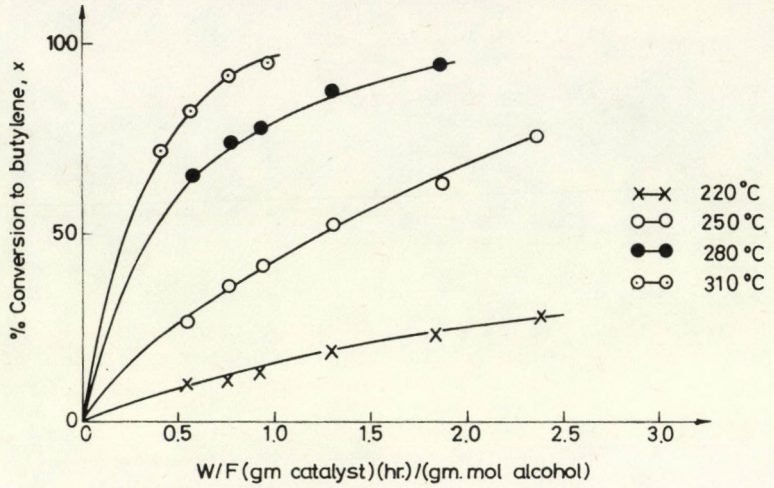

Fig. 4. Effect of Time Factor on Conversion. Alcohol: *s*-butanol, catalyst: 10×M.S.

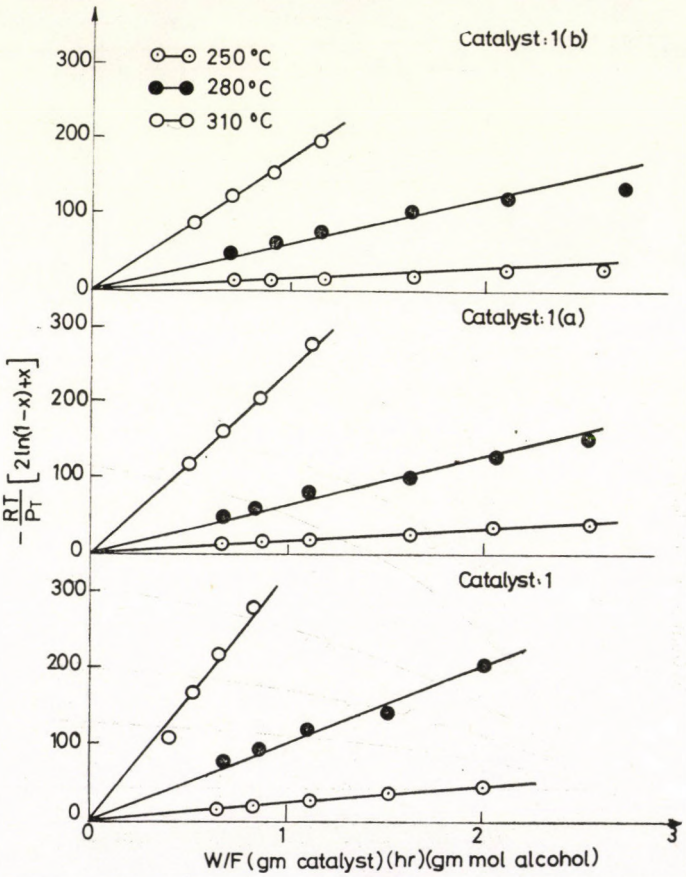

Fig. 5. Plot for First Order Rate Constant. Alcohol: *iso*-propanol

The validity of the above expression was checked by plotting (W/F) vs. the r.h.s. expression in Eq. (1). Straight line plots passing through the origin were obtained in all the cases. Representative plots are given in *Fig. 5* and *6*. Individual values of the reaction velocity constant calculated by linear regression analysis are reported in *Tables 2* and *3*. The correlation coefficient in all the cases was found to lie between 0.98–1.00, thereby showing that the linear relationship in Eq. (1) is statistically significant. The reaction velocity constants were related for the temperature effect by means of ARRHENIUS equation. The corresponding activation energies and pre-exponential factors determined by linear regression analysis are reported in *Tables 4* and *5*. The validity of Eq. (1) was checked by substituting the pertinent values and back calculating the values of x. Calculated and experimental values of conversion are found to be in good agreement. Representative plots are presented in *Fig. 7* and *8*.

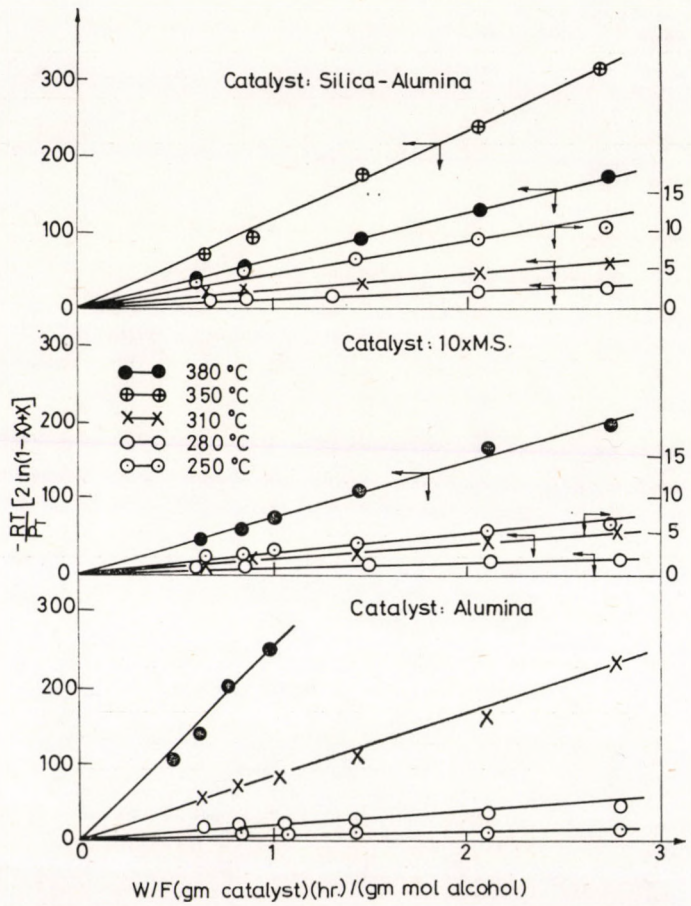

Fig. 6.
Plot for First Order Rate Constants. Alcohol: *iso*-butanol

Table 2.

Values of reaction velocity constant (k) for isopropanol

Catalyst	k(litres/hr.g. catalyst) Temperature °C			
	250	280	310	350
Catalyst 1	24.36	105.07	328.11	—
Catalyst 1(a)	17.24	63.93	243.41	—
Catalyst 1(b)	11.01	55.95	173.80	—
Catalyst 1(c)	11.79	78.77	267.16	—
Catalyst 2	8.65	32.30	69.02	179.26
Catalyst 3	8.52	31.55	73.91	166.54

Table 3.

Values of reaction velocity constants for butanols:

Alcohol	Catalyst	k(litres/hr.g-catalyst) Temperature, °C						
		220	250	280	310	350	380	410
n-butanol	1	—	—	—	149.01	376.66	—	—
n-butanol	2	—	—	—	8.51	44.61	82.29	123.47
n-butanol	3	—	—	—	7.31	24.27	44.07	77.73
iso-butanol	1	—	5.65	18.43	81.54	246.94	—	—
iso-butanol	2	—	2.61	6.82	20.43	74.83	—	—
iso-butanol	3	—	4.16	9.66	20.70	62.44	114.76	—
s-butanol	1	6.40	55.39	127.52	282.22	—	—	—
s-butanol	2	7.18	39.11	130.78	269.86	—	—	—
s-butanol	3	3.89	18.68	61.44	113.50	—	—	—
t-butanol	1	12.10	60.48	190.75	460.07	—	—	—
t-butanol	2	86.60	176.98	306.13	384.95	—	—	—
t-butanol	3	114.38	217.29	398.42	566.63	—	—	—

Table 4.

Values of activation energy (E) and frequency factor (A) for iso-propanol

Catalyst	A(litres/g.cat.hr.)	E(k.cal./g.mol)
Caralyst 1	2.43×10^{12}	26.30
Catalyst 1(a)	2.42×10^{12}	26.71
Catalyst 1(b)	5.45×10^{12}	27.94
Catalyst 1(c)	2.06×10^{14}	31.61
Catalyst 2	1.39×10^{11}	25.08
Catalyst 3	9.74×10^{8}	19.13

Table 5.

Values of activation energy (E) and Frequency factor (A) for butanols

Alcohol	E, K.cal./g.mole			A, litres/hr.g.cat.		
	Cat. 1	Cat. 2	Cat. 3	Cat. 1	Cat. 2	Cat. 3
n-butanol	24.94	21.29	18.65	8.29×10^{10}	9.84×10^{8}	7.61×10^{7}
iso-butanol	25.12	21.91	17.53	1.74×10^{11}	3.42×10^{9}	8.37×10^{7}
s-butanol	24.22	23.18	21.70	4.01×10^{11}	1.58×10^{11}	1.87×10^{10}
t-butanol	23.08	9.65	10.34	2.31×10^{11}	1.77×10^{6}	4.48×10^{6}

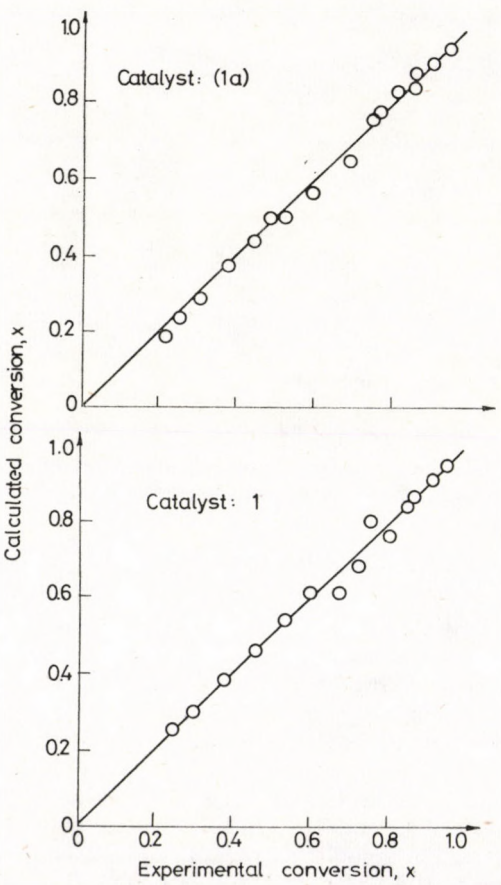

Fig. 7.
Plot of Experimental vs. Calculates Conversions. Alcohol: *iso*-propanol

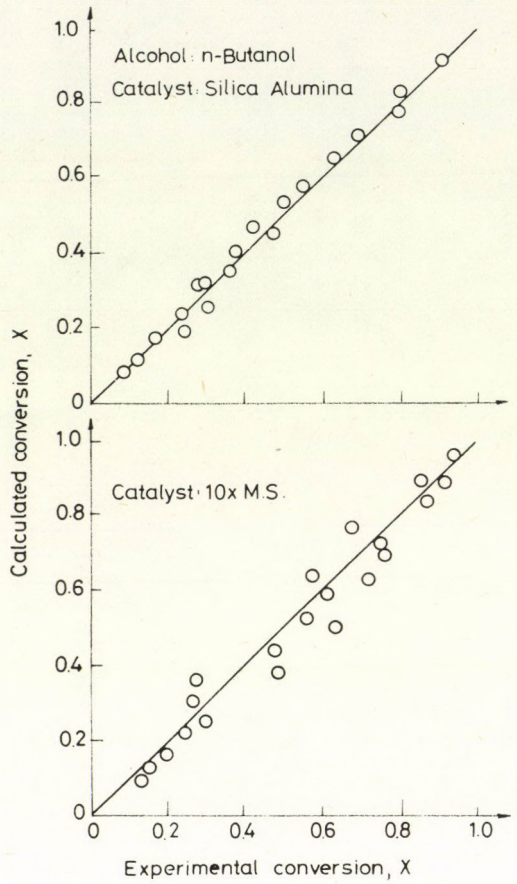

Fig. 8.
Plot of Experimental vs. Calculated Conversions. Alcohol: *n*-butanol

Discussion

In general, in investigations of this type involving a large number of reactants and catalysts, the effect of catalyst texture on reaction rate could be assessed by relating some kinetic parameter such as reaction velocity constant, reaction rate or activation energy with some intrinsic property of the catalyst, such as specific surface area, acidity or electrical conductivity. It is a common practice to identify activation energy for the reaction as an index of catalyst activity and a lower value as indicative of higher activity. However, a decrease in the value of the activation energy does not necessarily result in an increase in the value of the reaction velocity constant, since it is also frequently accompanied by a decrease in the value of the preexponential factor. Consequently, while assessing the effect of catalyst texture, the reaction velocity constants were taken as representativ of catalyst activity.

Effect of Catalyst Acidity

In the present investigation, acidity of the catalysts was measured at a pk_a values of +3.3. It was found that heat treatment reduces the specific surface area as well as the acidity of the catalyst (See *Table 1*, catalysts 1, 1a, 1b). The catalytic activity of the heat trated catalysts also followed a similar trend. Acidity of these catalysts when plotted against the reaction velocity constants in the case of iso-propanol *(Fig. 9)* showed a direct proportionality between the two.

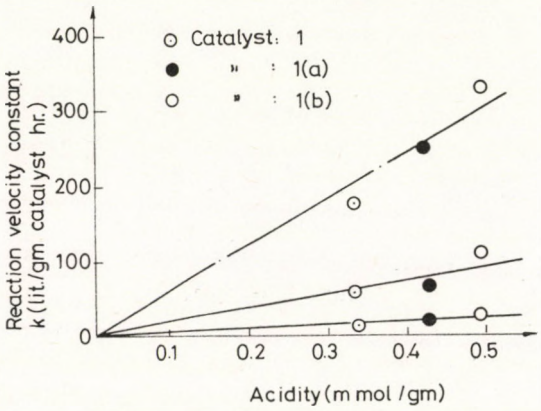

Fig. 9.
Effect of Acidity on Catalyst Activity for *iso*-Propanol Dehydration

Linear Free Energy Relationships (LFER)

A quatitative description of relationships between the structural parameters of solid catalysts on the one hand, and reaction rates on the other, are important in understanding the precise way in which catalysts function.

HAMMETT [30] found that the relative rate or equilibrium constants of meta- and para- substituted benzene derivatives for aromatic reactions can be empirically related by the following equation:

$$\log k_{\text{relative}} = \varrho\sigma \tag{2}$$

where ϱ is a proportionality factor characterising the reaction and σ is a constant characterising a substituent in the meta or para position. Values of ϱ have been derived from dissociation constants of substituted benzoic acid for which the value of ϱ was taken as unity. In the above equation, the reference compound is an unsubstituted benzene derivative i.e. $\sigma_H = 0$.

TAFT [31] proposed a similar equation for correlating the aliphatic reaction rates as follows:

$$\log k_{\text{relative}} = \varrho^+\sigma^+ \tag{3}$$

where ϱ^+ is a proportionality factor, and
σ^+ is a constant characterising a substitutent for aliphatic reactions.

In this equation the reference compound is a methylated derivative, i.e. $\sigma^+_{CH_3} = 0$.

Correlations between the substrate structure and its reactivity are qualitative or semiquantitative in the case of solid catalysts. In a recent review, KRAUS [32] reported some reactions for which the HAMMETT and TAFT equations were applicable. It was found that for the dehydration of ethanol, *n*-propanol, *n*-butanol, amylalcohol and hexanol on alumina at 380 °C, the TAFT equation was valid and the value of ϱ^+ to be -15.79. This value was on the higher side according to the authors themselves. Negative value of ϱ^+ indicates that the reaction proceeds by a carbonium ion or a highly polar mechanism. A high negative value of ϱ^+ is observed by a more polar transition state with a positive charge on the carbon atom. KIBBY and HALL [33] studied the structure reactivity relationships for alcohol elimination reactions over two well characterised hydroxy apatite catalysts and the rate constants for the dehydration of 15 acylic alcohols were correlated with TAFT equation for substitution at alpha carbon atom. KOCHLOEFL et al. [34] applied the TAFT equation for the dehydration of four secondary alcohols and the results were interpreted in terms of reaction mechanism and surface acidity.

In the present investigation, rate data collected on the dehydration of alcohols over the various catalysts were tested for the validity of the TAFT equation. The equation can be written as:

$$\log k/k_0 = \varrho^+ \sigma^+. \tag{4}$$

The reaction velocity constants are already reported in *Tables 2* and *3*. The sum of Taft σ^+ values for the alkyl groups at the alpha carbon, relative to $\sigma_\alpha^+ = 0.0$, for the three methyl groups based on *t*-butanol as the reference compound are evaluated. The relative rate constants are plotted against σ^+ in *Fig. 10* and *11*. Calculated values of ϱ^+ along with σ^+ and $\log(k/k_0)$ are reported in *Table 6*.

It was found that the TAFT equation is valid for the dehydration of all the alcohols over silica-alumina and 10×M.S. catalysts, except that in the later

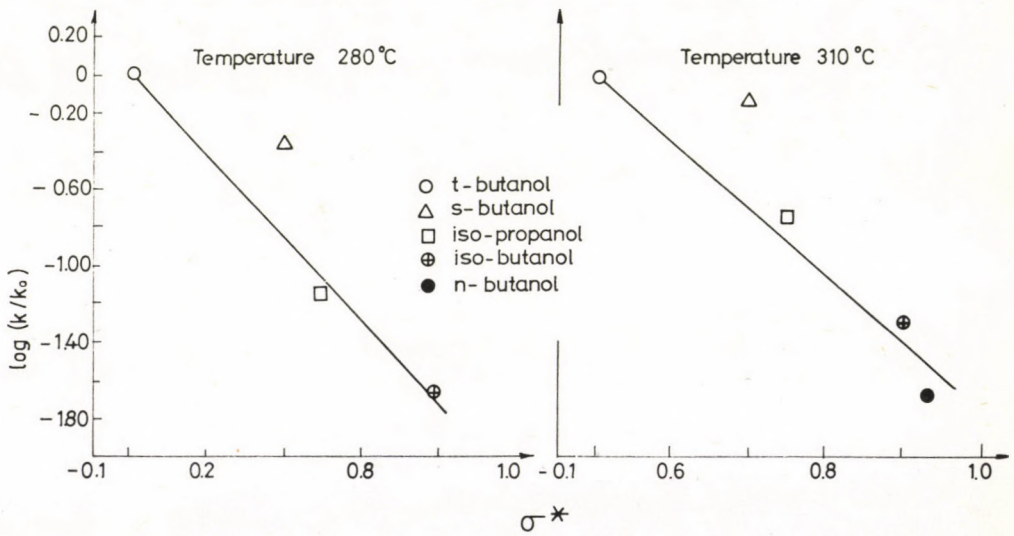

Fig. 10.
Variation of Alcohol Dehydration Rate with Taft σ^* Values. Catalyst: Silica-Alumina

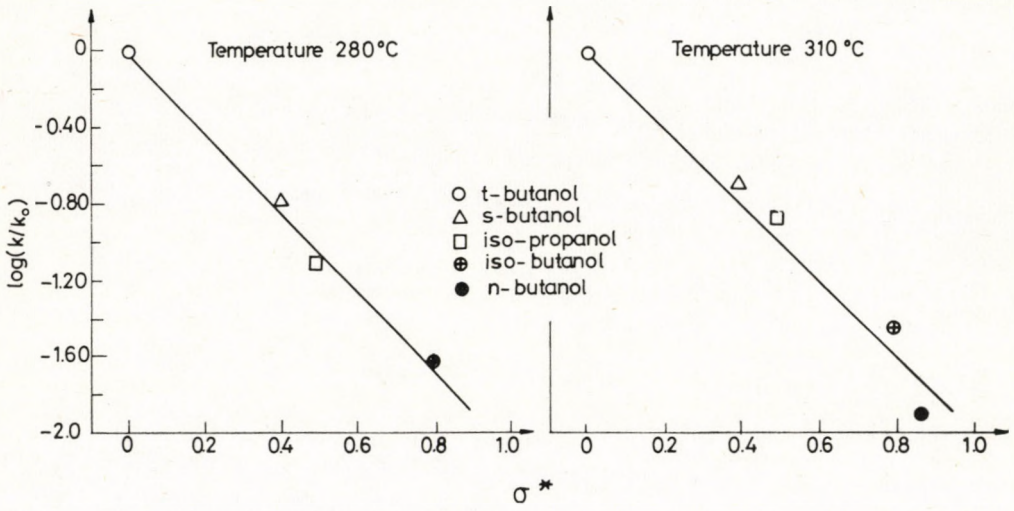

Fig. 11.
Variation of Alcohol Dehydration Rate with Taft σ^* Values. Catalyst: 10×M.S.

Table 6.
Effect of alpha-methyl substitution on dehydration of alcohols

Alcohol	σ^+	$\log k/k_0$	
		280 °C	310 °C
	Catalyst: Silica alumina		
n-butanol	0.86	—	− 1.89
iso-butanol	0.79	− 1.62	− 1.44
iso-propanol	0.49	− 1.10	− 0.88
s-butanol	0.39	− 0.81	− 0.70
t-butanol	0.00	0.0	0.0
ϱ^+	—	− 2.10	− 1.97
	Catalyst: 10×M.S.		
n-butanol	0.86	—	− 1.66
iso-butanol	0.79	− 1.65	− 1.28
iso-propanol	0.49	− 1.14	− 0.75
s-butanol	0.39	− 0.37	− 0.15
t-butanol	0.00	0.0	0.0
ϱ^+	—	− 2.12	− 1.74

case *s*-butanol falls away from the line. With an alumina catalyst no such correlation could be established. Values of ϱ^+ reported by various investigators for the dehydration of alcohols along with those obtained in the present investigation are reported in *Table 7*.

Table 7.

Values of ϱ^+ reported in literature for the dehydration of alcohols

Reference	Alcohol	Kinetic parameter used for correlation	Catalyst	Temp. °C	ϱ^+
33	15 alcohols	Rate constant k	Stoichiometric calcium hydroxy apatite	282	−2.3
				395	−2.5
			Non-stoichio-metric calcium hydroxy apatite	230	−5.1
				282	−4.5
				350	−3.9
34	4 secondary	Rate constant k	SiO_2	200	−2.8
			TiO_2	200	−0.8
32	6 primary alcohols	Reaction rate r	Alumina	380	−15.79
Present authors	*n*-butanol *iso*-butanol *iso*-propanol *s*-butanol *t*-butanol	Rate constant k	Silica-alumina	280	−2.10
				310	−1.97
			10×M.S.	280	−2.11
				310	−1.74

Stability of Carbonium Ions

It is now accepted that during dehydration, the alcohol molecule reacts with an acid centre (whether LEWIS or BRØNSTED) on the surface of the catalyst forming a carbonium ion. The stability of the carbonium ion is a measure of the reaction rate, provided that the same mechanism is operating throughout the catalyst. It was reported [35] that ionization potentials are a measure of the stability of the carbonium ions. The ionization potential, I, is designated as the energy required to remove an electron from a molecule or an atom as:

$$R \Rightarrow R^+ + e \quad \Delta H = I. \tag{5}$$

Table 8.

Effect of ionization potential on reaction rate

Alcohol	Ionization potential (k.cal./mol)	ln k(litres/hr.g.cat.)			
		280 °C		310 °C	
		Silica-alumina	10×M.S.	Silica-alumina	10×M.S.
n-butanol	199.24	—	—	1.99	2.14
iso-butanol	192.55	2.27	1.92	3.30	3.02
iso-propanol	182.17	3.45	3.10	4.30	5.23
s-butanol	182.87	4.12	4.87	4.73	5.60
t-butanol	171 10	5.99	5.72	6.34	5.95
Slope of the plot on ln k vs ionisation potential	—	−0.17	−0.18	−0.15	−0.13

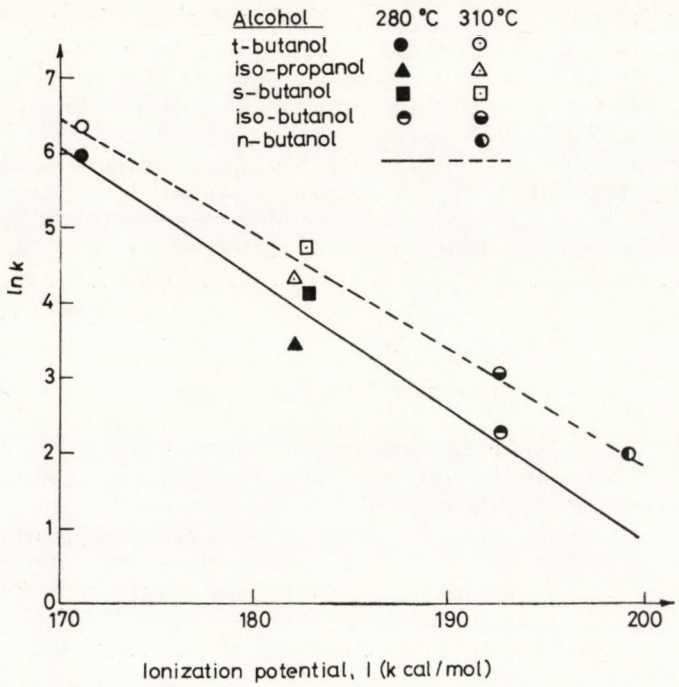

Fig. 12. Plot of Ionization Potencial vs. ln. *k*. Catalyst: Silica-alumina

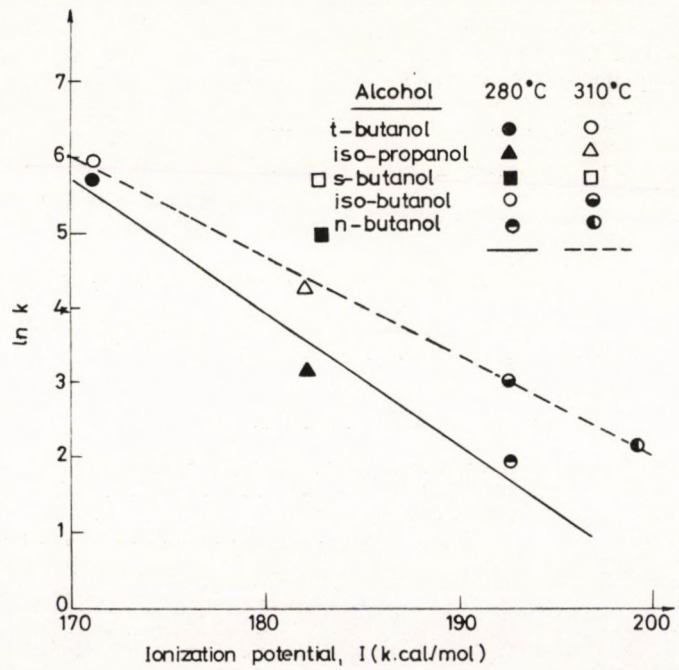

Fig. 13. Plot of Ionization Potencial vs. ln *k*. Catalyst: 10×M.S.

The ionization potentials of various alkyl radicals by electron impact method have been reported by LOSSING et al. [35] In the present investigation, the ionization potentials are plotted against ln k for the different alcohols in *Figs. 12* and *13* in the case of silica-alumina and 10×M.S. catalysts. The data are presented in *Table 8*.

With silica-alumina as well as 10×M.S. the reaction velocity constants are in good agreement with the ionization potentials, or, in other words, with the stabilities of the carbonium ions of the respective alcohols. Thus the higher the ionization potential, the lower the reactivity of the alcohol. These findings were similar to those found in the case of linear free energy relationships.

Summary and Conclusions

Dehydration of *iso*-propanol, *n*-butanol, *iso*-butanol, *s*-butanol and *t*-butanol over alumina, silica-alumina and molecular sieve catalysts suggests that acidity of the catalyst per unit surface has significant influence over the reaction rate. A direct proportionality between catalyst acidity and dehydration activity was observed. Rates of dehydration of the various alcohols were compared by linear free energy relationships and the stabilities of carbonium ions. The TAFT equation was found to be valid for the alcohols studied. The reaction velocity constants were correlated with the stabilities of carbonium ions.

SYMBOLS

A	frequency factor, litres/g. cat. hr.
C	constant in Eq. (2); litres/g. cat. hr.
E	activation energy; k.cal./mole.
I	ionisation potential, k.cal./mole.
k	reaction velocity constant, litres/g. cat. hr.
k_{relative}	dimensionless
m	constant Eq. (2); g.moles/k. cal.
P_T	total pressure, atm.
R	gas constant, appropriate units.
T	absolute temperature, K.
W/F	time factor, g. cat. hr./g.mole
ϱ	reaction parameter in HAMMETT equation for aromatic reactions
ϱ^+	reaction parameter for polar effects in TAFT equation
σ	substitutent parameter in HAMMETT equation for aromatic reactions
σ^+	polar substituent parameter in TAFT equation

REFERENCES

1. KNOZINGER, H. and KOHNE, R.: J. Catal., *1964*, 3, 559.
2. BUTT, J. R., BLISS, H. and WALKER, C. A.: A. I. Ch. E. J., *1962*, 8, 42.
3. TANABE, K. and WATNABE, Y.: J. Res. Inst. Catal., Hokkaido Uni., *1963*, 11, 65.
4. DE MOURGUES, L., PEYRON, F., TRAMBOUZE, Y. and PRETTRE, M.: J. Catal., *1967*, 7, 117.
5. KNOZINGER, H., BUHL, H. and RESS, E.: J. Catal. *1968*, 12, 121.
6. FIGUERAS ROCA, F., DE MOURGUES, L. and TRAMBOUZE, Y.: J. Catal. *1969*, 14, 107.
7. GOTTIFREDI, J. C., YERAMIAN, A. A. and CUNNINGHAM, R. E.: J. Catal. *1968*, 12, 345.
8. BUTLER, J. D., POLES, T. C. and WOOD, B. J.: J. Catal, *1970*, 16, 239.
9. DZISKO, V. P.: Proc. Int. Congr. Catal, 3rd (Amsterdam) I. 422, (1965).
10. ROY, N. C. and BOSE, N. K.: Indian Chem. Enggr., *1964*, 6, 36.

11. De Boer, J. H., Fahim, R. B., Linsin, B. G., Vessern, W. J. and De Viesschauwer. W. F. N. M.: J. Catal., *1967*, 7, 163.
12. Mezaki, R. and Butt, J. R.: Ind. Eng. Chem. Fundamentals, *1968*, 7(1), 120.
13. Solomon, H. J., Bliss, H. and Butt, J. R.: Ind. Eng. Chem. Fundamentals *1962*, 6, 325.
14. De Boer, J. H. and Vissern, W. J.: Catal. Rev., *1971*, 5, 55.
15. Fahim, H. B.: J. Appl. Chem., *1969*, 19, 356.
16. Aslop, B. P. and Dowden, D. A.: J. Chem. Phys., *1954*, 51, 678.
17. Garner, W. E.: Advn. Catal., *1957*, 9, 184.
18. Wolkenstein, Th.: Advn. Catal., *1960*, 12,189.
19. Whitmore, F. C.: J. A. C. S., *54*, 3274 (1932).
20. Ross, R. A. and Bennett, D. E. R.: J. Catal., *1967*, 8, 289.
21. Topchieva, K. V., Yun-Pin, K. and Smirnova, J. V.: Advn. Catal., *1957*, 9, 799.
22. Bremner, J. G. M.: Research (London), *1948*, 1, 281.
23. Dowden, D. A.: J. C. S., *1950*, 342.
24. Winsfield, M. E.: "Catalysis" (Ed. Emmett, P. H.) Vol. VII, p. 93, Reinhold Pub. Corpn., N.Y., 1960.
25. Noller, H. and Klading, W.: Catal Rev., *1976*, 13, 149.
26. Pines, H. and Haag, W. O.: J. A. C. S., *1960*, 82, 2471.
27. Ravindram, M. and Murthy, K. S.: J. Appl. Chem. Biotechnol. *1977*, 27, 181.
28. Yoshida, F., Ramaswami, D. and Hougen, D. A.: A. I. Ch. E. J., *1962*, 8, 5.
29. Miller, D. N. and Kirk, R. S.: A. I. Ch. E. J., *1962*, 8, 183.
30. Hammett, L. P.: "Physical Organic Chemistry", McGraw Hill, N.Y., 1940.
31. Taft, R. W. Jr.: J. A. C. S., *1952*, 74, 3120, *1953*, 75, 4231.
32. Kraus, M. S.: Advan. Catal., *1967*, 17, 75.
33. Kibby, C. L. and Hall, W. K.: J. Catal., *1973*, 29, 144.
34. Kochloefl, K., Kraus, M. and Bazant, V.: Proc. Int. congr. Catal., 4th Moscow, *1971*, 11, 490.
35. Bethell, D. and Gold, V.: "Carbonium ions: An introduction", p. 62 Academic Press, N.Y., 1967.
36. Lossing, F. P. and De Sousa, J. B.: J. A. C. S., *1969*, 81, 281.

РЕЗЮМЕ

Авторами изучено обезвоживание изопропанола, *n*-бутанола, изобутанола, *s*-бутанола, *t*-бутанола с помошью катализаторов на основе глинозема, силико-глинозема и молекулярных фильтров и установили, что удельная по поверхности кислотность катализаторов значительно влияет на скорость реакции. Установлена линейная зависимость между активностью дегидрационного прцесса и кислотностью катализатора. Скорость дегидрации исследованных алкоголев сопоставили линейными функциями свободной энергии ионов карбониумов и их стабильностью. Находили, что для исследованных алкоголев действительна функция Тафта. Установлена коррелационая связь между постоянными скоростей и стабильностью ионов карбониумов.

HUNGARIAN JOURNAL
OF INDUSTRIAL CHEMISTRY
VESZPRÉM
Vol. 9. pp. 365–384 (1981)

OPTIMIERUNG DER VERWERTUNG UNGARISCHER ROHBRAUNKOHLEN. I.

PROBLEMATIK WASSERVERLUSTFREIER PROBENAHME UNGARISCHER ROHBRAUNKOHLE VON HOCHEM WASSERGEHALT*

Z. Schultheisz, L. Pleva und L. Bartha
(Technische Universität für schemische Industrie Veszprém, Ungarn)

Eingegangen am 25. Juli, 1981.

Korrekte Qualitätsbestimmung ungarischer Rohbraunkohlen hochen Wassergehaltes ist durch große Wasserabgabefähigkeit beeinträchtigt. Es wird gezeigt, welche Fehlerquellen die automatische Probeentnahmevorrichtung aufweist und welche Verluste an Wasser während der Aufbereitung der Proben auftreten können. Zur quantitativen Beschreibung des Trocknungsprozesses der Rohbraunkohle wurde unter Ausnutzung der Analogie zwischen der Diffusion und Wärmeleitung eine mathematische Methode entwickelt, wodurch sich der unvermeidliche Verlust an Wasser während der Probeentnahme und der Aufbereitung bestimmen läßt.

Das Kraftwerk J. Gagarin bei Gyöngyösvisonta (Ungarn) verwendet etwa $6 \cdot 10^6 - 8 \cdot 10^6$ Jahrestonnen Rohbraunkohle (Wassergehalt 40—50%, Aschegehalt 15—25%, unterer Heizwert 6 500—8 500 kJ/kg) für Erzeugung elektrischer Energie mit einer Kapazität von 800 MW. Die aus Oberpannon (Pliozen) stammende und im Tagebau gewonnene Rohbraunkohle hat eine ziemlich große Wasserabgabefäigkeit so, daß ein meßbarer Verlust an Adhesionswasser schon am Förderband zu verzeichnen ist.

In diesem Fall handelt es sich um eine sehr große Fördermenge, deshalb ist die wasserverlustfreie Probenahme der Rohbraunkohle von großer Bedeutung. Eine Unsicherheit der Wassergehaltsbestimmung entspricht einer Menge von 60 000—80 000 Jahrestonnen Rohbraunkohle oder einem entsprechenden Verrechnungsfehler zwischen dem Berg- und Kraftwerk. Was die Wasserabgabefähigkeit andererseits betrifft, wäre es sehr wünschenswert die Rohbraunkohle vor Aufbereitung z. B. durch Zwischenlagerung austrocknen zu lassen und dadurch ökonomisch günstigere Betriebsführung zu erzielen.

* Diese Forschungsarbeit wurde im Auftrag des Berg- und Kraftwerks Visonta erarbeitet mit besonderer Rücksicht auf die vasserverlustfreie Probenahme der Rohbraunkohle.

Aufbereitung der Rohbraunkohle

Die Rohrbraunkohle gelangt aus dem 2—5 km fern liegenden Tagebau durch Förderbänder direkt ins Aufbereitungswerk *(Bild 1)*. Die Rohbraunkohle wird vermahlen, und dies bringt das öftere Festfahren der Schlagmühlen (SM-1, -2, -3) mit sich, falls die Lagerstätte minderwertig oder zu naß ist. Während der Behebung der Betriebsstörung wird der Abbau oder nur die Förderung unterbrochen. Zur Minderung der Betriebsstörung sind zwei Aufbereitungsstraßen ausgebaut.

Die Menge der Rohbraunkohle wird durch Förderbänderwaagen (FW-1, FW-2) laufend registriert. Aus dem Mahlgut entnimmt die automatische Probenahmevorrichtung (PNV) alle 3,5 Mimuten Proben, die in einer kleineren Schlagmühle (SM-4) weiter zerkleinert werden. Um die fortlaufende Probenahme auch beim Festfahren dieser Mühle sichern zu können, sind die automatischen Probenahmevorrichtungen mit Zwischenbehältern (ZB) ausgestattet.

Ein Becherwerk (BW) — bestehend aus 10 Bechern — entnimmt aus dem anfallendem Mahlgut mengenmäßig proportional verminderte Durchschnittsproben (*D*) (8 Becher) und Proben für die Wassergehaltsbestimmung (W) (2 Becher). Bei diesem Ausbau sollte das Verhältnis der Durschnitsprobe (*D*) zu Wassergehaltsprobe (W) der Relation 4:1 entsprechen. Diesbezügliche

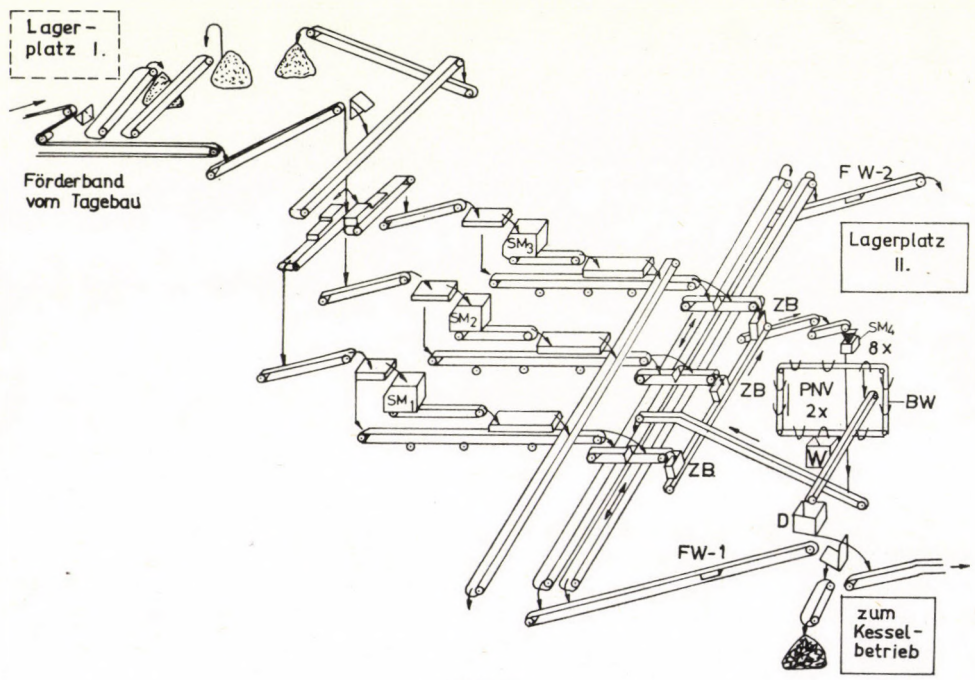

Bild 1.
Aufbereitung und Probenahme der Rohbraunkohle

Tabelle 1.

Betriebsdaten der autometischen Probenahmevorrichtung

Dauer der Probenahme Stunde	Menge der Probe, kg			Verrechnete Braunkohlemenge t	Unterer Heizwert kcal/kg	Wassergehalt %	Aschegehalt %	Gesamtprobe bezogen auf 100 t Rohbraunkohle kg	Probe f. WG
	für Wassergehaltsbestimmung	Durchschnittsprobe	insgesamt						Probe %
1	2	3	4	5	6	7	8	9	10
06—10	8,4	63,3	71,7	1 879	1 948	49,30	18,74	3,82	11,7
10—14	8,0	70,0	78,0	2 353	1 826	49,01	20,64	3,31	10,3
14—18	7,6	67,0	74,6	2 160	1 935	50,02	18,14	3,45	10,2
18—22	5,2	37,5	42,7	1 100	1 966	49,88	17,95	3,88	12,2
22—02	9,7	68,0	77,7	2 464	1 867	49,74	19,13	3,15	11,5
02—06	6,8	52,3	59,1	3 013	1 873	49,53	19,40	1,96	11,5
14—18	—	—	—	2 711	1 967	49,88	18,10	—	—
18—22	10,7	53,6	64,3	2 538	1 922	49,74	18,68	2,53	16,6
22—02	3,9	25,5	29,4	1 299	1 879	49,00	19,87	2,26	13,3
02—06	6,5	32,4	38,9	2 362	1 834	48,72	20,89	1,64	16,7
06—10	7,4	41,9	49,3	2 465	1 857	49,21	20,07	2,00	15,0
10—14	8,0	45,0	53,0	2 671	1 791	47,92	22,54	1,98	15,1
14—18	7,2	40,0	47,2	2 696	1 810	48 42	21,99	1,75	15,2
18—22	5,5	29,6	35,1	3 352	1 845	48 42	20 73	1,05	15,7
22—02	9,4	54,4	63,8	3 201	1 833	48,50	21,19	1,99	14,7
02—06	9,0	55,0	64,0	3 140	1 802	48,50	21,52	2,04	14,1
06—10	7,0	32,5	39,5	2 545	1 834	49,09	19,62	1,55	11,8
10—14	—	—	—	1 710	1 967	49,08	18,48	—	—
14—18	—	—	—	2 169	1 910	47,51	20,97	—	—
18—22	4,8	22,5	27,3	1 681	1 874	48,10	20,79	1,62	17,6
22—02	4,2	23,6	27,8	1 834	1 735	45,91	25,15	1,51	15,1
02—06	5,1	25,0	30,1	2 647	1 834	47,52	22,02	1,14	16,9
06—10	8,6	40,2	48,8	2 416	1 946	49,24	18,74	2,02	17,6
10—14	4,8	19,0	23,8	1 581	2 023	48.71	18,03	1,50	20,2
14—18	8,8	49,5	58,3	1 781	1 876	48,13	29,87	3,27	15,1
18—22	3,7	17,5	21,2	2 980	1 702	47,32	23,31	0,71	17,4
22—02	5,2	32,9	38,1	2 523	1 855	49,22	20,31	1,51	13,6
02—06	3,9	25,3	29,3	1 933	1 742	47,56	23,55	1,51	13,3

Meßergebnisse sind in der *Tabelle 1* zusammengestellt. Die Dauer der Probenahme beträgt etwa 4 Stunden.

Die Spalten 9 und 10 der *Tabelle 1* zeigen, daß die auf 100 t Rohbraunkohle entfallende Menge der Gesamtprobe (D) sich von 0,71 bis 3,88 kg ändert, während die für die Wasserbestimmung gesammelter Probe (W) 10,2—20,2% der Gesamtprobe beträgt.

Die Prüfung der Ursachen dieser Streuung lieferte folgende Resultate.

Die in die Probenahmevorrichtung eingebaute Schlagmühle (SM-4) ist gegenüber den Schwankungen der Qualität besonders den des Wassergehaltes der Rohbraunkohle empfindlich. Übersteigt der Wassergehalt der geförderten

Rohbraunkohle einen kritischen Wert, so fährt sich die Mühle fest. Während der Reinigung der Mühle ist die Aufarbeitung der Probe unterbrochen, die Probenahme wird aber fortgesetzt. Falls die Zwichsenbehälter (ZB) während der Behebung der Betriebsstörung vollgefüllt werden, so sollten im Prinzip sowohl die Probenahme als auch die Förderung abgestellt werden. Dies bedeutet Produktionsausfall, deshalb ist man gezwungen auch während der Betriebsstörung weiter zu fördern, und dies führt zur Verschiebung der obengenannten Mengenverhältnisse.

Diese Fehlermöglichkeit könnte durch Einbau einer zweiten Schlagmühle beseitigt werden. Das Problem konnte noch besser durch den Bau des zwischen dem Tagebau und Aufbereitungswerk liegenden Zwischenlagerplatzes (Lagerplatz I) gelöst werden, wo die auch für die Verstopfung der großen Schlagmühlen verantwortliche Rohbraunkohle hochen Wassergehaltes durch Liegenlassan vorgetrocknet werden sollte.

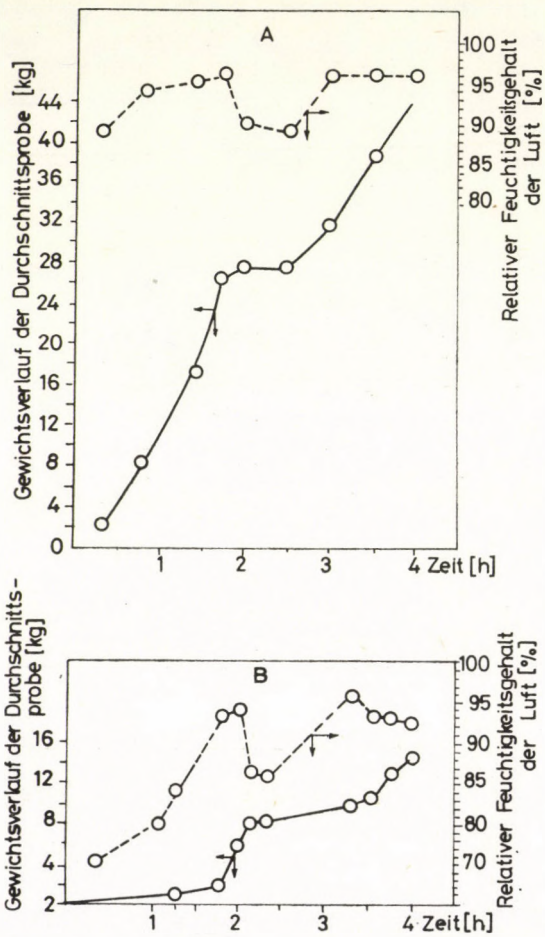

Bild 2.
Anhäfung der Rohbraunkohle in der Probenahmevorrichtung

Weiterhin untersuchten wir die Materialanhäufung im Durchschnittsprobebehälter (*D*), und machten die Beobachtung, daß zwischen Anhäufungsgeschwindigkeit und relativer Luftfeuchtigkeit enge Korrelation nachzuweisen ist. Bei einer relativen Luftfeuchtigkeit von 60% im Aufbereitungswerk und bei großer Materialanhäufungsgeschwindigkeit steigt die Luftfeuchtigkeit im Durchschnittsprobebehälter rasch bis auf 95% zu *(Bild 2/A)*, nimmt bei Betriebsstörung steil ab, und steigt wieder nach der Behebung der Betriebsstörung. Bei kleiner Anhäufungsgeschwindigkeit *(Bild 2/B)* ist der Fall ähnlich, nur die Luftfeuchtigkeit im Behälter nimmt langsamer zu, nimmt aber ebenso rasch bei Betriebsstörung ab, wie im ersten Fall.

Die obengeschilderten Beobachtungen sprechen dafür, daß in der Braunkohleprobe ein schneller Trocknungsprozeß stattfindet. Die Trocknung ist in erster Linie in der obersten mit der Luft in Berührung stehenden Schicht des Braunkohlehaufens beträchtlich. Das Maß der Trocknung ist im Falle einer Betriebsstörung das größte, deshalb ist eine betriebsstörungsfreie Materialanhäufung eine Vorbedingung für die einwandfreie Probenahme.

Das stark feuchte Mikroklima wirkt entgegen der Trocknung, deshalb ist es zweckmäßig, eine Materialanhäufungsgesschwindigkeit zu wählen, die im Probebehälter eine Luftfeuchtigkeit um 90% sichert.

Tabelle 2.

Vergleich der Wassergehaltsbestimmungen

Momentprobe			4 stündige Durchschnittsprobe		
Nr.	Wassergehalt	Durchschnittlicher Wassergehalt	Nr.	Wassergehalt	Abweichung am Wassergehalt
	%			%	
1	48,34 49,41 51,40 50,30 51,51 51,94 52,62 48,98	50,56	1	50,18	+0,38
2	51,46 52,13 52,52	52,03	2	51,38	+0,65
3	52,75 50,47 51,44	51,61	3	48,81	+1,80
4	49,15 50,62 50,41 49,19	49,84	4	49,04	+0,80

Zur Ermittlung des vermutbaren Wasserverlustes während der Probenahme haben wir die Wassergehaltswerte von Momentproben und Durschnittsproben für gleichen Zeitraum verglichen *(Tabelle 2)*. Der durchschnittliche Wassergehalt der Momentproben liegt um 0,38—1,80% höher als der der Durchschnittsproben.

Wasserverlust durch Lagerung

a) *Im geschlossenen Zustand*

Die Rohbraunkohle gibt auch in dichter Verpackung bei Lagerung Wasser ab, das auf die Innenseite des Behälters oder der Plastiktüte ausscheidet. Zur Bestimmung der durch Lagerung abgegebenen Wassermenge wurden 24

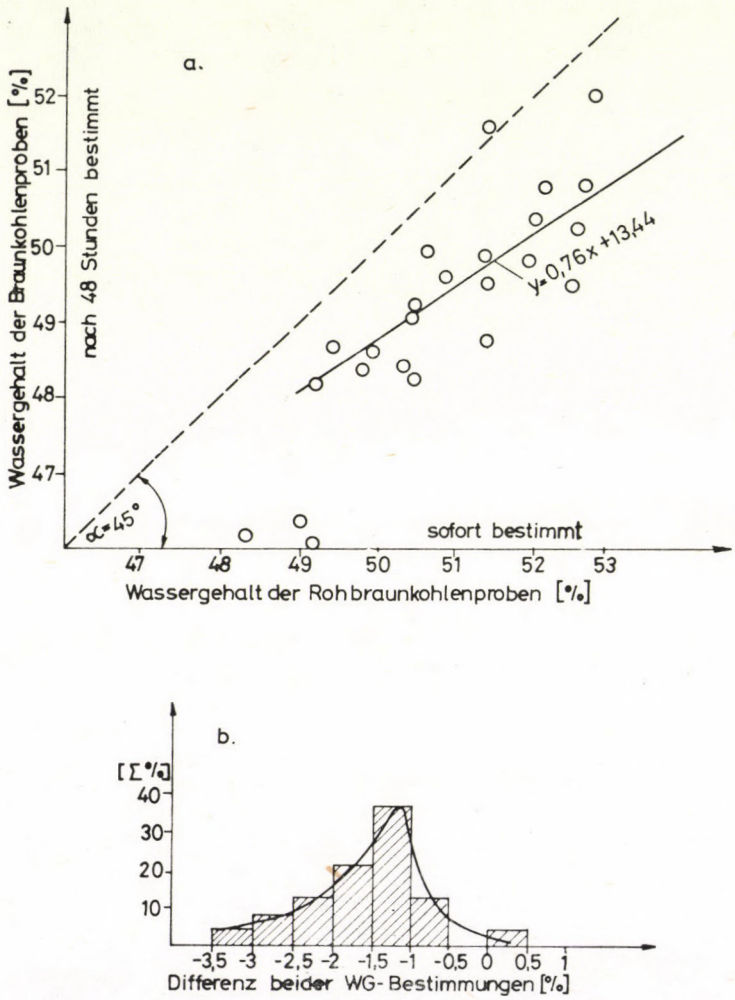

Bild 3.
Einfluß der Lagerung auf den Wassergehalt der Rohbraunkohle

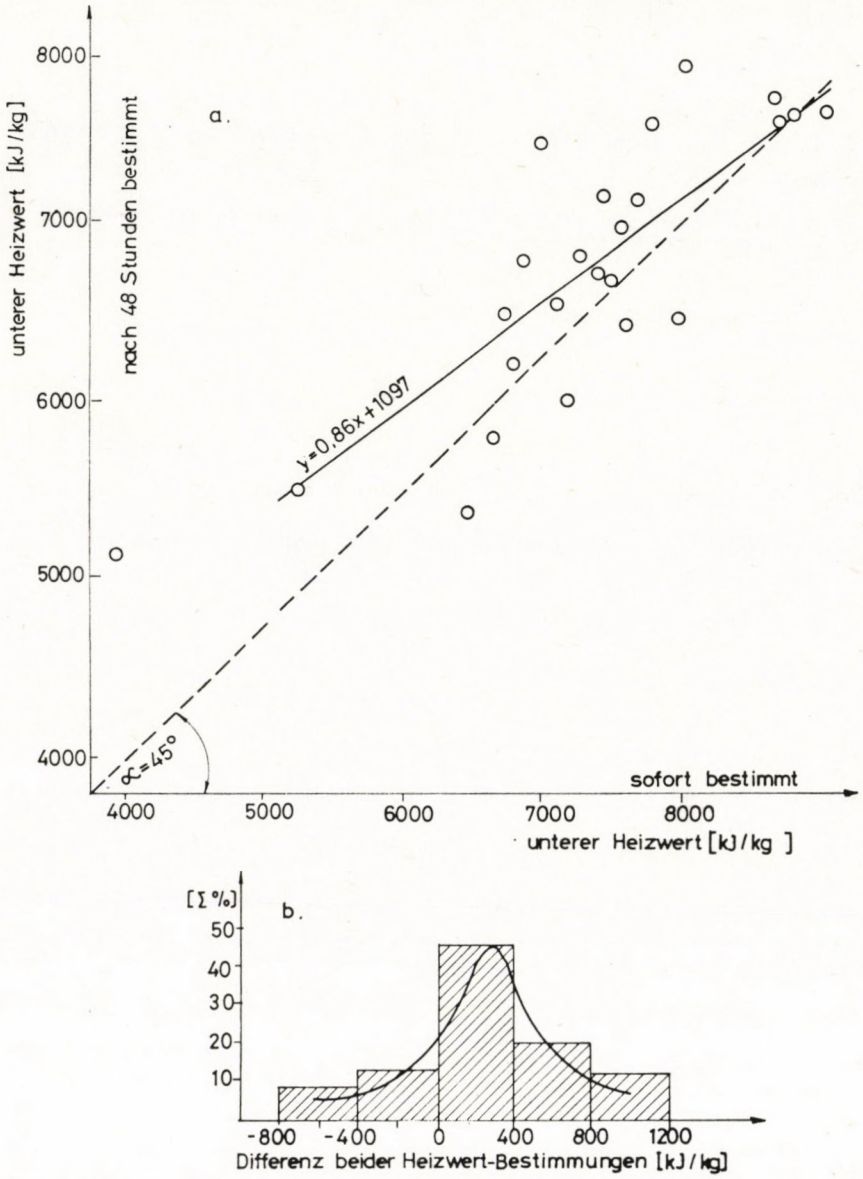

Bild 4.
Einfluß der Lagerung auf den unteren Heizwert der Rohbraunkohle

Momentproben gezogen und einmal sofort, dann nach 48 Stunden Lagerung auf Wassergehalt und Heizwert untersucht *(Bild 3—4)*.

Ohne Wasserverlust sollten die Wassergehaltswerte im Bild 3/A etwa simmetrisch zu Gerade

$$y = ax + b$$

$$a = \operatorname{tg} \alpha, \qquad \alpha = 45°, \qquad a = 1, \qquad b = 0 \tag{1}$$

liegen. Die Punkte streuen aber auf die rechte Seite obiger Gerade, und die stochastisch errechnete Gleichung lautet:

$$y = 0{,}76x + 13{,}44. \tag{2}$$

Aus den Differenzen beider Wassergehaltsbestimmungen liegt der Wasserverlust während der geprüften Lagerungszeit mit größter Wahrscheinlichkeit höher als 1,5%.

Aufgrund der Heizwertsbestimmung gelangt man zu ähnlichem Bild, das zeigt, durch Wasserabgabe nimmt der untere Heizwert scheinbar um etwa 330 kJ/kg (80 kcal/kg) zu *(Bild 4)*.

b) *Im offenen Zustand*

Die Wasserabgabe eines Rohbraunkohlehaufens hängt bei konstanten Umständen (Temperatur, Luftfeuchtigkeit und -strömung) und bei gleichen Materialeigenschaften von der freien Oberfläche bzw. von der Flächenbedeckung ab.

Zur Prüfung der Trocknungsbedingungen der Rohbraunkohle wurden auf Schalen einer Fläche von 1/16 m² (625 cm²) Probemengen aufgetragen, die einer Flächenbedeckung 0,1—1,3 g/cm² enstprechen. Die Ergebnisse zeigen *(Bild 5)*, die obere Schicht des Haufens wird ziemlich schnell bis zum Gleich-

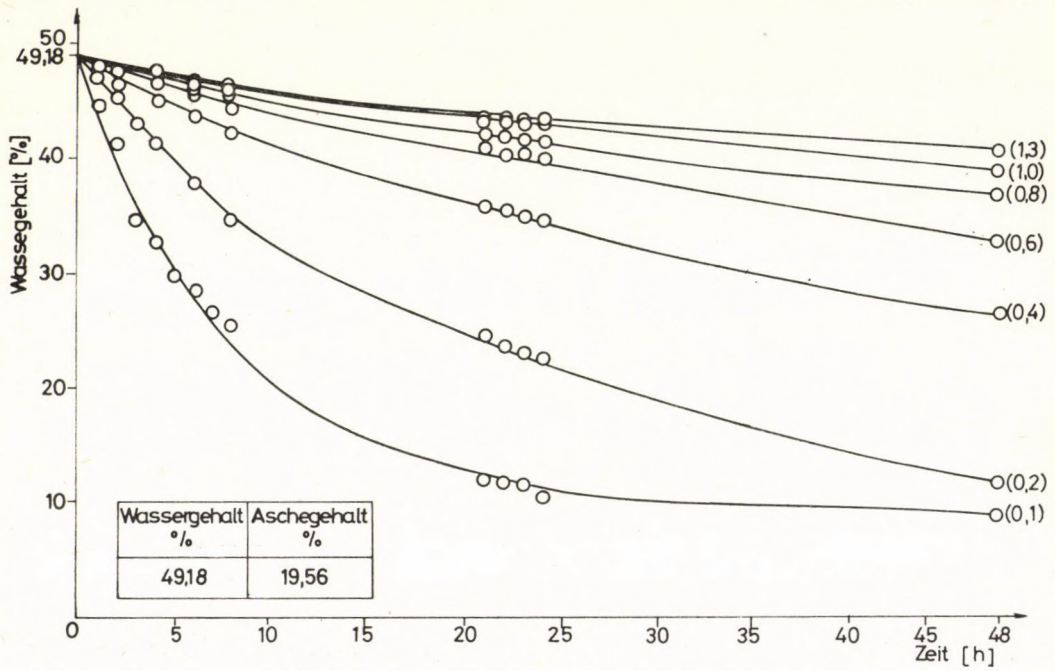

Bild 5.
Trocknungsverlauf der Rohbraunkohle in Abhängigkeit der Flächenbedeckung

gewichtswassergehalt austrocknen. Das ist der Fall im Probenamesammler, wo sich die freie Oberfläche ständig erneuert. Die Trocknung dickerer Schichte verläuft aber von einer Flächenbedeckung von etwa 0,8—1,0 g/cm² an praktisch linear.

Quantitative Beschreibung des Wasserverlustes der Rohbraunkohle

Anhand der Meßergebnisse versuchten wir den Trocknungsprozeß der Rohbraunkohleproben mit hinreichender Genauigkeit mathematisch zu beschreiben. Dazu nützten wir die zwischen der Diffusion und Wärmeleitung bestehende Analogie aus *(Bild 6)*. Die auf den Probenahmeschalen ausgebreitete Rohbraunkohle gibt ihren Wassergehalt an die sie umgebende Luft ab.

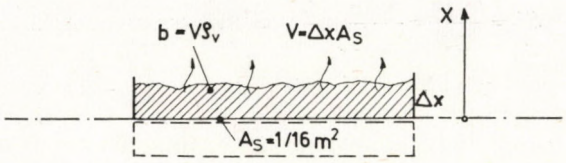

Bild 6.
Schalenmodell

Die Differentialgleichung der instationären Diffusion lautet:

$$-\operatorname{div}[D_w \operatorname{grad} c] + \omega\beta\Delta C = -\frac{\partial c}{\partial \tau} \quad \frac{\text{kg}}{\text{h}\cdot\text{m}^3} \tag{3}$$

Die Wasserabgabe eines Braunkohlehaufens ist als ein instationärer Diffusionsprozeß analog zur Wärmeabgabe einer sich abkühlenden Masse *(Bild 7)*.

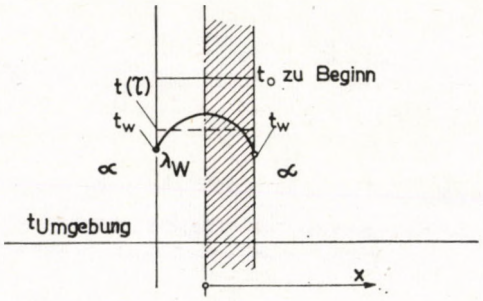

Bild 7.
Örtlicher Konzentrationsverlauf als Analogon eines örtlichen Temperaturverlaufes

Weil die Gesamtoberfläche (A) der Kohlenkörner unbekannt ist

$$A = V\cdot\omega = \Delta x\cdot A_S\cdot\omega \quad \text{m}^2 \tag{4}$$

scheint es für zweckmäßig zur Ersetzung der spezifischen Einwaage (E/A_S) und der Schichthöhe (Δx)

$$\frac{E}{A_S} = \Delta x\cdot\varrho_v = \Delta x^* \quad \text{kg/m}^2 \tag{5}$$

im Betracht der Dimensionsfreiheit der FICKschen Zahl vorläufig einen neuen

Diffusionskoeffizienten einzuführen:

$$D_w^* = D_w \cdot \varrho_w^2 \quad \text{kg}^2/\text{m}^4 \cdot \text{h} \tag{6}$$

So läßt sich schreiben

$$Fi = \frac{D_w \cdot \Delta\tau}{\Delta x^2} = \frac{D_w^* \cdot \Delta\tau}{\Delta x^{*2}} \quad \text{FICKsche Zahl} \tag{7}$$

und

$$Sh = \frac{\beta \cdot \Delta x}{D_w} = \frac{\varrho_v \cdot \beta \cdot \Delta x^*}{D_w^*} \quad \text{SCHERWOODsche Zahl} \tag{8}$$

Da für uns die erste mit einem Wasserverlust von 1—2% verbundene Periode der Trocknung maßgebend war, und es uns mehr auf die Ausarbeitung einer für die Praxis brauchbare Berechnungsmethode, und nicht auf eine vollständige Analyse ankam, haben wir die Korngrößeninhomogenitäten vernachläßigt.

Die Lösung des Problems liefert die Ermittlung der Funktion

$$\Psi' = \varphi_1(Sh,\ Fi) \tag{9}$$

Die erwähnte Analogie ermöglichte die Verwendung der für die Wärmeleitung gültigen Gleichung

$$\Psi = \varphi(Bi,\ Fo) \tag{10}$$

und die Benutzung des Diagrames 5 des VDI-Wärmeatlas' (1956. Ed. 3).

Die Formelzeichnen des abgewandelten Diagrammes von *Bild 8:* sind in der Verzeichnisliste zusammengefaßt.

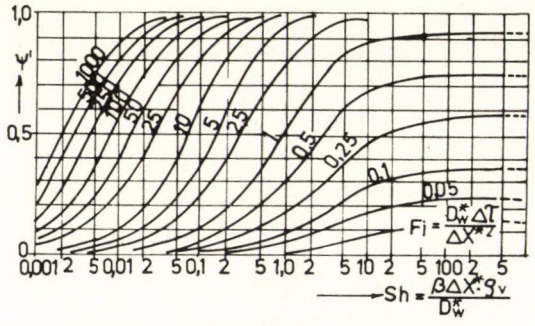

Bild 8.
Reduzierte Feuchtigkeit als Funktion von *Sh* und *Fi*

Als Einheit wurde eine Einwaage von 62,5 g gewählt, das heißt:

$$\Delta x^* = 1 = \frac{62{,}5}{1/16} \simeq 1000 \text{ g/m}^2 = 1 \text{ kg/m}^2. \tag{11}$$

Um das Diagramm graphoanalytisch benutzen zu können, konstruierten wir dazu ein verschiebbares Hilfsdiagramm auf Transparentpapier und von gleicher Größe *(Bild 9).*

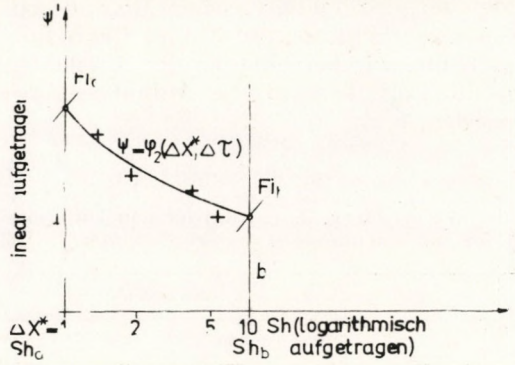

Bild 9.
Verschiebbares Hilfsdiagramm zur Bestimmung von Sh_a und Fi_a

Aus den Meßergebnissen *(Tabelle 3)* läßt sich die Funktion

$$\Psi' = \varphi_2(\Delta x^*, \Delta\tau) \tag{12}$$

ermitteln.

Parameter	Bedingungen
P	B
$\cdot Sh$	$\cdot \Psi' = \varphi_1(Sh, Fi)$ *(Bild 8)*
$\cdot Fi$	$\cdot \Psi' = \varphi_2(\Delta x^*, \Delta\tau)$ *(Bild 9)*
$\cdot Fi_a$	$\cdot \Psi' = \dfrac{\Delta G_{\Delta\tau}}{\Delta G_{48}}$
$\cdot Fi_b$	$\cdot \left[\dfrac{Sh_b}{Sh_a}\right]^2 = \dfrac{Fi_a}{Fi_b}$
$\cdot Sh_a$	$\cdot \left[\begin{array}{l} Fi_a = D_w^* \Delta\tau \\ Sh_a = \dfrac{\varrho_v \beta}{D_w^*} \\ \text{falls } \Delta x^* = 1 \end{array}\right.$
$\cdot Sh_b$	
$\cdot \varrho_v \beta$	
$\cdot D_w^*$	$\cdot Sh = \dfrac{\Delta x^* \cdot \varrho_v \cdot \beta}{D_w}$
$\cdot \Delta\tau$	$\cdot \Delta G_{\Delta\tau} = \varphi_3(\Delta\tau)$ (Aus Meßdaten der *Tab. 3*)
$\cdot \Delta x^*$	$\cdot Fi = \dfrac{D_w^* \Delta\tau}{\Delta x^{*2}}$
$\cdot \Delta G_{\Delta\tau}$	$\cdot \dfrac{Sh_b}{Sh_a} = 10$ (in unserem Fall)
$\cdot \Psi'$	
$P = 12$	$B = 11$

Definitionsgemäß: $F = P - B = 1$.

Um die Rechtigkeit der graphoanalytischen Methode zu beweisen, verwendeten wir den zwischen den Parametern P und Bedingungen B bestehenden Zusammenhang, das heißt, wir berechneten den Freiheitsgrad F.

Durch Festlegung der Zeit $\Delta\tau$ wird die Aufgabe bestimmt, $\varrho_v \cdot \beta$ und D_w können berechnet werden.

Tabelle 3.

Berechnung des Wertes für $\varrho_v \cdot \beta$ und des für den Diffusionskoeffizienten D_w^* der Rohbraunkohle (Durchschnittsprobe Nr. 131)

$\Delta G_{\Delta\tau} = \varphi_3(\Delta\tau)$	Einwaage, g					
	62,5	125	250	375	500	625
Δx^*	1	2	4	6	8	10
ΔG_4 $\Delta\tau = 4$ h	10,8	10,2	11,2	10,2	11,8	12,3
ΔG_8 $\Delta\tau = 8$ h	16,5	17,5	18,7	17,6	18,7	20,5
ΔG_{24} $\Delta\tau = 24$ h	24,2	39,4	39,5	35,0	37,6	43,5
ΔG_{48}	25,1	49,8	69,6	57,1	56,5	73,7
$\Psi'_1 = \Delta G_4 / \Delta G_{48}$	0,430	0,208	0,160	0,178	0,208	0,167
$\Psi'_2 = \Delta G_8 / \Delta G_{48}$	0,657	0,358	0,268	0,308	0,330	0,278
$\Psi'_3 = \Delta G_{24} / \Delta G_{48}$	0,964	0,805	0,568	0,613	0,665	0,590

$$\text{Wird die Bedingung } \left[\frac{Sh_b}{Sh_a}\right] = \frac{Fi_a}{Fi_b} \tag{13}$$

erfüllt, so kann anhand der Meßergebnisse von *Tabelle 3* für den Fall $\Delta\tau = 4$ h die Funktion

$$\Psi'_1 = \frac{\Delta G_4}{\Delta G_{48}} = \varphi_2(\Delta x^*, \Delta\tau) \tag{14}$$

im $\psi' = \varphi_1$ *(Sh, Fi)* Feld dargestellt werden *(Bild 10)*.

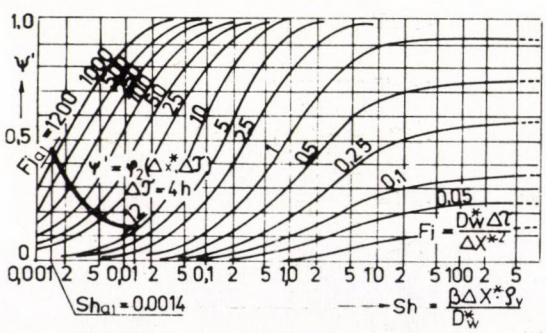

Bild 10.
Die Erfüllung der Bedingung (13)

Mit Hilfe einer vorgegebenen Zeit $\Delta\tau$ und $\Delta x^* = 1$

$$D_w^* = \frac{Fi_a}{\Delta\tau} \text{ und} \tag{15}$$

$$\varrho_v \cdot \beta = Sh_a \cdot D_w^* \tag{16}$$

Unter Zuhilfenahme der Meßdaten von *Tabelle 3:*

$$Fi_{a_1} = 1200 \qquad D_{w_1}^* = \frac{1200}{4} = 300 \text{ kg}^2/\text{m}^4 \cdot \text{h}$$

$$Fi_{a_2} = 1200 \qquad D_{w_2}^* = \frac{1200}{8} = 150 \text{ kg}^2/\text{m}^4 \cdot \text{h}$$

Tabelle 4.

Die $\varrho_v \cdot \beta$-Werte von Rohbraunkohleproben bei Zugrundelegung einer Trocknungszeit von 48 und 72 Stunden

Probe			
Nummer	Trocknungszeit	Korngröße	
		gemahlen	stückig
		$\varrho_v \cdot \beta$	
140	24/48	0,365	0,350
140	8/48	0,376	0,328
140	4/48	0,437	0,280
138	24/48		0,396
138	8/48		0,375
138	4/48		0,375
132	24/48		0,388
132	8/48		0,403
132	4/48		0,330
131	24/48		0,469
131	8/48		0,405
131	4/48		0,420
141	24/48		0,364
141	8/48		0,450
141	4/48		0,375
142	24/48		0,416
142	8/48		0,438
142	4/48		0,438
143	24/48		0,469
143	8/48		0,400
143	4/48		0,375
Durchschnitt		0,393	0,392

Probe		
Nummer	Trocknungszeit	Korngröße
		stückig
		$\varrho_v \cdot \beta$
140	24/72	0,208
140	8/72	0,175
140	4/72	0,200
138	24/72	0,209
138	8/72	0,156
138	4/72	0,207
132	24/72	0,182
132	8/72	0,219
132	4/72	0,275
Durchschnitt		0,203

$$Fi_{a_3} = 250 \qquad D^*_{w_3} = \frac{250}{24} = 10{,}4 \text{ kg}^2/\text{m}^4\cdot\text{h}$$

$$Sh_{a_1} = 0{,}0014 \qquad \varrho_v \cdot \beta_1 = 0{,}0014 \cdot 300 = 0{,}420 \text{ kg/m}^2\cdot\text{h}$$

$$Sh_{a_2} = 0{,}0027 \qquad \varrho_v \cdot \beta_2 = 0{,}0027 \cdot 150 = 0{,}405 \text{ kg/m}^2\cdot\text{h}$$

$$Sh_{a_3} = 0{,}0045 \qquad \varrho_v \cdot \beta_3 = 0{,}0045 \cdot 10{,}4 = 0{,}469 \text{ kg/m}^2\cdot\text{h}$$

Der Diffusionskoeffizient D^*_w nimmt mit dem Fortschreiten der Trocknung stark ab *(Tabelle 5)*, während $\varrho_v \cdot \beta$ praktisch konstant bleibt *(Tabelle 4)*.

Tabelle 5.

Berechnung des Wertes für $1-\Psi'$ und des für den Diffusionskoeffizienten D_w bei Zungrundelegung einer Trocknungszeit von 48 Stunden, zwischen den Grenzen $\Delta x^* = 1$ und $\Delta x^* = 10$

Nummer der Probe	$\psi' = \frac{\Delta G_{\Delta\tau}}{\Delta G_{48}}$	$1-\psi'$				D^*_w
		$\Delta x^*=1$	$\Delta x^*=2$	$\Delta x^*=4$	$\Delta x^*=10$	
131 stückig	24/48	0,036	0,195	0,432	0,410	10,4
	8/48	0,343	0,642	0,732	0,722	150
	4/48	0,570	0,792	0,840	0,833	300
132 stückig	24/48	0,098	0,282	0,382	0,409	31,2
	8/48	0,427	0,640	0,705	0,705	175
	4/48	0,655	0,804	0,854	0,835	250
138 stückig	24/48	0,044	0,307	0,298	0,447	20,8
	8/48	0,396	0,636	0,672	0,719	125
	4/48	0,648	0,806	0,823	0,850	250
140 stückig	24/48	0,185	0,403	0,362	0,426	83,5
	8/48	0,536	0,720	0,704	0,781	219
	4/48	0,716	0,846	0,831	0,888	350
140 gemahlen	24/48	0,201	0,248	0,381	0,380	41,6
	8/48	0,417	0,619	0,696	0,706	188
	4/48	0,690	0,817	0,842	0,847	437
141 gemahlen	24/48	0,040	0,276	0,380	0,406	10,4
	8/48	0,417	0,619	0,704	0,710	225
	4/48	0,651	0,790	0,824	0,837	300
142 gemahlen	24/48	0,048	0,265	0,373	0,385	20,8
	8/48	0,400	0,620	0,710	0,669	219
	4/48	0,652	0,801	0,841	0,831	438
143 gemahlen	24/48	0,048	0,261	0,362	0,383	10,4
	8/48	0,393	0,323	0,675	0,698	125
	4/48	0,663	0,806	0,826	0,837	375

Mit Hilfe der Meßwerte von Tabelle 5 wurde die Funktion

$$D_w^* = \varphi_4(1 - \Psi', \Delta x^*) \tag{17}$$

in einem Parameterfeld dargestellt *(Bild 11)*, in dem der Diffusionskoeffizient zu Beginn der Trocknung D_{w0}^*, wo also $1 - \Psi \cong 1$ ist, bestimmt werden konnte.

$$D_{w0}^* \cong 700 \text{ kg}^2/\text{m}^4 \cdot \text{h}$$

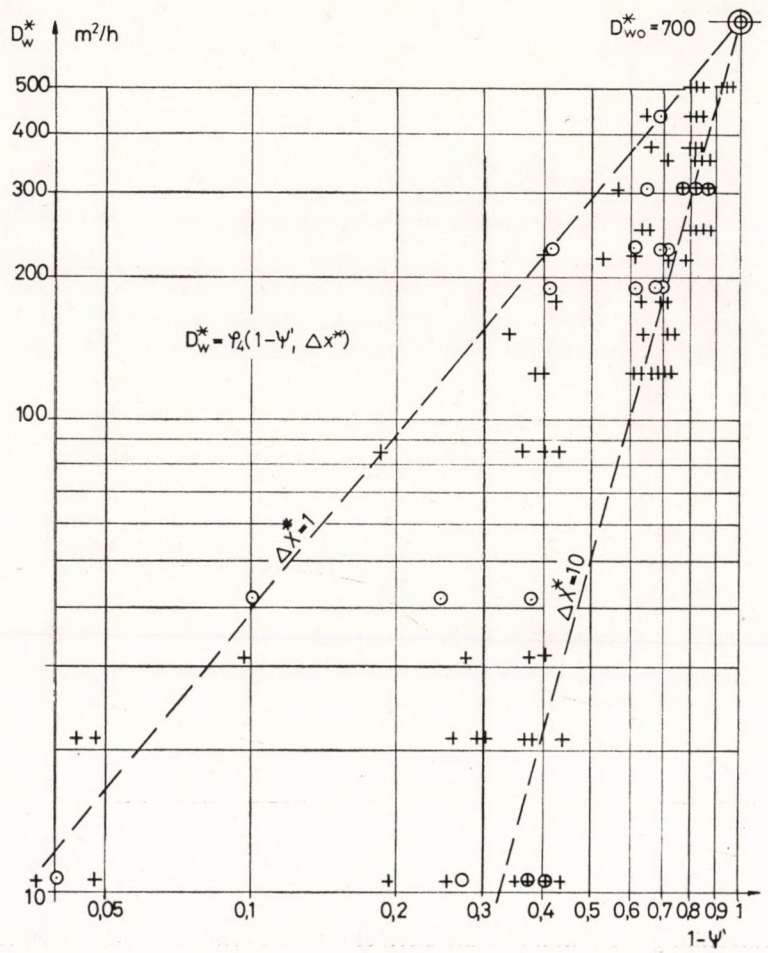

Bild 11.
Bestimmung des Diffusionskoeffizienten D_{w0}^* anhand der Meßergebnisse einer Trocknungsversuchsperiode von 48 Stunden

Da unsere Überlegungen nur auf einen Wasserverlust von 1—2% abgestellt sind, kann dieser Wert mit hinreichender Sicherheit benutzt werden.

Die Werte um $\Psi = 0{,}01$ können aus *Bild 8* und 10 nur ungenau entnommen

werden, deshalb ist es zweckmäßig, für technische Berechnungen eine Näherungsformel anzugeben

$$Fi = \text{konst} \quad \Psi' = P(Fi) \cdot \frac{1}{\frac{1}{k(Fi)} \cdot Sh - b^{(Fi)+1}} \tag{18}$$

Die Darstellung dieser Funktion kann unter Zuhilfenahme von *Bild 8* in einem Parameterfeld erfolgen, wo die Parameter die Funktionen der Fickschen Zahl sind *(Bild 12)*.

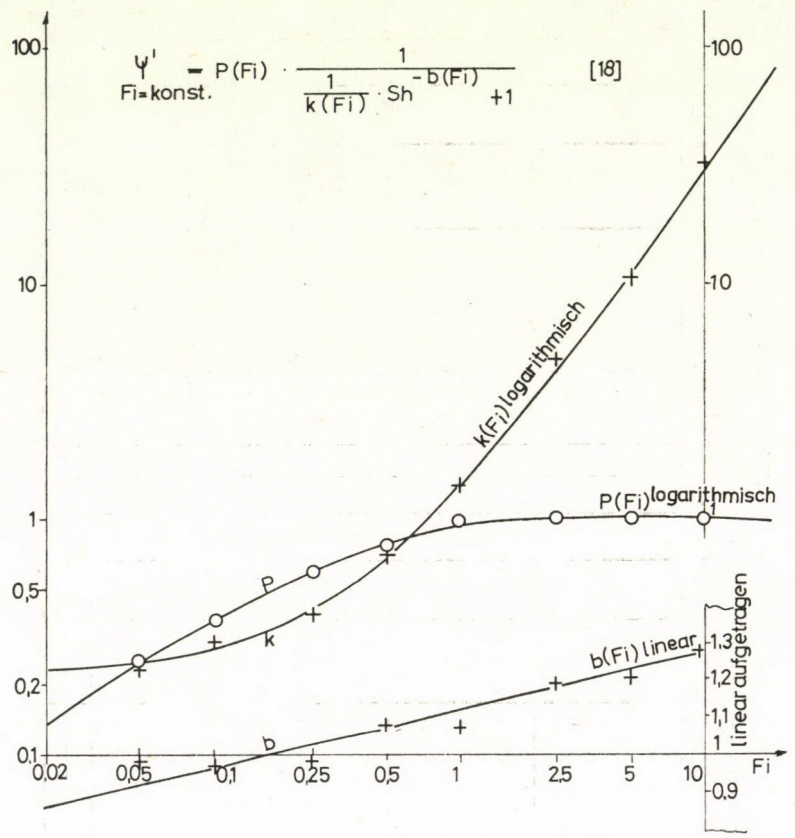

Bild 12.
Darstellung der Parameter der Formel (18) in Form von *Fi*-Funktionen

Einfluß des unbeständigen Betriebes und der Entleerungshäufigkeit des Behälters (*Bild 13/A*)

$$G_d = \frac{1}{\tau_1 - \tau_0} \left[G \int_{\tau_0}^{\tau^*} \tau_d \tau + G^* \int_{\tau^*}^{\tau_1} d\tau \right] \tag{19}$$

hieraus

$$G_d = G_g \cdot \eta(1 - \eta/2) \tag{20}$$

Betriebsparameter

$$\eta = \frac{\tau^* - \tau_0}{\Delta\tau}$$

Falls $\tau^* = \tau_1$; $\eta = 1$ dann $G_d = G_g/2$ *(Bild 13/B)* und falls $\tau = \tau_0$ dann $\mathring{G} = 0$. Hiernach ist der Ersatzparameter für die Schichthöhe:

$$\Delta x^* = \frac{G_d}{A_D} = \frac{G_g}{A_D} \cdot \eta(1 - \eta/2) \tag{21}$$

(21) und (18) dienten zur Berechnung der reduzierten Feuchtigkeit für $\eta = 1 \ldots 0{,}4$ *(Bild 13/C)*.

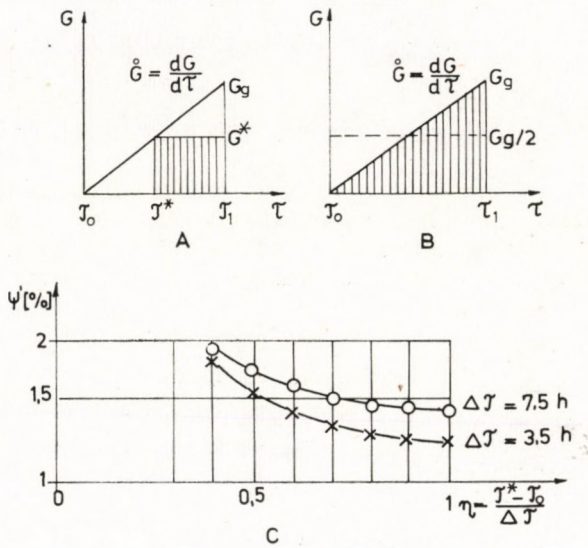

Bild 13.
Einfluß der unbeständigen Betriebsführung und der Häufigkeit der Probenahme auf die reduzierte Feuchtigkeit

Die Berechnungsanlage enthält *Tabelle 6.*

Aus *Bild 13/C* ist zu ersehen, daß die Wahl einer Probenahmezeit von $\Delta\tau = 7{,}5$ Std statt $\Delta\tau = 4{,}5$ Std keine nennenswerte Änderung mit sich bringt. Diese Änderung ist mit dem Wasserverlust vergleichbar, der durch die Betriebstörungen der Probenahmevorrichtung hervorgerufen wird.

So beträgt z. B. die reduzierte Feuchtigkeit einer Rohbraunkohleprobe mit $N = 36\%$ Wassergehalt und bei einem Betriebsparameter von $\eta = 0{,}7$ flächenförmig ausgebreitet 1,5, falls $\Delta\tau = 7{,}5$ Std.

Tabelle 6.

Hilfsparameter zum Bild 13/C

$\Delta\tau = 3{,}5$ h; $G_g = 51{,}6$ kp; $A = 0{,}25$ m²; $D_w = 700$ kg²/m⁴·h; $\varrho_v\beta = 0{,}384$ kg/m²·h

$\eta = \frac{\tau^*}{\tau_1}$	1	0,9	0,8	0,7	0,6	0,5	0,4
Δx^*	103,2	102,17	88,07	93,91	86,69	77,4	66,05
Fi	0,230	0,235	0,250	0,278	0,326	0,409	0,561
Sh	0,0581	0,0575	0,0557	0,0528	0,0488	0,0436	0,0372
$P(Fi)$	0,570	0,575	0,585	0,610	0,650	0,720	0,810
$k(Fi)$	0,400	0,410	0,425	0,450	0,510	0,600	0,800
$b(Fi)$	1,020	1,022	1,028	1,033	1,045	1,058	1,078
Ψ' %	1,22	1,25	1,25	1,30	1,38	1,53	1,82

Diese Rohbraunkohle verliert bei der Probenahme

$$W = \frac{\Psi'}{100} \cdot N = 0{,}015 \cdot 36 = 0{,}54\%$$

ihrer groben Feuchtigkeit.

Bei der kegelförmigen Anhäufung muß mit dem drei- bis vierfachem dieses Wertes gerechnet werden.

Das beschriebene Berechnungsverfahren muß noch verfeinert und weniger zeitaufwendig gemacht werden, bis es zum Standardverfahren erklärt werden kann. Es stellte sich aber heraus, daß es für die Aufklärung der Fehlerquellen der derzeitigen Probenahmemethode und zur Erfassung deren Einflüsse geeignet ist.

BEZEICHNUNGEN

E Einwaage, kg
C Konzentration, kg/m³
D_w Diffusionskoeffizient, m²/h
D_w^* eingeführter Diffusionskoeffizient, kg²/m⁴·h
β Stoffübergangszahl, m/h
ω spezifische Stoffaustauschfläche, m²/m³
ϱ_v Volumendichte der Rohbraunkohle, kg/m³
τ Zeit in Stunden, h
$\Delta\tau = \tau_1 - \tau_2$ Zeit zwischen den aufeinanderkommenden Entleerungen der Durschnittsprobebehälter, h
A Gesamtoberfläche der Kohlekörner, m²
A_S Grundfläche der Schale (1/16 m²), m²
A_D Grundfläche der Durschnittsporbebehälter, m²
Δx Schichthöhe, m
Δx^* Ersatzparameter für die Schichthöhe $\left(\Delta x^* = \frac{E}{A_S} = \varrho_v \cdot \Delta x\right)$, kg/m²
V Volumen der Kohleschichte, m³
Fi FICKsche Zahl
Sh SHERWOODsche Zahl
Bi BIOTsche Zahl
Fo FOURIERsche Zahl
Ψ' reduzierte Feuchtigkeit
$\Delta G_{\Delta\tau}$ während der Zeit $\Delta\tau$ abgegebene Wassermenge, kg

ΔG_{48} Wasserabgabe innerhalb von 48 Stunden $\Psi' \cong 1$
$\varphi_1, \varphi_2, \varphi_3, \varphi_4$ Funktionen
$\dot{G} = dG/d\tau$ geschwindigkeit der Probenahme, kg/h
G_g Menge der Kohleprobe bei störungsfreiem Betrieb
G_g^* Menge der Kohleprobe bei unbeständigem Betrieb
τ_0 Anfang der Probenahme, h
τ_1 Ende der Probenahme, h
τ^* Zeitdauer der Betriebsstörung, h
b, P, K Parameter der Gleichung (18)
$\tau^* - \tau_0$ Dauer der beständigen Betriebsperiode, h
η Betriebsparameter
Indices
a, b gültig für die Grenzkoordinaten im *Bild 9*
1, 2, 3 gültig für gegebene Gewichtsänderung ΔG
4, 4, 24, 48 gültig für Gewichtänderungen innerhalb bestimmter Zeit $\Delta G_{\Delta\tau}$
d durchschmittlich

РЕЗЮМЕ

Определению теплотворности лигнитов высокого влагосодержания ископаяемых в Венгрии препятствует большая их склонность к дегидрации. Авторы обсуждают вопросы связанные раскрытием источников ошибок аппарата автоматического анализа проб и вопросы возникающие насчет потери влаги в стадии приготовления проб. Для количественного описания кинетики сушки сырого лигнита авторы разработали математический метод пригодный для определения потери влаги на аналогии процесса диффузии и теплопроводности.

HUNGARIAN JOURNAL
OF INDUSTRIAL CHEMISTRY
VESZPRÉM
Vol. 9. pp. 385–396 (1981)

OPTIMIERUNG DER VERWERTUNG UNGARISCHER ROHBRAUNKOHLEN. II.

INSTATIONÄRE TROCKUNG PERIODISCH AUFGETRAGENER HAUFEN

L. Pleva und Z. Schultheisz

(Technische Universität für chemische Industrie Veszprém, Ungarn)

Eingegangen am 25. Juli, 1981.

Aufgrund der Versuchsergebnisse [1] wurde für die Verfolgung des Trocknungsprozesses der Kohlehaufen von verschiedenen Formen ein allgemeingültiges Rechenprogramm erarbeitet. Die mit Hilfe des Rechenprogramms gewonnenen Werte für Trocknungsverhalten ungarischer Rohbraunkohlen stimmen gut mit den praktisch gefundenen Ergebnissen überein.

Bei meisten Anhäufungen z. B. in Kegelform von verschiedenartigen Stoffen ist problematisch, neben der periodischen Iteration des Auftragens, die mathematische Beschreibung des Trocknungsprozesses in der Zeit.

Die fürs mathematische Modell gültige Differentialgleichung liefert die Lösung, unter Anwendung der Differenzmethode, in Form von Algorithmus. Es besteht die Möglichkeit die Randbedingungen z. B. den Böschungswinkel zu verändern, und das so aufgebaute Komputerprogramm ermöglicht das gegebene Problem allgemeingültig zu erfassen. Dieses Verfahren führt, parallel mit den theoretischen Rechnungen und nach der Kontrolle von Spezialfällen, zur in breitem Anwendungskreis verwertbaren Lösung.

Infolge der Analogie zwischen der Diffusion und Wärmeleitung ist es durchaus möglich die oben dargestellte Methode auch auf Systeme mit Wärmeströmen zu erweitern.

Die Verfasser beschäftigten sich mit der Lösung des bei der Probenahme von Rohbraunkohlen beobachteten Trocknungsproblems. Man stößt überall auf ähnliche Fälle, wo es sich um die Trocknung und Wärmeabgabe granulierter Stoffe im Falle kontinuirlicher oder periodischer Anhäufung handelt.

Mathematisches Modell

Die Aufgabe ist die mathematische Beschreibung der instationären Stoffübergabe und Diffusion für folgende Fälle:

a) symmetrische Planwand,

b) unendlicher Zylinder und
c) kegelförmige Körper.

Zur Lösung des Problems wurde die Diefferenzmethode verwendet.

Allgemeine Bedingungen:

c_{f1} Konstante (Konzentration des Fluidums)
c_t Konzentration der Stoffzellen im Zeitpunkt $\tau = 0$ (Anfangsbedingung)
D_w Diffusionskoeffizient
β Komponentenübergangskoeffizient
n Anzahl der Zellen und ausgewählter Punkte (auch als Index verwendet)
$c_1 = c_{f1}$ (Randbedingung), $c_2 = c_w$

Symmetrische Planwand

(Nur auszugsweise wegen der Übernahme der BINDER-SCHMIDTschen These)

$$\frac{\beta \cdot \Delta x}{D_w} = \frac{1}{\varphi} = Sh \tag{1}$$

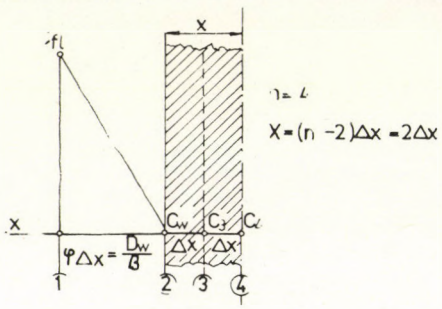

Bild 1.

Im Falle

$$\frac{\Delta^2 c}{\Delta x^2} = 0 \text{ ist } \quad \frac{\Delta c}{\Delta \tau} = 0 \tag{2}$$

$$c_w = \frac{Sh \cdot c_{f1} + c_3}{Sh + 1} \tag{3}$$

$$D_w = \frac{\Delta^2 c}{\Delta x^2} = \frac{\Delta c}{\Delta \tau} \tag{4}$$

Im Falle (4) lautet die Lösung der Differenzgleichung:

$$\frac{\Delta \tau \cdot D_w}{\Delta x^2} = \left[\frac{c_{f1a}}{\varphi} + c_{3a} - \frac{c_{wa}}{\varphi} - c_{wa}\right] = c_{wb} - c_{wa} \tag{5}$$

beziehungsweise

$$\frac{\Delta \tau \cdot D_w}{\Delta x^2} = [Sh \cdot c_{f1a} + c_{3a}] - (Sh + 1) c_{wa} = c_{wb} \tag{6}$$

Nach Umordnung der Gleichung (6) bekommt man

$$(Sh+1)\frac{\Delta\tau\cdot D_w}{\Delta x^2}\left[\frac{Sh}{Sh+1}\cdot c_{f1a}+\frac{c_{3a}}{Sh+1}-c_{wa}\right]+c_{wa}=c_{wb} \tag{7}$$

$$\text{Sei } (Sh+1)\frac{\Delta\tau\cdot D_w}{\Delta x^2}=1 \text{ (Bedingung der Übertragung)} \tag{8}$$

dann läßt sich aus der Konzentrationsverteilung im Zeitpunkt „a" die Wandkonzentration im Zeitpunkt „b" ermitteln.

$$c_{wb}=\frac{Sh\cdot c_{f1a}+c_{3a}}{Sh+1} \tag{9}$$

Für instationäre Diffusion ist nach obiger Analogie im Falle $\varphi=1$

$$Fi=\frac{\Delta\tau\cdot D_w}{\Delta x^2}=\frac{1}{2} \text{ (Bedingung der Diffusion)} \tag{10}$$

Um für den Fall der Übertragung (8) die mathematische Differenzmethode anwenden zu können, ist es notwendig, unter Berücksichtigung der Bedingung der Diffusion (10), daß

$$Sh=1, \quad \text{beziehungsweise } \Delta x=\frac{D_w}{\beta} \text{ und } \varphi=1 \tag{11}$$

sein muß, um die Gleichungen $Sh\neq 1$ auch in Originalform verwendbar zu bleiben.

Werden die Bedingungen für instationäre (3) und stationäre Berechnungsmethode (9) im Auge behalten, dann ist die Analogie bzw. die Ähnlichkeit kaum zu versehen.

Unendlicher Zylinder

(Ausführlich wegen der gegebenen Schwierigkeiten).

Instationäre Diffusion:

$$D_w\left[\frac{1}{r}\frac{\partial c}{\partial r}+\frac{\partial^2 c}{\partial r^2}\right]=\frac{\partial c}{\partial \tau}; \quad N\geqq 1 \tag{12}$$

Ordnen vir die Differenzgleichung bezogen auf den Zylindermantel $n=4$, dann bekommt man

$$\Delta\tau\cdot D_w\left[\frac{1}{N\cdot\Delta r}\cdot\frac{\Delta c}{\Delta r}+\frac{\Delta^2 c}{\Delta r^2}\right]+c_{4a}=c_{4b} \tag{13}$$

beziehungsweise

$$\frac{\Delta\tau\cdot D_w}{\Delta r_2}\left[\frac{c_{3a}}{N}-\frac{c_{4a}}{N}+c_{3a}+c_{5a}-2c_{4a}\right]+c_{4a}=c_{4b} \tag{14}$$

$$\frac{2N+1}{N}\cdot\frac{\Delta\tau\cdot D_w}{\Delta r^2}\left[\frac{N\cdot c_{5a}+(N+1)\cdot c_{3a}}{2N+1}-c_{4a}\right]=c_{4b} \tag{15}$$

Sei

$$\frac{2N+1}{N}\cdot\frac{\Delta\tau\cdot D_w}{\Delta r^2}=1 \text{ (Bedingung der Diffusion)} \tag{16}$$

dann läßt sich aus der Konzentrationsverteilung im Zeitpunkt „a“

$$c_{4b} = \frac{N \cdot c_{5a} + (N+1) \cdot c_{3a}}{2N+1} \tag{17}$$

ermitteln.

Auf der Abszisse X ist im Punkt $N = 0$ aus Simmetriegründen z. B.

$$c_{6b} = c_{5a} .$$

Aus der Prüfung der Bedingung (16) ist es ersichtlich, im Falle $N \to \infty$ bekommt man die für die Planwand gültige Bedingung (10).

Bei instationärer Diffusion und im Bereich $N \geqq 1$ sind ausgehend aus Gleichung (16)

$$Fi = \frac{D_w \cdot \Delta\tau}{\Delta r^2} = \frac{N}{2N+1} \tag{18}$$

und wenn D_w bekannt ist, zwei Lösungswege einzuschlagen.

a) Sei $\Delta\tau$ gegeben (Fall der Homochronität)

$$\Delta r(N) = \sqrt{\frac{(2N+1)}{N} \cdot D_w \cdot \Delta\tau} \tag{19}$$

wo die Einteilung von Δr von der dimensionsfreien Schichtzahl abhängig ist.

b) Sei Δr = konstant

$$\Delta\tau = \frac{\Delta r^2}{D_w} \cdot \frac{N}{2N+1} \tag{20}$$

wo bei der Berechnung nach (17) die Teilpunkte keine Gleichzeitigkeit bedeuten. In den Teilpunkten ist der Zeitverlauf nämlich verschieden: für Teilpunkte bzw. für Kegelschnitte in der Nähe der Achse ist der Zeitverlauf langsamer als der für die ferner liegenden, wo $\Delta\tau(N)$ ist.

Analog wie im Falle der Planwand betrachten wir auch hier die Schicht, wo die Übertragung stattfindet unter Angabe der Sherwoodschen Zahl als Diffusions-Wandelement. Das Problem wird in Form grad c an der Grenzoberfläche gelöst.

Lösen wir die Differentialgleichung (12) unter den bekannten Anfangsbedingungen und schaffen wir Formel für die Berechnung von c_w.

Bilden wir den Differenzquotienten für Kegelschicht $n = 2$.

$$\left(\frac{\Delta c}{\varphi \cdot \Delta r}\right)_{1\_2} = \frac{c_{f1} - c_w}{\varphi \cdot \Delta r} \tag{21}$$

$$\left(\frac{\Delta c}{\Delta r}\right)_{2\_3} = \frac{c_w - c_3}{\varphi \cdot \Delta r} \tag{22}$$

$$\frac{\Delta^2 c}{\Delta r^2} = \frac{1}{\Delta r}\left[\left(\frac{\Delta c}{\varphi \Delta r}\right)_{1\_2} - \left(\frac{\Delta c}{\Delta r}\right)_{2\_3}\right] = \frac{1}{\Delta r^2}\left[\frac{c_{f1}}{\varphi} - \frac{c_w}{\varphi} + c_3 - c_w\right] \tag{23}$$

Unter Berücksichtigung der Werte im Zeitpunkt „a“ und „b“ bekommt man nach der Analogie (13)

$$\Delta\tau \cdot D_w\left[\frac{1}{N \cdot \Delta r} \cdot \left(\frac{c_{f1a} - c_{wa}}{\varphi \cdot \Delta r}\right) + \frac{1}{\Delta r^2}\left(\frac{c_{f1a}}{\varphi} - \frac{c_{wa}}{\varphi} + c_{3a} - c_{wa}\right)\right] + c_{wa} = c_{wb} \tag{24}$$

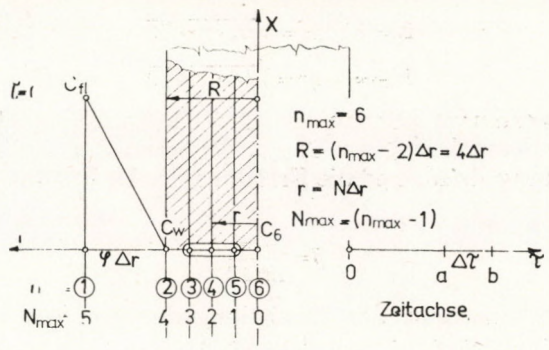

Bild 2.

Im *Bild 2* ist $N = 4$.

Nach Zusammenziehen und unter Berücksichtigung $Sh = \frac{1}{\varphi}$ folgt

$$\frac{1}{N} \cdot \frac{\Delta\tau \cdot D_w}{\Delta r^2} \{Sh \cdot (N+1) \cdot c_{f1a} + N c_{3a} - [Sh(N+1) + N] c_{wa}\} + c_{wa} = c_{wb} \tag{25}$$

Nach Ausklammern bekommt man

$$\frac{[Sh \cdot (N+1) + N]}{N} \cdot \frac{\Delta\tau \cdot D_w}{\Delta r^2} \left[\frac{Sh \cdot (N+1) \cdot c_{f1a} + N c_{3a}}{Sh \cdot (N+1) + N} - c_{wa} \right] - c_{wa} = c_{wb} \tag{26}$$

Sei

$$\frac{Sh \cdot (N+1) + N}{N} \cdot \frac{\Delta\tau \cdot D_w}{\Delta r^2} = 1 \quad \text{(Bedingung der Übertragung)} \tag{27}$$

dann läßt sich aus der Konzentrationsverteilung im Zeitpunk „a“

$$c_{wb} = \frac{Sh \cdot (N+1) \cdot c_{f1a} + N \cdot c_{3a}}{Sh \cdot (N+1) + N} \tag{28}$$

ermitteln.

Dividiert man Nenner und Zähler durch N, dann ist es ersichtlich, daß im Falle $N \to \infty$ die für die Planwand gültiger Zusammenhang (9) vor uns steht.

Berücksictigen wir in der Bedingung der Übertragung (27) die Bedingung der Diffusion (16) und (18), dann läßt sich schreiben

$$\left[\frac{Sh \cdot (N+1) + N}{N} \right] \frac{N}{2N+1} = 1 \tag{29}$$

Zur Vereinfachung soll auch hier $Sh = 1$ sein.

Obige Bedingung scheint von Ortskoordinaten unabhängig zu sein, weil die Gleichungen $Sh \neq 1$ auch hier in ihrer Originalform zu verwenden sind.

Bei den Berechnungen ist ez zweckmäßig die Bedingung der Homochronität zu berücksichtigen. Aus der Gleichung (19) läßst sich $\Delta r(N)$ ermitteln, und bei bekannten Werten von D_w und $\Delta\tau$ bekommt man:

wenn

$$N=1 \quad \Delta r=\sqrt{D_w\cdot\Delta\tau}\cdot\sqrt{3}$$

$$N\to\infty \quad \Delta r=\sqrt{D_w\cdot\Delta\tau}\cdot\sqrt{2}$$

Nach diesem Verfahren können wir den Überganskoeffizienten β bestimmen, wozu die Substituirung von M_{max}. gehörend zur Zylinderschicht $n=1$ sowie die Anwendung $\Delta r(N)$ und die Erfüllung der Bedingung $Sh=1$ notwendig sind.

$$\beta=\frac{D_w}{\Delta r(N)} \tag{30}$$

Vorteilhaft ist im Interesse der Ermittlung der Konzentrationsmittelwerte von Stoffzellen und wegen der Einstufung nach der Zeit die Homochronität im Auge zu behalten. Die Schwierigkeit besteht hier darin, daß $\beta[\Delta r(N)]$ in Form einer Funktion vorliegt.

Symmetrischer Kegel

In diesem Falle betrachten wir nur die Endlösungen, wenn die diffusive Massenstrom $\mathring{m}$ nach außen zeigt. Die Differenzgleichung, wobei aus dem Bezugsintervall der Spitzenpunkt des Kegels π_0 und die Kreispunkte π_N ausgenommen sind, lautet wie folgt

$$D_w\left[\frac{\Delta^2 c}{\Delta x^2}+\frac{1}{r}\cdot\frac{\Delta c}{\Delta r}+\frac{\Delta^2 c}{\Delta r^2}\right]=\frac{\Delta c}{\Delta\tau}\,; \qquad N\geqq 1 \tag{31}$$

Die Lösung bezogen auf den Innenraum des Kegels, vorausgesetzt wenn

$$\left(\frac{2N\psi^2+2N+1}{N}\right)\cdot\frac{D_w\cdot\Delta\tau}{\Delta r^2}=1 \text{ (Bedingung der Diffusion)} \tag{32}$$

läßt sich aus der Konzentrationsverteilung im Zeitpunkt „a" unter Anwendung der Bezeichnungen des *Bildes 3* ermitteln.

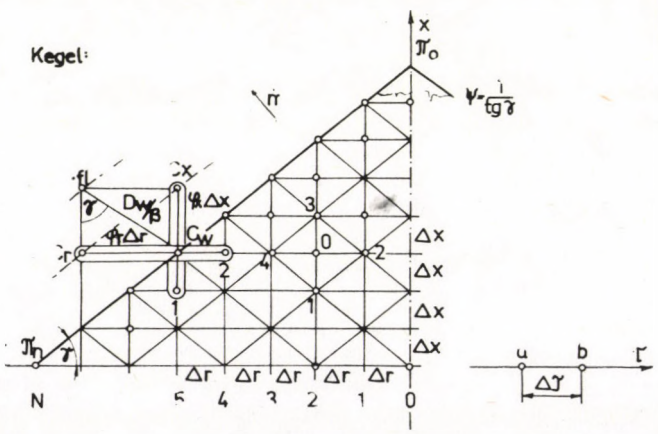

Bild 3.

$$c_{0b}=\frac{N\psi^2(c_{1a}+c_{3a})+(N+1)c_{2a}+Nc_{4a}}{2N\psi^2+2N+1} \tag{33}$$

Die Gleichung (33) ist auch im Falle $N=0$ gültig.

Betrachten wir bei der Übertragung bisherige Methode, so bekommen wir nach obiger Abbildung

$$\varphi_r\cdot\Delta r=\frac{D_w}{\beta}\sin\gamma \tag{34}$$

Daraus folgt

$$\frac{1}{\sin\gamma}\cdot\frac{\beta\cdot\Delta r}{D_w}=\frac{1}{\varphi_r} \tag{35}$$

wo

$$Sh_r=\frac{\beta\cdot\Delta r}{D_w} \tag{36}$$

Bei gleichzeitiger Erfüllung der Bedingung der Übertragung

$$\left(\psi^2+\frac{Sh_r}{\sin\gamma}+\frac{1}{N}+1\right)\cdot\frac{D_w\cdot\Delta\tau}{\Delta r^2}=1 \tag{37}$$

läßt sich die Wandkonzentration c_{wb} im Zeitpunkt „b" aus der Konzentrationsverteilung im Zeitpunkt „a" unter Anwendung der Bezeichungen des *Bildes 3* ermitteln.

$$c_{wb}=\frac{\psi^2\cdot c_{1a}+c_{2a}+\frac{Sh_r}{\sin\gamma}\cdot c_{f1a}}{\psi^2+\frac{Sh_r}{\sin\gamma}+\frac{1}{N}+1} \tag{38}$$

wobei der durch Einbeziehung der Bedingungen für Diffusion (35) und Übertragung (37) gewonnene Zusammenhang

$$Sh_r=(\psi^2+1)\cdot\sin\gamma \tag{39}$$

zu berücksichtigen ist. Z. B. sei $\gamma=90°$, $\psi^2=\frac{1}{\mathrm{tg}^2\,\gamma}=0$ und $Sh_r=1$, so bekommt man den für den unendlichen Zylinder gültigen Wert. Nach Gleichung (39) nimmt Sh_r bei abnehmendem Winkel γ zu, wie es auch unsere Versuche bestätigen, die wir für Kegelhaufen von gleichem Volumen aber von verschiedenem Böschungswinkel gewonnen haben [1].

Obige für den Kegel gültige Beschreibung beinhaltet den Fall der Homochronität nicht, weil daraus weitere Komplikationen auftreten würden.

Zuerst sollte die Einteilung für Δr inhomogen sein. Die Werte in der Nähe der Achse wären dadurch größer, andere dagegen kleiner.

Bei priodischem Stoffanfall, wobei die Oberfläche des Kegelhaufens immer von neuen und den Anfangsbedingungen entsprechenden und gleichmäßig verteilten Schichten bedeckt wird, wirkt störend auch das Radialwachstum des Kegels in Richtung r. Es ist nämlich einzusehen, bei konstanter Förderkapazität werden die entstehenden neuen Schichten immer dünner. Aus diesem Grund beschränkten wir die Untersuchungen auf den Fall $N\to\infty$, wobei das Problem in einem auf die Parallelwand transportierten System behandelt werden konnte.

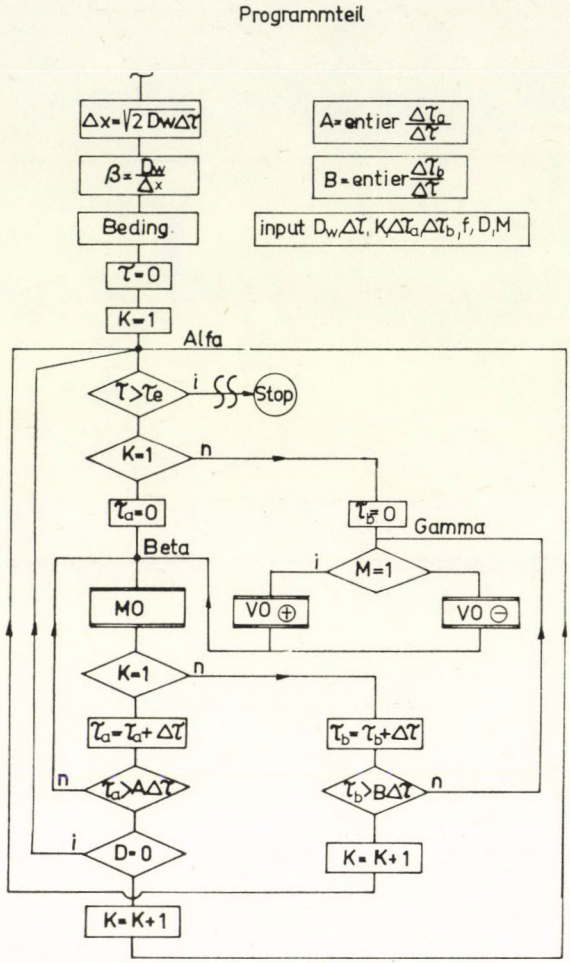

Bild 4.

Die Bescreibung des mathematischen Modells und das Funktionsschema des Rechenprogramms werden im *Bild 4* dargestellt. Bei Gestaltung des Modells wurde auf Vielseitigkeit geachtet, so ist das Programm für Untersuchung von Kegelhaufen für Komponentenübertragung-Diffusion, Wärmeübertragung-Wärmediffusion mit

a) konstaten,
b) zunehmenden oder
c) abnehmenden Parametern geeignet.

Als allgemeingültige Bedingung wurde $c_{f1} = \text{konstant}$ gewählt. Zur Grundlage der Funktion des Rechenprogramms dient eine Matrixoperation (*MO*) mit einer Häufigkeit von $\Delta\tau$, derer FALKsche Verteilung bezogen auf die Symmetrieachse $n=4$, $c_1 = c_{f1}$, c_4 im *Bild 5* dargestellt ist.

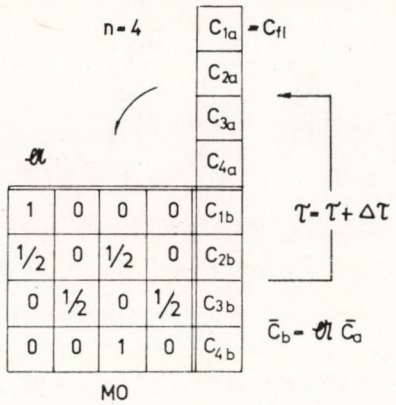

Bild 5.

Der Algorithmus trägt die Daten der mit Anfangsbedingungswerten beladenen Schicht (z. B. Konzentration oder Temperatur) in einen Block r über, und errechnet sowohl den mathematischen als auch den Integralmittelwert.

$$\left[\begin{array}{l} s=0 \\ \text{copy}/n,\ t[1],\ r[1] \\ \text{for i}=2 \text{ step 1 until } (n-1) \text{ do begin} \\ t[\text{i}]=(r[\text{i}-1]+r[\text{i}+1]\times 0.5 \\ s=s+t[\text{i}] \text{ end} \\ t[\text{n}]=r[n-1] \\ s=(s+t[n])/(n-1) \end{array}\right] MO$$

Wenn eine zunehmende Schicht mit einer Häufigkeit von $\Delta\tau$ beschrieben wird, dann bekommt man:

$$\left[\begin{array}{l} n=n+f \\ \text{for i}=2 \text{ step}-1 \text{ until } (f+1) \text{ do} \\ t[\text{i}]=tt \\ \text{for i}=n \text{ step}-1 \text{ until } (f+2) \text{ do} \\ t[\text{i}]=t[j-f] \end{array}\right] \text{VO}+$$

$$\left[\begin{array}{l} n=n-f \\ \text{for i}=2 \text{ step}-1 \text{ until } n \text{ do} \\ t[\text{i}]=t[\text{i}+\text{c}] \end{array}\right] \text{VO}-$$

Unter Beachtung, daß die Werte für Fi und Sh mit einer Dichte Δx des Mikrosystems gebildet worden sind, wozu im allgemeinen ein geometrisches Makromaß $x=(n-2)\cdot\Delta x$ zu berücksichtigen ist, so bekommt man für Planwand und für Mikrosystem unter Beachtung der zu unserer Berechnungsmethode erforderlichen Diffusions- (10) bzw. Übergangsbedingungen (11)

$$Fi=\frac{D_w\cdot\Delta\tau}{\Delta x^2}\cdot\frac{1}{(n-1)^2} \tag{40}$$

und

$$Sh = \frac{\beta \cdot \Delta x(n-2)}{D_w} \tag{41}$$

wo $(n-2)$ die Anzahl der Schichten bedeutet.

Mit Berücksichtigung der Gleichungen (40) und (41) sowie (10) und (11) ergibt sich für ein Makrosytem

$$Fi \cdot Sh^2 = 0{,}5. \tag{42}$$

Die Beschaffenheiten des Rechenprogramms sind in der *Tabelle 1* zusammengestellt.

Tabelle 1.

Beschaffenheiten des Rechnenprogramms

	Anzahl der Schichten des Kegelhaufens		
	konstant	abnehmend	zunehmend
Abkühlung oder Trocknung	$t_{fl} < tt$ $D = 0$	$t_{fl} < tt$ $D \neq 0$ $M \neq 1$	$t_{fl} < tt$ $D \neq 0$ $M = 1$
Aufwärmung oder Wasseraufnahme	$t_{fl} > tt$ $D = 0$	$t_{fl} > tt$ $D \neq 0$ $M \neq 1$	$t_{fl} > tt$ $D \neq 0$ $M = 1$

Die mit Hilfe des Rechenprogramms gewonnen Werte für Trocknungsverhalten ungarischer Rohbraunkohlen stimmen gut mit den praktisch gefundenen Ergebnissen überein.

BEZEICHNUNGEN

t[i] Konzentration oder Temperatur im gegebenen Zeitpunkt
r[i] Konzetration oder Temperatur im vorangehenden Zeitpunkt
c_{fl} oder t_{fl}: Anfangskonzentration oder Anfangstemperatur des Fluidums
tt Anfangstemperaturen oder Anfangskonzentrationen der Zellen
n Anzahl der aktuellen Schichten oder Zellen
f zunehmende oder abnehmende Schichtenzahl innerhalb der Zeit von $\Delta\tau$
s Summe oder die Zelle der Integralmitte
$\mathcal{A}$ Matrix
$\bar{c}_a$, $\bar{c}_b$ Konzentration oder Temperatur der Schichten in einem Zeitpunkt „a“ oder „b“
τ aktueller Zeitintervall
$\Delta\tau$ elementarer Zeitintervall zwischen Zeitpunkten „a“ und „b“
$\Delta\tau_a$ vorgeschriebene Zeitdauer ohne Zu- oder Abnahme
τ_a aktuelle Zeitdauer ohne Zu- oder Abnahme
$\Delta\tau_b$ Zeitdauer der vorgeschriebenen Zu- oder Abnahme der Schichte n
τ_b Zeitdauer der aktuellen Zu- oder Abnahme der Schichte n
MO Matrixoperation
$VO+$ Schichtenoperation bei Zunahme
$VO-$ Schichtenoperation bei Abnahme
c_{fl} Konzentration des Fluidums

c_t Anfangskonzentration einer Zelle im Zeitpunkt $\tau = 0$
$c(i)$ Zellenkonzentration
β Komponentenübergangskoeffizient
D_w Diffusionskoeffizient
φ Umsetzungsfaktor
x, r Koordinaten
$\Delta x, \Delta r$ Schichthöhe
X halbe Wanddichte (bei Planwand)
R Radius (beim symmetrischen Kegel)
N Schichtenlaufzahl in zylindrischem Raum
Sh SHERWOODsche Zahl
Fi FICKsche Zahl
α Wärmeübergangskoeffizient
λ_w Wärmeleitungskoeffizient der Wand bzw. des Haufens
A abgerundete Zahl im Zeitpunkt ohne Zu- oder Abnahme
B abgerundete Zahl im Zeitpunkt mit Zu- oder Abnahme
D, K, M Entscheidungsparameter des Programms
Bi BIOTsche Zahl
F_0 FOURIERsche Zahl
$\dot{m}$ Massenstrom
φ_r Faktor für Wärmeübergang in Richtung r
φ_x Faktor für Wärmeübergang in Richtung x
c_r Konzentration der Übergangsschichte in Richtung r
c_x Konzentration der Übergangsschichte in Richtung x
γ Böschungswinkel
$\psi = 1/\mathrm{rg}\ \gamma$

Indices

e vorgeschrieben
a, b Werte im Zeitpunkt „a“ und „b“
w bezogen an die Oberfläche
r in Richtung r
x in Richtung x

LITERATUR

1. Schultheisz, Z., Pleva, L. und Bartha, L.: Hung. J. Ind. Chem., *1981*, 9, 365.

РЕЗЮМЕ

На основе результатов предыдущих исследований процесса сушки сыпучих масс угла авторы разработали вычислительный алгоритм для расчета скорости сушки. Результаты расчета хорошо согласуются с измеренными данными.

HUNGARIAN JOURNAL
OF INDUSTRIAL CHEMISTRY
VESZPRÉM
Vol. 9. pp. 397–406 (1981)

APPLICATION OF DIFFERENT REGULATORS FOR STIRRED TANK REACTOR CONTROL

SIMULATION STUDY

MRS. K. M. HANGOS

(Computer and Automation Institute, Hungarian Academy of Sciences, Budapest, Hungary)

Received: October 1, 1981.

The advantages of previous simulation investigation were shown in preparing the control of a perfectly stirred tank reactor. Simulation investigations were carried out on two typical examples for determining the most suitable input variables and the amplitude of the reactor output noise using the sensitivity method and for determining the discrete linear regulator parameters of the reactor. Conventional PID and discrete linear adaptive stochastic regulators were compared from the viewpoint of regulation quality.

Introduction

The use of modern digital control algorithms is very important, but this is a difficult task with regard to chemical plants, because they often have a nonlinear and/or nonstationary character from a control viewpoint even in the case of perfectly stirred objects. This is the reason why the method, commonly used during the implementation of a control algorithm is of the "black box" type. However, a chemical engineer working in a chemical plant has plenty of information about it. Unfortunately, this information is not in a suitable form for control engineers, and this is the reason why they do not use it. The simulation method seems to be suitable for overcoming this difficulty i.e., to transfer information of a physico-chemical nature to a form suitable for modern control theory. Here, it will be shown how the simulation method can be used during the process of selecting the most suitable regulator for stirred tank reactor control.

Reactors studied

Two liquid phase, perfectly stirred chemical tank reactors with water cooling/heating were chosen as illustrative examples in order to show the methods and problems occurring in the case of a control object having stationary and non-stationary characters, respectively.

The first reactor was a continuous stirred tank reactor (CSTR) in which a single $2Q \rightarrow T$ type 2nd order reaction takes place with the reaction rate:

$$z_1 = -pe^{-\frac{E}{RT}} \times c^2. \tag{1}$$

In order to obtain simple mathematical equations, it was supposed that the physico-chemical properties of the reaction mixture, of the inlet mixture and of the reactor, as well as the parameters of the reaction are constant and the change in the intensity of heating or cooling can be modelled by changing T_H. These are the same assumptions, as in references [4] and [5].

By these assumptions the model equations are the following [10]:

$$\frac{dc}{dt} = 2 \cdot z_1 + \frac{v_B}{V}\left(c_{B1} - \frac{\varrho_B}{\varrho} c\right) \tag{2}$$

$$(G_R + c_p \varrho V) \times \frac{dT}{dt} = -K_T F(T - T_H) + 2z_1 \times H \times V + v_B c_{PB} \varrho_B (T_B - T) \tag{3}$$

$$V = V^0 \tag{4}$$

$$F = k_1 V^0 \tag{5}$$

with the initial conditons:

$$c(t_0) = c^0; \quad T(t_0) = T^0; \quad V(t_0) = V^0. \tag{6}$$

The second reactor was a semi-continuous, perfectly stirred tank reactor (SSTR) in which a methylization reaction occurred using dimethyl-sulphate (DMS) and sodium hydroxide as reagents. This reaction was strongly exothermic and can be regarded as a reaction with infinite reaction rate constant, i.e., the reaction rate was determined by the feed rate only. During the operation, DMS and NaOH solution was continuously added to the reaction mixture containing the reagent to be methylized. The control task was to keep the temperature at prescribed constant level (also applying water cooling). It was assumed that the reaction is a single:

$$\sum_{i=1}^{i} v_i A_i = 0$$

type ($v_i > 0$ denoting reagent, $v_i < 0$ denoting the product) with infinite rate constant, i.e., with reaction rate:

$$z_2 = -\frac{v_B c_{B1}}{V}, \tag{1'}$$

determined by the feed rate (v_B) and the inlet concentration of the first component (c_{B1}) only. (The inlet matter immediately reacts independently of the temperature.) Further assumptions were the same as in the case of CSTR above.

Thus the model equations are very similar to Equations (2–6)

$$\frac{dc_i}{dt} = v_i z_2 + \frac{v_B}{V}\left(c_{Bi} - \frac{\varrho_B}{\varrho} c\right), \qquad i = 1, \ldots, k, \tag{2'}$$

$$\frac{dV}{dt} = v_B \times \frac{\varrho_B}{\varrho} \tag{4'}$$

$$F = \frac{2}{r} \times V + \frac{2r^2\pi}{3} \tag{5'}$$

with the initial conditons:

$$c_i(t_0) = c_i^0; \quad i = 1, \ldots, k, \quad T(t_0) = T^0; \quad V(t_0) = V^0. \tag{6'}$$

[Eq (3′) is the same as Eq (3).]

The parameters of the models for the CSTR and for the SSTR are summarized in *Table 1.*

Table 1.

Comparison of the reactor model coefficients for the CSTR and SSTR

Parameter name	Unit	CSTR [Eqs (1–6)]	SSTR [Eqs (1′–6′)]
k	—	—	5
v_1, v_2, v_3	—	—	
v_4, v_5	—	—	−1
K_T	J/m²·s·K	779.0	1500.0
ϱ	kg/m³	1.105×10^3	2.25×10^3
ϱ_B	kg/m³	1.105×10^3	1.39×10^3
c_P	J/kg	3.836×10^3	5.8×10^3
c_{PB}	J/kg	3.836×10^3	5.0×10^3
G_R	J/kg	1.428×10^5	1.4×10^5
k_1	l/m	3.07	—
r	m	—	0.6
H	J/kmol	-5.732×10^7	-2.0×10^8
E	J/kmol	8.0×10^7	—
P	m³/s·kmol	1.174×10^{10}	—
V°	m^3	2.0	0.6
T°	K	323.15	288.2
v_B	m²/s	2.75×10^{-3}	1.475×10^{-4}
C°	kmol/m³	1.1	0.0, 1.042, 11.36, 0.672, 0.0
c_B	kmol/m³	2.1	6. 72, 6.08, 0.0, 0.0, 0.0
T_B	K	293.15	288.2

Analysis of Non-Controlled Reactor Behaviour from a Control Viewpoint

Some results are reported on here, which help to answer some questions in the constructing the control of reactors:

— how to choose the most suitable control variables?
— what are the properties of the reactor output noise?

In order to answer the above two questions, it is necessary to know what is the influence of the reactor parameters or variables (those, what are potentional inputs or potentional noise sources) on the chosen output. This influence is characterized by the sensitivity functions of the output variable with respect to the reactor parameters or variables. The definition and the method of computation of the sensitivity functions are described in detail in reference [4]. Here the application of these functions to the above control problem is shown.

Tables 2 and *3* contain the values of the relative sensitivity functions of the system variables c and T, with respect to the most important reactor parameters and variables starting from the stationary state of the CSTR as a function of time. The values multiplied by the relative change of the parameter or vari-

Table 2.

Relative concentration sensitivity functions for the CSTR $\Psi_{\alpha}^{C} \cdot \alpha$ (kmol/m³)

τ(s)	$\alpha=E$	$\alpha=p$	$\alpha=K_T$	$\alpha=v_B$	$\alpha=T_H$	$\alpha=c_B$
10.0	-4.72×10^{-1}	-1.57×10^{-2}	-9.16×10^{-5}	1.58×10^{-2}	-7.55×10^{-4}	2.89×10^{-2}
20.0	-9.11×10^{-1}	-3.02×10^{-2}	-3.65×10^{-4}	3.10×10^{-3}	-3.01×10^{-3}	5.80×10^{-2}
30.0	-1.32	-4.38×10^{-2}	-8.15×10^{-4}	4.55×10^{-2}	-6.72×10^{-3}	8.71×10^{-2}
40.0	-1.70	-5.64×10^{-2}	-1.44×10^{-3}	5.95×10^{-2}	-1.18×10^{-2}	1.16×10^{-1}
50.0	-2.05	-6.81×10^{-2}	-2.23×10^{-3}	7.30×10^{-2}	-1.83×10^{-2}	1.46×10^{-1}
60.0	-2.38	-7.90×10^{-2}	-3.18×10^{-3}	8.58×10^{-2}	-2.62×10^{-2}	1.75×10^{-1}
70.0	-2.69	-8.90×10^{-2}	-4.29×10^{-3}	9.81×10^{-2}	-3.54×10^{-2}	2.05×10^{-1}
80.0	-2.97	-9.83×10^{-2}	-5.56×10^{-3}	1.10×10^{-1}	-4.59×10^{-2}	2.35×10^{-1}
90.0	-3.23	-1.07×10^{-1}	-6.99×10^{-3}	1.21×10^{-1}	-5.76×10^{-2}	2.65×10^{-1}
100.0	-3.47	-1.15×10^{-1}	-8.56×10^{-3}	1.32×10^{-1}	-7.06×10^{-2}	2.95×10^{-1}

Table 3.

Relative temperature sensitivity functions for the CSTR $\Psi_{\alpha}^{T} \cdot \alpha$ (K)

τ(s)	$\alpha=E$	$\alpha=p$	$\alpha=K_T$	$\alpha=v_B$	$\alpha=T_H$	$\alpha=c_B$
10.0	6.39	2.12×10^{-1}	2.41×10^{-1}	5.86×10^{-1}	1.98	-3.29×10^{-3}
20.0	12.57	4.17×10^{-1}	4.75×10^{-1}	1.15	3.92	-1.31×10^{-2}
30.0	18.55	6.15×10^{-1}	7.02×10^{-1}	1.70	5.79	-2.91×10^{-2}
40.0	24.35	8.07×10^{-1}	9.23×10^{-1}	2.24	7.61	-5.14×10^{-2}
50.0	29.96	9.93×10^{-1}	1.14	2.75	9.38	-7.96×10^{-2}
60.0	35.42	1.17	1.35	3.25	11.10	-1.14×10^{-1}
70.0	40.73	1.35	1.55	3.74	12.78	-1.49×10^{-1}
80.0	45.91	1.52	1.75	4.21	14.40	-1.99×10^{-1}
90.0	50.97	1.69	1.94	4.66	15.99	-2.50×10^{-1}
100.0	55.92	1.85	2.13	5.10	17.53	-3.06×10^{-1}

able [for example $\Delta T_H/T_H$] gives the absolute possible change in the system variables caused by the parameter variations after the time interval τ. The reactor parameters in *Tables 2* and *3* are divided into two parts with a double line.

Parameters E, p and K_T, which cannot be influenced, are in the first group, i.e., they are potential noise sources. Because of the simplifications in the model construction, the variations caused by the imperfect stirring, and heterogeneity, etc., can be modelled only formally via variations of the reaction and the heat transfer parameters (p, E and K_T). It can be seen from the values of the sensitivity functions with respect to these parameters, that in the range of their real change [the frequency of changing is greater than 0.1/s, the mean amplitude of changing is in the magnitude of 10%/(0.1)] only the effect of the change in the parameter E will be greater than the measurement error range (~ 0.06 K or 1.10^{-3} kmol/m^3, respectively). In this way it can be seen that in the case of the CSTR, the reactor is to be regarded as a stochastic control object only when stochastic change in the activation energy (i.e. change in a reaction mechanism for example in the case of imperfectly stirred heterogeneous systems) occurs.

The variables (v_B, c_B, T_H) which can be influenced, are in the second group, i.e., they are potential control (input) variables. It can be seen from the values of the sensitivity functions that in the range of typical discretization time (10–90 s) the most effective control (input) variable for the concentration control is the inlet concentration c_B, which has negligible influence on the temperature. On the other hand, for temperature control, the temperature of the water (T_H) seems to be most suitable and the influence on the concentration is negligible. Thus it can be seen that in the case of simultaneous concentration and temperature control it is possible to implement two independent single input-single output control circuits for the two tasks, respectively. It can also be seen from the data in *Tables 2* and *3* that the inlet volume rate (v_B) is also an effective input variable for both cases. For example, if it is not possible to influence the inlet concentration (c_B), the inlet volume rate can be chosen as the input variable for concentration control. Then the effect caused by the variation of v_B on the temperature cannot be neglected, thus the two control circuits will be coupled. In this case, a multiple (two) input multiple (two) output regulator is needed.

It should be noted that in the case of the SSTR, the method is much more complicated, because of the nonstationarity of the reactor. As the reactor has no stationary state, the values of the sensitivity functions along all working trajectories are needed. This means that the sensitivities become functions with several independent variables. Thus the result of the choice of the suitable input variable depends on the state of a reactor.

It may happen that the sensitivity functions have maximum or minimum values. In that case, applying discrete regulators, the choice of the most suitable discretizetion time can be determined according to this maximum.

It should also be noted that in order to design stochastic regulators, much more information is needed concerning the noise characteristics than merely its amplitude. This problem needs further investigation, however, some simulation results have already been reported [5].

Tuning and Selecting Suitable Discrete Regulators

Discrete linear control algorithms are commonly used in industry, especially since the characteristics (price, size, and computation time) of their microprocessor implemented versions come into the range of conventional PID-controllers. A self-tuning stochastic discrete linear controller seems to be suitable for the control of chemical systems [3, 7] having a nonlinear and/or nonstationary character. General theoretical investigation (convergence or stability) of nonlinear and nonstationary systems (e.g. nonstationary stirred tank reactors) is not yet available, so it is reasonable to carry out simulation investigations on the model of a concrete system before the application, in order to choose the suitable controller and its parameters, and estimate the behaviour of the controlled system. Results of such a simulation investigation will be shown here for the SSTR. The control task is to maintain the temperature of a reactor on a constant $T^* = 318.2$ K level, while the reactor is perturbed with 7% noise in the cooling water temperature (T_H). The reactor works at this state until the component to be methylized is used up (until $c_3 = 0$). *Fig. 1* shows the temperature of the reactor (T) and the concentration of the component to be methylized (c_3) in time without control.

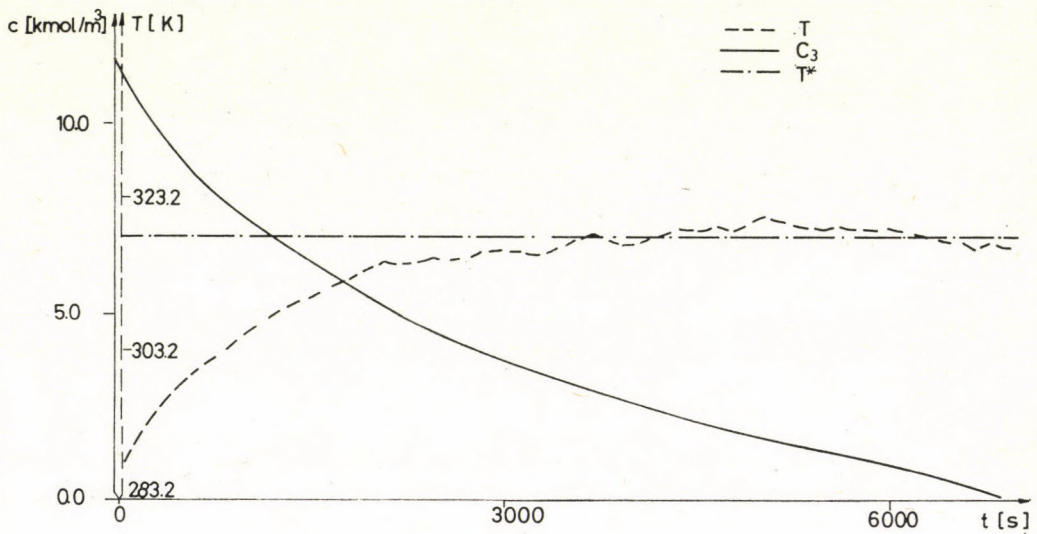

Fig. 1.
The temperature of the reactor (T) and the concentration of the component to be methylized (c_3) for the SSTR

First a sensitivity investigation was carried out according to the previous paragraph. On the basis of these results, the inlet flow rate was chosen as control variable and a noise caused by 20 K fluctuation in the cooling water temperature was in the magnitude of 1 K in the reactor temperature. After this, some preliminary identification investigations were carried out in order to determine the suitable regulator parameters. The PID regulator parameters

were determined from the unit step response functions according to CHIEN, HRONES and RESWICK [2]. It should be noted that this PID regulator tuning mode is not optimal, but is widely used. As the state of the reactor is non-stationary, several unit step response functions were computed using the temperature of a "non-controlled reactor" as a reference value.

The coefficients of a time-varying, discrete, linear, stochastic ÅSTRÖM-type [1] model were also indentified applying an adaptive version of the Second Extended Matrix Method, which can be regarded as an approximate model of the reactor. In this case, the adaptive character of the algorithms was used in order to handle the nonlinearity and nonstationarity of the reactor. The polynomial orders needed for the discrete linear stochastic control algorithms were computed from the results of the model identifications. In some simplified special cases, the polynomial orders can be determined analytically from the physico-chemical model as reported in reference [5].

It is also important to know that all these identification results are valid only in the neighbourhood of the non-controlled reactor trajectory. Thus, as

Table 4.

Comparison of some discrete regulators acting on the SSTR ($\pi = 30$ s; input bounded)

No.	Algorithm	Parameters	$s^2_{(T-T^*)}$ $t>50$	Remarks
1	Without control	—	5.19	
2	P regulator	$K = 1.5 \times 10^{-5}$	0.84	
3	PID regulator	$K = 5.6 \times 10^{-4}$ $T_I/\pi = 54.0$ $T_D/\pi = 0.47$	0,67*	Practically PI regulator *Switched on 50 steps later
4	LS-type self-tuning	$d = 1,\ n = 2,\ m = 1$ $q = 0.99$	0.74	3 estimated regulator coefficients
5	LS-type self-tuning	$d = 1,\ n = 1,\ m = 0$ $q = 0.99$	0.81	1 estimated regulator coefficient
6	LS-type self-tuning	$d = 1,\ n = 1,\ m = 1$ $q = 0.99$	0.68	2 estimated regulator coefficients
7	ELS-type self-tuning	$d = 1,\ na = 1,$ $nb = 0,\ nc = 0,$ $q = 0.99$	0.75	2 estimated coefficients
8	ELS-type self-tuning	$d = 1,\ na = 2,$ $nb = 0,\ nc = 0$	0,58	3 estimated coefficients
9	ELS-type self-tuning	$d = 1,\ na = 2,$ $nb = 1,\ nc = 1,$ $q = 0.99$	0.70	5 estimated coefficents

the controlled reactor will be led to another trajectory, these results have only an informatory character for the controlled case.

In order to compare various discrete linear regulators, simulation investigations were carried out using discrete P and PI regulators with constant parameters and discrete linear stochastic adaptive Least-squares (LS) [8] and Extended-least-squares (ELS) type [9] regulators. In *Table 4*, the parameters of the regulators applied and the empirical standard deviation of the output (T–T^*) beginning with the 50th sample (after $t=1{,}500$ s) are summarized. The discretization time (π) was equal to 30 sec and the input variable (inlet flow rate) was bounded:

$$1.175\times 10^{-4}\ \mathrm{m^3/s} \leq v_B \leq 1.775\times 10^{-4}\ \mathrm{m^3/s}.$$

As shown by the data of *Table 4*, the quality of control in almost all cases is practically the same; i.e., the task performed by simple P or PI regulators is well in the neighbourhood of the temperature T^*.

It is important to note that the bounded input, the relative long initial transient period and a finite operating time disturbed the normal operation of the discrete PID, as well as the adaptive stochastic regulators. Thus, in order to overcome the transient response of the discrete PID regulator on the initial period, it was necessary to switch on this regulator 50 steps later, when the initial period has already ended.

Among the adaptive stochastic regulators the LS-type regulator seems to be better than the ELS-type one for this task and this is the simplest one from computational viewpoint. Their simplest versions (No. 5 or 6) have the advantages of adaptivity and are also rather simple to implement on a microprocessor. The storage needed by the LS-type self-tuning regulator is about 2-times grater than that of a discrete PID algorithm (both cases included the floating point arithmetic routines), and the computation time of the LS algorithm with 1 estimated coefficient (No. 5) is about 4-times, and with 2 estimated coefficients (No. 6) about 10-times greater than that of the PID algorithm on the Z80 microprocessor [6].

Conclusion

The use of the simulation method was shown in several stages of the regulator design process for a stirred tank reactor control.

The sensitivity method is able to provide information about the most effective input variables, the potentional noise sources and the most suitable discretization time in the first stage of the regulator design.

In the last stage, when several regulators have been already selected, it is very useful to make a simulation investigation with them on a detailed model of the chemical reactor. This is extremely important in those cases when the regulator design was performed under hard restriction (bounded input, transient and after near steady state behaviour, and finite operation time), as indicated in the second part of this paper.

Both of the above investigations are rather simple, even in the case of more complicated perfectly stirred chemical control objects and they are rather efficient. But the advantages of this and similar investigations were increased when these simulation possibilities were collected into a consistent simulation

system containing both chemical and control theoretical elements, and this system can be used by chemical and control engineers.

SYMBOLS

$c_i(t)$ concentration of the i-th component (i = 1, 2, 3)
c_i^0 initial values for the concentration
c_{Bi} concentration of the i-th component in the inlet
c_P specific heat of the reaction mixture
c_{PB} specific heat of the inlet mixture
d time lag
E activation energy
F surface of heat exchange
G_R thermal capacity of those parts of the reactor which get warm
H reaction heat
k number of components
k_1, k_2 constants
K_T parameter of heat conductance
K coefficient for the proportional term in the PID regulator
m, n, na, nb, nc polynomial orders
p pre-exponential factor
q exponential forgetting factor
r radius of the reactor
R universal gas constant
$s^2_{(T-T^*)}$ empirical variance of the temperature output $(T - T^*)$
t time
$T(t)$ temperature of the reaction mixture
t_0 initial moment
T^0 initial value for the temperature
T_B temperature of the inlet
T_H temperature of the heating or cooling medium
T_I, T_D parameters of the PID regulator, coefficients for the integral and differentiel terms, resp.
T^* reference value of the reactor temperature
$V(t)$ volume of the reaction mixture
V^0 initial value for the volume
v_B volumetric inlet rate
v_k volumetric outlet rate
z_1, z_2 reaction rates
ϱ density of the reaction mixture
ϱ_B density of the inlet mixture
π discretization time
$\Psi^x_\alpha(t)$ sensitivity function of the variable x with respect to the parameter α

REFERENCES

1. Åström, K. J.: Introduction to the Stochastic Control Theory. Academic Press, New York, 1964.
2. Chien, K. L., Hrones, J. A., and Reswick, J. B.: A.S.M.E., *1952*, 74, 175.
3. Clarke, D. W. and Gawthrop, J.: Proc. IEE, *1979*, 126, 633–640.
4. Hangos, K. M.: Hung. J. Ind. Chem., *1980*, 8, 25–34.
5. Hangos, K.: Investigation of Stirred Tank Reactor Control. Preprints of the CHEMPLANT '80 Symposium, Hévíz, Hungary 1980. pp. 1110–1121.

6. HANGOS, K. M.: Investigation of the Peterka-Type Self-Tuning Regulators by Simulation.
Preprints of the 6th IFAC/IFIP Conference on Digital Computer Application to Process Control held in Düsseldorf, FRG, 1980.
7. ISERMAN, R.: Parameter Adaptive Control Algorithms — A Tutorial. Preprints of the 6th IFAC/IFIP Conference on Digital Computer Application to Process Control held in Düsseldorf, FRG, 1980.
8. PETERKA, V.: Adaptive Digital Regulation of Noisy Systems, IFAC Symposium on Identification, Prague, Czechoslovakia, 1970.
9. ASTRÖM, K. J., and WITTENMARK, B.: Automatica, *1973*, 9, 185–199.
10. PERLMUTTER, D. D.: Stability of chemical reactors. Prentice Hall, Englewood Cliffs, New Jersey, 1974.

РЕЗЮМЕ

В сообщении показаны преимущества симуляционного исследования регулирования сосудов идеального смешения. На двух типовых задачах иллюстрируется выбор наиболее подходящего входного сигнала (input variable), и амплитуды выходного шума (output noise). Для этого применен метод чуствительности (sensitivity method) и установлены дискретные линейные параметры регулирования (discrete linear regulator parameters). С точки зрения качества регуливования сравнены обыкновенные ПИД и дискретные линейные адаптивные стохастические регуляторы (discrete linear stochastic regulators).

HUNGARIAN JOURNAL
OF INDUSTRIAL CHEMISTRY
VESZPRÉM
Vol. 9. pp. 407–416 (1981)

CALCULATION OF ENTHALPY AND ENTROPY OF GASES BY MODIFIED REDLICH–KWONG EQUATION OF STATE

A. Mihajlov*, B. Djordjević and A. Tasić

(Department of Chemical Engineering, Faculty of Technology and Metallurgy, University of Belgrade, 1100 Belgrade, Karnegieva 4, Yugoslavia and *Faculty of Technology, University of Novi Sad, 21000 Novi Sad, Vlejka Vlahovića 2, Yugoslavia)

Recived: November 16. 1981.

Enthalpy and entropy of pure nonpolar, slightly polar and polar gases (carbon monoxide, propylene, hydrogen sulphide and ammonia) were calculated by two different procedures. One of them is based on the original Redlich–Kwong (RK) equation of state and the other on the RK equation with optimal parameters (for each isotherm separately — Ω_{cal}, and as temperature dependent values — Ω_{cor}).

2063 P-v-T data points of 124 isotherms were used to compute enthalpy and entropy of four investigated substances, with respect to the ideal gas reference state. Values of the properties, calculated by two procedures, were compared with experimental and smoothed results.

Introduction

Reliable thermodynamic properties of fluids are necessary for the appropriate design and rational operation of chemical processes. Since these data are not often readily available, especially for polar substances, considerable effort has been expended to increase the accuracy of the methods used for their analytical prediction.

Values of enthalpy and entropy are used in making equilibrium calculations and heat balances in reactors, separation equipment, heat exchangers, and power cycles, etc. These thermodynamic properties are becoming of increasing interest in geothermal, coal and other related technology. In this sense, the development of predictive methods for the properties mentioned above is of particular significance. The use of an equation of state, among which Redlich–Kwong's and their modifications represent a very popular two-parameter model, is one of the most suitable approaches.

In previous papers the capability of the Redlich–Kwong (RK) equation of state for correlating and predicting the thermodynamic properties was

demonstrated, such as compressibility factors [1, 2], heat capacities [3, 4] and second virial coefficients [5] of various substances using optimal values of the constants obtained for each available isotherm of P-v-T data. In this work the study of evaluation of thermodynamic properties is continued and attention is focused on the calculation of enthalpy and entropy of some nonpolar, slightly polar and polar gases.

Data reduction

The ability of the RK equation to predict volumetric, phase equilibrium and other properties was considered [7–10].

The RK equation of state (6) is as follows:

$$Z=\frac{v}{v-b}-\frac{a}{RT^{1.5}(v+b)} \tag{1}$$

where the constants a and b are related to the critical proterties by:

$$a=\Omega_a R^2 T_c^{2.5}/P_c \tag{2}$$

$$b=\Omega_b RT_c/P_c \tag{3}$$

REDLICH and KWONG recommended two universal dimensionless constants for Ω_a and Ω_b which are valid for all temperatures and pressures. For the conditions of critical point $(\partial P/\partial v)_{Tc}=(\partial^2 P/\partial v^2)_{Tc}=0$ they obtained $\Omega_a=0.4275$ and $\Omega_b=0.08664$. However, it is now generally accepted that these parameters are temperature dependent and vary from substances to substances.

The method used in this study was proposed previously [1–3] as follows. Parameters Ω_a and Ω_b of RK equation were determined from P-v-T data of gases at each available isotherm separately (Ω_{cal}). For each temperature, the optimal values of these dimensionless parameters were found. The NEWTON–RAPHSON procedure [11] was used to minimize the objective function F defined by:

$$F=\sum_{i=1}^{n}(Z_{exp}-Z_{cal})_i^2 \tag{4}$$

where Z_{exp} stands for the values of factor compressibility obtained from P-v-T data, and Z_{cal} stands for the right hand side of Eq. (1). As shown in the cited articles, in all cases the proposed method was to be preferred to the results of other applied modifications of RK equation.

Enthalpy and entropy of investigated gases were evaluated by two different procedures. One of them was based on the original RK equation with constants which require the critical data of compounds (Eq. 2 and 3) and the other one with optimal parameters for each available isotherm. Enthalpy and entropy were estimated according to the original RK equation by:

$$H_{RK}=H_0+\frac{1.5a}{T^{0.5}b}\ln\frac{v}{v+b}+RTZ+\frac{1.5a}{T^{0.5}b}\ln\frac{v_0+b}{v_0}-RTZ_0 \tag{5}$$

$$S_{RK}=S_0+R\ln\frac{v-b}{v_0-b}+\frac{0.5a}{T^{1.5}b}\ln\frac{v(v_0+b)}{v_0(v+b)} \tag{6}$$

Enthalpy and entropy obtained with optimal parameters were calculated by:

$$H = H_{RK} + FH$$
$$S = S_{RK} + FS \tag{7}$$

where FH and FS are as follows:

$$FH = -RT^2(\partial b/\partial T)\left(\frac{1}{v-b}-\frac{1}{v_0-b}\right)-\frac{T^{0.5}}{b}\,(\partial a/\partial T)\,\ln\frac{v(v_0+b)}{v_0(v+b)}+$$
$$+\frac{aT^{0.5}}{b^2}\,(\partial b/\partial T)\left(\ln\frac{v(v_0+b)}{v_0(v+b)}+\frac{b}{v+b}-\frac{b}{v_0+b}\right) \tag{9}$$

$$FS = -RT(\partial b/\partial T\left(\frac{1}{v-b}-\frac{1}{v_0-b}\right)-\frac{1}{bT^{0.5}}\,(\partial a/\partial T)\,\ln\frac{v(v_0+b)}{v_0(v+b)}+$$
$$+\frac{a}{b^2T^{0.5}}\,(\partial b/\partial T)\left(\ln\frac{v(v_0+b)}{v_0(v+b)}+\frac{b}{v+b}-\frac{b}{v_0+b}\right) \tag{10}$$

In these expressions, H_0 and S_0 are given with respect to the ideal gas reference state. To calculate H and S by means of the modified method, the parameters Ω_a and Ω_b were considered two way: as established values at available isothermal conditions — for each isotherm separately (Ω_{ca_i}), and as temperature dependent parameters given by corresponding temperature correlations (Ω_{cor}).

The functions Ω_{cor} depend on $T_R(T_R = T/T_c)$. For each gas individually, in therms of two ranges of temperature ($T_R < 1$ and $T_R \geq 1$), the following empirical fitting of Ω_{cor} applied on the Ω_a and Ω_b:*

$$\Omega = C_0T_R + C_1T_R^2 + C_2T_R^3 + C_3T_R^6 \tag{11}$$

$$\Omega = C_0 + (C_1/T_R) + (C_2/T_R^2) + (C_3/T_R^3) \tag{12}$$

$$\Omega = \frac{C_0}{T_R}+\frac{C_1}{T_R^2}+\frac{C_2}{T_R^3}+\frac{C_3}{T_R^6} \tag{13}$$

$$\Omega = C_0+\frac{C_1}{1-T_R}+\frac{C_2}{(1-T_R)^2}+\frac{C_3}{(1-T_R)^3} \tag{14}$$

$$\Omega = C_0 + C_1(1-T_R) + C_2(1-T_R)^{1/3} + C_3(1-T_R)^{2/3} \tag{15}$$

$$\Omega = C_0 + C_1\left(1-\frac{1}{T_R}\right) + C_2\left(1-\frac{1}{T_R}\right)^{1/3} + C_3\left(1-\frac{1}{T_R}\right)^{2/3} \tag{16}$$

$$\Omega = T_R^{1.5}\left(\frac{C_0}{T_R}+\frac{C_1}{T_R^2}+\frac{C_2}{T_R^3}+\frac{C_3}{T_R^6}\right) \tag{17}$$

The coefficients C_0, C_1, C_2 and C_3 were determined by means of the least squares method. For tested gases: carbon monoxide, propylene, hydrogen sulphide and ammonia their values are listed in *Table 1*. The *P-v-T* data are collected from literature [12–15].

* In this consideration, the following correlations are included for comparison purposes: $\Omega = C_0 + C_1T_R + C_2T_R^2 + C_3T_R^3$ and $\Omega = C_0(1-T_R) + C_1(1-T_R)^2 + C_2(1-T_R)^3 + C_3(1-T_R)^6$. However, in all cases these relations did not give satisfactory results.

Table 1.

Coefficients of equations (11) – (17)

SUBSTANCE	$T_R<1$				$T_R \geq 1$			
	Ω_a		Ω_b		Ω_a		Ω_b	
	$s^{(a)}$	$C_j^{(c)}$	$s^{(a)}$	$C_j^{(c)}$	$s^{(a)}$	$C_j^{(c)}$	$s^{(a)}$	$C_j^{(c)}$
Carbon-monoxide	(15)[b]	0.428 191	(14)	0.084 702 25	(13)	– 1.190 624	(16)	0.086 732 32
		5.684 563		0.002 556 05		6.414 374		– 0.044 792 46
	0.21×10^{-2}	1.943 668	0.41×10^{-6}	– 0.000 821 6	0.54×10^{-4}	– 5.917 375	0.41×10^{-6}	– 0.041 359 11
		– 6.486 775		0.000 072 7		1.123 073		0.088 609 38
Propylene	(16)	– 6.524 891	(13)	– 1.413 908	(16)	– 6.524 891	(12)	0.093 057 86
		24.491 15		2.281 383		24.491 15		0.000 434 66
	0.25×10^{-2}	– 21.101 12	0.83×10^{-2}	– 0.773 392 6	0.61×10^{-3}	– 21.101 12	0.15×10^{-4}	0.000 015 626
		3.566 014		– 0.029 555 1		3.566 014		0.000 000 07
Hydrogen sulphide	(17)	6.392 852	(13)	3.869 417	(12)	2.579 578	(14)	0.086 686 5
	0.43×10^{-3}	– 13.652 54	0.13×10^{-2}	– 8.751 409	0.28×10^{-2}	– 9.059 434	0.54×10^{-8}	0.000 005 2
		8.175 424		5.335 808		13.143 69		0.000 002 37
		– 0.495 5399		– 0.373 809 8		– 6.248 141		0.000 000 14
Ammonia	(11)	28.268 77	(14)	0.090 129 47	(16)	0.427 8759	(16)	0.086 641 71
	0.49×10^{-3}	– 77.014 49	0.58×10^{-3}	– 0.005 647 11	0.19×10^{-4}	– 0.695 8895	0.11×10^{-6}	– 0.151 073 1
		57.153 91		0.000 503 18		– 0.422 5502		– 0.116 093 8
		– 7.974 042		– 0.000 005 8		0.930 0377		0.234 312 6

$(a) = \sum_{i=1}^{n} (\Omega_{cal} - \Omega_{cor})_i^2$, (b) = all brackets refer to the correlation equations (11) ÷ (17), $(c) = C$, $j = 0, 1, 2, 3$ coefficients of equations (11) – (17)

Table 2.

Mean absolute deviation in enthalpy and entropy for four investigated gases

Substance	μ (debyes)	Number of data points	Number of isotherms	Ref.	T_R		$\delta H(\%)$					$\delta S(\%)$				
					min	max	RK	SB	ChAR	RK (Ω_{cal})	RK (Ω_{cor})	RK	SB	ChAR	RK (Ω_{cal})	RK (Ω_{cor})
Carbonmonoxide	0,10	496	22	12	0.62	5.06	0.56	1.3	1.3	1.296	1.182	0.61	0.60	0.61	0.554	0.562
Propylene	0.35	737	50	13	0.91	1.43	0.48	0.49	0.51	0.486	0.492	0.20	0.23	0.29	0.213	0.306
Hydrogen sulphide	0.93	436	58	14.15	0.92	2.62	0.67	0.77	0.89	0.982	0.988	0.23	0.24	0.49	0.591	0.583
Ammonia	1.46	493	14	12	0.74	1.43	3.6	3.3	3.6	3.467	2.110	1.5	0.91	1.5	0.908	0.917

Results and discussion

The Ω_{cal} and Ω_{cor} were used to evaluate the enthalpy and entropy. The calculated results were compared with the original RK equation, where constants a and b were treated as universal values. The results for gases mentioned above are summarized in *Table 2*. In addition to these treatments, the SIMONET and BEHAR [16] and CHAUDRON, ASSELINEAU and RENON [17] modifications were also included in the analysis. All comparisons in this *Table* were realized for the same arbitrarily selected isotherms of volumetric and enthalpy and entropy data.

Table 2 indicates that all procedures give good agreement between the calculated and observed values of enthalpy and entropy. Howeveer, as indicated in the previous paper [1], factor compressibilities of some substances calculated by the original RK, SB and ChAR equations were considerably worse than those obtained by this method. Consequently these poor results were not reflected in the enthalpy and entropy calculations. Total mean absolute percentage deviation between calulated and experimental results was 1.14 and 0.56 for enthalpy and entropy respectively, when original RK parameters were used. When the properties were calculated employing optimal RK parameters (Ω_{cal}), the corresponding deviations for enthalpy and entropy were 1.16 and 0.51. Deviations for enthalpy and entropy using Ω_{cor} were 1.07 and 0.51 respectively. In the case of the SB and ChAR equations, the errors in H were

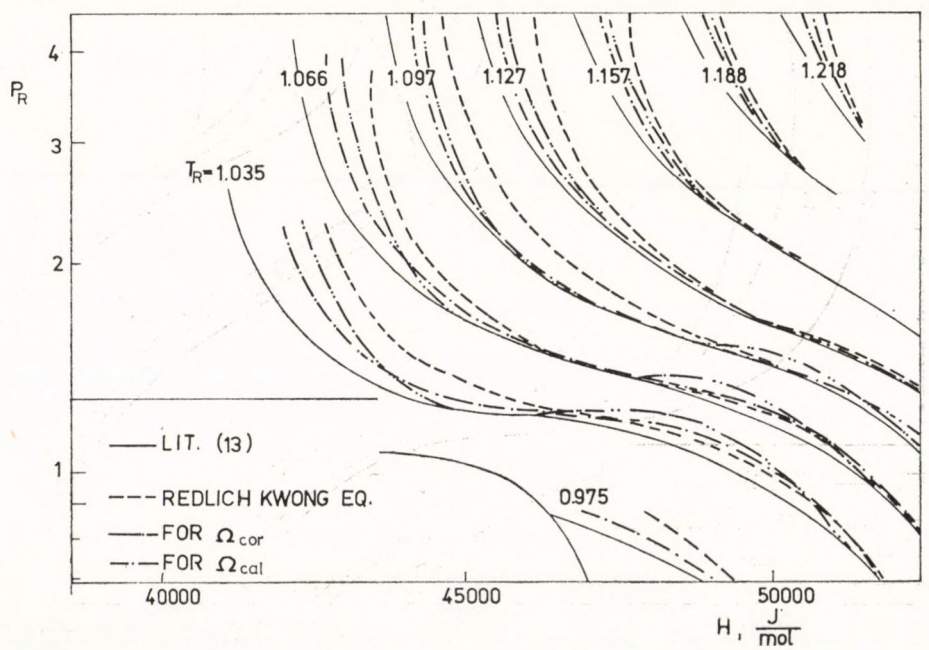

Fig. 1.

Enthalpy of Propylene. ——— denotes literature values [13]

1.46% and 1.56% respectively. Deviations for S were 0.50% and 0.73%, respectively.

In order to illustrate the validity of the proposed methods the predicted values of enthalpy and entropy are graphically given in *Fig. 1–3.*

From the results obtained for enthalpy and entropy of nonpolar and slightly polar gases, it could be concluded that this method does not improve its

Table 3.

Absolute deviation in enthalpy and entropy for isotherms in the vicinity of the critical point up to $P_{R_{max}}$

Substance[a]	T_R	$P_{R_{max}}$	δH(%)		δS(%)	
			RK	RK (Ω_{cal})	RK	RK (Ω_{cal})
Carbon monoxide	1.002	5.794	6.212	1.206	0.537	0.967
Propylene	1.035	2.643	2.940	2.281	0.711	0.964
Ammonia	0.995	1.714	47.664	6.775	3.701	2.702

(a) Available pressure of Hydrogen sulphide is not sufficiently high.

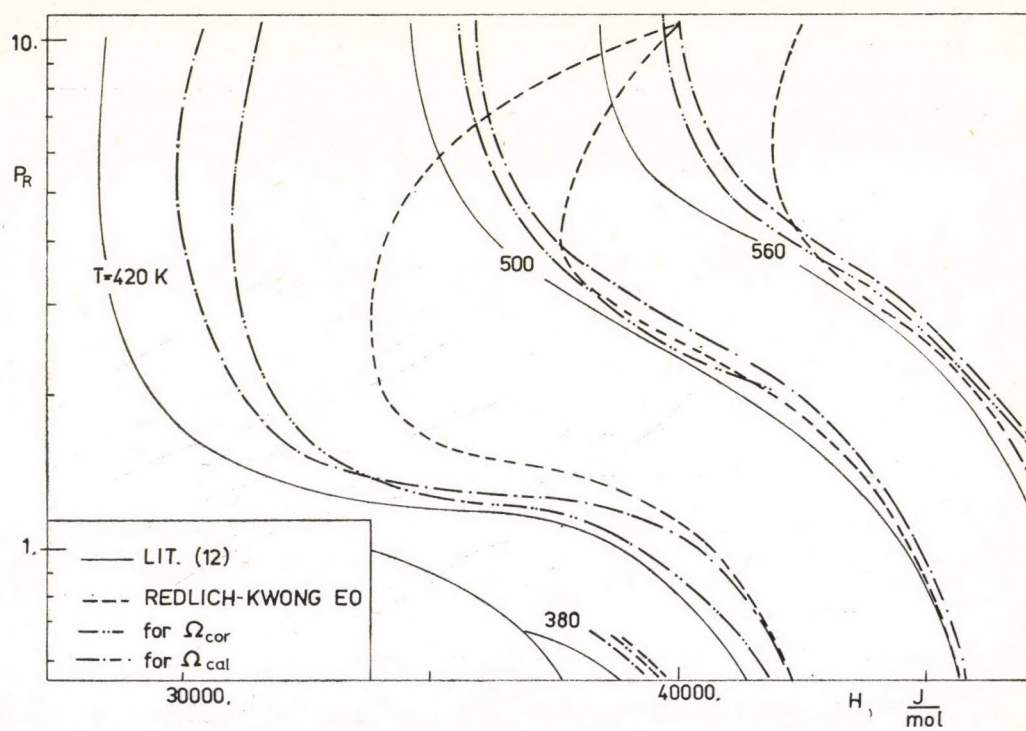

Fig. 2.

Enthalpy of Ammonia. ——— denotes literature values [12]

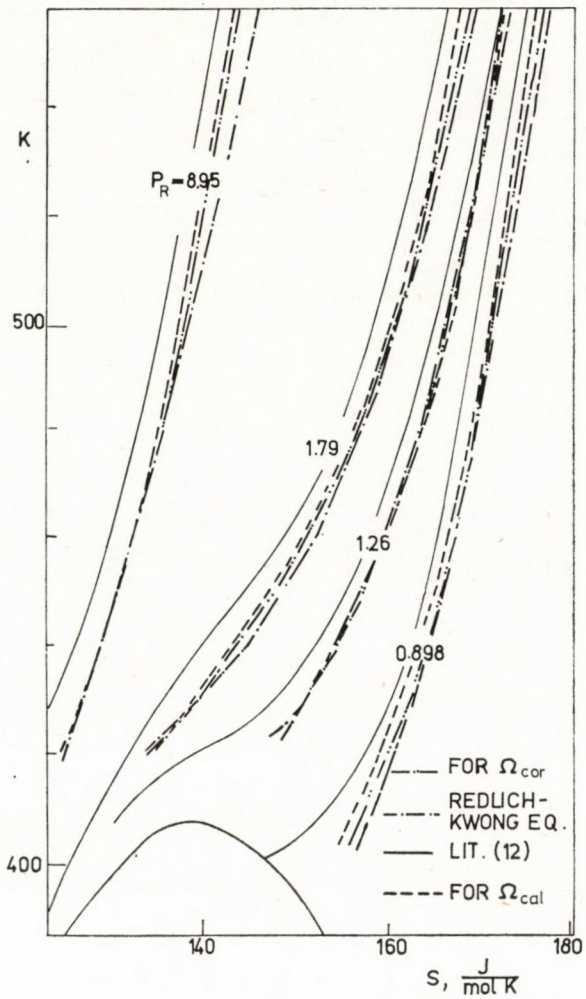

Fig. 3.

Entropy of Ammonia. ——— denotes literature values [12]

capability over the original form of RK equation. The exception is ammonia which is a polar compound.

Although the calculated results for enthalpy are not represented in detail, from *Table 3* it can be noticed that this procedure with calculated parameters (Ω_{cal}) is preferred to the results of the original RK equation at high pressures and in the critical, very sensitive region. When the calculated entropy, obtained on the basis of Ω_{cal} values, were compared with those evaluated by the original RK equation, the results were comparable and satisfactory.

On the other hand, when this procedure with correlated parameters (Ω_{cor}) was applied to the temperature in the vicinity of the critical point, in some

cases (for CO, $T_R = 0.926$ and 1.002 and for NH_3, $T_R = 0.986$) the results obtained indicated that the derivatives of the dimensionless parameters with respect to temperature were too sensitive for the evaluation of enthalpy and entropy. For this reason, these isotherms were excluded from consideration.

Conclusions

The REDLICH–KWONG equation of state is suitable for enthalpy and entropy calculations of nonpolar, slightly polar and polar gases, regardless of whether original or modified form with optimal temperature dependent parameters are applied. However, for a highly polar compound, such as ammonia, better results are obtained with the modified form.

The procedure used in this work for correlation equations of the dimensionless parameter Ω_a and Ω_b in function of T_R produces only a small loss of accuracy in the calculation of thermodynamic properties mentioned above.

ACKNOWLEDGMENT

This work was supported by a grant from the Scientific Research Fund of the SR Serbia and the Faculty of Technology and Metallurgy, Belgrade.

SYMBOLS

a, b parameters of REDLICH–KWONG equation of state
C_0, C_1, C_2, C_3 coefficients of Equations (11)—(17)
F objective function
H enthalpy
n number of data points
P pressure
R universal gas constant
S entropy
T temperature
v molar volume
Z compressibility factor

Greek symbols

Ω_a, Ω_b — dimensionless parameters of the REDLICH-KWONG equation

Subscripts

c critical property
o property given with respect to the ideal gas reference state
R reduced property
RK proparty given with respect to the original REDLICH–KWONG equation of state

REFERENCES

1. DJORDJEVIĆ, B. D., MIHAJLOV, A. N., GROZDANIĆ, D. K. TASIĆ, A. Ž. and HORVATH, A. L.: Chem. Eng. Sci., *1977*, 32, 1103.
2. MIHAJLOV, A. N.: Evaluation on Modified Constants in the Redlich–Kwong Equation of State. Correlation of P-v-T Data of Pure Nonpolar and Polar Gases. M.S. thesis, Faculty of Technology and Metallurgy, University of Beograd, 1977.
3. DJORDJEVIĆ, B. D., MIHAJLOV-DUDUKOVIĆ, A. N. and TASIĆ, A. Ž.: Chem. Eng. Sci., *1980*, 35, 752.

4. Djordjević, B. D., Mihajlov-Đuduković, A. N., Jovanović, S. DJ. and Tasić, A. Ž.: Applicability of the RK Equation of State with Temperature Dependent Parameters to the Evaluation of Heat Capacity of Gaseous Ammonia and Carbon Monoxide, 2nd Yugoslav–Italian–Austrian Chemical Engineering Conference, Bled (Yugoslavia), 1980. Proc. Symp., u. 29–35.
5. Djordjević, B. D., Mihajlov-Đuduković, A. N. and Tasić, A. Ž.: A.I.Ch.E. Journal, *1980*, 26, 858.
6. Redlich, O. and Kwong, J. N. S.: Chem. Rev., *1949*, 44, 233.
7. Djordjević, B. D., Mihajlov, A. N., Grozdanić, D. K., Tasić, A. Ž. and Malić, D.: Chem. Ind (Beograd), *1975*, 29, 291.
8. Tsonopoulos, C. and Prausnitz, J. M.: Cryogenics, *1969*, 9, 315.
9. Horvath, A. L.: Chem. Eng. Sci., *1974*, 29, 1334.
10. Mihajlov-Đuduković, A. N., Djordjević, B. D. and Tasić, A. Ž.: Calculations of the Thermodynamic Properties of Real Gases and Liquids by Modified RK Equation of State, Advances in Separation Science, Trieste (Italy), 1978. Proc. Symp., p. 200–209.
11. Rosenbrock, H. H. and Storey, C.: Computational Techniques for Chemical Engineers. Pergamon Press, Oxford. 1966.
12. Din, F.: Thermodynamic Functions of Gases, Butterworths, London. 1956.
13. Vaughan, W. E., Graves, N. R.: Ind. Eng. Chem., *1940*, 32, 1252.
14. Reamer, H. T., Sage, B. H. and Lacey, W. N.: Ind. Ent. Chem., *1950*, 42, 140.
15. West, J. R.: Chem. Eng. Progr., *1948*, 44, 287.
16. Simonet, R. and Behar, E.: Chem. Eng. Sci., *1976*, 31, 37.
17. Chaudron, J. Asselineau, L. and Renon, H.: Chem. Eng. Sci., *1972*, 38, 839.

РЕЗЮМЕ

В сообщении описаны различные методы расчета энтальпии и энтропии чисто неполярных менее пплярных и полярных газов/двуокись углерода, пропилен, сереводород и аммония). Первый метод основан на оригинальном уравнении состояния РЕДЛИХА—КВОНГ-а (РК), а второй метод на уравнении РК с оптимальными параметрами/значения-Ω_{cal} для всех изотерм, а значения-Ω_{cor} зависящие от температуры).

Для расчета энтальпии и энтропии четырех исследованных газов использованы 2063 p-V-T данных 124 изотерм.

HUNGARIAN JOURNAL
OF INDUSTRIAL CHEMISTRY
VESZPRÉM
Vol. 9. pp. 417-425 (1981)

BIOCIDES FROM HALOGENATED BENZENES. I.

SOME NEW SUBSTITUTED ANALIDES OF DICHLOROBENZENE SULPHONIC ACIDS AND THEIR BIOCIDAL ACTIVITIES

A. Marei,* M. M. A. El-Sukkary,** F. I. El-Dib**
and O. H. El-Sayed***

(* Chem. Dept., Riyadh University, Riyadh, Saudi Arabia,
** Petrochem. Dept., Petroleum Research Institute, Cairo, Egypt.
and *** Chem. of Microorganisms Lab., National Research
Centre, Cairo, Egypt.)

Received: November 24. 1981.

Six different substituted anilides from every dichlorobenzene sulphonyl chloride isomer were prepared and their bactericidal and fungicidal activities were screened. The relation between their toxicity and their chemical structure was investigated.

Introduction

It was established that toxicity to bacteria and fungi can result from two aryl groups linked by —SO_2—NH— bridge [1–3]. In the present investigation, it was planned to synthesize a number of such compounds, to screen their toxicity towards microorganisms and to study their variation with the chemical structure.

Experimental

Preparation of 2,3-dichlorobenzene sulphonyl chloride

2,3-Dichloronitrobenzene was prepared according to [4, 5]. It was reduced to 2,3-dichloroaniline [6] which was diazotized and its diazonium compound was treated with a saturated solution of SO_2 in glacial acetic acid containing $CuCl_2$ [7] to produce the title compound, b.p. 124 °C/15 mm Hg, n_D^{20} 1.5919.
$C_6H_3O_2Cl_3S$, Calculated: C 29.35; H 1.23; Cl 43.32; S 13.06
Found: C 30.05; H 1.11; Cl 43.71; S 13.12
IR absorption: (wave length im cm^{-1}) 1,460 for 1,2,3-trisubstituted aromatic nucleus, 840 for C—Cl, 1,185 and 1,360 for SO_2—Cl.

Preparation of 3,4-,2,5 and 2,4-dichlorobenzene sulphonyl chlorides

These were prepared as in [8]. The starting materials (*a*), solvent (*b*), reaction temp. and time (*c* & *d*) and the products (*e*) are:

(a)	*(b)*	*(c)*	*(d)*	*(e)*
1,2-dichlorobenzene	$CHCl_3$	180 °C	16 hrs	3,4-dichlorobenzene sulphonylchloride
1,4-dichlorobenzene	$CHCl_3$	150 °C	1 hrs	2,5-dichlorobenzene sulphonylchloride
1,3-dichlorobenzene	$CHCl_3$	18 °C	4 hrs	2,4-dichlorobenzene sulphonylchloride

Preparation of 2,6-dichlorobenzene sulphonylchloride

2,6-Dichloroaniline was prepared from sulphanilamide according to [9]. It was then diazotized and converted into 2,6-dichlorobenzene sulphonyl chloride as given in [7].

Preparation of 3,5-dichlorobenzene sulphonyl chloride

3,5-dichlorobenzene sulphonamide was prepared according to [7] and on treating with $ClSO_3H$ and $SOCl_2$, 3,5-dichlorobenzene sulphonyl chloride was obtained.

Preparation of N-substituted dichlorobenzene sulphonamides

Equimolecular amounts (0.05 mol.) of each dichlorobenzene sulphonyl chloride isomer and the used amine (*o*, *m*, *p*-anisidenes, *o*, *m*, *p*-phenetedines) were mixed and heated with vigorous stirring at 60–70 °C; NaOH solution (0.05 mol., 0.7 N) was then added dropwise over a period of $^1/_2$ hour. Heating and stirring were continued for a further $^1/_2$ hour. On cooling, a solid product separated, it was filtered, washed with dilute HCL and with water, dried and finally crystallized from aqueous ethanol, *Tables 1–6.*

Antibacterial and antifungal activities of the prepared compounds

The cup-plate method (10) was adopted with some modification:

a) The spore suspension of the test organism was prepared in inoculating flasks; each contained 50 ml of sporulating medium of the following composition (g/l): peptone, 3.0, meat extract, 3.0 and distilled water 1,000 ml.
The flasks were incubated for 6 days at 30 °C on a rotary shaker, then pasteurized at 80 °C for 10 minutes, this can be used for any spore forming bacteria, but in the case of nonsporulating bacteria, this technique can also be allowed without pasteurization after the sixth day of incubation.

b) A solid medium containing the following ingredients (g/l); peptone 6.0; yeast extract 3.0; meat extract 1.5; glucose 1.0; and agar 15.0 was sterilized and divided while hot (50–60 °C) in 15 ml portions among sterile petri-dishes of 9 cm diameter.

c) One ml of the spore suspension was placed on the surface of the cold solid medium in the petri-dishes and spread over the surface.

Table 1.

No. of comp.	Nomenclature	M.P. °C
I_1	*N-o*-anisyl-2,4-dichloro-benzene sulphonamide	122-3
I_2	*N-m*-anisyl-2,3-dichloro-benzene sulphonamide	133-4
I_3	*N-p*-anisyl-2,3-dichloro-benzene sulphonamide	145-6
I_4	*N-o*-phenetyl-2,3-dichloro-benzene sulphonamide	124-5
I_5	*N-m*-phenetyl-2,3-dichloro-benzene sulphonamide	120-1
I_6	*N-p*-phenetyl-2,3-dichloro-benzene sulphonamide	118-9

Table 2.

No. of comp.	Momenclature	M.P. °C
II_1	*N-o*-anisyl-3,4-dichloro-benzene sulphonamide	94-5
II_2	*N-m*-anisyl-3,4-dichloro-benzene sulphonamide	164-5
II_3	*N-p*-anisyl-3,4-dichloro-benzene sulphonamide	87-8
II_4	*N-o*-phenetyl-3,4-dichloro-benzene sulhponamide	82-3
II_5	*N-m*-phenetyl-3,4-dichloro-benzene sulphonamide	72-3
II_6	*N-p*-phenetyl-3,4-dichloro-benzene sulphonamide	110-1

Table 3.

No. of comp.	Nomenclature	M.P. °C
III_1	*N-o*-anisyl-2,5-dichloro-benzene sulphonamide	111-2
III_2	*N-m*-anisyl-2,5-dichloro-benzene sulphonamide	110-1
III_3	*N-p*-anisyl-2,5-dichloro-benzene sulphonamide	96-7
III_4	*N-o*-phenetyl-2,5-dichloro-benzne sulphonamide	136-7
III_5	*N-m*-phenetyl-2,5-dichloro-benzene sulphonamide	128-9
III_6	*N-p*-phenetyl-2,5-dichloro-benzene sulphonamide	109-10

Table 4.

No. of comp.	Nomenclature	M.P. °C
IV_1	*N-o*-anisyl-2,4-dichloro-benzene sulphonamide	112-3
IV_2	*N-m*-anisyl-2,4-dichloro-benzene sulphonamide	111-2
IV_3	*N-p*-anisyl-2,4-dichloro-benzene sulphonamide	98
IV_4	*N-o*-phenetyl-2,4-dichloro-benzene sulphonamide	137
IV_5	*N-m*-phenetyl-2,4-dichloro-benzene sulphonamide	129
IV_6	*N-p*-phenetyl-2,4-dichloro-benzene sulphonamide	110-11

Table 5.

No. of comp.	Nomenclature	M.P. °C
V_1	*N-o*-anisyl-2,6-dichloro-benzene sulphonamide	145-6
V_2	*N-m*-anisyl-2,6-dichloro-benzene sulphonamide	118-9
V_3	*N-p*-anisyl-2,6-dichloro-benzene sulphonamide	116-7
V_4	*N-o*-phenetyl-2,6-dichloro-benzene sulphonamide	97-8
V_5	*N-m*-phenetyl-2,6-dichloro-benzene sulphonamide	134-5
V_6	*N-p*-phenetyl-2,6-dichloro-benzene sulphonamide	106-7

Table 6.

No. of comp.	Nomenclature	M.P. °C
VI_1	*N-o*-anisyl-3,5-dichloro-benzene sulphonamide	77-8
VI_2	*N-m*-anisyl-3,5-dichloro-benzene sulphonamide	121-2
VI_3	*N-p*-anisyl-3,5-dichloro-benzene sulphonamide	78-9
VI_4	*N-o*-phenetyl-3,5-dichloro-benzene sulphonamide	102-3
VI_5	*N-m*-phenetyl-3,5-dichloro-benzene sulphonamide	117-8
VI_6	*N-p*-phenetyl-3,5-dichloro-benzene sulphonamide	149-50

d) The test substances were dissolved in a few drops of acetone, then completed to the appropriate volume with distilled water to make colloidal suspensions of different concentrations which were 50, 100, 200, 500, 1,000 and 2,000 μg/ml.

e) In a petri-dish containing the culture of one of the chosen microorganisms seven small pits were made in positions widely separated from each other. These were marked on the bottom of the dish. One of these pits was filled with acetone and water mixture as a blank test and the other pits were filled with the solutions of the test substances with different concentrations. The petri-dishes were incubated at 5 °C for 1–2 hours to permit good diffusion and then trasferred to an incubator at 28 °C for 4–8 hours. Methylene blue was added to the medium before solidification to give more definite and restricted zones. The inhibition zone is transparent blue, in contrast to the background, which is opaque due to the thin or thick growth of the organism. The zone of inhibition was well defined and the margin between it and the bacterial growth was sharp, allowing easy measuring of the diameter.

The activity of each of the prepared substances against four microorganisms representing gram + ve and − ve bacteria, fungus and yeast (Bacillus subtilis, Escherichia coli, Aspergillus niger and Candida albicans respectively) was first investigated. The activity of the test substances at different concentrations towards any test organism was expressed as follows:

+ + +	at concentration of	50	μg/ml
+ +	at concentration of	100 − 500	μg/ml
+	at concentration of	1,000 − 2,000	μg/ml

If no activity was noticed with a solution of 2,000 μg/ml concentration, the substance was considered inactive and this inactivity was expressed with −. The substances with activity of the order + + + or + + towards any of these four organisms (Tables 7–10) were then screened with the other six species of bacteria and yeast in the same manner *(Tables 11–16)*.

Discussion

The six isomers of dichlorobenzene sulphonyl chlorides were prepared. Each sulphonyl chloride was converted to six anilides with the following structure:

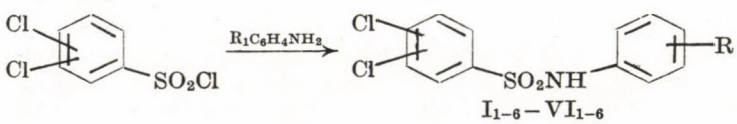

$I_{1-6} - VI_{1-6}$

R_1 = *o*- or *m*- or *p*-OMe; *o*- or *m*- or *p*-OEt

The chemical structure of the prepared new compounds was elucidated by microanalysis and infrared light absorption measurement. The compounds which have analogous structure, absorbed this light at nearly the same wave lengths. The following results were obtained from some compounds which can be considered as representatives of their classes in the present work.

Table 7.

Position of Cl_2	Toxicity to B. subtilis					
	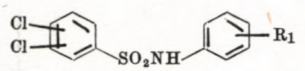					
	R_1=					
	o-OMe 1	*m*-OMe 2	*p*-OMe 3	*o*-OEt 4	*m*-OEt 5	*p*-OEt 6
2.3- I	–	–	–	–	–	–
3.4- II	–	–	+++	+	+++	–
2.5- III	–	–	+	–	–	–
2.4- IV	–	+	–	–	–	–
2.6- V	–	–	–	–	–	–
3.5- VI	–	++	+	–	+++	–

Table 8.

Position of Cl_2	Toxicity to Escherichia coli					
	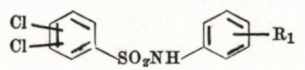					
	R_1=					
	o-OMe 1	*m*-OMe 2	*p*-OMe 3	*o*-OEt 4	*m*-OEt 5	*p*-OEt 6
2.3- I	–	–	–	–	–	–
3.4- II	–	–	–	–	–	–
2.5- III	–	–	–	–	–	–
2.4- IV	–	–	–	–	–	–
2.6- V	++	–	–	–	–	–
3.5- VI	–	–	+	–	++	–

Table 9.

Position of Cl_2	Toxicity to Aspergillus niger					
	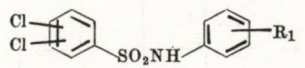					
	R_1=					
	o-OMe 1	*m*-OMe 2	*p*-OMe 3	*o*-OEt 4	*m*-OEt 5	*p*-OEt 6
2.3- I	–	–	–	–	–	–
3.4- II	–	–	–	–	–	–
2.5- III	–	–	–	–	–	–
2.4- IV	–	–	–	–	–	–
2.6- V	–	–	–	–	–	–
3.5- VI	–	–	–	–	+	–

a) The Table indicates that Cl_2 is active in the positions 3,4- & 3,5-.

b) Comparison of VI2 with VI5 shows *m*-OEt > *m*-OMe inactivity.

These two tables show that Cl_2 is inactive in all positions.

Table 10.

Position of Cl_2	Toxicity to Candida albicans 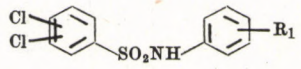 R_1=					
	o-OMe 1	*m*-OMe 2	*p*-OMe 3	*o*-OEt 4	*m*-OEt 5	*p*-OEt 6
2.3- I	–	–	–	–	–	–
3.4- II	–	–	–	–	–	–
2.5- III	–	–	–	–	–	–
2.4- IV	–	–	–	–	–	–
2.6- V	–	–	–	–	–	–
3.5- VI	–	–	–	–	–	–

All compounds were found non-toxic to this organism.

Table 11.

Position of Cl_2	Toxicity to Bacillus cereus 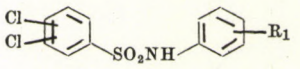 R_1=					
	o-OMe 1	*m*-OMe 2	*p*-OMe 3	*o*-OEt 4	*m*-OEt 5	*p*-OEt 6
2.3- I						
3.4- II			+++		+++	
2.5- III						
2.4- IV						
2.6- V	–					
3.5- VI		++			+++	

Table 12.

Position of Cl_2	Toxicity to Micrococcus sp. 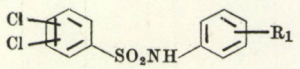 R_1=					
	o-OMe 1	*m*-OMe 2	*p*-OMe 3	*o*-OEt 4	*m*-OEt 5	*p*-OEt 6
2.3- I						
3.4- II			+++		++	
2.5- III						
2.4- IV						
2.6- V	++					
3.5- VI		++			+++	

From these two Tables it can be seen that

a) Cl_2 is active in positions 3,4- and 3,5-
b) Vi_2 and Vi_5 show *m*-OEt > *m*-OMe inactivity.

Table 13.

Position of Cl_2	Toxicity to Salmonella sp.					
	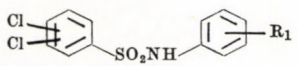					
	R_1=					
	o-OMe 1	*m*-OMe 2	*p*-OMe 3	*o*-OEt 4	*m*-OEt 5	*p*-OEt 6
2.3- I						
3.4- II			+++		+++	
2.5- III						
2.4- IV						
2.6- V	–					
3.5- VI		+++			+++	

Cl_2 is active in the positions 3,4- and 3,5-.

Table 14.

Position of Cl_2	Toxicity to Sarcine sp.					
	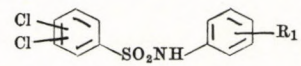					
	R_1=					
	o-OMe 1	*m*-OMe 2	*p*-OMe 3	*o*-OEt 4	*m*-OEt 5	*p*-OEt 6
2.3- I						
3.4- II			+++		+++	
2.5- III						
2.4- IV						
2.6- V	–					
3.5- VI		–			–	

Table 15.

Position of Cl_2	Toxicity to Staphylococcus aureus					
	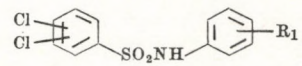					
	R_1=					
	o-OMe 1	*m*-OMe 2	*p*-OMe 3	*o*-OEt 4	*m*-OEt 5	*p*-OEt 6
2.3- I						
3.4- II			+++		+++	
2.5- III						
2.4- IV						
2.6- V	+					
3.5- VI		–			++	

These two Tables indicate that Cl_2 is active in the position 3,4- only.

Table 16.

Position of Cl_2	Toxicity to Saccharomyces cerevisiae 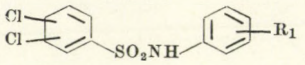 R_1=					
	o-OMe 1	*m*-OMe 2	*p*-OMe 3	*o*-OEt 4	*p*-OEt 5	*p*-OEt 6
2.3- I						
3.4- II			+++		+++	
2.5- III						
2.4- IV						
2.6- V	++					
3.5- VI		++			++	

Cl_2 is active in the position 3,4-.

N-p-anisyl and N-p-phenetyl dichlorobenzene sulphonamides

These absorbed the infrared light at the following wave lengths in cm^{-1}: 1,490 for 1,4-disubstituted, 1,2,3-, 1,2,4- and 1,3,5-trisubstituted aromatic nucleus, 840 for C—Cl aromatic, 1,356 and 1,180 for SO_2—N— group, and 3,310 for —N—H.

Antibacterial and antifungal activity of the prepared compounds

There is no single test which is suitable for general evaluation of the germicidal cemicals.

In the present work, the antibacterial and antifungal activity of the prepared compounds was measured as described in the experimental part. The results are shown in *Tables 7–16*. The activities of the compounds against a particular organism are compared in these *Tables*, in order to find out the effects of the chlorine position in the molecule, the nature and position of the other substituents R_1 and the nature of the bridge between the two aromatic nuclei. Activity and inactivity towards the test organism were met with among compounds with the same position of chlorine, but with different —NH— substitution and compounds with the same—NH—substitution, but with different position of chlorine. This indicated the interference of the influences of chlorine position, the nature of the —NH— substituent and the position of substitution in the latter on the toxicity of these compounds to the test organisms.

Table 17.

Prepared compounds which have a biological effect on the test organisms

Organism	Compound
Bacillus subtilis	$II_{3,5}$, VI_5
Bacillus cereus	$II_{3,5}$, VI_5
Micrococcus sp.	II_3, VI_5
Salmonella sp.	$II_{3,5}$, $VI_{2,5}$
Sarcina sp.	$II_{3,5}$
Staphylococcus aureus	$II_{3,5}$
Saccharomyces cerevisiae	$II_{3,5}$

REFERENCES

1. Runge, F. and El-Hewehi,: J. Prakt. Chem. *1962* 16, 297.
2. Marei, A. et al.: Bull. NRC, Egypt. *1979*, 4 (4) (in press).
3. Marei, A. et al.: Bull. NRC, Egypt. *1980*, 5 (2) (in press).
4. Kaufman: Ber. *1909*, 42, 3480.
5. Chester, B., Kremer, and Bendich, A.: J. Am. Chem. Soc. *1939*, 61, 2658.
6. Hodgson: J. Chem. Soc. *1929*, 2922
7. Somasekhara, S. et al.: Indian J. Chem. *1968*.
8. Stewart: J. Chem. Soc. *1922*, 121, 2555.
9. Seikel: Org. Synth. *1944*, XXIV, 47.
10. Abou Zeid, A. A. and Shahata, Y. M.: Indian J. of Pharmacy *1969*, 31 (3) 72–75.

РЕЗЮМЕ

Авторами изготовлены изомеры шести различно замещенных анилидев диклоро-бензол-сульфонил-клорида и изучены их бактерицидные и фунгицидные свойства. Изучено далее взаимосвязь между химической структурой и токсичностью.

HUNGARIAN JOURNAL
OF INDUSTRIAL CHEMISTRY
VESZPRÉM
Vol. 9. pp. 427–440 (1981)

BIOCIDES FROM HALOGENATED BENZENES. II.

SOME *N*-SUBSTITUTED DICHLOROBENZENE SULPHONAMIDES AND THEIR BIOLOGICAL ACTIVITIES

*A. Marei, **M. M. A. El-Sukkary, **F. I. El-Dib
and ***O. H. El-Sayed

(*Chemistry Dept., Riyadh University, Riyadh, Saudi Arabia;
**Petrochemical Dept., Petroleum Research Institute, Cairo,
Egypt. and ***Chem. of Microorganisms Lab., National
Research Centre, Cairo, Egypt.)

Received: November 24. 1981.

A number of *N*-substituted dichlorobenzene sulphonamide were prepared and their biocidal activity towards bacteria and fungi was screened.

Introduction

The structure —SO_2NHCO— has proved to be of high biochemical significance on bacteria and fungi [1, 2]. The present investigation involves the preparation of some new *N*-substituted dichlorobenzene sulphonamides and the correlation of their biocidal activities with their structures.

Experimental

Preparation of 2,3-dichlorobenzene sulphonamide

This was prepared from 2,3-dichlorobenzene sulphonyl chloride and NH_4OH according to [3]; m.p. 224–225 °C, from aqueous ethanol;

$C_6H_5Cl_2NO_2S$, Calculated: C, 31.88; H, 2.23; N, 6.19; Cl, 31.36; S, 14.18
Found: C, 32.00; H, 2.14; N, 6.51; Cl, 31.67; S, 14.88

IR absorption at wavelengths 1,460 cm^{-1} for 1,2,3-trisubstituted aromatic nucleus, 480 cm^{-1} for C—Cl, 1,180 and 1,360 for SO_2—N— group and 3,310 for —N—H.

Preparation of 3,4-, 3,5-, 2,4-, 2,5- and 2,6-dichlorobenzene sulphonamides

These were prepared from the corresponding dichlorobenzene sulphonyl chlorides with NH_4OH according to [3].

Preparation of N-Substituted dichlorobenzene sulphonamides

a) Each dichlorobenzene sulphonamide isomer (0.005 mol), the aliphatic acid chloride (0.007 mol) and glacial acetic acid (5 ml) were mixed and heated on boiling water-bath for $^1/_2$ hr under reflux condenser. The excess acid chloride was then evaporated and the residue was poured on ice cold water (100 ml). The solid product was filtered, dissolved in $NaHCO_3$ solution (100 ml) and then filtered. The filtrate was acidified with glacial acetic acid. The solid product which separated was filtered and crystallized from ethanol.

Tables 1–6; Compounds I_{7-9}, II_{7-9}, III_{7-9}, IV_{7-9}, V_{7-9} and VI_{7-9}.

b) Each dichlorobenzene sulphonamide isomer (0.005 mol) and the used aromatic acid chloride (0.005 mol) were mixed and heated at 180–190 °C for 1 hr. The mixture was taken in ethanol (100 ml) and heated with charcoal under reflux for $^1/_2$ hr. After filteration, concentration of the filterate and cooling the separated product was filtered and recrystallized from ethanol.

Tables 1–6; Compounds I_{10-18}, II_{10-18}, III_{10-18}, IV_{10-18}, V_{10-18} and VI_{10-18}.

Antibacterial and antifungal activities of the prepared compounds

This activity was measured in the same manner as described in Part I of this investigation [4].

Discussion

The structures 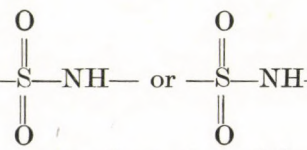 have proved to be of high biochemical significance on bacteria and fungi [1, 2] hence it was planned to prepare a number of substituted and unsubstituted aromatic compounds having such groupings, to screen their toxicity towards microorganisms and to study the variation of the degree of toxicity with the nature and position of the substituent. Dichlorobenzene sulphonyl chlorides and sulphonamides were chosen as starting materials in the present synthesis.

Dichlorobenzene sulphonamides

A scheme for the synthesis of the six isomers of dichlorobenzene sulphonyl chlorides and dichlorobenzene sulphonamides, which form the mother substances of the prepared N-substituted dichlorobenzene sulphonamides is given

Table 1.

No. of comp.	Nomenclature	M.P. °C
I_7	N-acetyl-2,3-dichloro-benzene sulphonamide	114-5
I_8	N-propionyl-2,3-dichloro-benzene sulphonamide	130-1
I_9	N-buteryl-2,3-dichloro-benzene sulphonamide	137-8
I_{10}	N-benzoyl-2,3-dichloro-benzene sulphonamide	75-6
I_{11}	N-*o*-chlorobenzoyl-2,3-dichlorobenzene sulphonamide	133-4
I_{12}	N-*m*-chlorobenzoyl-2,3-dichlorobenzene sulphonamide	116-7
I_{13}	N-*p*-chlorobenzoyl-2,3-dichlorobenzene sulphonamide	128-9
I_{14}	N-*o*-methoxybenzoyl-2,3-dichlorobenzene sulphonamide	140-1
I_{15}	N-*m*-methoxybenzoyl-2,3-dichlorobenzene sulphonamide	110-1
I_{16}	N-*p*-methoxybenzoyl-2,3-dichlorobenzene sulphonamide	91-2
I_{17}	N-*m*-nitrobenzoyl-2,3-dichlorobenzene sulphonamide	60-1
I_{18}	N-*p*-nitrobenzoyl-2,3-dichlorobenzene sulphonamide	52-3

Table 2.

No. of comp.	Nomenclature	M.P. °C
II_7	N-acetyl-3,4-dichloro-benzene sulphonamide	148-9
II_8	N-propionyl-3,4-dichloro-benzene sulphonamide	120-1
II_9	N-buteryl-3,4-dichloro-benzene sulphonamide	82-3
II_{10}	N-benzoyl-3,4-dichloro-benzene sulphonamide	165-6
II_{11}	N-*o*-chlorobenzoyl-3,4-dichlorobenzene sulphonamide	106-7
II_{12}	N-*m*-chlorobenzoyl-3,4-dichlorobenzene sulphonamide	168-9
II_{13}	N-*p*-chlorobenzoyl-3,4-dichlorobenzene sulphonamide	178-9
II_{14}	N-*o*-methoxybenzoyl-3,4-dichlorobenzene sulphonamide	150-1
II_{15}	N-*m*-methoxybenzoyl-3,4-dichlorobenzene sulphonamide	119-20
II_{16}	N-*p*-methoxybenzoyl-3,4-dichlorobenzene sulphonamide	230-1
II_{17}	N-*m*-nitrobenzoyl-3,4-dichlorobenzene sulphonamide	153-4
II_{18}	N-*p*-nitrobenzoyl-3,4-dichlorobenzene sulphonamide	173-4

Table 3.

No. of comp.	Nomenclature	M.P. °C
III_7	N-acetyl-2,5-dichloro-benzene sulphonamide	213-4
III_8	N-propionyl-2,5-dichloro-benzene sulphonamide	139-40
III_9	N-buteryl-2,5-dichloro-benzene sulphonamide	137-8
III_{10}	N-benzoyl-2,5-dichloro-benzene sulphonamide	141-2
III_{11}	N-*o*-chlorobenzoyl-2,5-dichlorobenzene sulphonamide	134-5
III_{12}	N-*m*-chlorobenzoyl-2,5-dichlorobenzene sulphonamide	190-1
III_{13}	N-*p*-chlorobenzoyl-2,5-dichlorobenzene sulphonamide	205-6
III_{14}	N-*o*-methoxybenzoyl-2,5-dichlorobenzene sulphonamide	193-4
III_{15}	N-*m*-methoxybenzoyl-2,5-dichlorobenzene sulphonamide	125-6
III_{16}	N-*p*-methoxybenzoyl-2,5-dichlorobenzene sulphonamide	230-1
III_{17}	N-*m*-nitrobenzoyl-2,5-dichlorobenzene sulphonamide	234-5
III_{18}	N-*p*-nitrobenzoyl-2,5-dichlorobenzene sulphonamide	214-5

Table 4.

No. of comp.	Nomenclature	M.P. °C
IV_7	N-acetyl-2,4-dichloro-benzene sulphonamide	165-6
IV_8	N-propionyl-2,4-dichloro-benzene sulphonamide	176-7
IV_9	N-buteryl-2,4-dichloro-benzene sulphonamide	175-6
IV_{10}	N-benzoyl-2,4-dichloro-benzene sulphonamide	212-3
IV_{11}	N-*o*-chlorobenzoyl-2,4-dichlorobenzene sulphonamide	165-6
IV_{12}	N-*m*-chlorobenzoyl-2,4-dichlorobenzene sulphonamide	130-1
IV_{13}	N-*p*-chlorobenzoyl-2,4-dichlorobenzene sulphonamide	167-8
IV_{14}	N-*o*-methoxybenzoyl-2,4-dichlorobenzene sulphonamide	166-7
IV_{15}	N-*m*-methoxybenzoyl-2,4-dichlorobenzene sulphonamide	164-5
IV_{16}	N-*p*-methoxybenzoyl-2,4-dichlorobenzene sulphonamide	160-1
IV_{17}	N-*m*-nitrobenzoyl-2,4-dichlorobenzene sulphonamide	218-9
IV_{18}	N-*p*-nitrobenzoyl-2,4-dichlorobenzene sulphonamide	200-1

Table 5.

No. of comp.	Nomenclature	M.P. °C
V_7	N-acetyl-2,6-dichloro-benzene sulphonamide	178-9
V_8	N-propionyl-2,6-dichloro-benzene sulphonamide	165-6
V_9	N-buteryl-2,6-dichloro-benzene sulphonamide	128-9
V_{10}	N-benzoyl-2,6-dichloro-benzene sulphonamide	169-70
V_{11}	N-*o*-chlorobenzoyl-2,6-dichlorobenzene sulphonamide	215-6
V_{12}	N-*m*-chlorobenzoyl-2,5-dichlorobenzene sulphonamide	194-5
V_{13}	N-*p*-chlorobenzoyl-2,6-dichlorobenzene sulphonamide	188-9
V_{14}	N-*o*-methoxybenzoyl-2,6-dichlorobenzene sulphonamide	197-8
V_{15}	N-*m*-methoxybenzoyl-2,6-dichlorobenzene sulphonamide	165-6
V_{16}	N-*p*-methoxybenzoyl-2,6-dichlorobenzene sulphonamide	212-3
V_{17}	N-*m*-nitrobenzoyl-2,6-dichlorobenzene sulphonamide	245-6
V_{18}	N-*p*-nitrobenzoyl-2,6-dichlorobenzene sulphonamide	203-4

Table 6.

No. of comp.	Nomenclature	M.P. °C
VI_7	N-acetyl-3,5-dichloro-benzene sulphonamide	187-8
VI_8	N-propionyl-3,5-dichloro-benzene sulhponamide	144-5
VI_9	N-buteryl-3,5-dichloro-benzene sulphonamide	103-4
VI_{10}	N-benzoyl-3,5-dichloro-benzene sulphonamide	134-5
VI_{11}	N-*o*-chlorobenzoyl-3,5-dichlorobenzene sulphonamide	117-8
VI_{12}	N-*m*-chlorobenzoyl-3,5-dichlorobenzene sulphonamide	170-1
VI_{13}	N-*p*-chlorobenzoyl-3,5-dichlorobenzene sulphonamide	236-7
VI_{14}	N-*o*-methoxybenzoyl-3,5-dichlorobenzene sulphonamide	137-8
VI_{15}	N-*m*-methoxybenzoyl-3,5-dichlorobenzene sulphonamide	225-6
VI_{16}	N-*p*-methoxybenzoyl-3,5-dichlorobenzene sulphonamide	183-4
VI_{17}	N-*m*-nitrobenzoyl-3,5-dichlorobenzene sulphonamide	134-5
VI_{18}	N-*p*-nitrobenzoyl-3,5-dichlorobenzene sulphonamide	227-8

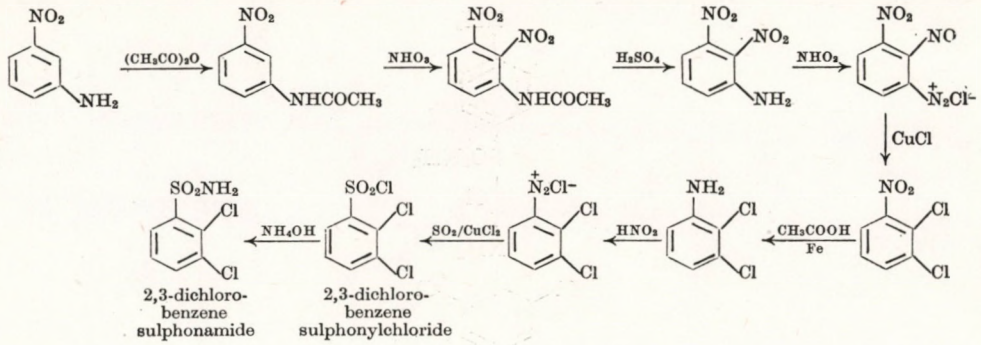
NO2
NH2
(CH3CO)2O
NHCOCH3
NHO3
NO2
H2SO4
NO
+
N2Cl-
CuCl
SO2NH2
Cl
SO2Cl
NH4OH
SO2/CuCl2
HNO2
CH3COOH
Fe
2,3-dichloro-
benzene
sulphonamide
2,3-dichloro-
benzene
sulphonylchloride

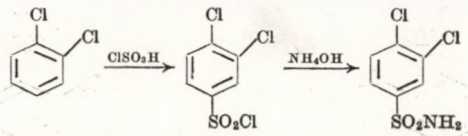
Cl
ClSO3H
SO2Cl
NH4OH
SO2NH2

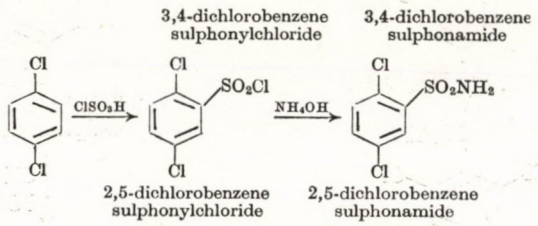
3,4-dichlorobenzene
sulphonylchloride
3,4-dichlorobenzene
sulphonamide
Cl
ClSO3H
SO2Cl
NH4OH
SO2NH2
2,5-dichlorobenzene
sulphonylchloride
2,5-dichlorobenzene
sulphonamide

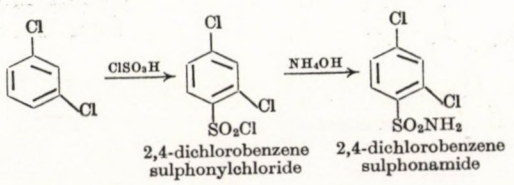
Cl
ClSO3H
SO2Cl
NH4OH
SO2NH2
2,4-dichlorobenzene
sulphonylchloride
2,4-dichlorobenzene
sulphonamide

Fig. 1

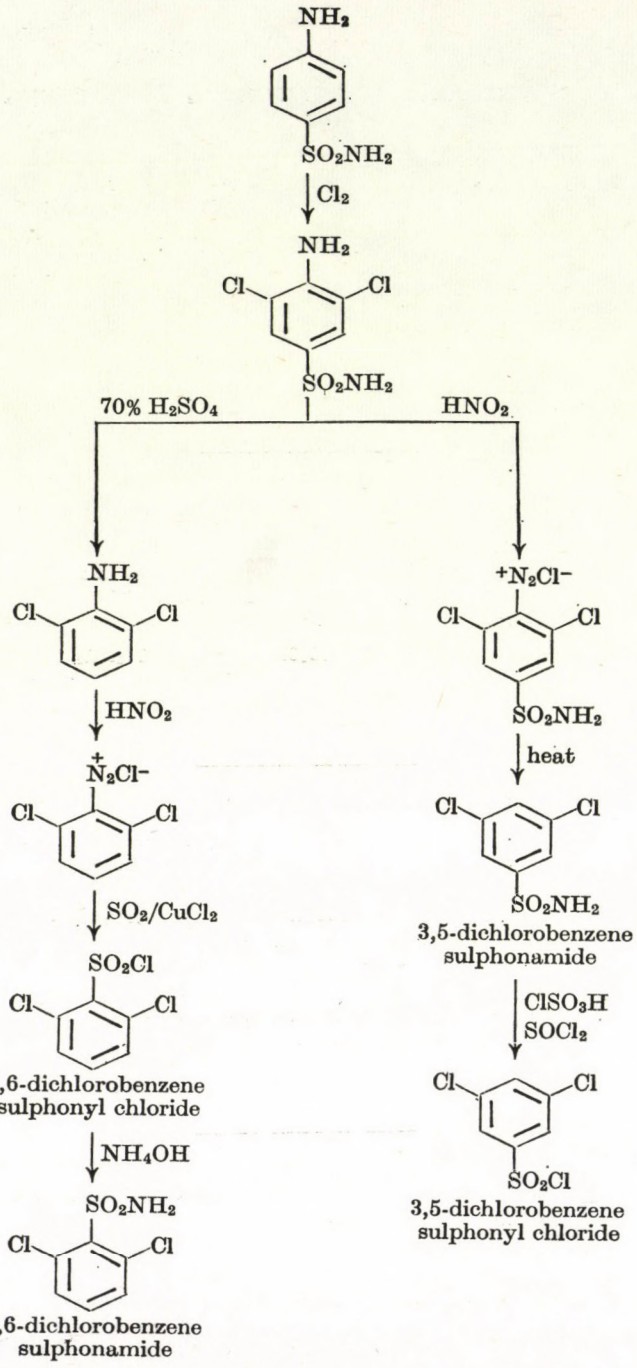
NH2
SO2NH2
Cl2
NH2
Cl
Cl
SO2NH2
70% H2SO4
HNO2
NH2
Cl
Cl
HNO2
+N2Cl−
Cl
Cl
SO2NH2
heat
+N2Cl−
Cl
Cl
SO2/CuCl2
Cl
Cl
SO2NH2
3,5-dichlorobenzene sulphonamide
SO2Cl
Cl
Cl
ClSO3H
SOCl2
2,6-dichlorobenzene sulphonyl chloride
Cl
Cl
SO2Cl
3,5-dichlorobenzene sulphonyl chloride
NH4OH
SO2NH2
Cl
Cl
2,6-dichlorobenzene sulphonamide

Fig. 2

in the following charts. The preparations were carried out according to the references [3–10].

Each sulphonamide was converted to twelve N-substituted dichlorobenzene sulphonamides with the following stfuctures:

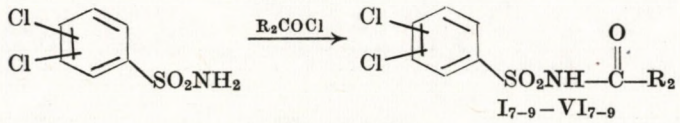

$I_{7-9} - VI_{7-9}$

R_2 = Me; Et; Prop.
(tables 1–6)

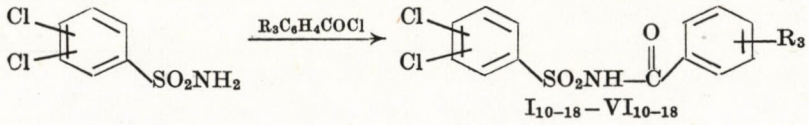

$I_{10-18} - VI_{10-18}$

R_3 – H; *o*- or *m*- or *p*-Cl; *o*- or *m*- or *p*-OMe; *m*- or *p*-NO_2
(tables 1–6)

The chemical structures of the prepared new compounds were elucidated by microanalysis and infrared light absorption measurments. The compounds which have analogous structure absorbed this light nearly at the same wavelengths. The following results were obtained from some compounds which can be considered as representatives of their classes in the present work.

N-acetyl, N-benzoyl, N-p-chlorobenzoyl, N-p-methoxybenzoyl and N-p- nitrobenzoyl-2,5-dichlorobenzene sulphonamides

These absorbed infrared light at the following wavelengths in cm^{-1}: 1,460–1,475 for 1,4-disubstituted and 1,2,4-trisubstituted aromatic nucleus, 840 for C—Cl aromatic, 1,350 and 1,180 for SO_2—N-group, 3,310 for —N—H, 1,480–1,575 and 1,650–1,710 for —NH—CO—, 1,315 for C—NO_2.

Antibacterial and Antifungal Activity of the Prepared Compounds

In the following Tables a comparison is made between the compounds which are active against a particular organism to find out the effects of chlorine position in the molecules, of nature and position of the other substituents R_2, R_3 and of the nature of the bridge between the two aromatic nuclei. The activity and inactivity towards the test organism were met with among compounds with the same position of chlorine, but with different —NH— substitution and compounds with the same —NH— substitution, but different position of chlorine. This indicates the interference of the influences of chlorine position, of the nature of the —NH— substituent and also of the position of substitution in the latter on the toxicity of these compounds to the test organisms.

Position of Cl_2	Activity of the test compounds against Bacillus subtilis											
	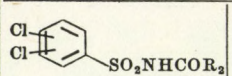			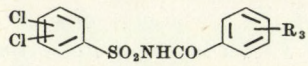								
	R_2=			R_3=								
	Me 7	Et 8	Prop. 9	H 10	*o*-Cl 11	*m*-Cl 12	*p*-Cl 13	*o*-OMe 14	*m*-OMe 15	*p*-OMe 16	*m*-NO_2 17	*p*-NO_2 18
2,3- I	–	–	+ + +	+ + +	–	–	+ + +	+ +	+ + +	+ + +	–	+ + +
3,4- II	+ + +	+ +	+ + +	+ + +	–	–	+ +	–	+ + +	–	+ + +	+ +
2,5- III	–	–	–	–	+ +	–	+ + +	+ +	+ + +	+ +	+	–
2,4- IV	–	+	–	+ + +	–	+ + +	–	+ +	–	+ + +	+ + +	–
2,5- V	+	–	+	+ + +	+ + +	+ + +	+ +	+	+ + +	+ + +	–	–
3,5- VI	–	+ + +	+	–	–	–	–	–	+ + +	+ + +	–	+ + +

1 — Cl_2 is active in the positions: 2,3-, 3,4- and 3,5 (Cpds: $I_{7-9}-V_{7-9}$)

2 — *p*-Cl *p*-OMe (Cpds: III_{13}, III_{16})
p-OMe *p*-Cl (Cpds: V_{13}, V_{16})

3 — *p*- and *m*-OMe *o*-OMe (Cpds: I_{14}, I_{15}, I_{-16})
m-NO_2 *p*-NO_2 (Cpds: II_{17}, II_{18})
p-Cl *o*-Cl (Cpds: III_{11}, III_{13})
m-OMe *o*- & *p*-OMe (Cpds: II_{14}, III_{15}, III_{16})
p-OMe *o*-OMe (Cpds: IV_{14}, IV_{16})
o- and *m*-Cl *p*-Cl (Cpds: V_{11}, V_{12}, V_{13})

4 — -SO_2NHCO- SO_2NH- (Cpds: VI_2, VI_{15})

Position of Cl_2	Activity of the test compounds against Escherichia coli											
	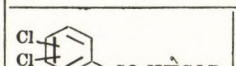			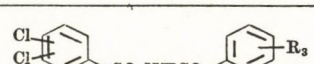								
	R_2=			R_3=								
	Me 7	Et 8	Prop. 9	H 10	*o*-Cl 11	*m*-Cl 12	*p*-Cl 13	*o*-OMe 14	*m*-OMe 15	*p*-OMe 16	*m*-NO_2 17	*p*-NO_2 18
2,3- I	–	–	+ +	+ +	–	–	–	–	–	–	–	+ + +
3,4- II	+ + +	+ + +	+ + +	–	–	–	+ + +	–	–	–	–	+ +
2,5- III	–	–	–	–	–	–	+ +	–	–	+ + +	–	–
2,4- IV	–	+ +	–	–	–	+ +	–	+ +	–	+ +	–	–
2,6- V	–	–	+ + +	+	–	–	+ +	–	+ +	–	–	–
3,5- VI	–	–	–	–	–	–	–	–	–	–	–	–

1 — Cl_2 is active in the positions 2,6-, 3,4- (Cpds: $I_{7-9}-VI_{7-9}$)
Cl_2 is active in the positions 2,3-, 2,5-, 3,4- (Cpds: I_{10-18}–VI_{10-18})

2 — *p*-Cl > *p*-NO_2 (Cpds: II_{13}, $II_{18}z$)
p-OMe > *p*-Cl (Cpds: III_{13}, III_{16})

Position of Cl_2	Activity of the test compounds against Aspergillus niger											
	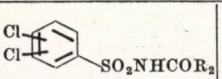			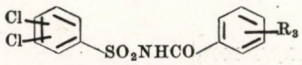								
	R_2=			R_3=								
	Me 7	Et 8	Prop. 9	H 10	*o*-Cl 11	*m*-Cl 12	*p*-Cl 13	*o*-OMe 14	*m*-OMe 15	*p*-OMe 16	*m*-NO_2 17	*p*-NO_2 18
2,3- I	–	–	++	+	–	–	+++	+++	+++	++	–	+
3,4- II	–	–	+++	–	–	–	–	–	–	–	+	–
2,5- III	–	–	–	–	–	–	+++	–	–	–	–	–
2,4- IV	–	–	–	+++	–	–	–	–	–	–	–	–
2,6- V	–	–	++	–	–	–	+++	–	–	–	–	–
3,5- VI	–	–	–	–	–	–	–	–	–	+++	–	+

1 — Cl_2 is active in position 3,4- only (Cpds: $I_{7-9}-VI_{7-9}$)
Cl_2 is inactive in position 3,4- (Cpds: $I_{10-18}-VI_{10-18}$)

2 — *p*-Cl > *p*-OMe (Cpds: I_{13}, I_{16})

3 — *o*- and *m*-OMe > *p*-OMe (Cpds: I_{14}, I_{15}, I_{16})

Position of Cl_2	Activity of the test compounds against Candida elbicans											
	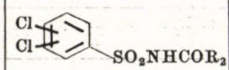			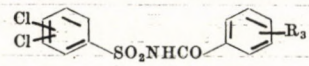								
	R_2=			R_3=								
	Me 7	Et 8	Prop. 9	H 10	*o*-Cl 11	*m*-Cl 12	*p*-Cl 13	*o*-OMe 14	*m*-OMe 15	*p*-OMe 16	*m*-NO_2 17	*p*-NO_2 18
2,3- I	–	–	–	–	–	–	–	–	–	–	–	+++
3,4- II	–	–	–	–	–	–	–	–	–	–	–	+++
2,5- III	–	–	–	–	–	–	+	–	–	–	–	+
2,4- IV	–	–	–	–	–	–	–	–	–	+	–	–
2,6- V	–	–	–	–	–	–	+	–	–	–	–	–
3,5- VI	–	–	–	–	–	–	–	–	–	+	–	–

Only I_{18} & II_{18} were found to be toxic to this organism. Both of them contain *p*-NO_2 and the Cl atoms are in the position 2,3- and 3,4.

Position of Cl_2	Activity of the test compounds against Bacillus cereus											
	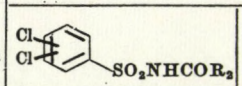			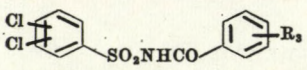								
	R_2=			R_3=								
	Me 7	Et 8	Prop. 9	H 10	*o*-Cl 11	*m*-Cl 12	*p*-Cl 13	*o*-OMe 14	*m*-OMe 15	*p*-OMe 16	*m*-NO_2 17	*p*-NO_2 18
2,3- I			++	+++			++	+++	+++	+++		++
3,4- II	+++	+++	+++	+++			++		+++		++	+++
2,5- III					++		+++	+++	+++	+++		
2,4- IV		+++		+++		++		+++		+++	+++	
2,6- V			+++	+++	++	++	+++		+++	+++		
3,5- VI		++							+++	+++		++

1 — Cl_2 is active in positions 2,4-, 2,6- and 3,4- (Cpds: $I_{7-9}-VI_{7-9}$)
No change in the activity with variation of Cl_2 position (Cpds: $I_{10-18}-VI_{10-18}$)

2 — *p*-OMe > *p*-Cl and *p*-NO_2 (Cpds: I_{13}, I_{16} and I_{18})
p-NO_2 > *p*-Cl (Cpds: II_{13} and II_{18})
o-OMe > *o*-Cl (Cpds: III_{11} and III_{14})
m-NE_2 > *m*-Cl (Cpds: IV_{12} and IV $_{17}$)
m-OMe > *m*-Cl (Cpds: V_{12} and V_{15})
p-OMe > *p*-NO_2 (Cpds: VI_{16} and VI_{18})

3 — *p*-NO_2 > *m*-NO_2 (Cpds: II_{17} and II_{18})
p-Cl > *o*-Cl (Dpds: III_{11} and III_{13})
p-Cl > Cl (Cpds: V_{11}, V_{12} and V_{13})

4 — SO_2CO- > -SO_2NH- (Cpds: VI_2 and VI_{15})

Position of Cl_2	Activity of the test compounds against Micrococcus sp.											
	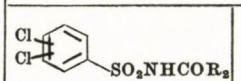			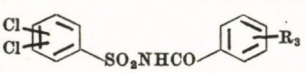								
	R_2=			R_3=								
	Me 7	Et 8	Prop. 9	H 10	*o*-Cl 11	*m*-Cl 12	*p*-Cl 13	*o*-OMe 14	*m*-OMe 15	*p*-OMe 16	*m*-NO_2 17	*p*-NO_2 18
2,3- I			+++	+++			++	++	++	+++		+++
3,4- II	+++	+++	+++	+++			+++		+++		+++	+++
2,5- III					–		++	++	++	+++		
2,4- IV		+++		+++		++		++		++	++	
2,6- V			+++	+++	++	+++	+++		+++	+++		
3,5- VI		+++							+++	+++		+++

1 — Cl_2 is inactive in the position 2,5- (Cpds: $I_{7-9}-VI_{7-9}$)
Variation of toxicity with Cl_2 position cannot be traced (Cpds: $I_{10-18}-VI_{10-18}$)

2 — *p*-OMe > *p*-Cl (Cpds: I_{13}, I_{16} and III_{13}, III_{16})
p-NO_2 > *p*-Cl (Cpds: I_{13}, I_{18})

3 — *p*-OMe > *m*- & *o*-OMe (Cpds: I_{14}, I_{15}, I_{16} and III_{14}, III_{15}, III_{16})
p- and *m*-Cl > *o*-Cl (Cpds: V_{11}, V_{12}, V_{13}).

Position of Cl_2	Activity of the test compounds against Salmonella sp.											
	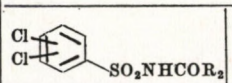			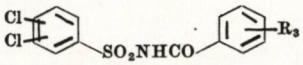								
	R_2=			R_3=								
	Me 7	Et 8	Prop. 9	H 10	*o*-Cl 11	*m*-Cl 12	*p*-Cl 13	*o*-OMe 14	*m*-OMe 15	*p*-OMe 16	*m*-NO_2 17	*p*-NO_2 18
2,3- I			+ + +	+ + +			+ +	+ +	+ +	+ + +		+ + +
3,4- II	+ + +	+ + +	+ + +	+ + +			+ + +		+ + +		+ +	+ + +
2,5- III					+ + +		+ + +	−	+ +	+ + +		
2,4- IV		+ + +		+ + +		+ + +		+ + +		+ + +	+ + +	
2,6- V			+ + +	+ + +	+ +	+ +	+ +		+ + +	+ + +		
3,5- VI		+ + +				.			+ + +	+ + +		+ + +

1 — Cl_2 is inactive in the position 2,5- (Cpds: $I_{7-9}-VI_{7-9}$)
No change of toxicity with variation of Cl_2 position (Cpds: $I_{10-18}-VI_{10-18}$)

2 — *p*-OMe and *p*-NO_2 > *p*-Cl (Cpds: I_{13}, I_{16}, I_{18})
m-OMe > *m*-NO_2 (Cpds: II_{15}, II_{17})
m-OMe > m-Cl (Cpds: V_{12}, V_{15})
p-OMe > *p*-Cl (Cpds: V_{13}, V_{16})

3 — *p*-OMe > *o*-OMe (Cpds: I_{14}, I_{16})
p-OMe > *m*-OMe (Cpds: I_{15}, I_{16} and III_{15}, III_{16})
p-NO_2 > *m*-NO_2 (Cpds: II_{17}, II_{18})

Position of Cl_2	Activity of the test compounds against Sarcina sp.											
	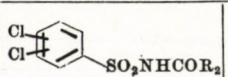			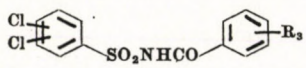								
	R_2=			R_3=								
	Me 7	Et 8	Prop. 9	H 10	*o*-Cl 11	*m*-Cl 12	*p*-Cl 13	*o*-OMe 14	*m*-OMe 15	*p*-OMe 16	*m*-NO_2 17	*p*-NO_2 18
2,3- I			−	+ + +			−	+ +	+ + +	+ + +		+ +
3,4- II	+ +	+ + +	+ + +	+ +			+ +		+ + +		+	+ + +
2,5- III					−		+ +	+ + +	+ + +	+		
2,4- IV		+ +		+ + +		−		+ + +		−	+ + +	
2,6- V			−	−	−	+ +	+ + +		+ + +	+ + +		
3,5- VI		+ + +							−	+ + +		+

1 — Cl_2 is active in the position 3,4- and 3,5- (Cpds: $I_{7-9}-VI_{7-9}$)
No variation of toxicity with Cl_2 position (Cpds: $I_{10-18}-VI_{10-18}$)

2 — *p*-OMe > *p*-NO_2 > *p*-Cl (inactive) (Cpds: I_{13}, I_{16}, I_{18})
p-NO_2 > *p*-Cl (Cpds: II_{13}, II_{18})
m-OMe > *m*-Cl (Cpds: V_{12}, V_{15})
Propyl and ethyl > methyl (Cpds: II_7, II_8, II_9)

3 — *p*- and *m*-OMe > *o*-OMe (Cpds: I_{14}, I_{15}, I_{16})
p-Cl > *m*-Cl (Cpds: V_{12}, V_{13})

Position of Cl_2	Activity of the test compounds against Staphylococcus aureus											
	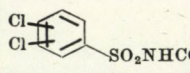			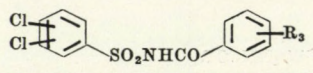								
	R_2=			R_3=								
	Me 7	Et 8	Prop. 9	H 10	*o*-Cl 11	*m*-Cl 12	*p*-Cl 13	*o*-OMe 14	*m*-OMe 15	*p*-OMe 16	*m*-NO_2 17	*p*-NO_2 18
2,3- I			+ + +	+ + +			+ + +	+ + +	+ + +	+ + +		+ + +
3,4- II	+ +	+ +	+ + +	+ + +			+ + +		+ + +		+ +	+ + +
2,5- III					+ +		+ + +	+ +	+ + +	+ + +		
3,4- IV		+ + +		+ + +		−		+ +		+ + +	+ + +	
2,6- V			+ + +	+ + +	+ + +	+ + +	+ + +		+ + +	+ + +		
3,5- VI		+ + +							+ +	+ + +		+ + +

1 — Cl_2 is inactive in position 2,5- (Cpds: $I_{7-9}-VI_{7-9}$)
No change in toxicity with Cl_2 position (Cpds: $I_{10-18}-VI_{10-18}$)

2 — Propyl > ethyl and methyl (Cpds: II_7-II_{18})

3 — *p*-NO_2 > *m*-NO_2 (Cpds: $II_{17}-II_{18}$)
p-Cl > *o*-Cl (Cpds: III_{11}–III_{13})
p-OMe > *o*-OMe (Cpds: III_{14}, III_{16} and IV_{14}, IV_{16})
p-OMe > *o*-OMe (Cpds: VI_{15} and VI_{16})

Position of Cl_2	Activity of the test compounds againts Saccharomyces cerevisiae											
	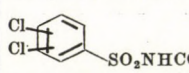			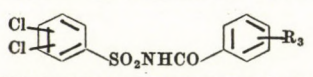								
	R_2=			R_3=								
	Me 7	Et 8	Prop. 9	H 10	*o*-Cl 11	*m*-Cl 12	*p*-Cl 13	*o*-OMe 14	*m*-OMe 15	p-OMe 16	*m*-NO_2 17	*p*-NO_2 18
2,3- I			+ + +	+ + +			+ +	+ + +	+ + +	+ + +		+ +
3,4- II	+ + +	+ + +	+ + +	+ + +			+ + +		+ + +		+ + +	+ + +
2,5- III					−		+ +	+ +	+ + +	+ + +		
2,4- IV		+ + +		+ + +		+ +		+ + +		+ + +	+ + +	
2,6- V			+ + +	+ + +	+ + +	+ + +	+ + +		+ +	+ + +		
3,5- VI		+ + +							+ + +	+ + +		+ +

1 — Cl_2 is inactive in the position 2,5- and active in the position 3,5- (Cpds: $I_{7-9}-VI_{7-9}$)
No variation of toxicity with Cl_2 position (Cpds: $I_{10-18}-VI_{10-18}$)

2 — *p*-OMe > *p*-Cl (Cpds: I_{13}, I_{16} and II_{13}, III_{16})
p-OMe > *p*-NO_2 (Cpds: I_{16}, I_{18} and VI_{16}, VI_{18})
m-NO_2 > *m*-Cl (Cpds: IV_{12}, IV_{17})

3 — *p*-OMe > *m*-OMe (Cpds: III_{15}, III_{16} and V_{15}, V_{16})
p-OMe > *o*-OMe (Cpds: III_{14}, III_{16})

4 — -SO_2NHCO- > -SO_2NH- in (compounds VI_2 and VI_{15})

Prepared compounds which have a biological effect on the test organisms

Organism	Compound
Bacillus subtilis	$I_{9,10,13,15,16,18}$; $II_{7,9,10,15,17}$; $III_{13,15}$; $IV_{10,12,16,17}$; $V_{10,11,12,15,16}$; $VI_{8,15,16,18}$
Escherichia coli	I_{18}; $II_{7,8,9,13}$; III_{16}; V_9
Aspergillus niger	$I_{13,14,15}$; II_9; III_{13}; IV_{10}; V_{13}; VI_{16}
Candida albicans	I_{18}; II_{18}
Bacillus cereus	$I_{10,14,15,16}$; $II_{7,8,9,10,15,18}$; $III_{13,14,15,16}$; $IV_{8,10,14,16,17}$; $V_{9,10,13,15,16}$; $VI_{15,16}$
Micrococcus sp.	$I_{9,10,16,18}$; $II_{7,8,9,10,13,15,17,18}$; III_{16}; $IV_{8,10}$; $V_{9,10,12,13,15,16}$; $VI_{8,15,16,18}$
Salmonella sp.	$I_{9,10,16,18}$; $II_{7,8,9,10,13,15,18}$; $III_{11,13,16}$; $IV_{8,10,12,14,16,17}$; $V_{9,10,15,16}$; $VI_{8,15,16,18}$
Sarcina sp.	$I_{10,15,16}$; $II_{8,9,15,18}$; $III_{14,15}$; $IV_{10,14,17}$; $V_{13,15,16}$; $VI_{8,16}$
Staphylococcus aureus	$I_{9,10,13,14,15,16,18}$; $II_{9,10,13,15,18}$; $III_{13,15,16}$; $IV_{8,10,16,17}$; $V_{9,10,11,12,13,15,16}$; $VI_{8,16,18}$
Saccharomyces cerevisiae	$I_{9,10,14,15,16}$; $II_{7,8,10,13,15,17,18}$; $III_{15,16}$; $IV_{8,10,14,16,17}$; $V_{9,10,11,12,13,16}$; $VI_{8,15,16}$

REFERENCES

1. Swiss Patent, 247–867 1948; C.A. *1949*, 43, 7960.
2. Raffa, L. et al.: Formaco Parria, Ed. Sci. *1965*, 20, (11) 786–799.; C.A. *1966*, 65, 13592.
3. Somasekhara, S. et al.: Indian J. Chem. *1968*, 6, (1) 19–23.
4. Marei, A. et al.: Hung. J. Ind. Chem. *1981*, 9, 000–000.
5. Kaufmann: Ber. *1909*, 42, 3480.
6. Chester, Kremer, B. and Bendich, A.: J. Am. Chem. Soc. *1939*, 61, 2658.
7. Hodgson: J. Chem. Soc. *1929*, 2922.
8. Stewart: J. Chem. Soc. *1922*, 121, 2922.
9. Seikel: Org. Synth. *1944*, XXV, 47.
10. Marei, A. et al.: Bull. NRC., Egypt, *1979*, 4, (4) (in press).

РЕЗЮМЕ

Авторами изготовлены *N*-замещенные производные сульфонамида диклоробензола и изучены их бактерицидные и фунгицидные свойства.

Egyetemi Nyomda — 82.7281 Budapest, 1981. Felelős vezető: Sümeghi Zoltán igazgató

CONTENTS

Ára: 250 Ft

THE FOLLOWING ARE PLEASED TO ACCEPT SUBSCRIPTIONS TO THIS JOURNAL:

AUSTRALIA

C.B.D. Library and Subscription Service
Box 4886 G.P.O.
Sydney 2000

Cosmos Book and Record Shop
145 Acland Street
St. Kilda 3182

Globe and Co.
694—696 George Street
Sydney 2000

AUSTRIA

Globus (VAZ)
Höchstädtplatz 3
A—1200 Wien XX

BELGIUM

"Du Monde Entier" S. A.
Rue du Midi 162
B—1000 Bruxelles

Office International de Librairie
Avenue Marnix 30
B—1050 Bruxelles

CANADA

Pannonia Books
P.O. Box 1017
Postal Station "B"
Toronto, Ontario M5T 2T8

DENMARK

Munksgaard's Boghandel
Norregade 6
DK—1165 Copenhagen K

FINLAND

Akateeminen Kirjakauppa
Keskuskatu 2, P.O.B. 128
SF—00 100 Helsinki 10

FRANCE

Office International de Documentation et Librairie
48 Rue Gay Lussac
75 Paris 5

GERMAN FEDERAL REPUBLIC

Kubon und Sagner
Pf 68
D—8 München 34
BRD

GREAT BRITAIN

Bailey Bros and Swinfen Ltd.
Warner House, Folkestone
Kent CT 19 6PH England

HOLLAND

Martinus Nijhoff
Periodicals Department
P.O. Box 269
The Hague

Swets and Zeitlinger
Keizersgracht 487
Amsterdam C

ITALY

Licosa
P.O.B. 552, Via Lamarmora 45
50121 Firenze

JAPAN

Igaku Shoin Ltd.
Foreign Department
Tokyo International P.O. Box 5063
Tokyo

Maruzen Co. Ltd.
P.O. Box 5050
Tokyo International 100—31

Nauka Ltd.
Yasutomi Bldg. 5F 2—12 Kanda
Jinbocho, Chiyoda-ku
Tokyo 101

NORWAY

Tanum—Cammermayer
Karl Johangt. 41—43
Oslo 1

SWEDEN

Almqvist and Wiksell Förlag A. B.
Box 2120
S—103 13 Stockholm 2

Wennegren—Williams AB
Subscription Department Fack
S—104 Stockholm 30

SWITZERLAND

Karger Libri A. G.
Petersgraben 31
CH—4011 Basel

USA

Ebsco Subs. Services
1 st Ave North at 13th street
Birmingham, Ala. 35201